IAEA-TECDOC-921

Behaviour of LWR core materials under accident conditions

Proceedings of a Technical Committee meeting held in Dimitrovgrad, Russian Federation, 9–13 October 1995

INTERNATIONAL ATOMIC ENERGY AGENCY IAEA

The IAEA does not normally maintain stocks of reports in this series. However, microfiche copies of these reports can be obtained from

INIS Clearinghouse
International Atomic Energy Agency
Wagramerstrasse 5
P.O. Box 100
A-1400 Vienna, Austria

Orders should be accompanied by prepayment of Austrian Schillings 100,— in the form of a cheque or in the form of IAEA microfiche service coupons which may be ordered separately from the INIS Clearinghouse.

The originating Section of this publication in the IAEA was:

Nuclear Fuel Cycle and Materials Section
International Atomic Energy Agency
Wagramerstrasse 5
P.O. Box 100
A-1400 Vienna, Austria

BEHAVIOUR OF LWR CORE MATERIALS UNDER ACCIDENT CONDITIONS
IAEA, VIENNA, 1996
IAEA-TECDOC-921
ISSN 1011–4289

Printed by the IAEA in Austria
December 1996

FOREWORD

At the invitation of the Government of the Russian Federation, following a proposal of the International Working Group on Water Reactor Fuel Performance and Technology (IWGFPT), the IAEA convened a Technical Committee Meeting on Behaviour of LWR Core Materials Under Accident Conditions from 9 to 13 October 1995 in Dimitrovgrad to analyse and evaluate the behaviour of LWR core materials under accident conditions with special emphasis on severe accidents. In-vessel severe accidents phenomena were considered in detail, but specialized thermal hydraulic aspects as well as ex-vessel phenomena were outside the scope of the meeting.

Forty participants representing eight countries attended the meeting. Twenty- three papers were presented and discussed during five sessions.

Under the auspices of the IWGFPT many different aspects of fuel behaviour in normal, off-normal and accident conditions have been considered at Specialists and Technical Committee meetings convened by the IAEA. Details of the work are recorded in the following publications:

Water Reactor Fuel Safety and Fission Product Release in Off-Normal and Accident Conditions (IWGFPT/16);

Water Reactor Fuel Behaviour and Fission Products Release in Off-Normal and Accident Conditions (IWGFPT/27);

Water Reactor Fuel Element Computer Modelling in Steady State, Transient and Accident Conditions (IWGFPT/32);

Behaviour of Core Materials and Fission Product Release in Accident Conditions in LWRs (IAEA - TECDOC-706).

The OECD/NEA has issued a publication on safety aspects of fuel behaviour in off-normal and accident conditions, resulting from a joint meeting with the IAEA.

Since the last meeting in the IAEA series, significant progress has been made in the understanding of fuel behaviour under design-basis accidents such as LOCA and RIA, and in the identification of the sequence of events that occurs during the disintegration of fuel elements and assemblies during severe fuel damage. These issues became important again as a result of new trends in LWR fuel utilization such as burnup extension and utilization of MOX fuel. In this field, the lack of comprehensive data is obvious and further international effort will be required.

EDITORIAL NOTE

In preparing this publication for press, staff of the IAEA have made up the pages from the original manuscripts as submitted by the authors. The views expressed do not necessarily reflect those of the governments of the nominating Member States or of the nominating organizations.

Throughout the text names of Member States are retained as they were when the text was compiled.

The use of particular designations of countries or territories does not imply any judgement by the publisher, the IAEA, as to the legal status of such countries or territories, of their authorities and institutions or of the delimitation of their boundaries.

The mention of names of specific companies or products (whether or not indicated as registered) does not imply any intention to infringe proprietary rights, nor should it be construed as an endorsement or recommendation on the part of the IAEA.

The authors are responsible for having obtained the necessary permission for the IAEA to reproduce, translate or use material from sources already protected by copyrights.

CONTENTS

FUEL BEHAVIOUR IN SEVERE FUEL DAMAGE CONDITIONS (Session C)

FUEL BEHAVIOUR IN RIA CONDITIONS (Session D)

SUMMARY OF THE TECHNICAL COMMITTEE MEETING

INTRODUCTORY SESSION: GENERAL OVERVIEW

CHAIRMEN: R. A. Moore, USA
N.B. Sokolov, Russian Federation

In accordance with the recommendations of the previous Technical Committe meeting held in France, 1992, the present meeting focussed on behaviour of LWR core materials under severe accident conditions and did not consider specialized thermal hydraulic aspects or ex-vessel phenomena. The papers and comments presented in this session discuss the programs in place to deal with these in-vessel severe accident phenomena.

In the USA, the Department of Energy program has focused on core melt progression and in-vessel retention topics of advanced light water reactor (ALWR) safety. The research and development work supports the understanding of severe accidents and is available for design certification of ALWRs in the regulatory review process. Currently this program, known as the Advanced Reactor Severe Accident Program (ARSAP), supports the US AP-600 reactor design.

Three challenges to vessel integrity are considered: in-vessel steam explosion; vessel wall ablation by melt jet streams; and coolability of in-vessel retained melt. The first two challenges are design-specific to the nuclear design, while in-vessel melt coolability does not depend upon specific accident sequences. The experimental database, as well as relevant information from the TMI-2 accident, were reported. Important conclusions are that the analytical capability to model the first two challenges is being steadily improved through code development and experimental approaches, and that the AP-600 design will achieve an in-vessel coolable melt debris configuration with external water cooling of the lower reactor vessel head.

In Japan, the study of core material behaviour during severe accidents became one of the major research efforts in the 1980s at the Japan Atomic Energy Research Institute (JAERI). Small-scale severe fuel damage experiments in steam and helium environments and debris coolability experiments performed in the Nuclear Safety Research Reactor (NSRR) were typical examples. PBF-SFD, ACRR-DF and LOFT-LP experiments in the United States, Phebus-SFD experiments in France, and CORA experiments in Germany were typical international projects in this stage.

Current research activities in JAERI relating to core material behaviour under accident conditions are as follows:

(1) Fuel quench tests at NSRR
(2) Core materials interaction tests
(3) TMI-2 debris examinations
(4) Reactivity Initiated Accidents (RIA) tests with high burnup fuels at NSRR
(5) Mechanical properties measurements for hydrided cladding.

(1) -(3) are for severe accident study and (4)-(5) are for design- basis accident (RIA).

Fuel quench tests at NSRR were performed to study fuel behaviour during delayed reflooding. Core materials interaction tests have aimed at obtaining quantitative information for evaluating the phenomena observed in the large scale bundle tests and in TMI-2. JAERI participated in the TMI Vessel Investigation Project (TMI-VIP) organised by the OECD/NEA, obtained many TMI-2 debris samples, and performed detailed examinations to identify physical properties of the debris. These efforts will be completed in the very near future.

Recent major issues in LWR safety are fuel burnup extension and utilisation of plutonium as a mixed-oxide (MOX) fuel material. These concerns bring some research subjects relating to design-basis accidents (LOCA and RIA), and current safety guidelines for LOCA and RIA must be examined for high burnup fuel and MOX fuel.

In France, a wide range of research activities is being conducted analytically and experimentally in the framework of international programs on the two following fields:

- Fuel behaviour in severe fuel damage (SFD) conditions and related fission product (FP) release and behaviour;
- Reactivity initiated accident (RIA).

Regarding the first field, the Phebus FP program is the centre piece of research aimed at the late phase of core degradation and related FP release and behaviour in the reactor and containment vessel. This international program, which is mainly funded by IPSN and the European Community, is supported by several separate-effect tests such as VERCORS and EMAIC tests for FP release and Ag-In-Cd control rod aerosol production. An

important analytical effort is also conducted focussing on the development and validation of the mechanistic SFD ICARE 2 code recently coupled to the thermal-hydraulic CATHARE code. The priority is on the late phase of core degradation and FP release including debris bed formation, evolution to molten pool and final relocation of corium to the lower head. Simplified models are derived and included in the ESCADRE code system used for source term calculations.

Complementary experimental and analytical efforts are being devoted to study the behaviour of molten materials in the lower head and the related impact on the vessel wall. In these areas separate-effect tests are underway in parallel with modelling development efforts.

The mechanical behaviour of irradiated clads under quenching conditions is under study in the TAGCIR separate-effect experiments.

IPSN participates in the framework of OECD/CSNI - PW2 to the production of the validation matrix for Severe Fuel Damage (SFD) codes. This document gives a complete overview of the existing database and an assessment of each test for code validation. Finally, IPSN was involved in the Re-inforced Concerted Actions (RCA) launched by the European Commission, particularly regarding core degradation and FP release. This co-operative programme between European and Eastern countries enable the production of a revised State-of-the-Art Report (SOAR) on core degradation, other activities concerned database, code development and code benchmark and validation.

Regarding the RIA field, the co-operative CABRI-REP-Na program between IPSN and the French utility EDF is underway using standard PWR and MOX fuel. Supporting separate effect tests are being performed such as PATRICIA(heat transfer between clad and cooling fluid) and PROMETRA (mechanical properties of irradiated Zr). The analytical effort is aimed at developing the SCANAIR code for LWR fast power transients taking into account the FP gases and the rim zone.

In Russia, an extensive research program is underway for core material behaviour in VVER-440 and WWER-1000 accident studies. The behaviour of core component materials (fuel elements, spacer grids, guide tubes, control rods) in accident situations is part of the comprehensive investigations into power plant safety. Studies of two-component interactions include high temperature liquid-solid interactions and gas-liquid interactions. A major portion of Russian research into solid-gas and solid-solid interactions has been completed; study of interactions of B_4C with stainless steel and with Zr-1%Nb is scheduled to be completed. More in-pile fuel assembly experience and experimental evidence on the design-basis and severe fuel damage accidenty are needed.

The code modelling program is two-fold: the adaptation of foreign codes like SCDAP, MELCOR, ICARE and ATHLET; and the development of Russian codes such as the ARSRIIM fuel code RAPTA-SFD.

The major objectives of further Russian experiments are:
- refining criteria characteristic of fuel element and bundle failure with special emphasis on irradiation impacts;
- correcting fuel parameters specifying variations in the geometry and composition under severe accidents;
- studying hydrogen release in reflooding damaged fuel;
- defining the rate and composition of fission products more exactly.

Recommendations

Core material behaviour under severe accident conditions has been extensively studied so far by large-scale/small-scale in-pile/ out-of-pile experiments and a quite large data base has been accumulated. However, there still remain subjects to be studied in more detail:

1) FP release behaviour from damaged fuel rod or degraded core materials at very high temperature. Amount of FPs released, particularly low volatiles and actinides and their chemical forms should be determined with better accuracy.

2) Determination of properties of degraded core materials with reasonable accuracy for the analytical models.

3) Extension of the experimental database to higher burnups (up to 60 MW·d/kg U) and to MOX fuel.

4) Continuation of global experiments for the late phase of core degradation and related FP release, and for defining criteria for reactivity initiated accidents (RIA).

5) Separate-effect tests in support of global experiments for specific model developments and for two-component reactions.

6) Parallel efforts on modelling improvements and validation based on recent experimental results.

7) Confirmatory experiments on in-vessel melt retention and cooling, and complementary analysis or experiments to identify and quantify additional debris cooling modes at TMI-2 which are not accounted for in present analyses.

Research of fuel rod behaviour under design-basis accidents such as LOCA and RIA became important again due to new trends in LWR utilization such as extension of fuel burnup and potential utilization of MOX fuels. In this field, the lack of a comprehensive database is obvious and further international efforts will be required.

SESSION A: MATERIAL AND ALLOY PROPERTIES AND THEIR INTERACTION

CHAIRMEN: K. Ishijima, JAERI, Japan
V.N. Golovanov, Russian Federation

Good knowledge of materials properties including materials interaction behaviour at very high temperature is very essential to develop a better understanding of the phenomena encountered in case of severe accident.

Five presentations in this category were given in this session. Four papers covered experimental work on the fission product release and material interaction. One paper was devoted to the development of technology for in-pile experiments wich simulate severe accident conditions.

The paper from Czech Republic had the objective to review experimental data on high-temperature oxidation of B_4C and to assess B_4C oxidation from the point of view of heat and hydrogen release.

The analysis of literature data on non-irradiated and non-enriched B_4C have shown that the reaction kinetics in steam (or air) was not yet published for temperatures above 1000°C. This fact generates an uncertainty in modelling of B_4C oxidation in severe accident codes such as MELCOR, SCDAP/RELAP5 or ICARE2. The paper shows that B_4C is a comparable heat source with respect to the Zr/steam reaction (unit length of rods in PWR design). The formation of boric acids in steam from B_2O_3 does not drastically increase the total heat release from the B_4C oxidation.

Four papers were presented from Russia.

V. Dvoretsky made a presentation "Methodical Approach to Study of Corium Properties in Spent Fuel up to 2200°C". The in-cell facility for melting of the irradiated fuel and change of the corium generation parameters was described. The experimental results obtained from the first corium samples exhibited axial redistribution of the fission products and cladding components. Further investigations in this area are important to understand the corium generation mechanism and thermal effects following it.

V. Smirnov made a presentation "Investigation of Fission Products Release and Structural Changes of the WWER Spent Fuel at Elevated Temperatures". The main aim of the investigations was to gain information on the dynamics of the fission product release in the process of high temperature heatup of the irradiated fuel and changing of its structure and properties. The experiments related to the fission products release during heating up of high burnup fuel were described.

V. Ovchinnikov made a presentation " Methods of Performing the Power Ramping Experiments with WWER Fuel Rods at Different Burnups". The main experimental capabilities of the MIR reactor for investigations of the irradiated fuel behaviour in the severe accident conditions are presented.

N. Sokolov reported on high-temperature interaction of fuel rod cladding material (Zr 1% Nb alloy) with oxygen-containing mediums. The experimental data on Zr 1% Nb oxidation kinetics at atmospheric pressure steam in the temperature range (500-1600)°C are presented. The oxidation rate acceleration is marked at 1500°C. The deformation of cladding enhances the steam/zirconium reaction rate. However, for temperature and time parameters of design basis accidents is shown that the recommended correlation is conservative in the case of deformation. The effect of air and nitrogen concentrations in mixtures with steam on steam/zirconium reaction is estimated at temperature between 800 and 1200°C. The null effect of hydrogen concentration (up to 90% vol.) in mixture with steam is marked at temperatures up to 1200°C. The effect of increased steam pressure (up to 8 MPa) on oxidation kinetics is experimentally shown at temperatures up to 1100°C.

Recommendations

Progress in the research field relating to material properties applicable to severe accident conditions is remarkable in these days. However, there still remain subjects to be covered for improving understanding and simulation capability on the physical phenomena during severe accidents.

It is necessary to carry out further in-reactor experiments with various materials such as zirconium alloys, irradiated nuclear fuel and absorbing materials under various irradiation conditions to improve accuracy of materials properties and interaction data base.

For Zr-based alloy oxidation by steam:

1) To complete study of steam pressure influence on oxidation kinetics.

2) As for severe fuel damage accident, it is important to study oxidation kinetics of molten Zr and Zr-rich melts.

SESSION B: FUEL BEHAVIOUR IN LOCA CONDITIONS

CHAIRMEN: P. Balakrishna, India
N.B. Sokolov, Russian Federation

Significant progress has been made in research in the field of fuel behaviour in LOCA conditions since the last meeting in 1992. Further, licensing policies of various countries are increasingly demanding incorporation of advanced safety features in new reactor systems. This session provided a forum for exchange of new information. Five papers dealing with LOCA problems code were presented in the session.

The paper from India (S.M.Chaudhri et al) analysed the behaviour of a GE 6x6 BWR clad in a design basis LOCA initiated by break of one recirculation line. Fuel and clad temperatures were calculated and fission gas pressure estimated as a function of burn up. Plastic strains were determined by a computer code NISA using the finite element technique. The clad was estimated to experience tangential strains of about 20 per cent resulting in a maximum subchannel blockage of about 45%. This value is within acceptable limits and does not obstruct coolant flow during the emergency core cooling phase.

The paper from Moscow, Russia (Yu.K.Bibilashvily et al) reported on RAPTA-5 code used for licensing calculations to validate the compliance requirements for VVER fuel safety in design basis accidents. The main results of verification calculations were presented. Use was made of the results of the laboratory experiments modelling high-temperature processes (oxidation, straining and rupture of fuel rod cladding) as well as results of rig and in-pile integral experiments.

The paper from Obninsk, Russia (V.Troyanov et al.) presented the accident analysis activities of IPPE along eight main directions. These are (1) ballooning and failure behaviour of fuel element cladding and control rods (2) investigation of residual mechanical properties of cladding (3) analysis properties of steel and effect of molten corium (4) investigation of chemical interaction between structurals in the presence of steam (5) analysis of corium and structure-property correlations (6) study of the interaction between molten corium and structural materials (7) investigations of thermal physical properties of various types of corium (8) strength analysis of pressure vessel lower head under molten pool in nonstable conditions.

Another paper from Obninsk, Russia (A.D. Yefanov et al.) presented the results of an investigation of heat and mass transfer phenomena under accident conditions, associated with the partial uncovering of heated rods, consequent steam zirconium reaction and bundle reflooding. It was established that the effect of nonuniform power generation was rather strong. The presence of fuel assembly shrouds raised the coolant levels in high power bundles, augmenting heat transfer to the uncovered rods.

The paper from Dimitrovgrad, Russia (V. Makhin et al.) described the condition of the first experimental WWER type fuel assembly after a small break LOCA test with dryout and reflooding of a bundle in the MIR reactor. Post-irradiation examination of the bundle has shown that VVER fuel rods remained intact after testing in steam-water environment, with heat up of the upper cladding part up to 500-950°C in 72 minutes. The pellet temperature was 200-400°C higher than the cladding temperature at maximum linear heat rating of 90-95 W/cm. This work is a significant step towards code verification and the feasibility of reactor core repair after an accident of the type described. Unfortunately, Mr. Makhin did not submit paper for the publication in these proceedings.

Recommendations

Cladding strain rates (especially in transient conditions) need to be determined more accurately. The effect of oxide layer in reducing clad thickness and the strenghtening of the clad wall by diffused oxygen should be investigated.

The investigations of the irradiated core materials properties in the wide temperature range (thermophysical, thermomechanical, corrosion, straining, rupture) need to be done. Integral experiments, modelling the design basis accident conditions with irradiated fuel rods need to be performed. Coordination between the experimenters and the code developers in order to obtain the informative experimental results, will be useful for code.

The investigations of material structure and properties should be continued with respect to corium, structural materials and absorber materials. Structure mechanics analysis and accident loading (e.g., strength of lower head under molten pool) need to be studied.

There is good scope for updating and upgrading the existing codes with inputs from results of various participating countries.

Further work is called for in testing bundles in different accident scenarios to establish the feasibility of core repair after an accident.

A recommendation made at the IAEA Technical Committee Meeting held in France in 1992 still applies and is worth reporting.

Integral experiments should cover the whole domain of LOCA. If a considerable amount of irradiated fuel has been tested, the range must be extended to high burn-up, that is, 49-60 MW·d/kg U for PWRs. In these experiments, in order to obtain a good description of fission product release, it is necessary to have a good description of the reflooding and post-accident cooling phases in water. Other types of transients, including off-normal operations also have to be performed for these high burn-up fuels.

SESSION C: FUEL BEHAVIOUR IN SEVERE FUEL DAMAGE CONDITIONS

CHAIRMEN: B. Adroguer, France
V. Smirnov, Russian Federation

Summary

Seven papers were presented in this session. Four papers concerned experimental work on fuel degradation behaviour (CORA W2, PHEBUS FPT0 and FP release (VERCORS)). Two papers were devoted to code assessment and validation. One paper described code modelling regarding radial relocation of melt between fuel rods. These papers indicate that an important effort is being presently made both in experimental and analytical areas including the early phase but also the late phase of core degradation. In this general sense some recommendations expressed in the previous meeting held in Aix-en-Provence in 1992 have received a positive answer.

1. Phebus FPT0 brings significant results on the progression of the core degradation toward the late phase, including the related impact of degradation on FP release.

2. The database on VVER material properties and core behaviour was significantly re-inforced both with separate effect test ($Zr1\%Nb/UO_2$, $Zr1\%Nb/SS$, SS/H_2O, B_4C/SS) and global tests (in cooperation between FZK and Russian researchers) such as CORA W2 and W1 respectively with and without B_4C. The behaviour of a VVER - type bundle under SFD conditions was found to be very similar to the behaviour of the PWR-type bundle in similar conditions.

3. An International Standard Problem (ISP36) was organized by OECD/CSNI on CORA W2 test. The large number of destructive examinations performed on this test enabled a rather complete quantification of key parameters of the degradation : clad oxidation, blockage formation, melt relocation, UO_2 dissolution. This data base enabled the assessment and validation of main SFD codes.

4. Progress has been made regarding post-irradiation examination of degraded bundles. This was illustrated by the tomographs performed on PHEBUS FPT0. This non-destructive examination enables a rather rapid and precise overview of the final degradation. These results facilitate the definition of cutting zones for further destructive examinations. Improvements are still foreseen for the next test FPT1.

5. A large effort on FP release has been performed on an extended area of conditions to re-inforce the data base mainly on volatile FP release and on some non-volatile FP up to 2600 K: VERCORS (CEA), VI (ORNL) and RIAR FP tests and the in-pile global test PHEBUS FPT0. Priority is now on the release of low volatile FPs and actinides for which the data base is poor. In this area, high temperatures up to the melting point of fuel are foreseen to be investigated in future VERCORS, VEGA and PHEBUS FP tests.

6. Regarding the FP release modelling, current models give reasonable results for calculating the volatile FPs when there is no significant rod degradation. Improvements are still necessary for modelling the impact of degradation on FP release or for modelling the non-volatiles and actinides release.

7. Progress has been made regarding code development and assessment particularly on the early phase of degradation. This analytical effort was illustrated by the development of new mechanistic models in ICARE2 (IBRAE RAS in co-operation with IPSN): UO_2-Zr-H_2O interactions based on diffusion, melt relocation, mechanical behaviour of cladding. Comparative calculations indicate that the oxidation model based on diffusion gives good agreement on the oxidation for isothermal and transient conditions. These calculated results indicate an improvement compared to the parabolic approach.

8. Code validation efforts were presented on ICARE2 and RAPTA-SFD codes. These codes gave reasonable prediction of the early phase as was illustrated by the code-to-data comparisons between RAPTA and CORA W2 or by the ICARE 2 calculation of the early oxidation phase of the PHEBUS FPTO test.

9. The preparation of FPT0 test was performed in an international frame using the main SFD codes. These codes which were validated for the early phase were not able to predict the late phase aspects observed after the oxidation phase such as the loss of rod geometry and the formation of a molten pool. Post test calculations using standard versions of codes indicate, even after tuning, the same tendency.

10. Recent progress has been achieved regarding specific models on the late phase degradation. In particular new models were mentioned to be under development in the framework of the ICARE2 code development regarding the radial spreading of corium between rods, crust stability, debris bed formation and behaviour up to a molten pool, and on upward radiative transfer from a pool.

Recommendations

Additional efforts are requested regarding experiments and code modelling in the following areas :

1. The experimental database on the degradation must be improved regarding late phase aspects up to relocation of melt into the lower head. In this area high temperature and high burn-up must be investigated.

2. Additional experimental work is recommended on core material interactions at high temperature using irradiated fuel, in particular for fuel dissolution by molten Zr and silver-Zr-mixtures, oxidation of Zr-rich melt and material properties of U-rich mixtures.

3. New specific experiment are necessary both for PWR and VVER regarding the reflooding of degraded cores. Current knowledge is not sufficient for modelling the rod embrittlement and the large oxidation escalation that could be induced by core quenching.

4. The priorities regarding FP release is on the non-volatiles FP and actinides release. Of particular interest is the release under air atmosphere.

5. The chemical form of iodine keeps a high degree of priority in the future studies in order to predict the transportation far away beyond the core.

6. Code development and validation is recommended mainly on the transition toward late phase up to the relocation of melt into the lower head, including the thermal and mechanical interaction between corium and vessel. Model assessment is recommended as well for irradiated fuel rods.

7. Future code developments should be performed keeping in mind that the final objective of codes is plant applications. It is recommended to check the sensitivity of new models on reactor accident transients to assess the real benefit for practical situations.

8. The effort on post-irradiation techniques, either non-destructive or destructive should be carefully prioritized in order to obtain good qualitative and quantitative results for code assessment.

SESSION D: FUEL BEHAVIOUR IN RIA CONDITIONS

CHAIRMEN: J.P. Breton, France
A.V. Goryachev, Russian Federation

Three sorts of power burst experiments with high burnup fuel simulating RIA conditions in PWRs/WWERs were overviewed during the session:

-NSRR experiments with irradiated PWR fuel rods with burnup up to 50 MWd/kgU conducted in NSR reactor (JAERI, Japan). Tested fuel rod was placed into a capsule with stagnant water at atmosphere pressure ; power pulse half-width was of 4.4-6.9 ms and energy deposition of up to 310 cal/g (fuel enthalpy- up to 74 cal/g);

-CABRI experiments with irradiated PWR fuel rods with burnup up to 63.8 MWd/kgU conducted in a sodium loop of CABRI reactor (IPSN, France). Sodium coolant rate was 4 m/s; power pulse half-width was of 9.5-60 ms and energy deposition of up to 211 cal/g (fuel enthalpy- up to 206 cal/g);

-IGR experiments with irradiated WWER fuel rods with burnup up to 50 MWd/kgU conducted in IGR reactor (Kurchatov Institute, Russia). Tested fuel rod was placed into a capsule with stagnant water or air at atmosphere pressure; power pulse half-width was up to ~1s and energy deposition of more than 400 cal/g.

Separate fuel rods failed during power burst experiments including:

-NSRR HBO-1 test - at energy deposition of ~60 cal/g;

-CABRI REP Na 1 test- at fuel enthalpy of ~29 cal/g;

-IGR tests- at energy deposition of~ 239 cal/g (in water) and ~ 147cal/g (in air).

PIE demonstrated that possible rod failure mechanism was low temperature PCMI of hydrided during basic irradiation cladding (PWR) or high temperature cladding plastic deformation of ballooning type (WWER).

It was agreed that condition of irradiated rod (burnup, rim layer, cladding hydrating, etc.) and experiment conditions (pulse half-width, type and parameters of coolant, etc.) should be taken into account in order to rightly plan, evaluate and use (for modeling) results of the above-mentioned experiments. Big difference in enthalpy threshold values could only be explained by differences in either initial rod condition or methods of experiment. For example, the failed fuel rod in REP Na 1 test was initially strongly corroded, even ZrO_2 spallation was observed.

Unfortunately, Ms. Egorova did not submit paper for the publication in these proceedings. Therefore some data on fuel fragmentation thresholds from her presentation are given below:

-420 cal/g for fuel rods cooled with water,
-280 cal/g for fuel rods cooled with air.

GENERAL CONCLUSIONS AND RECOMMENDATIONS

An important effort has been performed both in experimental and analytical areas including the early and the late phase aspects of core degradation and fission product release.

Future efforts should be focused on high burn-up, high temperatures and degradation up to the final interaction between corium and the vessel wall. Nevertheless the current database is not sufficient for improvement of code modelling.

Research on fuel rod behaviour under design-basis accidents such as LOCA and RIA became important again due to new trends in LWR utilisation such as extension of fuel burn-up

The main recommendations are:

- Perform experiments on both separate effects and global tests which combine degradation and fission product release in conditions representative of the late phase degradation, including determination of degraded core material properties. In this area the current data base is insufficient.

- Regarding the early phase there are some remaining issues unresolved due to the lack of experimental data: interaction between absorber material (Ag-In-Cd and B_4C) and surrounding rods, possible oxidation of B_4C by steam, oxidation of Zr rich melts impact of quenching on degraded rods and material interactions with irradiated fuel.

- Code modelling effort on mechanistic SFD codes and integrated codes is necessary to take advantage of experimental data expected in the near future: PHEBUS FP programme and separate effect tests such as VERCORS and VEGA

- Code development and validation effort must be done considering also plant applications. The assessment of sensitivity of codes on reactor accident transients (total H_2 production, volatile FP release, total amount of relocated melt...) is recommended in order to priorities developments and assess the real benefits on practical situations.

- Perform experiments modelling LOCA and RIA conditions with high burn-up fuel.

GENERAL OVERVIEW

(Introductory Session)

Chairmen

R.A. MOORE
USA

N.B. SOKOLOV
Russian Federation

RESEARCH PROGRAM FOR CORE MATERIAL BEHAVIOUR IN SEVERE VVER ACCIDENTS

N.B. SOKOLOV
All-Russian Institute of Inorganic Materials,
Moscow, Russian Federation

Abstract

An overview is presented of studies to be performed on the behaviour of water-cooled power reactor core materials under abnormal conditions. No consideration is given to interactions with the reactor vessel and to out-of-pile gas routes.

Introduction

The behaviour of core component materials (fuel elements, spacer grids, guide tubes, control rods) forms a part of comprehansive investigations into power plant safety. In recent years much effort has been directed worldwide toward this problem, because accident impacts are dependent on the state of the core in emergency.

Materials of the VVER type cores are covered. Some results hold true for other Russian reactors like RBMK.

Table 1. lists materials which are currently in service in VVER - 440 and VVER - 1000 cores.

TABLE 1. MAJOR MATERIALS OF THE VVER FUEL ASSEMBLY COMPONENTS

Element of FA	Material
Fuel pellets (VVER - 1000)	Sintered UO_2, $UO_2 + Gd_2O_3$
Fuel Rod Claddings Spacer grids for VVER - 440 Spacer grids for VVER - 1000 (experiment)	Zr1%Nb
Guide tube Spacer grids for VVER - 1000 Control rod claddings	X18H10T
Control rod material	B_4C

Tests of Zr1%Nb spacer grids and of Gd_2O_3 as a burnable adsorber are now in progress on a pilot-plant scale at the Balakovskaya power plant.

1. General characteristics of accident phases.

Depending on temperature and boundary conditions within the core and in the primary circuit, severe reactor accidents can be divided into several phases.

1.1. *Thermohydraulic phase.*

It is commonly accepted that a severe reactor assident originates in design basis abnormal conditions followed by contingency (failure or malfunction).

This phase involves the drying (probably partial) of the core and the growth of fuel clad temperature up to 1200°C. The phase features:

- deformation of a fuel cladding (balooning or collapse) and rupture by pressure drop;
- oxidation of a fuel cladding and stainless steel by steam;
- interaction between a pellet and a cladding (when in contact);
- cladding-spacer grid interaction;
- UO_2-steam interaction;
- B_4C-control rod cladding interaction.

By now all these processes are known in sufficient detail in Russia with the exception of oxidation of zirconium alloys and stainless steel by high-pressure (above 5 Mpa) steam and the B_4C-stainless steel interaction on long standing.

The phase can be arbitrarily characterized by no liquid phase in the core, although the binary phase diagrams for Fe-Zr, Ni-Zr, V-Zr suggest low eutectic temperatures, the lowest eutectic temperature being about 930°C for Fe-Zr. But simulated fuel element tests show the shift in the liquefaction temperature to the stainless steel melting temperature under oxidizing media (water steam).

1.2. *High - temperature material interaction*

This phase exhibits the formation of liquid eutectics, melting and liquid-solid interaction. The phase starts at a temperature of 1200°C (maximum temperature for design basis accidents) and ceases at the UO_2 melting temperature of about 2850°C.

With melting, interactions become much more complicated. First, flowing down liquid phases interact with steam to form oxides or complex solid solutions. Second, liquid phases can interact with materials of structural components. For instance, the flowing down eutectic resulting from the B_4C - stainless steel interaction becomes enriched with oxygen and can interact with zirconium or Zr oxides of fuel claddings.

In addition to processes listed in 1.1., this phase involves:

- cladding failure due to mechanical stresses from Zr oxidation ("flowering");
- UO_2 dissolution by liquid zirconium;
- formation of a-ZrO and ZrO_2 eutectics.

Increased hydrogen evolution during reflooding ("quench") contributes to these processes.

The study of fission product release is also of importance.

A major portion of Russia's research into solid-gas and solid-solid interactions has been completed. More in-pile fuel assembly experience and experimental evidence on the solid-liquid interaction is needed.

1.3. *Reactivity - initiated accidents (RIA)*

The time it takes for core processes to occur is responsible for special features of the RIA type accident. Pulse length and energy release are decisive parameters for fuel state in this case. Some 200 tests performed in Russia's "Hydra" and IGR reactors provided a considerable experimental database. But not much is known about irradiated fuel rods. Since 1995 a great deal of effort will be going into the investigation of the detailed nature of VVER irradiated fuel using the BIGR reactor of the Institute of Experimental Physics (the town of Arzamas).

2. Separate - effects tests

2.1.*Solid - gas reactions*

The study of kinetics of the clad-steam interaction over a wide range of pressures and temperatures is scheduled for the immediate future.

The effect of irradiation on the oxidation kinetics of cladding materials, the oxidation characteristics during reflooding ("quench"), hydrogen release among them, as well as the B_4C - steam interaction will be subjects of further investigations.

2.2. *Solid - solid interactions.*

The examination of interactions of B_4C with stainless steel and with Zr1%Nb is scheduled to complete.

Efforts will be directed towards studying the effect of thickness of oxide films on initial materials (stainless steel, zirconium alloys) on high-temperature interactions.

2.3. *Solid - liquid reactions*

The UO_2 dissolution by molten zirconium is of the topmost importance and planned for investigation.

The interaction of the B_4C-stainless steel eutectics with zirconium alloys is also of considerable interest.

2.4. *Liquid - gas reactions*

The molten core materials-steam interaction experiments can provide important evidence to treat a severe reactor accident analitically. Experimental data on this process, primarily the rate and other parameters, are due to be obtained.

TABLE 2. PLANNED TESTS WITH FUEL ELEMENT AND BUNDLE

Test object	Test type	Institute	Remarks
Single rod	out - of - pile	ARSRIIM -Moscow EKB Hydropress - Podolsk IPPE - Obninsk	
Single rod	in - pile	SB ENTEC - Sverdlovsk region	
Bundle	out - of - pile	OE NPO "Lutch" - Podolsk	7 - element bundle including control rod
Single rod, bundle	in - pile	RIAR - Dimitrovgrad	MIR reactor Loop 2 - LB LOCA, SB LOCA Loop3- SFD accident
Single rod, bundle	in - pile	RENC - TEP Arzamas - 16	Fast - neutron pulsed reactor (BIGR) RIA type tests

3. Tests of fuel elements and assemblies

High-temperature experiments with single fuel elements or fuel bundles are of great interest in terms of process interrelations. Two-component reactions cannot simulate the behaviour of fuel elements and assemblies under abnormal conditions in full measure. Besides, integral experiments are important for verification of computer codes.

Table 2 lists tests to be performed. It should be noted that a variety of experimental studies has been started. Results of some experiments will be reported at this meeting.

The major objectives of further experiments are:

- refining criteria characteristic of the fuel element and bundle failure with special emphasis on irradiation impacts;
- correcting fuel parameters specifying variations in the geometry and composition under severe accidents;
- studying hydrogen release, in reflooding damaged fuel included;
- defining the rate and composition of fission products more exactly.

4. Modelling and codes

The fuel element and core behaviour modelling program is twofold. In the first place, foreign codes like SCDAP, MELCOR, ICARE, ATHLET are of use in Russia. These codes are adapted to fit our power plants and verified within the database on severe reactor accidents. Domestic models to describe individual processes have been developed and integrated with existing codes.

On the other hand, a variety of Russian codes has been developed. The results of the International standart problem ISP-36 based on the German CORA-W2 experiment show a good prediction ability of the ARSRIIM fuel code RAPTA-SFD.

5. Candidate materials

The introduction of better radiation-resistant materials for core components is planned in the coming years. A zirconium alloy doped with Nb, Sn and Fe will be used as a material of fuel claddings. The alloy is also intended for application as control rod guide tubes. Experimental evidence reveals that in its high-temperature properties (oxidation, deformation) the alloy is as good as Zr1%Nb and Zircaloy-4 now in use.

Nowadays, spacer grids of the VVER-440 fuel assembly are made of Zr1%Nb. Soon this experience will be extended to VVER-1000.

Spacer grids of this sort are now being tested on a pilot-plant scale at the Balakovskaya power station. Near-term outlook involves the use of the Zr-Nb-Sn-Fe alloy for spacer grids.

Considerable changes are in store in control rods. A nickel-based XHM-1 alloy is a candidate as a cladding for longer lifetime of a control rod. Boron carbide with dysprosium titanate at the control rod bottom or hafnium are also kept in mind.

All these materials listed will be put to comprehensive tests ranging from two-component interactioins on a laboratory scale to in-pile fuel assembly experiments.

6. High burnup accident features

A vital issue in improving fuel is to achive high burnup (over 40 MWt/kgU as a medium value for a fuel element). Efforts have been recently directed toward discovering peculiariaties of oxide fuel at high burnup. Certain of them influencing the fuel behaviour in emergency are as follows:

- lower heat conduction of fuel (UO_2)
- better heat capacity of UO_2 (resulting in higher stored energy at the same linear power.

- rim-effect (it can cause a local decrease in the fuel-cladding heat conductance);
- high internal pressure within a fuel element (responsible for lower heat conductance at the fuel-cladding gap).

The main objective of high-burnup experiments to be performed is the failure mechanism under LOCA or RIA conditions. Accidents of the RIA type are known to change the failure mechanism as a result of high burnup. A purpose of the program to be executed is to obtain information about the failure enthalpy as a function of burnup with allowance made for design features of Russian fuel assemblies and fuel rods.

Conclusions

Research efforts to be performed in Russia on the core material behaviour in severe VVER accidents have been reviewed. Studies on individual two-components interactions and experiments with single fuel elements and fuel assemblies as well as participating research centres are listed. Particular emphasis will be placed on investigations into burnup impacts and on experimentation to introduce candidate materials as soon as possible.

XA9743286

RESEARCH ACTIVITIES AT JAERI ON CORE MATERIAL BEHAVIOUR UNDER SEVERE ACCIDENT CONDITIONS

H. UETSUKA, S. KATANASHI, K. ISHIJIMA
Department of Reactor Safety Research,
Japan Atomic Energy Research Institute,
Tokai, Ibaraki, Japan

Abstract

At the Japan Atomic Energy Research Institute(JAERI), experimental studies on physical phenomena under the condition of a severe accident have been conducted. This paper presents the progress of the experimental studies on fuel and core materials behavior such as the thermal shock fracture of fuel cladding due to quenching, the chemical interaction of core materials at high temperatures and the examination of TMI-2 debris.

The mechanical behavior of fuel rod with heavily embrittled cladding tube due to the thermal shock during delayed reflooding have been investigated at the Nuclear Safety Research Reactor(NSRR) of JAERI. A test fuel rod was heated in steam atmosphere by both electric and nuclear heating using the NSRR, then the rod was quenched by reflooding at the test section.

Melting of core component materials having relatively low melting points and their eutectic reaction with other materials significantly influence on the degradation and melt down of fuel bundles during severe accidents. Therefore basic information on the reaction of core materials is necessary to understand and analyze the progress of core melting and relocation. Chemical interactions have been widely investigated at high temperatures for various binary systems of core component materials including absorber materials such as Zircaloy/Inconel, Zircaloy/stainless steel, Zircaloy/(Ag-In-Cd), stainless steel/B_4C and Zircaloy/B_4C. It was found that the reaction generally obeyed a parabolic rate law and the reaction rate was determined for each reaction system.

Many debris samples obtained from the degraded core of TMI-2 were transported to JAERI for numerous examinations and analyses. The microstructural examination revealed that the most part of debris was ceramic and it was not homogeneous in a microscopic sense. The thermal diffusivity data was also obtained for the temperature range up to about 1800K.

The data from the large scale integral experiments were also obtained through the international cooperation such as Phebus-SFD, Phebus-FP and CORA programs to supplement the research at JAERI.

1. Severe Accident Research at JAERI

The wide range of research activities on the severe accident of light water reactors(LWRs) is conducted analytically and experimentally at Japan Atomic Energy Research Institute(JAERI). Outline of present research program at JAERI is shown in Fig.1. The program consists of four research fields, core melt progression, containment integrity, source term and piping integrity.

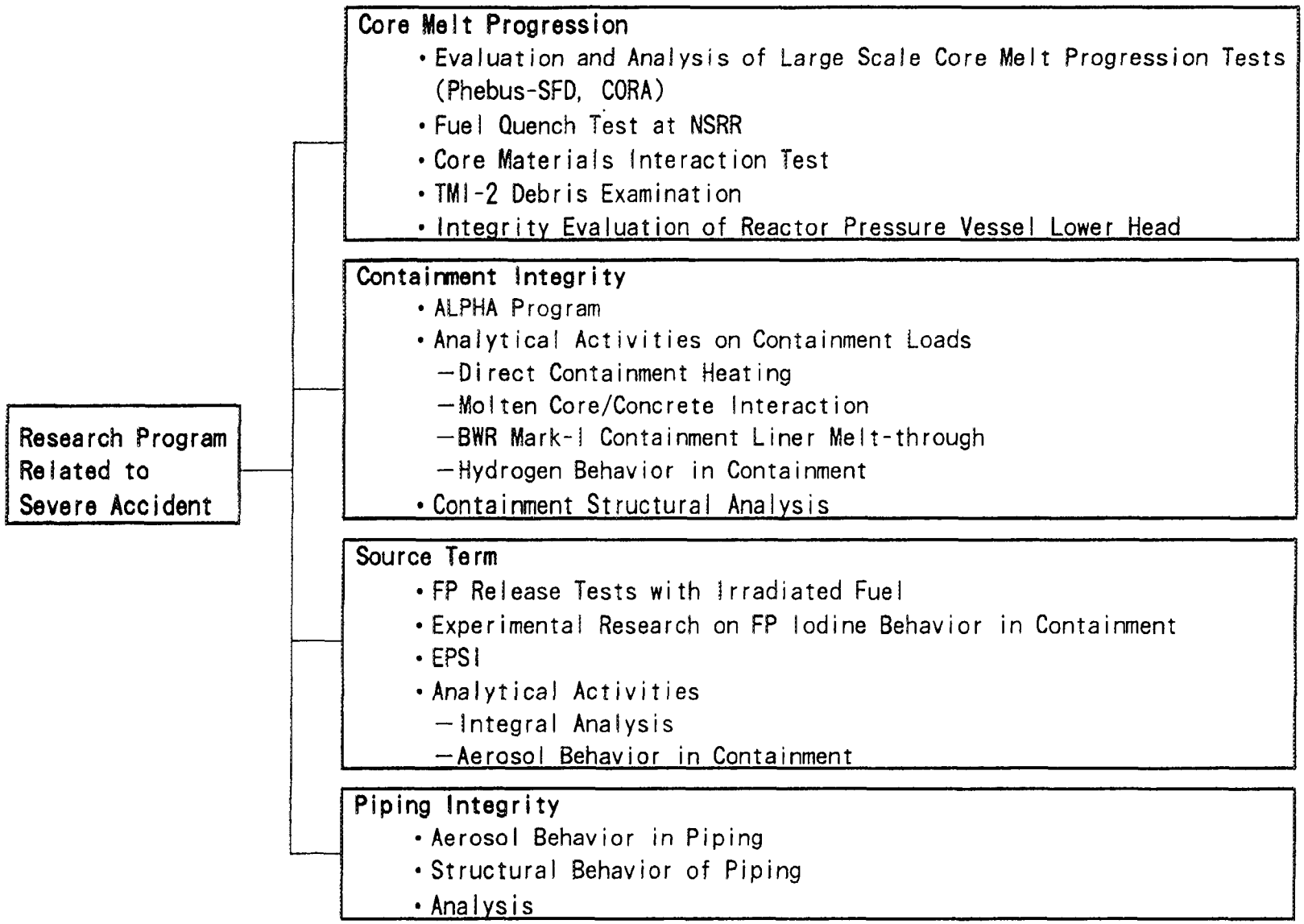

Fig. 1 Outline of present severe accident research at JAERI

The research on the behavior of LWR core materials under severe accident conditions is included in the first research item of core melt progression which is concerned with physical phenomena in the pressure vessel, such as melting behavior of fuel rod, thermal shock fracture of fuel rod by reflooding, core material interaction at high temperature, etc. In this field of research activities, fuel melt tests[1] and debris coolability tests at the Nuclear Safety Research Reactor(NSRR) are already finished and other experimental programs are still progressing. The examination of TMI-2 debris which provides valuable data for severe accident research is also conducted as well as laboratory scale experiments on core materials interaction. These researches at JAERI consist of relatively small scale experiments and analytical work. To supplement the research at JAERI, information from the large scale integral experiments have also been obtained through international cooperation such as Phebus-SFD and Phebus-FP programs in France and CORA program in Germany.

This paper describes the current status and main results of the experimental studies on fuel and core materials behavior, i.e., fuel rod fracturing by thermal shock, chemical interaction of core materials at high temperature and TMI-2 debris examination.

2. Fuel quench test at the NSRR

In a loss of coolant accident(LOCA) of a LWR, fuel rods will be heated by both decay heat and highly exothermic reaction between steam and Zry, if the emergency core cooling system(ECCS) does not work well by some accidental reason. In such case, fuel rod temperature

Table 1 Test conditions of fuel quench test at NSRR

Test No.	952	954
Test Fuel Rod		
Cladding Material	Zry-4	←
Cladding Outer Diameter(mm)	10.72	←
Cladding Tube Thickness(mm)	0.62	←
Pellet Material	UO_2	←
Pellet Diameter(mm)	9.29	←
Pellet Length(mm)	10.0	←
Enrichment(%)	10	20
Internal Pressure(MPa)	0.5	0.4
Pellet Stack Length(mm)	320	310
Linear Heat Rate of Test Fuel(W/cm)	18	23
Atmosphere	He, Steam	←
Wall Temperature of Test Section(K)	1,133	1,183
Operation Time of NSRR(min)	8	14

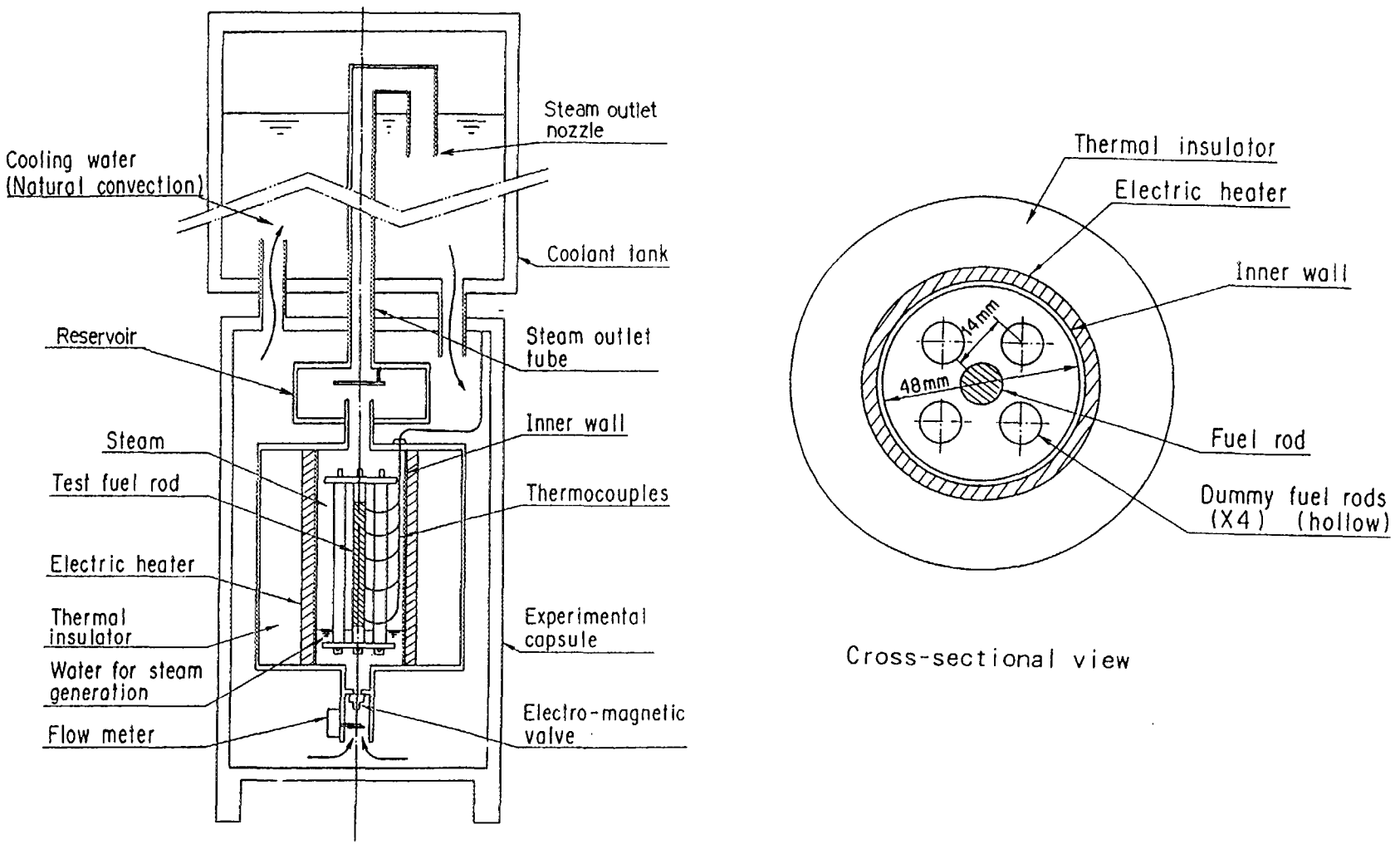

Fig. 2 Schematic of the test capsule for NSRR quench test

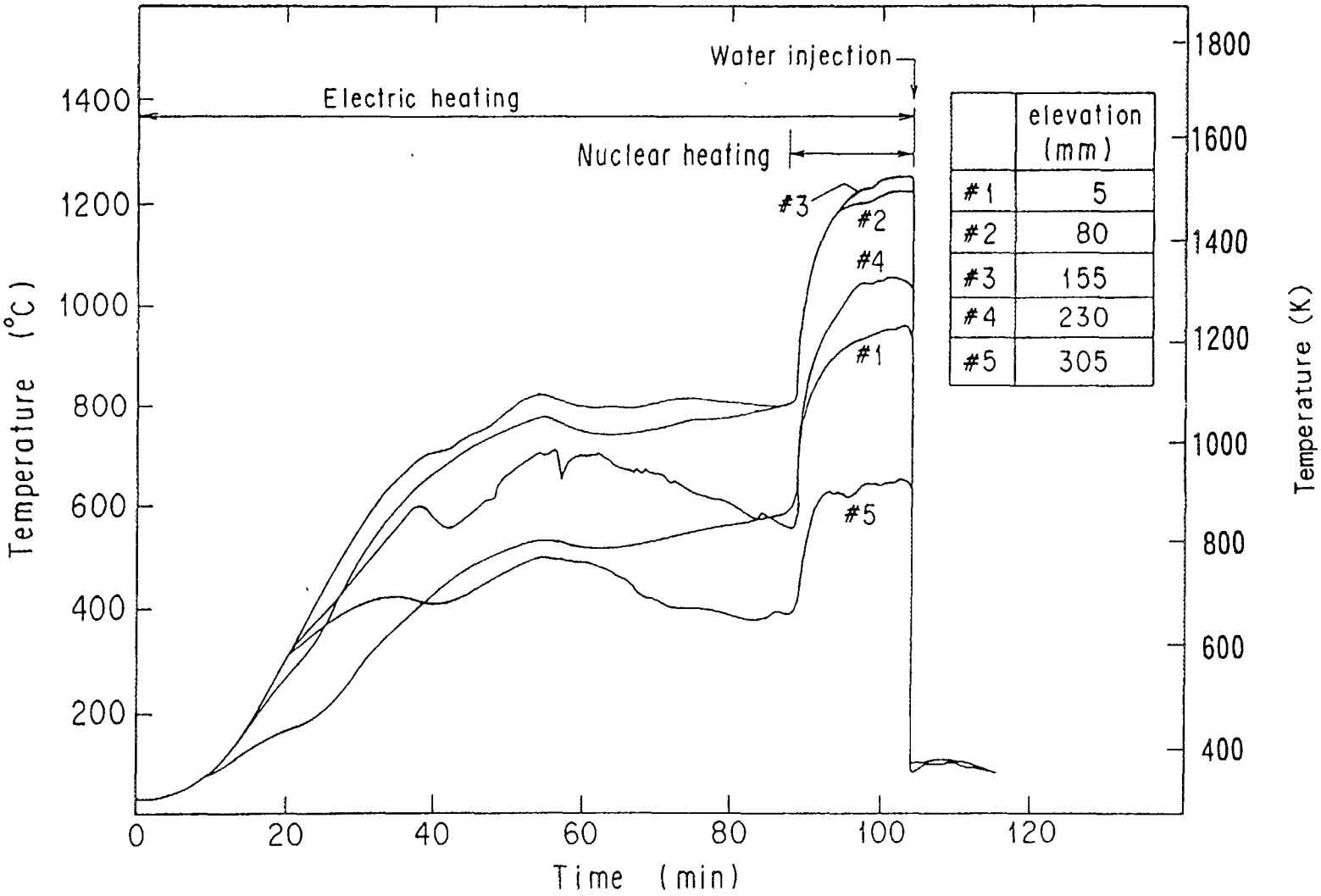

Fig. 3 Temperature histories of cladding outer surface at each elevation in test no. 954 (Maximum cladding temperature : 1533K)

would be raised to very high level beyond the temperature of the design basis event(DBE) criteria, and fuel rods might be damaged severely. Under such severe accident conditions, the cladding tube of fuel rod will rupture and be oxidized on its inner and outer surfaces by high temperature steam. Consequently, severe oxidation of the cladding tube may result in fuel degradation due to thermal shock if delayed reflooding occurs.

The in-pile tests on the fuel behavior during delayed reflooding were performed at the NSRR[2]. The objectives of these tests were to clarify the fuel behavior and degradation conditions during delayed reflooding after the cladding tube was heavily oxidized.

Conditions of the fuel quench tests at the NSRR are summarized in Table 1. A test fuel rod was a shortened PWR type fuel rod containing fresh UO_2 pellets. Initial internal pressure of the test fuel rod was 0.5 or 0.4MPa at the room temperature. With this pressure, the cladding tube is estimated to rupture when the cladding temperature reaches at the level of about 1300K.

Tests were conducted by using a high-temperature flooding capsule. Figure 2 shows a schematic drawing of the capsule. The test fuel rod was placed in the center of the test section. The test fuel rod and four dummy fuel rods were surrounded by an electric heater and a thermal insulator. This capsule with the test fuel rod was fixed at the experimental cavity of the driver core of the NSRR[3] and was irradiated. The environment of the fuel rod during heating was steam which was generated by evaporation of water at the bottom of the test section. An electro-magnetic valve was installed at the bottom of the test section in order to inject water into the test section to simulate reflooding.

Figure 3 shows temperature histories of cladding outer surface measured with thermocouples at each elevation in Test No.954 which exhibited the highest cladding temperature in the test series. The elevations, #1 to #5 denotes the axial position of fuel rod from the bottom of fuel stack. The fuel rod was heated initially only by the electric heater to the temperature beyond 1000K. Then, nuclear heating was started at the linear heat rate of 23W/cm, and the cladding surface temperature reached 1533K. The test was terminated by the water injection into the test section, and the fuel rod was quenched. Another test(Test No.952) was conducted under the same condition except for the linear heat rate.

In Test No.952 which exhibited lower maximum cladding temperature of 1300K, the cladding tube ballooned and ruptured at the middle elevation where the temperature was the highest as shown in Fig.4. Though whole surface of the cladding was oxidized, fragmentation of the cladding tube did not occur in this test. Sum of the oxide layer thickness on the outer and inner surfaces corresponded to about 10% of the cladding thickness which became thinner than the initial value due to ballooning. In contrast to this, the cladding tube ballooned and fractured into several pieces in Test No.954 as shown in Fig.5. These fragments of the cladding tube were 1 to 2cm long. Fragmentation occurred between the elevation of 32mm and 160mm where the temperature was the highest. Inner surface of cladding tube was heavily oxidized in the region above an elevation of 70mm, and its

metallic luster was lost there as shown in the magnified view in Fig.5. The sum of the oxide layer thickness of both surfaces reached 35% of the cladding thickness.

In the NSRR quench tests, cladding tube was broken into several fragments during quenching when the cladding temperature exceeded 1500K and the cladding was oxidized to the extent equivalent to 35% oxidation of cladding thickness after occurrence of ballooning. On the other hand, it did not fail in case of the temperature of around 1300K and oxide layer thickness of 10%. These results are in agreement with that of out-of-reactor tests such as Chung's study[4] which was obtained under isothermal oxidation conditions with no constraint force. After fragmentation of cladding tube, fuel pellets were exposed to the environment at the broken part of the cladding tube. This suggests a possibility of the enhancement of fuel degradation in the case of irradiated reactor core with cracked fuel pellets.

In this test series, some other tests have already been conducted and detail information will be obtained after post test examinations.

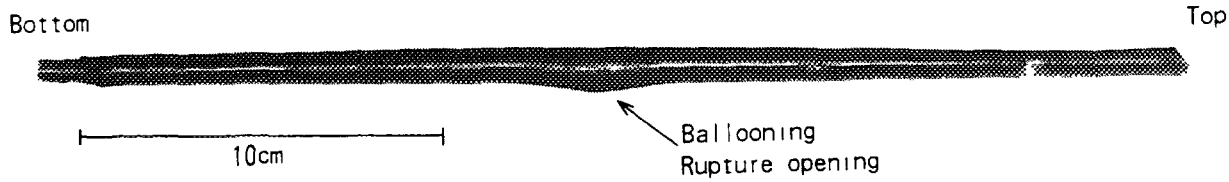

Fig. 4 Post test appearance of the fuel rod after test no. 952
(Max. cladding temperature:1300K, Oxide layer thickness: ~40μm)

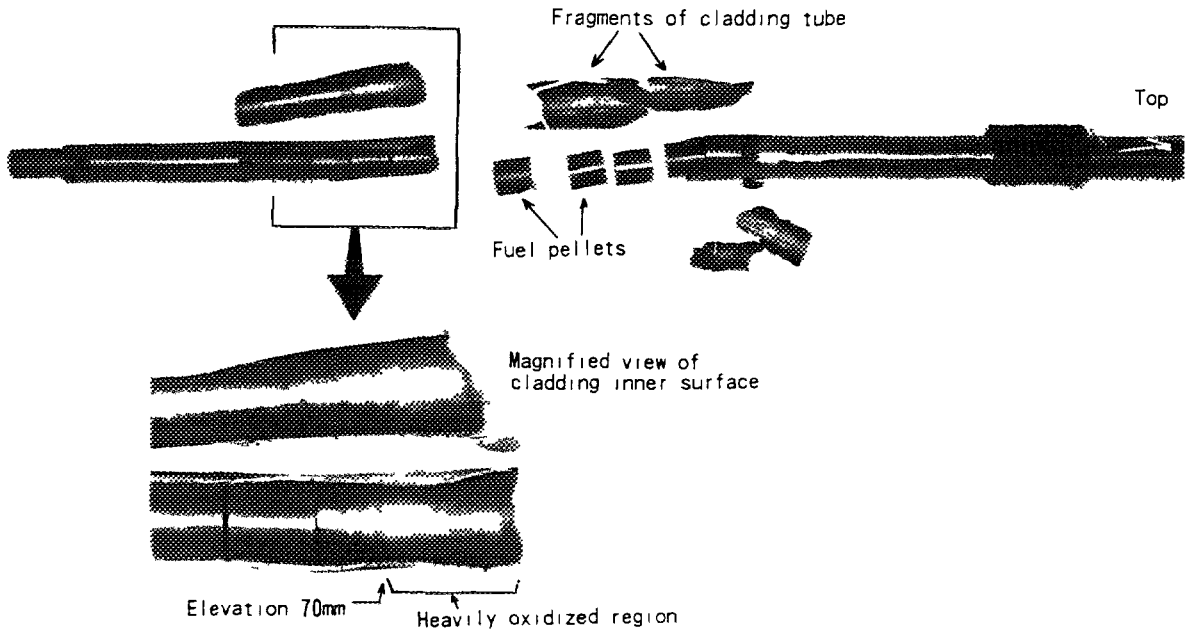

Fig. 5 Post test appearance of the fuel rod after test no. 954
(Max. cladding temperature:1533K, Oxide layer thickness:~200μm)

3. High Temperature Behavior of Fuel and Core Materials

The core of an LWR consists of many materials including UO_2 fuel, Zircaloy cladding, stainless steel, Inconel, and various control rod materials. The high temperature expected in a severe accident would cause fuel failures and core component material interactions. Therefore, extensive information concerning the high temperature behavior and interaction of core materials is required to evaluate and analyze the progression and extent of core damage.

The large scale bundle tests such as PBF-SFD, LOFT/LP-FP-2, PHEBUS-SFD, ACRR-DF, CORA etc. have been performed in many countries. In these experiments, the fuel bundles composed of UO_2 fuel, Zircaloy cladding, spacer grids and control rods were heated up to very high temperatures above 2100K. The experiments have produced significant information that is essential to understand the phenomena that occur in fuel assemblies under a severe accident condition.

In parallel to the large scale bundle tests, out-of-pile separate effect tests focused on the individual interaction between core materials have been performed at Forschungszentrum Karlsruhe(FZK) and JAERI. These tests have aimed to obtain more quantitative information for

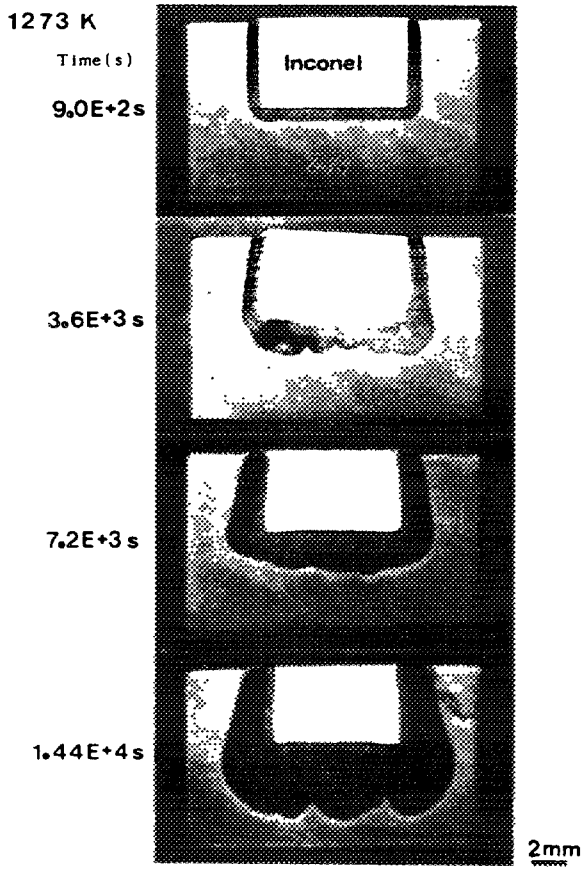

Fig. 6 Macrophotographs of Zry/Inconel diffusion couples isothermally heated at 1273K

Table 2 Kinetics for materials interaction measured at JAERI

Reaction System	Temperature Range (K)	Kinetics $K(m^2/s)=K_0\exp(-Q/RT)$	Applicable Temperature Range (K)
Metal / Metal			
Zry-4/Inconel-718	1248 - 1523	$K=2.69\times10$ exp(-259/RT)	1248 - 1423
		$K=5.33\times10^{-1}$ exp(-192/RT)	1473 - 1523
Zry-4 /SS-304	1273 - 1573	$K=3.11\times10^{9}$ exp(-496/RT)	1273 - 1573
Zry-4/Ag-In-Cd	1273 - 1473	$K=6.30\times10^{3}$ exp(-331/RT)	1273 - 1473
Metal / Ceramics			
SS-304/B_4C	1073 - 1623	$K=1.49\times10^{-2}$ exp(-250/RT)	1073 - 1473
		$K=1.40\times10^{10}$ exp(-549/RT)	1498 - 1623
Zry-4/B_4C	1173 - 1953	$K=2.42\times10^{-8}$ exp(-173/RT)	1173 - 1773
		$K=8.79\times10^{43}$ exp(-1965/RT)	1498 - 1623
Zry-4/(20wt%-B_4C+ 80wt%-SS-304)	1473 - 1923	$K=7.04\times10^{-9}$ exp(-41.3/RT)	1473 - 1673
		$K=7.01\times10^{10}$ exp(-666/RT)	1773 - 1923
Fuel / Metal			
UO_2/(Zry-4+silver)	1473 - 1703	$K=5.98\times10^{-12}$ exp(-34.9/RT)	1473 - 1573
		$K=2.10\times10^{-10}$ exp(-675/RT)	1618 - 1703

Kinetics were measured for decrease in Zry thickness (ex.SS-304 in SS-304/B_4C, UO_2 radius in UO_2/(Zry+silver) reaction), R=8.314 J/mol/K, Q:activation energy in kJ/mol

evaluating the phenomena observed in the large scale bundle tests and TMI-2 accident. The experiments have been conducted under well-defined conditions and reaction rates have been evaluated based on the measurement data. Many reaction systems, Zircaloy/Inconel, Zircaloy/SS, Zircaloy/Ag-In-Cd, SS/B_4C etc. were investigated in the temperature range from 1073 to 1953K at JAERI. Figure 6 shows an example of Zircaloy/Inconel interaction at 1273K. To estimate the reaction rate, the extent of reaction was measured as the thickness of reaction layer formed at the interface of reaction couple and/or the decrease in the material thickness by the reaction. The reaction approximately obeyed the parabolic rate law in every case of reaction system in the examined temperature range, so that the parabolic rate law constant for each system was determined and the Arrhenius equation was obtained. The kinetics data obtained at JAERI and the applicable temperature range is summarized in Table 2. The reaction rates for the various reaction systems are compared with each other in the Arrhenius type plotting in Fig.7. The reaction between materials used in the core of PWR, Zircaloy/Inconel and Zircaloy/Ag-In-Cd, showed the highest rates. The drastic change in the reaction rate at certain temperature level seen for some reaction systems indicates the change of reaction mechanism and this could be related to the eutectic formation occurs at this temperature. For the some reaction systems, the effect of oxidizing atmosphere on the reaction rate was partly investigated and the qualitative information was obtained, which indicated the increase in the initiation temperature of eutectic formation.

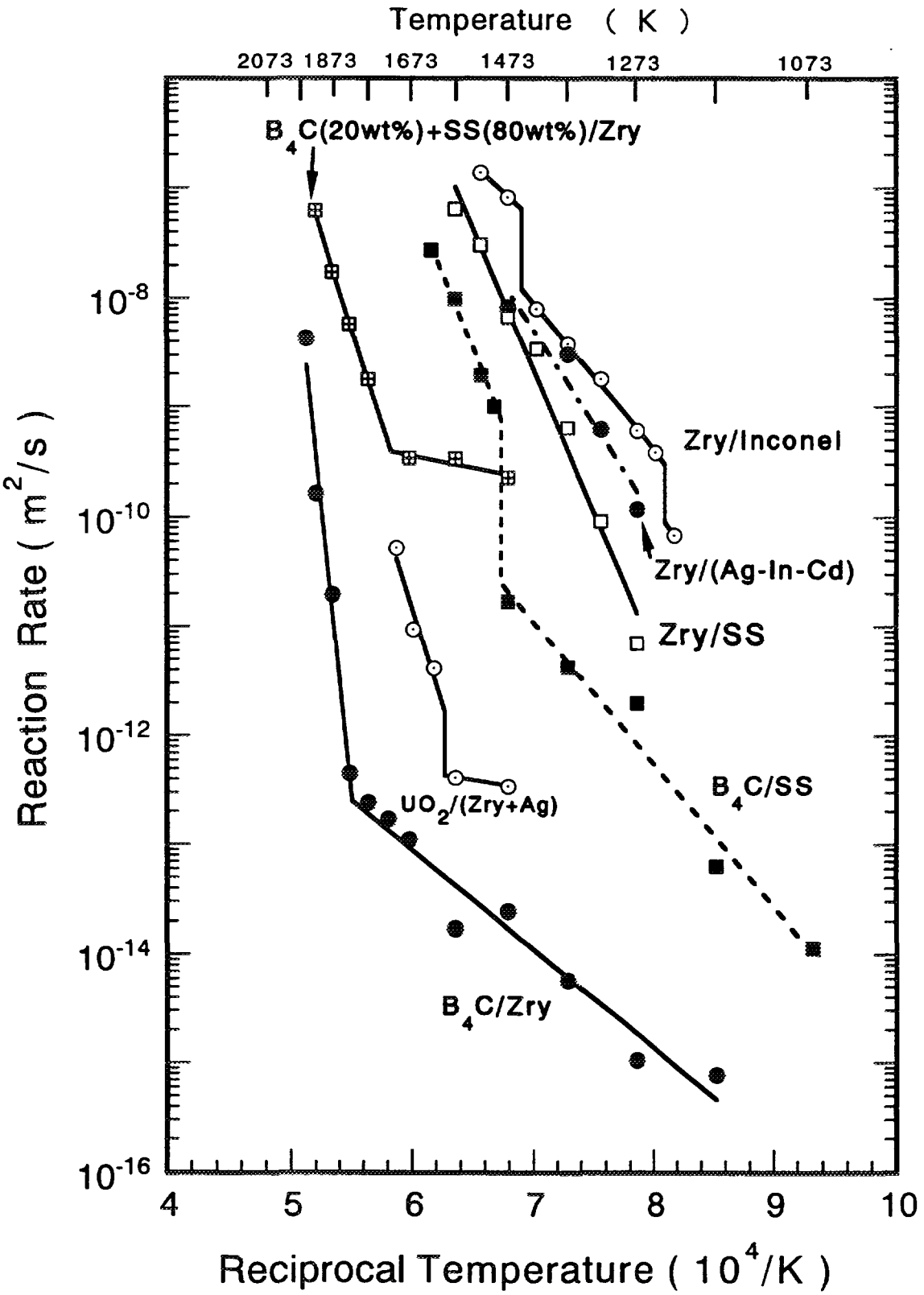

Fig. 7 Comparison of reaction rates between core materials measured at JAERI

The obtained kinetics has been incorporated into computer codes such as ICARE2 which predict the fuel degradation such as melt formation and progression in the bundle under a severe accident condition.

4. TMI-2 debris examination

The TMI-2 reactor accident in March 1979 resulted in severe fuel damage, including melting, interaction and relocation of reactor core materials. About 19 tons of molten core material was assessed to have relocated onto the lower head of the reactor vessel during the accident. JAERI has participated in the TMI-2 Vessel Investigation Project conducted by the OECD-NEA and has obtained sixty samples including ten companion samples from locations adjacent to the lower head. Many examinations and analyses such as ceramography, SEM/EPMA analysis, γ-ray spectrometry and thermal property measurement are being performed at the Reactor Fuel Testing Facility(RFTF) of JAERI. These examinations are being performed to obtain behavioral data for fuel and core materials under LWR severe accident conditions.

Visual examinations indicated that the samples were composed primarily of once molten ceramics. They were generally dull grey in appearance. The histogram of debris density for the 30 measurements data is shown in Fig.8. The density ranged from 6.3 to 9.3g/cm^{3}and the average

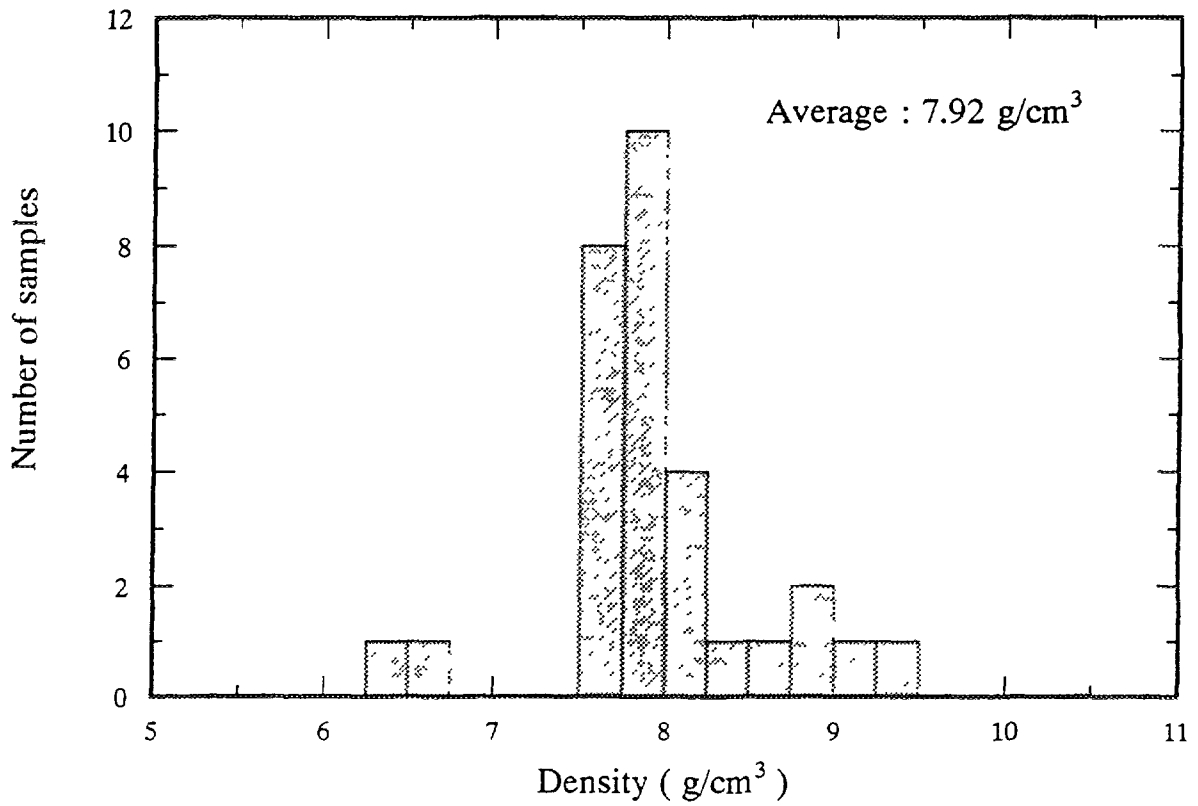

Fig. 8 Histogram of debris density

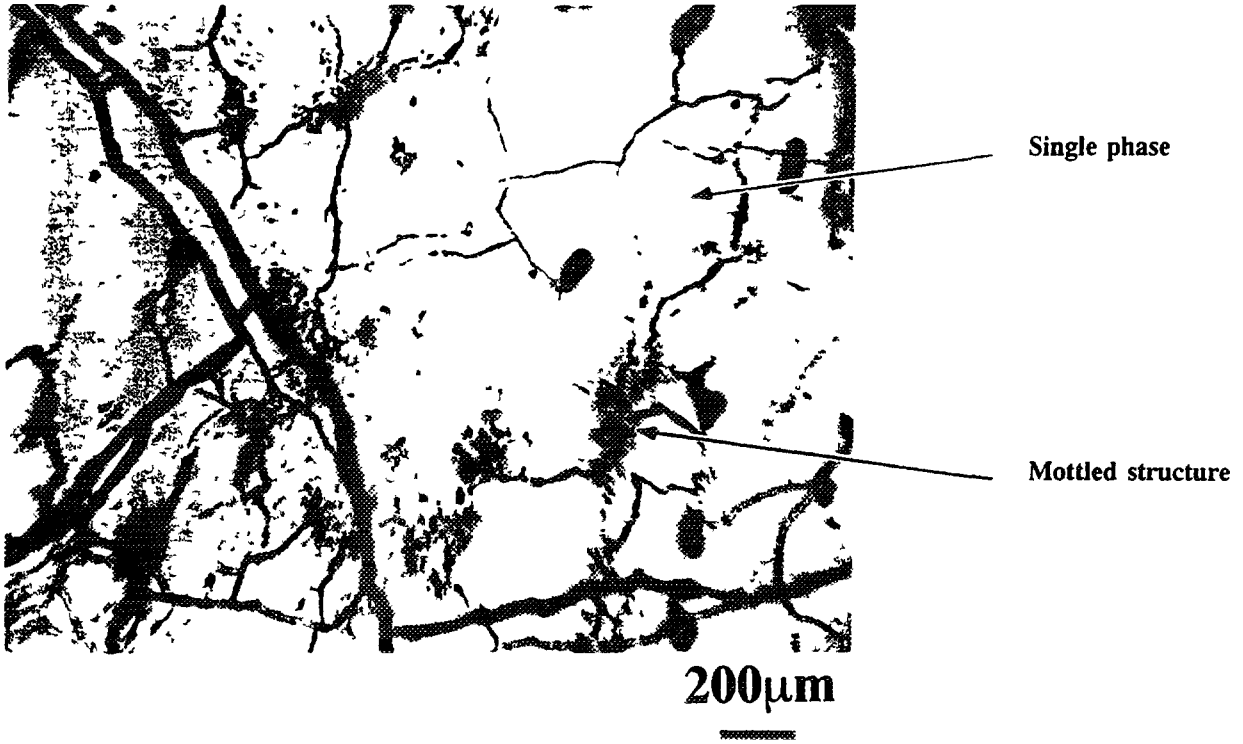

Fig. 9(A) Microstructure of ceramic debris(VIP-12A)

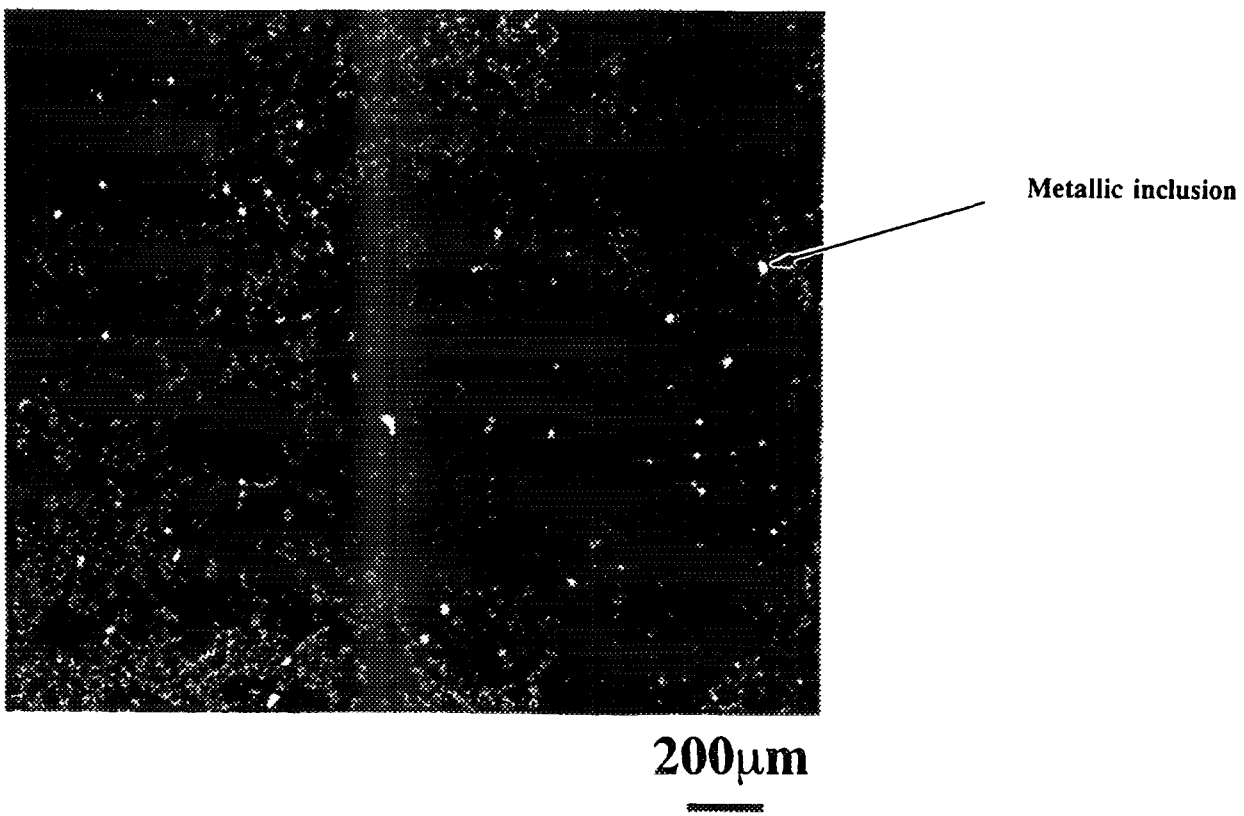

Fig. 9(B) Metallic inclusions dispersed in ceramic debris(VIP-12A)

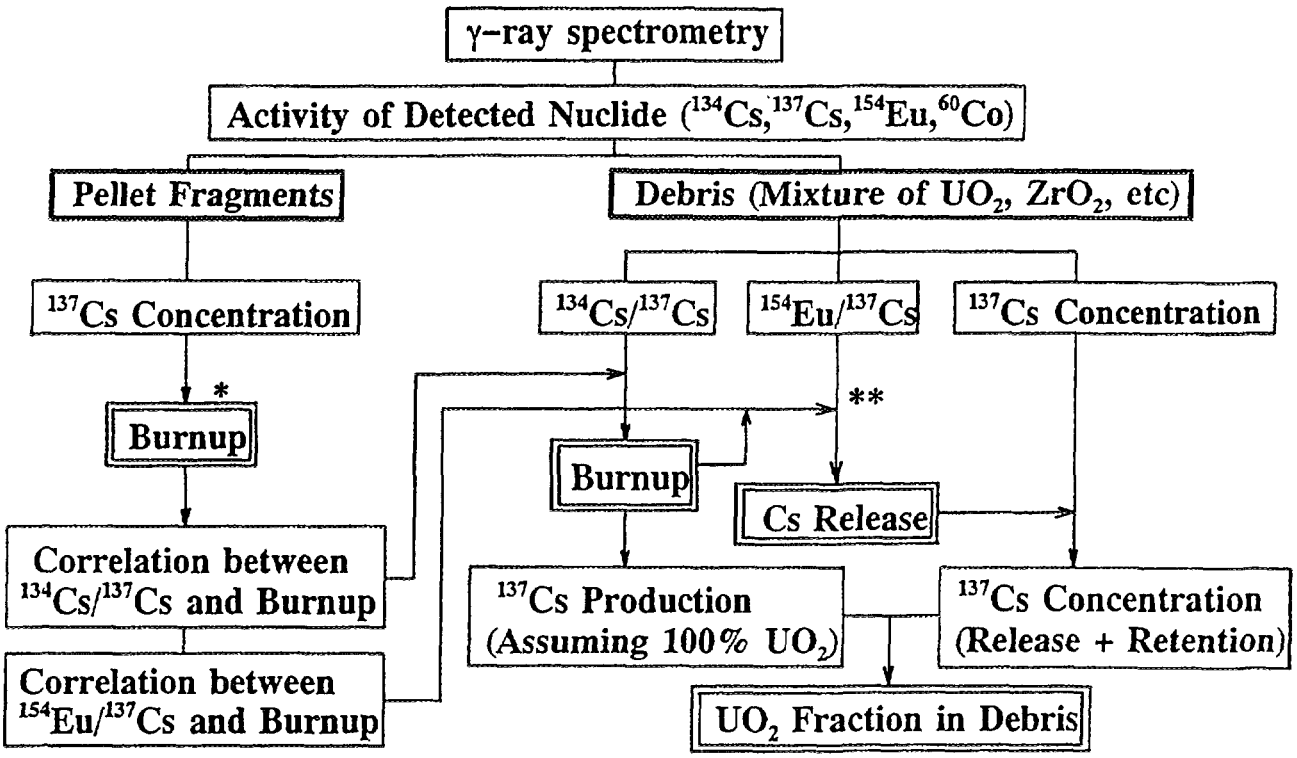

Fig. 10 Flow diagram of estimation for Burnup and Cs retention of TMI-2 debris

Table 3 Burnup, Cs retention and UO_2 fraction in debris

Sample	*Burnup [MWd/t]*	*Cs Retention [%]*	*UO_2 Fraction [%]*
E9-4	*3300*	*0.4*	*64.5*
H8-1	*3700*	*4.2*	*72.5*
VIP-9H-a	*3500*	*5.3*	*79.4*
VIP-9H-b	*3500*	*3.3*	*83.3*
VIP-10C-a	*3600*	*3*	*76.7*
VIP-10C-b	*3600*	*5.9*	*73.9*

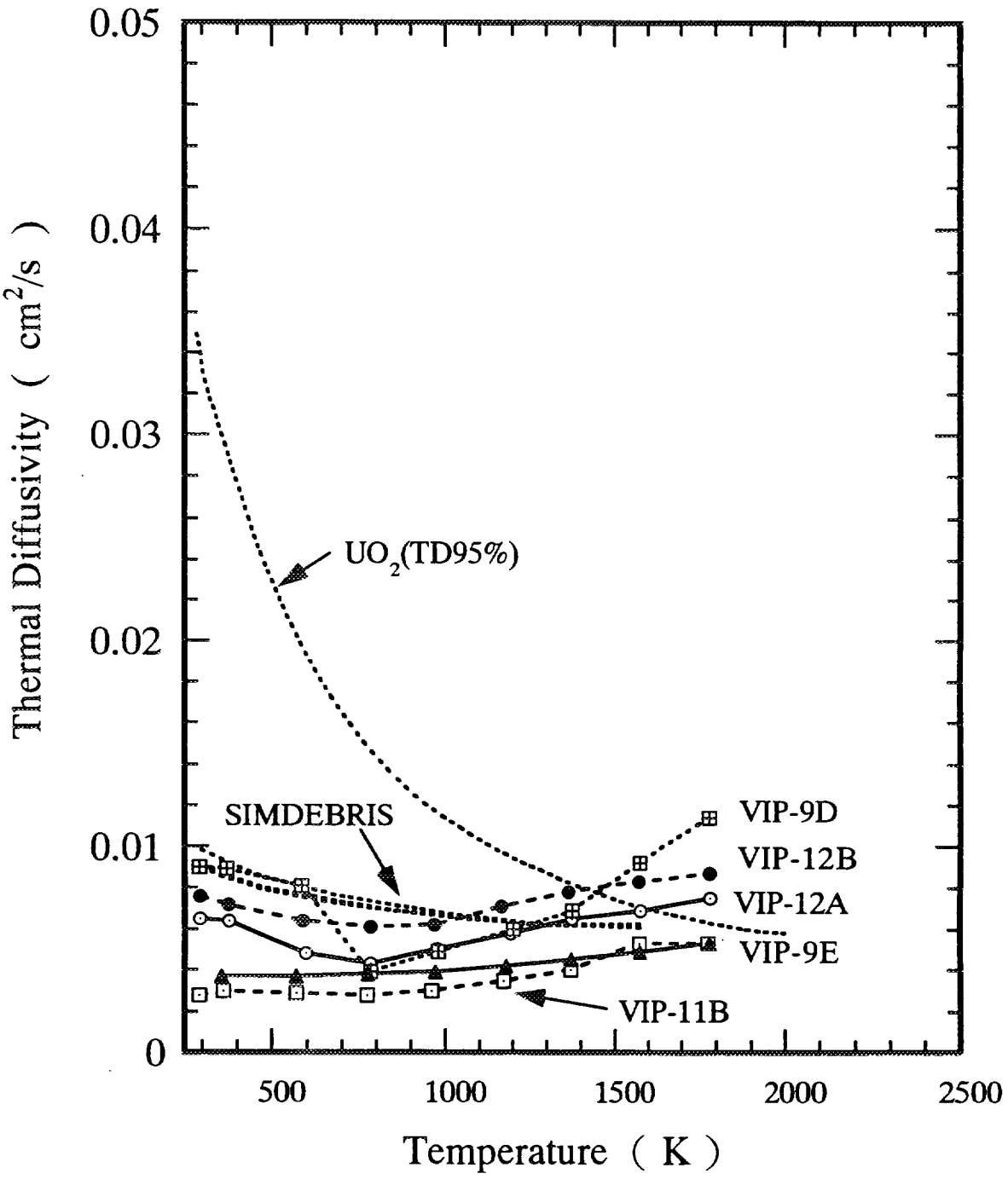

Fig. 11 Thermal diffusivity of TMI-2 debris measured with the laser flash method

density was about 7.9g/cm^3. Figure 9(A) is a high magnification photograph that shows the typical microstructure of ceramic debris. The structure is composed of both the clear single-phase region and the mottled region. The SEM/EPMA analysis revealed that the single-phase was uranium-rich $(U,Zr)O_2$ phase and the secondary phase consisted of microporosity and ceramic two-phase structure, uranium-rich $(U,Zr)O_2$ phase and zirconium-rich $(Zr,U)O_2$ phase. The metallic inclusions were sometimes found in the ceramic debris as shown in Fig.9(B). These melts are probably silver-rich metallic particles.

In the γ-spectrometry, four nuclides of Cs-134, Cs-137, Eu-154 and Co-60 were detected for each sample. The retention of Cs, burnup of fuel and fuel fraction in debris were estimated based on the measurement data and by the method shown in Fig.10. The results of present estimate are summarized in Table 3. The burnup of fuel contained in debris was estimated to be in the range of 3,300 - 3,700MWD/t. The retention of Cs in debris was quite low, it ranged from 0.4 to 5.9%. This indicates debris experienced very high temperature during the accident. In the experiments at ORNL, 37% Cs retention was measured after the heating at 2300K for 60min in steam. The UO_2 fraction in debris was estimated in the range between 64.5% and 83.3%.

Thermal diffusivity of debris was measured with a LASER flash equipment in the temperature range from room temperature to 1773K. Fig.11 summarizes the measurement data showing the correlation between the thermal diffusivity and the temperature. The data of 95%-TD UO_2 and simulated fuel debris(SIMDEBRIS) having similar chemical composition to TMI-2 debris is also plotted in the figure for comparison. The thermal diffusivity of debris is much lower than that of UO_2 at relatively low temperature range, while the data becomes comparable each other in the highest range of examined temperature. There was large difference in diffusivity among debris samples. It was confirmed that the difference in thermal diffusivity between samples was caused by the difference in chemical composition and microstructure.

5. Summary and future plan

To investigate the core materials behavior under severe accident conditions, fuel quench tests at the NSRR, core materials interaction tests at high temperature and TMI-2 debris examination were conducted at JAERI. Experimental data to determine the boundary condition of the fuel fracturing upon quenching have been obtained through fuel quench tests. Chemical interactions have been widely investigated at high temperatures for various binary systems of core component materials. Also, valuable information on the TMI-2 debris was obtained through debris examination. The NSRR quench test program will be finished after information on the additional oxidation by steam generation during reflooding is obtained through post test examination. The experiments on the materials interaction and TMI-2 debris examination are planned to be finished in this year, 1995.

As a next phase of the experimental study on material behavior at JAERI, Verification Experiment of Gas/Aerosol Release(VEGA program) is planned. Objective of this program is to investigate the fission product(FP) release behavior and materials interactions by heating tests of

burnup fuels. JAERI's participation in the international collaboration of Phebus-FP program will be continued in order to obtain the information from large scale experiments on FP behavior under severe accident conditions.

REFERENCES

[1] Saito, S., et al., Severe Fuel Damage in Steam and Helium Environments Observed in In-reactor Experiments, Fifth International Meeting on Thermal Nuclear Reactor Safety, Karlsruhe, September, 1984

[2] Katanishi, S., et al., Quenching degradation in-pile experiment on an oxidized fuel rod in the temperature range of 1000 to 1260, Nucl. Engrg. Des. 132(1991)239-251

[3] Saito, S., et al., Measurement and evaluation on pulsing characteristics and experimental capability of NSRR, J. Nucl. Sci. Technol. 14(3)(1977)226-238.

[4] Chung, H. M., et al., Embrittlement criteria for zircaloy fuel cladding applicable to accident situations in light-water reactors : Summary report, NUREG/CR-1344 (January 1980).

A REVIEW OF THE DOE/ARSAP CORE MELT PROGRESSION PROGRAM SUPPORTING DESIGN CERTIFICATION FOR ADVANCED LIGHT WATER REACTORS

B.W. SPENCER
Argonne National Laboratory

S.W SORRELI, R.A. MOORE
US Department of Energy

USA

Abstract

An important element of the safety approach for AP600 is in-vessel retention (IVR). System design features are provided which enable the reactor cavity to be flooded in the event of a core melt accident. The ARSAP is performing work demonstrating that core melt materials would be retained and cooled within the vessel by means of this cavity flooding, and that ex-vessel threats to the containment are thereby avoided. This paper addresses in-vessel melt progression analyses being performed by ARSAP which are providing input to IVR-related issues such as in-vessel steam explosion and melt stream impingement/vessel wall ablation. (The issue of melt coolability in the vessel lower head, by virtue of external water cooling, is not sensitive to details of core melt progression and has been handled separately.) This paper also reviews the in-vessel core melt progression database as well as results from the TMI-2 accident which are the foundation of the current analyses for AP600.

INTRODUCTION

The U.S. Department of Energy (DOE) currently sponsors research and development work on selected topics of advanced light-water-reactor (ALWR) safety. The specific work is selected on the basis of its value as base technology supporting understanding of the safety-related behavior of advanced LWR designs, notably under accident conditions which are beyond the design basis. There has been a commitment to consider such accidents as part of the ALWR design certification process in the U.S., and hence, the results of this R&D work are available for use by the industrial vendor design teams as they participate in U.S. Nuclear Regulatory Commission (NRC) reviews. The DOE organizational unit responsible for identifying and carrying out this R&D work is the Office of Nuclear Energy, Science and Technology's Advanced Reactor Severe Accident Program (ARSAP).

Among the activities currently underway in the U.S. through ARSAP, and most noteworthy from the standpoint of the subject of this paper, is the in-vessel retention (IVR) program. In-vessel retention refers to the permanent termination of a core melt accident within the reactor vessel by passive means; i.e., the core meltdown materials are permanently coolable inside the reactor vessel via external cooling. This was the outcome that was achieved in the accident at Three-Mile Island Unit-2 (TMI-2), albeit that success was achieved through the ability to achieve coolant water flow into the reactor vessel. Strictly speaking, IVR requires no sustained availability of cooling water flow into the vessel, and hence it is a very robust safety approach. With respect to IVR implementation, there are four main system-related requirements of the ALWR design: 1) high reliability reactor depressurization system, 2) large water inventory inside containment for flooding the reactor cavity such that at least the bottom region of the reactor pressure vessel is covered with water, 3) vessel thermal insulation design which does not preclude necessary heat dissipation from the vessel to water in the cavity, and 4) containment cooling and liquid pathway designs such that a heat reflux cycle can be established to achieve removal of decay heat from the containment and return condensate to the cavity pool. With a nuclear power plant (NPP) design that meets these main requirements, the questions relevant to IVR are:

1) What is the spectrum of challenges to vessel integrity during in-vessel core melt progression which bear on the success of achieving IVR, and
2) What is the capability of the vessel to remain intact under the spectrum of loads?

To answer these questions requires understanding of basic aspects of core melt progression in the specific-design NPP.

Currently, analyses are underway under ARSAP sponsorship addressing in-vessel retention and related issues for AP600. Three specific challenges to vessel integrity have been identified:

1) *In-Vessel Steam Explosion (IVSE)* -- The relocation of molten core material from the core region to the lower plenum occurs via water-filled pathways and through water in the lower plenum itself. At TMI, about 23,000 Kg of molten core materials (corium) flowed from the core region over a 1-2 minute period, of which 19,000 Kg collected on the vessel bottom head. Although no steam explosion occurred at TMI as a result of this process, the hypothetical energetics of such an event is nonetheless being examined in the ARSAP program as well as the vessel structural response to such an event.

2) *Vessel Wall Ablation* -- The relocation of molten core material from the core region to the lower plenum is being investigated to determine whether melt stream impingement on structures (notably the vessel wall itself) may pose an ablation-related threat to vessel integrity. Evidence at TMI indicated that such a melt stream cut through internal, vertical core baffle plates and that, while importantly influencing the melt relocation pathway, did not itself threaten either the vessel sidewall nor lower head. Nonetheless, this process is being examined in the ARSAP program for the specific melt relocation behavior and configuration of AP600.

3) *In-Vessel Melt Coolability* -- The coolability of a heat generating corium pool in the vessel bottom head is being investigated in the ARSAP program. The program is addressing the limiting internal heat flux distribution from the convecting pool to the vessel wall together with assessments of external heat removal capability as well as vessel structural integrity where wall thinning is indicated.

It is important to recognize that the ARSAP approach to resolving in-vessel melt coolability does not depend upon details of core degradation, core melting, and melt relocation. It focuses on the limiting state of a stratified oxide pool with an overlying molten metal layer, where the masses encompass the entire corium inventory plus all steel internal structure embedded by the pool depth. This approach provides the largest corium mass and therefore the largest thermal load to the vessel bottom head.

In-vessel steam explosion and vessel wall ablation, on the other hand, are closely related to the core melting and melt relocation processes. In order to quantify the steam explosion process, it is necessary to know the conditions associated with corium flow into the water. Similarly, the melt jet ablation issue requires knowledge of the melt relocation flowrates and pathways in the specific NPP design. The remainder of this paper focuses on the ARSAP approach to quantifying the core melting and melt relocation processes for input to resolution of the jet impingement and steam explosion threats.

CORE MELT PROGRESSION DATABASE

Programs in the U.S. which have investigated core degradation and core melt phenomena in LWR's were initiated in the 60's [1] and have mainly been completed. Among these programs were several which utilized varying size bundles of varying lengths of real fuel subjected to nuclear heating in test reactors. Notable among these are the following:

1) *Severe Fuel Damage (SFD) Tests [2]* -- There were four early post-TMI tests conducted in the Power Burst Facility (PBF) at Idaho National Engineering Laboratory (INEL). Each test consisted of PWR-type fuel elements, one meter in length, using inconel grid spacers. Tests SFD1-ST and SFD1-1 utilized 32 unirradiated fuel elements, and tests SFD1-3 and SFD1-4 utilized 26 fuel elements irradiated to nominally 36,000 MWD/t and two instrumented fresh fuel elements. The pressure was 7 MPa. The fuel was fission heated at decay heat level by the PBF reactor. Initial cladding heatup rate was ~1° K/s, (except the Scoping Test, 0.1 K/s) characteristic of small-break LOCA conditions. Steam flow was provided by water boiloff in the channels. The first test in the series had a simulated reflood transient.

2) *Damaged Fuel (DF) Tests* [3] -- Four tests were conducted in the Annular Core Research Reactor (ACRR) at Sandia National Laboratories (SNL). These tests utilized from eight to fourteen unirradiated fuel elements 0.5 m in length. The first two tests utilized nine PWR-type fuel elements with inconel spacer grid. They attempted to parameterize on the amount of oxidation preexisting on the cladding. Fission heating was used to heat the elements at an initial rate of ~1° K/s. Steam flow was provided through the bundle.

3) *Full-Length High Temperature (FLHT) Tests* [4] -- Four tests were performed by Pacific Northwest Laboratories (PNL) in the National Research Universal (NRU) reactor at Chalk River, Canada. These tests consisted of bundles of 12 full-length (3.7 m) PWR-type fuel elements having inconel spacer grids at 0.5 m spacing (the last test had four inconel and four zircaloy spacer grids). The first two tests utilized unirradiated fuel; the last two tests incorporated one element irradiated to 28,000 MWD/t and one stainless steel rod. The pressure was 1.4 MPa. Steam was provided to the bundles by boiloff of water delivered at constant flowrate at the bundle inlet. The fuel elements were fission heated in NRU such that the initial cladding heatup rates ranged between 2.6 - 3.5 °K/s, which is faster than would be expected even for large-break LOCA conditions.

4) *Loss of Fluid Test (LOFT) LP-FP-2* [5] -- Often referred to as the LOFT "destructive test", this was a large, single test conducted in a specially-designed center fuel module in the LOFT reactor core. The test bundle consisted of one hundred 1.68 m long PWR-type fuel elements internally pressurized to 2.41 MPa, plus eleven Ag-In-Cd stainless-steel clad control rods in zircaloy guide tubes plus six empty zircaloy guide tubes. The bundle incorporated five inconel spacer grids separated by ~0.45 m. The fuel had low burnup of 448 MWD/t. The system pressure was 1.1 MPa; initial cladding heatup was ~1° K/s. The steam flowrate through the bundle resulted from a combination of coolant flashing and boildown. The test was terminated by a rapid core reflood.

5) *CORA Experiments* [6] -- A major contribution to understanding core degradation and early melting has resulted from the extensive CORA series of out-of-pile experiments at KfK in Germany. These tests employed bundles of from 18 to 59 Western PWR-type fuel elements (BWR and VVER-1000 type fuel have also been tested). The bundles consist of electrically heated fuel element simulators (tungsten heater elements in the center of annular UO_2 pellets), unheated fuel elements, and absorber rods. The test bundles are 2 meters in length with a heated length of 1.0 m. The nominal initial cladding heatup rate is 1° K/s, and small-break LOCA conditions are simulated. Steam from a steam generator and superheater is delivered to the bottom of the bundle. After heatup, the test is terminated either slowly with argon gas or rapidly by a rising front of water.

KEY FINDINGS PERTAINING TO IN-VESSEL MELT PROGRESSION

It is beyond the scope of this paper to review results from these various programs. This has been accomplished in recent survey papers such as [7]. However, it is useful to remark on general and consistent findings which relate to a broad range of accident conditions encompassing early to late uncovery time and low to high vessel pressure. Following core uncovery, early fuel element degradation results from zircaloy oxidation by available steam in the channels. Early melting at temperatures as low as ~1000 C results from eutectic reactions between zircaloy and iron-bearing materials such as Inconel and stainless steel. By the time 1200 C is reached, molten materials are found to drain, typically to spacer grids or water elevation, where they form partial channel blockage. The draining melt may also include absorber material Ag-In-Cd (T_m ~800 C) when released from its stainless steel cladding. Blockage formation is typically incomplete during this stage due to noncoherence and relatively small masses, so steam flow continues into the degraded core region, and cladding oxidation continues. When the cladding temperature reaches ~1200 C, the exothermic oxidation rate becomes very rapid, and the oxidation energy source begins to surpass the nuclear (decay heat) energy source. With this chemical heating the heatup rate of the fuel-cladding material can reach up to 20 C/s. At this point, the temperature attains the cladding melting range (1860-1975 C, depending on oxygen content) in only a few minutes. The cladding will melt and typically find an available path to run down, dissolving and carrying some limited amount of the fuel with it. This material will freeze in the lower bundle region forming a largely metallic blockage with some fuel material in it. This blockage is also typically found to be incomplete such that some steam can continue to pass up into the degraded core zone while other steam is directed radially to peripheral channels which may have little or no damage due to the radial power profile and/or radial heat losses. At this point, the degraded core consists of intact stacks or jumbled fuel pellets together with oxidized cladding shards (ZrO_2). With continued heating, the formation of an oxide melt begins at ~2600 C, and, with time, the UO_2/ZrO_2 materials in this zone can be liquefied completely. The liquefied oxide material is retained initially by completion of the lower blockage which had been formed largely of metallic materials. Hence, through this stage, little molten material except possibly a limited amount of the low melting eutectics passes below the fuel element support structure.

KEY FINDINGS FROM THE TMI-2 ACCIDENT [8-12]

While the above scenario is based largely on results of experiment programs, the depiction is consistent with the TMI-2 accident, albeit core melt progression at TMI-2 continued well beyond the ability of the relatively small scale, separate-effects tests to address. At TMI-2, the bottom blockage (i.e., crust) was about 10 cm thick and was composed primarily of various Zr-based metallic compounds, plus Ag-In-Cd and some fuel. The blockage was dish shaped, located at the first grid spacer elevation in the central region, ~0.5 m above the bottom of the core. There was a radial crust roughly one-to-two fuel assemblies from the edge of the core. Initially, the mainly (U,Zr) O_2 oxide melt was held within the crust boundary. This corium mass was growing by the progressive ingression from above of pellet and cladding rubble collapsed from the upper region of the core, and supported by an impermanent upper crust. During the TMI-2 recovery, this upper crust was found to have been 1-3 cm in thickness and comprised of both metallic and ceramic material. A large void region formed between the top fuel assembly grid and the rubble bed, resulting from the collapse of the upper pellet stacks and cladding fragments as well as their ingression into the molten pool.

The core melt progression continued at TMI-2 until the molten oxide pool was ~3 m diameter and ~1.5 m deep in the central region. The pool contained ~56 tonnes of mainly (U, Zr) O_2 ceramic material including small quantities of other oxides (mainly Cr_2O_3 and Fe_3O_4) and metals (primarily Ag, Sn, and Ni). This pool was supported at the bottom by about 0.5 m fuel element stubs, surrounded everywhere by crust, and supported an 0.8 m deep rubble bed atop the top crust. Although immersed in water during much of the melt progression process, this oxide pool was not a coolable configuration. At 224 min into the accident, instrumentation indicated that an abrupt relocation of melt was initiated. This relocation process involved ~23,000 Kg of melt which flowed from a breach in the pool crust of which 19,000 Kg poured to the vessel lower plenum. The crust

was breached at an upper location along the side of the pool. Hence, not all the available melt flowed out; ~33 tonnes remained in the melt pool at elevation below the crust breach. The corium ejection from the breach appears to have been vigorous, aided perhaps by upper crust collapse under the weight of the upper rubble bed. The melt flowed into adjacent, intact, fuel assemblies and drained downward, essentially filling the available channel space in four assemblies. However, this melt appeared to freeze at the bottom of the assemblies, and relocation to the lower head by this pathway apparently did not occur. The melt jet emanating from the breached pool penetrated laterally through two adjacent fuel assemblies and subsequently ablated through the core former assembly locally. In doing so, the melt gained access to a roughly annular region formed by a series of horizontal baffle plates with varying size holes (3.3 cm typical diameter) for coolant passage. The corium used this annular pathway to drain downward to the lower plenum. As the melt drained onto successive former plates, it spread laterally, gaining access to flow holes through which it drained down onto the next lower former plate. Indeed, the melt flowed laterally in this annulus to extend about three quarters of the way around the vessel circumference. As this relocation process occurred entirely under water, it is not surprising that melt froze and remained in this relatively narrow annulus, causing subsequently released material to flow laterally as well as downward. When this melt emerged at the bottom of the annulus, it encountered the lower internal structure consisting of lower grid, grid forging, and flow distributor plates. Hence, the melt drained through the numerous holes in these structures in draining to the lower head. Insofar as the melt contacted these structures at their radial extremity, the melt streams emerging from the distributor plate holes impinged upon the hemispherical head at a relatively high elevation, whereupon the melt flowed down the head inner surface and collected at the bottom.

This process left a debris layer in the lower head which amounted to 19 tonnes and mainly consisted of (U, Zr) O_2. The depth of the hard layer (resolidified melt) plus overlying loose debris ranged to as much as 0.81 m. Based on results of the Vessel Investigation Project (VIP) [10-12], the picture of melt relocation that emerges consists of progressive, discernable flows emanating from the radial extremity of the core support and flow distributor structures from varying azimuthal location as corium relocated, froze, and progressively diverted around the annular space surrounding the core former. The entire 19 tonnes of corium relocated to the lower head in from 1 to 2 minutes, most likely less than 1 1/2 minutes. Hence, the flowrate of corium into water in the lower head was between 160 and 320 Kg/sec. A steam spike occurred from this corium-water mixing which resulted in system pressure increase of 1.4 MPa; however, there was no steam explosion at the prevailing system pressure of 10.5 MPa. Based on meltoff of lower head instrument nozzles, it has been interpreted that the initial molten fuel layer spreading on the bottom head froze and cooled rapidly, forming an insulating crust layer that protected the lower head and many of the nozzles from damage. This frozen material was very hard but did not adhere to the underlying vessel wall. Subsequent material flowing into the head region may have been hotter. Evidence indicates its temperature was at least 2600 C. It flowed over quenched layers building up depth and resulting in nozzle melting at high elevations in some places. In one region of the lower head approximately 1 m x 0.8 m in dimension, a "hot spot" was formed at the vessel surface which reached a temperature of ~1100 C. It was speculated that this hot spot occurred where the initial curst layer was either absent or lacked sufficient thickness to protect the head.

From the standpoint of core melt progression, the TMI-2 accident was stabilized after this relocation event. The corium relocation event at 224 minutes had redistributed the corium from the single original pool, reducing the melt mass in the original pool region to 33 tonnes, spreading corium into adjacent fuel assemblies, into the core former annulus, and into the lower head. The corium was coolable in this configuration given the continuous presence of water in the system.

APPLICATION TO AP600 VESSEL INTEGRITY CHALLENGES

The DOE/ARSAP is addressing details of in-vessel core melt progression to the extent necessary to quantify the vessel integrity challenges posed by 1) in-vessel steam explosion, and 2) melt-stream impingement and ablation of the vessel wall. The reference accident scenario for the

passive plant is the analog of the S2B sequence, which is a small break loss-of-coolant-accident (SBLOCA) with failure to achieve passive water injection into the primary system. The ARSAP approach is to use MAAP 4.0 code analyses through core uncovery and early degradation. Separate analyses were performed based on the MAAP-calculated reactor conditions to determine realistic, upper bound conditions of melt relocation from the in-core pool to the lower head. These realistic, upper bound flowrate conditions are used to assess the impingement-related threat to vessel integrity, and they are used as input to the corium fragmentation/quenching code THIRMAL as well as the corium-coolant mixing code PM-ALPHA in order to evaluate corium-water coarse premixing in the lower plenum. The latter information is used as input to the steam explosion propagation code ESPROSE.m which calculates pressure-time history from an explosive interaction. The resulting pressure-time history is the source term for vessel structural response analyses.

The core melt progression analyses are based on the results of experiments as well as the TMI-2 accident described previously. The analyses are specific to the geometry and core design of AP600 albeit ignoring the passive safety features of that reactor intended to prevent such an accident from occurring. The analyses prominently include the effects of radial noncoherrence attributable mainly to radiation heat loss to the reflector during the accident. The initial fuel/cladding heatup occurs at $\sim 1°$ C/s, typical of PWR and SBLOCA conditions. Upon reaching 1200 C cladding temperature, the heatup rate escalates to 10-20 C/s such that zircaloy cladding begins melting in only a very few minutes. Overall cladding oxidation to ZrO_2 is about 70%; the 30% Zry runs down and forms a blockage at the water level near the bottom of the core. The UO_2 fuel and ZrO_2 cladding continue heatup at ~ 0.5 K/s to melting. The oxide melt flows down forming a crust layer at the bottom metallic blockage. Additional melting oxide flows radially and forms a crust in the outermost fuel assembly. This crust takes on a thickness of 2-6 cm. Upper material rubblizes during the downward melting process. Soon a state of oxide pool is attained whose crust boundaries extend downward virtually to the bottom of the core and radially to near the steel reflector. Initially the oxide pool temperature is at or near its liquidus (2650 C). With continued internal heat generation, the pool temperatures become superheated.

The Steinberner and Reineke [13] as well as the Churchill and Chu [14] correlations were used to calculate natural circulation heat transfer from the pool to its boundaries. The boundaries were calculated to grow radially owing to this natural convection heat flux. In fact, the lateral erosion eventually penetrates into the steel reflector itself. In doing so, the melt gained access to the reflector coolant channels. Molten metal and oxide flowed down into these channels (1.6 and 1.9 cm dia) where it froze and plugged. No corium mass exited at the bottom into the lower plenum by this path, and the corium mass depleted thereby was relatively small. Sideward pool growth continued until the reflector wall was fully beached. This occurred at the elevation of the molten stainless steel layer atop the corium pool, and the metal subsequently drained into the reflector-to-core-barrel gap region, depleting ~ 7000 Kg of molten metal from the pool. Eventually, the core barrel itself was breached by the radial pool growth at the top of the oxide pool. An initial breach 7 cm high by 7 cm wide was used which was progressively enlarged by erosion of the corium efflux. The melt ejected from the breach flows down the core barrel-to-vessel channel (downcomer) and enters the lower plenum directly. The melt relocation rate is determined primarily by the rate of reflector downward melting which is sensitive to the vertical temperature distribution in this structure as it evolved during the entire accident.

The current assessment is that the realistic, upper bound corium relocation rate is ~ 500 Kg/s (compared to the range 160-320 Kg/s interpreted from TMI-2 instrument response and VIP examinations). The corium pool consists of $\sim 96{,}000$ kg of oxide at the time relocation is initiated. Interestingly, at the stage of the accident when oxide melt is released to the lower plenum, it takes as little as 17,000 Kg of melt to completely boil off remaining water. Hence, it is only the very early stage of melt relocation that is relevant to in-vessel steam explosion owing to rapid depletion of the water inventory.

The ARSAP will soon complete evaluation of melt coolability in the vessel lower head with external vessel cooling [15], including international peer review. Currently, the peer review process is in its second round of review comments. All comments are expected to be received by the middle of October, 1995. The necessity of an additional round of comments will be evaluated in the near future. As mentioned previously, this specific work was not dependent on details of core-melt progression. Work described above pertaining to core melt progression is used for vessel ablation evaluation and is a part of the in-vessel steam explosion evaluation headed by Professor Theofanous of the University of California at Santa Barbara.

FUTURE NEEDS

In-vessel retention (IVR) via external cavity flooding is a severe accident mitigation approach adopted by Westinghouse for use in their AP600 design. Interactions with the Nuclear Regulatory Commission's Office of Nuclear Reactor Regulation is expected to begin in the very near future. Questions not satisfactorily answered as a result of the peer review process will be discussed in detail to develop a consensus between the regulator, the designer, and the researcher. Ultimately, the issue of in-vessel retention is resolved when the regulator agrees with the designer's accident mitigation approach.

Independent of any regulatory or peer reviewer input at this time, DOE/ARSAP is planning to conduct two confirmatory tests further proving the concept of in-vessel retention. Those two tests are called ACOPO and PACOPO. The first test (called ACOPO for axisymmetric COPO) saw its genesis in a smaller version of the experiment called mini-ACOPO that was conceived by Professor Theofanous at the University of California at Santa Barbara (UCSB) in support of the IVR effort [15]. The second test (called PACOPO for prototypic axisymmetric COPO) is an extension of the ACOPO experiment and involves the use of prototypic reactor materials.

The basic concept of the ACOPO experiment involves a cooldown of simulant material within a hemispherical volume rather that a heatup of the same in order to establish, and measure, convective heat transfer in the contained volume at Rayleigh numbers of interest. Detailed analyses has shown that for a large enough volume, a controlled cooldown transient approximates a quasi-steady process at any instant in time. For the mini-ACOPO efforts conducted in support of the IVR report [15], a 1/8 scale model of the AP600 lower heat was constructed of 1/4 inch copper tubing that was coiled and brazed into a hemispherical shape. The inside surface of the tubing was filled with a solder to create a smooth internal boundary with a diameter of 0.44 m. The copper tubing was separated into nine distinct cooling circuits - each with inlet and outlet controlled to maintain specific energy transfer to each of the loops. An extension of this concept to 1/2 scale is called ACOPO and is currently under construction at UCSB.

The PACOPO test program bridges the gap from simulant to prototypic materials by employing the use of uranium thermite in a large hemispherical volume that is cooled externally in a water bath - much like the situation hypothesized to occur in the AP600; that is, a core melt residing in the lower head of the vessel being cooled externally by cooling water. The concept for this test will be peer reviewed at UCSB in late October, 1995. Because the test will use uranium thermite, the experiment will be conducted at Argonne National Laboratory. These two tests, ACOPO and PACOPO, are expected to be the final confirmatory tests of the efficacy of in-vessel retention of a core melt by means of external vessel cooling.

ACKNOWLEDGEMENT

The authors wish to express their appreciation to Dr. James J. Sienicki for his review and helpful comments on this paper. The manuscript was typed by Ms. Lois Ondracek.

REFERENCES

[1] T. J. Thompson and J. G. Beckerly (Eds.), The Technology of Nuclear Reactor Safety," The MIT Press, Cambridge, MA (1973); See especially L. Baker, Jr. and R. C. Liimatainen, "Chemical Reactions", V. 2, p. 419.

[2] D. A. Petti, Z. R. Martinson, R. R. Hobbins, and D. J. Osetek, "Results from the Power Burst Facility Severe Fuel Damage Test 1-4: A Simulated Severe Fuel Damage Accident with Irradiated Fuel Rods and Control Rods," Nuclear Technology, V. 94 (1991).

[3] R. D. Gasser, C. P. Fryer, R. O. Gauntt, A. C. Marshall, K. O. Reil, and K. L. Stalker, "Damaged Fuel Experiment DF-1," NUREG/CR-4668, SAND 86-1030, U.S. Nuclear Regulatory Commission (1990).

[4] N. J. Lombardo and F. E. Panisko, "Principle Results of Severe Damage Tests on Full Length Nuclear Fuel Rods," Proc. Intl. Topical Meeting on Safety of Thermal Reactors, Portland, Oregon, 21-25 July 1991.

[5] "The OECD/LOFT Project--Achievements and Significant Results," Proc. Open Forum by the OECD Nuclear Energy Agency, Madrid, Spain, 9-11 May 1990.

[6] P. Hofmann, S. Hagen, V. Noack, G. Schonz, G. Schumacher, and L. Sepold, "Essential Experimental Results of the CORA Test Program on Severe Core Damage Phenomena," Kemtechnick, 59, (1994).

[7] R. R. Hobbins, D. A. Petti, D. J. Osetek, and D. L. Hagrman, "Review of Experimental Results on Light Water Reactor Core Melt Progression," Nuclear Technology, 95, September 1991.

[8] J. M. Broughton, P. Kuan, D. A. Petti, and E. L. Tolman, "A Scenario of the TMI-2 Accident," Nuclear Technology, 87, August 1989.

[9] D. W. Akers and R. K. McCardell, "Core Materials Inventory and Behavior," Nuclear Technology, 87, August 1989.

[10] A. M. Rubin and E. Beckjord, "Three Mile Island-New Findings 15 Years After the Accident," Nuclear Safety, 35, No. 2, July-December 1994.

[11] J. R. Wolf, D. W. Akers, and L. A. Neimark, "Relocation of Molten Material to the TMI-2 Lower Head," Nuclear Safety, 35, No. 2, July-December 1994.

[12] D. W. Akers and B. K. Schultz, "Physical and Radiochemical Examinations of Debris from the TMI-2 Lower Head," Nuclear Safety, 35, No. 2, July-December 1994.

[13] U. Steinberner and H.-H. Reineke, "Turbulent Buoyancy Convection Heat Transfer with Internal Heat Sources," Heat Transfer 1978, V. 2 (1978).

[14] S. W. Churchill and H. H. S. Chu, "Correlating Equations for Laminar and Turbulent Free Convection from a Vertical Plate," International Journal Heat and Mass Transfer, 18, (1975).

[15] T. G. Theofanous, et. al., "In-vessel Coolability and Retention of a Core Melt," DOE/ID-10460, July 1995. (2 Vols.)

MATERIALS AND ALLOY PROPERTIES AND THEIR INTERACTION

(Session A)

Chairmen

K. ISHIJIMA
Japan

V.N. GOLOVANOV
Russian Federation

HEAT RELEASE FROM B_4C OXIDATION IN STEAM AND AIR

L. BELOVSKY
Nuclear Research Institute Rez Plc,
Rez, Czech Republic

Abstract

BWR and some PWR cores contain boron carbide (B_4C) as neutron absorber. During a severe accident, the B_4C can potentially react with steam under release of heat and hydrogen. Although models for B_4C oxidation already exist in MELCOR and SCDAP/RELAP5, a development of a new model for another computer code seems to be difficult due to a missing comprehensive description of the current modelling methodology and scarce experimental data. The aim of this paper is to highlight the key points of the B_4C oxidation using the existing available experimental data and to perform a simple heat balance analysis of the B_4C/steam and B_4C/air chemical reactions.

The analysis of literature data shows that the B_4C oxidation phenomenon is qualitatively well described below 1000°C. However, no reliable data exist for the reaction kinetics especially above this temperature. It was found that the experimental results strongly depend on the experimental arrangement. The reaction heats, calculated in this study, indicate that the B_4C oxidation is an exothermic reaction, releasing more heat in air than in steam. The formation of boric acids from the boron oxide increases the heat release from B_4C by ~ 10 %, in the worst case. Although the total heat, released in a PWR core from the B_4C oxidation, is probably much smaller than the heat released from the Zr/steam reaction, it is not excluded that the B_4C oxidation can locally contribute to the damage of the control elements due to local overheating. Modelling of these phenomena is, however, very difficult due to the complex geometry of the liquefied control elements and due to absence of suitable data on the reaction kinetics.

1. Introduction

Boron carbide (B_4C) is one of the neutron absorber materials used in control elements of PWR's and BWR's. During a severe accident, the B_4C can react with steam (and air) under release of heat and hydrogen. This reaction thus contributes to the core damage. From this reason, B_4C oxidation models were included into computer codes SCDAP/RELAP5 [1] and MELCOR [2]. These models can be used only for BWR geometry. In spite of existence of these models, a comprehensive description of the current modelling methodology (often based on unknown data) is missing. It is also not known, how deeply the current models were verified against experimental data. In this situation, the development of a new model (e.g. for PWR geometry) for another computer code requires a new thorough analysis of all, the B_4C oxidation phenomenon, the available data and the current modelling.

The aim of this paper is to analyse the B_4C oxidation phenomenon (data and models) and to perform a simple heat balance study of the related reactions in order to draw conclusions for a potential development of a new PWR and/or BWR model.

2. About oxidation of B_4C

The discovered capability of B_4C to absorb neutrons led to the first irradiation tests in the middle 50s. The use of B_4C as neutron absorber in LWR's and in other applications as well is, however, limited by poor corrosion and oxidation resistance of the B_4C in oxygen-containing environment at elevated temperatures. From this reason, the oxidation behaviour of B_4C was experimentally studied at atmospheric pressure in air, oxygen, steam or in their mixtures by many authors up to temperatures ~1200-1300°C. Above these temperatures *"a catastrophic oxidation of B_4C starts, accompanied by a considerable thermal effect"* [3]. More information about the application and properties of B_4C can be found in [4-6].

In experiments, the B_4C was usually used in form of powder (~100 μm), ultrafine powder (~2-4 μm), hot-pressed pellets with low porosity or in form of flat blocks or thin coupons. It can be concluded that results strongly depend on material composition and test configuration. Especially the reaction kinetics is very sensitive to the mentioned parameters. Unfortunately, no data were found for pressureless sintered B_4C pellets with open porosity of ~70 % theoretical density, typical for the PWR design [5]. Owing to the sensitivity of results to the form of the tested materials, configuration and boundary conditions, it is very difficult to extrapolate the range of validity of the measured results to different materials and temperatures. Therefore, a direct application of such data in models, used in severe accident codes, must be handled with care. One have to take in mind that the B_4C oxidation can be considerably modified by the molten or solidified B_4C/SS/Zircaloy metallic mixtures, formed after the B_4C containing control element has failed at temperatures above 1200°C.

In the following chapter, the main characteristics of the B_4C oxidation will be described.

2.1 Oxidation of B_4C in oxygen and dry air

It is known that oxidation of B_4C powder in oxygen starts near 600°C [7] and in air at 450°C [8]. Ultrafine B_4C powders (~0.4 μm) start to oxidize in air at ~540°C [9]. From a thermodynamic point of view the most probable reaction is in eq.(1) [8]:

$$B_4C + 4O_2 \Rightarrow 2B_2O_3 + CO_2 \qquad (1)$$

The boron oxide (B_2O_3), as reaction product, is liquid at the considered temperatures. The melting point of the crystallic B_2O_3 is 450°C [10] and 577°C of the amorphous B_2O_3 [11]. The B_2O_3 has a relatively high vapor pressure [12]. At room temperature the B_2O_3 is glassy and before hydratation by moisture from air also transparent. The B_4C oxidation results in weight gain up to ~1100°C. At higher temperatures, the B_2O_3 intensively vaporizes so that weight loss of the samples can be observed. The reaction is thus a result of two simultaneous processes. The B_4C oxidation leads to the weight gain whereas the B_2O_3 vaporization results in weight loss. Between 600-1000°C, a protective B_2O_3 film is formed. In this case, the oxidation rate is limited by the diffusion of the oxygen and carbide components through the oxide film (i.e. by the diffusion of boron and carbon from the B_4C matrix through the B_2O_3, and not by the diffusion of the oxygen into the material substrate). The linear rate of weight gain, observed in dry air, indicates that the rate of transport of oxygen through the B_2O_3 is greater than the oxidation rate.

Lawrenko [13] measured reaction kinetics of B_4C in oxygen on sintered coupons of low porosity (<2 %) between 700-1200°C. The kinetics was initially parabolic (first 50-60 min) after which it became linear. The sharp rise in the oxidation rate, observed above 1100°C, was probably caused by intensive evaporation of the B_2O_3. The measured preferential depletion of carbon in the substrate near the B_4C/scale interface occured probably due to higher diffusion rate of carbon than that of boron at temperature. Although carbon monooxide is thermodynamically the most probable specie, it was not detected, probably because of excess oxygen. It seems to be possible that CO oxidized to CO_2 either on the surface of the oxide scale or in the system, immediatelly after it has formed.

Nazarchuk [7] performed tests with B_4C powder (62-74 μm) of different carbon content at temperatures between 500-1300°C. He observed that formation of the B_2O_3 oxide scale at 1100°C inhibited the complete oxidation of B_4C. The B_4C oxidized completely only at 1200-1300°C. Samples with higher carbon content oxidized more intensively.

Yefimenko [14] studied the oxidation kinetics of high-dense hot-pressed B_4C (1 % porosity) in air at temperatures between 630-930°C. The reaction kinetics for weight gain was approaching the parabolic law with activation energy of 108 kJ/mol. This value is much smaller than 188 kJ/mol, measured by Litz [8] on granular material. The porosity strongly influenced the reaction kinetics. The parabolic character of the reaction kinetics in air was also observed by Meyerson [15] at 1000°C. Lavrenko [16], on the other hand, observed between 800-1000°C a logarithmic increase of weight gain. Above 1200°C, a linear loss of weight can be seen in all experiments.

2.2 Oxidation of B_4C in steam

The B_4C oxidation in water-containing environment is more complicated due to formation of volatile boric acid in the reaction of water with B_2O_3:

$$B_4C + 8H_2O \Rightarrow 2B_2O_3 + CO_2 + 8H_2 \quad \text{and/or} \quad (2)$$

$$B_4C + 7H_2O \Rightarrow 2B_2O_3 + CO + 7H_2 \quad (3)$$

$$B_4C + 6H_2O \Rightarrow 2B_2O_3 + CH_4 + 4H_2 \quad (4)$$

The B_2O_3 reacts with steam to form some combination of acids, depending on conditions (on the partial steam and hydrogen pressure):

$$B_2O_3 + H_2O \Rightarrow 2HBO_2 \quad \text{(metaboric acid)} \quad \text{and/or} \quad (5)$$

$$B_2O_3 + 3H_2O \Rightarrow 2H_3BO_3 \quad \text{(orthoboric acid)} \quad (6)$$

$$3B_2O_3 + 3H_2O \Rightarrow 2(HBO_2)_3 \quad \text{(trimer of metaboric acid)} \quad (7)$$

The reactions (2), (5) and (6) were proposed by Litz [8], reaction (7) is reported by Randall [17]. Reactions (2), (3) and (4) are used in the MELCOR model, reaction (3) is considered in the older SCDAP/RELAP5 model. The newer model is, unfortunately, not described in the manual.

A comprehensive source of data for oxidation of B_4C powder at temperatures between 200-750°C was published by Litz [8]. The reaction of B_4C with steam in air-water and

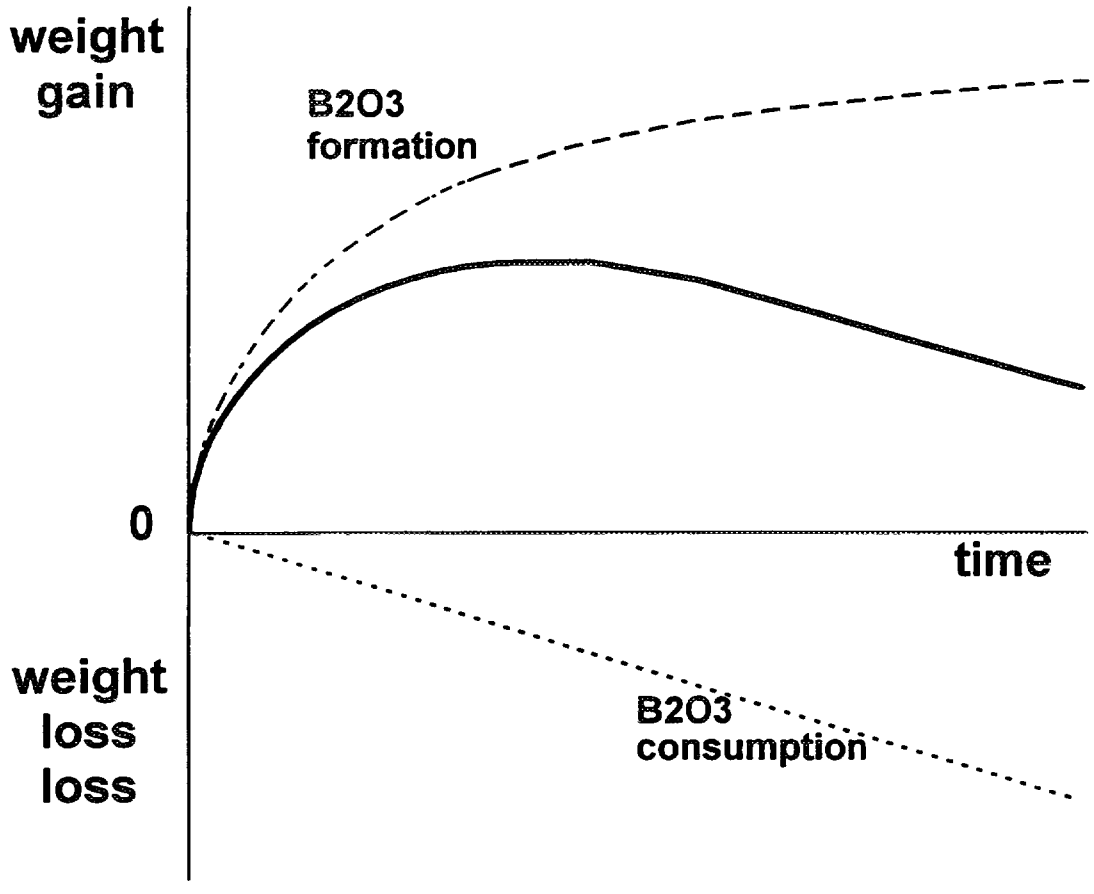

Figure 1 **Schematic representation of total weight change of B_4C specimen in steam as a function of time at constant temperature. Shown separately are weight change due to production of B_2O_3 and of volatile acids (consumption of B_2O_3). This schema was taken from [12].**

argon-water mixtures above ~600°C was characterized by an initial weight gain (formation of B_2O_3) followed by a weight loss (consumption of B_2O_3 by steam). Litz explains this mechanism as follows, Fig. 1:

"As long as the equivalent rate of transport of HBO_2 (gas) exceeds the rate of formation of B_2O_3, the weight loss curves directly depict the oxidation rate. However, when the oxidation rate exceeds the rate of removal of B_2O_3 , a film of the oxide will build up on the surface, and a net weight gain may result. As the thickness of the oxide film increases, the oxidation by H_2O is inhibited, and the rate of oxidation will decrease until a point is reached where the film thickness is constant due to equivalent rates of formation and transport of B_2O_3. Once the oxidation rate becomes fixed by the constant thickness of the B_2O_3 film, the system will again lose weight in a linear fashion".

Below ~600°C, the removal of B_2O_3 by water vapor occured faster than is the oxidation rate so that a clean boron carbide surface was maintained. This continuous weight loss is characterized by an activation energy of ~45 kJ/mole (compared to ~188 kJ/mole in dry air). Moreover, Litz observed in the air-water system a linear dependence of the reaction rate on the partial pressure of water p_{H2O} (mm H_2O). The fraction, reacted per hour, of

initial weight can be expressed as (temperature T in this and the following equations is in Kelvin):

$$\textbf{Oxidation rate} = 0.0617 \cdot p_{H2O} \cdot \exp(\frac{-5360}{T}) \quad [\text{hour}^{-1} \tag{8}$$

The measured reaction rates, however, may not apply to other specimens, because the character of the surface may play a significant role in determining the reaction kinetics. The study of Litz provides further interesting results:

- A measurable reaction of B_4C with water vapor can be observed at temperatures as low as 250°C (450°C in dry air).
- In dry air, a continuous weight gain was observed with complete loss of carbon and with the boron remaining on the unreacted B_4C as B_2O_3.
- When a layer of B_2O_3 exists over the B_4C, inhibition of the water reaction rate occurs but the presence of B_2O_3 does not inhibit the oxidation rate in dry oxygen.

Woodley [18] measured reaction kinetics on small blocks of boronated graphite (5 wt % boron) with water vapor / helium mixture in the temperature range 830-930°C, i.e. when steady state B_2O_3 layer thickness existed. The resulting reaction rate can be expressed in units of fractional weight change per minute, where C_{H2O} is the water vapor concentration in volume parts per million (total pressure was 1 atm):

$$\textbf{Oxidation rate} = 2.82 \cdot 10^{-4} \cdot C_{H2O}^{0.48} \cdot \exp(\frac{-8958}{T}) \quad [\text{min}^{-1} \tag{9}$$

Elrick [12] studied the B_4C/steam reaction at ~1000°C using thin B_4C coupons. The measured oxidation rate was seven times greater than the calculated one from eq.(8) and ten times greater than the rate from eq.(9). One reason for the difference can be in different flow conditions in the system and different material compositions.

Tests performed by Fujii [11] with B_4C powder and pellets (2.31 g/cm^3) in helium-water mixture (0.65 % H_2O) showed that the oxidation rates did not monotonously increased with temperature due to the behaviour of molten B_2O_3, acting as a physical barrier against diffusion of H_2O. In these tests, small concentrations of CH_4 and CO_2 were detected besides the main reaction products H_2 and CO.

The MELCOR model determines the relative extent of each of the three mentioned reactions (eqs.2-4) using the steam and hydrogen partial pressures and the B_4C temperature under assumption of chemical equilibrium between reaction products. The reaction energies for each reaction are shown in Fig. 2. The reaction kinetics, taken from Litz [8], is however, that for dry air. The B_4C oxidation rate is expressed as fractional change in the initial (intact) M^o_{B4C} mass:

$$\frac{d\left(M_{B4C}/M^o_{B4C}\right)}{dt} = \frac{9.973 \cdot 10^6}{60} \cdot \exp(\frac{-22647.2}{T}) \quad [\text{s}^{-1} \tag{10}$$

In the SCDAP/RELAP5, there are two models for BWR geometry. The older one is an exponential oxidation model, calculating the B_4C consumption M_{B4C}/M^o_{B4C} during time step Δt, where M^o_{B4C} is the available B_4C at the beginning of the time step:

$$M_{B4C} = M^{o}_{B4C} \cdot \exp[-(C \cdot T + D) \cdot \Delta t] \quad \textbf{[kg]} \tag{11}$$

where C = 0.001 and D = -1.7, according to the manual. In the SCDAP/RELAP5 source, C = 0.0005 and D = -0.35 are coded. It is interesting to note that this model calculates a decreasing reaction rate (M_{B4C}/M^{o}_{B4C}) with increasing temperature T.

In the newer BWR blade/box component model, developed at ORNL, the B_4C oxidation is derived from an advanced $B_4C/H_2/H_2O$ chemistry package, based on the SOLGASMIX code [19]. SOLGASMIX calculates equilibrium compositions in systems containing one gaseous phase, condensed mixtures, and condensed phases of invariant or variable stoichiometry.

The examples, shown above, illustrate that the B_4C oxidation in steam is a complex process. Competition of the two reactions (B_2O_3 formation and B_2O_3 consumption) makes it difficult to directly quantify the reaction kinetics of the real B_4C consumption, from which the heat and hydrogen release could be deduced. No reaction rate eqations for B_4C in steam were found in literature for temperatures above 1000°C.

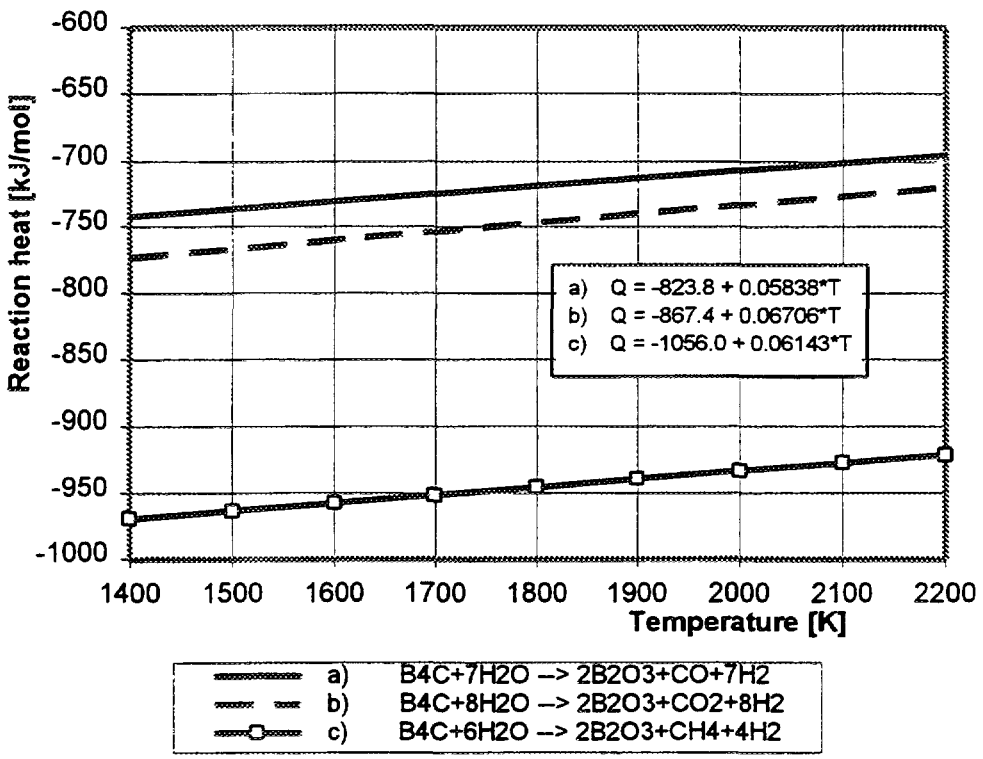

Figure 2 Reaction heat of B_4C oxidation in steam, used in MELCOR [2]. The minus sign means exothermic reaction.

2.3 Oxidation of B_4C in Severe Fuel Damage (SFD) Tests

A relatively small number of integral tests was performed with the B_4C absorber: two tests in the NIELS Facility [20], one test (DF-4) in the ACRR reactor, [21] and seven tests in the CORA Facility [22]. Results of these tests do not show any directly observable reaction of B_4C with steam. The reason can be in the fact that after rupture of the absorber rods (or blades) due to B_4C / stainless steel / Zircaloy chemical interaction, only a small fraction of the boron carbide particles is in direct contact with steam.

However, it cannot be excluded that during the damage progression, the B_4C can be locally in contact with steam, releasing heat and hydrogen. Hence, the B_4C oxidation could enhance the damage of the control elements without observable impact on the global temperature response of the whole bundle. A question thus arises, whether the modelling efforts can result in a realistic simulation of the complex B_4C / melt / steam behaviour without too much conservatism. The development of new B_4C-oxidation model must address the following areas:

- Heat and hydrogen release from B_4C oxidation.
- Reaction kinetics.
- Area of B_4C surface exposed to oxidation.

In this study, the first item will be analyzed from the point of view of heat balance during the oxidation process. The remaining items are out of scope of this paper and will be analyzed elsewhere.

3. Heat release from B_4C oxidation

In this chapter, the reaction heat of 1 mole B_4C in steam and air will be calculated for reactions, described by eqs. (1) - (7), under atmospheric pressure and temperatures 1400 - 2200 K. The contribution of boric acids, not reported in literature, will be taken into account. The upper bound of the total reaction heat in steam will be estimated from combinations of the six particular reactions (2) -(7).

3.1 Methodology

In this study, the reaction heat was calculated under assumption that the heat of formation ΔH^f is known at 298.15 K for each reaction specie. The following steps were performed for each reaction equation:

Left-hand-side of reaction equation	*Right-hand-side of reaction equation*
Cooling of species from the chosen temperature to 298.15 K.	Formation of reaction products from stable compounds at 298.15 K
Decomposition of species to stable compounds at 298.15 K.	Heating of reaction products from 298.15 K to the chosen temperature.

The reaction heat Q is the sum of energies, consumed or released during each of the above mentioned steps:

$$Q = \sum_{i=1}^{m} -m_i \cdot \left(H_i - H_i^{298} + \Delta H_i^f\right) + \sum_{k=1}^{n} n_k \cdot \left(H_k - H_k^{298} + \Delta H_k^f\right) \quad \textbf{[kJ / mol B}_4\textbf{C]} \qquad (12)$$

where:

- m and n is number of initial species and reaction products, respectively
- m_i and n_i is the corresponding number of moles of initial species and reaction products, respectively
- $(H - H^{298})$ is the enthalpy difference during cooling or heating

To avoid confusion with signs, the following rules were applied:

- Energy consumed is (+), energy released is (-).
- Energy consumed by formation = energy released by decomposition
- Energy released by formation = (-1) · energy consumed by formation

The heat of formation ΔH^f at 298.15 K and the enthalpic difference H - H(298.15) were taken from the following references: B_4C [23] and [24], B_2O_3, HBO_2, H_3BO_3, H_2O, H_2, and O_2 [10], $(HBO_2)_3$ [17], CO, CO_2 and CH_4 [25]. The data are summarized in Table 1. Data were not found only for the trimer of metaboric acid $(HBO_2)_3$. The ΔH^f at 298.15 K was replaced by the available value ΔH^f at 0 K. The difference is expected to be not significant. The missing enthalpy difference was replaced by the enthalpy of HBO_2 multiplied by factor 3. It is to note that possible decrease of this enthalpy will increase the calculated reaction heat for the reaction (7).

For demonstration, the reaction heat at 1500 K is calculated for eq.(3) as example:

$$\mathbf{B_4C + 6H_2O \Rightarrow 2B_2O_3 + CH_4 + 4H_2}$$

Cooling of B_4C from 1500 to 298.15 K : $Q_C^{B4C} = -127.6$ kJ

Cooling of $6H_2O$: $Q_C^{H2O} = -6 \cdot 48.3 = -289.8$ kJ

Decomposition of 1 mole of B_4C : $-n \cdot \Delta H_{B4C}^f = (-1) \cdot (-71.5) = 71.5$ kJ

Decomposition of $6H_2O$: $-n \cdot \Delta H_{H2O}^f = (-6) \cdot (-241.8) = 1450.8$ kJ

Formation of $2B_2O_3$: $m \cdot \Delta H_{B2O3}^f = (2) \cdot (-1273.5) = -2547$ kJ

Formation of CH_4 : $m \cdot \Delta H_{CH4}^f = 1 \cdot (-74.6) = -74.6$ kJ

Formation of $4H_2$: $m \cdot \Delta H_{H2}^f = 4 \cdot 0 = 0$ kJ

Heating of $2B_2O_3$: $Q_H^{B2O3} = 2 \cdot 163.2 = 326.4$ kJ

Heating of CH_4 : $Q_H^{CH4} = 80.2$ kJ

Heating of $4H_2$: $Q_H^{H2} = 4 \cdot 36.3 = 145.2$ kJ

$$Q = -127.6 - 289.8 + 71.5 + 1450.8 - 2547 - 74.6 + 326.4 + 80.2 + 145.2 = \mathbf{-964.9\ kJ / mol\ B_4C} \qquad (13)$$

Table 1 **Heat of formation ΔH^f at 298.15 K and enthalpy difference H-H(298) [kJ/mol] at various temperatures.**

Specie	ΔH^f(298) [kJ/mol]	1400	1500	1600	1700	1800	1900	2000	2100	2200
		Temperature [K]								
B4C	*-71.5*	115	127.6	140.5	153.6	167	180.5	194.4	208.4	222.7
HBO2	*-563.2*	69.2	76.6	84	91.5	99	106.7	114.3	122.1	129.8
(HBO2)3	*-2248.9*	207.6	229.8	252	274.5	297	320.1	342.9	366.3	389.4
H3BO3	*-1004.3*	125.6	139.2	153	167	181	195.3	209.6	224.1	238.6
B2O3	*-1273.5*	150.3	163.2	176	188.8	201.6	214.4	227.2	240	252.8
CO	*-110.5*	35.3	38.8	42.4	45.9	49.5	53.1	56.7	60.4	64
CO2	*-393.5*	55.9	61.7	67.6	73.5	79.5	85.4	91.46	97.5	103.6
CH4	*-74.6*	71.3	80.2	89.5	98.9	108.6	118.4	128.5	138.7	149
O2	*0*	37	40.6	44.3	48	51.7	55.4	59.2	63	66.8
H2	*0*	33.1	36.3	39.5	42.8	46.2	49.5	52.9	56.4	59.9
H2O	*-241.8*	43.6	48.3	53.1	58	62.9	68	73.1	78.3	83.6

The calculated reaction heat for the reactions (1) - (7) are summarized in Table 2. The (-) sign indicates an exothermic reaction. The only endothermic reaction is the formation of HBO_2 from B_2O_3. The results are in good agreement with the data used in MELCOR. It is to note that between 1400-2200 K the reaction heat is almost independent on temperature. In this temperature range a constant value of reaction heat can be used for all studied reactions without any significant error.

3.2 Heat release from B_4C in oxygen (or dry air)

This study indicates that oxidation of 1 mole B_4C in oxygen or in dry air at 1500 K releases about 2771 kJ, i.e. ~50155 kJ/kg B_4C, Table 2. This value is about **7.7** times higher than heat, released during complete oxidation of 1 kg Zr in steam (~6500 kJ/kg Zr). The reaction heat of B_4C in oxygen was not found in literature, so that comparison with existing data could not be made.

The amount of this heat is demonstrated on the following example. The VVER-1000 core with russian fuel contains approximately 272 kg of B_4C powder. Complete oxidation of this

Table 2 Heat in [kJ/mol B_4C] released during various reactions of B4C with steam and air.

	Temperature [K] →	1400	1500	1600	1700	1800	1900	2000	2100	2200
	B4C oxidation in dry air									
(1)	B4C + 4O2 → 2B2O3 + CO2	-2775.5	-2770.9	-2767.1	-2763.5	-2760.1	-2756.9	-2754.3	-2751.9	-2749.7
	B4C oxidation in steam									
(2)	B4C + 8H2O → 2B2O3 + CO2+8H2	-777.1	-770.1	-764.3	-758.7	-752.5	-748.9	-744.74	-740.7	-737.7
(3)	B4C + 7H2O → 2B2O3 + CO+7H2	-746	-739.8	-734.7	-729.9	-724.6	-721.5	-718.1	-714.7	-712.4
(4)	B4C + 6H2O → 2B2O3 + CH4+4H2	-971.6	-964.9	-958.9	-953.2	-947.1	-942.6	-937.8	-933.2	-929.4
	B2O3 oxidation in steam									
(5)	2B2O3 + 2H2O → 4HBO2	666.8	661.2	655.6	650.2	644.8	639.8	634.4	629.6	624.2
(6)	2B2O3 + 6H2O → 4H3BO3	-79	-79	-78	-77	-76	-75	-74	-73	-72
(7)	2/3*(3B2O3+3H2O) → 2/3*2(HBO2)3	-78.9	-84.5	-90.1	-95.5	-100.9	-105.9	-111.3	-116.1	-121.5

Table 3 Total reaction heat [kJ/mol B4C] in steam, as combination of reactions (2) to (7).

2+5	-110.3	-108.9	-108.7	-108.5	-107.7	-109.1	-110.34	-111.1	-113.5
2+6	-856.3	-848.9	-842.3	-835.7	-828.5	-823.9	-818.74	-813.5	-809.9
2+7	-856.0	-854.6	-854.4	-854.2	-853.4	-854.8	-856.1	-856.8	-859.2
3+5	-79.2	-78.6	-79.1	-79.7	-79.8	-81.7	-83.7	-85.1	-88.2
3+6	-825.2	-818.6	-812.7	-806.9	-800.6	-796.5	-792.1	-787.5	-784.6
3+7	-824.9	-824.3	-824.8	-825.4	-825.5	-827.4	-829.4	-830.8	-833.9
4+5	-304.8	-303.7	-303.3	-303	-302.3	-302.8	-303.4	-303.6	-305.2
4+6	-1050.8	-1043.7	-1036.9	-1030.2	-1023.1	-1017.6	-1011.8	-1006	-1001.6
4+7	-1050.5	-1049.4	-1049.0	-1048.7	-1048.0	-1048.5	-1049.1	-1049.3	-1050.9

absorber in dry air would produce $\sim 13.6 \cdot 10^6$ kJ. Assuming an adiabatic process, this heat is sufficient to heat-up ~ 50 % of the core from ~ 1500 K (failure temperature of B_4C control rods) to the melting temperature of Zr-based fuel claddings. The presence of water, fortunately, decreases the reaction heat, as will be shown in the next chapter.

3.3 Heat release from B_4C in steam

The calculation of reaction heat in a water containing environment (steam) is more complicated due to the presence of larger number of reactions and due to the existence of an intermediate compound, the B_2O_3. Three reactions are considered to participate in the formation of B_2O_3 as well as three reactions in its consumption. In reality, the partitioning of the process between the reaction depends on actual boundary conditions, i.e. on partial pressure of steam and hydrogen. A method for determination of the relative extent of each reaction is available in MELCOR for reactions (2)-(4) and in [12] for reactions (5)-(7). In this study, the limiting cases only were examined, i.e. cases, when only one reaction participates in the formation of B_2O_3 and only one reaction in its consumption. In this way, 9 combinations were obtained.

The results for reactions (2) to (4) in Table 2 are in excellent agreement with the data used in MELCOR, shown in Fig. 1. The temperature independent value of -11.1 MJ/kg B_4C (-613 kJ/mol), coded in the SCDAP/RELAP5/MOD3.1 source, seems to be also acceptable, especially when the formation of boric acids is taken into account as will be discussed below.

For the total reaction heat (including boric acids), the maximum value of $\sim$(-1050) kJ/mol B_4C was found for the combination of reactions (4) and (7), Table 3. This is by factor ~ 2.5 smaller than for the reaction in air but still ~ 3 times larger than for the reaction Zr-H_2O. The high endotermicity of the formation of HBO_2 causes a wide spread of total values, nevertheless being still exothermic. According to [12], the HBO_2 is the dominant species at very low steam pressures. This means that under rich-steam conditions, mainly the exothermic reactions will take place.

3.4 Hydrogen release

A comment to the hydrogen release seems to be suitable at this point. The amount of hydrogen, released during formation of B_2O_3, can be directly calculated from eqs. (2) to (4). One mole of B_4C produces 4 to 8 moles of H_2, i.e. 0.145-0.290 kg H_2 per 1 kg B_4C. The standard VVER-1000 core thus can produce $\sim$(40-80) kg of hydrogen from the B_4C-steam reaction. This is a relatively negligible mass, compared with ~ 980 kg H_2 that can be produced in the same core from the Zr-H_2O reaction. In reality, the B_4C will produce much less hydrogen than the above calculated, because not all B_4C will be in contact in steam, as was discussed in chapter 2.3.

4. Conclusions

The present study reviewed the B_4C oxidation in steam and dry air. A simple heat balance analysis of the reaction heat of B_4C with steam and air was performed. The main results are the following:

- Experimental data are available mainly below 1000°C. The extrapolation of these data to SFD conditions is very difficult, especially for the reaction kinetics. The use of inadequate data can easily produce misleading results.
- This study confirmed that the B_4C oxidation in steam and dry air is an exothermic reaction, releasing more heat in air. In steam, the B_4C oxidation can be an important heat source only locally, accelerating the damage of control elements.
- The B_4C oxidation in steam is a relatively negligible source of hydrogen, producing in a PWR core one order less hydrogen than the Zr-steam reaction.
- The development of a new B_4C oxidation model is related to availability of data on reaction kinetics in SFD conditions.

REFERENCES

[1] Davis, K.L. (Editor), "SCDAP/RELAP5/MOD3.1 Code Manual. Volume II: Damage Progression Model Theory", NUREG/CR-6150 (1993).

[2] Cole Jr.R., et al., "MELCOR Computer Code Manuals, Version 1.8.3", NUREG/CR-6119 (1995).

[3] Gogotsi, G.A., Groushevsky, Ya.L., Dashevskaya, O.B., Gogotsi, Yu.G., Lavrenko, V.A., "Complex investigation of hot-pressed boron carbide", Journal of the Less Common Metals, No. 117 (1986) 225-230.

[4] Ridgway, R.R., "Boron carbide, a new crystalline abrasive and wear-resisting product", Transactions of the Electrochemical Society, Vol. 65 (1934) 117-134.

[5] Reinmuth, K., Lipp, A., Knoch, H., Schwetz, K.A., "Borhaltige keramische Neutronenabsorberwerkstoffe", Journal of Nuclear Materials 124 (1984) 175-184.

[6] Thevenot, F., "A review on boron carbide", Key Engineering Materials, Volumes 56-57 (1991) 59-88.

[7] Nazarchuk, T.N., Mekhanoshina, L.N., "On the oxidation of boron carbide" (in russian), Poroshkovaya Metallurgija No. 2 (1964) 46-50.

[8] Litz, L.M., Mercuri, R.A., "Oxidation of Boron Carbide by Air, Water and Air-Water Mixtures at Elevated Temperatures", Journal of the Electrochemical Society, Vol.110, No. 8 (1963) 921-925.

[9] Krutsky, Yu.L., Galevsky, G.V., Kornilov, A.A., "Oxidation of ultradispersion powders of boron, vanadium and chromium carbides" (in russian), Poroshkovaya Metallurgija No. 2 (1983) 47-50.

[10] Cordfunke, E.H.P., Konings, R.J.M. (Editors), "Thermochemical Data for Reactor Materials and Fission Products", North-Holland, Elsevier Science Publishers (1990).

[11] Fujii, K., Nomura, S., Imai, H., Shindo, M., "Oxidation behaviour of boronated graphite in helium, containing water vapor", Journal of Nuclear Materials 187 (1992) 32-38.

[12] Elrick, R.M., Sallach, R.A., Ouellette, A.L., Douglas, S.C., "Boron Carbide - Steam Reactions with Cesium Hydroxide and with Cesium Iodine at 1270 K in an Inconel 600 System", NUREG/CR-4963 (1987).

[13] Lavrenko, V.A., Pomytkin, A.P., Kislyj, P.S., Grabchuk, B.L., "Kinetics of High-Temperature Oxidation od Boron Carbide in Oxygen", Oxidation of Metals, Vol. 10, No. 2 (1976). 85-95.

[14] Yefimenko, L.N., Lifschitz. E.V., Ostapenko, I.T., Snezhko, I.A., Shevyakova, E.P., "Oxidation of hot-pressed boron carbide" (in russian), Poroshkovaya Metallurgija No. 4 (1987) 56-60.

[15] Meyerson, G.A., Kiparisov, S.S., Gurevich, M.A., Den Fen-Sian, "Investigation of conditions for obtaining solid alloys of the pseudobinary system B_4C-B4Si and some of their properties" (in russian), Poroshkovaya Metallurgija No. 3 (1965) 62-68.

[16] Lavrenko, V.A., Gogotsi, Yu.G., Frantsevich, I.N., "High-temperature oxidation of hot-pressed boron carbide" (in russian), Doklady Akad. Nauk USSR, No. 275 (1984) 114-117.

[17] Randall, S.P., Margrave, J.L., "Vapour equilibria in the B_2O_3-H_2O system at elevated temperatures", Joumal of Inorganic and Nuclear Chemistry, Vol. 16 (1960) 29-35.

[18] Woodley, R.E., "The reaction of boronated graphite with water vapor". Carbon, Vol. 7 (1969) 609-613.

[19] Eriksson, G., "Thermodynamic Studies of High-Temperature Equilibriums, SOLGASMIX, a Computer Program for Calculation of Equilibrium Compositions in Multiphase Systems", Chemica Scripta, Vol. 8, No. 3 (1975) 100-103.

[20] Hagen, S., Hofmann, P., "Physical and Chemical Behaviour of LWR Fuel Elements up to very High Temperatures", KfK 4104 (1987).

[21] Gauntt, R.O., Gasser, R.D., Ott, L.J., "The DF-4 Duel Damage Experiment in ACRR with a BWR Control Blade and Channel Box", NUREG/CR-4671 (1989).

[22] Hofmann, P., Schanz, G., Hagen, S., Noack, V., Sepold, L., Schumacher, G., "CORA-Ergebnisse zum LWR-Brennelementverhalten bei schweren Reaktorstorfallen", KfK-Nachrichten Vol. 26, No. 3 (1994) 156-169.

[23] Barin, I., Knacke, O., "Thermochemical properties of inorganic substances", Springer Verlag 1973.

[24] Weast, R.C. (Editor-in-chief), "CRC Handbook of Chemistry and Physics", CRC Press, Inc., Boca Raton, Florida (1988).

[25] Glushko, V.P. (Editor), "Thermodynamical properties of individual compounds" (in russian), Vol. 2, Book 2, Izdatelstvo Nauka, Moscow (1979).

METHODICAL APPROACH TO STUDY PROPERTIES OF CORIUM PRODUCED FROM SPENT FUEL UP TO 2200°C

V.G. DVORETSKY, Y.Y. KOSVINTSEV, V.P. SMIRNOV
State Scientific Centre, Research Institute of Atomic Reactors,
Dimitrovgrad, Russian Federation

Abstract

Experimental investigation of severe accidents final stages with loss of coolant and melting of core fuel and structural materials with formation and motion of melt to reactor vessel has essential limitation on simulating opportunity in operating reactor facilities.

Model small-scale experiments on melt of core irradiated componentswith vessel material interaction on electric heated rigs in hot cells are most secure but rather informative.

This paper is concerned with technical capabilities and some results of CORIUM type experiments on electric heated rigs in RIAR hot cells as a stage of technical preparation to experiments of this type with WWER irradiated fuel.

INTRODUCTION

Experimental simulation of severe accidents with spent fuel on electric rigs in hot cells has been extended rather widely within recent years due to good instrumentation of rigs, high information content and acceptable adequacy to full-scale accidents parameters. In spite of numerous fullfilled and active programs of experimental investigations [1] of accidents stages with core melting deficit of information about physicochemical processes occurring in this case still exists. Parameters of these processes must be included into design codes of scenario. Late stages of core destruction characterized by formation of melt volumes, their motion and interaction with vessel in reactor lower part are investigated least of all on core spent elements. Because of problem difficulty but practically because of impossibility of simulation of full-scale late stages on reactor facilities maximum statistics of investigations is based upon experiments on "fresh" fuel. In this case presence of fission products and actinides which are capable to change properties of core elements melt (corium), action of sources term in melt determining corium energetics, interaction of fission products with each other and with other elements cannot be taken into consideration directly. All these peculiarities of irradiated fuel can cause manner of accident process different from that in models.

Electric heated rigs in hot cells can compensate deficit of experimental information about late stages of severe accidents of irradiated fuel by solution of the following problems:

· receiving "small-scale" corium by fusion of FEs irradiated fragments from standard FAs, structural and absorbing materials (stainless steel, Zr materials, boron carbide, etc.);

· determination of gaseous (GFP) and highly volatile (HVFP) fission products release in different stages of developing accident;

. investigation of corium energetics (motion of source term);

· receiving data about macro- and microstructure, phase composition and distribubon of solidified corium elements along volume;

- investigation of molten corium with vessel steel interaction (in particular - estimate of influence of chemically active FP on interaction intensity and melting rate).

1. CHOICE OF SCALE AND CONCEPTION OF MODEL EXPERIMENTS

All model accident experiments with spent fuel are connected with considerable fission products release. That is why even at technically solved problems of electric heating up and melting of fuel considerable mass on rigs radiactive security of experiments is great limiting factor.

According to preliminary estimates mass of irradiated fuel of about 500-1000 g participating in model accident experiment can be taken into consideration as radiactive secure for rig in hot cell and at the same time rather representative from the point of view of the process under investigation. Status of similar experiments can be determined as supporting experiments for integral experiments with unirradiated fuel for determination of possible differences in processes connected with presence of chemically active fission products in melt affecting vessel material.

Phenomenologically process of severe accident development has several stages inside the device under full-scale conditions. They are:

- dryout and heat up of core;
- FEs destruction and melting;
- formation and motion of core melt (corium);
- interaction of melt with constructions and reactor vessel.

Marked stages of severe accidents are characterized by peculiarities in fuel behavior, course of thermal and physicochemical processes and can be the base for breaking them down to stages simulated experimentally for investigation of some effects and phenomena (severe accident stages) on facilities of different scale as it is illustrated in fig.1.

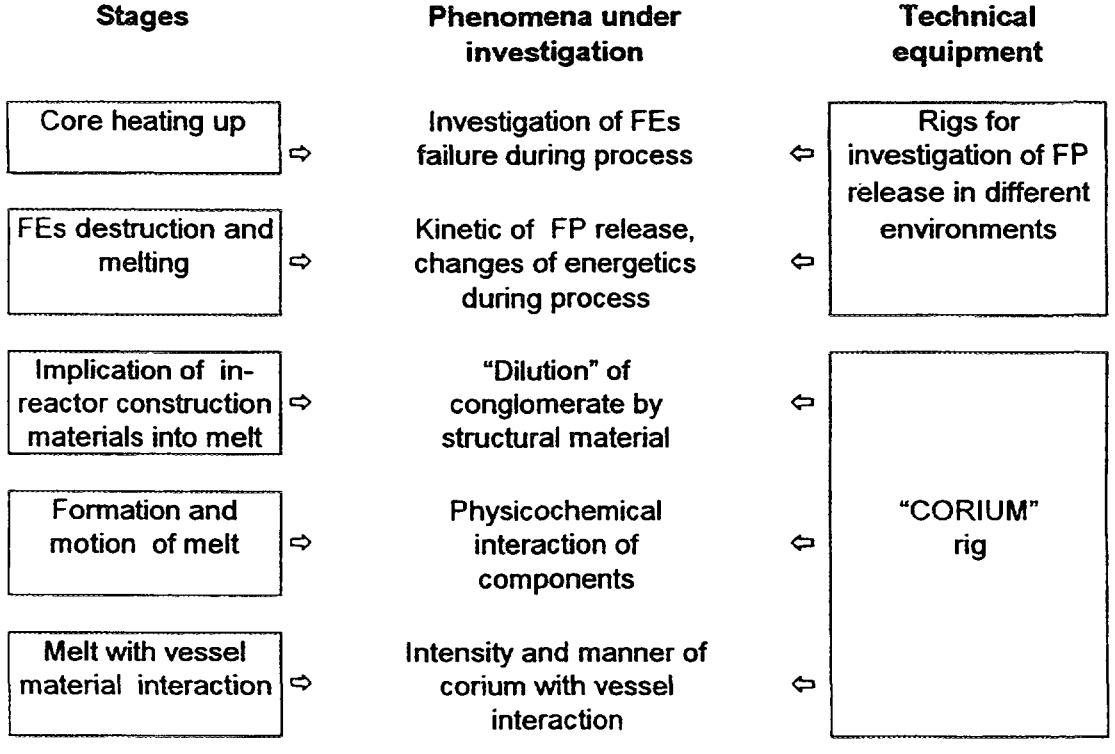

Fig.1. Stage-by-stage conception of CORIUM experiments onrigs in hot cells.

2. TECHNICAL EQUIPMENT OF CORIUM TYPE EXPERIMENTS ON SPENT FUEL

2.1. Electric heated rig in hot cells

Manufacturing technical devices for hot cell simulation of severe accidents with spent fuel is determined by scenario of accident stages under investigation, i.e. by necessary rates and values of heating temperatures, environment during heating, material composition and amount being investigated.

Experience of hot cell electric heated rigs development showed that rig surely includes the following systems:

- heating modulus;
- system of gas- preparation with lines of gas and aerosols transport;
- system of controlled power supply;
- system of FP release recording;
- system of aerosols filtration and utilization.

Because of difference of problems solved when using rig block structure consisting of remote - interchangeable modulus of heaters optimized for usable environment, samples geometry and volume was accepted.

2.2. Structure of high - temperature hot cell rig

Rig consists of the following components:

1. High - temperature heating device - electric furnace (heating modulus).
2. System of carrier gases supply and preparation of overheated water vapor into operating volume of heating modulus.
3. Recording system of released fission products (gaseous and volatile) from corium components.
4. System of anti-aerosol filters on rig output line.
5. Control panel with process instrumentation and rig power supply.

Fig.2 illustrates rig basic scheme. The main functional systems of rig are in hot cell. Control panel of rig is established in operator room.

2.3. Structure of heating modulus

Structure of heating modulus (fig.3,4) must provide the following:

- heating up of corium components weighing about 0,5 kg up to
  - 1900^0 C and heat time of 60 min.
  - 2200^0 C and heat time of 15 min.

  with heating rate (0.1 - 0.3)^0 C/s in the environment of inert gas, inert gas and water vapor, only water vapor;
- capability to operate in high radiative fields from sources with radioactivity up to 10^{14} Bq;
- full tightness of operating volume during corium melting;
- remote maintenance - loading and unloading of corium components and ingot, change of several joints and dismantling of the whole heating modulus.

Technical characteristics of heating modulus are given in tab.1.

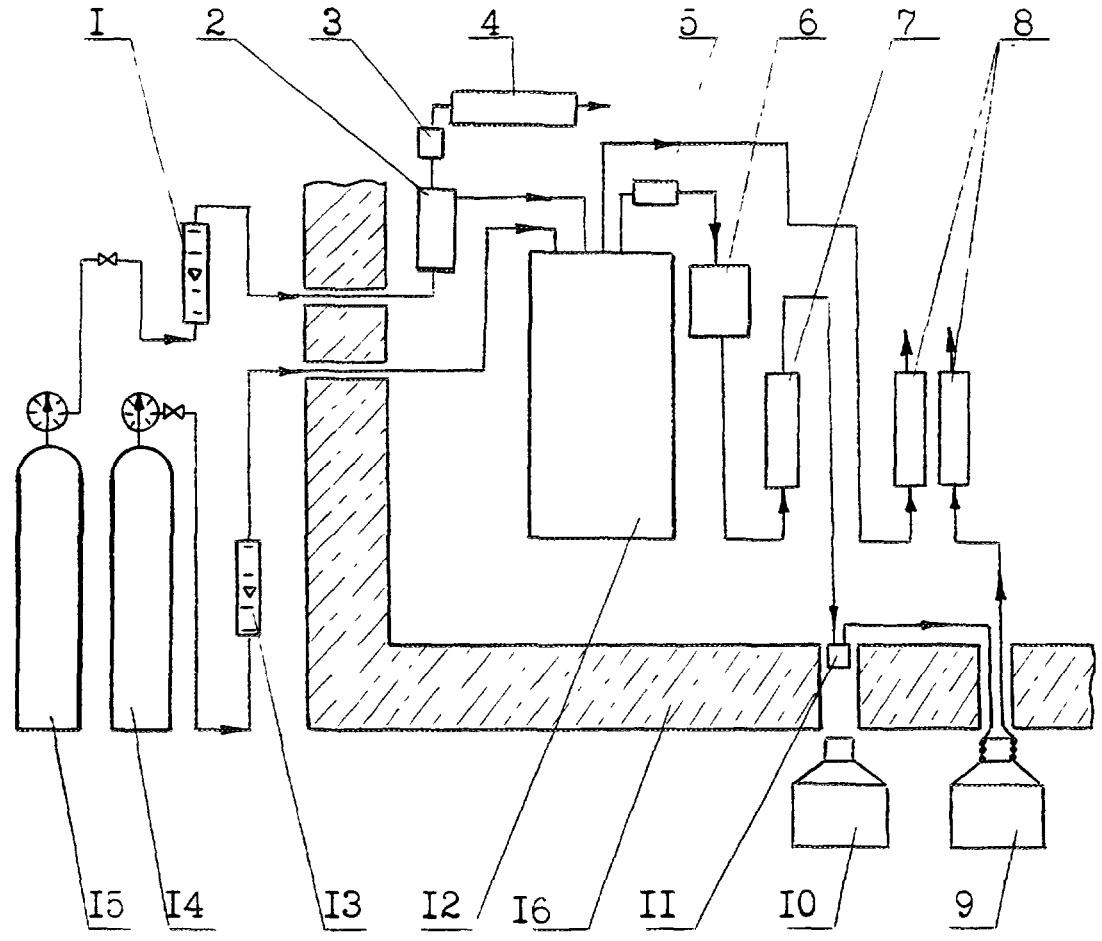

Fig 2. Basic scheme of hot rig cell:
1 - flowmeter; 2 - steam generator; 3 - safety valve; 4 - filter; 5 - measuring filter; 6 - separator; 7 - intermediate filter; 8 - anti - aerosol protection; 9 - detector of photon radiation; 10- detector of photon radiation from collimator; 11- measuring device for ^{85}Kr recording; 12- heating modulus; 13- rotameter; 14- vessel with argon; 15- vessel with carrier gas.

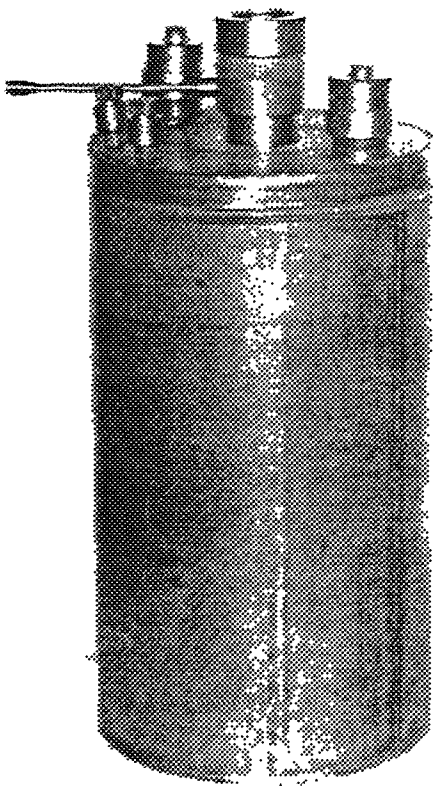

Fig 3. Appearance of CORIUM heating modulus

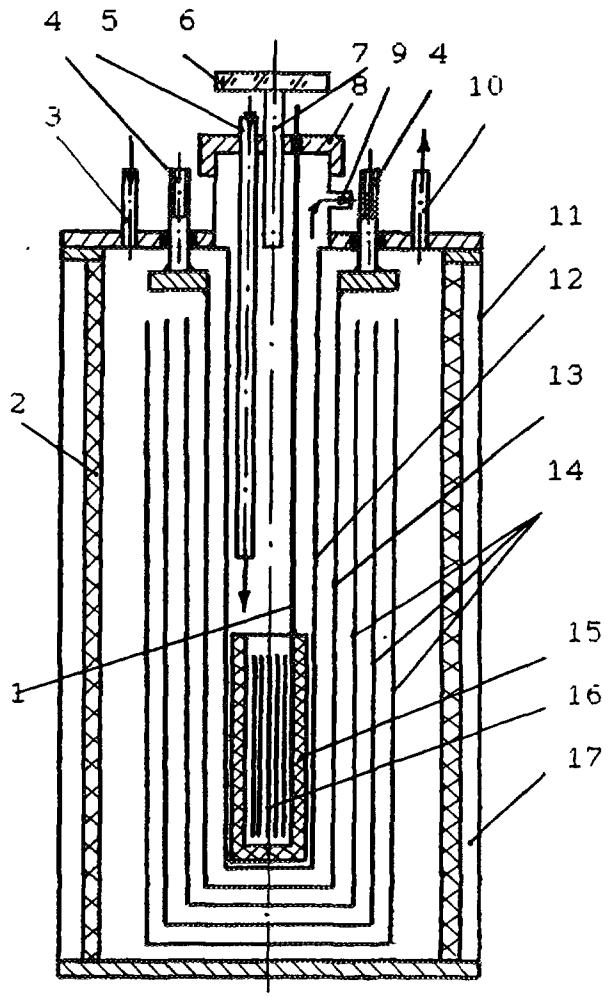

Fig 4. Structural scheme of CORIUM heating modulus

1 - thermocouple; 2 - heat insulator; 3 - input duct of argon supply; 4 - current leads; 5 - tube of carrier gas suuply; 6 - inspection hole; 7 - inspection tube; 8 - flange; 9 - release of carrier gas; 10- release of argon; 11- vessel; 12- protective jacket; 13- heater; 14- screen; 15- crucible; 16- sample; 17- jacket of water cooling.

Table 1

The main parameters of heating modulus

1. Maximum heating temperature	2200 ^{0}C
2. Rate of sample heating	(0.1 - 0.3) ^{0}C/s
3. Maximum power	14 kW
4. Maximum voltage of power source	20 V
5. Temperature inuniformity along sample length	±1.5%
6. Crucible length	20 cm
7. Crucible inner diameter	4 cm
8. Heating modulus height	48 cm
9. Heating modulus diameter	26 cm
10. Heating modulus weight	46 kg
11. Volumetric flow rate of carrier gases	(1 - 5)10^{-2} m^3 /h
12. Mass flow rate of water vapor	(5 - 20)10^{-2} kg/h

There were developed and tested several modifications of heating modulus.

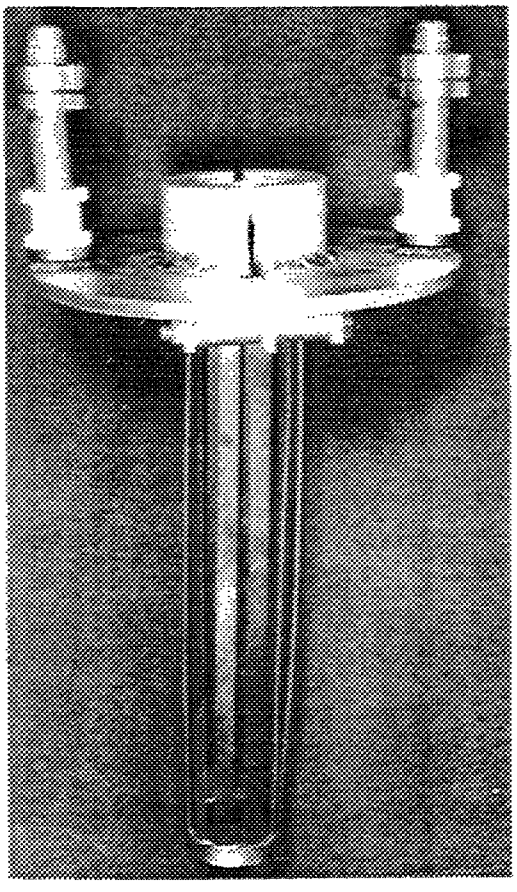

Fig.5. Heating item.
1 - current leads; 2 - electric insulator; 3 - heater.

Structure of resistance heater shown in fig.5 is of "squirrel cage" form cut into two halfs and fastened in lower part. Heater material is molybdenum of 0,5 mm width. Heater diameter is 52 mm, its length is 360 mm. Such heater construction allows to receive rather homogeneous temperature field in operating area extending over about 200 mm at rather small power.

To protect heater material from oxidation there is used inert gas - argon delivered to heater by input duct 3 (fig.2) and output duct 10.

Supply of electric power to heater 13 is performed by current lead 4 and in this case there are used ceramic rings with fluoroplastic bushings as electric insulators from vessel 11.

To decrease heat loss due to radiation eight cylindrical screens 14 were enclosed in device. Three inner screens are made of molybdenum of 0,5 width and others are made of 12X18HIOT stainless steel of 1 mm width.

Layer of slag cotton of 30 mm width is heat insulator.

Heating modulus is cooled by running water under o,25 MPa pressure in water jacket 17.

Heater 13 is separated from operating area with corium sample 16 by protective jacket made of zirconium dioxide, graphite or zirconium alloy depending on experiment conditions (with water vapor or without it).

Corium components are loaded into tungsten or graphite crucible 15.

2.4. System of steam and gas environment preparation

System is designed for formation of environment with assigned physico-chemical characteristics and consists of gas cylinders 15 and 14 (fig.2), flowmeters 1 and 13, steam generator with steam superheater 2, emergency valve designed for excessive 0,3 MPa pressure and filter 4 fixed at outlet of emergency valve for fission products absorption.

Steam generator volume is $0.5 \cdot 10^{-3}$ m^3 , gas flow rate is regulated by changing of power input in the range of $(5\text{-}20) \cdot 10^{-2}$ kg/h. Level of distilled water in steam generator is remote - controlled.

Steam enters steam superheater where it is heated up to 900 ^{0}C and then it is delivered to heating modulus.

Temperature in steam generator and steam superheater is controlled by alumel - chromel thermocouples.

2.5. System of fission products recording

This system removes solid fission products movable (^{106}Ru, ^{144}Ce) and highly movable compounds of radioactive ^{137}Cs, ^{134}Cs from ^{85}Kr radioactive gas for the following recording of ^{85}Kr.

System consists of the following items:

- measuring filter 5;
- steam separator 6;
- intermediate filter 7;
- measuring device for krypton recording 11;
- gamma radiation detector 10,9;

Measuring filter 5 is for localization of fission products released from heating modulus in solid phase. Filter structure consists of cylinder 10 mm in diameter and 80 mm in length. filled by aluminium oxide granules. Effectiveness of catching solid fission products is no less than 99.9%

Separator 6 is for localization of fission products which interacted with water vapor and are dissolved in water after steam condensation.

Intermediate filter 7 consists of cylinder 54 mm in diameter and 60 cm in length filled by silica gel mixtured with activated carbon. This filter removes radioactive impurified nuclides from krypton-85.

After passing intermediate filter krypton-85 with carrier gas enter measuring device 11 with inner volume of 50 cm^3. Gamma radiation with photons energy of about 512 keV released by krypton-85 is recorded by semiconductive germanium - lithium detector.

After measuring device gases mixture enters the next measuring device which is in operator room. Device has form of spiral from tube with 5 mm inner diameter rolled on germanium - lithium semiconductive detector external vessel and is for recording krypton-85 small samples. When measuring ^{85}Kr great activities device 9 is excluded from rig scheme.

2.6. System of antiaerosol filters

System of filters 8 is for catching radioactive aerosols which passed through intermediate filter 7 before release into hot cell. All the elements of filters system can be remote - assembled, dismantled, disactivated in special system and substituted if necessary.

Filters system consists of 4 sealed vessels 14 cm in diameter and 30 cm in height connected consequently. Vessel 1 (along gases motion) is filled by alkali (solution of caustic sodium), vessel 2 - by distilled water, vessel 3 - by silica gel, vessel 4 - by activated carbon.

3. DEVELOPMENT OF CORIUM PRODUCTION TECHNOLOGY

To work off corium receiving from irradiated materials on manufactured rig there were carried out technological experiments on relatively easily fusible components of dispertion type experimental FEs (uranium intermetallic compound in maxtrix made of aluminum alloys) in cladding from stainless steel.

Preliminary oxidation of corium samples (simulation of FEs oxidation at heating up by water vapor) is carried out on heating modulus with tubular ceremic canal (ZrO_2).

Later stages of accidents (fig.1) were simulated on CORIUM heating modulus.

Oxidation was performed in atmosphere of water vapor with carrier gas (nitrogen) with gradual temperature rise up to 1100 ^0C, with heat time of about 5 min and the following cooling with furnace.

Kinetic of FP release during experiment was recorded by gamma - spectrometric systems. Release of gaseous FP (^{85}Kr) and volatile (^{134}Cs, ^{137}Cs) in oxidation stage was ~25 % accumulated. If necessary oxidation degree was determined by quantitative metallography of samples.

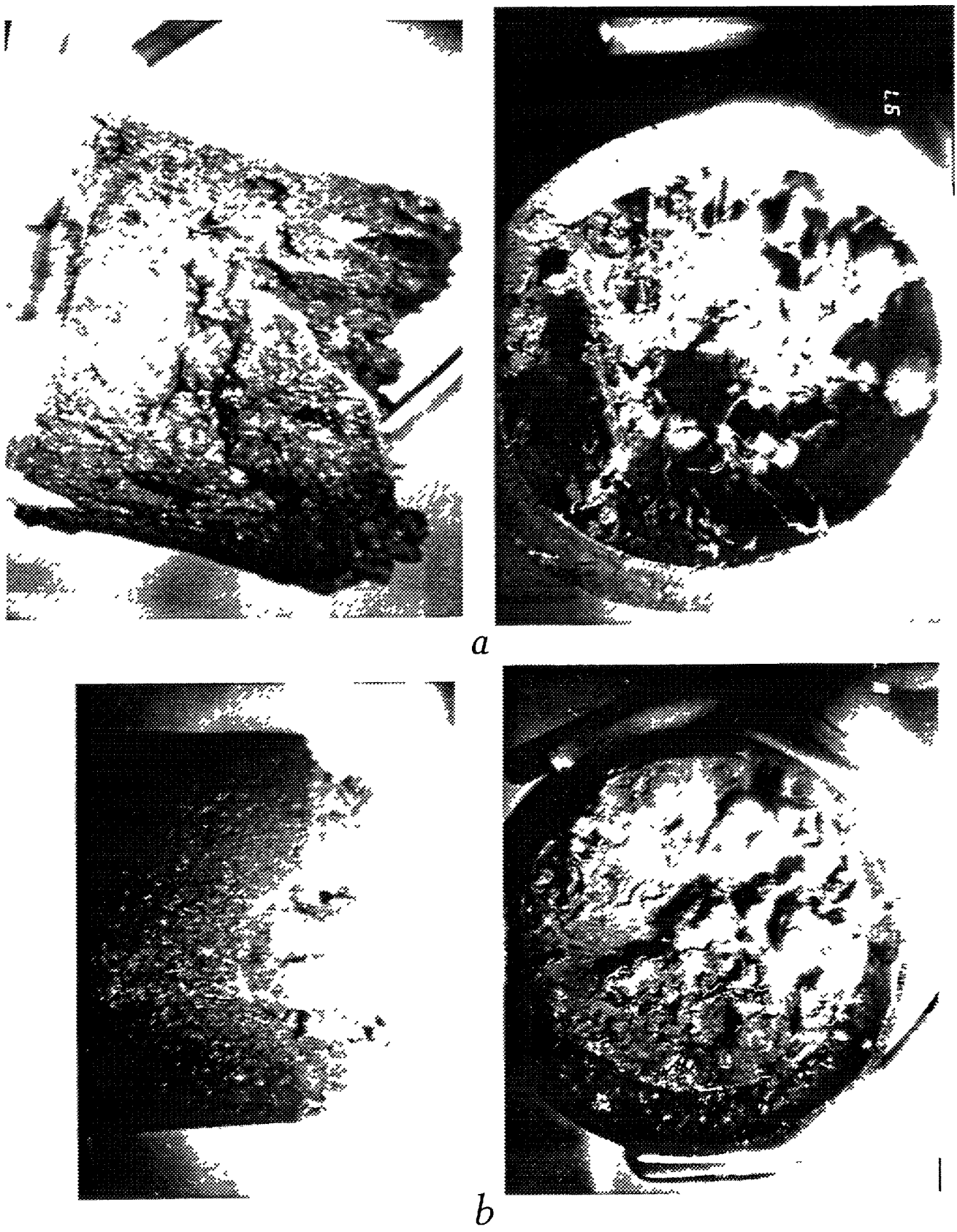

Fig.6. Corium conglomerate appearance.
a) after fusion (in the range of 1450 - 1510^0 C in argon environment);
b) after interaction with vessel steel (temperature is 1350^{0}C, time is 15min in nitrogen environment).

Fusion of oxidized samples was performed in heating modulus "Corium" in inert gas environment at linear growth of temperature up to maximum value of 1510 ^{0}C. Experiments showed presence of oxide film, absence of regular metallurgical contact of components to complicate process of eutectics formation and accordingly homogeneous corium melt.

Interaction of corium melt with reactor vessel material was simulated by arrangement of solidified cylindrical ingot of melt in crucible from vessel steel and remelting on CORIUM rig in inert gas environment at 1350 ^{0}C. This temperature is lower than temperature of vessel material melting.

Corium ingot received at working off of technology after stage of fusion of oxidized samples and after interaction with crucible manufactured from vessel steel material is illustrated in fig. 6a and 6b.

4. METHODICAL PROVISION OF CORIUM TYPE EXPERIMENTS

4.1. Composition of experiments methodical assurance

According to scheme of severe accidents stage - by - stage simulation system of electric heated rig with interchangeable heaters allows us to carry out the following:

- preliminary oxidation of samples of necessary parameters (fuel and structural) in steam and gas mixture;
- fusion of samples into compact conglomerate in inert environment;
- experiment on interaction of molten corium ingot with vessel material (crucible from vessel material).

In all consequant stages of experiment there was measured kinetic of FP release by gamma-spectrometric systems. Intermediate products, initial corium samples - oxidized samples - fusioned conglomerate can be investigated by active procedures directly and / or with samples selection.

Tab.2 presents summary data about methodical equipment of CORIUM type experiments during simulation and the following investigations.

4.2. Determination of corium components energy release

This paper represents experimental estimate of heat generation decrease in corium core caused by fission products release (entrainment) from materials bulk.

Problem of departure (entrainment) of energy release sources during developing severe accident (fig.1) in principle is open to experimental checking in small - scale experiments on hot - cell rigs. To demonstrate it experimentally there were measured heat releases of corium samples prior to and after oxidation stage by differential adiabatic calorimeter.

Table 2

Purpose and composition of methodical provision of CORIUM experiments

№	Processes, phenomena, properties under investigation	Used equipment, procedure	Procedure state
1	Kinetic of fission products release during oxidation and corium components melting	Recording gamma - spectrometric systems of rig	Used procedure
2	Hydrogen release during oxidation	Mass-spectrometer in on-line regime with rig	Used procedure
3	Investigation of changes of corium components energy release after different stages of accident on solid conglomerates	• Absolute gamma - spectrometric measurements • Calorimetry	Used procedure Used procedure
4	Structure - phase state of corium solidified conglomerate	• X-ray analysis • Quantitative metallography • Probe analytic methods	Used procedure Used procedure Experimental procedures
5	Redistribution of density and element composition along ingot volume	Gamma - tomography of corium ingot	Experimental procedure
6	Intensity and manner of interaction with corium material	Probe analytic methods	Experimental procedures

4.2.1. Calorimeter structure

Differential calorimeter designed to determine radiative energy release of corium components consists of two identical calorimeters. It is caused by its operating conditions in hot cell.

Basic part of each calorimeter (fig. 7) is lead absorber 1 of radiation in cylinder form. Its inner diameter is 50 mm; height is 105 mm, walls width is 55 mm. At the bottom it is closed by lead cover 60 mm wide and below it has bottom made of lead 61 mm wide. Such width of absorber walls provides (according to design data) complete absorption of alpha - and beta - radiation energy and absorption of 99,5% energy for corium gamma - radiation.

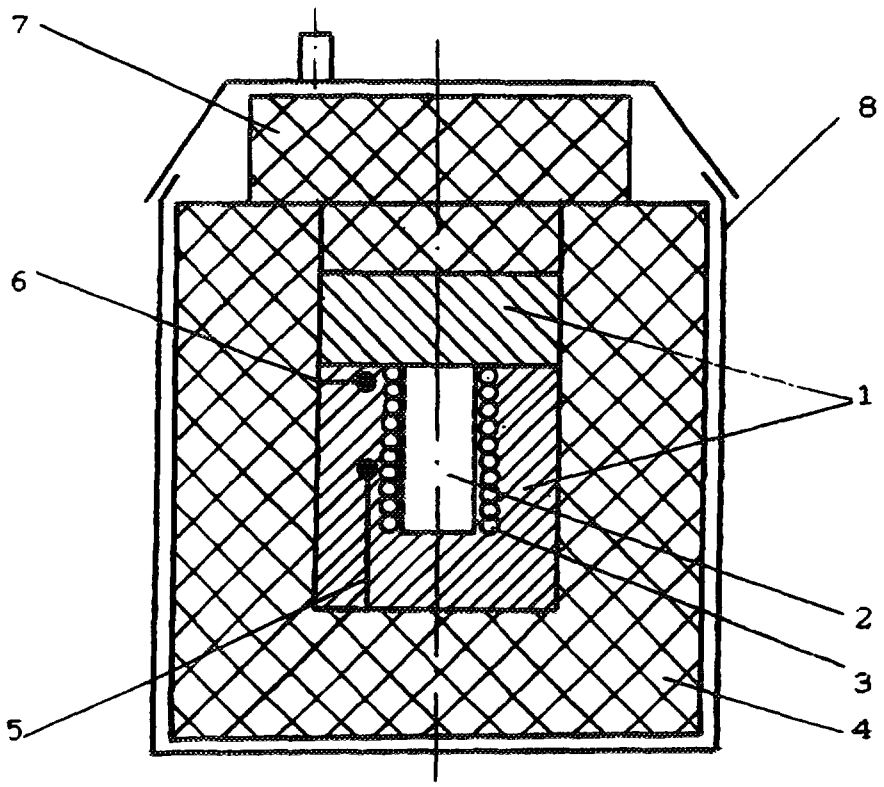

Fig.7. Calorimeter basic scheme.
1 - absorbing volume from lead; 2 - vessel; 3 - heater; 4 - heat insulator from foam plastic; 5 - thermistor; 6 - thermocouple; 7 - calorimeter cover from foam plastic; 8 - calorimeter vessel.

Absorber 1 is surrounded by layer of foam plastic (70 - 90) mm wide which serves as heat insulator 4. It is enclosed in cylindrical jacket 340 mm in height and 342 mm in diameter made from stainless steel 2 mm in width. Total weight of calorimeter is 42 kg.

Samples under investigation 2 constitute FEs fragments bundles of each corium located vertically in stainless glass vessel with inner diameter of 43 mm, height - 100 mm and walls width - 2 mm. It was enclosed into inner volume of operating absorber 1.

Temperature increase of operating absorber was recorded by thermocouple chromel - alumel 6, thermistor 5 with rated value of 680 Ω at 20 ^{0}C with temperature coefficient of about 0.03 deg^{-1}. Thermocouple readings were recorded by digital voltmeter.

Calorimeter N2 provided by thermocouple and thermistor was supporting and kept track of environment temperature in hot cell.

Thermistor of operating and supporting calorimeters were included into the scheme of direct current bridge.

Operating calorimeter was calibrated according to its power using heating element 3 fixed inside absorber 1 and made from nichrome wire with resistance of 30 Ω.

4.2.2. Procedure of energy release measurement

Using differential calorimeter there was determined power of corium samples radiative energy release prior to and after FEs fragments oxidation in water vapor environment. For it there were carried out four measurements. At each measurement there were determined decrease of operating thermistor resistance and increase of operating thermocouple E.M.F. depending on time when samples under investigation was in calorimeter. This time was 150 min.

Then there were compared rate of thermistor resistance changing (Ω/min) at heating up from samples under investigation with rate of resistance change of the same thermistor at heating up from heating element with definite power (0,6W). Using this comparison there was determined power of radiative energy release.

Such measurement procedure is caused by the fact that temperature of samples under investigation prior to their enclosing in calorimeter was 5 - 10 ^{0}C higher than calorimeter temperature in initial state. This case was determined experimentally in independent measurement and it is explained by samples self - heating from their own radioactive radiation.

According to calorimeter findings experimental value of radioactive energy release power of corium samples was the following:

- prior to oxidation $P_1 = (1.49 \pm 0.03)$ W,
- after oxidation $P_2 = (1.20 \pm 0.03)$ W.

Table 3

Contribution of energy release of several radionuclides (in %) to total energy release of corium components

№	Nuclide	Energy per act of decay, MeV	Corium-1 (prior to oxidation)		Corium-1	
			Activity $\cdot 10^{10}$ Bq (according to γ-spectr. measure-ments)	energy release W (calculation according to decay scheme)	prior to oxid.,%	after oxid., %
1	Ruthenium-106+ Rhodium-106	1.62	44	0.081	5.5	6.8
2	Cesium-134	1.71	128	0.251	16.8	14.8
3	Cesium-137+ Barium-137m	0.84	317	0.303	20.3	19.4
4	Cerium-144+ Praseodymium-144	1.32	245	0.376	25.2	31.3
5	Europium-154	1.50	6	0.011	0.7	0.9
6	Cobalt-60	2.60	10	0.030	2.0	2.5
7	Beta- and alpha-nuclides	-	-	-	29.5	24.3

There are given absolute errors of measurements with 95% of confidence probability received by method of minimum squares of experimental data processing.

There was a chance to determine fractional energy release of some radionuclides - gamma-emitter according to schemes of decay at measured absolute values of their activity. Design-experimental data for several gamma-radiating radionuclides in corium samples prior to their oxidation are given in tab.3. Based on balance of energy release measured by calorimeter (for all emitters including alpha-beta- and gamma-) and fractional energy release according to gamma-spectrometric data there were estimated contributions: fractional for gamma-radiating and summary for α , β - omitters. Data are given in tab.3.

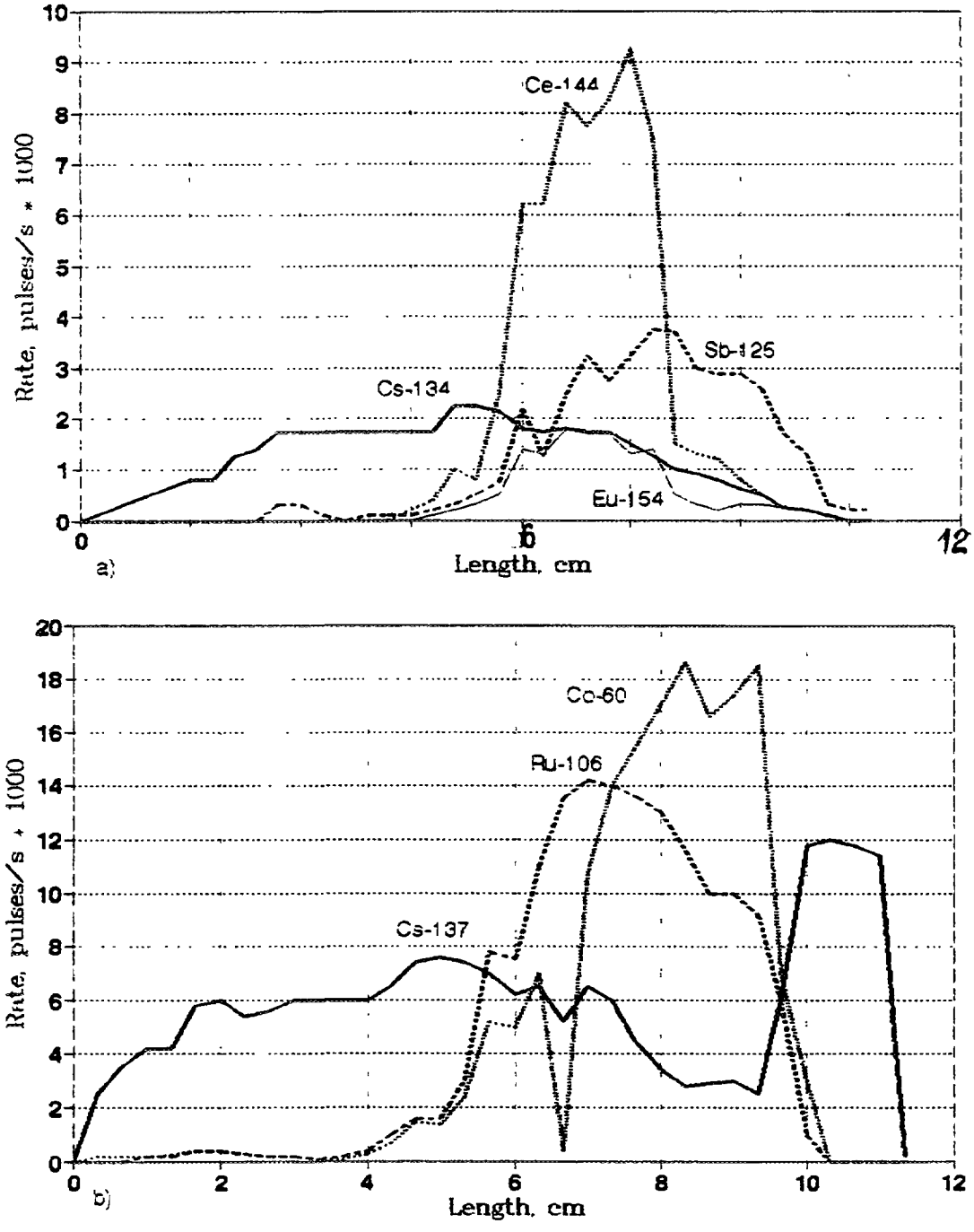

Fig. 8. FP distribution along height of corium conglomerate after fusion.

If investigation of energy release at the expense of short - term radionuclides is necessary the possibility exists of preliminary pre-irradiation of corium samples in MIR reactor.

For given values relative error with confidence probability is ±7%.

4.3. Investigation of element composition redistribution in solidified corium

It was determined by ingot axial gamma-scanning with graphite crucible that after procedure of corium conglomerate fusion (fig. 8a,b):

- essential axial motion of fission products and products of cladding occurred;
- fission products ^{137}Cs and ^{134}Cs in crucible volume had maximum spatial motion which are likely to be connected with absorption by graphite crucible (increased content along the whole depth of crucible bottom and side walls outside of ingot bulk);
- gravity centers of altitude distribution of ^{60}Co, ^{125}Sb, ^{144}Ce, ^{154}Eu and ^{106}Ru radionuclides do not coincide.

Altitude distribution of all irradiated radionuclides after procedure of remelting in crucible from vessel steel and following interaction with it changed practically insignificantly.

Complex analysis of gamma - spectrometric information testify to presence of mass transfer in melting corium with peculiarities caused by dissimilar thermo-chemical properties of different chemical elements. To investigate structural-phase composition of ingots different sections and on the interface of corium - vessel material there was planned preparation of sections by cutting out from ingot bulk according to scheme (fig. 9).

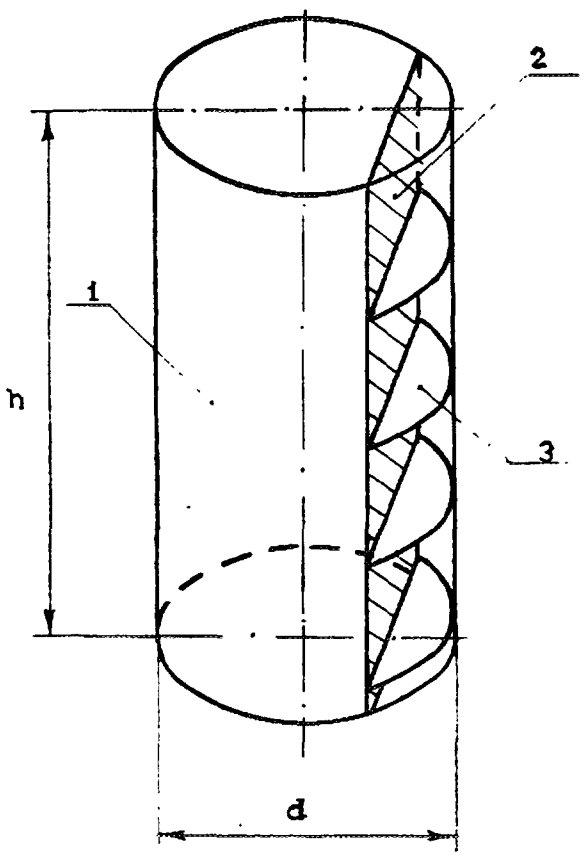

Fig.9. Scheme of ingot subdivision into samples under investigation.
1 - ingot; 2 - cut surface; 3 - samples.

Sections must be subjected to technological preparation (polishing, burnishing, etching) to use methods of quantitative metallography and / or probe analytic methodics (micro X-ray analysis, SIMS, etc.).

Conclusion

Simulation of final stages of severe accidents with melting of core spent elements on hot cell electric heated rigs is rather fruitful and informative basis for experimental support of design codes of scenario.

Fulfilled demonstration experiment on melting of irradiated dispersive fuel and its interaction with reactor vessel material (of bottom) allows to determine several regularities of proceeding phenomena:

- irregularity of components distribution in melting volume;
- regularities and quantitative characteristics of entrainment of energy release sources from melt;
- manner and intensity of corium melt with vessel material interaction.

Composition of applied methodics in CORIUM experiments allows to receive a number of quantitative parameters required for design codes of scenario of severe accidents.

Devised electric heated rig according to technical parameters allows to start investigation of final stages of severe accidents with spent fuel of WWER reactors.

REFERENCE

1. Popov S.G. Analysis of physicochemical processes occurring during accidents in LWR reactors core. Atomic technology abroad. N2, 1995, pag.7-16.

INVESTIGATION OF FISSION PRODUCTS RELEASE AND STRUCTURAL CHANGES OF WWER SPENT FUEL IN INERT AND OXIDIZING ENVIRONMENT

I.A. KUNGURTSEV, V.P. SMIRNOV, I.V. KUZMIN,
I.V. LEBEDUK, Y.I. PIMONOV, G.I. SOHCILIN, L.N. STUPINA,
V.V. CHESANOV, Y.A. SHTUCKERT, E.A. ZVIR
State Scientific Centre, Research Institute of Atomic Reactors,
Dimitrovgrad, Russian Federation

Abstract

At the Research Institute of Atomic Reactors in-cell experiments were carried out which were aimed at investigation of WWER spent fuel behavior under accident conditions. Gaseous and volatile fission products release and the influence of gaseous swelling, fuel interaction with the cladding and oxidation on it have been investigated.

At the present time, series of experiments in inert and air environments have been finished and the tests in steam environment have been carrying out. In all series the samples in the form of fuel pellets fragments and fuel elements pieces were used.

This report presents some results of annealing tests and investigations of the sample microstructure after annealing.

1. INTRODUCTION

This report presents some results obtained in the framework of SSC RIAR programme on investigation of fission products (FP) release and WWER fuel behavior under conditions of possible accidents. The programme aimed at formation of data basis on WWER fuel for design models as well as development of ideas about processes controlling FP release and resulting in structural changes in their interrelation. The programme assumes performing series of experiments in inert, air and steam environments. Experiments started in 1991. They are performed on hot cell electric heated installation using fuel samples selected from WWER reactor spent FEs. Basic regime of investigations is isothermic. It allows to obtain temperature and temporary dependences of FP release. To refine ideas about burst release of gaseous fission products (GFP) step-by-step heating up was used.

Annealings in inert environment were performed in the range of 1000 - 2600°C. The demand arose to widen a temperature range beyond temperatures at which fuel can be in inert environmentin accidents to obtain information about development of porosity and FP release. A special problem of experiments in the inert environment was investigation of influence of fuel-clading interaction on FP release.

Experiments in air environment were performed in the range of 600 - 1200°. Iodine and other FP release was investigated. In 1995 a series of experiments in steam environment started. Assumed temperature regime is from 600°C to 2200°C. Series of experiments in oxidizing environment aims at investigation of FP from WWER fuel with high burnup under accident conditions.

2. FUEL SAMPLES

Fragments of fuel pellets and FEs pieces that were cut out of the irradiated FEs of WWER-440 and WWER-1000 reactor were used as samples. Prior to FEs cut gamma-scanning, prophilometry and puncture with determination of GFP release under irradiation were performed. The samples were selected from parts with regular distribution of FP activity along the length. Total weight of one sample in fragments form was 3 - 5 gr, sample length in the form of FEs pieces was 12 mm or 45 mm. Characteristics of spent FEs, appearance of selected samples and annealing environment are given in tab. I. Material of FEs cladding is Zr +1% Nb.

Table I

FEs characteristics and appearance of selected samples

FEs type	Burnup, MWd/kgU	Type of samples	Annealing environment
WWER-440	64.0	pieces	Ar
WWER-440	59.8	fragments	Ar
WWER-1000	45.0	fragments	He
WWER-1000	15.8	fragments	Ar
WWER-1000	36.8*	fragments	air
WWER-1000	0*	fragments	air
WWER-440	51.7	pieces and fragments	steam+Ar

*Prior to annealing slight irradiation in WIR reactor for ^{131}J accumulation was performed.

3. EXPERIMENTAL EQUIPMENT

Scheme of the experimental installation is shown in fig 1. The main element of installation is a changeable heating modulus specialized for environment and temperature range. The modulus is installed on the movable platform. Heater material is tungsten. In the case of inert environment a channel of the tubular heater serves as a flow - type cavity where the fuel sample in tungsten crucible is located. In oxidizing environment a sample in the crucible of is Al_2O_3 or ZrO_2 located in the changeable ceramic channel of Al_2O_3 or ZrO_2 enclosed in the heater channel. Temperature was controlled by the thermocouples of *BP* and *XA* type. At temperatures beyond 1200°C in oxidizing environment thermocouples of BP type in the protective shroud of molybdenum covered by molybdenum dicilicide were used.

During annealing carrier gas was blown through the heating modulus continuously. It transported GFP releasing from the sample through the filters where volatile FPs deposited to the out-of-hot cell ^{85}Kr recording system.

The main filter is fixed at the outlet of heater channel. It operates at 200 - 600°C and changes after each annealing. Its material is porous ceramics and charcoal. The additional filter consists of porous ceramics, graphitized tissue and charcoal.

To perform the experiments in steam environment on the movable platform of the heating modulus a steam generator and condenser were assembled. The steam generator productivity is up to 100 gr/h. The Kr registration system consist of a spiral tybe arranged on Ge(Li) - detector. One more Ge(Li) - detector was installed on axis of collimation system assembled in the hot cell wall penetration. Change of the movable platform location allows to record either a decrease of FP activity of the fuel sample or its accumulation in the main filter during annealing.

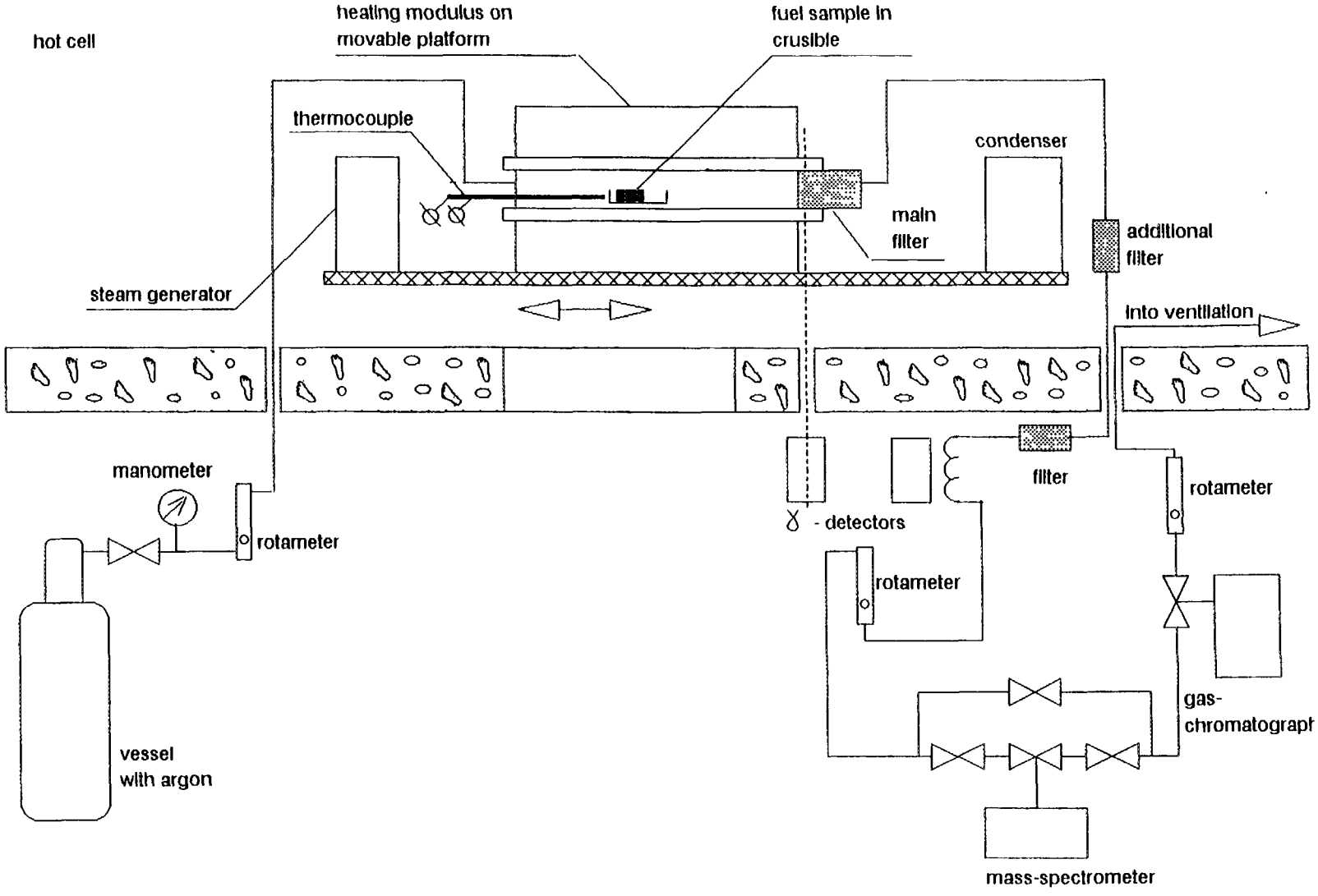

Fig.1 Scheme of experimental rig.

4. CONDUCTING OF EXPERINENTS

In all series of experiments prior to annealing the fuel samples were weighted and FP (^{137}Cs, ^{134}Cs, ^{106}Ru, ^{144}Ce, ^{154}Eu, ^{95}Zr, etc.) activities were measured. The FP activity was measured on single facility of gamma - spectrometry. A similar measurement was performed after annealing. According to difference of the FP activities prior to and after annealing a relative release of volatile FP was determined. To account for possible changes of the samples as the result of annealing activity of volatile FP was normalized with respect to nonvolatile FP (^{154}Eu or ^{95}Zr) when determining relative release.

During annealing there were measured ^{85}Kr activity in the carrier gas and increase of volatile FP activity (Cs, J, Ru) in the main filter. In the case when the samples in the form of FEs pieces were used a decrease of FP activity in samples was recorded. The temperature and time regimes of annealings are presented in tab. II.

Table II

Regimes of annealing

Environment	Temperature of isothermic annealing, °C	Heating up rate, C/sec	Time of isothermic regime, min	Flow rate of gas, ml/min	Flow rate of steam, ml/min
Ar or He	1000 -2600	13 - 20	45	190	-
air	600 - 1200	2.5	180	405	-
Ar + steam	600 - 2200*	1 - 2	45, 180	100	40 - 60

*At present instances of time experiments were performed in the range of 600-1200°C.

In the inert environment besides isothermic experiments there were performed those with step-by-step heating up.

During annealing in air environment changes of oxigen content in the flow which passed through the channel with the sample was controlled by gas chromatogragh. It presented information on oxidation kinetic. Oxidation of the fuel samples during annealing in the steam environment was determined by measurement of hydrogen content generated in reaction of sample oxidation by steam. On-line regime measurements were performed by means of gas-spectrometer.

To determine krypton relative release the krypton specific content in the annealed samples was measured. Measurements were performed by means of dissolution of the annealed sample in 5N HNO_3. Dissolving facility was connected to the experimental installation instead of the heating modulus. Registration of ^{85}Kr which releases during dissolution was performed on the same recording facility and in the same regimes which were used during annealing.

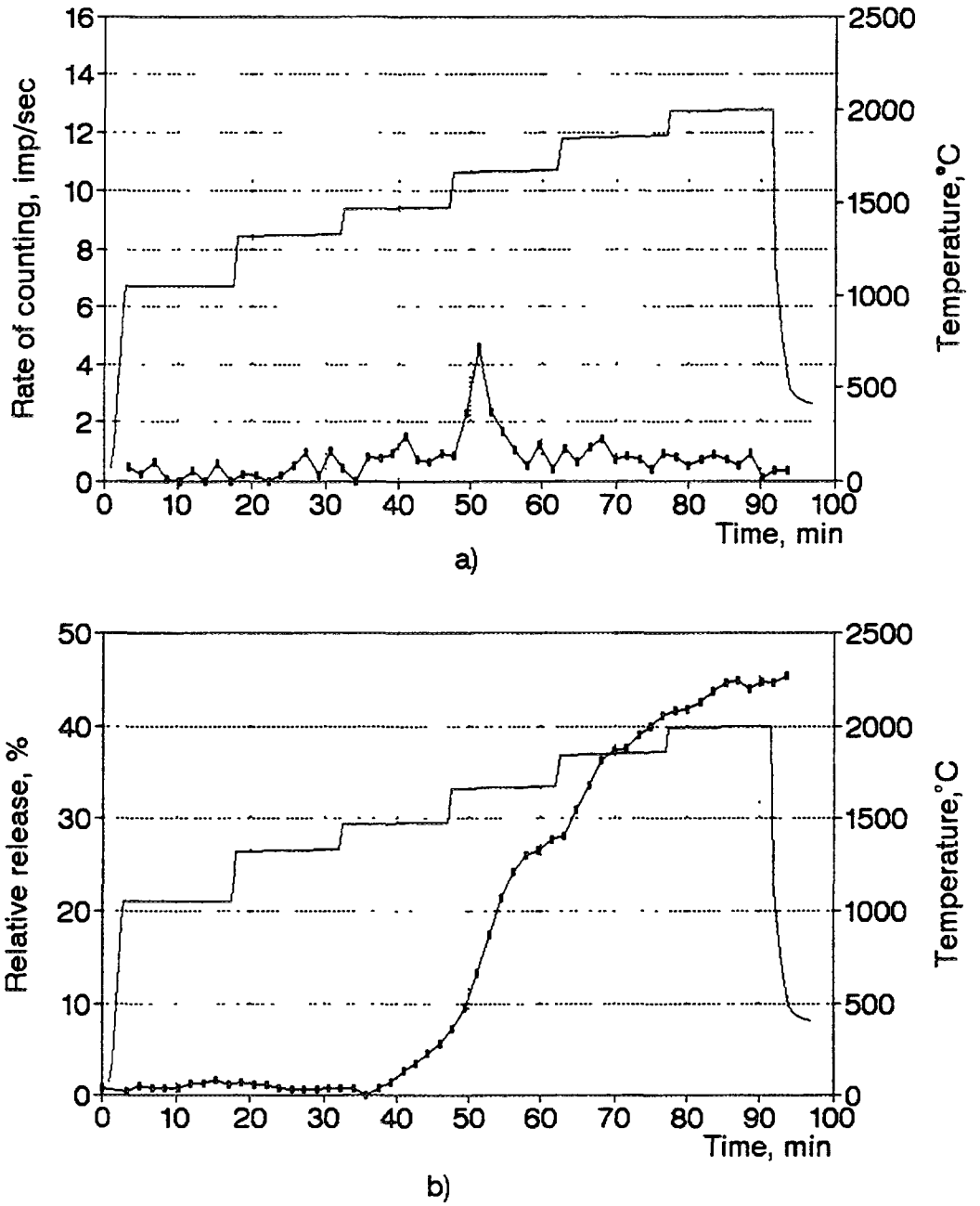

Fig.2 Kinetic of krypton (a) and cesium (b) release from sample with burnup of 59,8 MWd/kg U of at step-by-step increase of temperature in inert environment

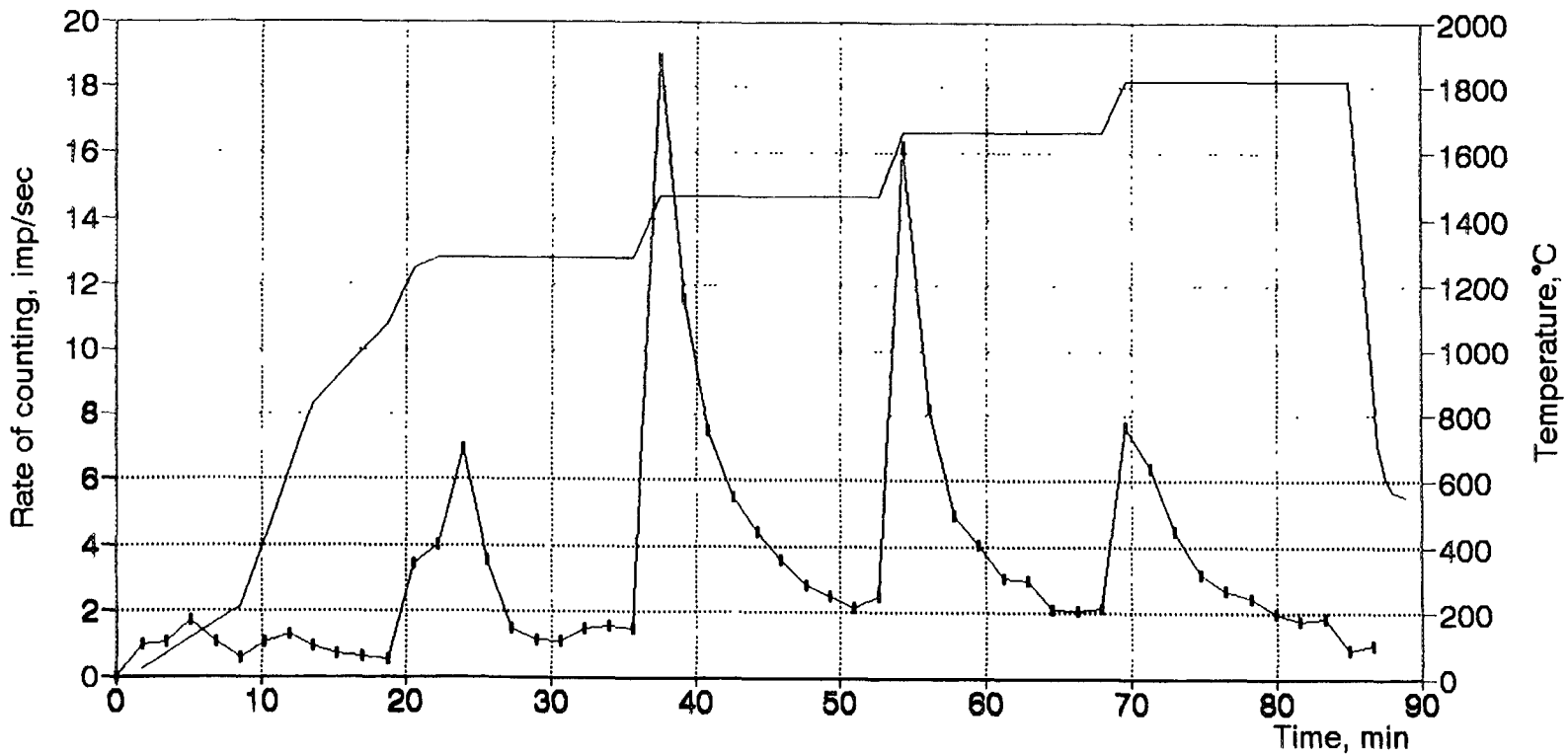

Fig. 3. Kinetic of krypton release from sample with burnup of 58.8 MWd/kg U at step-by-step temperature increase in inert environment.

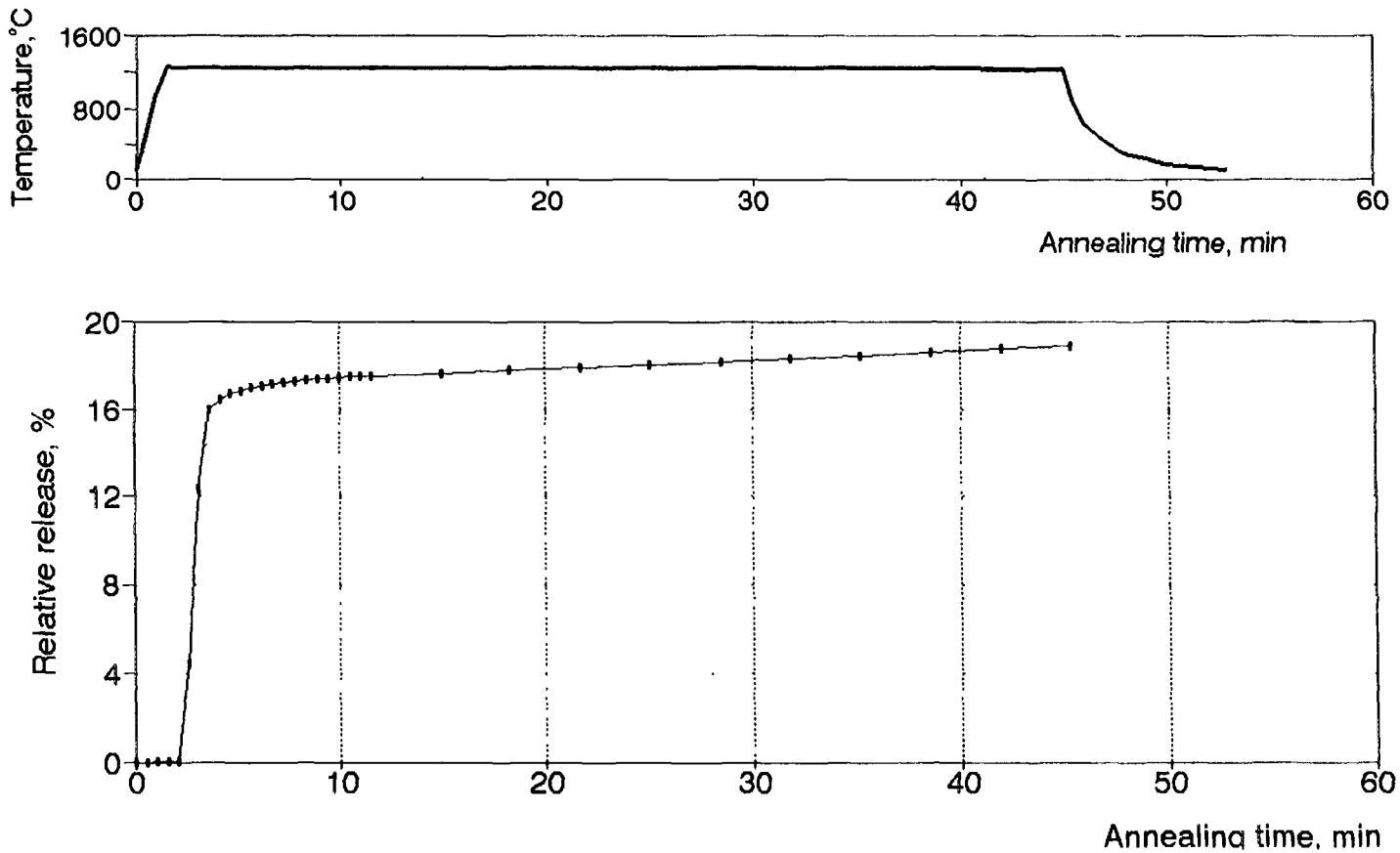

Fig. 4. Kinetic of krypton release from sample with burnup 59.8 MWd/kg U at annealing in inert environment.

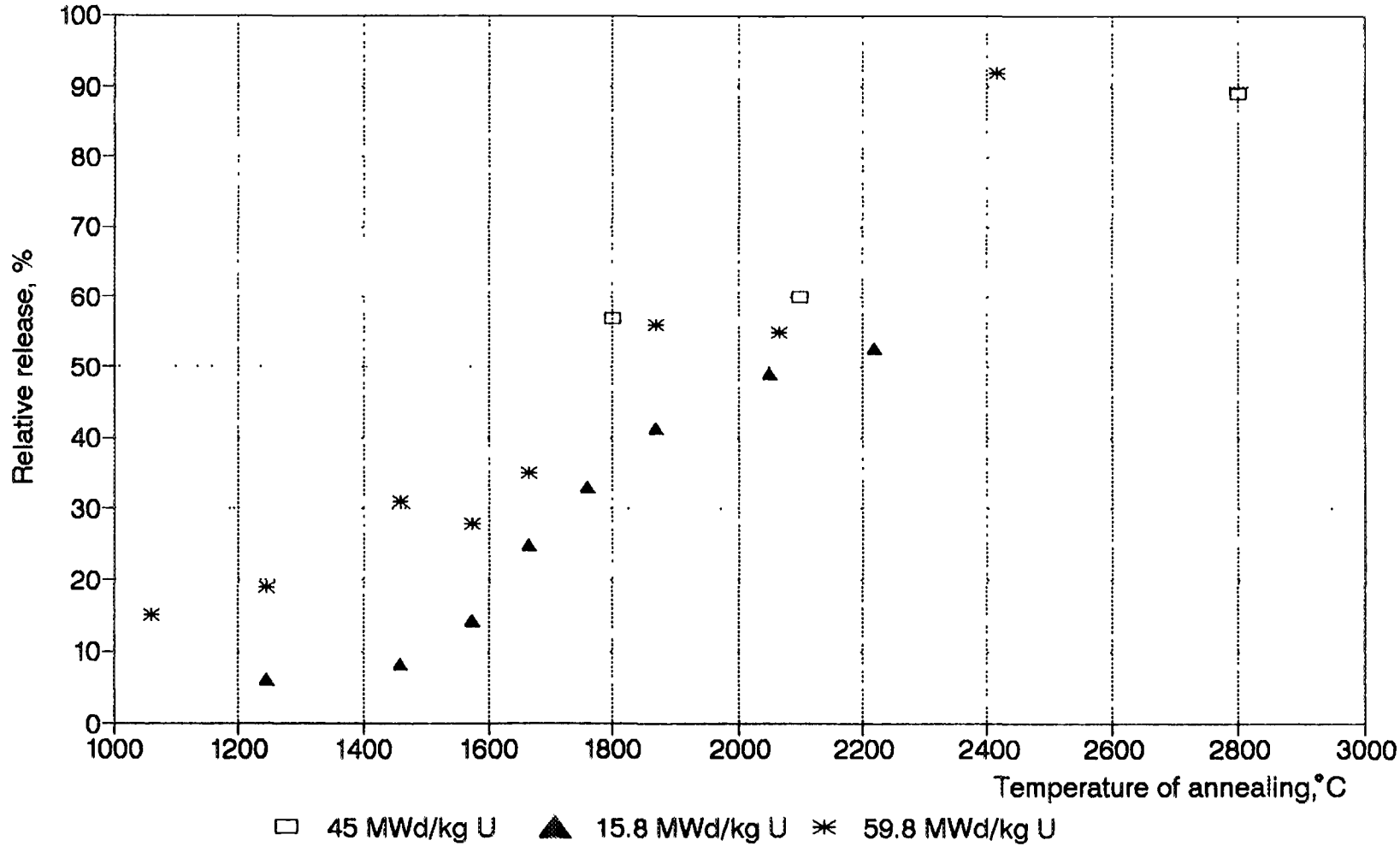

Fig 5. Dependence of release of krypton on annealing temperature. Time of annealing is45 min, environment is inert.

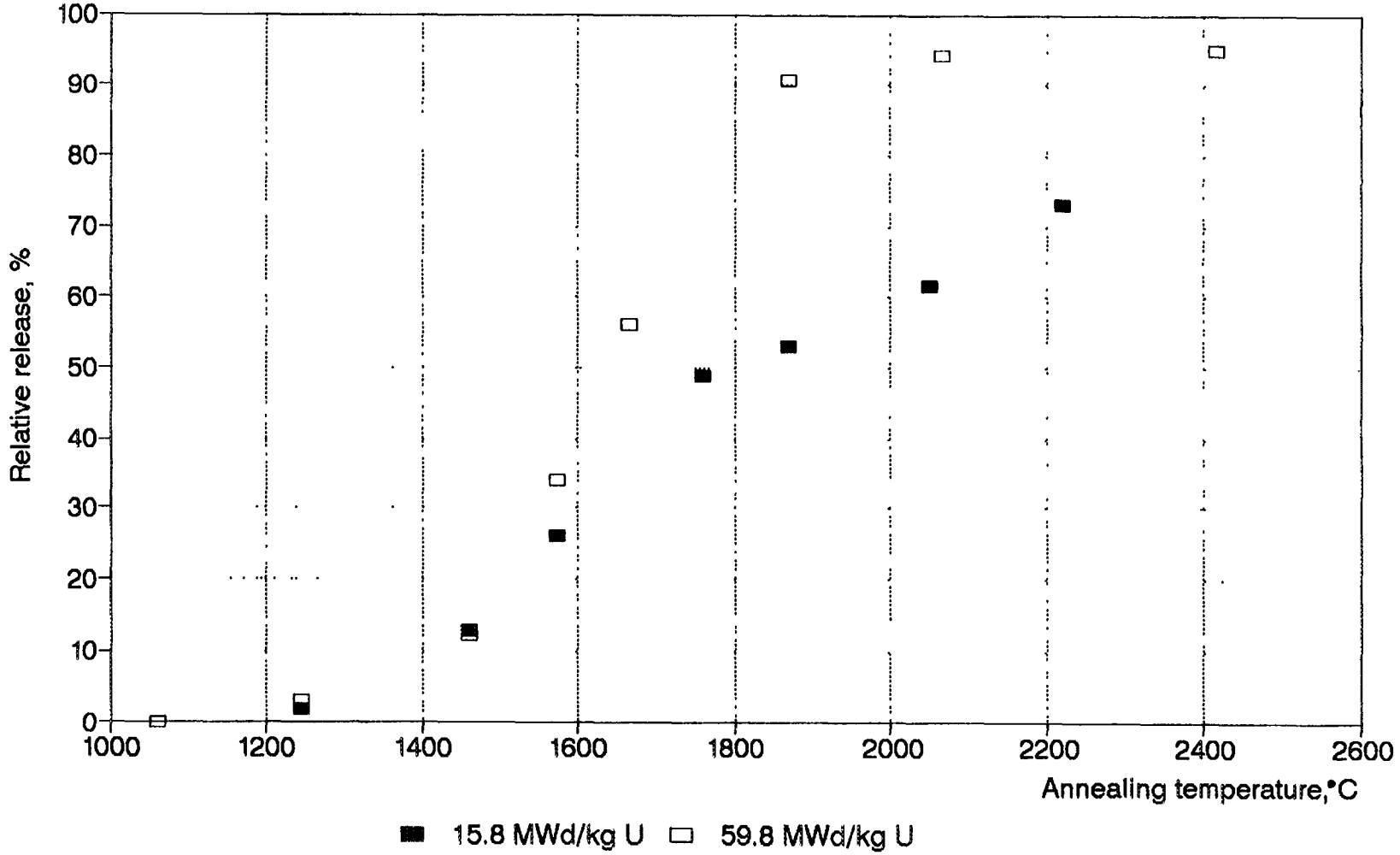

Fig 6. Dependence of cesium relative realise on annealing temperature.

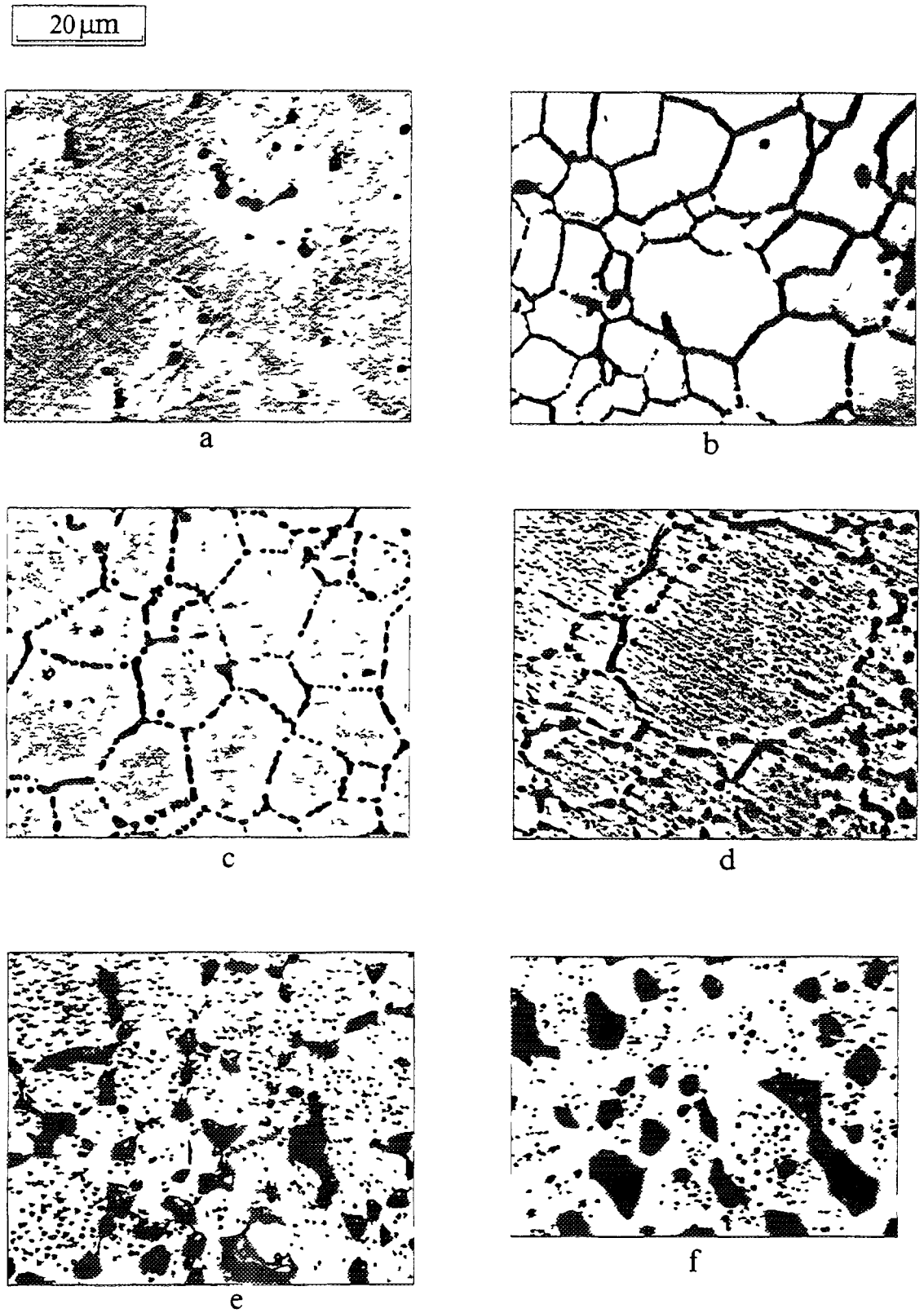

Fig.7 Microstructures of fuel fragments after annealing in inert environment. Burnup is 15,8 MWd/kgU. Annealing time is 45 min.
a) appearance before annealing, b) T=1460 °C, c) T=1660 °C,
d) T=1870 °C, e)T=2050 °C, f) T=2250 °C.

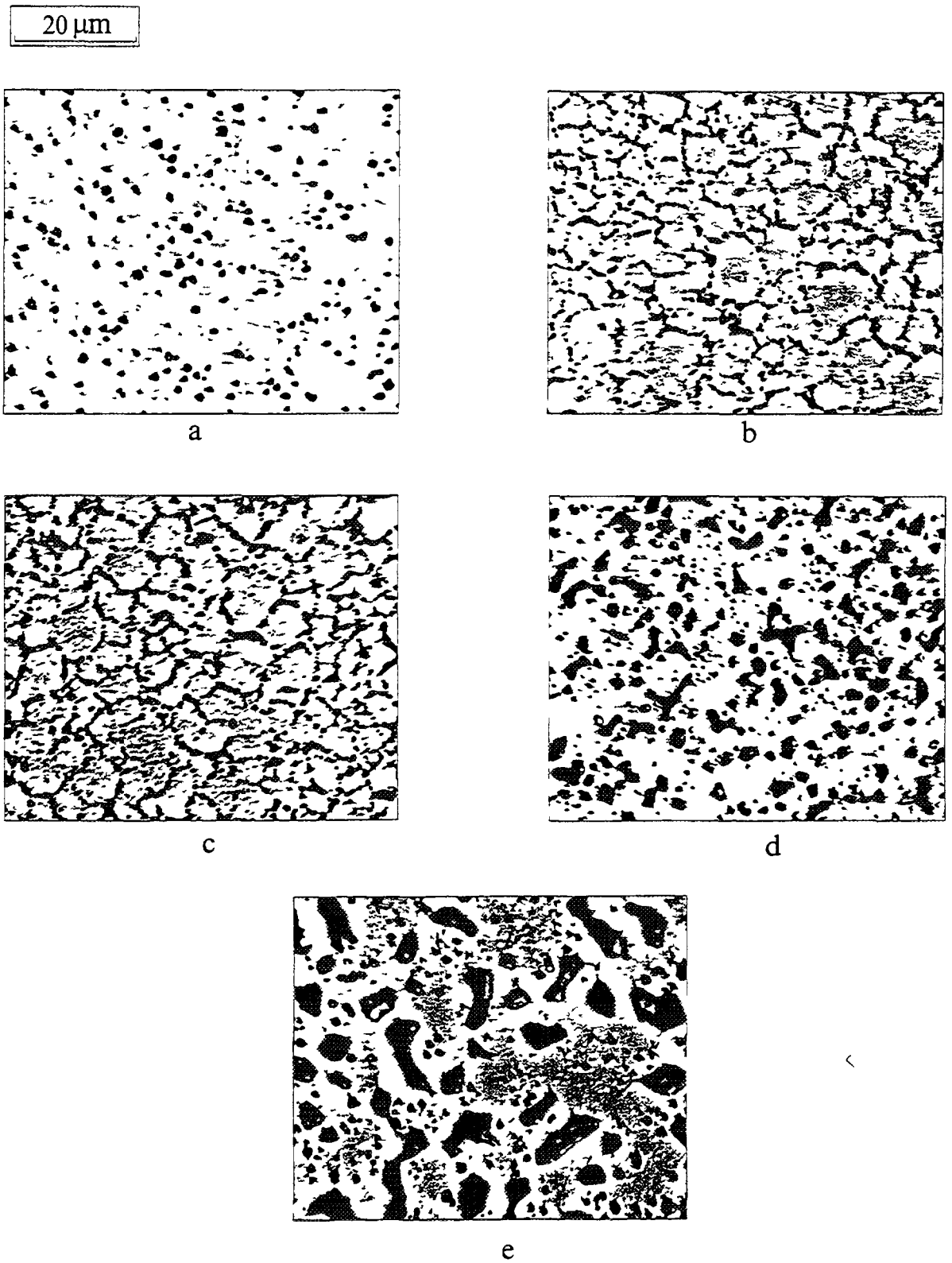

Fig.8 Microstructures of fuel fragments after annealing in inert environment. Burnup is 59,8 MWd/kgU. Annealing time is 45 min.
a) appearance before annealing, b) T=1460 °C, c) T=1665 °C,
d) T=1870 °C, e)T=2415 °C.

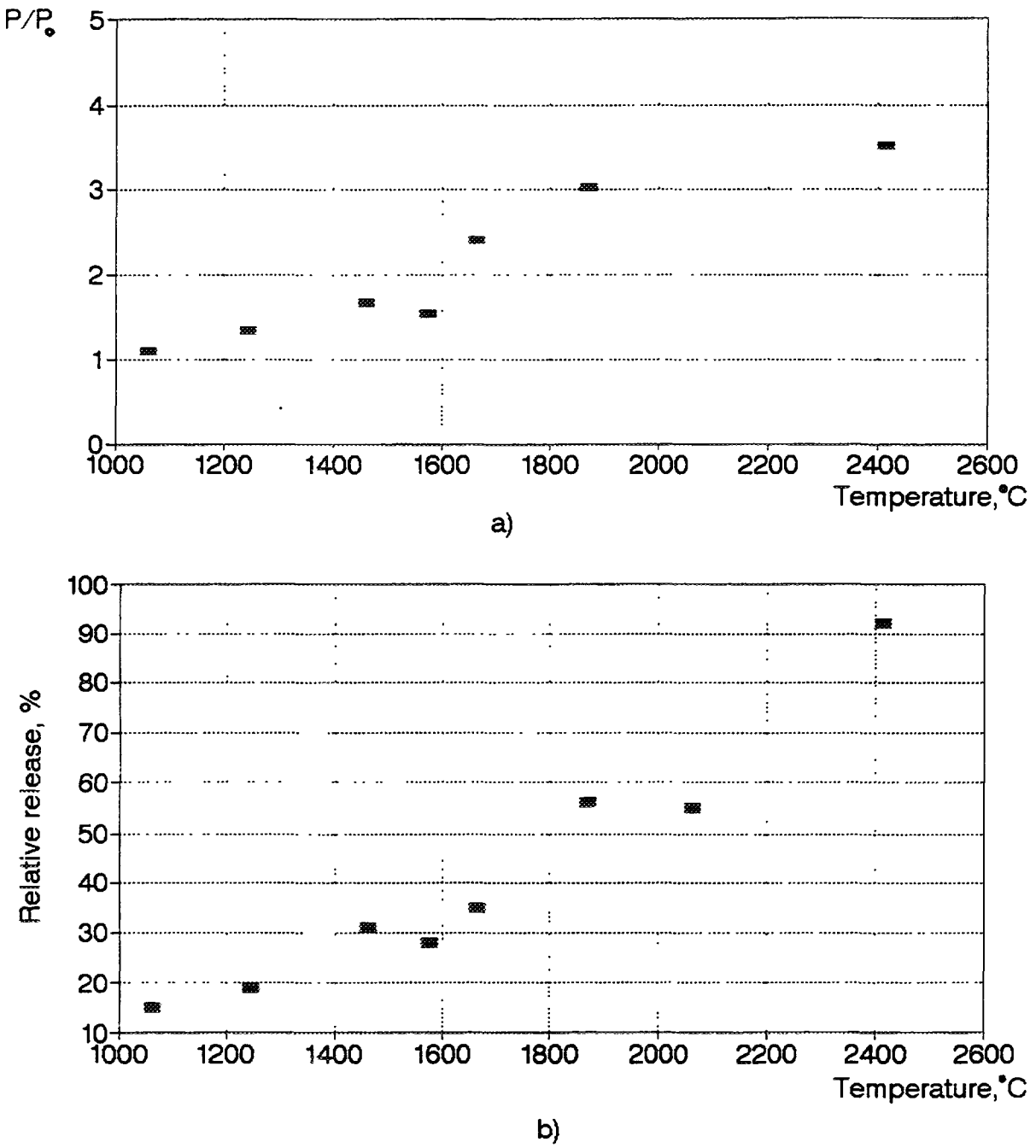

Fig. 9. Dependens of relative porosity (a) and krypton (b) on temperature annealing with burnup of 59.8 MWd/kg U. Time of annealing is 45 min, environment of inert.

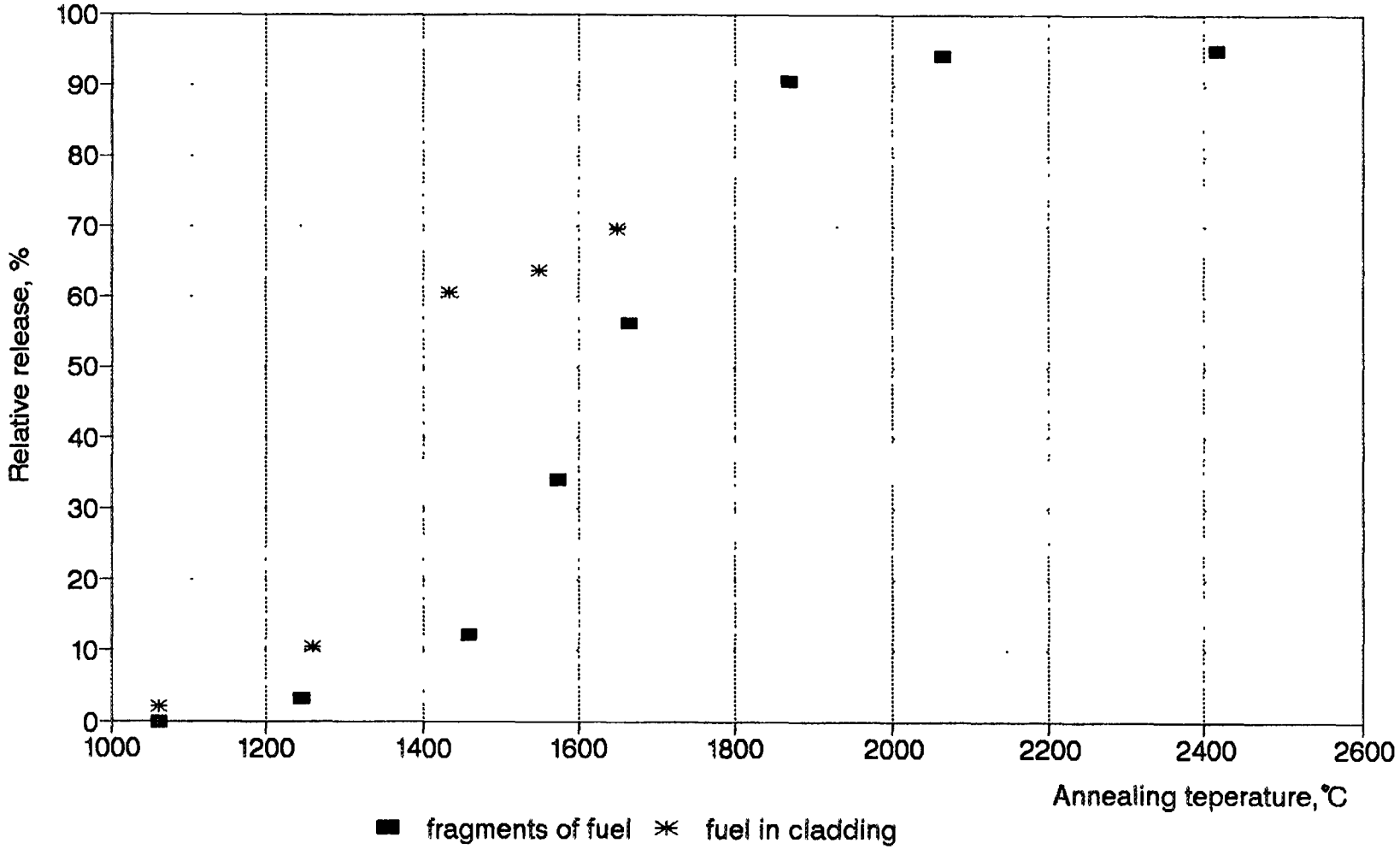

Fig 10. Dependece of cesium relative realise on temperature of annealing for samples as fragments of fuel and fuel in cladding. Time of annealing 45 min, environment is inert.

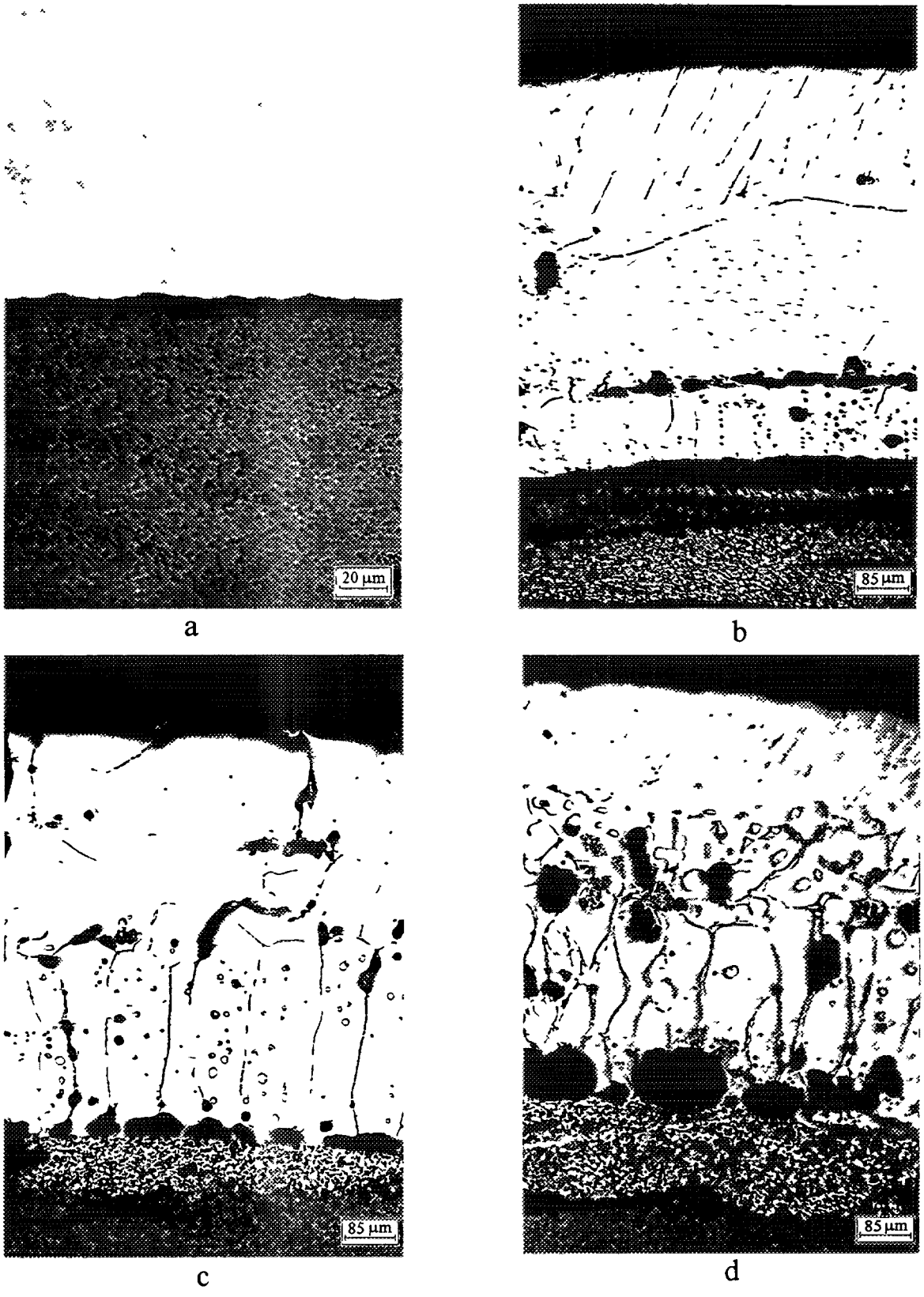

Fig.11 Parts of fuel-cladding interaction after annealing in inert environment. Burnup is 64,0 MWd/kgU, time of annealing is 45 min.
a) appearance before annealing,
b) T=1260 °C, c) T=1435 °C, d) T=1650 °C.

5. ANALYSIS OF SAMPLES MICROSTRUCTURE

Post - annealing investigations of the fuel samples are assumed the intergranular and intragranular porosity volume measurements by means of optical and scanning electron microscopes, and element analysis of the fuel - cladding interaction layers. The ceramographic investigation of samples using optical microscope was performed. The measurements of intergranular porosity are started.

6. RESULTS OF EXPERIMENTS AND DISCUSSION

6.1 Inert environment

Fig 2 and fig 3 illustrate krypton and cesium release at the step-by-step heating up test of the single fuel fragments at burnup of 15.8 and 59.8 MWd/kg U. The krypton burst release from the sample of slight burnup was observed at heating up from 1475°C to 1660°C. At the same time cesium release increased sharply. This release of krypton corresponds to release of gas accumulated during irradiation on grain boundaries /1/. For samples with burnup of 59.8 MWd/kg U burst release was observed at each temperature rise. Such manner of burst release is caused by both great accumulation of GFP on grain boundaries and samples cracking. Due to cracking recording of kinetic of cesium release from sample with high burnup failed.

At low temperature isothermic annealing of the samples at burnup of 59.8 MWd/kg U the burst release during the heat up represens the main part of krypton total release (fig 4).

Temperature dependence of cesium and crypton release in isothermic annealings has form of S-shaped curves (fig 5 and fig 6). In the temperature interval of 1500-1800°C sharp increase of the FPs release connected with formation of the tunnels system due to the development of gas porosity (given below).

Cesium release is higher than that of krypton. The exception is area of low temperatures when the burst release of GFP is higher than diffuse one. In area of high temperatures at tendency for 100% cesium release, in the temperature range of 1800-2200°C stabilization of krypton release at the level of 50-60% is observed. The temperature increase up to 2400°C results in almost total release of krypton. It points to insignificant isothermic dissolving of GFP from the intragranular gaseous pores up to 2200°C. A sharp increase of krypton release up to 93% at 2420°C is likely to be the result of the GFP release from the intragranular pores at the expense of phase transition into UO_2 at 2400°C /2/. To refine this effect additional experiments will be performed.

Cesium and krypton release from the samples at burnup of 59.8 MWd/kg U is higher than from the samples at burnup of 15.8 MWd/kg U. One of the reasons explaining it is smaller size of grains of the samples with high burnup. Possible influence of burnup will be defined at the following proceeding of results with determination of fractions of burst and diffuse releases as well as coefficients of diffusion.

Microstructure of fuel samples after isothermic annealings is illustrated in fig 7 and fig 8. Increase of the annealing temperature leads in enlargement of intergranular pores at first and then in redistribution of porosity from grains faces to edges and corners with loss of visibility of grains circuits.

Porosity as a function of annealing temperature for samples at burnup of 59.8 MWd/kg U is shown in fig 9. Values of porosity is given with respect to the sample porosity prior to annealing. Comparison of the porosity changing and krypton release confirms that increase of Kr release in the range of 1500-1800°C is connected with formation of the open linked porosity.

The fuel - cladding interaction results in essential increase of the cesium release. Fig 10 illustrates temperature dependence of the relative release of cesium from FEs fragments at burnup of 64.0 MWd/kg U. For comparison in this figure the results for fuel pellets fragments at burnup of 59.8 MWd/kg U is show. The state of the fuel cladding and the outer layer after

annealing is illustrated in fig 11. Peculiarity of presented structures in comparison with typical sequence of layers of interaction /3/:

$$[UO_2 + U] \rightarrow [\alpha - Zr(O) + (U,Zr)] \rightarrow (U,Zr) \rightarrow \alpha - Zr(O) \rightarrow \beta - Zr$$

is the presence of porosity between [UO_2+U] and [α-Zr(O)+(U,Zr)]. This porosity may be a result of GFP release and/or absence of external compression pressure. Also considerable content of metallic phase in UO_2 surface layer is observed. Composition of this layer is need to be determined. Its appearance is likely to be caused by absence of external pressure.

6.2 Oxidizing environment

Oxidation of UO_2 during annealing in the air environment results in destruction of fuel fragments. The samples of low burnup after slight irradiation in MIR reactor transformed into powder at all annealing temperatures in the range of 700-1100°C. The samples at burnup of 36.8 MWd/kg U were less subjected to destruction. Only at 600°C and 700°C a total transformation of the sample into powder was observed; at higher temperatures there was partial transformation.

Ruthenium release depends on degree of transformation into powder, i.e. on increase of open surface area. Ruthenium is low - volatile in UO_2 in inert environments and volatile in air environment due to the formation of volatile oxide. The kinetic of ruthenium release that is shown in fig 12 and fig 13 is likely to correspond to kinetic of the samples free surface increase. The result of these experiments at 995°C was total transformation of slightly irradiated sample into powder and partial one of sample at burnup of 36.8 MWd/kg U.

Fig 12 and fig 13 illustrate kinetic of the Kr, Cs and J release and change of oxigen content in air which passed through the heating modulus. During the first 10 - 20 minutes of isothermic annealing active absorbtion of oxigen by sample was observed. It may be explained by the sharp oxidation rate increase after achievement of some composition of UO_{2+x}. The similar effect was observed in steam environment. Fig 14 illustrates kinetic of the hydrogen generation and krypton release during annealing of the samples at burnup of 51.7 MWd/kg U at 1000°C. In 12 minutes after steam supply increase of hydrogen generation rate corresponding to increase of oxidation rate as well as increase of krypton release was observed. Hydrogen first peak is caused by desorption with surface.

Fig 15 illustrates temperature dependence of the cesium and iodine relative release in air environment. For samples with burnup of 36.8 MWd/kg U the hold manner of dependence of iodine release is evident. At temperatures beyond 900°C the iodine release reaches 90% and slightly depends on temperature. For slightly irradiated samples the release of iodine corresponds to that of cesium and release of cesium is equal for both burnups. Taking into consideration the transformation of the slightly irradiated samples into powder in the total temperature range the difference of iodine chemical forms in the slightly irradiated sample and in the sample at burnup of 36.8 MWd/kg U should be assumed. Temperature dependence processing of cesium release is realized according to model

$$F = 1 - \exp(-kt)$$

$$K = K_0 \exp\left(-\frac{Q}{Rt}\right)$$

where F is relative release;
k is constant of release rate, sec;
T is temperature, K;
t is time, sec;
Q is energy of activation;
R is gas constant.

The value of activation energy of 108 kJ/mol is obtained. It is close to the activation energy of UO_2 oxidation /4/.

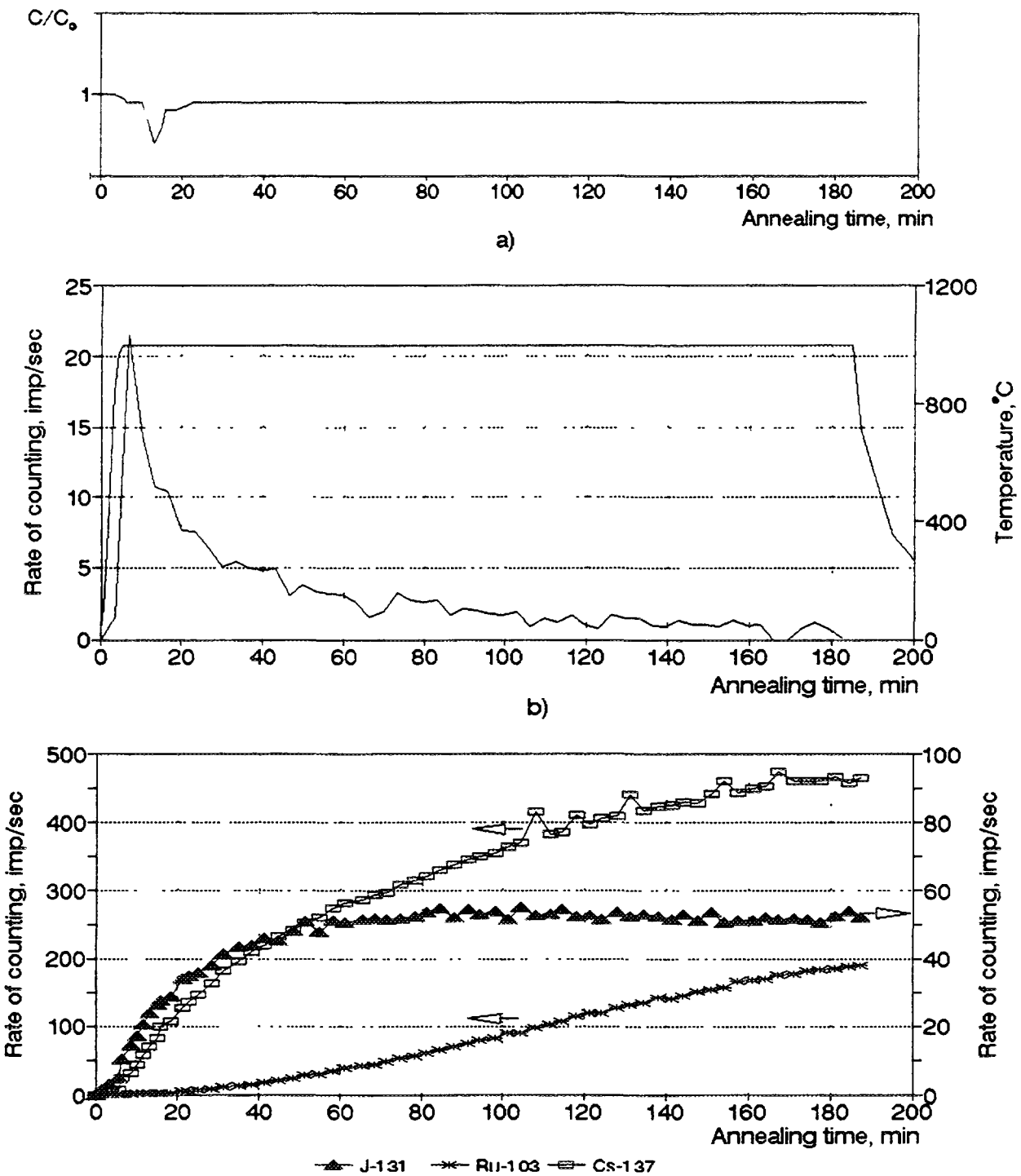

Fig.12. Results of sample annealing with burnup 36.8 MWd/kg U of uranium in air:
a) change of oxigen content;
b) kinetic of krypton release;
c) kinetic of ruthenium, cesium and iodine release.

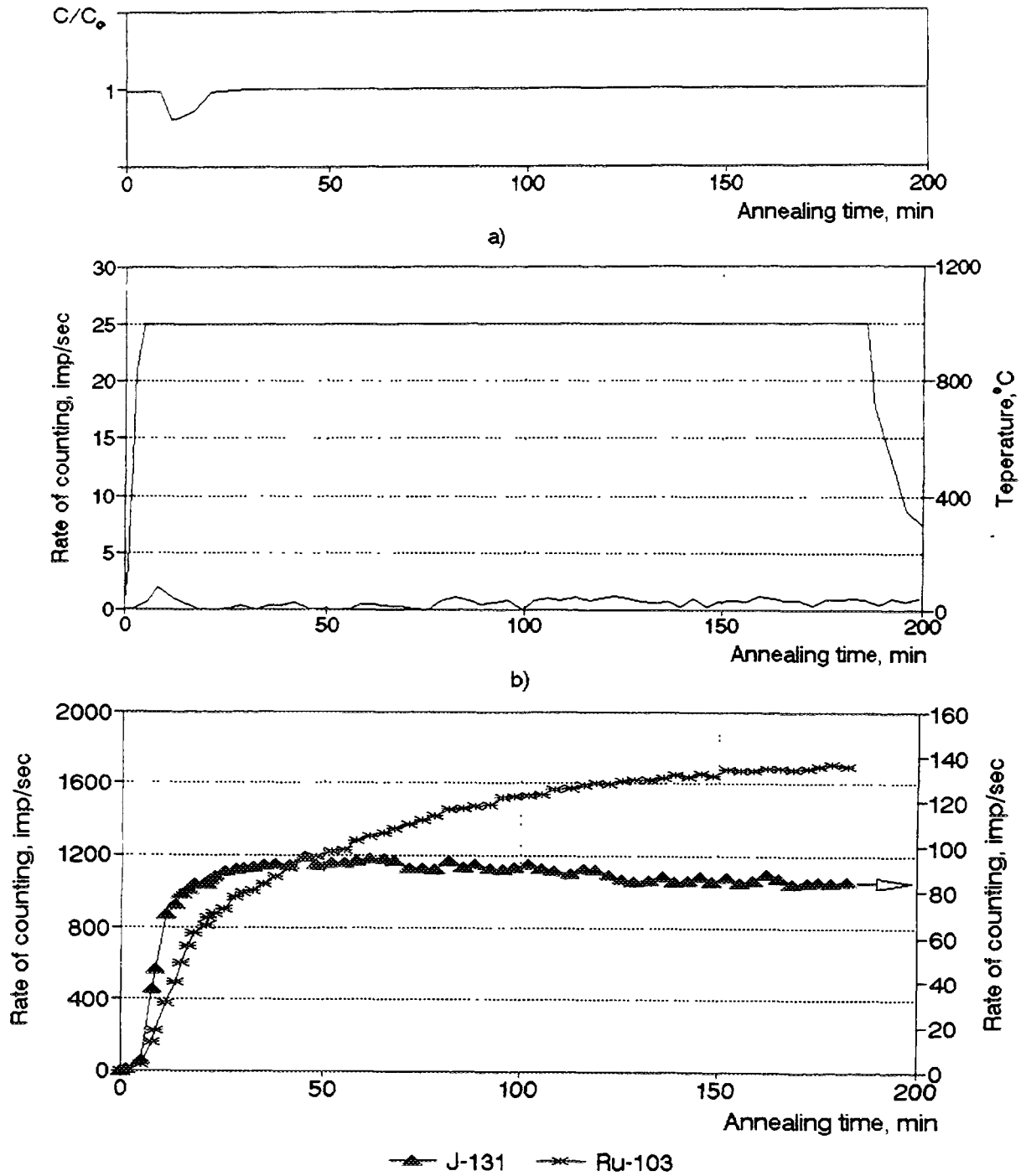

Fig.13. Results of annealing sligthly irradiated sample in air environment:
a) change of oxigen content;
b) kinetik of krypton release;
c) kinetic of ruthenium and iodine release.

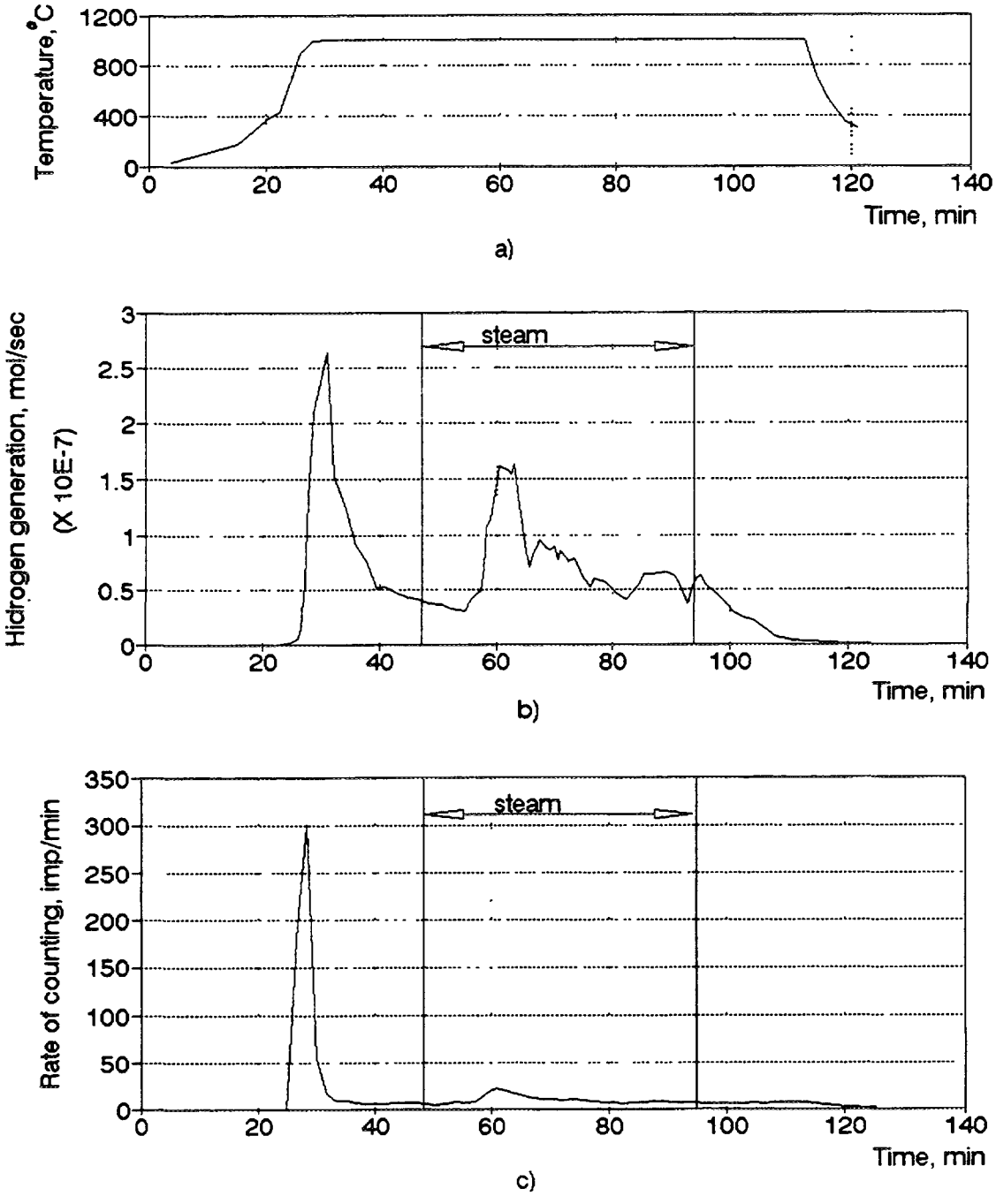

Fig. 14. Kinetic of hidrogen generation (b) and krypton realese (c) during annealing of sample with burnup 51.7 MWd/kg U.

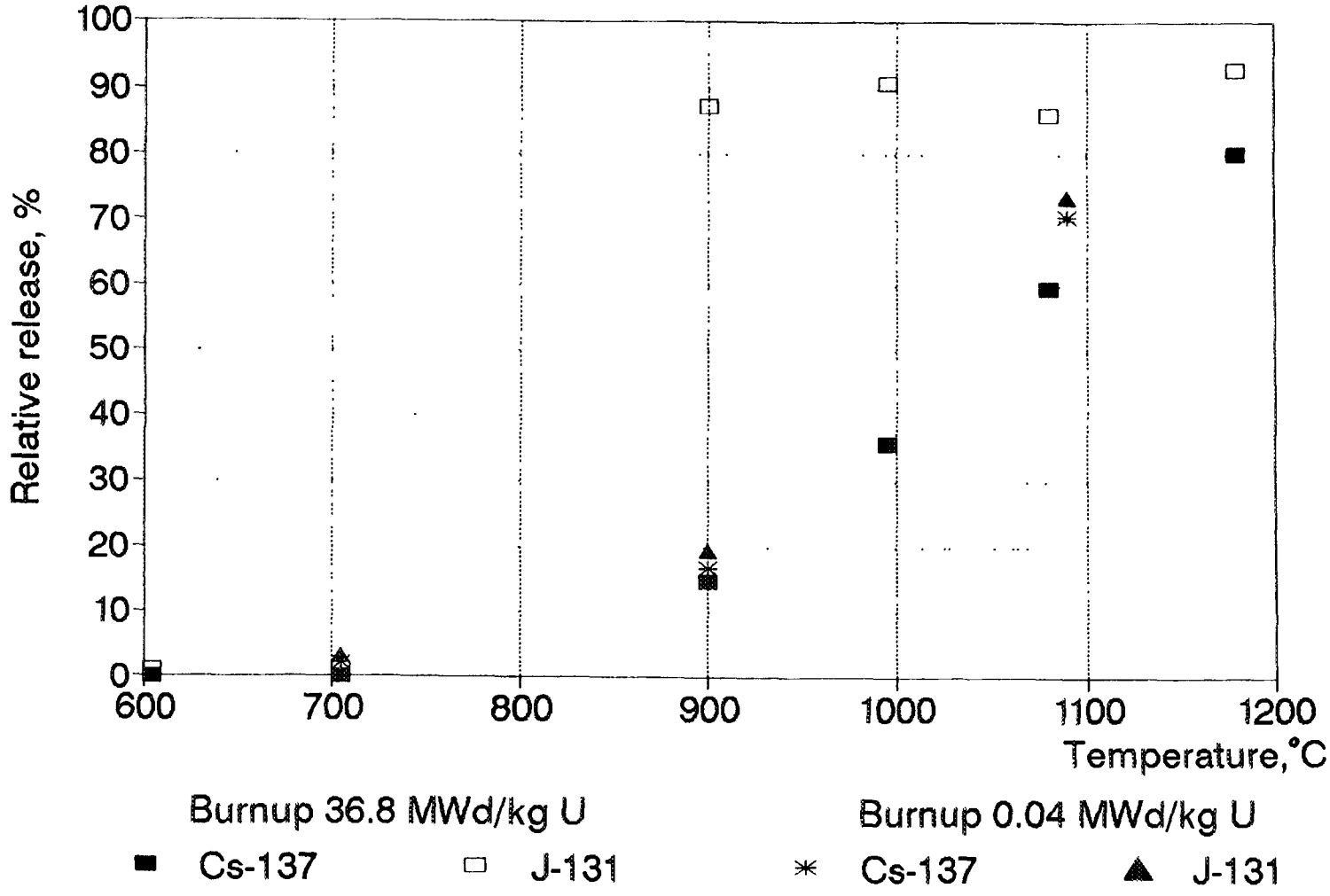

Fig. 15. Dependence of iodine and cesium relative release on temperature. Time of annealing is 180 min, air environment.

7. CONCLUSION

7.1. Inert environment

Isothermic annealing of WWER fuel with burnup of 15.8, 45 and 59.8 MWd/kg U are performed.

Relative release of krypton and cesium in the range of 1000 - 2600°C is measured.

Development of intergranular gaseous porosity in the range of 1500 - 1800°C results in sharp increase of cesium and krypton release.

In the range of 1800-2200°C krypton release changes slightly with temperature increase.

Heating up of samples with burnup of 59.8 MWd/kg U with rate of 13-20°C/sec results in burst release caused by both GPS release from grains boundaries and sample cracking.

The fuel - cladding interaction causes a considerable increase of cesium release at about 1400°C. With temperature increase cesium release from samples in cladding and without it comes close together.

7.2. Oxidizing environment

Isothermic annealing of WWER fuel in air environment in the range of 600 - 1200°C are performed; experiments in steam environment started.

A transformation of the fuel fragments into powder as the result of oxidation in the air environment influences ruthenium release essentially. It is caused by the volatile oxide formation.

During isothermic annealings in the air and steam environments in 10-20 min the rate of UO_2 oxidation increases sharply.

Dependence of iodine release from slightly irradiated samples and samples at burnup of 36.8 MWd/kg U on temperature during annealings in air environment differs essentially. In the slightly irradiated samples iodine behaves as cesium and increases a release from 15.7% at 705°C up to 70.5% at 1090°C. About 90% of iodine release from the spent fuel samples beginning from 900°C.

REFERENCES

[1] UNE K, KASHIBE S. Fission gas release during post-irradiation annealing of BWR fuels. - J. of Nucl. Science and Technol., 27, 1990, p.1002.

[2] LEIBOWITZ l. FUNK J.K. Phase transitions, creep, and fission gas behavior ın aktinide oxides. - J.of Nucl. Mat.,116, 1983, P.324

[3] HOFFMAN P., KERWIN - PECK D. UO_2 / Zircaloy-4 chemical interaction from 1000 to 1700°C under isotermal and transient temperature conditions. - J. of Nucl. Mat., 124, 1984, p.80.

[4] HARRISON K.T., PADGETT C., SCOTT K.T. The kinetic of oxidation of irradiated uranium dioxide in dry air. - J. of Nucl.Mat., 23, 1967, p.121.

METHODS OF PERFORMING THE POWER RAMPING EXPERIMENTS WITH VVER FUEL RODS AT DIFFERENT BURNUPS

Yu.K. BIBILASHVILI
State Scientific Center ASPRIIM,
Moscow

A.F. GRACHOV, V.A. KUPRIENKO, V.V. KALYGIN, N.P. MATVEYEV
State Scientific Center RIAR, Dimitrovgrad

V.V. NOVIKOV
State Scientific Center ASPRIIM,
Moscow

V.A. OVCHINNIKOV, I.S. POLYAKOV
State Scientific Center RIAR, Dimitrovgrad

Russian Federation

Abstract

In the present report an engineering of experiments " power ramp ", realized in RIAR till 1995 is considered. Included are methods and program of some experiments, scheduled for 1995.

TEST PROGRAM

The purpose: determination of safe linear heat generation rate (LHGR) at various burnup and safe speed of ramp.

Types of fuel rods:

- experimental (length 0,25-1 m)
  - cladding - Zr + 1 % Nb (110-alloy);
    - Zr + 1 % Nb + 1 % Sn + 0,5 % Fe (635-alloy);
  - fuel - UO_2 usual pellet;
- refabricated (length 1 m) and full-scale VVER-440 and VVER-1000 (lenght 2,5 and 3,8 m) at average and high burnup.

Main parameters:

- range LHGR ~ 150 - 700 W / cm;
- amplitude of ramps ~ of 200 %;
- time of power rise:
  - "slow" ramps - 2 min. and more;
  - " fast ramps " - 1-5 s;
- fuel rod burnup - 0-70 MW ·day / kg U;
- parameters of a coolant correspond to VVER parameters.

Experimental equipment :

- MIR reactor ;
- loops with water coolant (PVP-2, PV-1, PVK-2);
- special fuel rod rig and technological equipment.

The characteristics of the MIR reactor and its loop installations are indicated in tables 1,2. Chartogramm of a reactor core and arrangement of loop channels is shown in fig. 1. The arrangement

TABLE I. MAIN FEATURES OF THE MIR REACTOR

Thermal capacity		**up 100 MW**
Maximum neutron flux	**(E<0.68 eV)**	**5 x 10^{14} 1/cm^2 .s**
	(E>0.1 MeV)	**2 x 10^{14} 1/cm^2 .s**
Moderator		**Be, H_2O**
Reflector		**Be**
Coolant		**H_2O**
Water pressure		**1.24 MPa**
Coolant temperature		**40 - 83 o C**
Campaign duration		**30-40 days**
Fuel assemblies		**UO_2 - Al**
Number of Fuel assemblies		**48**
Number of control rods		**29**
Number of movable Fuel assemblies with compensating rods		**12**
Number of loop channels		**11**
Core height		**1 m**

of channels permits to create neutron flux, distinguished in 5-10 times in various channels. It is provided by
control facilities of reactor and loading burnup or new fuel assemblies of the MIR reactor about the loop channel.

The scheme of a loop is shown in fig. 2. For example, in the PVP-2 loop there are monitoring system of fuel rods tightness by activity of coolant, the system of coolant clearing, emergency cooling, disactivation, storage of active coolant and other. The loop has gauges of temperature on input and output from a channel, as well as gauges of heating, coolant pressure and flow rate.

For a example the scheme of realization of experiment is shown in fig. 3. The reading of loop gauges, results of determination of thermal losses and heat release in materials from gamma-radiation are used for determination of total power in fuel rods by a thermal balance method. Power distribution between fuel rods and along fuel rod is specifyied after post experimental gamma- scanning. In addition It is possible to use thermocouples and neutron detectors inside loop channel. The error of a linear power determination is 5-10 % depending on total power of fuel rods.

TABLE II. CHARACTERISTICS OF LOOPBACK INSTALLATIONS (LI) AT THE MIR REACTOR

Name LI	PV-1 PV-2	PVK-1 PVK-2	PVP-1	PVP-2	PG-1
Coolant	water	water, steam	water, steam	water, steam	helium, mixture of 2 gases
P, MPa	20	20	8.5	20	20
N, KW	2000	2000	100	2000	160
T, ^{o}C	340	340	500	500	550 (1000 in the core)
Q, kg / h	16000	14000	675	1000	
A, Bq / kg	3.7 e10	3.7 e10	3.7 e10	3.7 e10	3.7 e10

P - maximum pressure;
N - maximum capacity;
T - maximum temperature of a coolant;
Q - coolant flow;
A - maximally allowable activity of coolant.

NOTE: 1. Density of a flow of neutrons in channels

$E < 0.68$ eV - $(3-5) \cdot 10^{14}$ cm^{-2}.s^{-1};

$E > 0.1$ MeV - $(2-4) \cdot 10^{14}$ cm^{-2}.s^{-1}.

2. Maximum internal diameter of water channels of loopback installations - 74 mm.

It is possible to receive some different types of power ramping such as: "slow" or "fast". Methods are shown in fig. 4. They are follows: by change of reactor power for "slow" ramps , turn of fuel rods about the absorbing screen or movement of fuel rods from above downwards about screens ("fast" ramps). At moving of fuel rod about the screen it is possible to increase the non-uniformity of a neutron flux by arrangment of reactor control rods.

The characteristics of six "slow" ramps realized till 1995 are presented in table 3. In this case the ramps were performed by change reactor power (R6), reactor rods position (R1), or combination of these methods.

TABLE III. THE COMMON ITEMS OF INFORMATION ON THE R1-R6 EXPERIMENTS WITH VVER FUEL RODS ON THE MIR REACTOR

Name	R1	R2	R3	R4	R5	R6
Place of tests	PVK-2	PVK-2	PVK-2	PVK-2	PVK-2	PV-1
Quantity of fuel rods in irradiation rigs	10	9	10	12	11 + 6	12
Year of experiment realization	1990	1991	1993	1994	1994	1994
Length of fuel rods, mm	265	265	1075	265	265	1075
Burnup, MW.day / kg U	8.5-10	8-10.7	47	17	15-30	50
Amplitude of power ramp	1.9	2.8	1.9	2.2	2.2	2.2
Duration of capacity increaing, min.	8	13	2.5	8	10	113

In the latter case at first stage a reactor power was decreased, and simultaneously fuel rods power was supported constant by control rods, then reactor power was increased. So it is possible to realize ramp for a time more than two minutes. The results six "slow" ramp are presented in fig. 5. They were realized at different burnup. For a burnup of ~50 MW ·day / kg U the refabricated fuel rods were used. All fuel rods have saved tightness, no cracks detected on internal surface of a cladding after eddy current control and crossection investigation.

These "ramps" were realized in dismountable fuel assemblies , enabling to replace fuel rods. The ramps with a short fuel rod were realized in a test arrangment, shown in fig. 6. For fuel rods of 1 m long a test assemblies were used (fig. 7 and 8). Replacement of fuel rods in subassembly was performed in the shielding chambers, located in the reactor building. After "ramp" and gamma-scanning the fuel rods were sent for researches in other building, where there is a research laboratory.

Up to the end of 1995 and in the beginning 1996 some experiments were prepared for realization. There are "slow" ramps with using refabricated and full-scale fuel rods at burnup of 30-60 MW ·day / kg U, and one "fast" ramp for a time of 1-5 seconds with refabricated fuel rods (by turning about the screen) as well as "fast" ramp by moving of a fuel rod along screen. In the later case one can obtain the less depression of neutron flux with one fuel rod and the more linear power. In fig. 9 an assembly is shown, in which refabricated and full-scale fuel rods are placed together.

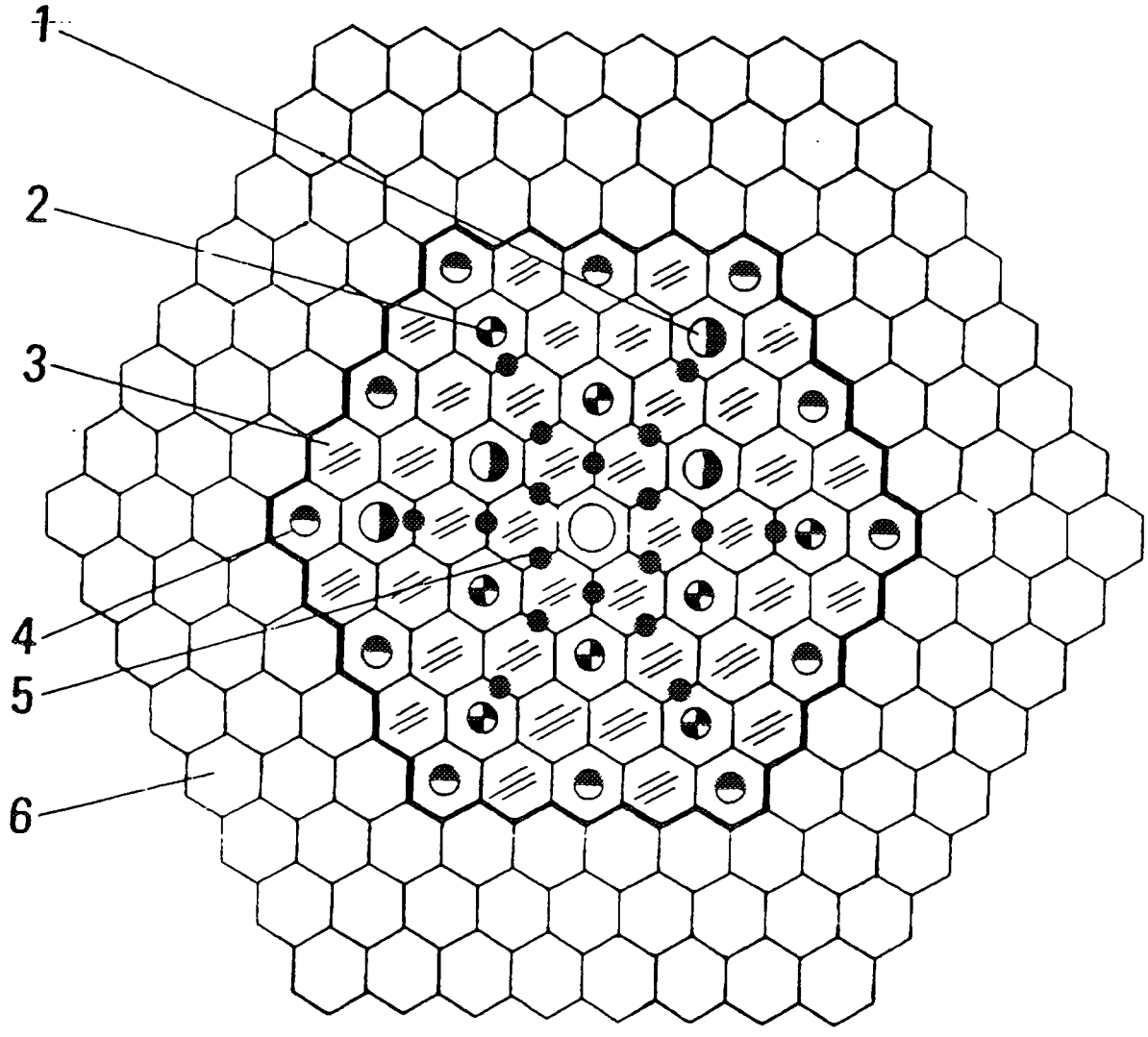

Fig. 1

Chartogram of the MIR reactor

1 - channels of PV-1 and PV-2 water loops;

2 - channels of other experimental loops;

3 - reactor working channels with drivung FA;

4 - control rods with fuel tails;

5 - control rods;

6 - reflector.

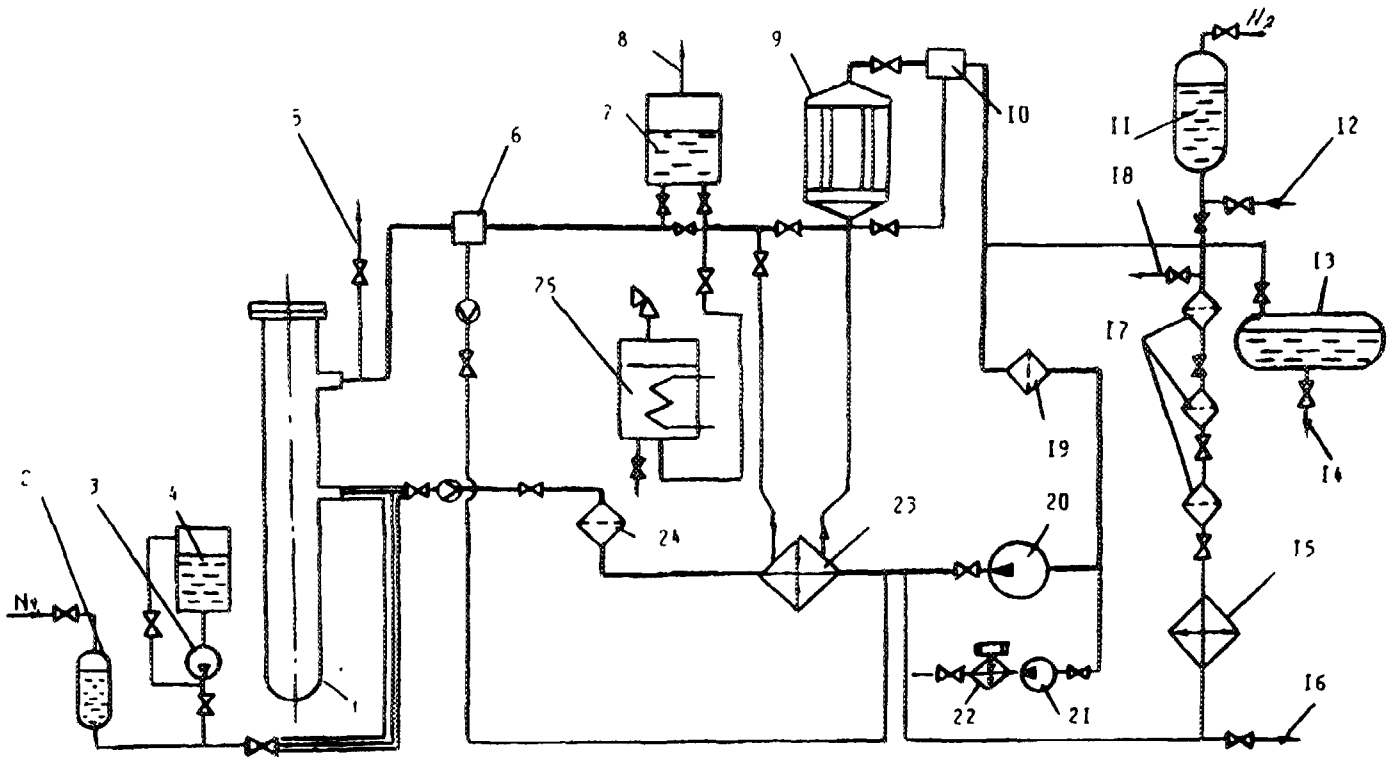

Fig.2

Scheme of the first circuit PVP-2 loop facility: 1 - loop channel; 2,3,4 - bottles, pumps and tanks of the System Emergency Cooling (1,2) correspondingly; 5,16,18 - sampling system; 6,10 - mixers; 7 - separator; 8 - pipe to the system of the hydrogen burn-up; 9,23 - main and regeneration heat exchange devices; 11 - volume compensator; 12 - distillat replenishment line; 13 - tanks for the long-term storage of the liquid radioactive waste (1,2); 14 - drainage to the waste piping; 15 - heat exchange device of the purification system; 17 - ion-exchange filters; 19,24 - gause filters; 20,21 - pumps; 25 - barbotage tank..

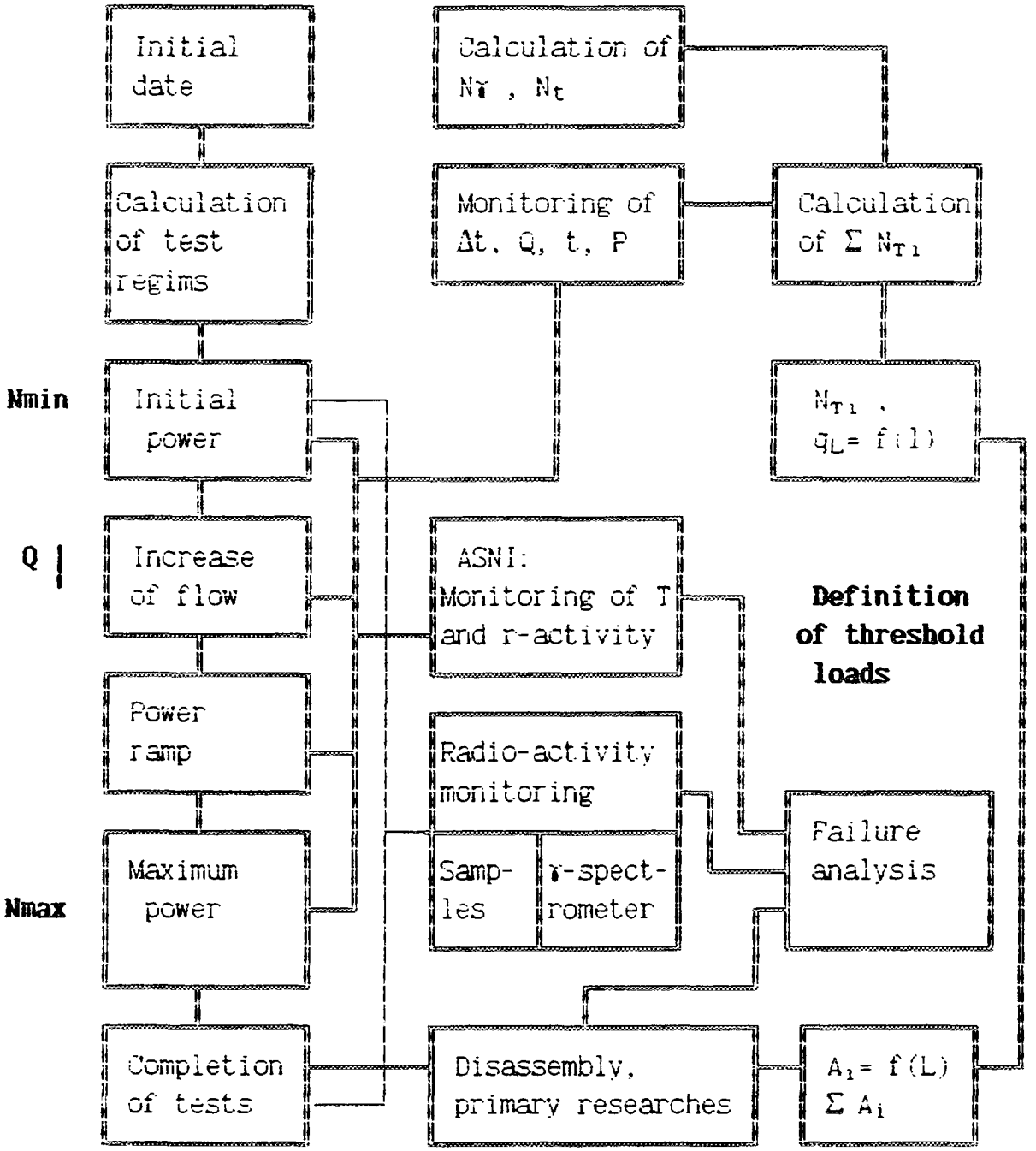

N_γ , N_t - energy of radiactivity heating and thermal losses;
Σ N_{Ti} - total power of assembliy;
N_{Ti} - power of fuel rod (i);
Δt, Q, T_{BX}, P - coolant parametrs;
$q_L = f(l)$ - linear heat generation rate;
$A_i = f(L)$ - γ-spectrum of fuel rod (i);
ASNI - automatic system of scientific investigations.

Fig. 3 Scheme of experiment's stages sequence and moving of information

Kind of tests

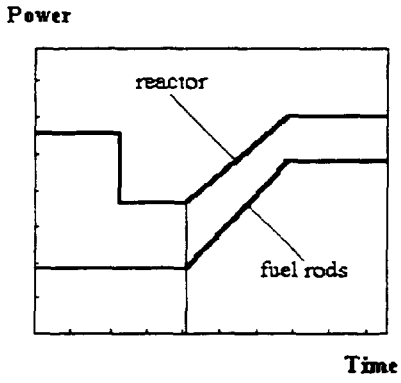

change of fuel rod power by change of reactor power.

"slow" power ramps

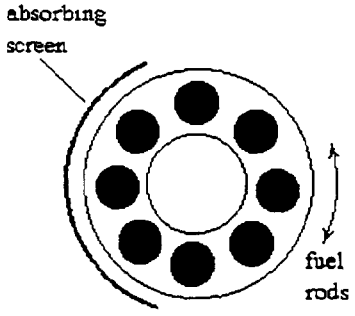

turning of a rig about absorbing screen

"fast" power ramps; prolonged tests with cyclic power change

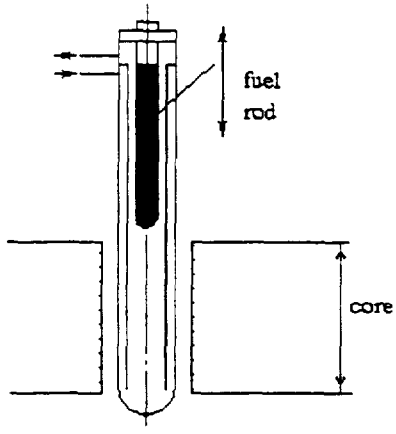

moving of fuel rod through the generated area with high neutron flux

pulsing changes of fuel rod power

Fig. 4 Methods of power change during tests

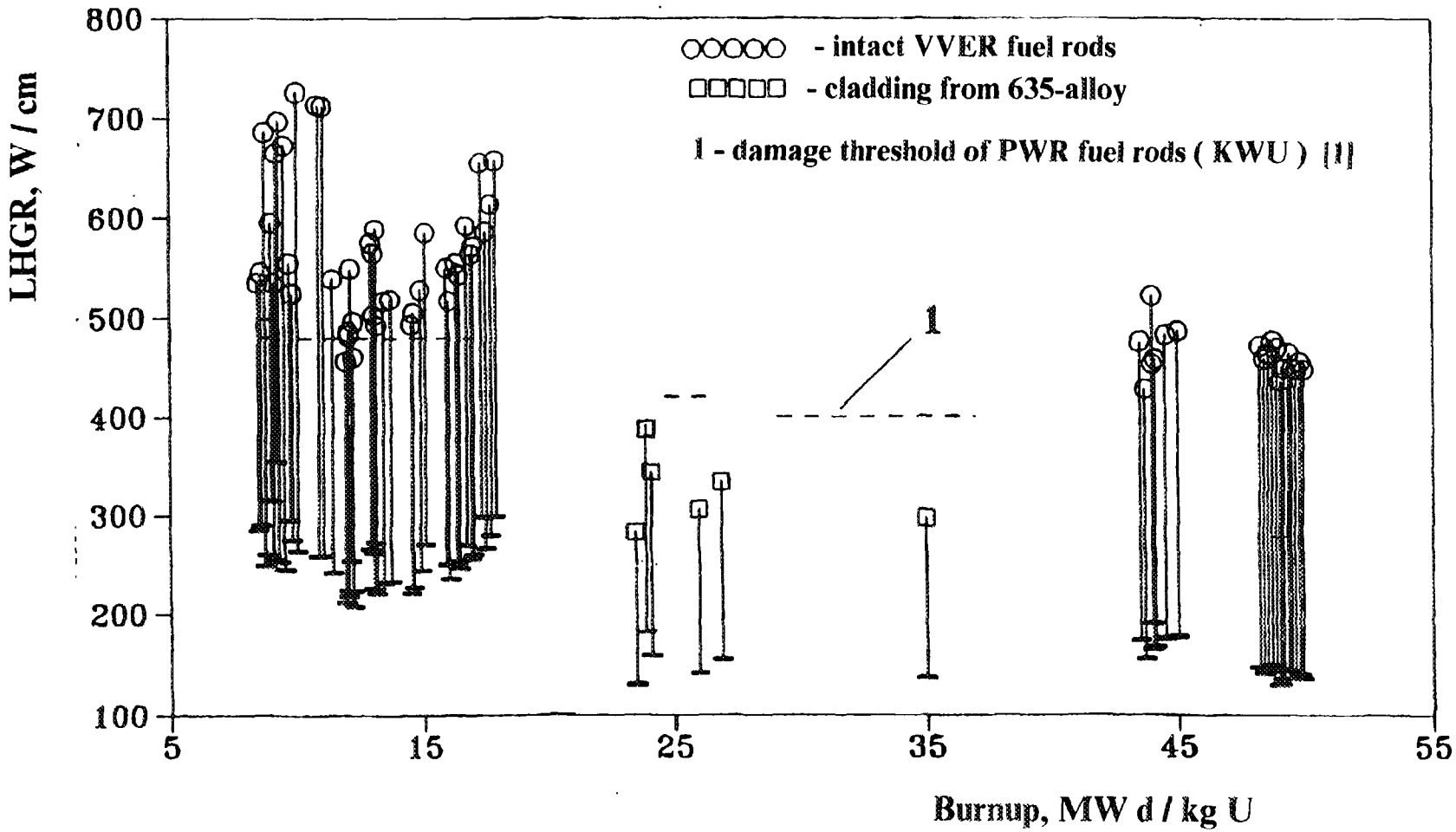

Fig. 5 Power RAMP tests in reactor MIR

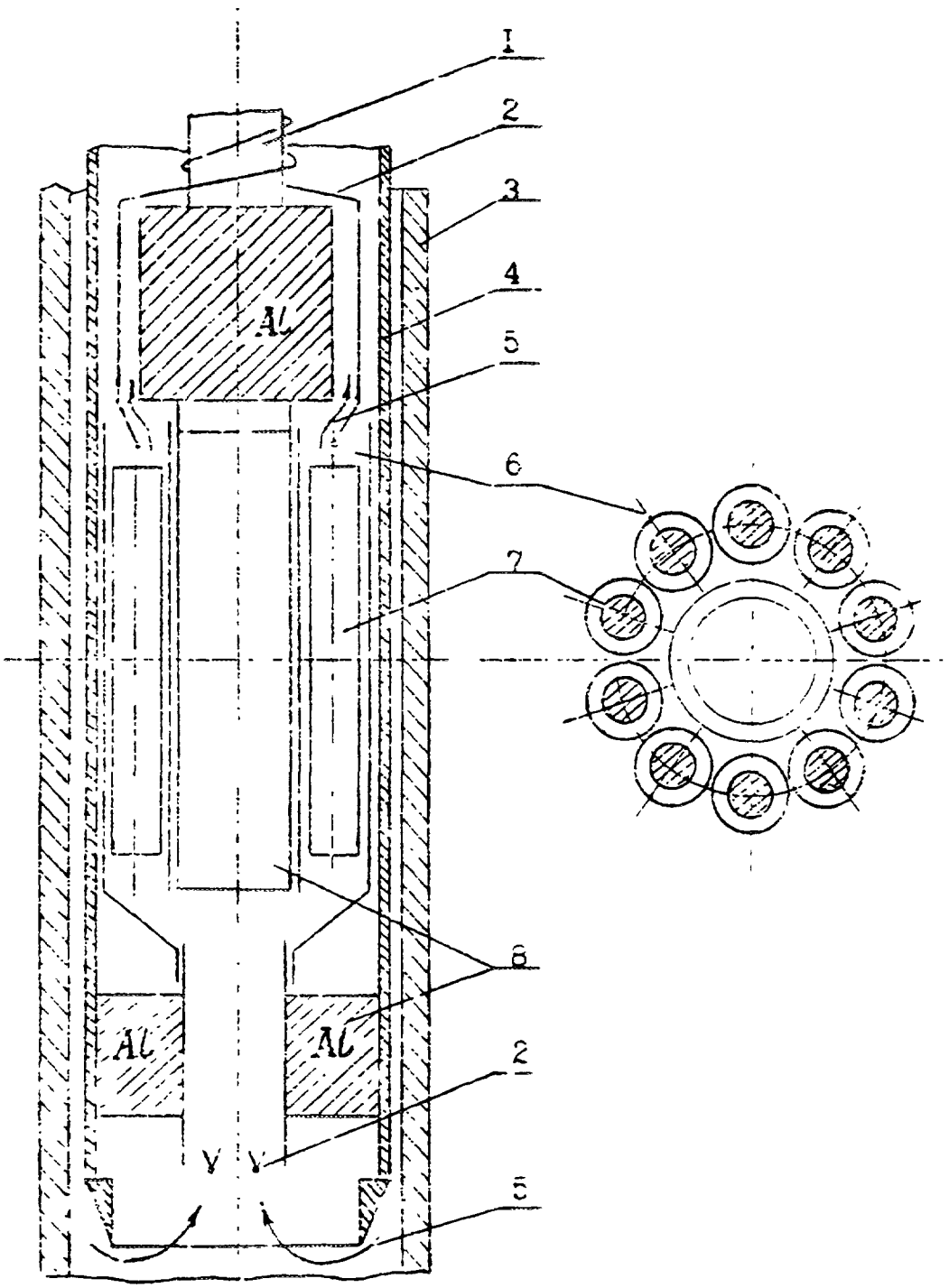

Fig. 6 The "TEST-1" irradiated rig

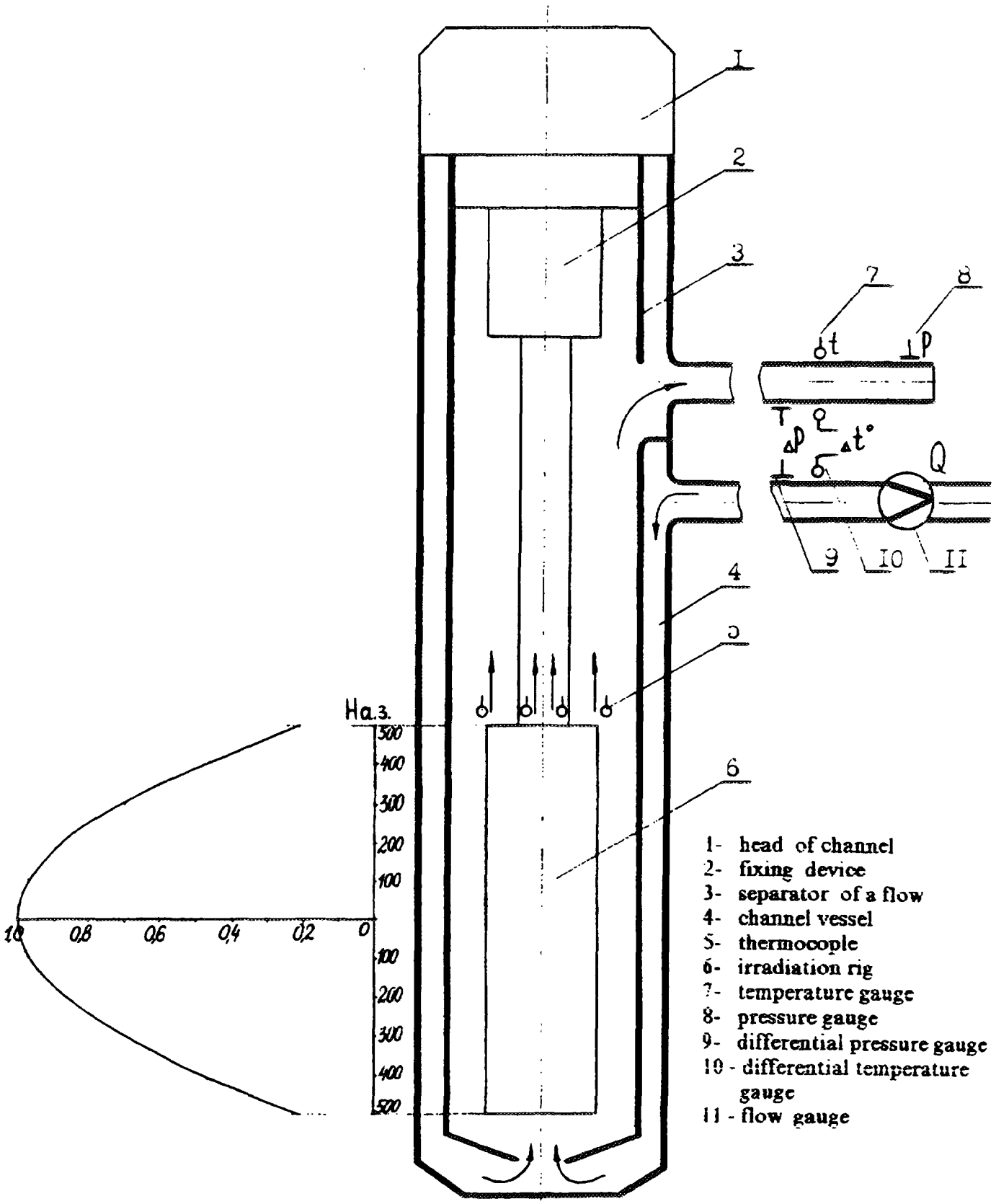

Fig. 7 Scheme of an irradiation rig accommodation in a loopback channel

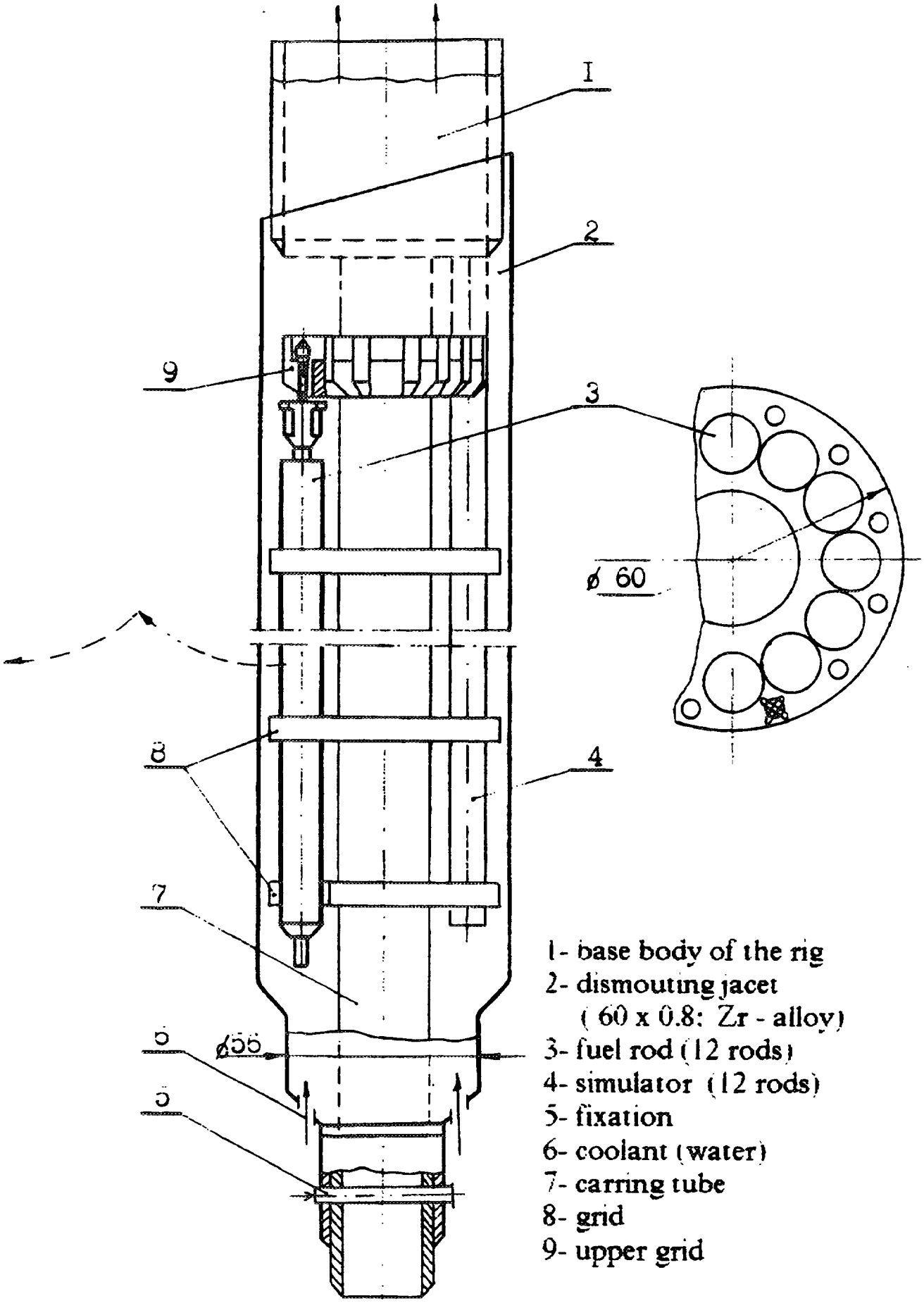

Fig. 8 The KMT irradiation rig

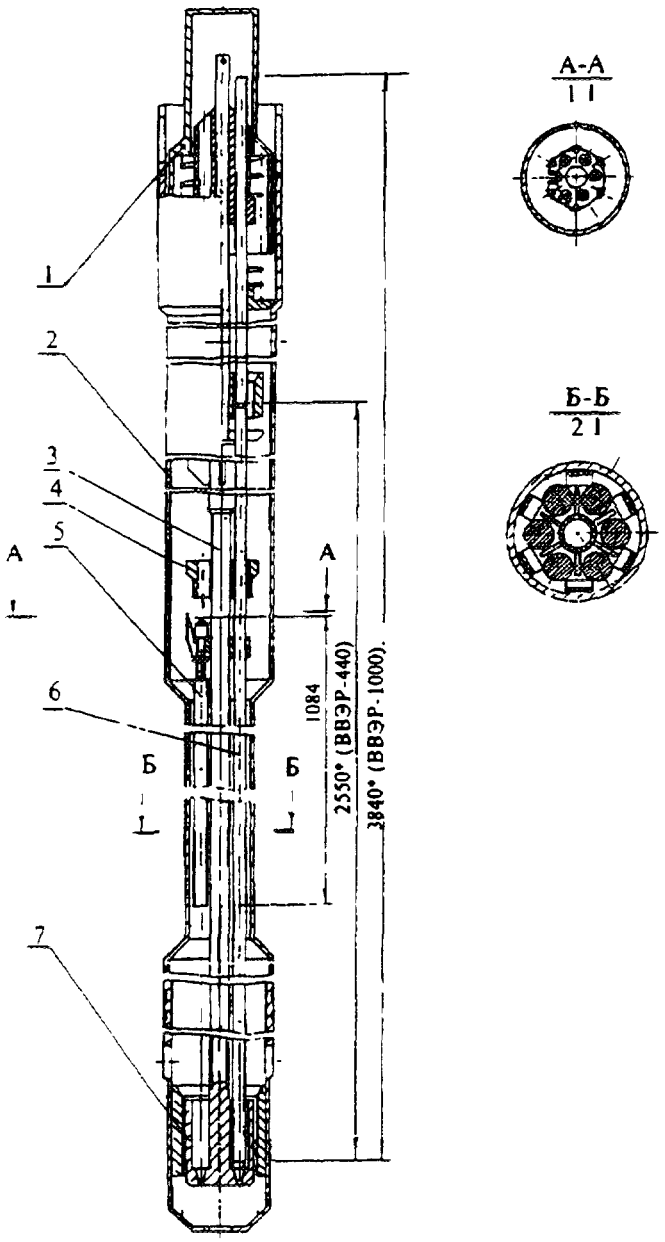

Fig. 9

Irradiation rig for test of refabricated and full-scale fuel rods:
1 - cowl; 2 - vessel; 3 - rod; 4 - leading grid; 5 - refabricated fuel rod; 6 - full-scale fuel rod; 7 - bed.

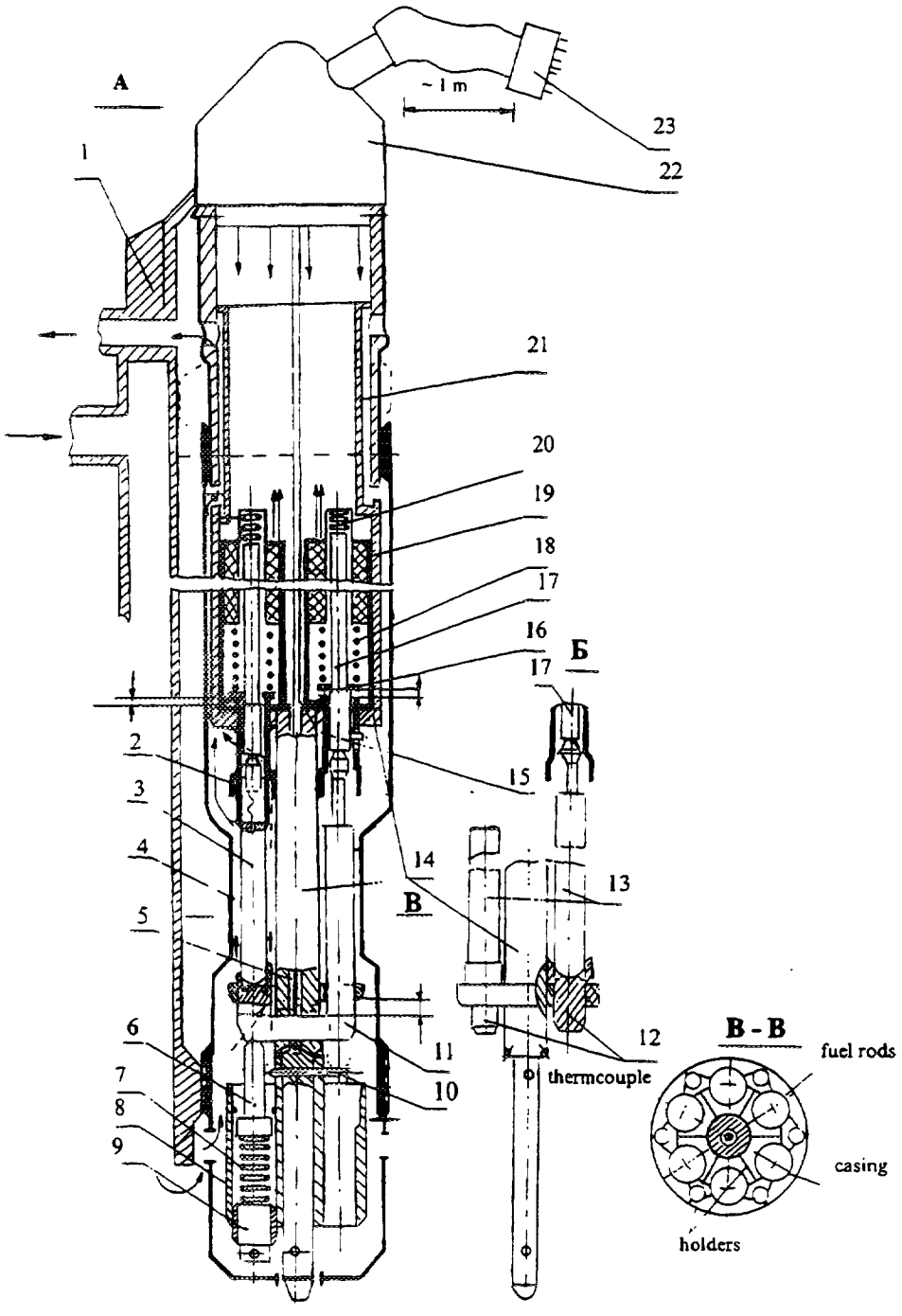

Fig. 10 The "GR" irradiated rig:
1- body of channel; 2 - case of gauge; 3 - fuel rod with pressure transducer; 4 - casing; 5 - thermocouple(input); 6 - pusher; 7 - spring; 8 - support demountable; 9 - screw; 10 - rod; 11 - Zr - rod; 12 - emphasis demountable; 13 - fuel rods; 14 - rig; 15 - thermocouple (output); 16 - ring; 17 - core; 18 - fixing spring; 19 - coil; 20 - spring of core; 21 - direction screen; 22 - head of channel; 23 - joint.

The simultaneous experiment with refabricated and full-scale fuel rods can determine difference in their behaviour. The full-scale fuel rods of VVER assemblies are used after nondistructive investigations of assembly in RIAR. In RIAR prepare the refabricated fuel rods are prepared from the same fuel rods.

The dismountable assembly with refabricated fuel rod is shown in fig. 10 The assembly has gauge of linear movement. The transducer of gas pressure into linear movment is located on the top of fuel rod. This assembly is used for several experiments. In this case the replacement of fuel rods is performed. Gas pressure and change of fuel rod length is simultaneously measured by this assembly Thermocouples are located at input and output from assembly .The experiment with such assembly is scheduled to perform at the beginning 1996. VVER refabricated fuel rods will be tested at the burnup of 50-60 MW · day / kg U.

As follows from the paper the equipment permits to test several various fuel rods in one assembly simultaneously It provides a good statistics with using a little number of experiments.

REFERENCE

1. M. Gartner and G Fisher. Survey of the power ramp performance testing of KWU's PWR UO_2 fuel. J. of nuclear materials. v. 149 (1987), p 29-40

HIGH-TEMPERATURE INTERACTION OF FUEL ROD CLADDING MATERIAL (Zr1%Nb ALLOY) WITH OXYGEN-CONTAINING MEDIUMS

Yu.K. BIBILASHVILI, N.B. SOKOLOV,
L.N. ANDREYEVA-ANDRIEVSKAYA, A.V. SALATOV
All-Russian Institute of Inorganic Materials,
Moscow

A.M. MOROZOV
JSC VTI, Moscow

Russian Federation

XA9743292

Abstract

The experimental data on kinetics of Zr1%Nb alloy oxidation in steam at atmospheric pressure in the temperature range 550 to 1600 °C are presented.

The effect of fuel rod claddings deformation on zirconium alloy interaction with steam is shown.

The estimates of influence of the additives of air, nitrogen and hydrogen in mixtures with steam at atmospheric pressure on kinetics of steam/zirconium reaction in the temperature range 800 to 1200 °C are presented.

The correlations for determination of weight gain with indication of area of applicability in space of parameters (temperature, time, deformation, pressure) are shown.

1. Introduction

The interaction of cladding material with oxygen-containing mediums is one of the main reasons of fuel rod damage in accidents accompaned by a fuel rod claddings temperature rise. Investigation of chemical interaction of fuel rod cladding material (Zr1%Nb alloy) with steam but also with steam mixtures with air, oxygen, nitrogen and hydrogen is important for determination and account for influence of the following factors:

- reduction of initial thickness of cladding metal,
- embrittlement of cladding material,
- energy release in the form of heat in steam/zirconium reaction (possibility of uncontrolled temperature rise in the active zone),
- hydrogen generation.

2. Oxidation in Steam at Atmospheric Pressure

By now, a large array of the results of experimental investigations of high-temperature oxidation kinetics of Zr1%Nb alloy VVER fuel rod claddings has been generated.

Some experimental data were submitted early in [1, 2, 3].

There are some methods of realization of such experiments. A special attention at development of the methods was paid on the following factors:

- accuracy of measurement of specimen temperature inspite of formation of oxide films of significant thickness and possible deformation of the specimen;
- quality of the steam (or other oxygen-containing medium) should not be changed during the experiment;
- possibility of establishing of isothermal conditions with given pressure and steam flow rate.

The oxidation of zirconium in steam is an exothermal reaction

$$Zr + 2H_2O \rightarrow ZrO_2 + 2H_2 + Q .$$

The reaction can become self-supporting at high temperatures, i.e. only at the expence of allocation of heat Q the reaction can proceed before complete transformation of Zr to ZrO_2.

2.1. Temperature Range 550 to 1300 °C

The buik of the data has been obtained on experimental rigs with well-thermostated work sections [1 - 6]. A great number of experimental data is recived on the rig with continuous recording of speciment weight gain during the steam/zirconium reaction [4].

Investigations of oxidation kinetics were performed with specimens 10, 30 and 60 mm length (in experiments on investigation of deformation influence) cut from VVER-type tubes. The temperature was measured by Pt - Pt/Rh thermocouples located in immediate proximity of the specimen.

As a measure of the reaction W the specimen weight gain was used. Thicknesses of layers of interaction of cladding material with steam (layer of ZrO_2, α-Zr stabilized by oxygen) were determined metallographically. Using weight gain as a measure of steam/zirconium reaction is more preferable due to possible spalling off oxide films but also not quite precisely determined thickness of α-Zr(O) layer (Fig. 1).

Duration of experiment for test temperatures above 700°C was from several seconds till 10 hours. The experiments lasted up to few tens of hours or lower values of test temperatures.

The smoothed curves "weight gain - time" obtained on the rig with continuous recording of specimen weight gain [4] (at temperatures above 700° C), and unpublished data received in autoclave long duration tests at temperatures 550, 600, 650°C) are presented in Fig. 2. Experimental data presented in Fig. 2 correspond to obtained average weight gains values.

Application of technique of continuous specimen weighting [4] in investigation of Zr1%Nb alloy oxidation has revealed existence of inflections on the "weight gain - time" curve. Metallographic investigations have confirmed the fact that oxidation acceleration is connected with spalling of oxide films ("breakaway"). A transition from parabolic to linear oxidation law has been observed at considerable exposure times at temperatures 700 to 850°C,. It is too complicated to approximate total oxidation kinetics curve, having inflections by a single dependence. Therefore the following approach was realized for selection of dependences. Oxidation kinetics in pre-inflection period is fairly described by parabolic dependence of the reaction measure on time. For post-inflection period of intensive destroying oxidation a linear dependence is chosen. Valuation of the transition time from parabolic to linear oxidation is the most important problem in determination of kinetic dependences.

On the basis of analysis of experimental data dependences describing Zr1%Nb alloy oxidation kinetics were obtained. A parabolic dependence is used for design estimates of oxidation kinetics of fuel rod in accidents of LOCA type

$$W^2 = K_p \tau \qquad (1)$$

where: $W = \Delta m / A$ - specific weight gain, mg/cm^2
K_p - reaction constant,
τ - time, s.

Dependence (1) for the temperature range 550 to 1200 °C has the form

$$\Delta m/ A = 920 \exp (-10410/T) \tau^{0,5} \qquad (2)$$

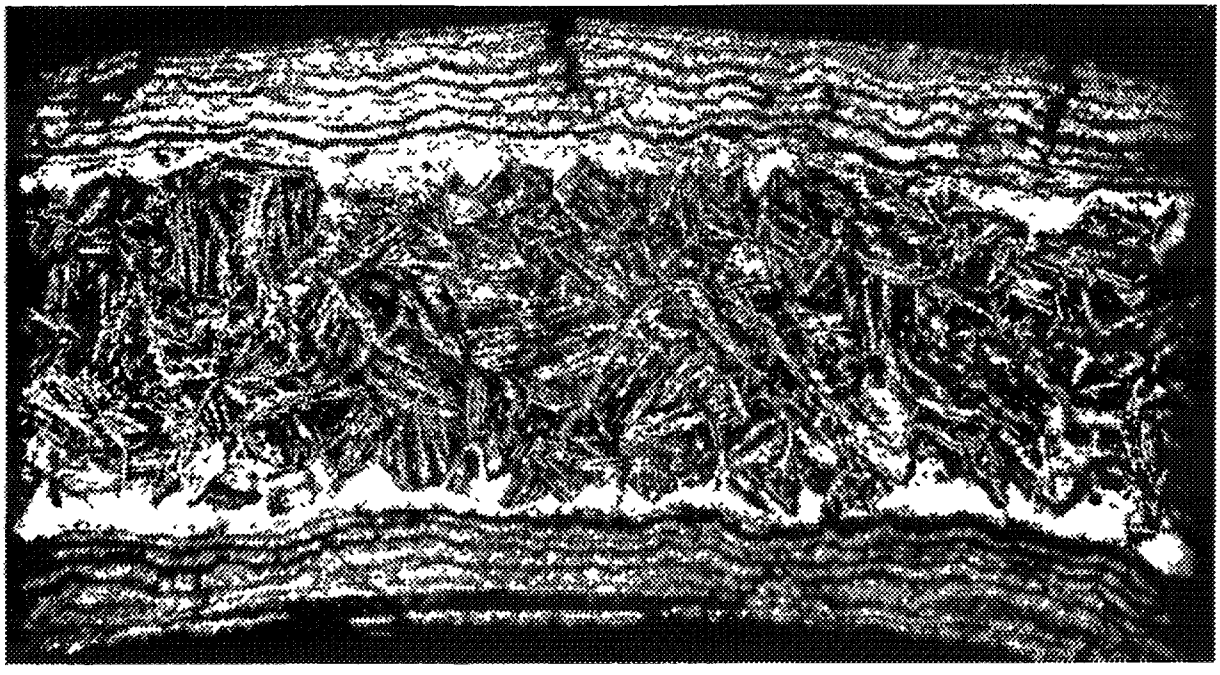

Temperature - 925°C. Exposure time - 9341 s. Weight gain - 24,06 mg/cm².

Fig.1 Microstructure of steam oxidized specimen

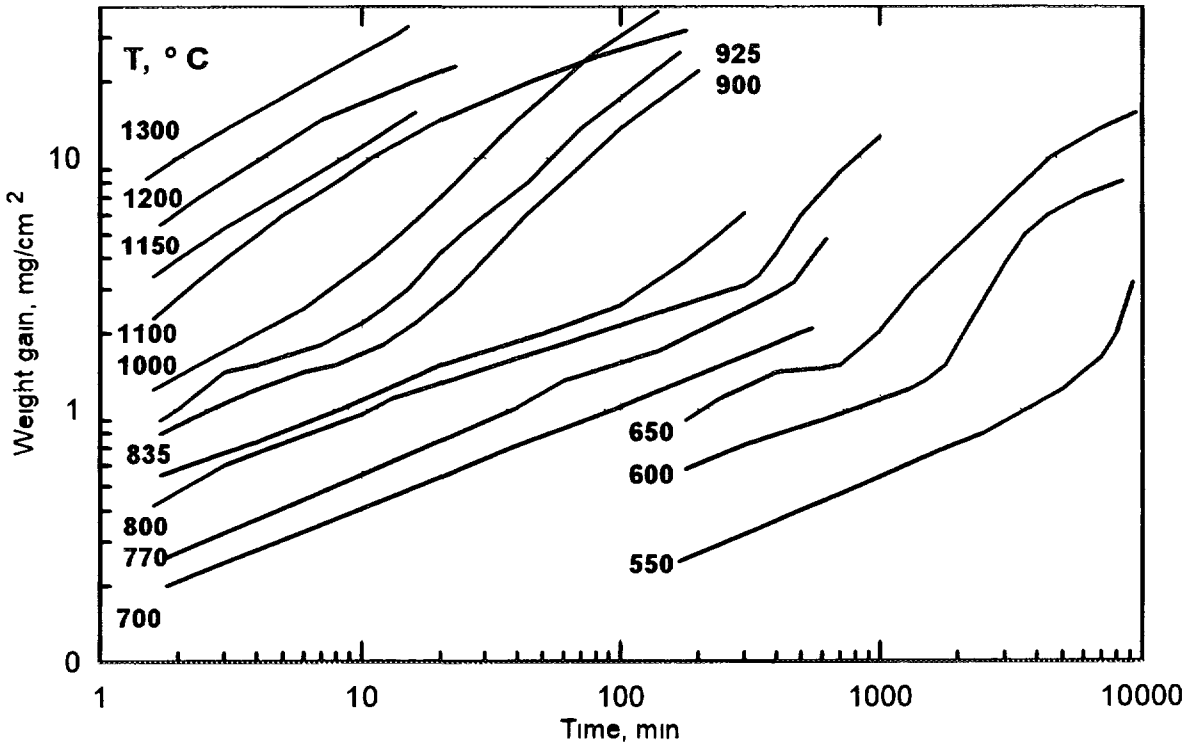

Fig. 2 Weight gains of VVER-type claddings oxidized in steam at atmospheric pressure

where: T - temperature, K
τ - time, s.

The dependence (2) is conservative at the following temperature/time parameters:
temperature range 550 to 650° C and time of interaction up to 10 hours;
temperature range 900 to 1100 ° C and time of interaction up to 900 seconds.

The multi-layered oxide films are formed at temperatures 900 to 1100 °C and isothermal exposures up to 900 s. Film spalling is possible accompanying by enhancing of reaction breakaway. However, the experimental data have shown that the transition from parabolic to linear oxidation law does not occur for this temperature/time range. Correlation (2) is conservative and for the case of spalling films in the specified limits.

Formation of multi-layered spalling-off oxide films is also characteristic at the temperature range 700 to 850 °C and interaction time up to 10 hours. The experimental data have revealed transition to destroying oxidation. The moment of transition from parabolic to linear oxidation is described for a conservative correlation by the following dependence
temperature range 700 to 850° C, time of exposure up to 10 hours

$$\tau = 7.867 \cdot 10^{7} / T - 44856,$$

where: T - temperature, K
τ - time, s.

After transition the kinetics is described by the dependence

$$\Delta m / A = 18.4 \exp (-11706/T) \tau$$

2.2. High -Temperature Oxidation

The research of chemical interaction of fuel rod cladding material with steam at temperatures above 1300°C is important for analysis of accidents with severe fuel damage from the viewpoints of:

- the energy released during steam/zirconium reaction;
- rate of the reaction;
- hydrogen generation.

In order to carry out such experiments a rig with indirect specimen heating in furnace made from high-temperature ceramics on the basis of aluminium oxide was built. The specimens tested were cut from VVER-type tubes. The experiments were performed at a constant temperature in steam at atmospheric pressure. The reaction rate was measured with hydrogen technique which provides continuous recording of hydrogen generation. The hydrogen technique was supplemented by specimen weighting in the end of the experiment but also by metallographic researches.

The analysis of experimental data has shown that stepwise increase in oxidation rate for Zr1%Nb alloy occurs at the temperature of 1500 °C. It is explained that at the temperature of 1500° C there is transition of ZrO_2 modification from tetragonal to cubic.

Data of experiments have shown that oxidation kinetics is described by parabolic law (1). As measure of the reaction, specific zirconium consumption was used

$$W = \Delta m_{Zr} / A , \qquad mg/cm^2 .$$

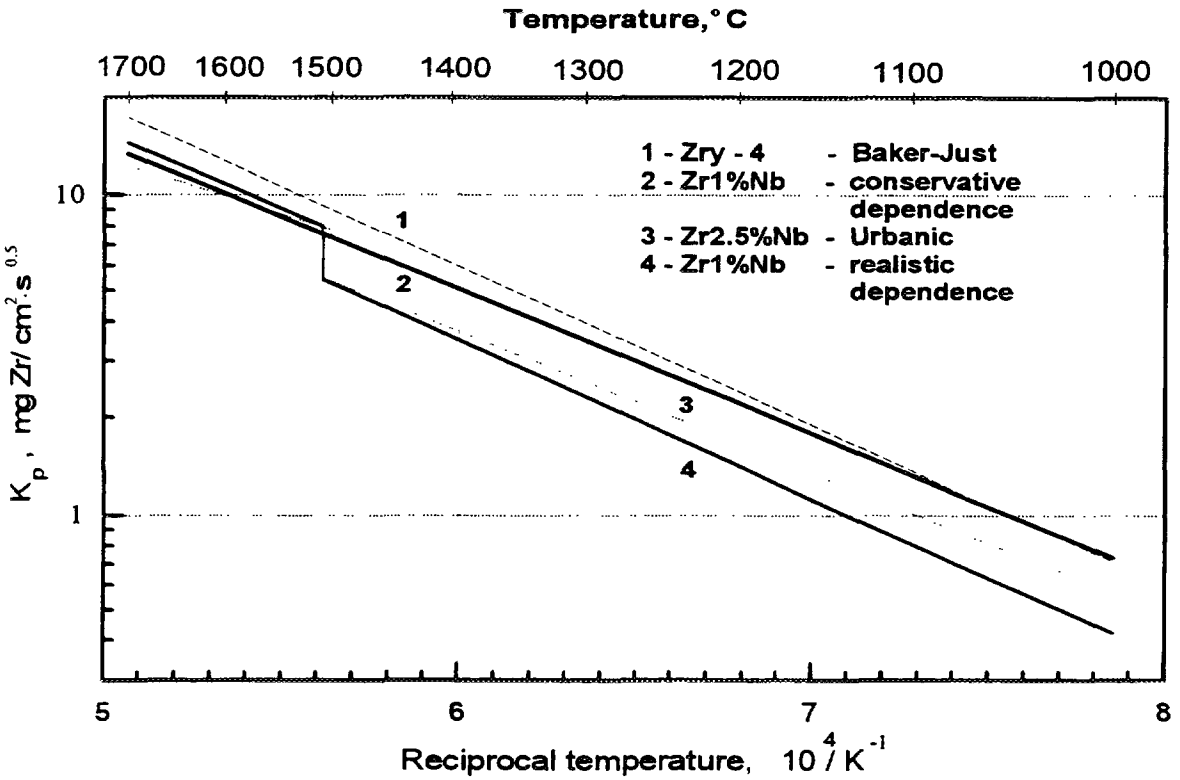

Fig.3 Temperature dependence of the rate reaction constants K_p for zirconium alloys

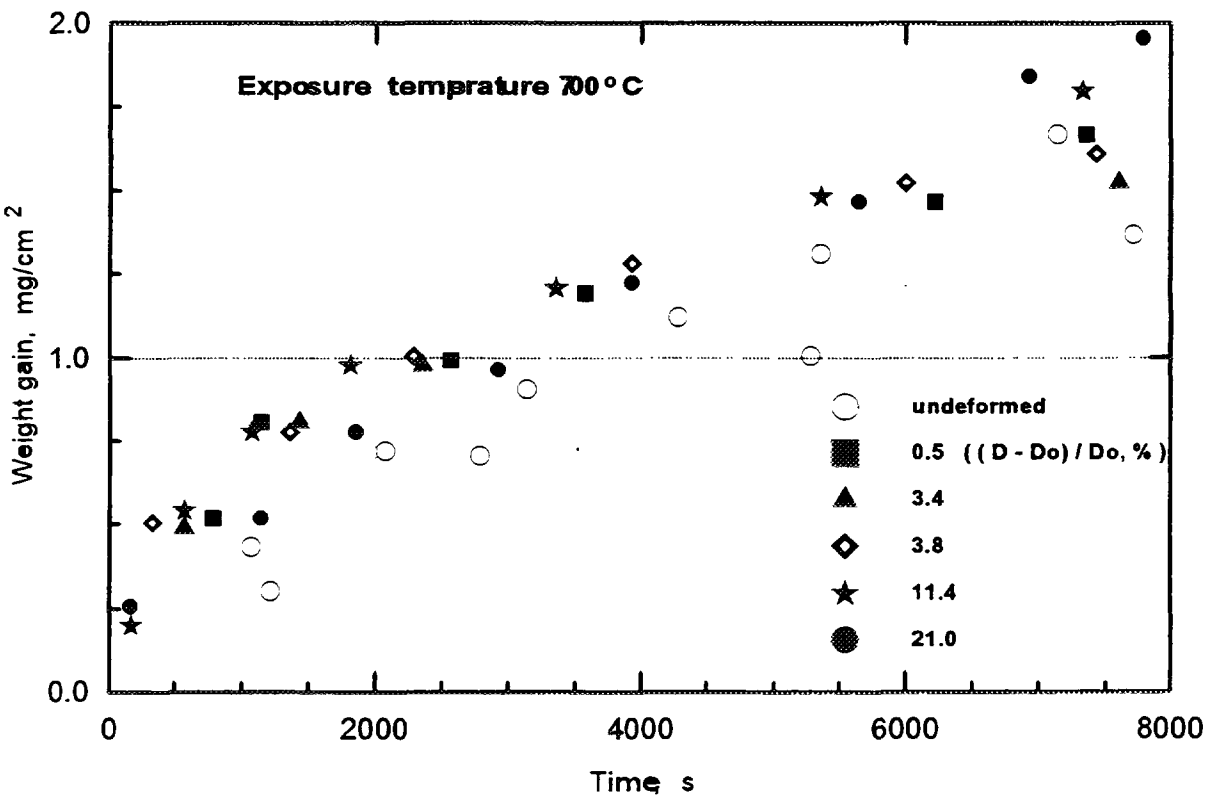

Fig.4 Weight gain of specimens on isothermal exposure in steam

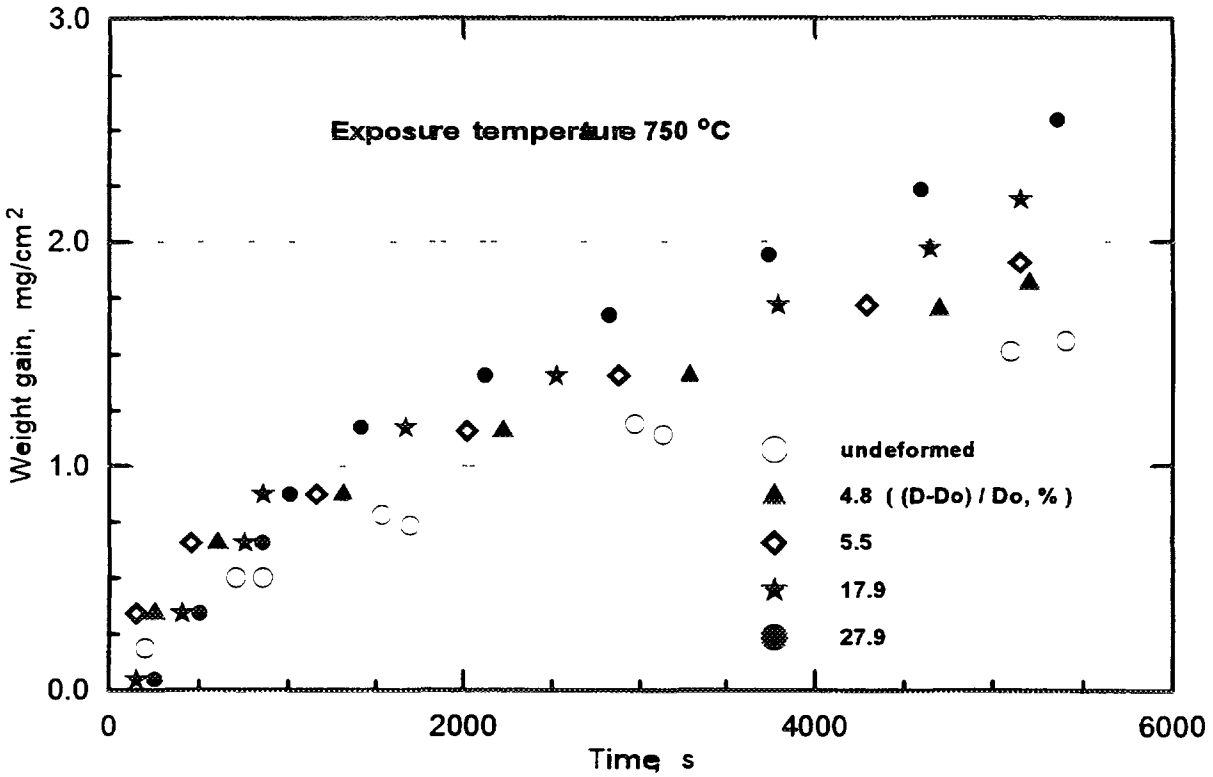

Fig.5 Weight gain of specimens on isothermal exposure in steam

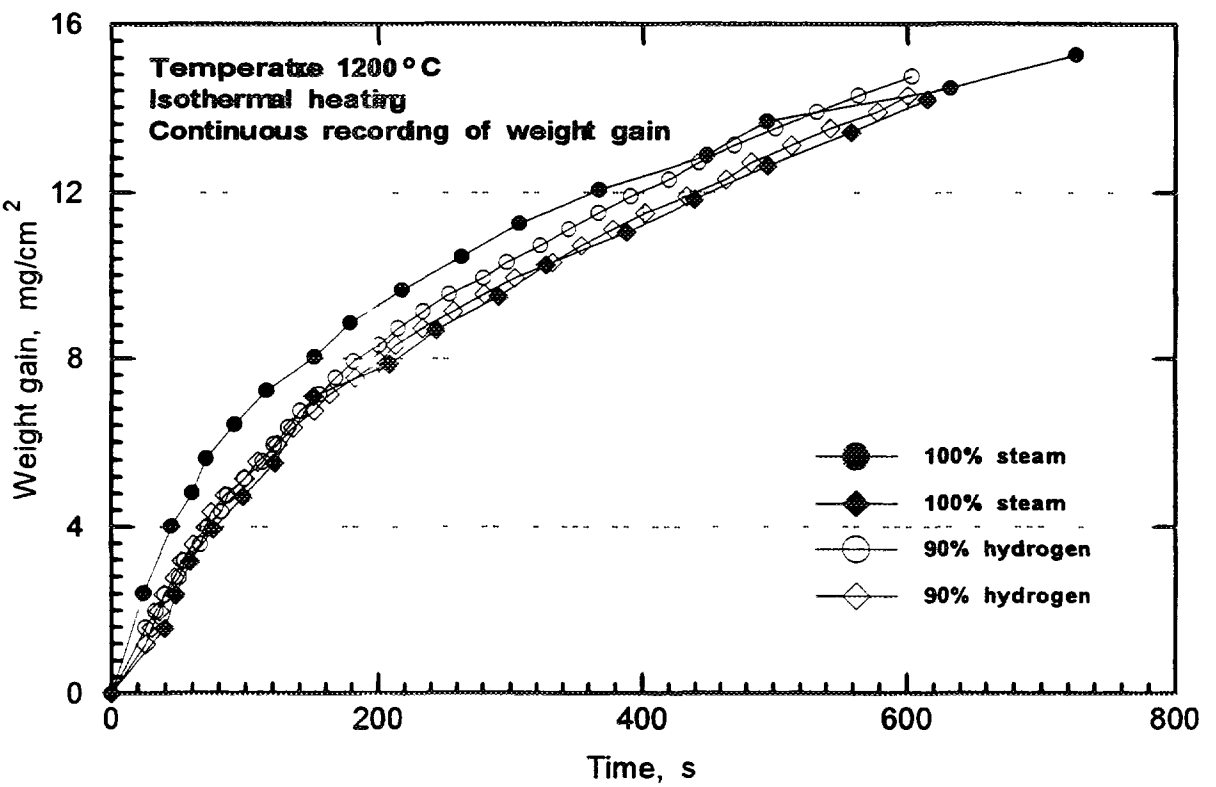

Fig.6 Oxidation kinetics of Zr1%Nb alloy specimens in steam and mixture hydrogen/steam

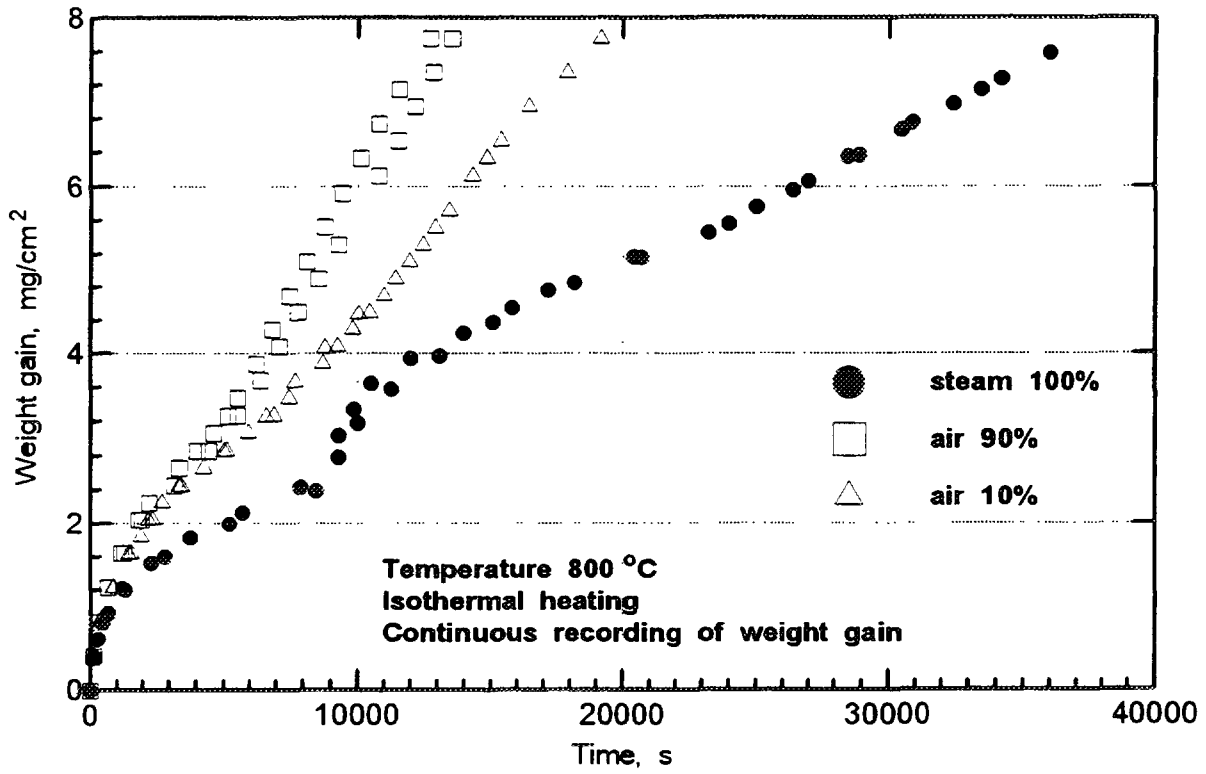

Fig.7 Oxidation kinetics of Zr1%Nb alloy specimens in steam and air/steam mixture

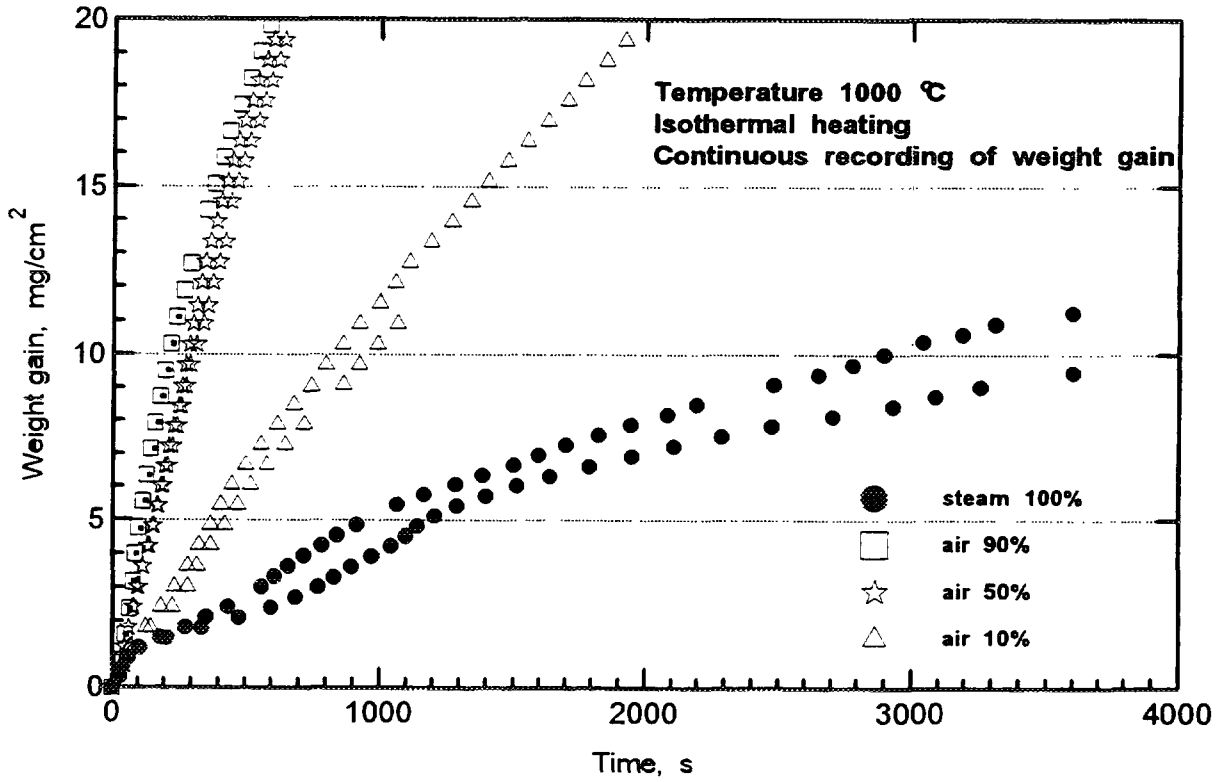

Fig.8 Oxidation kinetics of Zr1%Nb alloy specimens in steam and air/steam mixture

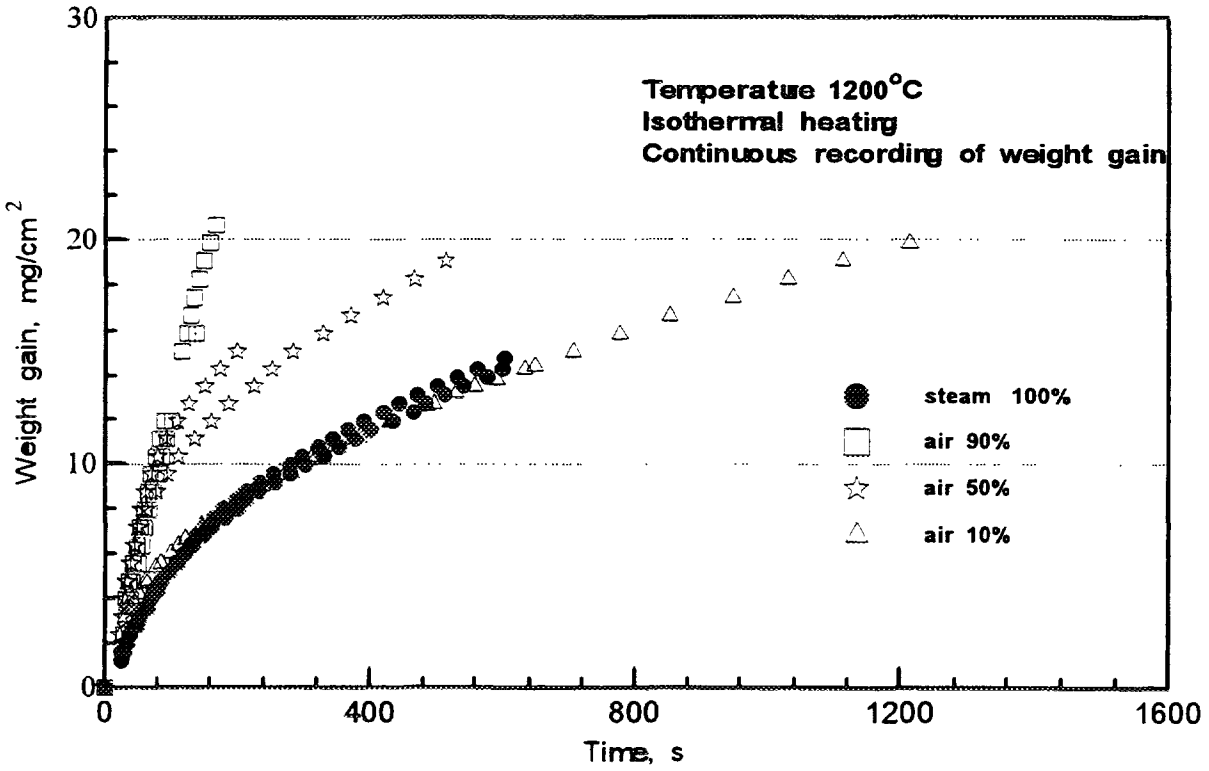

Fig.9 Oxidation kinetics of Zr1%Nb alloy specimens in steam and air/steam mixture

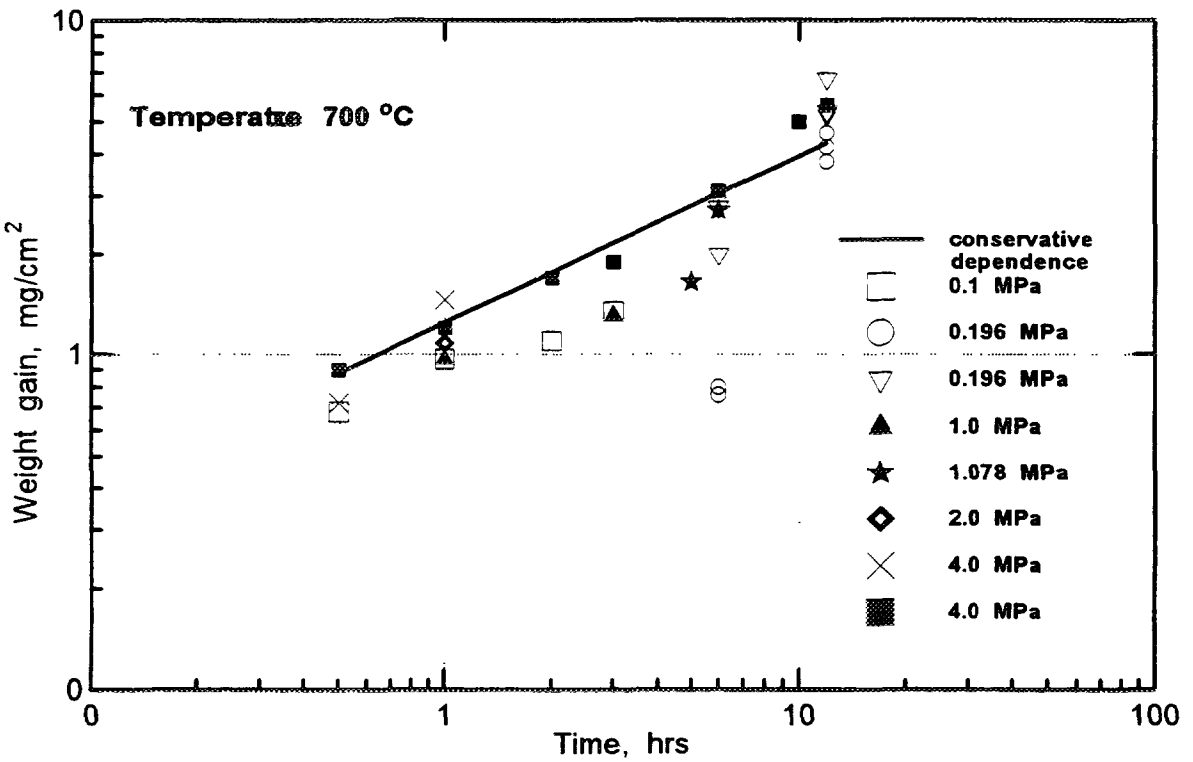

Fig.10 Weight gain of Zr1%Nb alloy fuel rod claddings at oxidation in steam at elevated pressure

The dependence for describing oxidation kinetics at high temperatures has the following form

at temperatures 1300 to 1500° C

$$K_p = 1.292 \cdot 10^7 \exp (-23040/T) \qquad (3)$$

at temperatures 1500 to 1600 ° C

$$K_p = 7.98 \cdot 10^6 \exp (-20800/T) \ .$$

The dependence of reaction rate constant (3) is indicated in Fig. 3., Baker - Just correlation for zirconium is also presented in Fig. 3. This relationship is recommended as conservative one for Zircaloy-4 alloy in the temperature range 1000 - 1850° C

$$K_p = 2025 \exp (-11456/T), \quad mg/cm^2 s^{0.5} \qquad (4)$$

The analysis oı the results presented in Fig. 3 showes that experimental data for Zr1%Nb and Zr2.5%Nb alloys (Urbanic [7]) are in a fair agreement.

3. Deformation Effect on Oxidation Kinetics

The experiments on study of influence of deformation on oxidation kinetics of Zr1%Nb alloy fuel rod claddings have shown that pre-straining insignificantly affects alloy oxidation kinetics independently of degree of cold deformation (2 to 10%).

The corrosion tests with simultaneous deformation of a specimen were carried out on pressure-tight specimens (ampoules) - sections of VVER tubes with butt-welded end pieces from Zr1%Nb alloy [5]. The specimens were filled in by inert gas of the necessary pressure. The surface area of the specimen changed, formation of cracks in oxide layer and cladding metal is possible, inner surface of the specimen is oxidized after cladding failure (loss of tightness) during the tests of such type.

The results of experiments at temperatures 700 and 750 °C are presented in Fig. 4 and 5. Specific weight gains were defined in relation to initial non-deformed specimen surfaces, i.e. the data presented in the figures are conservative. Dependence (2) determines cladding weight gain with a certain margin within the time interval up to 900 s.

The analysis of experimental data has shown that in case of cladding deformation weight gains are received large in comparison with weight gains of non-deformed specimens for equal oxidation times. It marked that after cladding failure, i.e. discontinuance of deformation, the difference in weight gain decreases. As appear, the increase in oxidation rate during deformation is explained by formation of cracks in oxide film. It enables to enter the interaction with steam the cladding metal, not yet oxidized.

Thus, one can assert that deformation increases the rate of interaction of cladding material - Zr1%Nb alloy - with steam. The oxidation rate is stabilized after termination of deformation approaching to oxidation rate of non-deformed specimens.

4. Oxidation in Mixtures of Steam with Hydrogen, Air and Nitrogen

The experiments on research of Zr1%Nb alloy oxidation kinetics in application to LOCA-type accidents are usually carried out in the water steam. The effect of hydrogen on kinetics of steam/zirconium reaction is possible due to intensive hydrogen generation. The assumption of possibility of "oxygen hunger" at high content of hydrogen in steam was suggested in the literature data. In non-design basis accidents entering the active zone of significant quantities of air and nitrogen is possible. Investigation of the effect of hydrogen, nitrogen, air additives in mixtures with steam on kinetics of steam/zirconium reaction is

carried out in connection with necessity of the analysis of proceeding of severe accidents conditions.

4.1. Effect of Hydrogen

The hydrogen is generated during steam/zirconium reaction, due to hydrazine decomposition, as a result of oxidation of materials and alloys contained in the active zone but also at water radiolysis under accident conditions, therefore the study of the effect of hydrogen on steam/zirconium reaction rate is important. However, only hydrogen generated during steam/zirconium reaction that can as appear affect the rate of the reaction.

The results of experimental investigation with Zircaloy-4 alloy have shown, that hydrogen renders influence kinetics of steam/zirconium reaction at its volume concentration in mixture with steam exceeding 90%.

The influence of hydrogen on Zr1%Nb alloy oxidation kinetics was investigated at temperatures of isothermal exposure 1000 and 1200 °C.

The volume concentration of hydrogen in steam/hydrogen mixture was 90%. Steam flow rate was 19.7 mg/cm^2/min. The specimen weight gains in function of time for test temperature 1200 °C are presented in Fig. 6.

The conducted tests have not revealed influence of hydrogen on the rate of steam/zirconium kinetics. The amount of steam is sufficient for the steam/zirconium reaction such of intensity rate as in water steam with given concentrations of hydrogen in steam/zirconium mixtures (up to 90%).

4.2. Effect of Air

The experiments on Zr1%Nb alloy specimens oxidation in steam mixtures with air were conducted on the modernized rig with continuous specimen weighing during the experiment. The system of air feeding into rig steam superheater was installed with the help of microprocessor. The air volume concentrations in these experiments were 10%, 50% and 90%. At 90% of air concentration in air/steam mixture steam flow rate was 8.4 mg/cm^2 /min.

The experimental data on weight gain for temperatures 800, 1000 and 1200 °C are presented in Fig. 7 - 9. Data analysis has shown that the availability of air considerably influences on kinetics of cladding material interaction with air/steam mixture. Increasing of air concentration leads to increasing of weight gain at equal exposures. It is marked that all curves are featured by characteristic inflection at temperatures up to 1000 °C. With increase of temperature distinction in weight gains at 10% air concentration mixture and pure steam decreases and for concentrations 50% and 90% is increased.

4.3. Effect of Nitrogen

The study of the effect of nitrogen concentration on oxidation kinetics was carried out according to the same procedure as for air/steam mixtures.

The analysis of experimental results has shown the similarity of Zr1%Nb alloy oxidation kinetics in air/steam and nitrogen/steam mixtures. The oxidation rate in steam mixtures with air or nitrogen is considerably higher than that in pure steam. The increase of reaction rate can be explained by activizing influence of nitrogen. In experiments with nitrogen/steam mixture the transition from parabolic to linear oxidation law occurs earlier than at oxidation in steam.

5. Effect of Steam Pressure

High-temperature oxidation of fuel rod cladding material at various types of accidents can occur both at atmospheric and high pressures of steam.

The experimental data on oxidation in high pressure steam are scarce. The data, obtained for Zry-4 alloy at test temperatures between 750 and 1100° C are known /8-10/. Exposure at 900° C made up to 45 minutes, at 1100° C - not more than 10 minutes. The results of the experiments have shown reducing influence of steam pressure on oxidation kinetics with increasing of temperature. The effect of pressure is considerably reduced at 1000° C , at 1100° C no effect has been observed.

In our country investigation of elevated pressure effect on oxidation was carried out in autoclaves and furnaces at test temperatures between 550 and 1100° C. Steam pressure maintained between atmospheric pressure and 8 MPa. The maximum exposure at test temperatures 1000 - 1100° C made 60 minutes, at 900° C - up to 3 hours, al lower temperatures - up to 10 hours. The experiments were carried out both with and without steam flow rate [6]. However, the experimental results for various flow rates have shown absence of flow rate effect on steam/zirconium reaction kinetics.

The data on weight gains for steam medium at elevated pressure are shown in Fig. 10. The results of calculation according to relation (2) are also plotted in Fig.10. Scatter in the experimental data is observed. The spalling of oxide film due to mechanical interaction of steam with oxidized specimen material could be one of the reasons of the data scatter.

The experimental data revealed a certain effect of elevated steam pressure on the oxidation of Zr1%Nb alloy. Dependence (2) is realistic at test temperatures 550 to 850°C and exposures up to 3 hours, at temperatures 900 to 1000 °C and exposures up to seconds. The null effect of steam pressure influence is observed at temperature 1100 °C.

The effect of steam pressure on oxidation kinetics of Zr1%Nb alloy is marked at higher temperatures and exposures in contrast to Zry-4 alloy.

6. Conclusion

The experimental data on Zr1%Nb alloy oxidation kinetics in atmospheric pressure steam in the temperature range between 550 and 1600 ° C are presented. Oxidation rate acceleration is marked at 1500° C.

The dependences, conservatively describing weight gains for Zr1%Nb alloy claddings of VVER fuel rods at oxidation in atmospheric pressure steam are suggested for the temperature range 550 - 1200 ° C and exposure up to 10 hours.

The deformation of fuel rod cladding enhances the steam/zirconium reaction rate. However, for temperature and time parameters of design accidents is shown, that the recommended dependence is conservative in the case of deformation.

The effect of air and nitrogen concentrations in mixtures with steam on steam/zirconium reaction kinetics is estimated at temperatures between 800 and 1200°C.

The null effect of hydrogen concentration (up to 90% volume) in mixture with steam is marked at temperatures up to 1200° C.

The effect of increased steam pressure (up to 8 Mpa) on fuel rod cladding oxidation kinetics is experimentally shown at temperatures up to 1100° C.

REFERENCES

[1] SOLYANY, V.I., BIBILASHVILI, Yu.K ., TONKOV, V. Yu. High temperature oxidation and deformation of Zr1%Nb alloy claddings of WWER fuels. In OECD-NEA-CSNI/IAEA specialists' meeting on water reactor safety and fission product release in off-normal and accident conditions. Summary report, Riso, Denmark, 16-20 May, 1983, pp. 163-174.

[2] SOLYANY, V.I., BIBILASHVILI, Yu.K ., DRANENKO, V. V., e.a. Steam oxidation of Zr1%Nb clads of WWER fuels in high temperature. In OECD-NEA-CSNI/IAEA specialists' meeting on water reactor fuel element performance and computer modelling. Summary report, Bowness-on-Windermere, UK, 9-13 April 1984. Vienna, 1984, pp. 261-269.

[3] SOLYANY, V.I., BIBILASHVILI, Yu.K ., DRANENKO, V. V., e.a. Characteristics of corrosion behaviour of Zr1%Nb WWER fuel claddings within 700-1000 ° C on long term exposure. In OECD-NEA-CSNI/IAEA specialists' meeting on water reactor safety and fission product release in off-normal and accident conditions. Summary report, Vienna, 10-13 November 1986, Vienna 1987, pp. 98-108.

[4] СОЛЯНЫЙ В.И., БИБИЛАШВИЛИ Ю.К., ДРАНЕНКО В.В. и др. Исследования коррозионного поведения оболочек твэлов из сплава Zr1%Nb в паре при высоких температурах. // Вопросы атомной науки и техники. Серия: Атомное материаловедение, 1988, вып. 2 (27), с. 89-95.

[5] БИБИЛАШВИЛИ Ю.К., СОКОЛОВ Н.Б., ДРАНЕНКО В.В. и др. Кинетика окисления оболочек твэлов типа ВВЭР в интервале температур 700-850 ° С с учетом деформирования под действием избыточного внутреннего давления. // Вопросы атомной науки и техники. Серия: Материаловедение и новые материалы, 1990, вып. 4 (38), с. 56-60.

[6] Ю.К. БИБИЛАШВИЛИ., Н.Б. СОКОЛОВ, В.С. МАРКЕШИН, О.П. ТАРАКАНОВ Влияние давления водяного пара на кинетику окисления оболочек твэлов типа ВВЭР в интервале температур 700-850 ° С. // Вопросы атомной науки и техники. Серия: Материаловедение и новые материалы, 1991, вып. 2 (42), с. 39-40.

[7] URBANIC, V.F. Oxidation of zirconium alloys in steam at 1000 to 1850 ° C. Zirconium in the Nuclear Industry, ASTM STP 633, 1977, pp. 168-181.

[8] PAWEL, R.E., CATHCARD, J.V., CAMPBELL, J.J. The oxidation of zircaloy-4 at 900 and 1100 ° C in high pressure steam // Journal of Nuclear Materials, 1979, v. 82, pp. 129-139.

[9] VRTILKOVA, V., VALACH, M., MOLIN, L. Oxiding and hydriding properties of Zr1%Nb cladding material in comparison with zircaloys. Technical committee meeting on influence of water chemistry on fuel cladding behaviour. Rez, Czech Republic, 4-8 October 1993.

[10] BRAMWELL, I., HASTE, T., WORSWICK, D., PARSONS, D. An experimental investigation into the oxidation of zircaloy-4 at elevated pressures in the temperature range 750-1000 ° C. AEA-RS-5438.

FUEL BEHAVIOUR IN LOCA CONDITIONS

(Session B)

Chairmen

P. BALAKRISHNA
India

N.B. SOKOLOV
Russian Federation

BWR FUEL CLAD BEHAVIOUR FOLLOWING LOCA

S.M. CHAUDHRY, K.N. VYAS, R. DINESH BABU
Bhabha Atomic Research Centre,
Trombay, Bombay, India

Presented by P. Balakrishna

Abstract

Flow and pressure through the fuel coolant channel reduce rapidly following a loss of coolant accident. Due to stored energy and decay heat, fuel and cladding temperatures rise rapidly. Increase in clad temperature causes deterioration of mechanical properties of clad material. This coupled with increase of pressure inside the cladding due to accumulation of fission gases and de-pressurization of coolant causes the cladding to balloon. This phenomenon is important as it can reduce or completely block the flow passages in a fuel assembly causing reduction of emergency coolant flow.

Behaviour of a BWR clad is analyzed in a design basis LOCA. Fuel and clad temperatures following a LOCA are calculated. Fission gas release and pressure is estimated using well established models. An elasto-plastic analysis of clad tube is carried out to determine plastic strains and corresponding deformations using finite-element technique. Analysis of neighbouring pins gives an estimate of flow areas available for emergency coolant flow.

1. INTRODUCTION

India has two BWR units at TAPS (Tarapur Atomic Power Station). The units have a capacity of 210 MWe each. The plant design is by General Electric of USA and belongs to an earlier generation of GE BWRs. Unlike modern BWRs, TAPS continues to use 6X6 type of fuel assembly with comparatively higher heat ratings. As the stored energy is higher, the clad temperatures tend to be higher during LOCA. This may cause clad ballooning, inspite of lower internal gas pressures. This paper describes calculations of clad surface temperatures during design basis LOCA and subsequenly clad deformations.

Table-I gives salient data of the TAPS fuel.

2. THERMAL HYDRAULICS ANALYSIS DURING LOCA[1]

Fig-1 shows the schematic of the BWR plant. As shown in the figure, the basic system consists of primary feed water entering the reactor through the feed water sparger. The water flows down, enters the reactor core and gets heated. Steam is taken out from the top via steam separator. The separated water also flows down and passes through recirculation loop consisting of a recirculation pump and secondary steam-generator. It mixes with the primary feed water at the bottom of the reactor pressure vessel. The design basis LOCA is the recirculation line break. Subsequent to LOCA , the core cooling is achieved by two independent, full capacity, core spray systems, which pump water directly on to the fuel assemblies in form of fine droplets.

During LOCA the scenario is as follows:

i) Recirculation line breaks resulting into depressurization of reactor vessel.
ii) During initial stages of LOCA, convective heat transfer co-efficients are relatively large.
iii) However, the heat transfer co-efficients drop rapidly within a period of 12 seconds to a very low value, and the fuel decay heat is transferred only by radiation.

TABLE I. SALIENT DATA OF TAPS FUEL

Fuel assembly configuration	6X6
Cladding outer diameter, mm	14.3
Cladding inner diameter, mm	12.52
Pellet diameter, mm	12.27
Active fuel length, mm	3613
Fuel element pitch, mm	17.81
Fill gas pressure, MPa	0.35
Peak linear heat rating, W/cm	550
Peak heat flux, W/cm^2	123

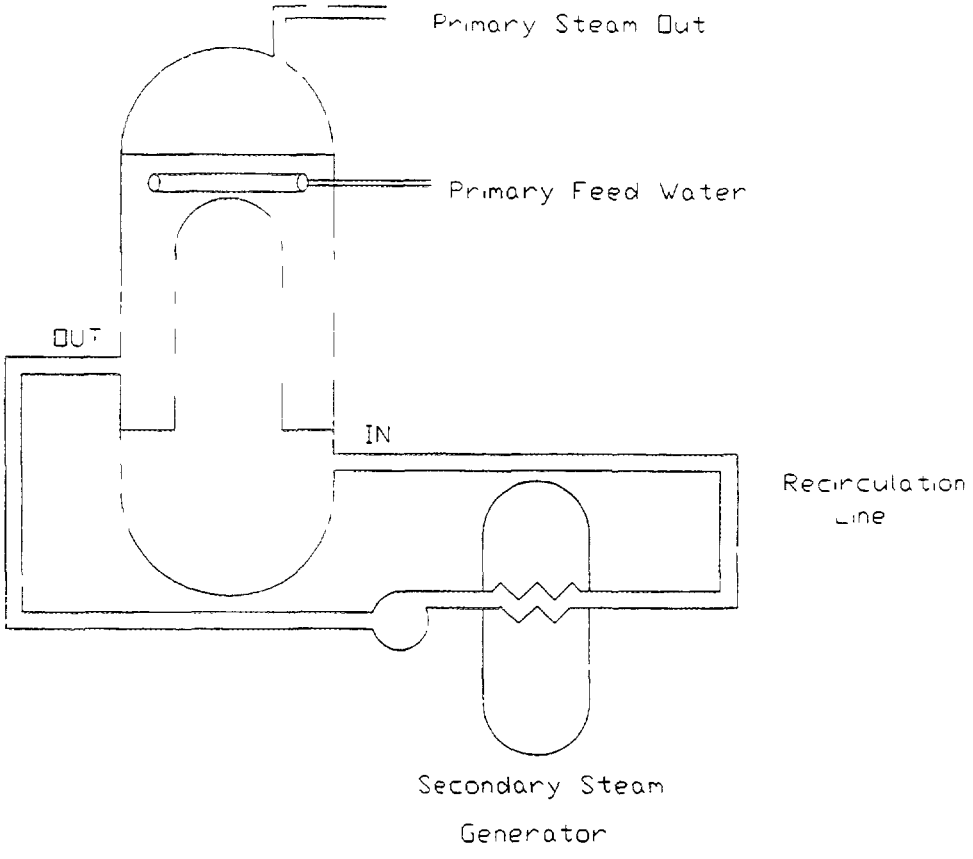

FIG. 1. BWR plant schematic.

iv) After 40 seconds, the core spray starts delivering full flow. This delay takes into account the time of reactor depressurization, core spray pump start-up and system valve opening times. As a result heat transfer improves.

v) After about 200 seconds, the fuel rewetting takes place and hence clad surface temperatures tend to fall.

For analysis a computer code HANU was developed and used for determining fuel clad temperature profile under LOCA. The code solves one dimensional heat conduction equation for a cylindrical geometry.

$$V_n \rho_n Cp_n \frac{dTn}{ds} = Q_n + S_n K_n \frac{dT_n}{dR} - S_{(n-1)} K_{(n-1)} \frac{dT_{(n-1)}}{dR}$$

TABLE II. GREY BODY SHAPE FACTORS USED FOR ANALYSIS

Source	Sink	Grey body shape factor (Source→Sink)
Rod Type 1	Channel	0.28
Rod Type 2	Channel	0.18
Rod Type 2	Rod Type 3	0.15
Rod Type 3	Rod Type 4	0.11

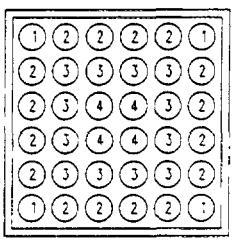

where,

Vn - Volume of n^{th} zone
ρ_n - Material density in the n^{th} zone
Cp_n - Material specific heat in the n^{th} zone
K_n - Material thermal conductivity in the n^{th} zone
S_n - Annular surface area in the n^{th} zone
R - Radius
T - Temperature
Q_n - Heat generated in the n^{th} zone

having the boundary conditions,

$$dT/dR_{(R=0)} = 0 \quad \text{and} \quad dT/dR_{(R=R0)} = h(T_n - T_w)/-K_n$$

where,

h - heat transfer co-efficient
Tw - Sink temperature

For evaluation of heat transfer co-efficient by radiative mode grey body shape factors shown in Table-II are used.

Fig-2 shows the clad surface temperature variation upto a period of 1000 seconds.

3. FUEL PERFORMANCE ANALYSIS

3.1 FUEL PERFORMANCE ANALYSIS DURING STEADY STATE

Fuel performance analysis is done using computer code COMTA[2] . It is a code which takes into consideration the heat genration profile as a function of burn-up till end of life. It also takes into consideration the axial flux profile along the length of the fuel element. The code performs one

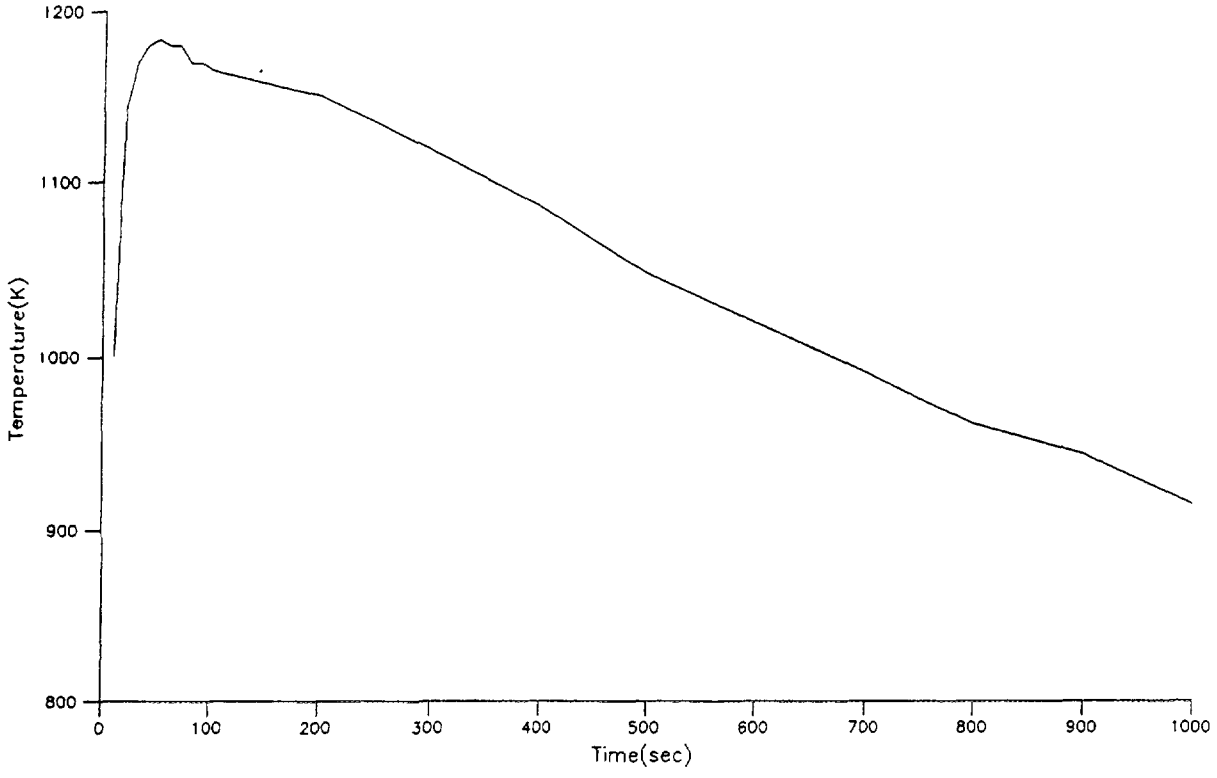

FIG. 2. Clad surface temperature variation during LOCA.

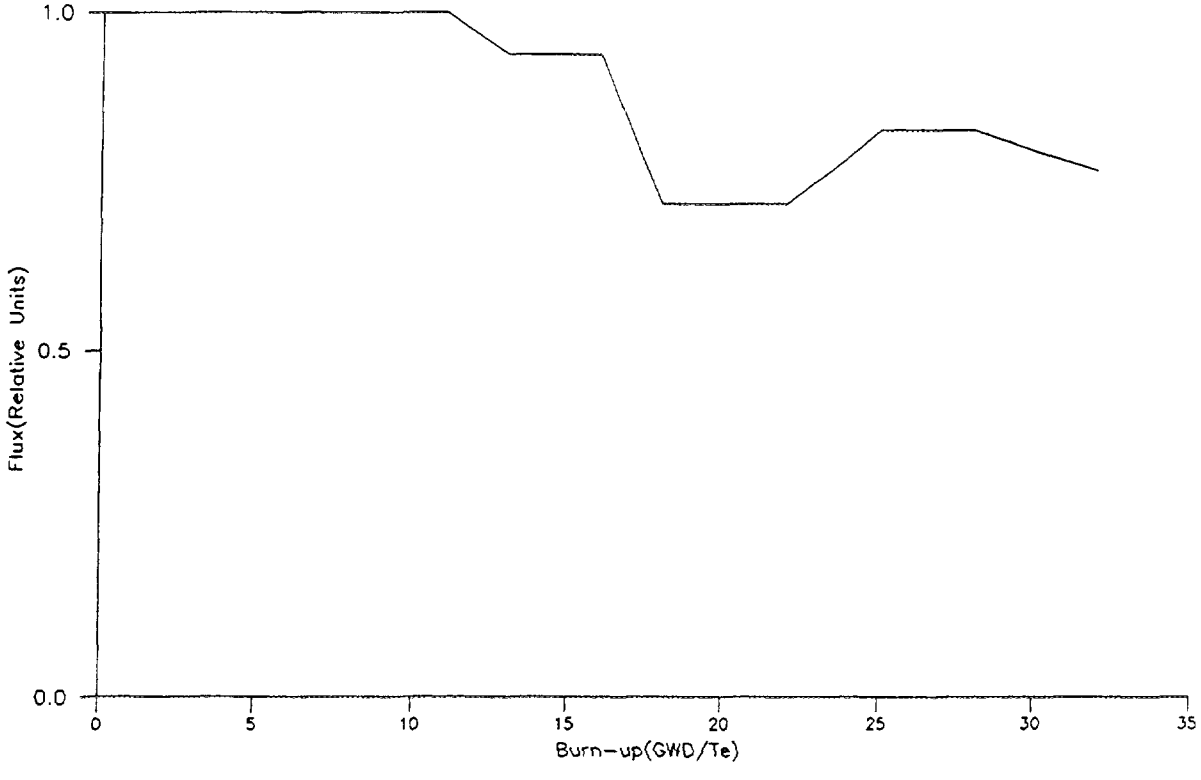

FIG. 3. Heat flux variation with burn-up.

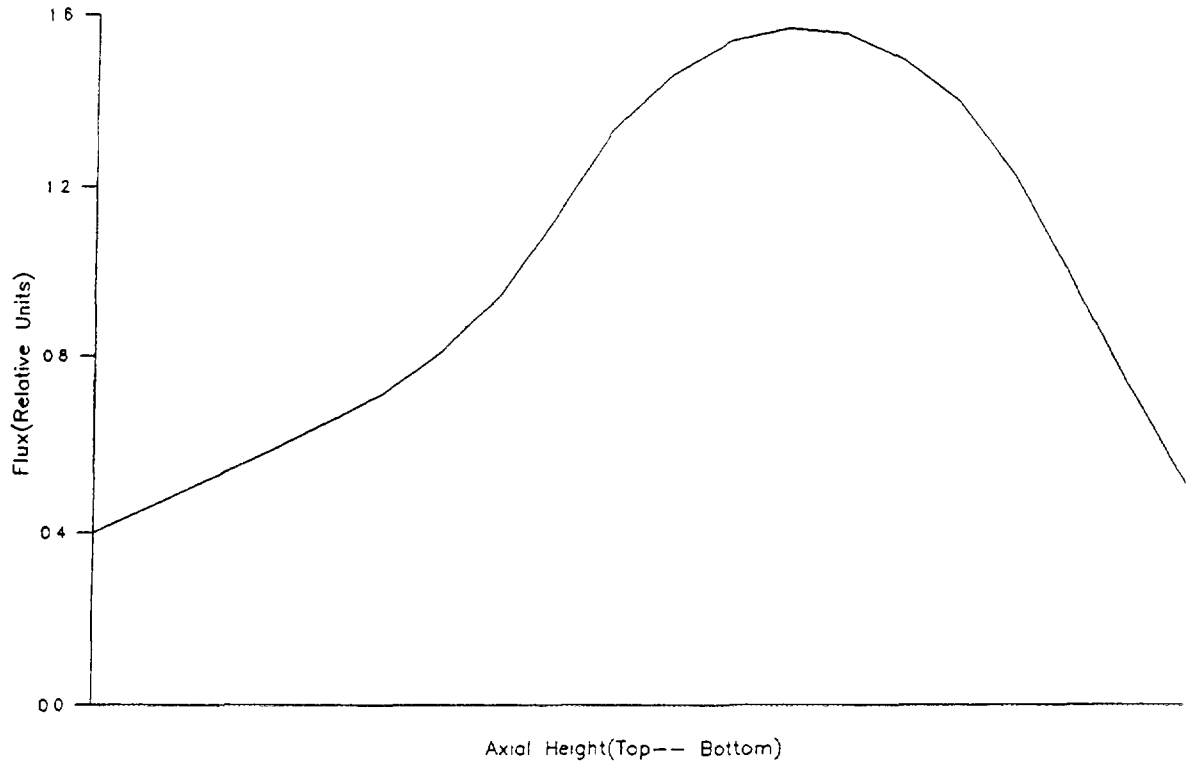

FIG. 4. Axial flux profile.

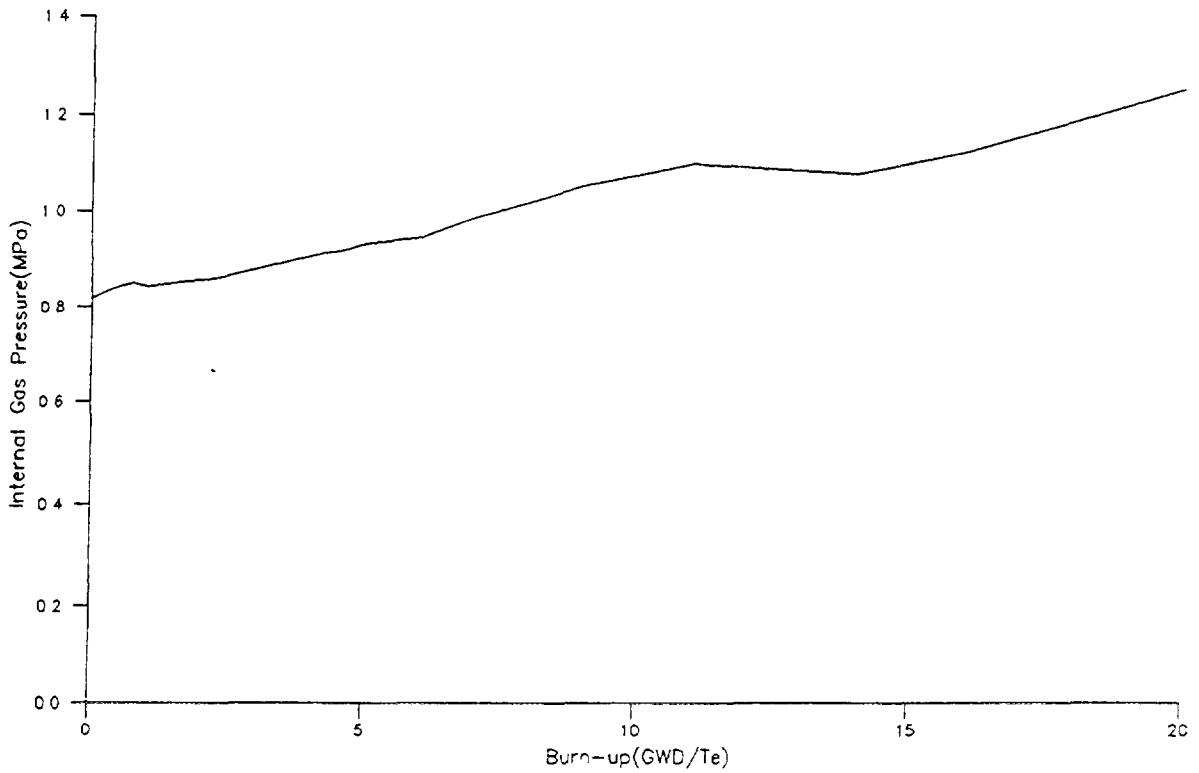

FIG. 5. Internal fission gas pressure build-up.

TABLE III. CONSTANTS FOR CREEP LAW

Phase	Temperature (K)	A ($MPa^{-n}s^{-1}$)	n	Q/R 1/K
α	$T \leq 1073$	2000	5.32	34220
β	$T \geq 1273$	8.1	3.79	17110

dimensional calculations at each axial node taking into consideration the following effects to evaluate pellet-cladding gap conductance:

i) Pellet-clad differential thermal expansion. At the maximum heat flux location pellet average temperature is about 850 °C higher than the cladding average temperature. In addition, the differences in the thermal expansion co-efficients are also taken into consideration.
ii) Pellet cracking and relocation. Temperature gradient across the pellet causes the pellets to crack. The cracked pellet relocates and causes a soft pellet-clad contact and increases gap conductance. The extent of relocation is dependent also on fuel burn-up.
iii) Pellet swelling. Pellet swelling both from solid and gaseous fission products is taken into consideration. Swelling also reduces the effective pellet-clad gap and increases the gap conductance.
iv) Clad inward creep due to external pressure. The computer code uses Nichol's[3] model for calculation of irradiation creep.
v) Fill gas dilution. Fill gas (helium) is diluted by the fission gases viz. xenon and krypton, having a lower thermal conductivity. This is a function of burn-up and fuel operating temperatures.

Gap conductance is calculated by using modified Ross and Stoute[4] correlation. Fuel temperatures are then obtained to calculate fission gas release and internal gas pressure. Other correlations used in the code are as given in MATPRO[5]. Fig-3 shows the heat flux variation against burnup at the peak location. Fig-4 shows the axial flux profile along the length of the pin. Fig-5 shows the internal pressure build-up in the fuel element up-to the pin average burn-up of 20 GWD/Te.

3.2 FUEL ANALYSIS SUBSEQUENT TO LOCA

The temperature profile (shown in Fig-2) and the internal pressure at the end of life (shown in Fig-5) are the forcing functions for clad ballooning. It can be seen that the cladding temperatures are high and the cladding is in $\alpha+\beta$ or β phase. Secondary creep laws following the Arrheneous expression are used to calculate the plastic deformation viz.:

$$\varepsilon = A\sigma^{n}\exp(-Q/RT)$$

where

ε - Strain rate (s^{-1})
A- Structure constant ($MPa^{-n}s^{-1}$)
σ - Stress (MPa)
n - Stress exponent
Q- Activation energy ($kJ\text{-}mol^{-1}$)
T - Temperature (K)
R - Universal gas constant ($kJ\text{-}mol^{-1}K^{-1}$)

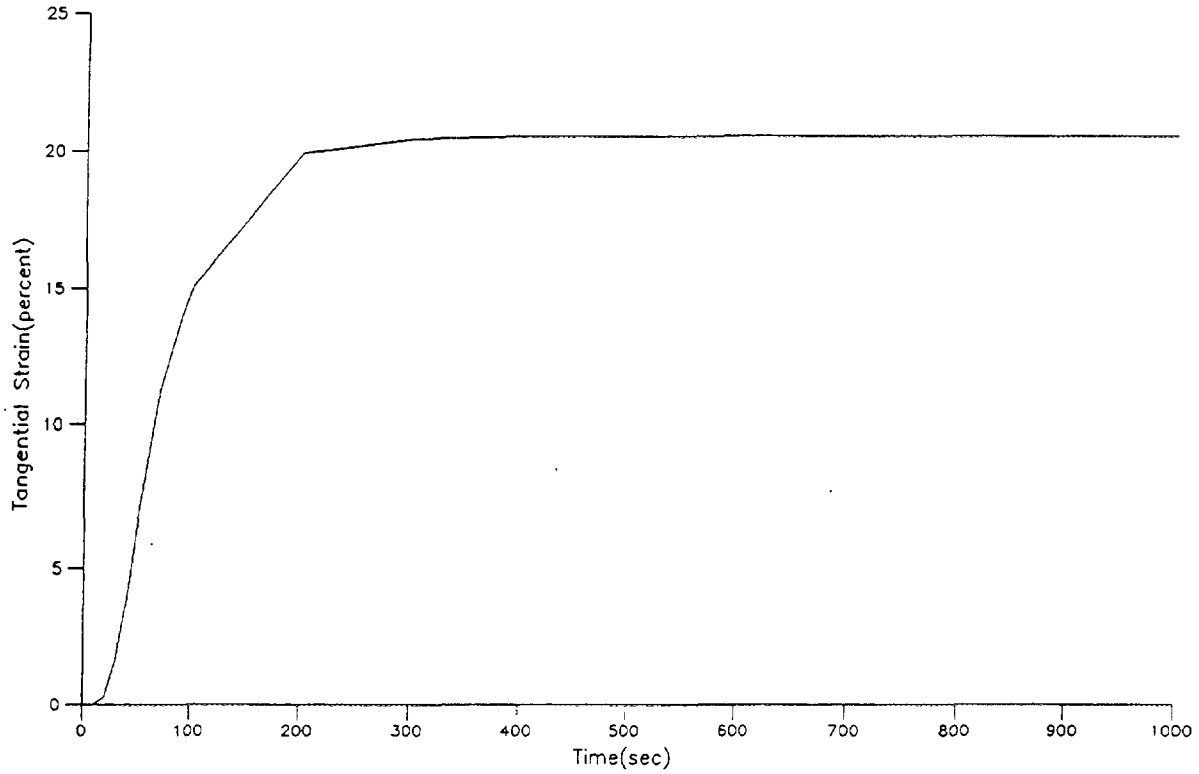

FIG. 6. Clad tangential variation with time.

For calculations, constants proposed by Rosinger & Bera[6] are used. The constants for α and β phases are shown in Table-3. For temperatures in the transition zone, values are obtained by interpolation.

Structural analysis is performed using a computer code NISA.[7] This a general purpose finite element code which supports different types of elements and can perform elasto-plastic analysis. A mesh consisting of 4 elements across the thickness and 16 elements along the circumference of semi-circular cladding segment was generated. Analysis was done using plane-strain elements. The package has a provision for describing the creep law constants. Pressure and temperature profiles were supplied as the forcing function. Fig-6 shows the percentage tensile strains produced in the cladding. It can be seen that cladding is in β phase for a very short period. During that period, strain rates are very high and a significant amount of strain is accumulated in that short period. It can also be seen that eventhough the internal pressure is low, accumulated creep strains are not very low.

4. CONCLUSIONS

During the LOCA, TAPS 6X6 cladding can experience the tensile strains of about 20%. This results into a maximum sub-channel blockage of about 45%. The value is within acceptable limits and does not cause a flow blockage during emergency core spray cooling. It is noticed that secondary creep rates are very sensitive to type of interpolation method used in $\alpha+\beta$ transition region. Choice of interpolation methods does not have a rigourous basis. Further investigations are being carried out to determine more accurate strain rates during transition region. The cladding temperatures are high and may result into cladding oxidation. The effect of oxide layer (i.e. reduction in effective thickness) as well the effect of diffused oxygen in strengthening of remaining layer is also being studied.

REFERENCES

1. GUPTA S. K. et. al., Effect of gap conductance on loss of coolant accident analysis of Tarapur Reactor. Internal report prepared at Reactor Analysis and Studies Section, Bhabha Atomic Research Centre.
2. BASU S. et. al., Computer code COMTA (Code for Mechanical and Thermal Analysis), Paper No. C3/11 presented at SMIRT-5, Berlin (1979).
3. NICHOLS F.A., On the mechanism of irradiation creep in zirconium base alloys, Journal of Nuclear Materials, (1970).
4. ROSS A. M. AND STOUTE R.L., Heat transfer co-efficient between UO_2 and Zircaloy-2, CRFD-1075, (1962)
5. MATPRO-11, Report No. NUREG/CR-0497, TREE-1280 (1979).
6. ROSINGER H.E. AND BERA P.C., Steady-state creep of zircaloy fuel cladding from 940 to 1873K, Journal of Nuclear Materials, 82 (1979), 286.
7. COMPUTER CODE NISA (Numerically Integrated System for Analysis), by M/S EMRC (Engineering Mechanics Research Center), (Release-93)

RAPTA-5 CODE: MODELLING BEHAVIOUR OF VVER-TYPE FUEL RODS IN DESIGN BASIS ACCIDENTS VERIFICATION CALCULATIONS

Yu.K. BIBILASHVILI, N.B. SOKOLOV,
A.V. SALATOV, L.N. ANDREYEVA-ANDRIEVSKAYA,
O.A. NECHAEVA, F.Yu. VLASOV
All-Russian Institute of Inorganic Materials,
Moscow, Russian Federation

Abstract

RAPTA-5 code used for licensing calculations to validate the compliance with the requirements for VVER fuel safety in design basis accidents. The characteristic results are given of design modelling experiments simulating thermomechanical and corrosion behaviour of VVER and PWR fuel rods in LOCA. The results corroborate the adequate predictability of both individual design models and the code as a whole.

1. Brief Description of Code

RAPTA-5 code is to be used for calculation of thermomechanical and corrosion behaviour of water cooled power reactor fuel rod in design basis accidents induced by degradation of heat transfer in a core or quick power changes and accompaned by a fuel cladding temperature rise (not higher than 1200 ° C).

The code has been under development since late 70 ns [1,2]. To-day the fifth version of the code has been developed.

The code makes use of the algorithm of the numerical integration of a system of non-steady equations of heat balance of elementary volumes of a multilayer cylindrical area taking account of its geometry changes at each time step. Geometry changes take into consideration thermoelastic strains of fuel and cladding, creep strain of cladding and oxide layer formation at inner and outer surfaces of cladding during oxidation.

To be used in the code a package of independent subprogrammes RAPTA-C (49 modules) has been made up to calculate temperature dependences of properties of the main core materials. They are based on experimental results of investigations of russian material properties and in some cases are supplemented with data taken from literature. The package represents thermophysical properties of UO_2 , Zr1%Nb alloy , ZrO_2 , inert gases, thermomechanical properties of fuel and cladding materials, equation of a cladding material condition in a wide range of stresses and temperatures, conservative and realistic models of Zr1%Nb oxidation kinetics also with the account for the effect produced by steam pressure.

The calculated results contain information on the thermophysical parameters of a fuel rod, strained condition of fuel and cladding, including an analysis of ballooning induced rupture of cladding, corrosion properties of cladding in the design range of time. The results are used to check up

the fulfilment of the criteria of the maximum design limit of fuel rod damages in accidents.

The major distinctions of the RAPTA-5 version from the previous one consist in the following:

1) Model of calculation of the local cladding deformation has been introduced with the account for height and azimuthal temperature non-uniformities [3,4];

2) Model has been introduced to calculate local cladding deformation upon symmetrical contact with claddings of adjacent fuel rods;

3) Design model of Zr1%Nb high temperature creep has been improved using experimental results [5,6,7] ;

4) Based on the supplemented array of experimental data on Zr1%Nb cladding failure effected by excess internal pressure at high temperatures new temperature dependences have been derived for rupture strains to be used in the deformation criterion of rupture;

5) The known conservative dependence used to calculate Zr1%Nb alloy oxidation in steam is supplemented with the model of the transition to the linear oxidation law at high exposure time;

6) A new design model of Zr1%Nb alloy oxidation has been introduced that is based on the realistic dependence of oxygen weight gain at temperatures up to 1600 ° C [8];

7) A design model of Zr1%Nb alloy oxidation has been introduced that takes account of a higher steam pressure at temperatures < 1100 ° C;

8) A feasibility is envisaged of randomly dividing a fuel rod into axial segments when forming a design array.

2. Main Results of Verification Calculations

The RAPTA-5 code was verified by design modelling a series of experiments. Use was made of the results of the domestic laboratory experiments aimed at studying the deformation behaviour, rupture parameters and oxidation of fuel rod claddings under unsteady temperature - force conditions of loading typical of design basis accidents. Use was also made of the results of foreign integral rig and in-pile experiments with PWR type fuel assemblies; the need material properties and design parameters having been corrected.

2.1. Kinetics of cladding steam oxidation

The most important aspect of a fuel rod behaviour under accident conditions is their high temperature steam oxidation. A large amount` of experimental and theoretical studies deal with corrosion behaviour of Zr1%Nb claddings and influence of oxidation on mechanical properties [8 - 11].

In the specific ranges of temperature and exposure time typical of LOCA there is square law dependence between oxygen weight gain and time that is true for isothermal conditions. Under non-isothermal

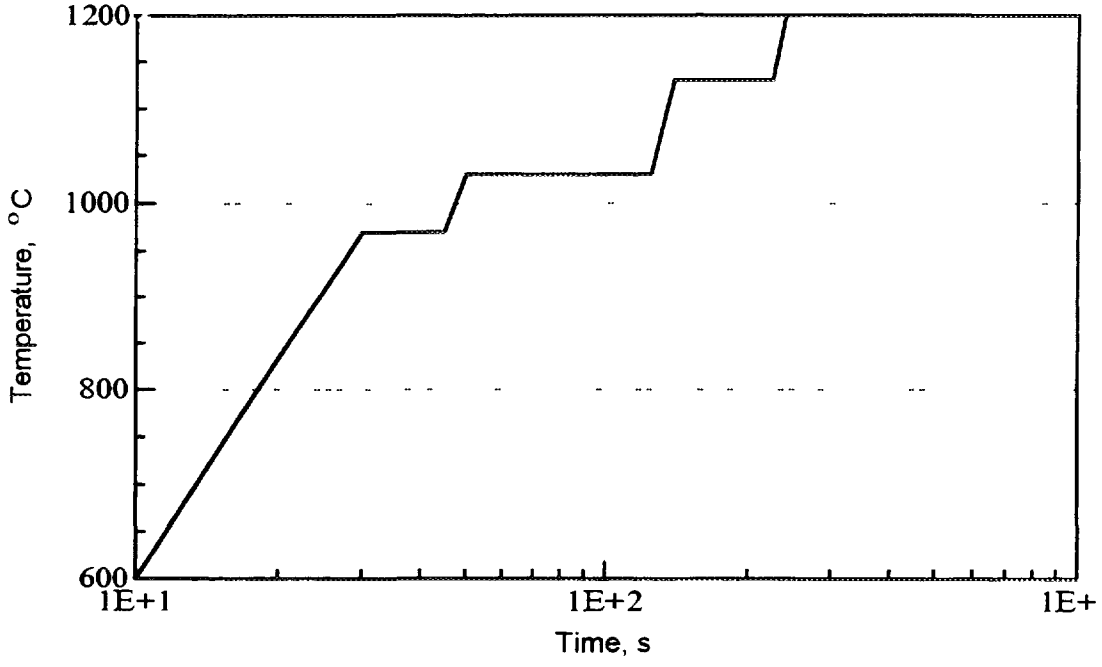

Fig.1 - Temperature evaluation of specimens 1, 2 during experiment

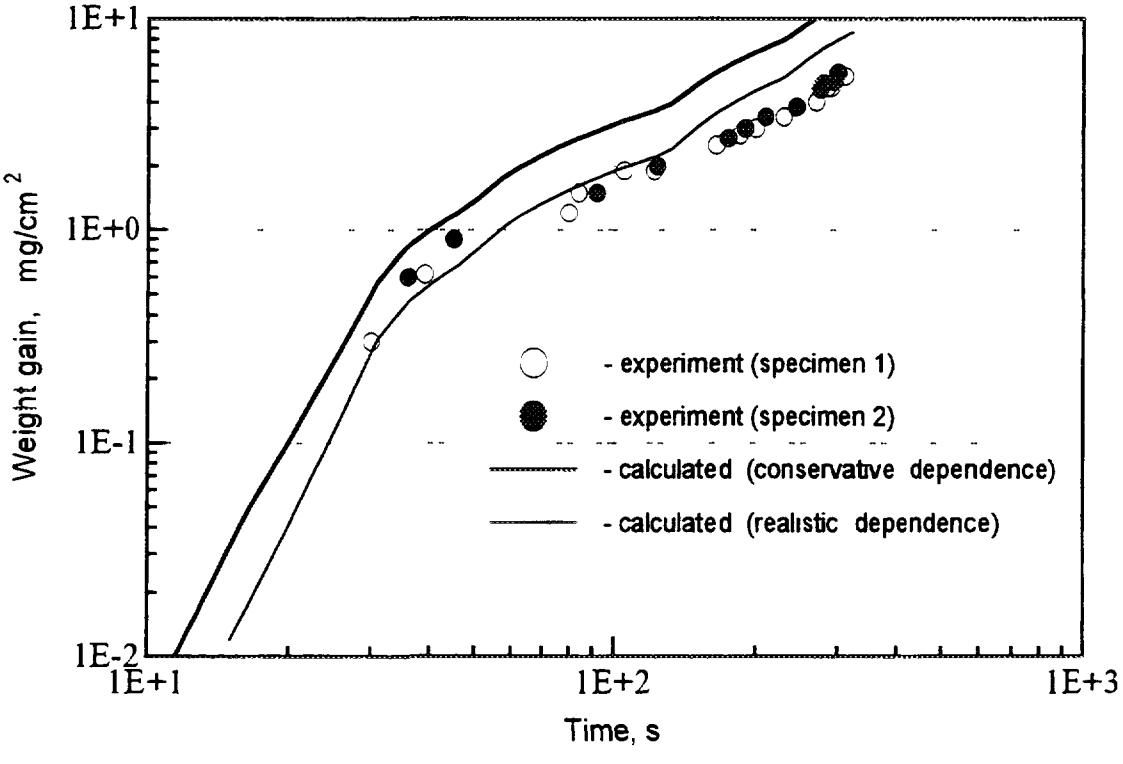

Fig.2 - Weight gain kinetics of specimens 1 and 2

conditions to find a weight gain a reccurent relationship is used taking account of the pre-history of the process

$$W^2 = K_p \tau,$$
$$K_p = A \exp(-Q/T),$$
$$W_i = (W_{i-1}^2 + K_{pi}(\tau_i - \tau_{i-1}))^{1/2},$$

where W - spesific weight gain of oxygen, mg/cm^2,
τ - time, s,
K_p - is reaction rate parameter, (mg/cm^2)^2 c^{-1},
T - absolute temperature,
A - empiric coefficient,
Q - reduced activation energy, K,
τ_{i-1}, τ_i - are limits of a time range within the temperature T_i is considered constant.

By now a large array of experimental data on Zr1%Nb alloy cladding oxidation has been generated (more then 1000 points); on its base conservative (used for licensing calculations) and realistic kinetic dependences were derived to determine the specific weight gain and release of hydrogen [1 , 8]

conservative $K_p^{1/2} = 920 \exp(-10410/T)$ at $T < 1773$ K,

realistic $K_p = 1.59 \cdot 10^6 \exp(-23040/T)$ at $T < 1773$ K,

$K_p = 9.825 \cdot 10^5 \exp(-20800/T)$ at $T \geq 1773$ K.

The verification of the model describing the interaction between a fuel rod cladding material and steam shows a good agreement of the oxidation kinetics derived using the realistic dependence with the results of non - isothermal experiments with the continuous recording oxygen weight gain in VVER - type fuel rod claddings (fig.1, 2). It was corroborated that the dependence of the kinetics of Zr1%Nb alloy cladding oxidation is conservative.

2.2. Cladding Deformation Behaviour and Loss of Tightness

The equations for Zr1%Nb alloy condition (creep law relating the strain rate to stresses and temperature) [5, 6, 7] were derived using the results of experimental studies in the stress range of 9 - 145 MPa and temperature range of 300 - 1500 K covering the range of the alloy phase transformation

1) for the α - region (temperature < 883 K)
in the stress range of 9 - 32 MPa

$$\varepsilon = 7.1 \cdot 10^5 \sigma^{2.2} \exp(-28900/T),$$

in the stress range of 32 - 90 MPa

$$\dot{\varepsilon} = 26\,\sigma^{5.1} \exp(-28900 / T),$$

at higher stresses

$$\dot{\varepsilon} = 2 \cdot 10^{9} \exp(0.05\,\sigma) \exp(-28900 / T),$$

2) for the β - region (temperature > 1070 K)

$$\dot{\varepsilon} = 0.09\,\sigma^{3.5} \exp(-13200 / T),$$

3) for the $(\alpha + \beta)$ region ($883 < T < 1070$ K) the model of parallel phase joining results in stress additivity:

$$\sigma = f_{\alpha}\sigma_{\alpha} + f_{\beta}\sigma_{\beta},$$

the model of successive phase joining results in strain rate additivity

$$\dot{\varepsilon} = f_{\alpha}\dot{\varepsilon}_{\alpha} + f_{\beta}\dot{\varepsilon}_{\beta},$$

where $\dot{\varepsilon}_{\alpha}, \dot{\varepsilon}_{\beta}$ – are straine rates of α– and β– phases,
$\sigma_{\alpha}, \sigma_{\beta}$ – are stresses in α– and β– phases,
f_{α}, f_{β} – are volume fractions of α– and β– phases.

The cladding failure parameters namely, time to rupture and tangential rupture strain of cladding are determined using the principle of linear summing elementary damages under conditions of isotermal steady loading. The elementary damage is determined as a ratio between a time pitch and time to rupture, the latter in determined from Garofalo criterion or as a ratio of a strain increment at a time pitch to a rupture strain under given isoconditions (deformation criterion)

$$\int_0^{\tau} d\varepsilon_{\theta} / \varepsilon_{\theta p} = 1 \qquad \text{or} \qquad \int_0^{\tau_{\theta}} d\tau / \tau_p = 1 .$$

The deformation criterion basis is formed by a large array of experimental data on rupture of Zr1%Nb claddings under the action of excess internal pressure at temperatures 600 - 1300 °C (some 1000 points).

To verify the model of excess internal pressure effected cladding local straining of in the area of a given temperature distribution over height use was made of the results of laboratory experiments with VVER fuel simulators with a 200 mm fuel column length heated by a center tungsten electrode. The heating rate was 20 K/s. The specimens were heated to the specified isothermal state until the cladding lost its integrity. The design of the rig provided the maximum temperature of the specimen central part and the temperature gradient of the 0.5 K/mm. Some results of the design

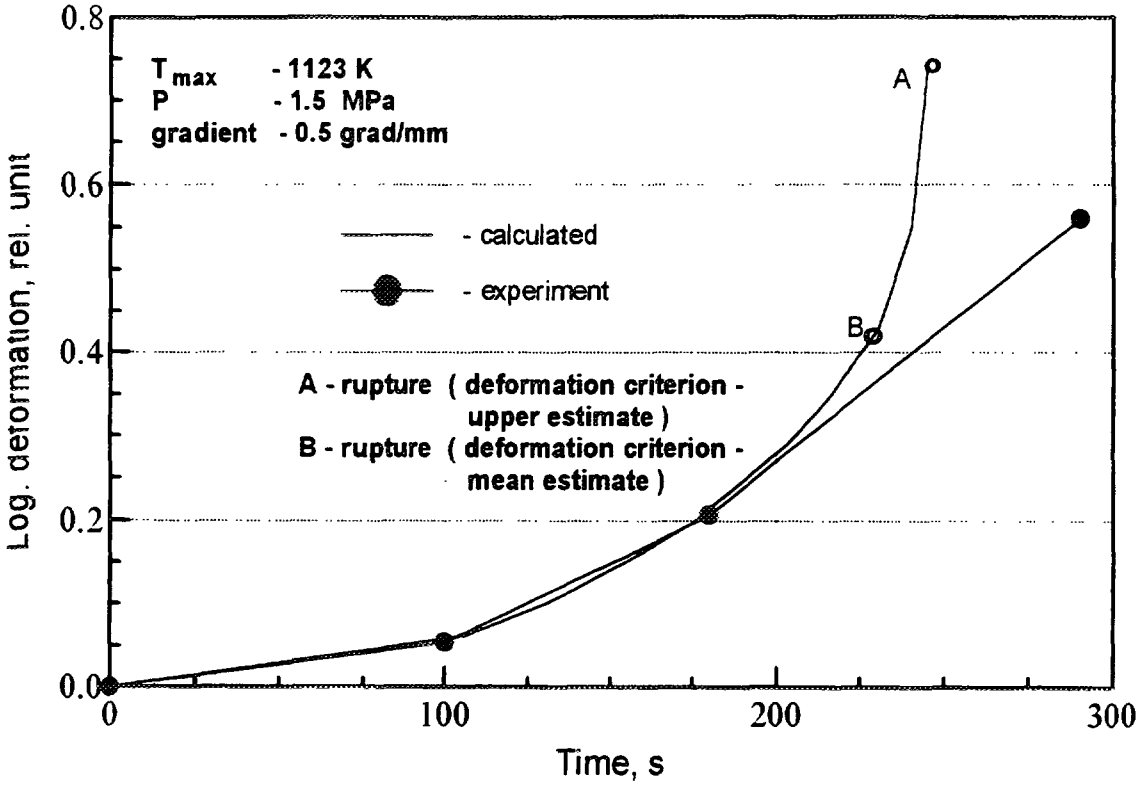

Fig.3 - Hoop strain kinetics (cladding hot cross section)

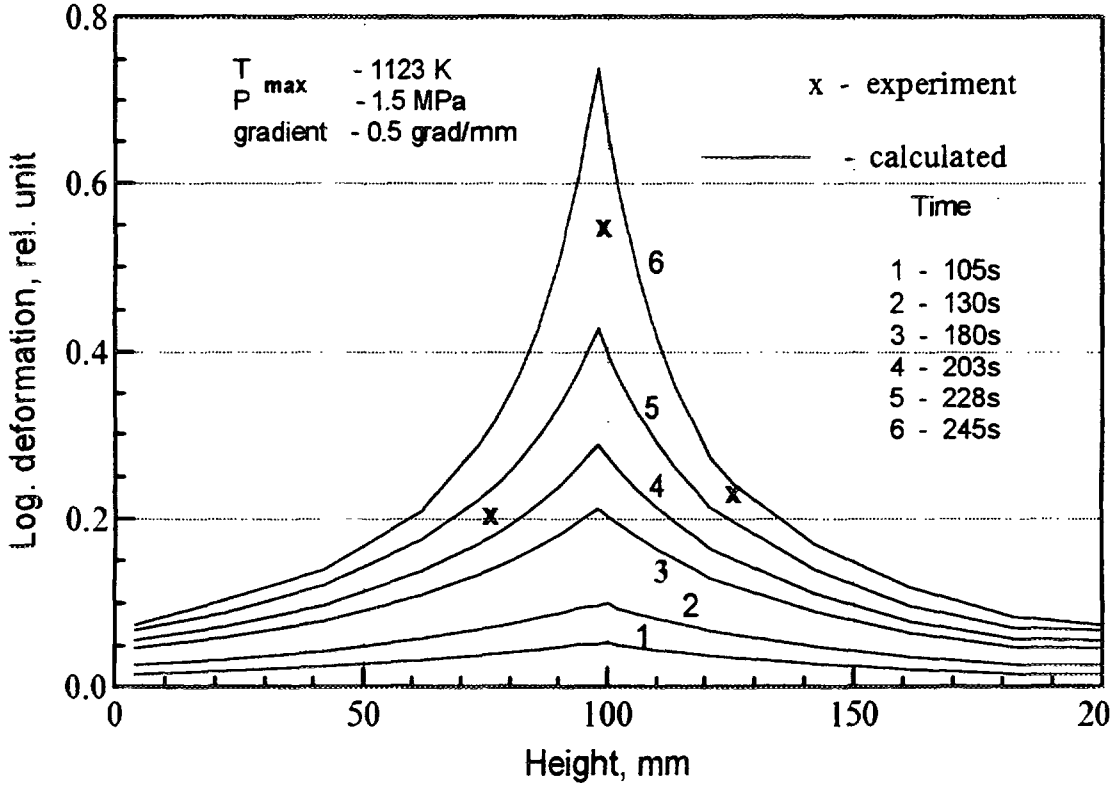

Fig.4 - Height distribution of hoop strain

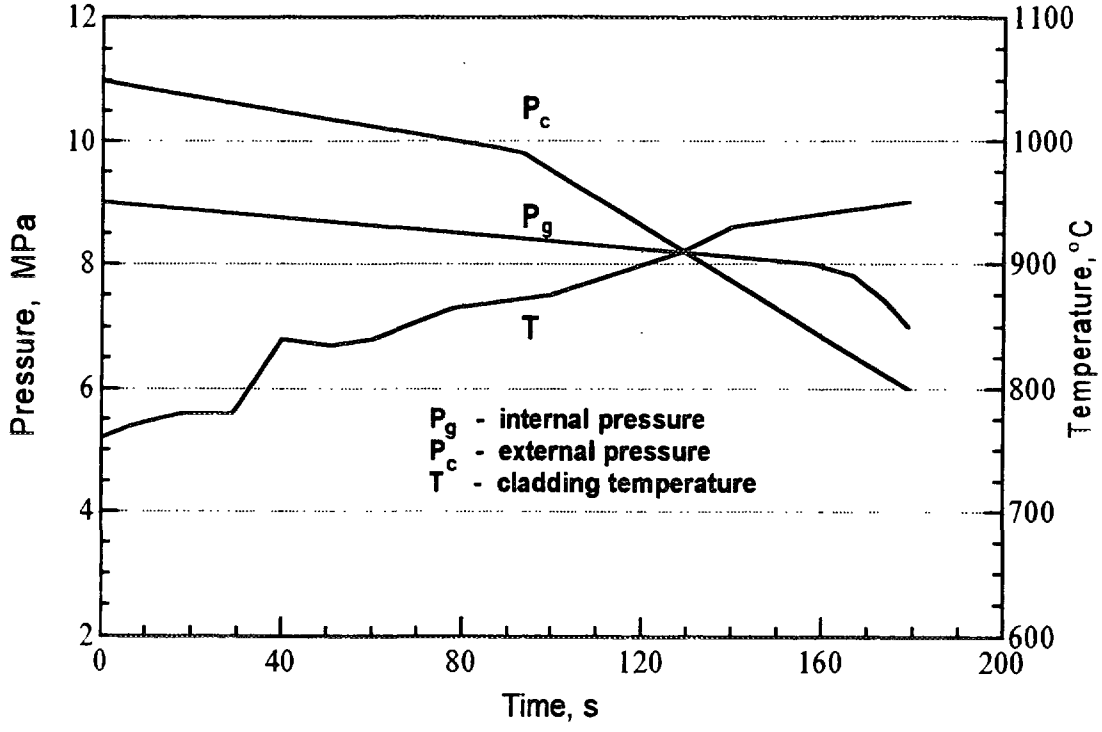

Fig.5 - Looding conditions of simulator (temperature, pressure)

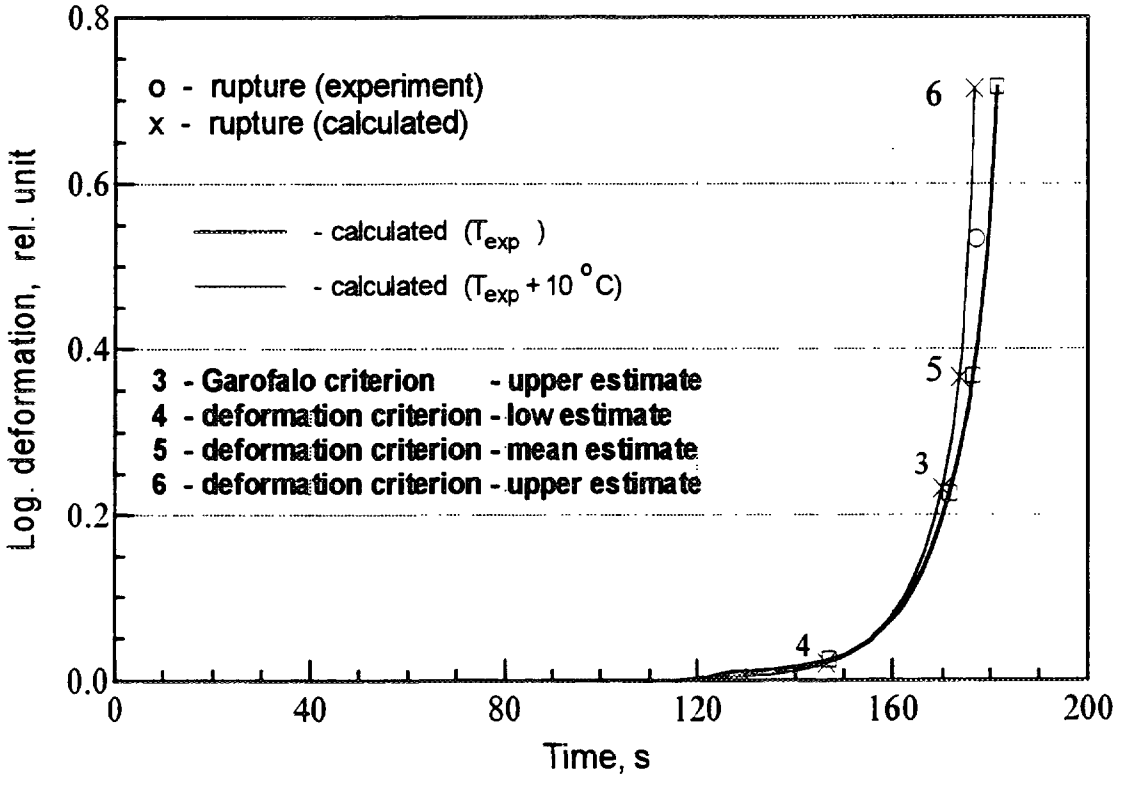

Fig.6 - Comparison of calculated and experimental rupture hoop strain

modelling in comparison to the experimental findings are given in figs. 3, 4. There is an adequate agreement parameters of a fuel cladding rupture and the strain distribution over the height.

The model of cladding rupture due to ballooning was verified using the results of the experiments carried out by OKB "Hydropress" with electrically heated (a molybdenum electrode in the centre) VVER fuel simulators 1.2 m long that had a higher power density zone 0.5 m long. In the experiments the parameters of non-steady loading conditions (cladding temperature, internal and external presssure) were measured. The loading conditions and the results of design modelling are illustrated in figs. 5, 6 for one of the experiments. The calculated cladding rupture parameters (time to rupture and a magnitude of hoop strain during rupture) are in adequate agreement with the experimantally found rupture parameters.

2.3. Blockage of Fuel Assembly Cross - Section

To verify the model of the restrained straining of cladding simmetrically contacting adjacent fuel rod claddings and of a fuel bundle cross-section blockage one of the experiments [12] was taken modelling the thermomechanical behaviour of PWR type fuel simulators in LOCA. In those experiments a (7 × 7) assembly of electrically heated simulators 0.9 m in height was cooled with superheated steam and conditions uniform

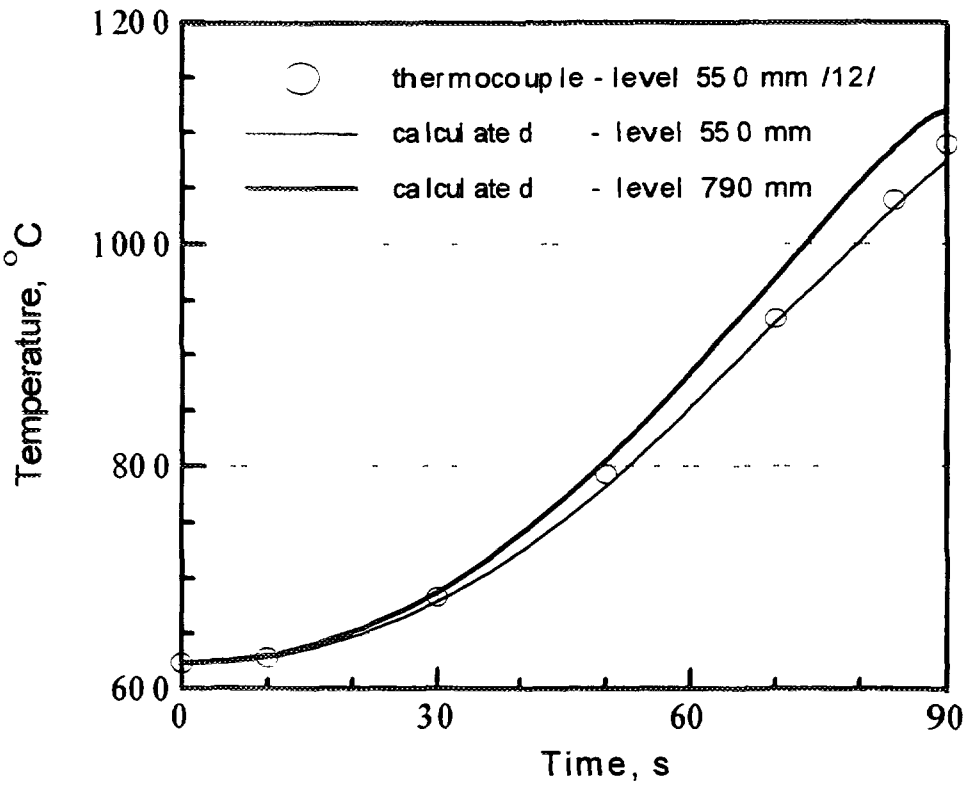

Fig.7 - Temperature during experiment

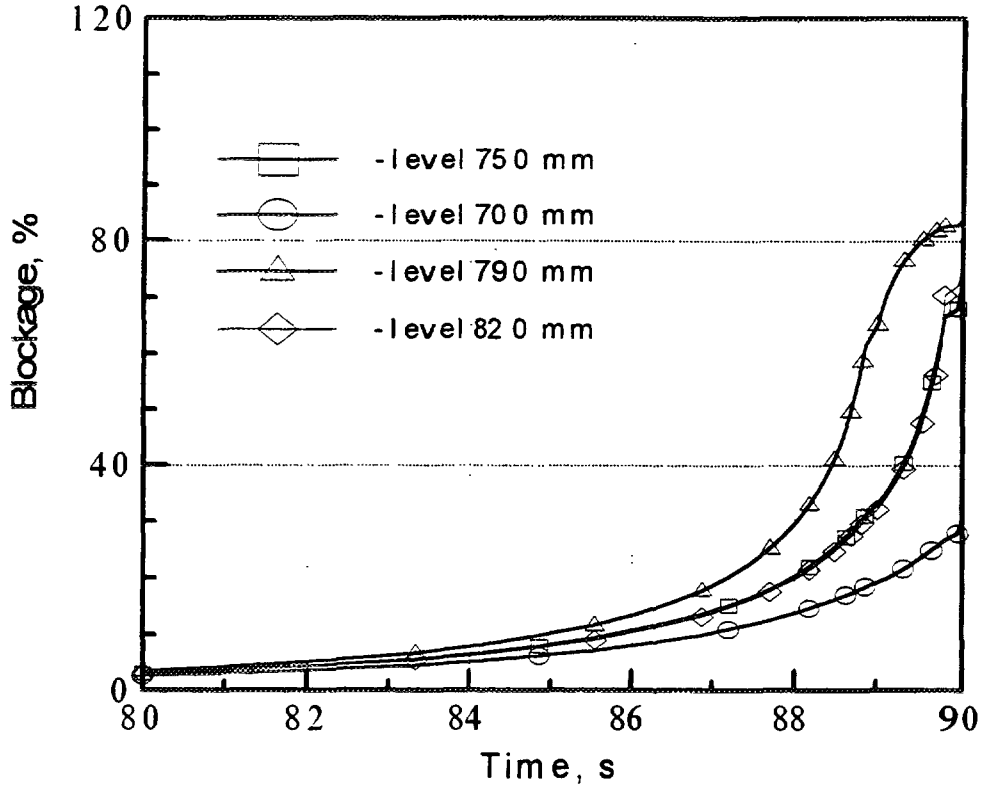

Fig.8 - Predicted blockage

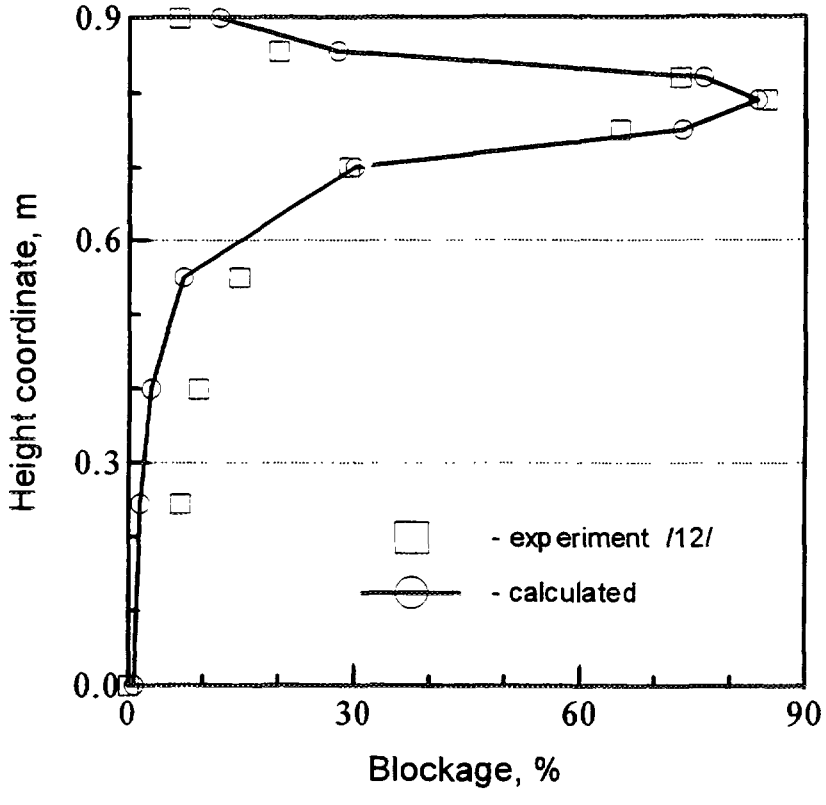

Fig.9 - Height distribution of blockage

across the assembly section were created under which all simulators experienced local ballooning at one and the same level of height. Essentially all claddings came into contact with the adjacent ones and their strain behaviour may be assumed to be similar. The programme was corrected when it was needed as applied to the material properties (the thermophysical properties of Zry-4, the high temperature creep law, the deformation criterion of rupture) and the account for the design feature of the assembly (arrangement of fuel rods in the angles of a square). Besides, also included was a model to calculate the heat transfer to the superheated steam flow. Thus, not only the deformation behaviour of cladding but also the temperature condition of a simulator were modelled. In this sense the modelled experiment is integral. As a result a good agreement was achieved between the calculated and experimental parameters, namely, temperature conditions of simulator claddings, blockage of bundle cross-section (figs. 7 - 9). Blockage was determined as a ratio between the changes in the assembly cross-sectional area and the initial one.

2.4. In - Pile Experiment Modelling

Presently the programme was also tested using the results of the in-pile experiments EOLO, MT-1, FR-2 carried out abroad. In these experiments the thermomechanical behaviour of PWR type fuel rods in LOCA was modelled. As an example, let us discuss the results of

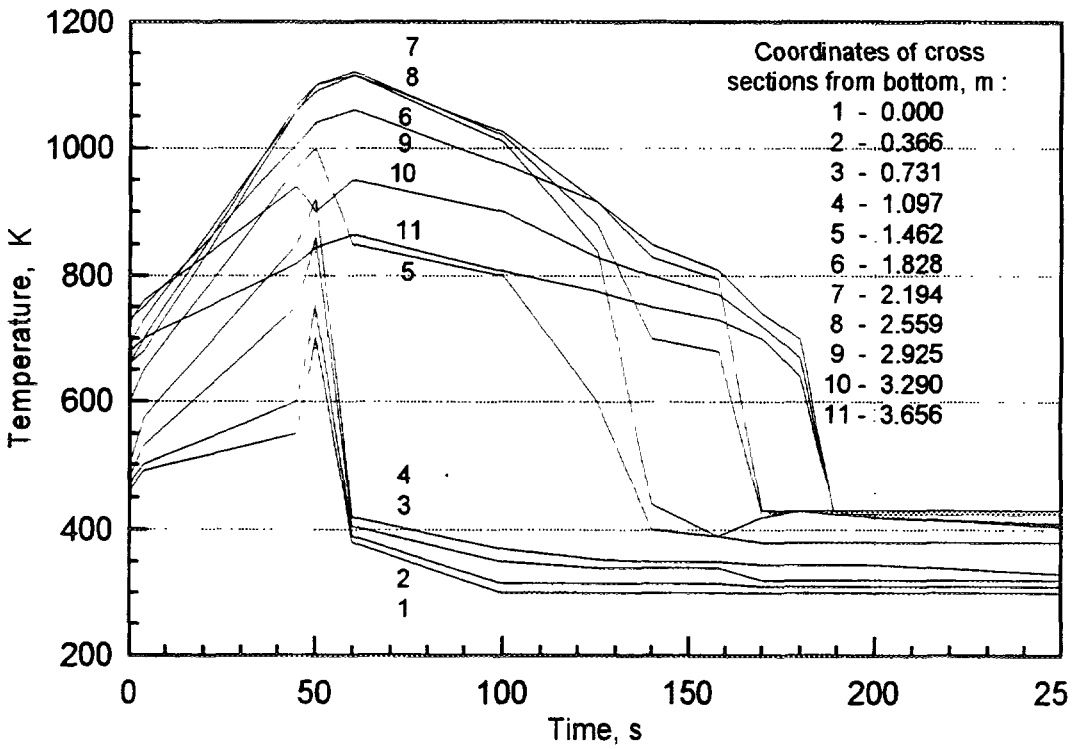

Fig.10 - Temperatures of cladding outer surface during experiment MT-1 (according to expert restore)

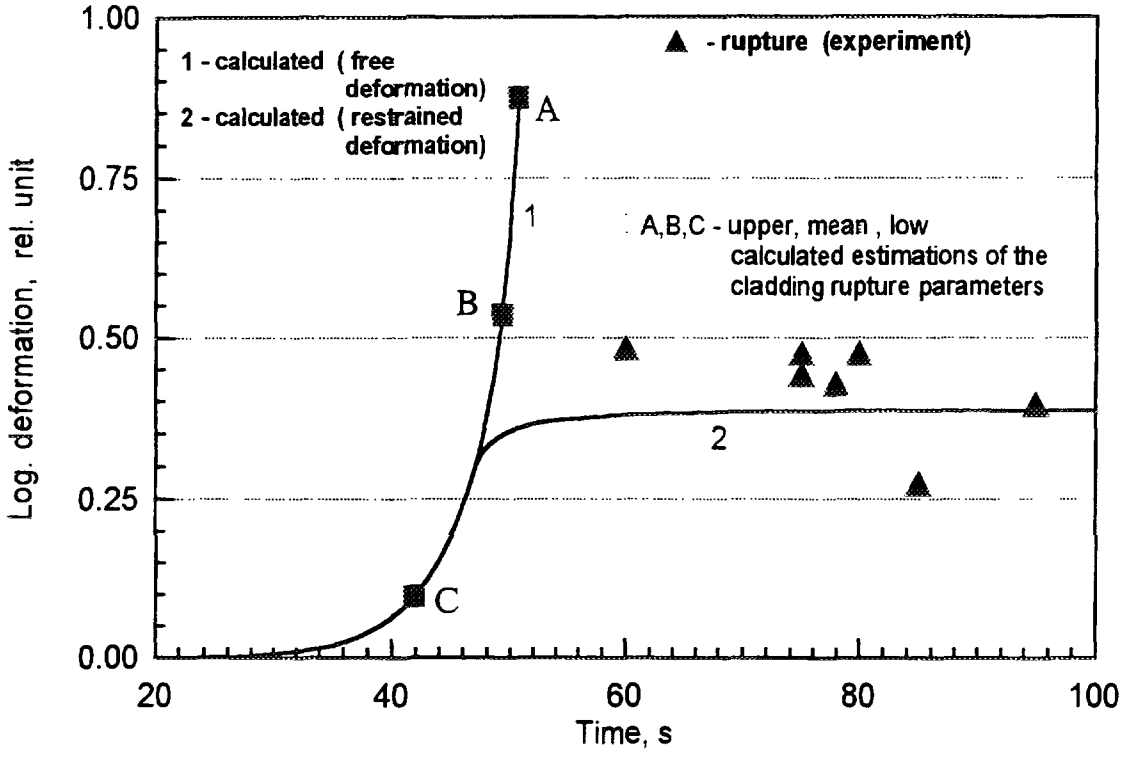

Fig.11 - Maximum hoop strain of cladding versus time

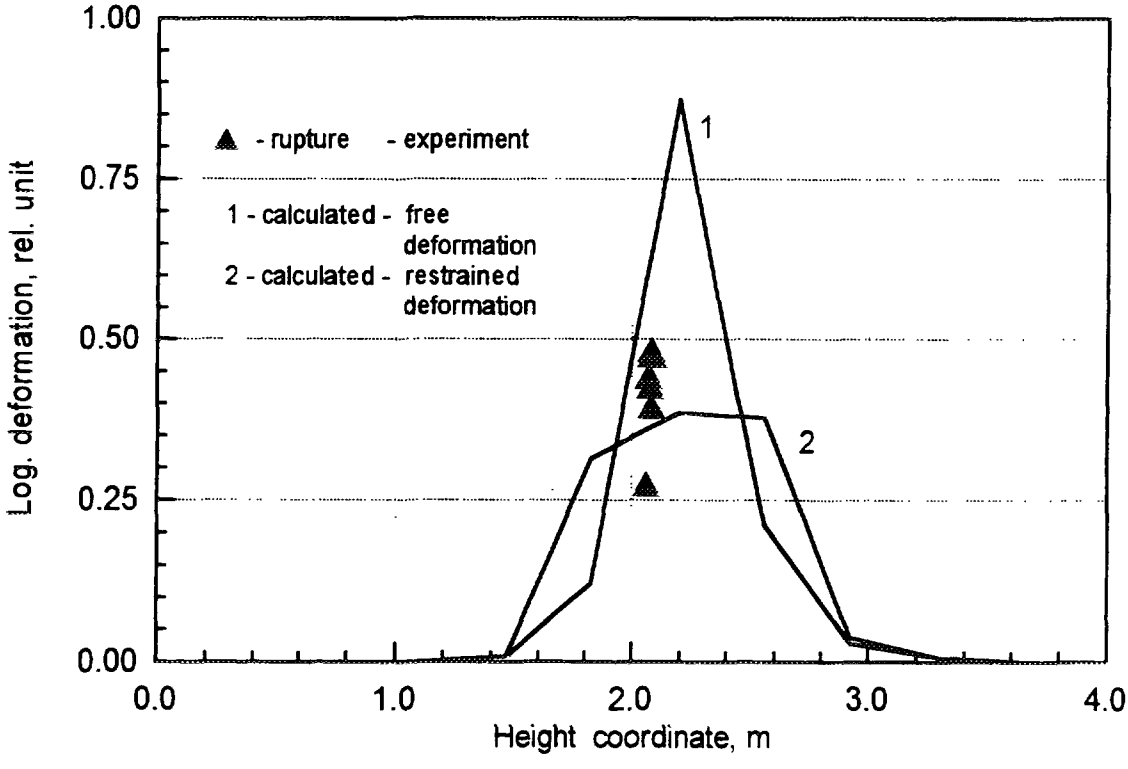

Fig.12 - Height distribution of hoop strain

modelling the experiment MT-1 (the reactor facility NRU, Canada) in which a (6 × 6) assembly (without fuel rods in the angles) of fuel-scale PWR fuel rods was tested. The experiment consisted of three phases, namely, simulation of a fuel rod operation under steady-state conditions, simulation of steady cooling with a steam flow on residual power rating, simulation of heating up as a result of a deficient heat transfer followed by flooding with water. The design modelling of phase 3 was carried out using the non-steady field of temperatures of an outer cladding surface as a boundary condition of the 1st kind (fig. 10). This field was reconstituted based on the published readings of thermocouples. Modelled were the fuel rod temperature field, kinetics of internal pressure, stress-strained condition and cladding rupture. In this instance as in Section 2.3., the programme was corrected as applied to cladding material properties and design features of assembly. The calculations were performed using two models of cladding deformation, namely free and restrained by symmetrical contact with adjacent claddings. As a result an adequate agreement was achieved between the calculated and experimental data on thermomechanical characteristics of fuel rod cladding failure : time to rupture, rupture location and maximum hoop strains. It can be seen from figs. 11 and 12 almost all experimental points of internally pressurized cladding rupture lie between two calculated curves that correspond to different versions of straining. It can be concluded that the free deformation model and upper estimate of the deformation criterion of rupture are too much conservative. Generally speaking, the maximum rupture strains of individual claddings are unrealistic under fuel rod assembly conditions. On the other hand, the restrained straining model not taking account of local superheating due to a contact gives a somewhat underestimated result.

3. Conclusion

Thus, the RAPTA-5 code was verified using results of laboratory experiments modelling high-temperature processes (oxidation, straining and failure of fuel rod cladding) as well as results of rig and in-pile integral experiments modelling conditions of loading in design basis accidents. The following conclusions can be drawn on the results of verification calculations :

- a good agreement was obtained between the design and experimental parameters of cladding oxidation and straining under specified conditions of temperature and force loading;
- the adequate agreement of cladding strain parameters in integral experiments evidences the adequate modeling of a non-steady temperature field in a fuel rod and of the parameters of the fuel rod filler gas condition;
- the code has conservative models of cladding oxidation, deformation behaviour and rupture that permit licensing calculations to validate the safety of VVER fuel with adequate reliability in design basis accidents.

REFERENCES

[1] RESHETNIKOV, F.G. GOLOVNIN, I.S., BIBILASHVILI, Yu.K. e.a. RAPTA-1 computer code for fuel behaviour accident analysis. In: Proceedings of CSNI specialists' meeting on the safety aspects of fuel behaviour in off-normal and accident conditions. Espoo, Finland, 1-4 September, 1980. Paris, 1981, pp. 511-529.

[2] Н.Б. СОКОЛОВ, В.И. СОЛЯНЫЙ РАПТА-4 - вычислительная программа для моделирования поведения твэлов энергетических водоохлаждаемых реакторов в аварийных ситуациях. // Вопросы атомной науки и техники. Серия: Атомное материаловедение, 1988, вып. 2(27), с.13-17.

[3] В.И. СОЛЯНЫЙ, Л.Н. АНДРЕЕВА-АНДРИЕВСКАЯ, Ю.К. БИБИЛАШВИЛИ и др. Блокировка проходного сечения ТВС реактора ВВЭР при аварии с потерей теплоносителя.// Атомная энергия, 1989, т.66, вып.6, с.383-388.

[4] V.I. SOLYANY, L.N. ANDREEVA-ANDRIEVSKAYA e.a. Influence of azimutal and axial non-uniformities of fuel clad straining on WWER type assembly. -Flow area blockage under accident conditions. -In: proc. of a Specialists' Meeting on Water Reactor Fuel Safety and Fission Product Release in Off-Normal and Accident Conditions, IAEA, Vienna, 1987, pp.89-98.

[5] М.И. АЛЫМОВ, Е.Н. ПИРОГОВ, Л.Л. АРТЮХИНА, О.В. КОМАРОВ Напряжение установившегося течения при растяжении сплава Н-1. - М.: Атомная энергия, 1987, т. 63, вып. 1, с. 50-51.

[6] М.И. АЛЫМОВ, Е.Н. ПИРОГОВ, Л.Л. АРТЮХИНА, О.В. КОМАРОВ Деформирование сплава Н-1 в интервале 1170 - 1370 К. - М.: Атомная энергия, 1988, т. 65, вып. 3, с. 227.

[7] Е.Н. ПИРОГОВ, М.И. АЛЫМОВ, Л.Л. АРТЮХИНА Ползучесть сплава Н-1 в области полиморфного превращения. - М.: Атомная энергия, 1988, т. 65, вып. 4, с. 293 - 294.

[8] SOKOLOV, N.B., ANDREEVA-ANDRIEVSKAYA, L.N., VLASOV, F.Yu., NECHAEVA, O.A., SALATOV, A.V., TONKOV, V.Yu., KARPOV, V.M. Kinetics of Interaction between Materials in Water-Cooled Power Reactor Core. Recomendations for Application within the Framework of the Intrnational Standard Problem for Cora-W2 Experiment. All-Research Institute of Inorganic Materials named after Academican A.A.Bochvar, 1993, - 18 p.

[9] SOLYANY, V.I., BIBILASHVILI, Yu.K., DRANENKO, V.V. e.a. Steam oxidation of Zr1%Nb clads of WWRE fuels in high temperature. In: OECD-NEA-CSNI/IAEA specialists' meeting on water reactor fuel element performance computer modelling. Summary report, Bowness-on-Windermere, UK, 9-13 April 1984. Vienna,1984, pp.261-269.

[10] BIBILASHVILI, Yu.K., SOLYANY, V.I., DRANENKO, V.V., e.a. Characteristics of corrosion behaviour of Zr1%Nb WWER fuel claddings within 700-1000°C on long term exposure. In: OECD-NEA-CSNI/IAEA specialists' meeting on water reactor safety and fission product release in off-normal and accident conditions. Summary report, Vienna, 10-13 November 1986, Vienna 1987, pp.98-108.

[11] СОЛЯНЫЙ В.И., БИБИЛАШВИЛИ Ю.К., ДРАНЕНКО В.В. и др. Исследования коррозионного поведения оболочек твэлов из сплава Zr1%Nb в паре при высоких температурах. //ВАНТ. Серия: Атомное материаловедение, 1988, вып.2(27), с.89-95.
[12] S. KAWASAKI, H. UETSUKA, T. FURUTA. Multirods burst tests under loss-of-coolant conditions. In: OECD-NEA-CSNI/IAEA Specialists' Meeting on Water Reactor Fuel Safety and Fission Product Release in Off-Normal and Accident Conditions. Riso, Denmark, 16-20 May 1983, IWGEPT/16, pp.17-28.
[13] JONES, P., MARKOVINA, A., RANDLES, J., SIMONI, O., ZEYEN, R. EOLO-JR: A singl rod burst test programme in the ESSOR reactor. Proceedings of a specialists' meeting organized by the IAEA, Preston UK, March 1982. Vienna, 1983.
[14] KARB, E.H., SEPOLD, L., HOFMANN, P., PETERSEN, C., SCHANZ, G., ZIMMERMANN, H. LWR fuel rod behaviour during reactor tests under loss-of-coolant conditions: results of FR-2 in-pile tests. J. of Nucl. Mat., 1982, v.107, pp.55-77.

EXPERIMENTAL STUDY OF THE CORE STRUCTURE BEHAVIOUR IN LOCA CONDITION

V. TROYANOV, E. ERSHOV, A. KOROLJOV, Yu. LIKHACHEV,
A. POMESCHIKOV, V. RUMJANTSEV, V. SUGONJAEV
Institute of Physics and Power Engineering,
Obninsk, Russian Federation

Abstract

The objective of this report is to describe the research program and its issues concerning to analysis of the in-vessel phase of accident. WWER types of materials and structures have been considered. All experiments have focused upon obtaining the data for core degradation modelling and reactor vessel strength analysis. Fuel rod ballooning and rupture under accident conditions including severe accidents, residual strength of claddings after high temperature oxidation, cladding spacer grid chemical interaction under steam presence, corium modelling, properties investigation, phase separation in melts, vessel lower head strength under high temperature loading are discussed. All of these laboratory-scale experiments are conducted in IPPE.

1. INTRODUCTION

There are no adequate calculation code for WWER core degradation simulation which would take into consideration all main phenomena inside fuel bundles or inside core under accident heating. As result it is impossible to develop exactly a scenario of severe accident upon in-vessel phase and, hence, to discuss a safety substantiation and possibility of the in-vessel accident localisation. Not only adequate core degradation code is absent up to now, but codes for next stage of accident (debris formation, molten pool formation, lower head high temperature loading) are absent too.

The main reason of that is insufficiency of experimental data about materials and structures behaviour such as chemical interaction under steam presence, liquefaction conditions, material properties including thermal-physical ones, high temperature strength and failure of structures, etc.

In IPPE the codes for analysis of the core degradation, molten pool behaviour, vessel lower head cooling and strength are under developing. Some experimental results for these codes support are discussed in this paper.

2. BALLOONING AND RUPTURE OF PRESSURISED FUEL ROD CLADDINGS

Ballooning and rupture of fuel rod claddings is considered both for Large Break Loss of Coolant Accident (LBLOCA) and initial stage of severe accident. Because of various scenarios of accidents can be realised, temperature evolution and duration of exposure can be varied, the dependencies of the time-to-rupture versus temperature for pressurised tubes have been obtained. Cladding material is Zr+1%Nb alloy. Results are shown in Fig.1. One of the objectives was the analysis of steam presence influence upon time to rupture and rupture strain. These characteristics of Zr+1%Nb alloy in vacuum are well known. As shown in Fig.1 the influence of steam is not catastrophical one. Initial absolute internal pressure of argon has been choozed 1.1, 2.0, 4.0 Mpa. Under uniform temperature distribution during the tests the rupture strains usually achieved a level up to 100% and more. These results have obtained upon the single tubes. In the cases of assemblies tests with low radial temperature gradient the strain localisation is happen and rupture deformation is reduced.

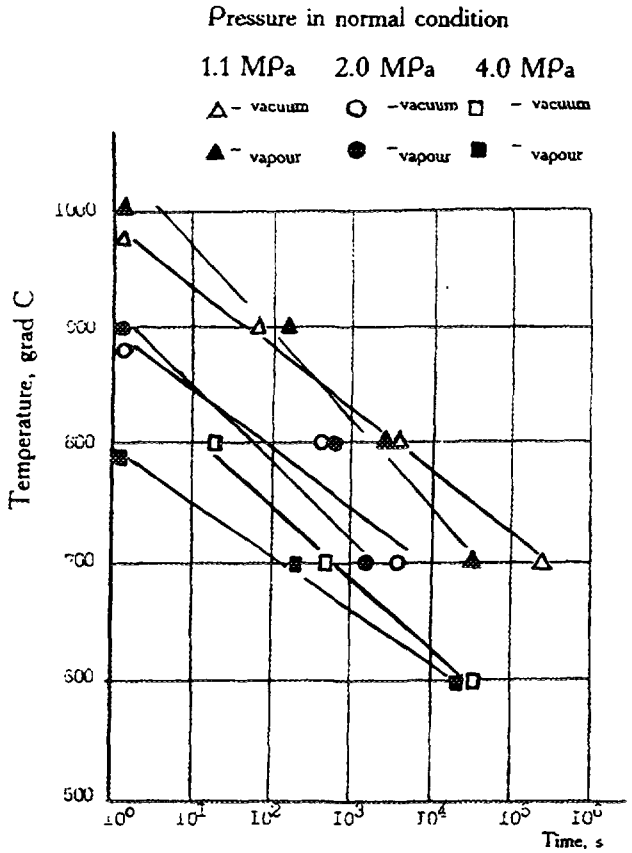

Fig. 1. Rupture of WWER pressurized claddings.

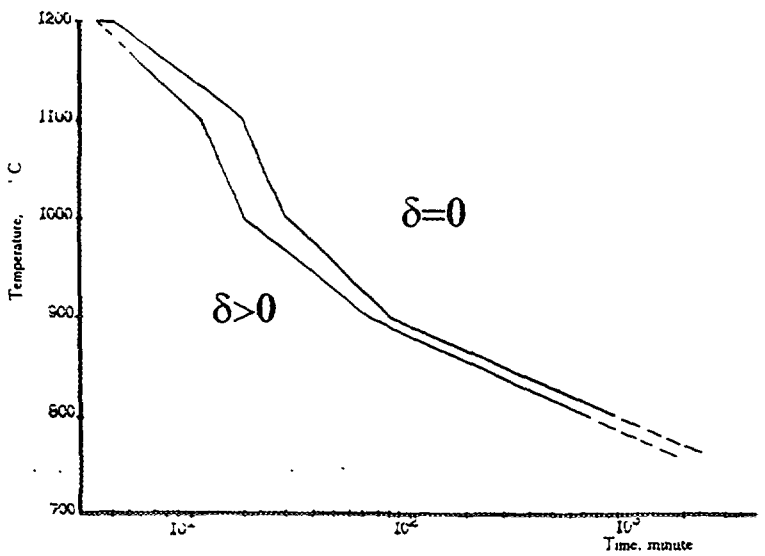

Fig. 2. The area of positive residual plasticity of oxidated claddings.

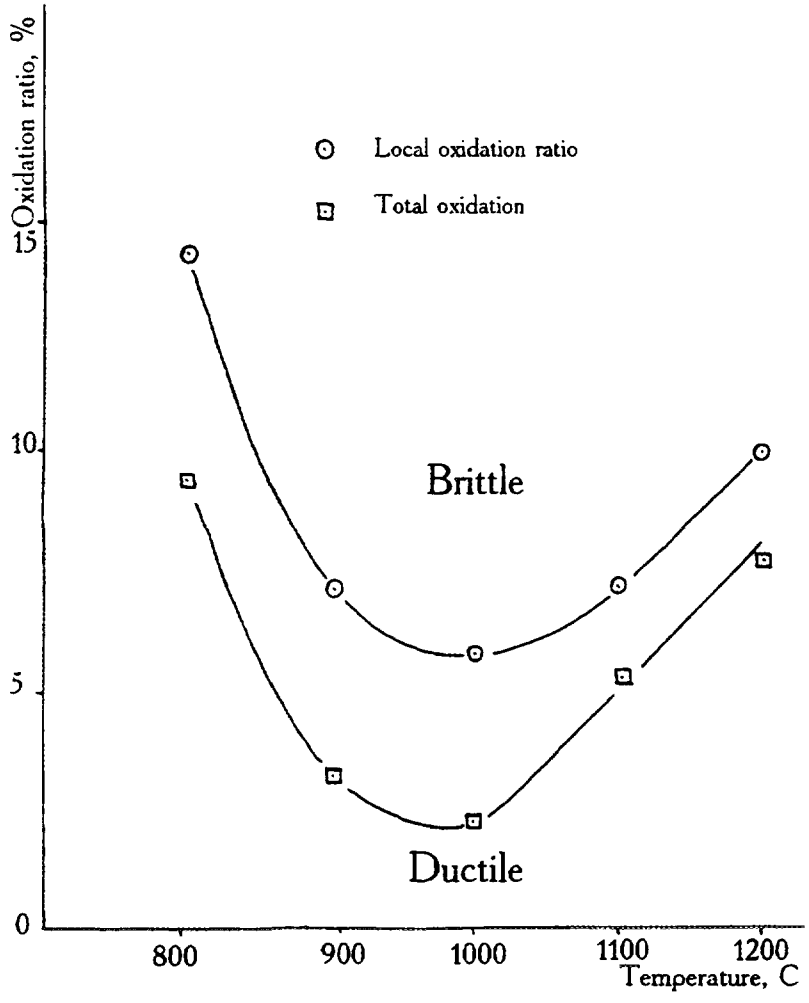

Fig. 3 The border between ductile and brittle failure of oxidised claddings as dependence of oxidation temperature and oxidation ratio.

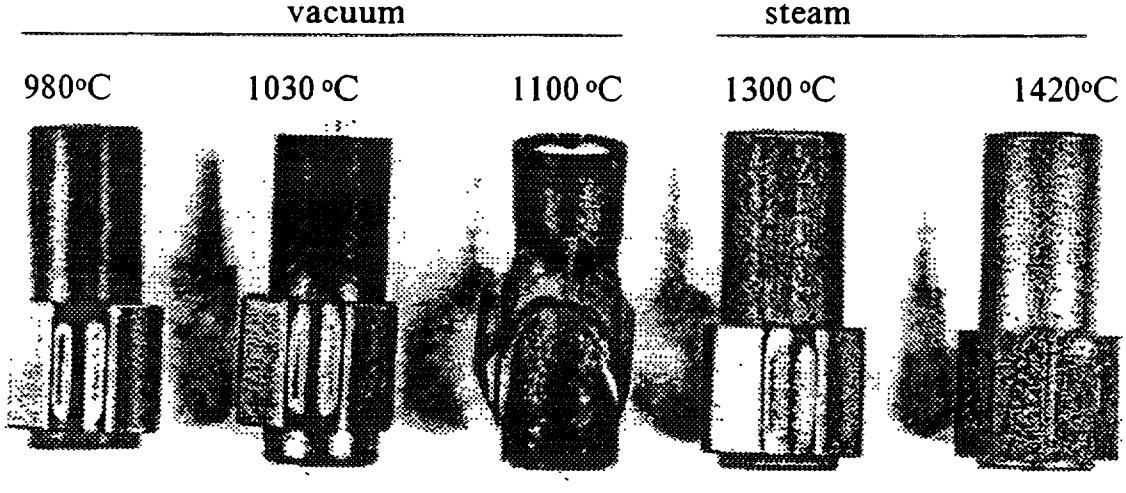

Fig.4 Chemical interaction between steel-made spacer grid cell and zirconium fuel rod cladding in various medium: vacuum and steam.

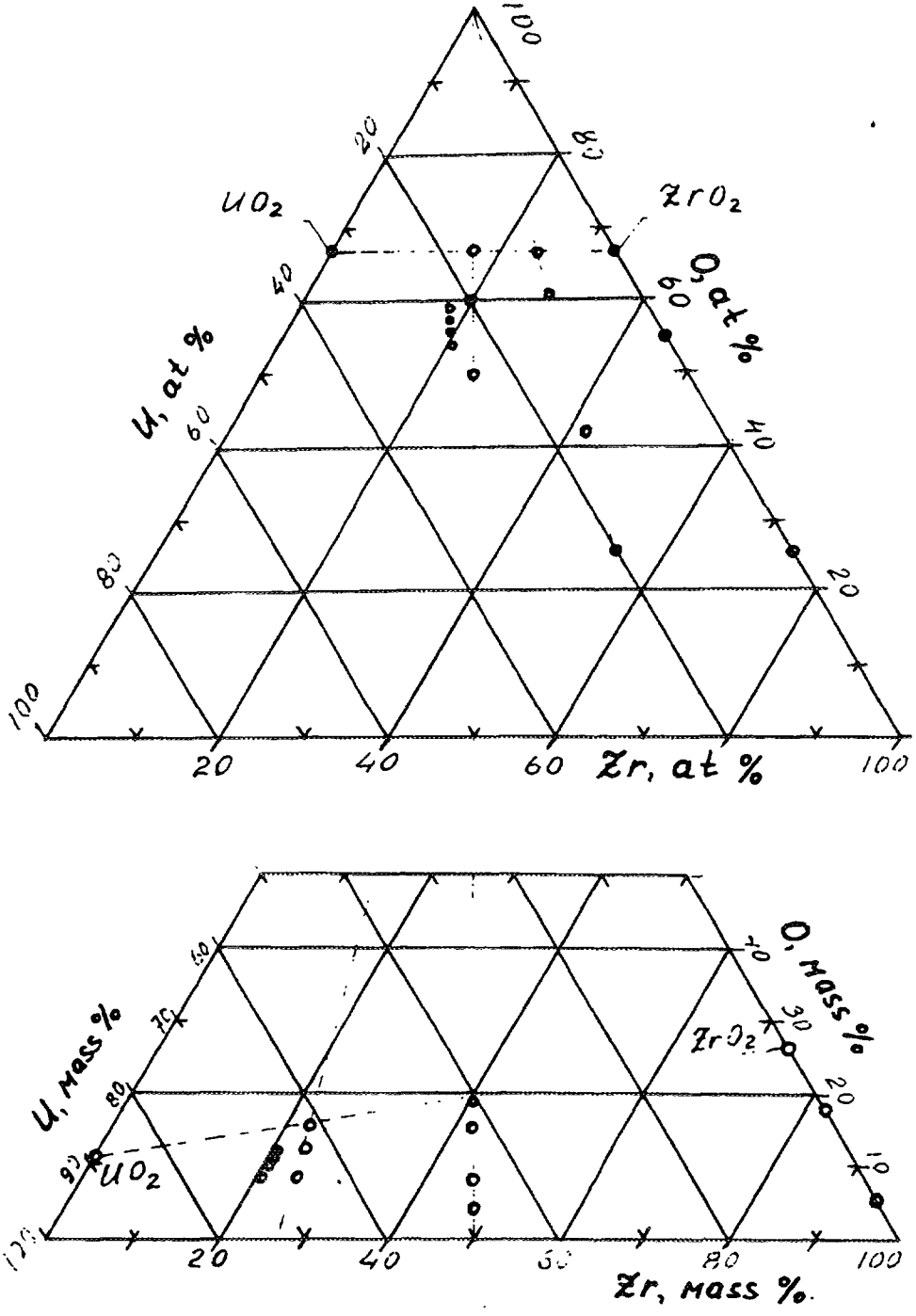

Fig.5 Position of choosed corium simulators on the 3-component diagram

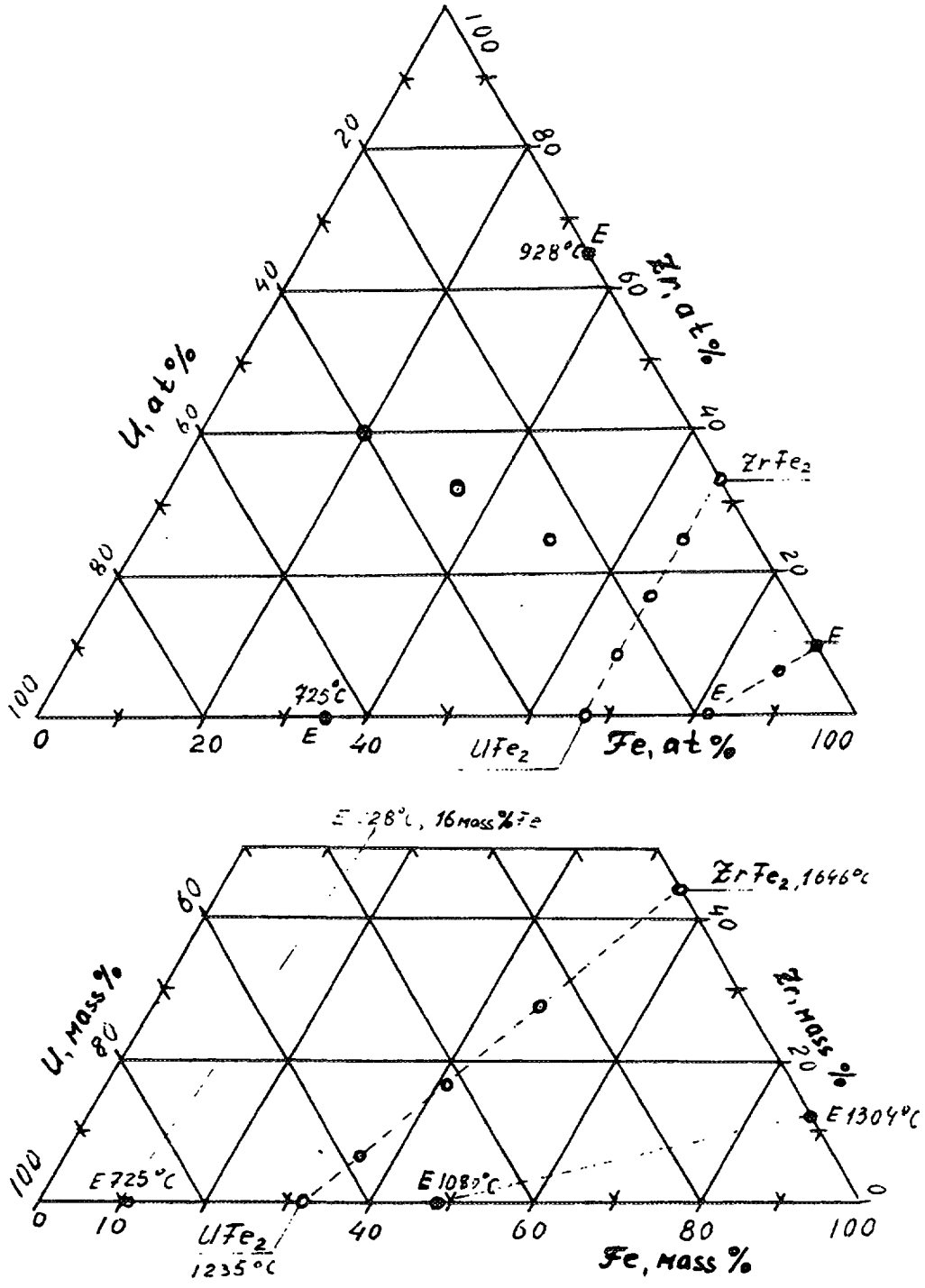

Fig.6 Position of choosed corium simulators on the 3-component diagram

Fig.7 The typical microstructure of the corium composition

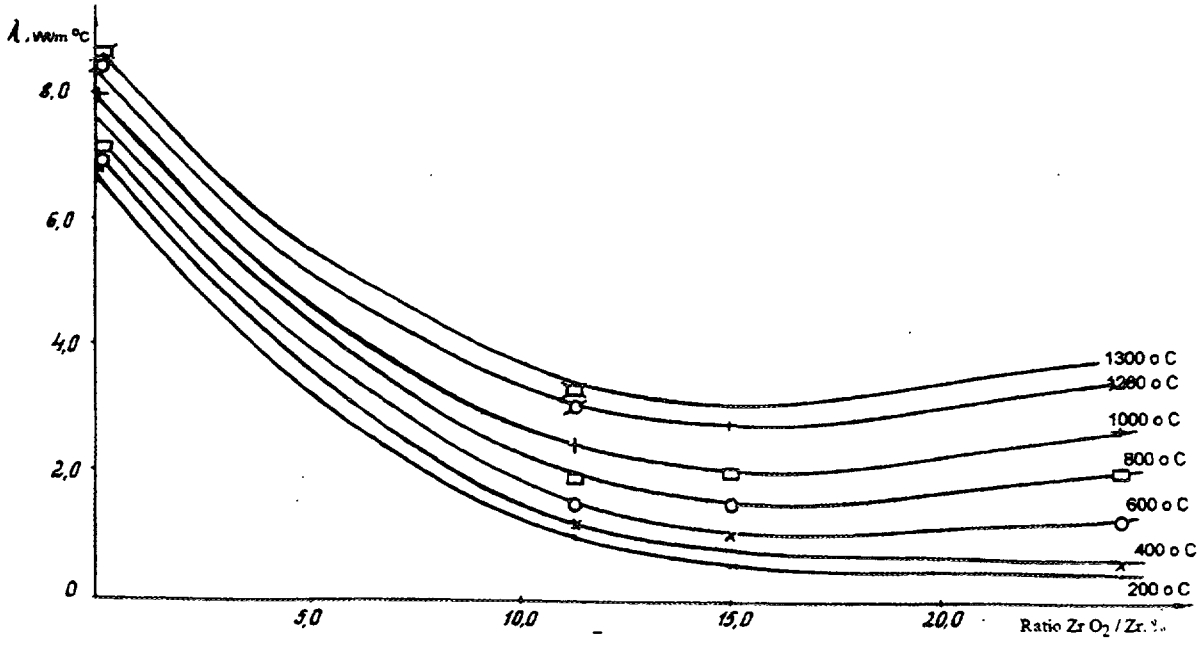

Fig. 8 Heat conductivity of UO_2-Zr -Zr O_2composition as a function of Zr O_2/Zr ratio

TABLE 1. EXAMPLES OF CORIUM SIMULATORS BEEN PREPARED IN IPPE

№	Share of component, % mass						Admixture	Note
	U	Zr	Fe	Cr	Ni	O	Si,Mn,Ti	
2		88	12	-	-	-	-	eutectic
3		45	55	-	-	-	-	$ZrFe_2$
4		45	38	10	5,5	-	1,5	Zr+1X18H10T
5		81,7	-	-	-	18,2	-	56at%O
6	18,6	64,4	-	-	-	16,9	-	UO_2+Zr
7	15	37,3	45,7	-	-	2,1	-	UO_2+Zr+Fe
8	45,8	15,1	33	-	-	6,2	-	UO_2+Zr+Fe
9		94,5	-	-	-	5,5	-	25at%O
10		89,5	-	-	-	10,5	-	40at%O
11		82,3	-	-	-	17,7	-	55at%O
12		30,7	46,6	12,2	7,5	1,8	2,6	Zr+ZrO_2+steel
13		30,1	45,7	11,9	6,6	3,5	2,0	-'-
14		29,3	44,4	11,6	6,4	6,3	1,9	-'-
15	68,1	-	31,9					UFe_2
16		44,9	55,1					$ZrFe_2$
17	24,8	28,6	46,4					25%UFe_2+75%$ZrFe_2$
18	43,1	16,5	40,4					50%UFe_2+50%$ZrFe_2$
19	57,0	7,3	35,7					75%UFe_2+25%$ZrFe_2$
20	65,9	25,2				8,9		UO_2+Zr
21	63,1	24,2				12,7		UO_2+ZrO_2+12%Zr
22	60,5	23,2				16,3		(U, Zr)O_2
23	48	48				4		UO_2+U+Zr
24	46	46				8		UO_2+ZrO_2+Zr
25	42	42				16		UO_2+ZrO_2+Zr
26	40	40				20		UO_2+ZrO_2
27	71,0	19,5				9,5		UO_2+Zr
28	70,5	19,3				10,2		UO_2+Zr+2,6%ZrO_2
29	70,0	19,2				10,8		UO_2+Zr+5,3%ZrO_2
30	69,5	19,1				10,4		UO_2+Zr+7,9%ZrO_2
31	68,3	18,7	3,8 Steel 1X18H10T			9,2		
32	67,8	18,6	-'-			9,8		
33	67,3	18,5	-'-			10,4		
34	66,9	18,4	-'-			10,9		
35	67,7	18,6	-'-			9,1	0,8 B4C	0% ZrO_2
36	67,3	18,4	-'-			9,7	-'-	2,5% ZrO_2
37	66,8	18,3	-'-			10,3	-'-	5,0% ZrO_2
38	66,4	18,2	3,7 Steel 1X18H10T			10,9	-'-	7,5% ZrO_2

TABLE 2. COMPONENT CONTENTS IN VARIOUS PHASES OF MELT No 8

	Fe, % mass	U, % mass	Zr, %mass
Crust (oxides)	0,01...0,44	64...70	26...29
Dendritic phase	55...60	7,5...9	20...31
Indendritic phase	43...50	44...55	3,5...6,4

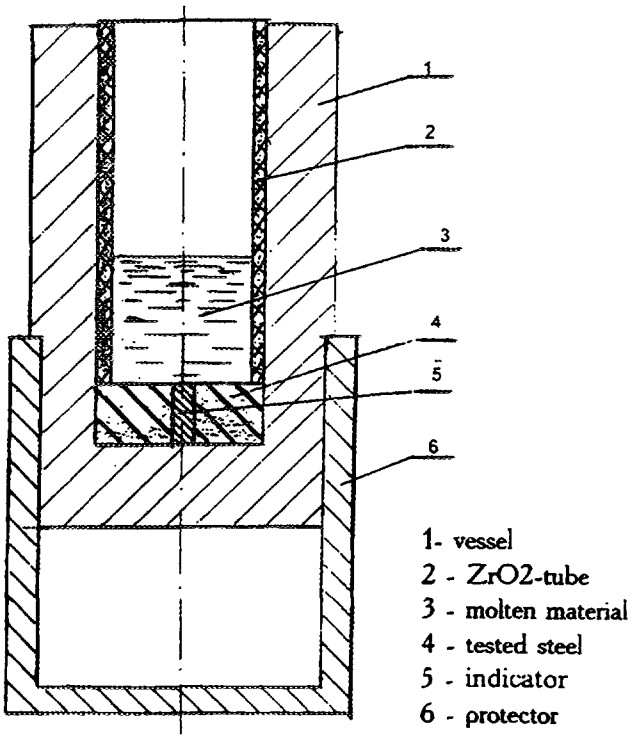

Fig. 9 Container for investigations of metallic phase-structure steel interaction

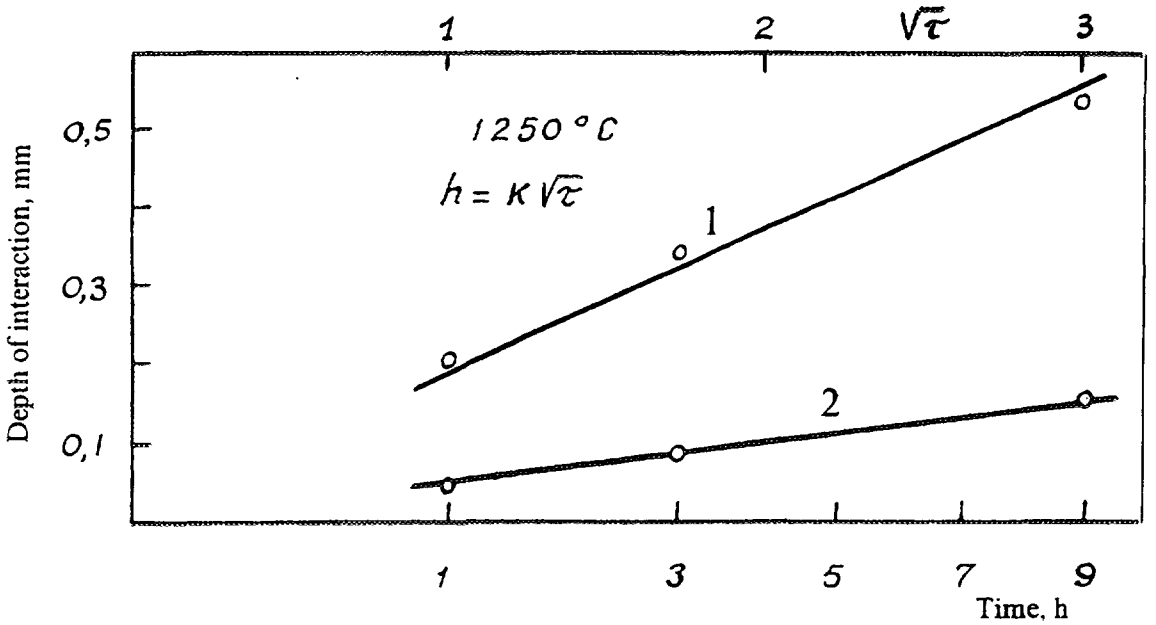

Fig.10 Depth of interaction between molted eutectie Zr-Fe-U and vessel steel
1. Intergranular penetration, 2. Total dissolution

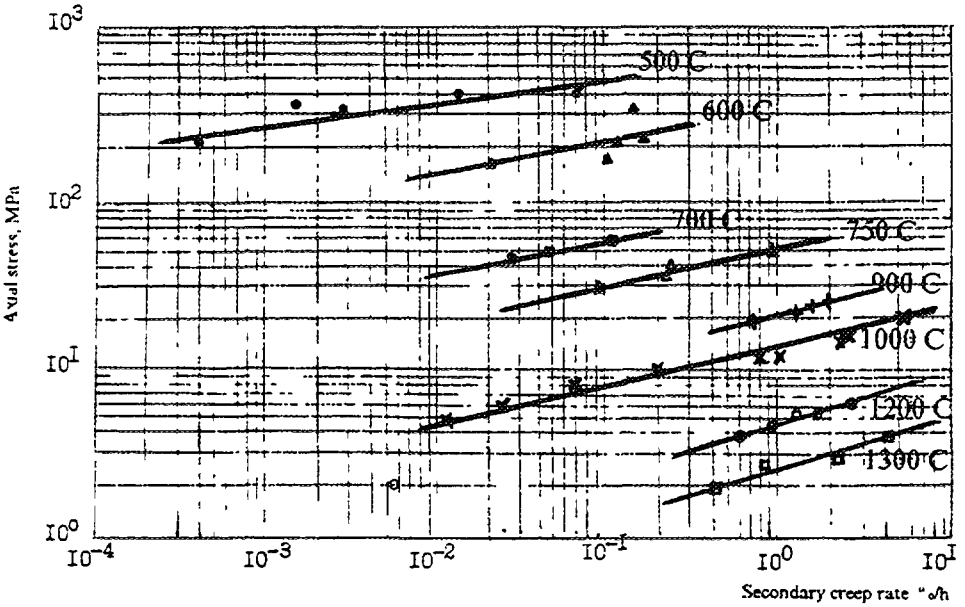

Fig.11 Experimental results on secondary creep tests

3. RESIDUAL MECHANICAL PROPERTIES AFTER CLADDING OXIDATION

Both for LBLOCA and for the first stage of severe accident it is important to know a residual mechanical properties of structure materials. It is sufficiently to demonstrate two examples:
- after LBLOCA it is necessary to demount a core and all structure elements including fuel rods should keep a strength;
- thermal shocks can take place under reflooding process and it is important to know whether structures will fail.

As a result of high temperature oxidation and structure evolution zirconium claddings lose the plasticity. In Figure 2 the border between ductile and brittle areas of residual properties is presented. This result is obtained by mechanical tests of ring specimens which have been cuted out from oxidised claddings.

The reasons of cladding embrittlement are oxygen solution into zirconium lattice and $\alpha Zr(O)$ phase formation and formation of hydride precipitations. These facts are confirmed by X-ray phase analysis and metallography.

In Figure 3 the area of residual plasticity is shown in dependence of test temperature and oxidation ratio. It is interesting to note that official limit of safe oxidation (18%) doesn't concern to residual embrittlement.

4. CORE MATERIAL LIQUEFACTION

The presence in fuel assembly compound of different materials such as zirconium alloy, stainless steel, boron carbide, uranium oxide makes possibility of premature liquefaction at the temperature level much less than melting point of materials. In principal liquid eutectic formation may be observed at the temperature about 940°C between iron and zirconium. Various liquids can be formed at temperature between 950 to 1400°C due to the chemical interaction between structure components.

However, oxidising can prevent to interaction. In fact in conditions of steam under temperature rising but below the point of liquefaction the protective oxide layer is appearing and liquefaction doesn't happen. The number of tests with interactive pairs (steel grid sells and zirconium tubes) have been conducted in vapour loop at various temperature levels. Illustrations of

results are shown in Fig.4. Liquefaction in vacuum is happen under temperature below 1100°C (initial zirconium tube oxidation increases liquefaction temperature) and liquefaction in steam is observed only above steel melting point.

Thus, in reality liquefaction between fuel rod cladding and steel spacer grid doesn't occurs. Only melting take place in this system. It is important to note that this conclusion is true for these structure configurations only and may be mistaken in generally.

Obviously, oxidation of interactive surfaces will prevent to chemical interactions between any core materials. At the same time oxidation can causes quite new phenomena under high temperature process. For instance, oxidising of the boron carbide can lead to significant reducing of melting point.

All of these phenomena should be studied more careful.

5. CORIUM FORMATION, CORIUM EVOLUTION, CORIUM PROPERTIES

Corium evolution and corium properties have been studied with the help of corium simulators.

More than 50 corium simulator ingots have been prepared in IPPE, Table 1. The main phase forming components are uranium, zirconium, oxygen, iron. In dependence of oxygen contain compounds may be separated into "oxide corium" and "metallic corium". The choose of initial corium compounds is shown with the help of 3-component diagrams, Fig.5,6. Points on these diagrams are prepared alloys.

Alloys have been melted in arc furnace at temperature higher
of oxide melting points. The typical microstructure of ingots is shown on Fig.7 (alloy ¹ 8 from Table 1). Usually separation of oxide phase (crust) and metallic phase (grey area) is observed. The content of original components in ingot is quite different one, Table 2.

Thermal-physical properties of the corium simulators are studied. In the Figure 8 the dependence of heat conductivity versus oxygen content for UO_2-Zr-ZrO_2 composition is presented. Temperature conductivity and irradiation capability are obtained too.

Also the interaction kinetic between molten metallic corium simulator and structure steel is studied, Fig.9. The interaction depth is indicated after test by metallography analysis. Example of experimental result is shown in the Fig.10. The molten corium simulator is (Zr-Fe) eutectic plus uranium 5%. Interaction is studied in isothermal condition.

6. STRENGTH ANALYSIS OF THE REACTOR VESSEL LOWER HEAD

Calculation model of thermal-hydraulic behaviour of the molten pool is under developing now. This model will present a temperature fields in reactor lower head wall under molten pool evolution. The strength model is developed. It demands characteristics of elastic-plastic-creep deformation of vessel steel at temperature range 600-1400°C.

The number of mechanical tests is conducted. Data bank is formed. As example the secondary creep is presented in the Fig.11. Creep rate and time-to-rupture including tests in liquid eutectic environment have been studied too.

Deformation of vessel lower head and its time-to-rupture have been calculated in various temperature conditions. The main results is: if temperature of inner surface of the lower head will be less that 800°C, the strength of pressure vessel will be secure. Of course, this conclusion is the previous one.

7. CONCLUSION

Safety analysis of nuclear power units demands to have an adequate calculation models for describing of the phenomena totality in ab-normal condition. These models and calculation codes concerning to thermal-hydraulic or material science problems are under development now. Some

processes are modelled better, but another ones require additional information concerning to materials and structure behaviour.

Presented framework has the objective to supply calculation models by necessary information about material properties and structure behaviour. This activity doesn't finished. Moreover, there are some questions which never been considered yet. For example, oxidation of molten corium in various stages of corium formation has never been studied. This is a task for the future. Also, the influence of fission products upon the corium properties and corium behaviour will be studied. It is necessary to learn in more details the significance of absorber presence for metallurgical phenomena.

Some questions are solved mainly now, such as cladding oxidation, cladding ballooning corium phase's separation et al. This experience demonstrates that many practical tasks may be solved by laboratory-scale experiments, and this scale allows to achive useful results. The combination of large-scale and laboratory-scale experiments must be optimum one, and large-scale integral tests must be implemented for code's verification mainly.

ACKNOWLEDGEMENTS

This work was supported by the Ministry for Atomic Energy of Russian Federation. The authors express thanks to the staff of IPPE laboratories for conducting of this work

STUDY OF HEAT AND MASS TRANSFER PHENOMENA IN FUEL ASSEMBLY MODELS UNDER ACCIDENT CONDITIONS

A.D. YEFANOV, C.G. KALYAKIN, V.M. LOSHCHININ,
R.S. POMET'KO, V.V. SERGEEV, R.V. SHUMSKY
Institute of Physics and Power Engineering,
Obninsk, Russian Federation

Abstract

The majority of the material in support of the thermal - hydraulic safety of WWER core was obtained on single - assembly models containing a relatively small number of elements - heater rods. Upgrading the requirements to the reactor safety leads to the necessity for studying phenomena in channels representing the cross - sectional core dimensions and non - uniform radial power generation. Under such conditions, the contribution of natural convection can be significant in some core zones, including the occurrence of reverse flows and interchannel instability. These phenomena can have an important influence on heat transfer processes. Such influence is especially drastical under accident conditions associated with ceasing the forced circulation over the circuit.

A number of urgent reactor safety problems at low operating parameters is related with the computer code verification and certification. One of the important trends in the reactor safety research is concerned with the rod bundle reflooding and verificational calculations of this phenomenon. To assess the water cooled reactor safety, the best fit computer codes are employed, which make it possible to simulate accident and transient operating conditions in a reactor installation. One of the most widely known computer codes is the RELAP5 / MOD3 Code. The paper presents the comparison of the results calculated using this computer code with the test data on 4 - rod bundle quenching, which were obtained at the SSCRF - IPPE.

Recently, the investigations on the steam - zirconium reaction kinetics have been performed at the SSCRF - IPPE and are being presently performed for the purpose of developing new and verifying available computer codes.

1. FLUID DYNAMICS AND HEAT TRANSFER IN MULTIASSEMBLY CORE MODELS

The tests were conducted on an integral WWER - 1000 primary circuit model including a 5 - assembly model shown in Fig.1. Each of the assemblies encomprises 14 indirectly heated 700 mm long heater rods 9.1 mm in diameter, i.e. the scale of height is 1 : 5. The heater rods were arranged in triangular array with a pitch of 12.75 mm. All five assemblies were encased into a test vessel with internal dimensions of 38 × 340 mm^2. The front and the back walls of the test vessel were manufactured of heat - resistant glass.

The partition presence or absence between the fuel assemblies makes it possible to simulate fuel assemblies with and without shrouds (WWER - 440 and WWER - 1000, respectively). In the area of the lower plenum, all fuel assemblies were in communication with each other, as it is in the case of a real reactor set - up.

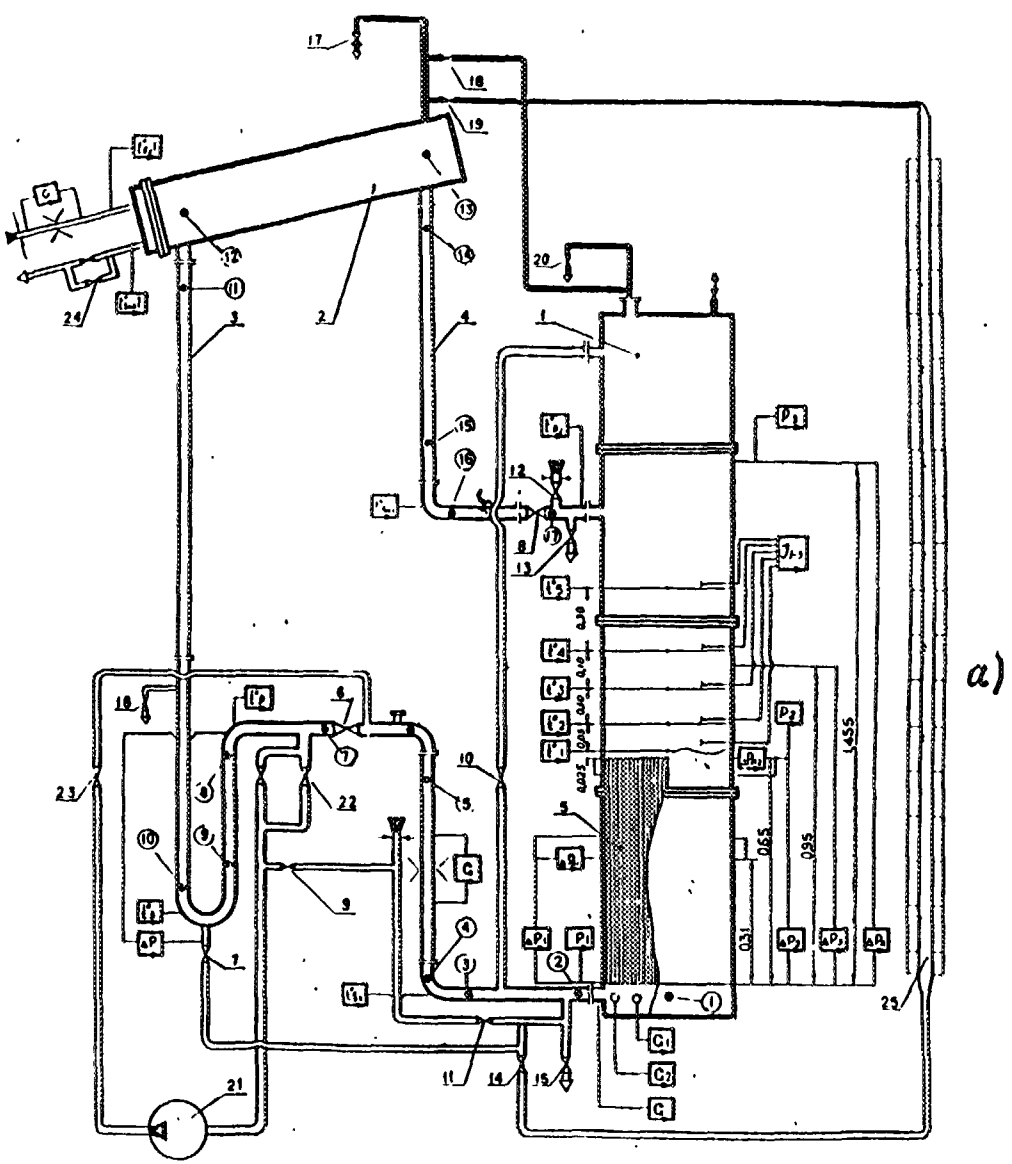

a)

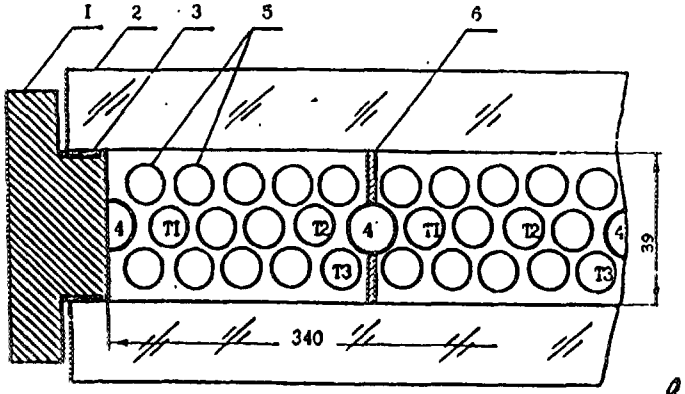

B)

Fig.1. Schematic Diagram of Test Section and Core Model Cross-section.

a) 1-5-assembly reactor model; 2-heat exchanger; 3- cold line; 4 - hot line; 5-fuel assemblies; 6-20 - control valves, providing coolant supply and discharge from circuit; 21-pump; 22,23-pump cut-off valves; ①-⑰ - pressure taps; 24-cooling water flow rate control valves; 25-measuring tube.

b) 1-test vessel; 2-front and back walls of test vessel; 3-seal; 4-non-heated rod; 5-heated rod; 6-baffle.

One of the limiting hydrodynamic phenomena occurring in WWER - type reactors under accident conditions with a water filled core is reflooding. It is characteristic of the situation under such conditions that there is no coolant flow rate at the channel inlet, with the upward steam flow and downward water flow within the channel itself. As the power supply to the channel increases, the flow rate of steam being generated goes up and conditions are reached, when water entering the channel from above is not capable to compensate its evaporation. From this moment, the channel dryout starts, which finally leads to the fuel element overheating.

The main goal of such researches is to obtain the test data on heat fluxes and cross - sections where the heater rod overheating origins under the conditions of nonuniform cross - sectional power generation.

A few of results obtained for the symmetric power generation profile and variable power of central fuel subassembly 3 are demonstrated in Fig.2. It is evident that in the presence of nonheated zone in the center of the model, the N_{cr} value is minimal (profile 1 in Fig.2). As the power of central fuel subassembly 3 (profiles 2,3 and 4) increases, the net power increases too. Fig.2 shows also the cross - sectional location of the CHF occurrence and the distance from the upper point of heating (z_{cr}) for each profile. As evident, the actual CHF location substantially varies with the profile changing. This fact may be explained by the variation in the natural convection intensity in this region as well as by changing its direction from upward to downward one as the central rod bundle power increases.

It is established also that the CHF location changes at the transition from shroud - covered fuel assemblies to those without shrouds: in fuel assembly models without shrouds, the CHF occurs in the area of heater rods being on the boundary of stable upward and downward convective flows; the CHF occurring not necessarily in the hottest fuel subassembly.

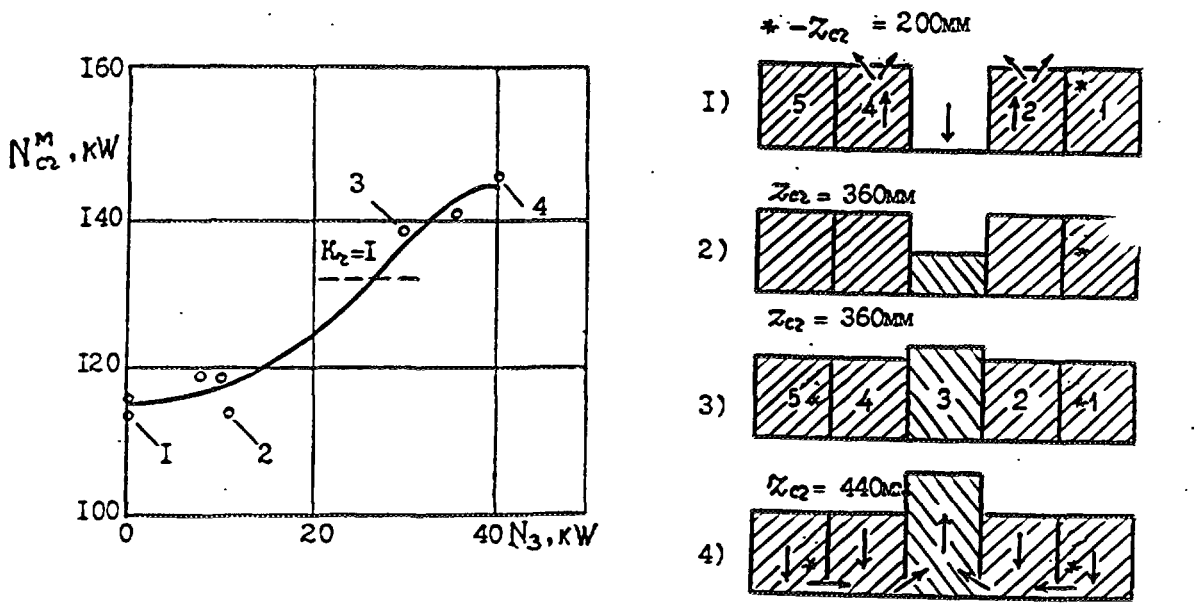

Fig.2. Critical Power of Core Model with Shroud-Covered Fuel Assemblies as a Function of Central Fuel Assembly Power. Z_{cr}-distance from CHF initiation to the top of heating. Arrows in Profiles 1-4 indicate the direction of convective flows.

The reflood test data obtained were compared with the results calculated using the correlations by Wallis, Tien, TsKTI and Bezrodny. In all cases, the TsKTI and Bezrodny correlations describe the data for multichannel systems best of all. The question is certainly about only a rough agreement of results at a power generation being close to the uniform cross - sectional one. In transition to rod bundles, the Wallis reflooding equation needs be substantially refined as it was done, for example, with the reflooding model for the RELAP5/MOD3 Computer Program. The results presented in Fig.2 as well as the other available test data on reflooding show a rather strong influence of the nonuniform cross - sectional power generation on the critical power value and the CHF occurrence point. Also it was established that these phenomena are significantly affected by fuel assembly shrouds. The fact of importance is actually the rod overheating in the area of downward flows, where maximum heat fluxes are not observed.

In a number of accidents accompanied by coolant leakage in the primary circuit, conditions under which the coolant level does not reach the top of the zone are possible. Such conditions can occur due to the absence or insufficient rate of feedwater supply, negative effect of hydraulic loop seal, etc.

In modeling situations like the abovementioned one, the following parameters were recorded along with the heater rod temperature: the power of each of 5 fuel assemblies, the mass and physical levels of coolant in each fuel assembly , the temperatures of the superheated steam above the upper edge of heater rods.

Based on the test results, the heat transfer coefficients, α_{exp}, were determined. The obtained results were compared with a few of correlations for laminar conditions in the uncovered zone.

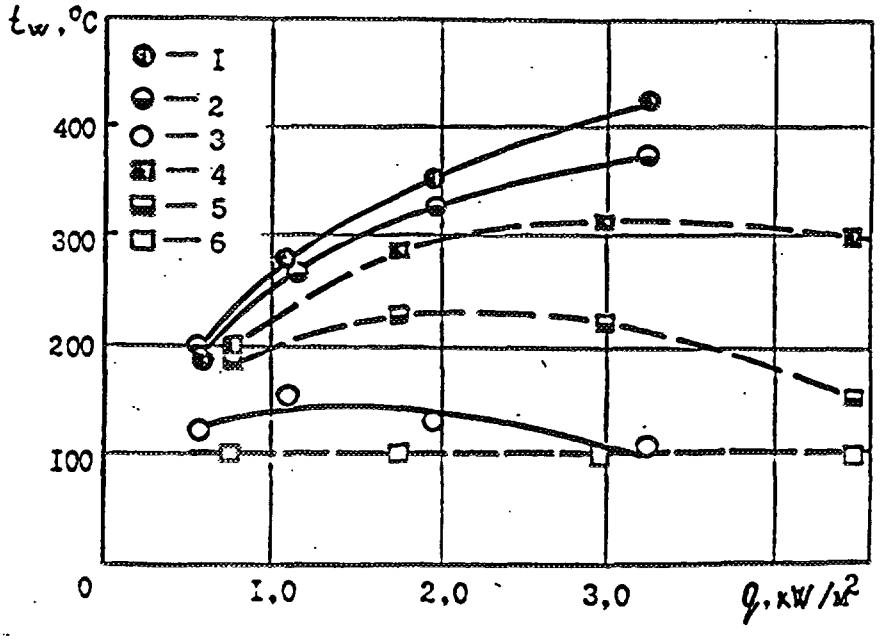

Fig.3. Heater Rod Wall Temperature in the Uncovered Zone as a Function of "Hot"Fuel Assembly Heat Flux. The height of the mass level is 400 mm; q_{max}/q_{min}=1.15; all fuel assemblies being heated. 1-3 - fuel assemblies without shrouds; 4-6 - with shrouds. The distance from the heating beginning: 1.4-630 mm; 2.5-570 mm; 3.6-440 mm.

In Fig.3, the comparison of some results on the heater rod temperature behavior in rod bundle systems simulating the fuel assemblies with and without shrouds is given. In both cases, the presented temperature values refer to the hottest fuel assemblies at a cross - sectional nonuniformity coefficient, $q_{max}/\bar{q}$, of 1.15. To judge by the results obtained in Fig.3, it can be noted that in the fuel assembly with shroud - covered assemblies more lower temperatures are observed in the uncovered region. The partition absence might be expected at first glance to lead to the occurrence of intensive cross - sectional flows and temperature level flattening at the nonuniform cross - sectional power generation. However, an opposite situation is actually observed: the temperature values in rod bundle models with shrouds are by 50 ÷ 150 °C lower under otherwise equal conditions.

The following is probably responsible for such behavior. First, in fuel assemblies splitted by partitions, the physical levels of coolant are very different at the nonuniform cross - sectional power generation, whereas in fuel assemblies without partitions, a certain flattening of the physical levels of coolant takes place. The more higher values of the physical levels in hot and partitioned fuel assemblies result in an increased amount of steam generation and augmented droplet entrainment and therefore can be the main cause of the heat transfer improvement in such fuel assemblies.

The second fact which seams to be responsible for more higher rod wall temperatures in the shroudless fuel assembly model is associated with the steam flow in the uncovered region. Not only water but also steam can leave the hotter fuel assemblies (or subchannels) due to higher pressure drops in the uncovered region. The reduction of steam flow rates over a hot fuel assembly in the uncovered region will favour its heating - up and increasing in heater rod wall temperature.

Thus, the information as obtained for heat transfer in uncovered region permits one to postulate that in the core consisting of fuel assemblies housed in shrouds, the fuel element overheating is lower. To judge by the fact that all domestic data on heat transfer in the uncovered region were produced on single fuel assemblies, these results may be expected to lead to more favourable results than they are in reality as applied to WWER - 1000 cores (consisting of shroudless fuel assemblies) without due account of cross - sectional flows.

2. COMPARISON OF RELAP5/MOD3 CALCULATIONS WITH TEST DATA ON 4 - ROD BUNDLE REFLOODING

The tests were conducted on a bundle of four heater rods. The flow area of the channel was the 32 by 32 mm square. The heater rods represented stainless steel 3008 mm long tubes with cross - sectional dimensions 13 × 1 mm, which were heated by direct current . Up to 10 thermocouples with 0.3 mm thermoelectrodes were installed on the internal surface of each of the four tubes by contact welding. The heater rods were centered in the channel by means of 15 mm high spacer grids. All in all 12 grids were arranged with a pitch of 245 mm; the first spacer grid being 49 mm distant from the heating start. The test facility was equipped with a IVK20 - and PC - based data acquisition system making it possible to record up to 100 channels with a frequency to 4 kHz.

The test procedure was as follows. Using the pressurizer, a pressure about 0.25 MPa was maintained in the test section outlet with a prescribed inlet water flow rate and temperature. After the circulation which proceeded during a few minutes and heating the equipment, the pumps were turned off and the test channel was cut from the circuit and drained. Then, the channel was jointed to the circuit; using gas from cylinder, the preset pressure was restored and electric power was

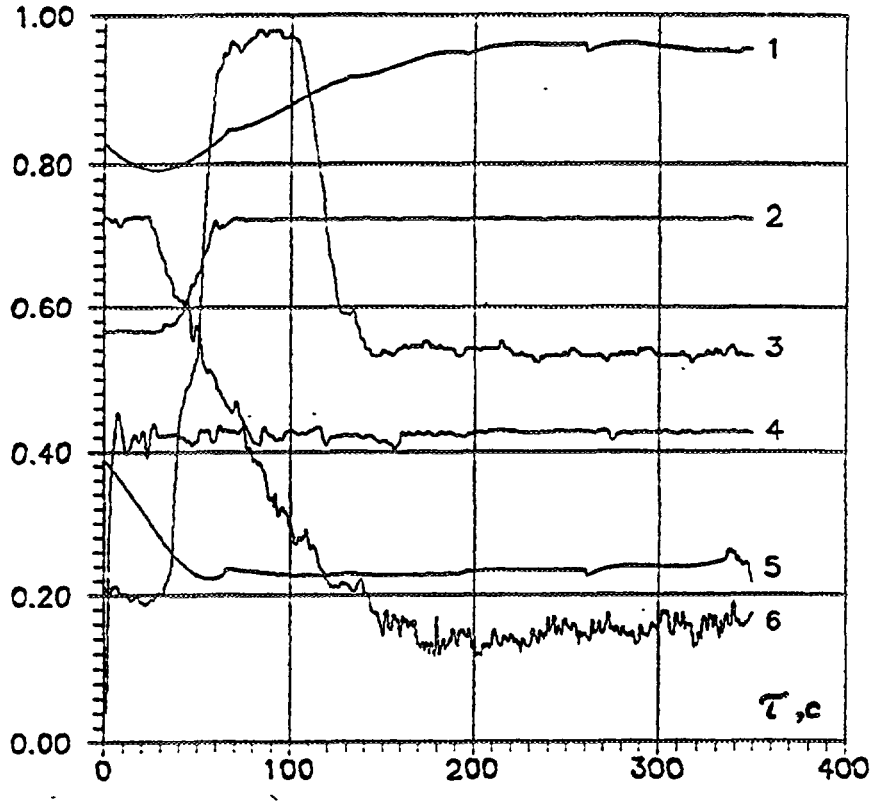

Fig.4. Operating Parameters Versus Time at Reflooding.
Test run 10. 1-power (N/25) kW; 2-pressure (P/4) bar; 3-outlet temperature (T/250)°C; 4-flow rate (G/200) kg/h; 5-inlet temperature (T/150)°C; 6-pressure drop on channel (Δ P/ 0.5) bar.

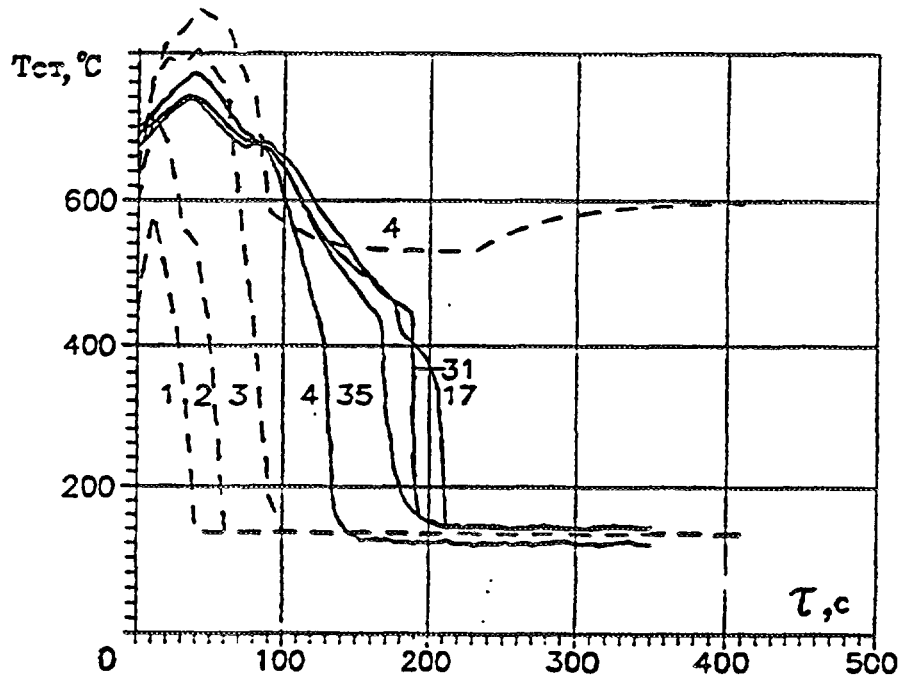

Fig.5. Test Section Surface Temperature Versus Time.
_____ test (4.35.31.17-distance from the heating beginning is 1568, 2138, 2488 and 2838 mm, respectively);
- - - - - calculation (1.2.3.4-distance from the heating beginning is 1075, 1505, 2150 and 2580, respectively).

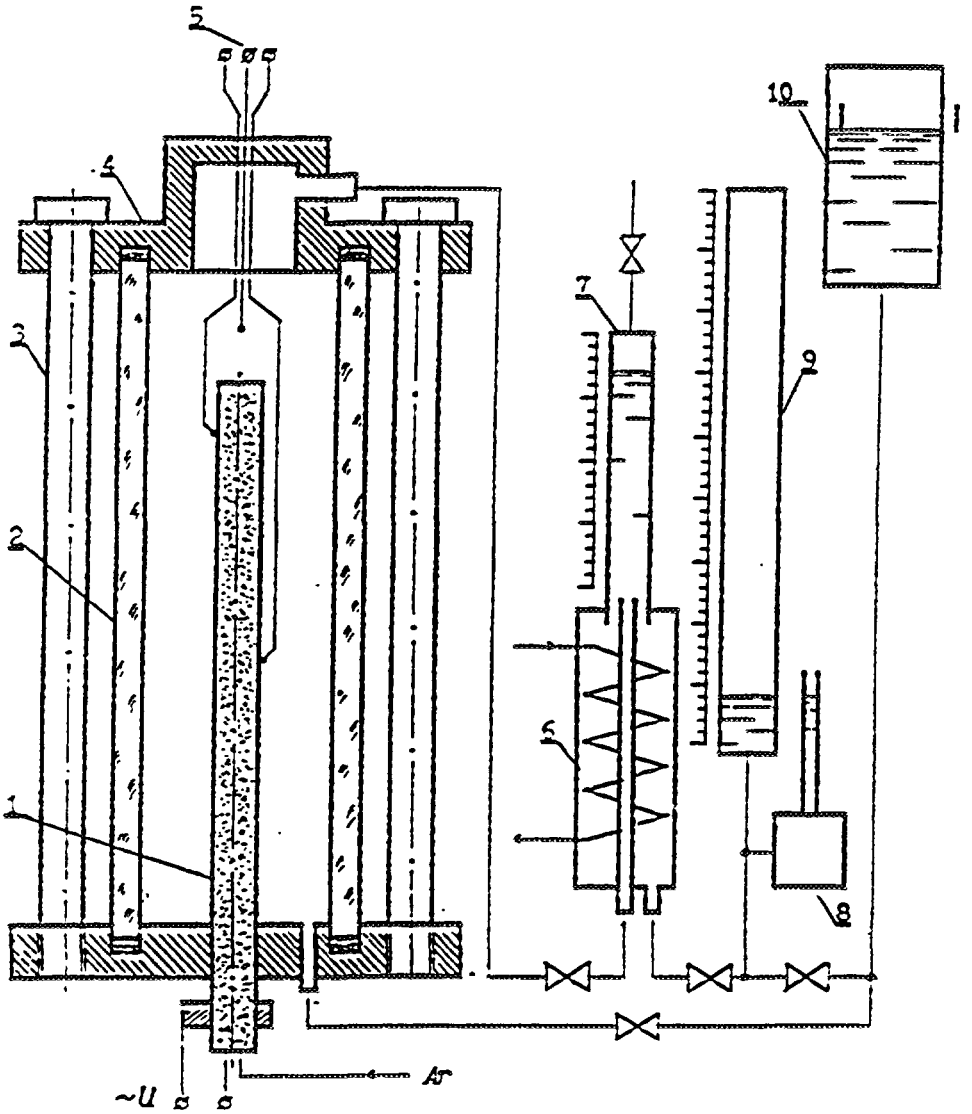

Fig.6. Schematic of Test Apparatus for Study of Hydrogen Release Kinetics during Steam-Zirconium Reaction on a Heater Rod.
1-heater rod; 2-transparent test vessel; 3-pillar; 4-flange; 5-thermocouples; 6-cooler; 7-hydrogen collector; 8-differential pressure gauge; 9-collecting tank; 10-water feed tank.

supplied to heater rods. After one of the thermocouples had reached the preset temperature (about 970 K), the data acquisition system was automatically put on and the coolant circulation was resumed. From this moment, the reflooding of the channel started. The quenching front went up and the channel inlet pressure rose due to the steam generation a little. With going over the preset level of pressure, steam was partially released into the atmosphere.

Using a specially developed program, the test data were averaged by means of base splines; and the heat flux, the heat transfer surface temperature and heat transfer coefficients in the unwetted region were determined according to the special programs.

The calculations were performed using the RELAP5/MOD3/V5M5 Code [2] The nodalization scheme of the test section consists of 7 components including the inlet chamber, pump, fuel

assembly, a simple fuel assembly junction to the outlet chamber, the outlet chamber, setting part and fuel assembly shroud.

The following parameters were initially preset in calculations: thermal power, pressure Po, and temperature $\bar{T}_o$ (in the fuel assembly), coolant flow rate at the inlet (being equal to zero), coolant flow rate at the outlet (being equal to zero), pressure, P_o = 2.7 bar, and steam quality, X_o = 1 (in outlet chamber).

If only in one of the sections the wall temperature, T, reached 973 K, the inlet flow rate varied stepwise from zero to the preset value (0.05 m/c). At this moment, the bundle was considered uncovered and from this moment, its reflooding started. The variation of main parameters in the course of the test is shown in Fig.4.

The comparison of calculated results with experimental data on heater rod surface temperature variation is demonstrated in Fig.5. As evident from the figure, the calculation substantially underestimates the time of the fuel assembly quenching in first 11 sections: at the same time, complete cooling does not occur in outlet sections. An attempt was made to improve the agreement of the results by taking account of the effect of the insulation material restricting the channel flow area. This made it possible to eliminate the quenching front blockage and reduce the peak wall temperatures to experimental values. However, the agreement in quenching time was actually not improved.

In the present authors opinion, the main causes of the discrepancy are as follows. To evaluate heat transfer in the uncovered zone, the code version under consideration employees the modified Brombey equation for a horizontal pipe at natural convection, where the tube diameter is substituted by the length of a quick - raising wave. Besides, to average the heat transfer coefficient within the wide range of two - phase flow qualities, a weight factor varying from 1 to zero is used. However, based on the available experimental results [3], the quality varying from zero to 1 actually does not exert any effect on the heat transfer coefficient. It is worth noting also that the data obtained by the present authors are in fair agreement with the results calculated by the Sacurai and Dhir formulae having the same form as the Bromley equation. Thus, the expression used in the Code for evaluating the heat transfer under the conditions of saturated film boiling (mod 8) and subcooled boiling (mod 7) is incorrect both from the viewpoint of its application for absolutely different conditions and from the viewpoint of quality accounting.

3. EXPERIMENTAL AND CALCULATIONAL STUDIES OF THERMAL - HYDRAULIC AND PHYSICAL - CHEMICAL PHENOMENA COUPLING IN UNCOVERED WWER CORE

The WWER core contains about 20 t of zirconium and zirconium melt capable of producing about 900 kg of hydrogen in the assumption of full oxidation. In principle, other core materials (like steel, Inconel, etc.) can be the additional source for hydrogen. Nevertheless, zirconium is the basic source of hydrogen in accident situations; the rate of its liberation being dependent on many conjugated phenomena.

The distruction of the oxide film on the zirconium surface is the factor which intensifies both the hydrogen release and the distruction of the shell itself. The free circulation in the emergency core also has an important bearing on the time of the hydrogen generation and its amount. A great influence on the hydrogen release rate is affected by the steam flow rate to the zirconium

surface. Thus the ingress of an additional amount of water into the zone, for instance, due to the personnel action may result in an augmentation of hydrogen release and thus, from this viewpoint, in worsening the situation in the core.

The studies of the steam - zirconium reaction kinetics were primarily restricted by integral characteristics and aimed at the development of new computer codes and verification of the available ones so far. However, in view of the sophistication and versatility of phenomena occurring in the accident core, the existing codes not always predict them adequately.

The differences are actually due to both the conditions of experimental simulation and discrepancy in the assessment of the contribution of separate components of phenomena occurring under the accident conditions in the core.

Thus, test data are urgently needed to refine the thermal - hydraulic models describing the hydrogen generation processes in the WWER core under the accident conditions.

The main goal of the present paper is to provide test data and develop computer codes giving account of the steam - zirconium reaction proceeding peculiarities and the effect of the two - phase mixture thermal - hydraulics on it during the WWER core uncovery.

The tests are expected to be conducted both using a single rod (a heater rod with internal heating) and a 3 and 7 rod bundle of zirconium tubes under the rod bundle uncovery conditions at the atmospheric pressure. The initial conditions are assumed to be as follows. The rod bundle is completely inserted into water (at a temperature of 20 $^{\circ}$C). The electric power is supplied to heaters installed inside rods. In the process of boiling, the water level goes down, the heater rods become uncovered and start to heat - up. At a certain temperature, the steam - zirconium reaction initiates. In the course of the experiment are recorded: the rod bundle temperature behavior, the rod bundle outlet steam temperature, the steam flow rate, the average void fraction, the local quality (the phase component measuring transmitter), the flow rate of steam generated, etc. If necessary, a water feed system is provided for the rod bundle.

These tests are planned to be extended by subsequent metallographic examination of heater rods and inspection of disturbances in the heater rod bundle (or separate heater rod) geometry. The schematic diagram of the test facility is presented in Fig.6. The basic components of the test facility are:

- a rod (heater rod) or rod bundle (3) with a 9.1 mm - 0.d., 1 m long zirconium shroud. The internal space of rods where a tungsten - niobium heater is positioned is filled with argon at a pressure of 0.7 ÷ 1.9 MPa. The rods are arranged in bundle in correspondence with the geometric parameters of WWER core. The temperature range of the external rod surface is 500 ÷ 1400 °C;
- the rod bundle vessel (1) is a pipe manufactured of quartz glass (for the visualization of the rod bundle uncovery phenomenon). If neces-sary, a stainless steel pipe may be used;
- a cooler (6);
- a calibrated vessel (5) for hydrogen collection;
- a tank (7) for collection of water forced out from the rod bundle;
- a tank (9) providing the test section with water feed.

If need be, the test section can be joined to the facility which makes it possible to deliver the superheated steam to the rod bundle and provide the hot rod bundle water reflooding, etc.

The main distinction of this paper from similar ones known from different literature sources is the wide range of phenomena under consideration, from the kinetics of the steam - zirconium reaction and the rod bundle thermal - hydraulics effect on it to the rod bundle configuration change being due to the rod deformation.

CONCLUSION

1. The test data on the multiassembly core models evidence that the non - uniform asymmetrical power generation has a strong influence on the critical heat flux at reflooding. In a model consisting of fuel assemblies without shrouds, the CHF is primarily observed to occur on the boundary of stable upward and downward convective flows; whereas in a model consisting of shroud - covered fuel assemblies, the CHF may occur in low power generation regions where downward flows are predominant.

2. It is established that at the nonuniform cross - sectional power generation, the core model consisting of fuel assemblies with shrouds provides more lower overheating of hot heater rods in the uncovered region as compared to that consisting of fuel assemblies without shrouds. This fact can be explained by a higher physical level of coolant in the first case in hottest fuel assemblies. As at reflooding, higher temperatures are observed in components indicating a lower level of power generation. This fact should be born in mind in planning studies on the fuel - coolant interaction.

3. The heater rod bundle quenching phenomenon has been investigated and the calculations of the quenching phenomenon have been performed using the RELAP5/MOD3/V5M5 Code. A rather large disagreement between the test data and calculational results in rod bundle quenching time results from the fact that the thermal - hydraulic part of this code version does not fit the phenomenon under consideration adequately.

REFERENCES

[1] ALEXEEV S.B., BALUNOV B.F., ILYKHIN A.N. et. al. The CHF in WWER Fuel Assemblies at Ceasing Forced Coolant Circulation /Proceedings of Int. Symposium "Thermophysics' 90" on Thermo-physical Aspects of WWER Safety, Obninsk, September 25-28, 1990.

[2] RELAP5/MOD3. Code Manual Models and Correlations (Draft). E. G. and G. Idaho / Inc. Idaho Falls, Idaho 83415. v.4.

[3] VOROB'YEV V.A., LOSHCHININ V.M. The Study of the Effect of Quality on Transient Heat Transfer at Film Pool Boiling. / The First Russian National Heat Transfer Conference. - M., 1994, v.4., p.59.

FUEL BEHAVIOUR IN SEVERE FUEL DAMAGE CONDITIONS

(Session C)

Chairmen

B. ADROGUER
France

V.P. SMIRNOV
Russian Federation

XA9743297

FUEL BUNDLE EXAMINATION TECHNIQUES FOR THE PHEBUS FISSION PRODUCT TEST

J.Y. BLANC
Commissariat à l'Energie Atomique,
Gif-sur-Yvette

B. CLÉMENT
Institut de Protection et de Sûreté Nucléaire
CEA/Cadarache, Saint-Paul-lez-Durance

P. VON DER HARDT
European Commission Joint Research Centre Ispra
CEA/Cadarache, Saint-Paul-lez-Durance

France

Abstract

Post-test analyses in the Phebus Fission Product experiments concentrate on the studies of the circuits where the fission products are transferred after leaving the core. Nevertheless, the examination of the degraded fuel bundle is a key feature when considering source term, mass balances, physical and chemical aspects of the molten fuel rods, and temperatures reached.

Post-irradiation testing of the first fuel bundle consisted of on-site non destructive examinations, sectioning in the Cadarache hot cells, and destructive examinations at Saclay. In future, the Transuranium Institute in Karlsruhe will participate through detailed investigations, including x-y gamma mapping, autoradiography, optical and electronic microscopy, Electron Probe Micro Analysis, and chemical analyses on microdrilled samples.

The paper will develop the non-destructive examinations, with a special emphasis on transmission tomography, performed in the Phebus facility, using a linear accelerator associated with a line scan camera based on PCD components. This particular technique enabled the high level of penetration to be obtained, necessary for this high density application. Spatial resolution is not far from the theoretical limit and the density resolution is often adequate.

This technique permitted : 1) to define beforehand the cuts on a precise basis, avoiding a long step-by-step choice as in previous in-pile tests, 2) to determine, at an early stage, mass balance, material relocations (in association with axial gamma spectrometry), and FP distribution, as an input into re-calculations of the bundle events.

However, classical cuttings, periscopic visual examinations, macrographies, micrographies and EPMA analyses remain essential to give oxidation levels (in the less degraded zones), phase aspect and composition, to distinguish between materials of identical density, and, if possible, to estimate temperatures. Oxidation resistance of sensors (thermocouples or ultrasonic thermometers) is also traced. The EPMA gives access to the molten material chemical analyses, especially in the molten fuel blockage area.

The first results show that an important part of the fuel bundle melted (which was one of the objectives of this test) and that the degradation level is close to TMI-2 with a molten plug under a cavity surrounded by an uranium-rich crust. In lower and upper areas fuel rods are less damaged. Complementarities between these examination techniques and between international teams involved will be major advantages in the Phebus FPT0 test comprehension.

1. INTRODUCTION

Post-test analyses in the Phebus Fission Product experiments [1,2] concentrate on the studies of the circuits where the fission products are transferred after leaving the core. Nevertheless, the examination of the degraded fuel bundle is a key feature when considering source term, mass balances, physical and chemical aspects of the molten fuel rods, and temperatures reached.

Post-irradiation testing of the first fuel bundle consists of on-site non destructive examinations, sectioning in the Cadarache hot cells, and destructive examinations at Saclay and Karlsruhe.

2. BRIEF SUMMARY OF THE PHEBUS FPT0 TEST

The FPT0 test, performed in December 1993, contained a 20 fuel rod bundle, with a central Ag-In-Cd absorbing rod. The fresh, 1 meter-long fuel rods were only irradiated during 9 days before the accident scenario. Degradation events included three heat up phases up to 900°C, from 900°C to 2000°C, and from 2000°C to 2800°C, followed by a late phase, and a cooling phase. Total duration of the transient was 5 h 40 mn.

The paper will develop the post-test non-destructive examinations on the fuel bundle, with a special emphasis on transmission tomography.

3. NON-DESTRUCTIVE EXAMINATIONS

In the Phebus reactor hall, a fuel examination facility, called "PEC" has been built for the FP project. After the FPT0 experiment, the test train was transferred to the "PEC". As the test bundle was not yet embedded in epoxy, special care has been taken during the transfer from the Phebus loop, using a very low speed overhead crane.

This facility has three possibilities of analyses : numerical radiography by translation of the test train, computed tomography by rotation and axial gamma-scanning.

For tomography and radiography (Fig. 1), a linear electron accelerator CGR Neptune 6 was rented. Its energy and dose rates are adapted to the significant amount of dense material to be penetrated, and to the sensitivity of camera optic sensors. Its main characteristics are the following : maximum energy = 5.5 MeV, average energy = 1.7 MeV, source of 2 mm^2, dose rate = 600 rads/mn at 1 m, primary collimation between source and bundle : height = 2 mm, depth = 300 mm.

The linear camera has two PCD components covered with scintillators, with 1024 photo-sensitive diodes per component. The width of each component is 51.2 mm (total width = 102.4 mm). The thickness of the scintillator layer is 0.3 mm. A personal computer, situated in the reactor hall, controlled the acquisitions and displacements of test train and camera.

A calibration in density was performed, using a lead cone to obtain density and distance as a polynomial fonction. Bundle attenuation is up to 9 cm lead equivalent.

Numerical radiography was performed by vertical translation of the bundle, with 1 projection per mm, 682 pixels/projection, and an acquisition time of 3 hours. In future tests, the resolution can be improved, by a reducing of the axial step.

Each tomography is built from 900 measurements acquired in one turn of the test train under the beam (i.e. one step each 0.4°). The test train has an overall width of 122 mm. The

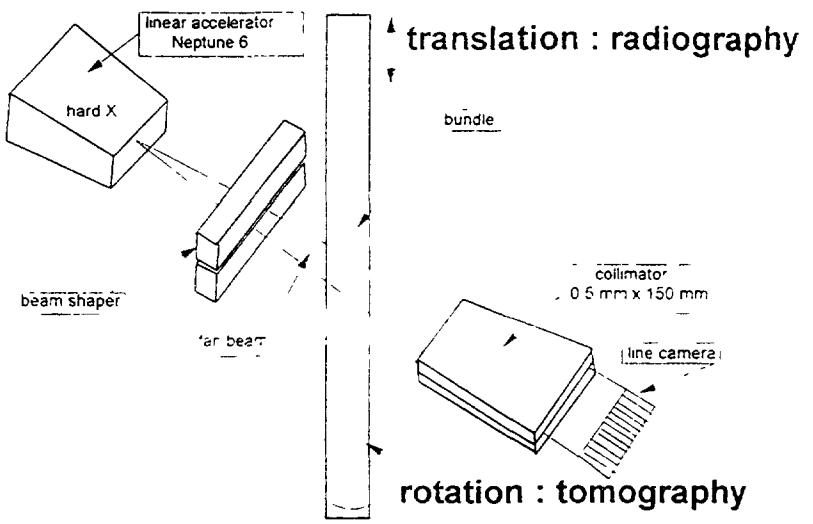

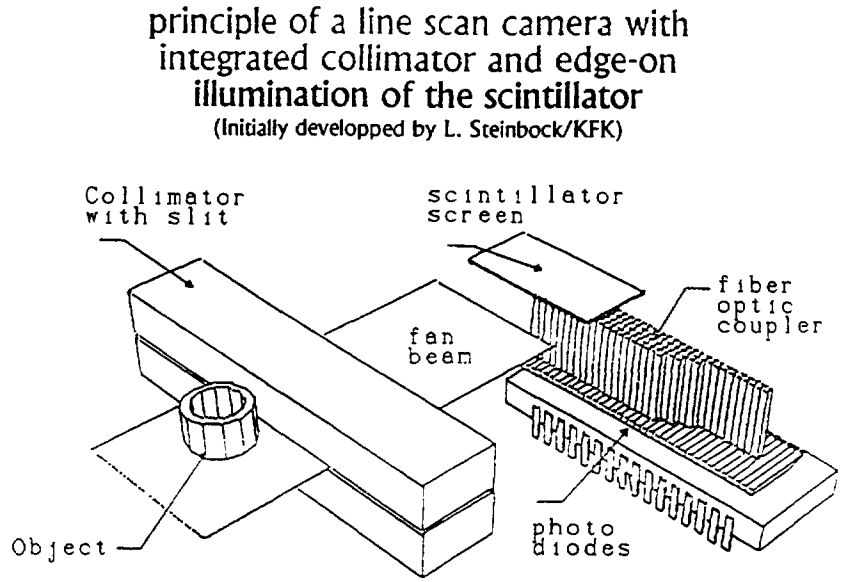

Fig. 1 : Phebus FPT0 - Computed tomography and numerical radiography.

electron beam has a width of 150 mm, but the camera is limited to 102.4 mm, so it was necessary to off-center the camera from 19 to 26 mm to see the whole object in one turn. Acquisition time of one projection lies between 6 and 22 s, depending of the section mean attenuation. As the camera has a limited dynamic, it was proceeded by accumulation of short duration acquisitions. For a single tomography, the acquisition time varied between 2 and 5 hours (in the molten pool area).

The result is a 2.5 Mbyte file, which is computed to give a tomographic reconstruction in about 11 mn on a PC DX2 66 MHz. Main steps of the computed tomography reconstruction are : 1) fan-beam correction, 2) Fourier transform, 3) filtering, 4) inverse Fourier transform, and 5) back -projection. The method was beforehand validated on two mock-ups, of similar geometry, realized with materials of similar density. The first mock-up was simulating a non degraded bundle, and the second a molten pool.

52 tomographies were taken, with excellent results. Three kinds of imperfections were detected : 1) edge problems, when the off-centering of the camera is poorly estimated : it leads to density error on the inconel tube, with no incidence on bundle results, 2) rotation problems, leading to poor image quality. 3) circular artefact, due to misalignment of the two PCD components and short acquisition times , this will be improved in the future test campaigns. Other improvements are under way, mainly concerning acquisition time reduction and density resolution by a new concept of line scan camera and also geometrical resolution by new computing environment.

It is also envisaged in future test to performed ECT · emission computed tomography (i.e. without an external source as transmission method), but the acquisition time is estimated to 1 week per section.

Gamma scanning of the bundle was performed, mainly looking for Zr-95 (fuel distribution), Co-60 (axial profile during irradiation phase), Ba-140, Nb-95, La-140, Ru-103 and Ag-110m. Cesium, iodine and tellurium were not measurable. Hypothesis were introduced about the localisation of the gamma emitters in the section of the bundle. These estimated self shielding coefficients were taken from the 50 tomodensitometries measured all along the bundle. If ECT is performed next time, an improvement of the quantitative estimation can be expected. A planning minimizing the decay time problem will also be looked for.

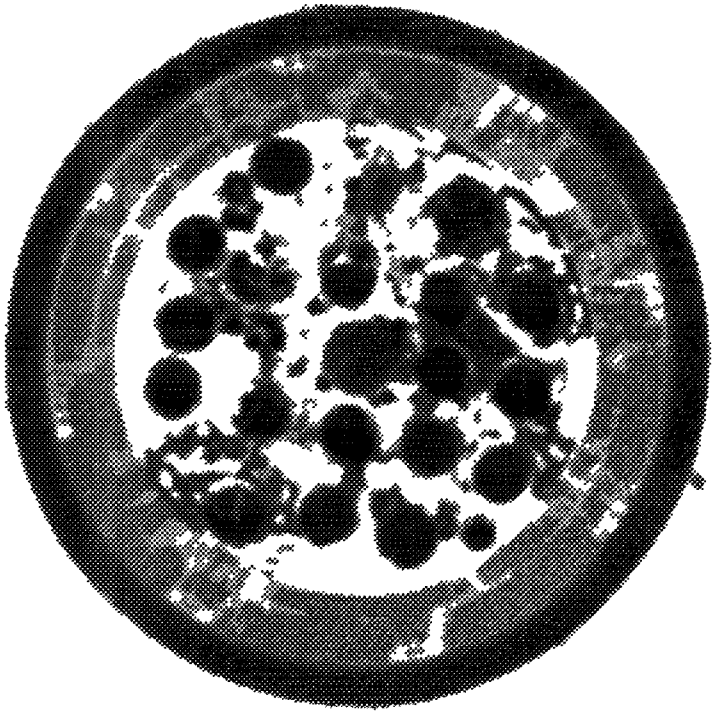

Fig. 2 : Phebus FPT0 - Computed tomography at level + 88 mm bfc.

Downward view Bundle orientation . North at the top

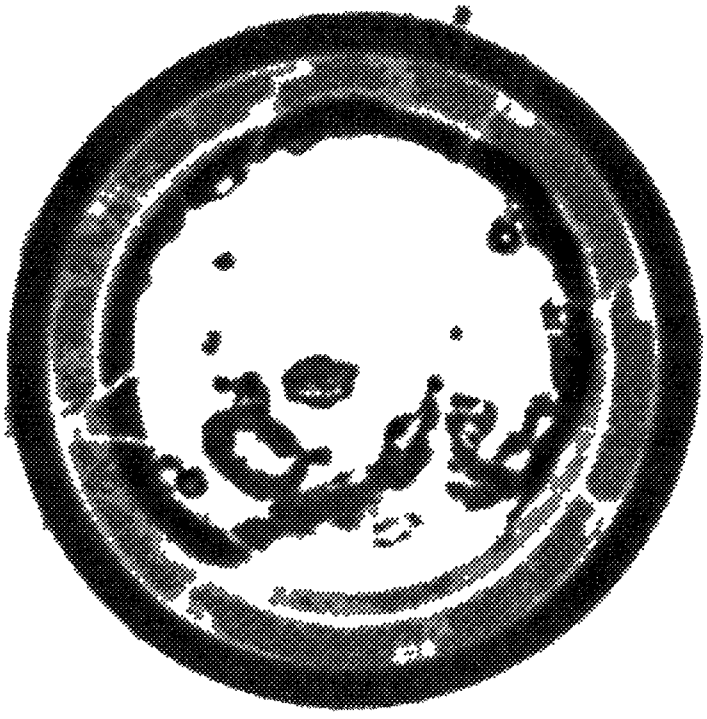

Fig 3 Phebus FPT0 - Computed tomography at level + 268 mm bfc

Downward view - Bundle orientation . North at left

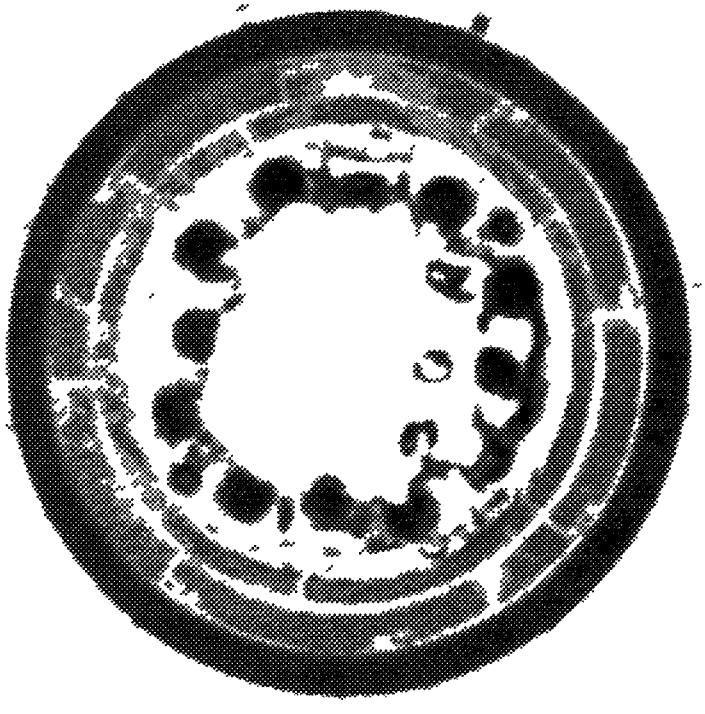

Fig 4 Phebus FPT0 - Computed tomography at level + 772 mm bfc

Downward view - Bundle orientation North at left

Results (Fig. 2 to 4), obtained from non-destructive examinations showed that the fuel bundle can be divided into 5 zones :
1) the lower part, with a nearly intact geometry (and presence of silver) ;
2) below the lower grid, with an accumulation of fuel and molten materials ;
3) from the lower grid to mid-plane, no more rods are present, but a pheripheral crust,
4) from mid-plane to the upper grid, only part of the external rods are visible,
5) the upper part, with rods with high dissolution rate.
Before the test, Zircaloy grids were located on either side of mid-plane : lower grid from 0.23 to 0.27 m and upper grid from 0.75 to 0.79 m from the bottom of fissile column (bfc).

An estimation of molten fuel amount has been done from these results : on each tomographic level, the amount of each rod which was not liquefied or molten was determined. It showed that an equivalent of about 13 rods out of 20 remained solid. Then, by integration, the amount of fuel which remained solid was obtained, and then the total amount of molten fuel. Mass balances used tomographies for materials with density > $6g/cm^3$, i.e. UO_2 + AgInCd + stainless steel. Conclusion of this work indicates that the molten pool near the lower grid can be evaluated to 2.4 +/- 0.5 kg of molten UO_2 not including molten ZrO_2.

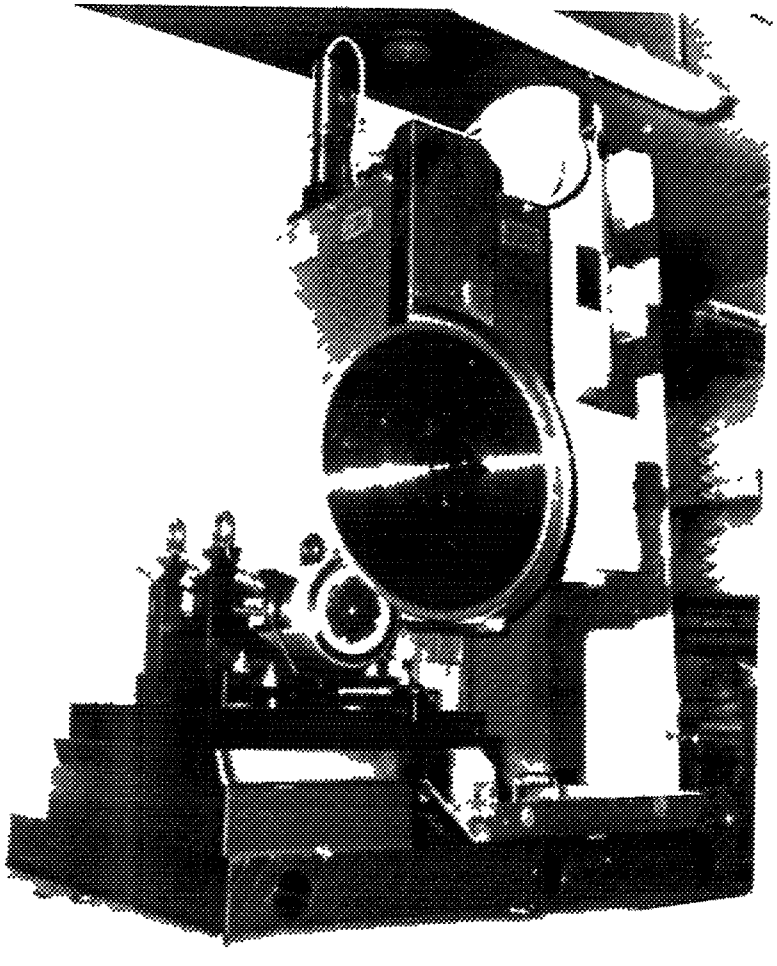

Fig 5 Cutting machine for Phebus destructive examinations before implementation in Saclay hot cells

These techniques, and especially the computed transmission tomography, permitted: 1) to define beforehand the cuts on a precise basis, avoiding a long step-by-step choice as in previous in-pile tests, 2) to determine, at an early stage, mass balance, material relocations (in association with axial gamma spectrometry), and FP distribution, as an input into re-calculations of the bundle events.

4. DESTRUCTIVE EXAMINATIONS

In fall 1994, the lower part of the test train, including the fuel bundle, was embedded in epoxy in the PEC facility, and transferred to the LECA hot cells at Cadarache. Besides cutting out some tube samples for deposit analyses in the upper part of the test train, two saw cuts were realized about 10 cm above and below the fuel rods. Then the bundle was sent to Saclay in early February 1995. It can be pointed out that the epoxy embedding gives some limitations in criticality allowance in hot cells.

At Saclay, two cuts were realized at first at the bottom of the fuel rods to define more precisely the original levels for future sectionning, then a mid-plane cut enabled an easier handling of the bundle. Finally, a total of 19 section cuts were done, with a majority in the lower areas showing highly oxidized cladding in the nearly intact geometry zone, and previously molten fuel in the molten pool area. A cutting saw using a 2 mm-thick diamond disk, with lubrication was employed (Fig. 5). Another cut, in vertical position is to be done in the molten pool area in the near future.

Periscopic photographies (x 1 to x 3) have been taken on all 19 slices both from the top and the bottom of each slice. The quality of the cut was sufficient to avoid polishing before photographies. Most of the cut levels being chosen from tomographic results, comparison between tomographies and photographies of cut at similar elevations are of particular interest (Fig. 6 to 9). It shows that the tomographies were representative of the real state of the bundle, although a better choice in the colours attributed to densities could be discussed.

However, cuts and photographs and further examinations remain essential to give oxidation levels (in the less degraded zones), phase aspect and composition, to distinguish between materials of identical density, and, if possible, to estimate temperatures. Oxidation resistance of sensors (thermocouples or ultrasonic thermometers) is also traced.

On the most interesting slices, areas are defined for further optical macrographies and micrographies (typically x 100 and x 400). Due to apparatus limitations, the sample is re-cut to approximately 20 mm x 20 mm. Two samples have been examined by June 1995: the first in the area above the blockage zone, where a void volume is surrounded by a crust, somewhat similar to TMI-2, and the second in the molten pool area, showing some metallic inclusions.

During discussions on micrographies, TransUranium Institute in Karlsruhe (TUI) suggested to perform a specific chemical etching on the previously molten materials, using a mixture of HNO_3 50%, H_2O_2 49% and HF 1% during 5 s to 2 mn. This etching was told to be useful for the two-phase system aZr(O) - $(U,Zr)O_{2-x}$.

After metallography, the sample is polished again, cut to limit its thickness (and radioactivity) and sent to the EPMA (Electron Probe Micro Analysis). This gives access to the molten material chemical analyses (either in weight per cent or atomic per cent), especially in the molten fuel blockage area. The zirconia shroud surrounding the fuel is useful as a standard for checking the EPMA results : actually, its chemical analyses before the test are perfectly well known, and as temperatures in this area were significantly lower that in the bundle itself, it can be hypothetized that shroud chemical composition remained stable.

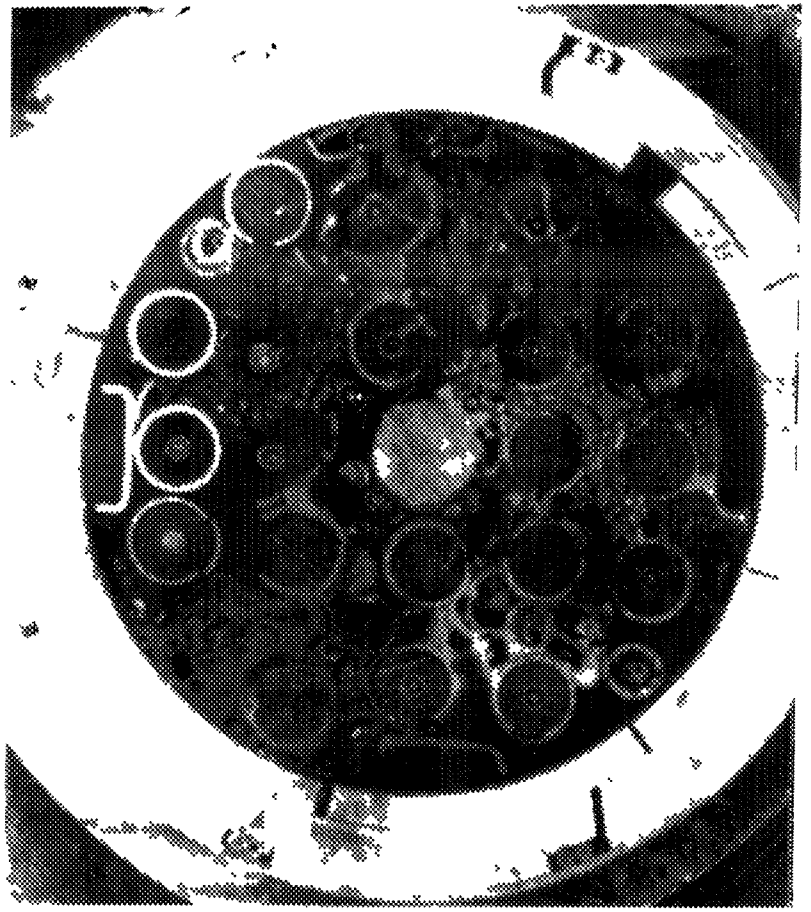

Fig 6 Phebus FPT0 Periscopic photography at + 89 mm bfc

Downward view Bundle orientation North at the top

Fig 7 Phebus FPT0 Periscopic photography at + 250 mm bfc

Downward view Bundle orientation North at left

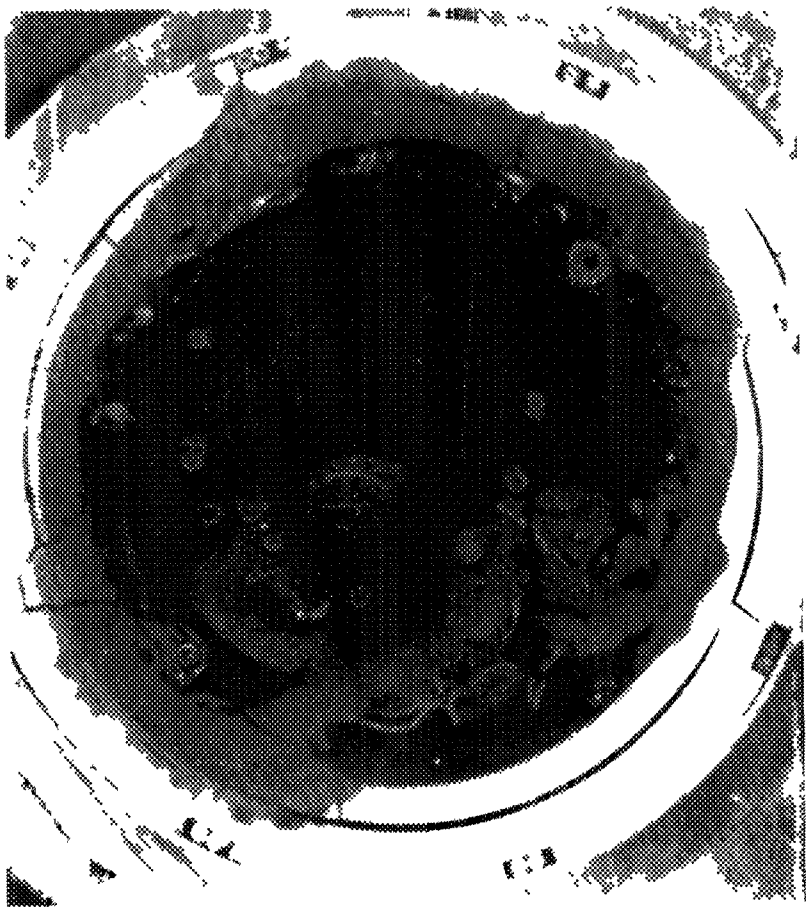

Fig 8 Phebus FPT0 Periscopic photography at + 268 mm bfc

Downward view Bundle orientation North at left

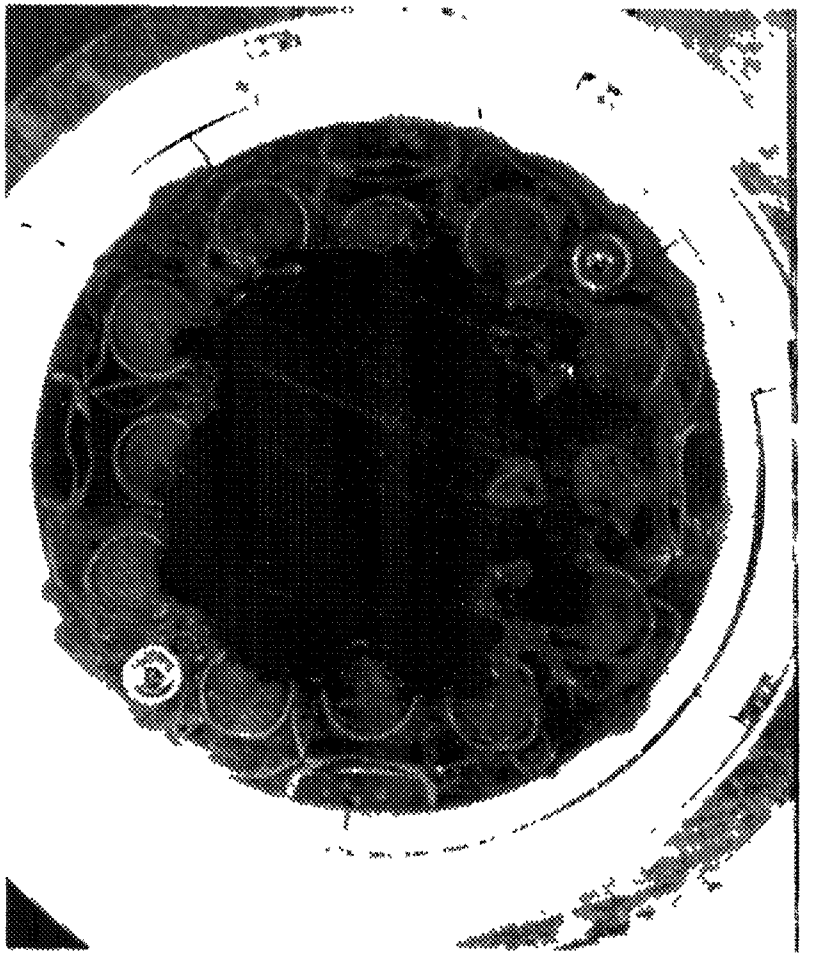

Fig 9 Phebus FPT0 Periscopic photography at + 773 mm bfc

Downward view Bundle orientation North at left

However, the epoxy embedding leads to some limitation in EPMA analyses, because epoxy is non-conductive. This difficulty is overcome by performing linescans on points selected manually, out of non-conductive areas (epoxy, void, porosities). The first results on the crust show a quite homogeneous previously molten material, composed of U, Zr and O. The specific etching, recommended by TUI, having revealed a limited area in the crust, some EPMA was performed in that part, but only an increase in iron (or steel) impurities was noticeable.

A second EPMA will be performed in the previously molten bath, essentially for its chemical composition, and for tracing the metallic particules, visible on metallography.

In fall 1995, a slice taken from the lower part of the bundle, in the area at the bottom of the molten pool will be shipped to the Transuranium Institute in Karlsruhe. This laboratory will participate through detailed investigations, including x-y gamma mapping, autoradiography, optical and electronic microscopy, Electron Probe Micro Analysis, and chemical analyses on microdrilled samples.

5. CONCLUSIONS

The first results show that an important part of the fuel bundle melted (which was one of the objectives of this test) and that the degradation level is close to TMI-2 with a molten plug under a cavity surrounded by an uranium-rich crust. In lower and upper areas fuel rods are less damaged.

Complementarities between these examination techniques and between international teams involved is a major asset for the understanding of the Phebus FPT0 test comprehension [3].

ACKNOWLEDGEMENTS

Most of the work described in the non-destructive part is taken out restricted reports from B. Cornu, I. Giacalone (tomography) and G. Répetto (bundle degradation). The principle of the line scan camera described above was initially developped by L. Steinbock/KfK. Destructive examination in Saclay are indebted to J. Y. Latarse, R. Cozler, J. M. Boyer, D. Gauvain and M. Perrot.

REFERENCES

[1] VON DER HARDT, P., TATTEGRAIN, A., " Phebus FP - An international severe accident research programme", International East-West Topical Meeting, Safety of Operating Nuclear Power Plants (TOPSAFE '95), Budapest, September 24-27, 1995.

[2] SCHWARZ, M., JONES, A.V., "Analytical interpretation of FPT0 and preparation of future PHEBUS FP tests", ibid.

[3] JAMOND, C., et al., "Phebus FPT0 test : Status of the interpretation of the bundle degradation using ICARE 2", IAEA Technical Committee Meeting on Behaviour of LWR Core Materials under Accident Conditions, Dimitrovgrad, Russia, October 9-13, 1995.

POST-TEST INVESTIGATION RESULT ON THE VVER-1000 FUEL TESTED UNDER SEVERE ACCIDENT CONDITIONS

A. GORYACHEV, Yu. SHTUCKERT, E. ZWIR, L. STUPINA
State Scientific Centre, Research Institute of Atomic Reactors,
Dimitrovgrad, Russian Federation

Abstract

The model bundle of VVER-type were tested under SFD condition in the out-of-pile CORA installation.

The objective of the test was to provide an information on the VVER-type fuel bundles behaviour under severe fuel damage accident conditions. Also it was assumed to compare the VVER-type bundle damage mechanisms with these experiensed in the PWR-type bundle tests with aim to confirm a possibility to use the various code systems, worked out for PWR as applied to VVER.

In order to ensure the possibility of the comparison of the calculated core degradation parameters with the real state of the tested bundle, some parameters have been measured on the bundle cross-sections under examination. Quantitative parameters of the bundle degradation have been evaluated by digital image processing of the bundle cross-sections. The obtained results are shown together with corresponding results obtained by the other paticipants of this investigation.

1.Introduction.

In 1993 two model bundles of VVER type were tested under severe core accident conditions including the bundle element melting. The planning and execution of the experiments have been carried out by a cooperative effort of Forschungszentrum Karlsruhe (FZK), Karlsruhe (formerly Kernforschungzentrum, KfK), Nuclear Safety Institute of the Russian Research Center "Kurchatov-Institute" (RRC "KI"), Moscow, Research Institute "Luch" Scientific and Industrial Association (SIA "Luch"), Podolsk and Bochvar Research Institute of Inorganic Materials (RIIM), Moscow.

The model bundle tests were carried out in the out-of-pile installation CORA (KfK). During the tests the model bundles were subjected to temperature transients of a slow heatup rate in a steam environment and experienced a temperature escalations due to the exotermal zirconium-steam reaction. After the experiments the bundles were encapsulated with epoxy resin and cut to the cross-sectional samples. Polished sumples were distributed to the Russian laboratories RRC "KI", RIIM, Research Institute of Atomic Reactors (RIAR) and to the KfK for the posttest examinations. The model bundle CORA-W2 was subjected to the most detailed post-test examinations because of the experimental results of CORA-W2 test serve as a data base for comparison with analytical predictions of the high-temperature material behaviour by various code systems in the frame of International Standard Problem (ISP-36).

CORA-W2 cross-section post-test investigation was carried out in a joint effort by FZKA, RRS "KI", RIIM and RIAR. Detail description of the post-test examination results is presented in [1]. This paper describes some quantitative bundle damage parameters obtained from the cross-section microstructural posttest investigation.

2. Description of the CORA Test Facility and experiment procedure.

Detail description of CORA facility and experimental conditions are presented in [2]. In this chapter the main characteristics of the facility and experiment scenario are briefly described.

2.1. *Description of the CORA Test Facility.*

Out-of-pile CORA facility was designed to LWR bundle tests simulate the bundle heatup phase due to decay heat under the cooling by the superheated slow flow rate vapour of about atmospheric pressure.

The general view of CORA facility is presented in Fig.1, the facility flow diagram is shown in Fig.2. The central part of the facility is the fuel rod bundle. The CORA-W2 bundle was enclosed in a Zr-1%Nb shroud with ZrO_2 fibre insulation. Additional heat insulation of the bundle was provided by a high temperature radiation shield, that provided a flat radial temperature profile.

The steam was produsedin the steam generator. Jointly with an additional argon flow steam was superheated and guided to the lower end of the bundle. The steam not consumed within the bundle was condensed in two parallel condensors and the residual argon-hydrogen mixture was fed to the off-gas system after dilution with air to attain a low hydrogen concentration.

2.2. *Bundle design.*

The CORA-W2 model bundle consisted of 18 fuel rod simulators and one absorber rod simulator (Fig. 3). From the outside the fuel bundle was surrounded by the shroud of 1,0 mm thick Zr-1%Nb

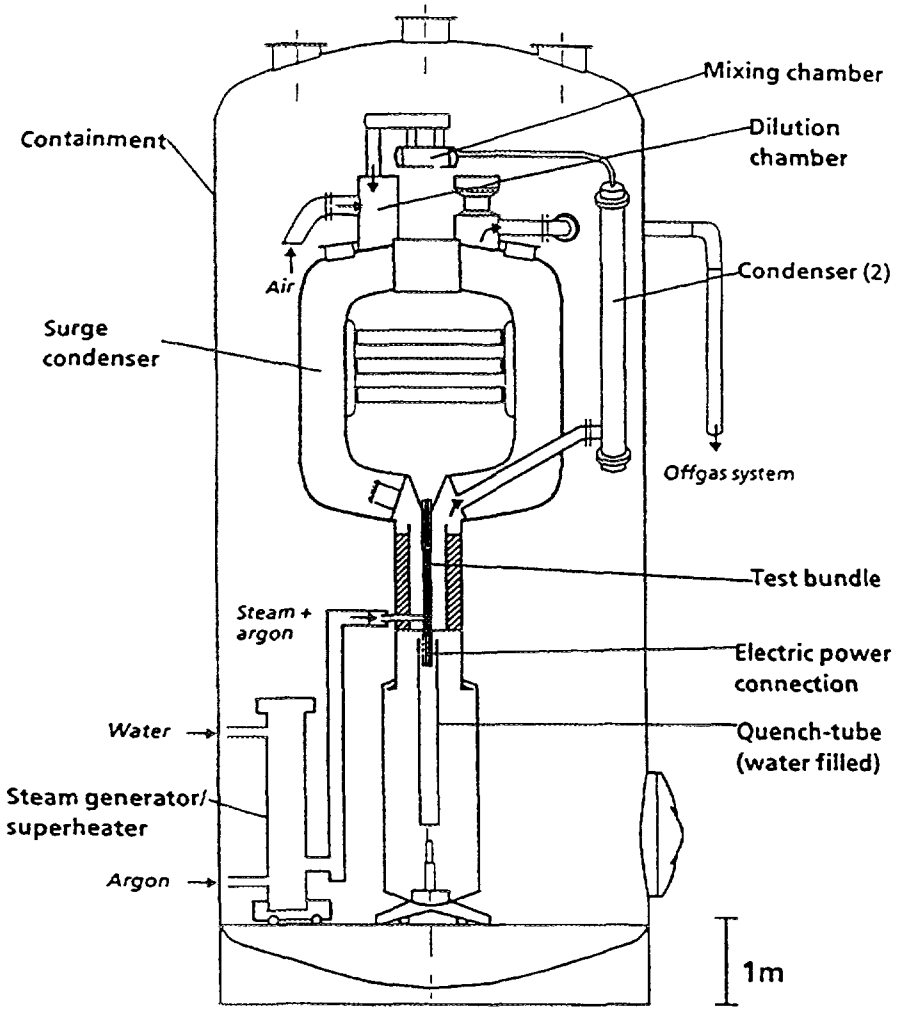

Fig. 1 SFD Test Facility CORA (Main components).

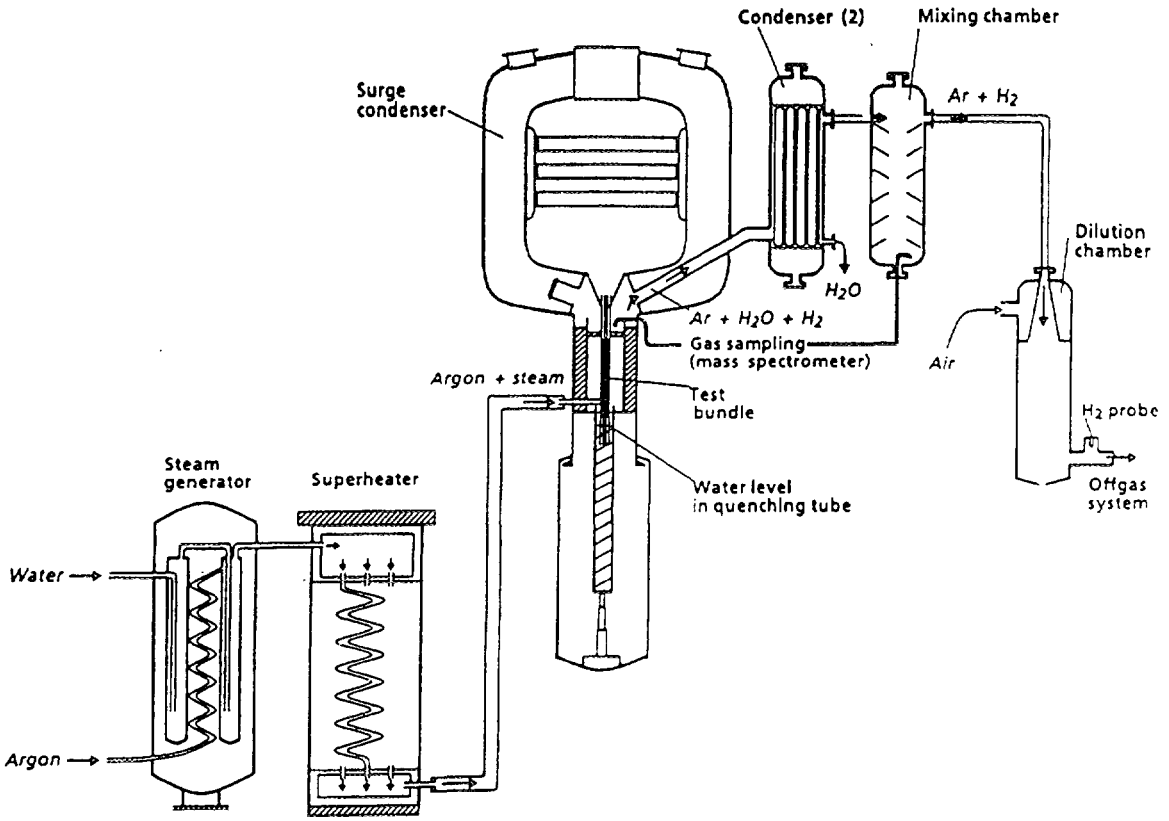

Fig. 2 SFD Test Facility (Simplified flow diagram).

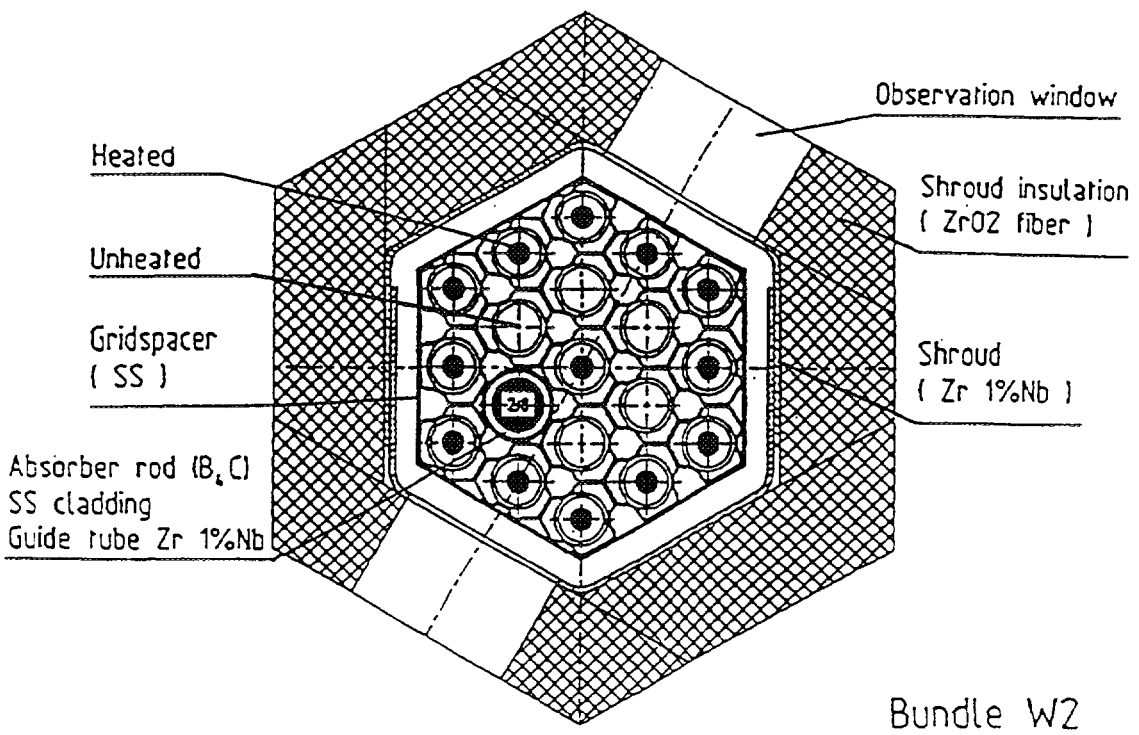

Fig. 3 Rod arrangement of bundle CORA-W2.

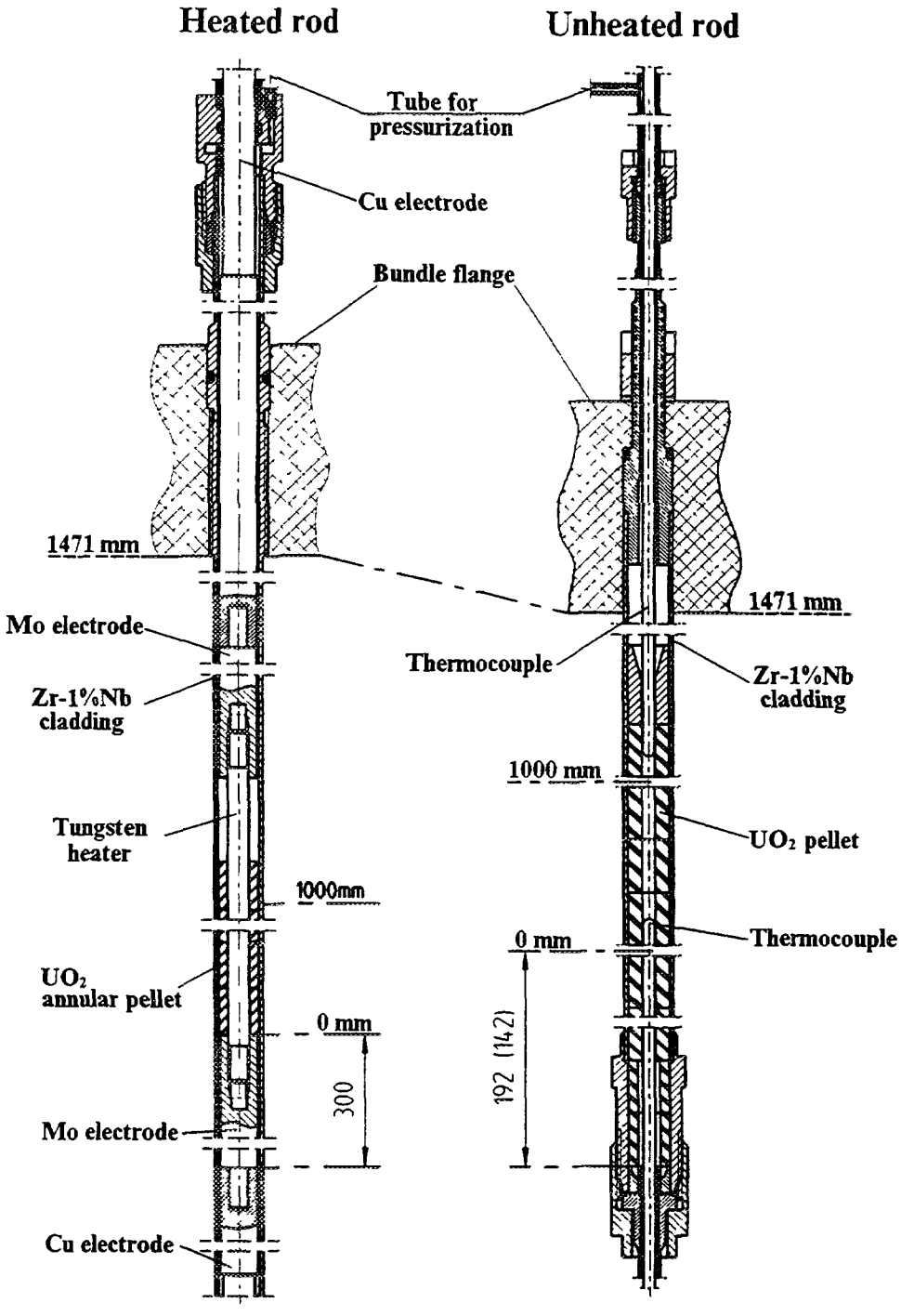

Fig.4 Rod types used in the CORA/WWER experiments.

alloy. The fuel element simulators were spased inside the shroud by means of three steel spacing grids manufactured according to the standard VVER-1000 technology and installed at marks - 5; 210; 610 mm. From the outer side the assembly shroud was equipped with the shroud insulation of fiber zirconium dioxide, that included two holes for the video monitoring of the experimental process.

The model CORA-W2 assembly used two types of fuel elements (Fig.4):

- heated rods - 13
- unheated rods - 5

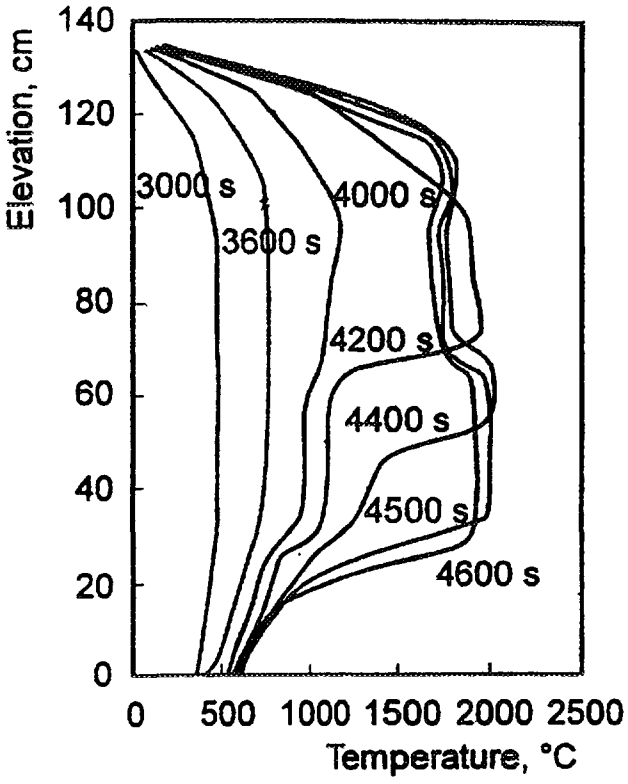

Fig.5 Axial temperature distribution along CORA/WWER-2 bundle.

The unheated rod simulators were of standard VVER-1000 design, radial dimensions and material composition. The column of fuel pellets in each of the heated rod simulators had the axial hole of 4.2 mm in diameter, where tungsten cylindrical heater of 4.0 mm in diameter was positioned.

The absorber rod consisted of the stainless steel guide tube and vibro compacted B_4C column in the SS cladding of standard VVER-1000 design.

2.3. Test Conduct and Initial Boundary Conditions.

The experiment scenario consisted of the following main phases:

1. 0-3000 s: pre heating of the assembly;
2. 3000-4500 s: heating phase;
3. 4500 s onwards: cooling phase.

During the first phase of the experiment, the pre-heated argon was supplied to the assembly at the flow rate of 8 ^{g}/s and low assembly electrical power of 0.5 kW. As a result the insulation temperature reached the level sufficient to prevent the vapour condensation. At 2760 s the argon flow rate was decreased to 6 ^{g}/s. At time of 3300 s the steam started to be supplied to the assembly at the flow rate of 4 ^{g}/s.

During the heating phase the bundle temperature was increased at the rate of about 1 ^{K}/s due to the electric power was increased from 2 kW to 14.5 kW. Experiment was terminated at 4500 s by the electrical heating switch off and termination of the steam supply.

The bundle axial temperature profiles is shown in the Fig.5.

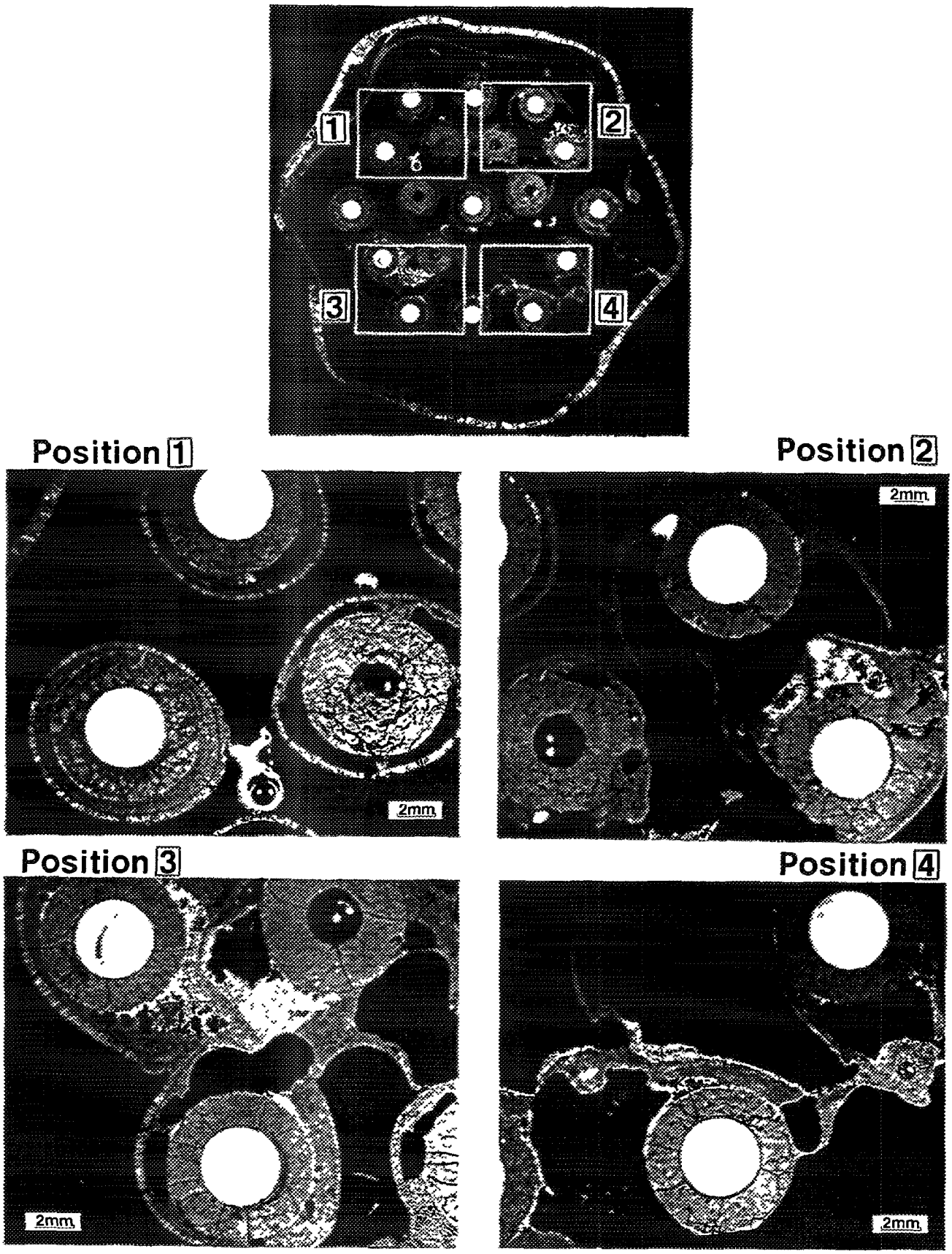

Fig 6 Cross-section W2-03 (bottom view)
Elevation 327mm

3. Posttest appearance of the fuel rod simulators.

The example of the bundle cross section, that was cut out at the 327 mm elevation, where the bundle materials were almost completely oxidized, is shown in the Fig. 6.

According to the results of the bundle cross-sections posttest microstructural investigation the next conclusion on the high temperature simulator damage mechanism may be done.

During the heating phase of the experiment the ZrO_2 layers were formed on the simulator cladding surfaces. After the melting point temperature of the Zr-1%Nb cladding have been reached, the internal metallic layer of the cladding formed a melt, that begun to dissolve the fuel pellet and outer ZrO_2 layer. The formed melt can flow in the gap between the pellet and outer oxide layer, that led to the ZrO_2 layer deformation (Fig.6, Pos.1).

The final appearance of the simulator is a result of two competitive processes: melt oxidation due to oxygen uptake from the vapour and outer ZrO_2 layer dissolution. In the case of the outer oxide layer is not sufficiently thick, it is ruptured and liquid melt flow down on the simulator surface (Fig.6, Pos. 3). Following oxidation of the inner cladding surface lead to the flattening of the cladding, so called "flowering" (Fig.6, Pos.2). In the other case the liquid melt is completely oxidized in the gap between the fuel pellet and outer ZrO_2 layer (Fig.6, Pos.1).

A strong impact on the fuel rod simulator damage process have an interaction of the cladding and stainless steel, that lead to the eutectic formation with a melting point ($\sim 1200°C$) far below the melting point of Zr-1%Nb alloy. This interaction lead to the more intensive process of the outer ZrO_2 layer dissolution and cladding damage (Fig.6, Pos.4).

In general, the cladding failure mechanisms revealed in the CORA-W2 bundle test is very similar to those experienced in the PWR model bundle tests [3].

4. Quantitative measurements of the bundle damage parameters.

Quantitative estimation of the bundle damage parameters was made on the basis of the bundle structural element and melted material phase area measurements by means of the cross-section fragment image processing. In Fig.7 the example of the cross-section fragment image processing is shown. The phase types selected for the quantitative analysis is also shown in this figure.

As a result of the various phase cross-section area measurements the following parameters were estimated:

- core blockage formation;
- fuel pellets dissolution by the cladding melt;
- axial distribution of cladding oxidation;
- axial distribution of core melt.

4.1. Core blockage formation.

In order to evaluate a core blockage formation the total core material area was measured on each of the tested cross-sections. Materials, were identified as belonging to the bundle shroud, were not taken into account. The bundle cross-sectional area axial distribution is shown in the Fig.8.

These data reflect only an area occupied by the bundle material excluding material porosity. Therefore, the cross-sectional area available for the vapour flow may be overestimated, because of some of the pores, that may be seen on the cross-sections, may appear to be the closed pores inside a bundle material and their cross-sectional area are not available for a vapour flow. In view of this assumption the additional measurements were made. In this case the area of pores, which look like

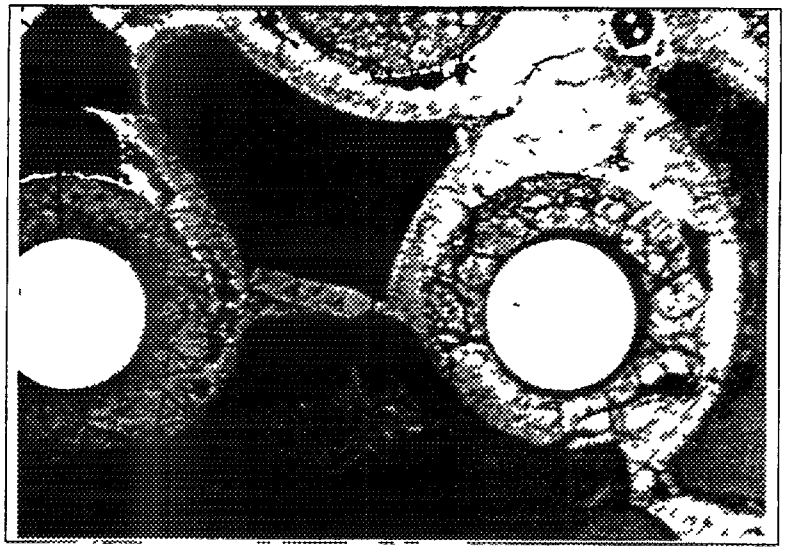

Original view

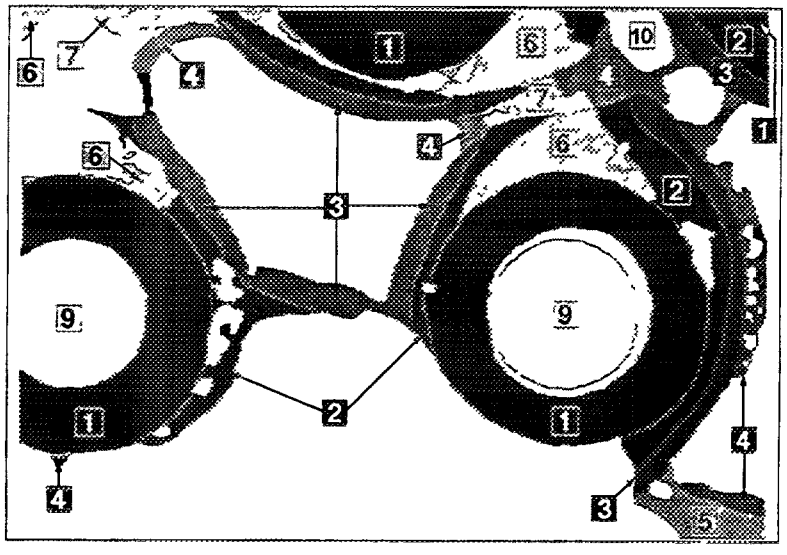

View reformed for analysis

1 Pellet remnants
2 Oxidized melt
3 ZrO_2 layer
4 Oxidized melt
5 Oxidized shroud
6 Metallic melt
7 Metallic melt
8 Metallic phase of the shroud
9 Tungsten heater
10 Thermocouple

Fig.7 Image processing of the cross-section fragment.

closed in the cross-section, i.e. have no visible leakage to the area among the fuel rod simulators, was added to the core material area. The resulting data is also shown in the Fig.8. Obviously, two group of the obtained data represent the extreme estimations. The real value of the core blockage must be in the range limited by these estimations.

As can be seen from the Fig.8, the axial redistribution of the core melt led to creation of two local core blockages at the marks correspond to the positions of the spacer grids. The lower blockage is created by the stainless steel melt originated from the absorber rod cladding and guide tube and contains a small amount of uranium and zirconium. The upper blockage is created by the melt, originated from the fuel rod simulators material, and is significantly polluted by the stainless steel components.

The remarkable fact is, that despite of the upper spacer grid was completely melted early in the bundle temperature ramp, it affected on the following core melt redistribution.

In general, CORA-W2 bundle material redistribution is of the same character that was observed in the absorber material bearing PWR model bundles tests.

4.2. ZrO_2 axial distribution and cladding oxidation profile.

In order to evaluate the cladding oxidation and final ZrO_2 distribution the zirconia layers area was measured on the bundle cross-sections. The results is shown in the Fig. 9. It should be taken into account that this data reflect only area of the ZrO_2 layers formed on the outer cladding surfaces during solid state oxidation of the claddings. In the most cases this outer oxide layers retained only partially due to mechanical failure and dissolution by the melt. In order to obtain a more realistic picture of the cladding oxidation profile formed during the solid state oxidation phase, the measurements of the average oxide film thickness was made. The thickness of the zirconia layers or their remnants were calculated as a ratio of the each measured object area to the half of its perimeter. As a result the average thickness of each measured layer were obtained. The result is not influensed by the missing of the some parts of the oxide layer from the cladding surface. The results of this measurements is shown in the Fig. 10. In the upper cross-sections of the bundle cladding oxidation have a smooth profile. The extreme value at the mark of 270 mm may be explained by the fact, that in this cross-section the cladding melting point temperature was reached late, than in the upper cross-sections and therefore, the solid state oxidation phase were longer.

4.3. Fuel pellets dissolution.

In order to evaluate the final uranium redistribution along the bundle the fuel pellet remnants area was measured in the each cross-section. The results of the fuel pellet remnants area measurements is shown in the Fig. 11. It should be noted, that no any fuel pellet damage mechanisms other than pellet dissolution by the melt were observed in the course of the microstructural investigations. The comparison of the heated and unheated simulator fuel pellets dissolution is shown in the Fig. 12. The averaged over the cross-section fuel pellet dissolution is not exceed of 17 %, but the fuel pellets of the individual simulators were experiensed a dissolution to a great extent, that, obviously, may be explained by the non uniform radial distribution of the melt in the bundle.

4.4. Axial distribution at the core melt.

The cross-sectional area of the melted material, that have not been definitely attributed to any of initial materials of the bundle and consisted of the complex mixture of the initial bundle materials, was measured in order to evaluate the core blockage formation and final core material distribution. The results of the measurements are shown in the Fig. 13. In order to

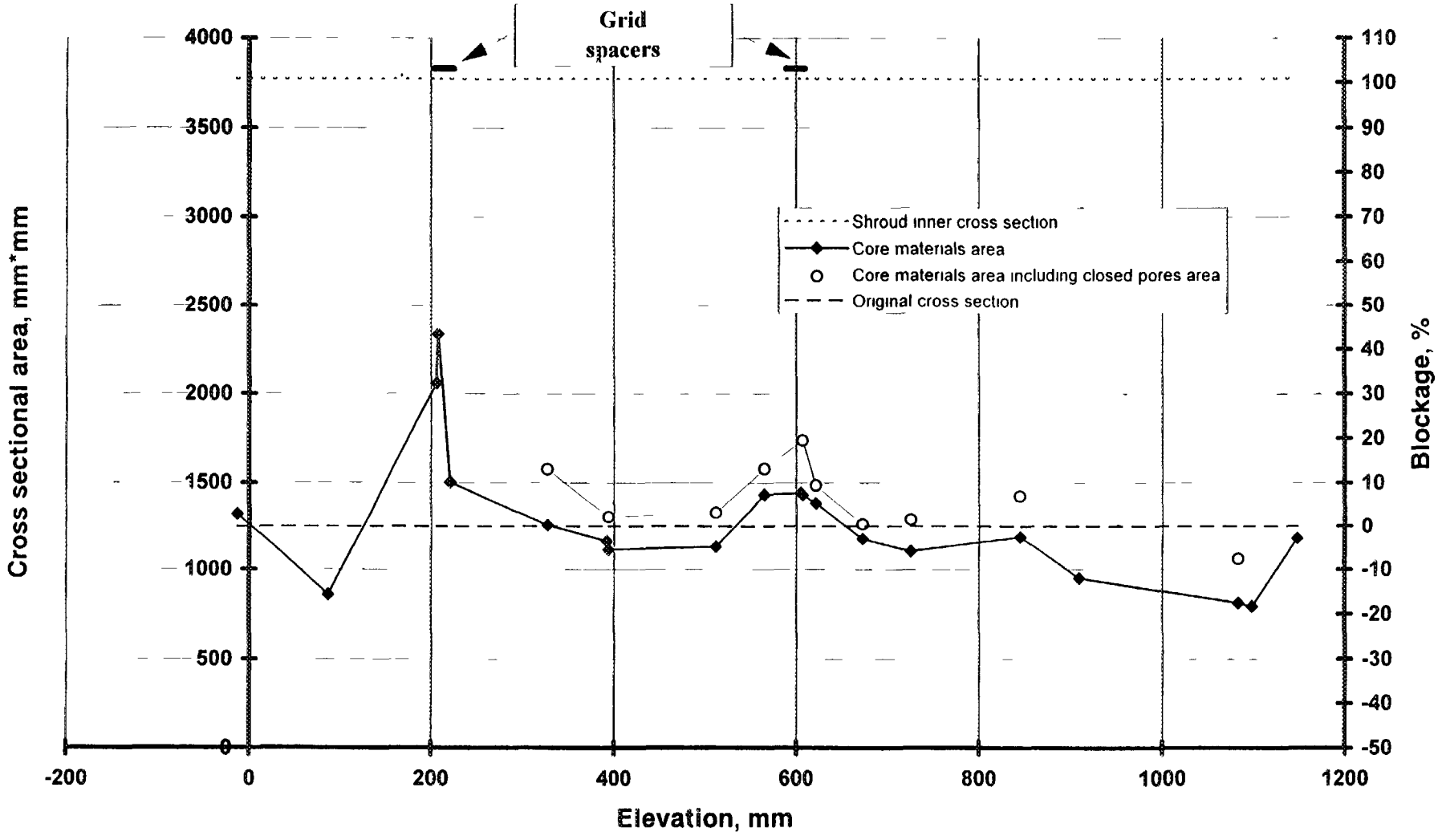

Fig.8 Profile of the cross-sectional areas after test CORA-W2.

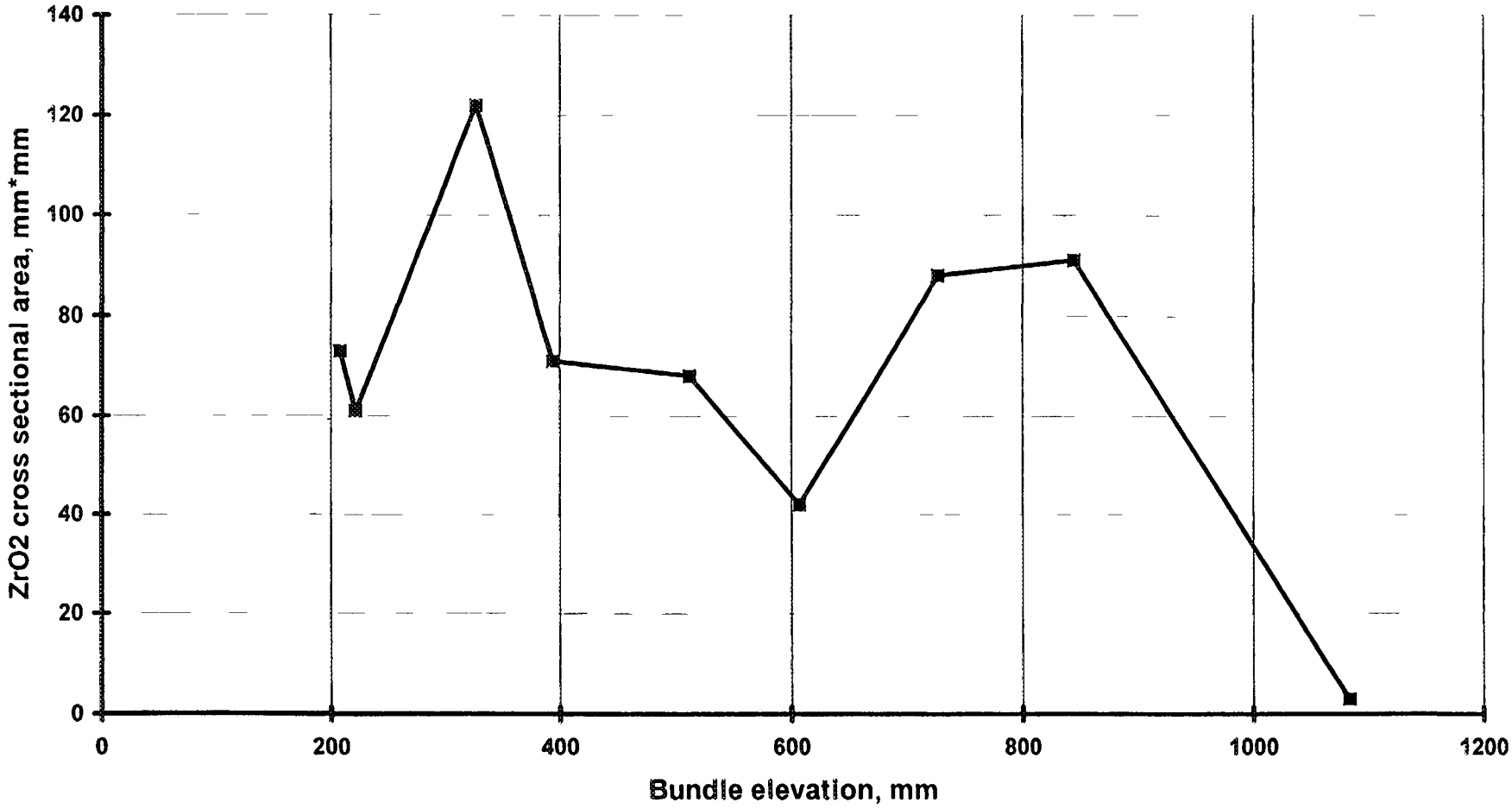

Fig.9 Axial profile of the remained cladding ZrO2 scales cross sectional area.

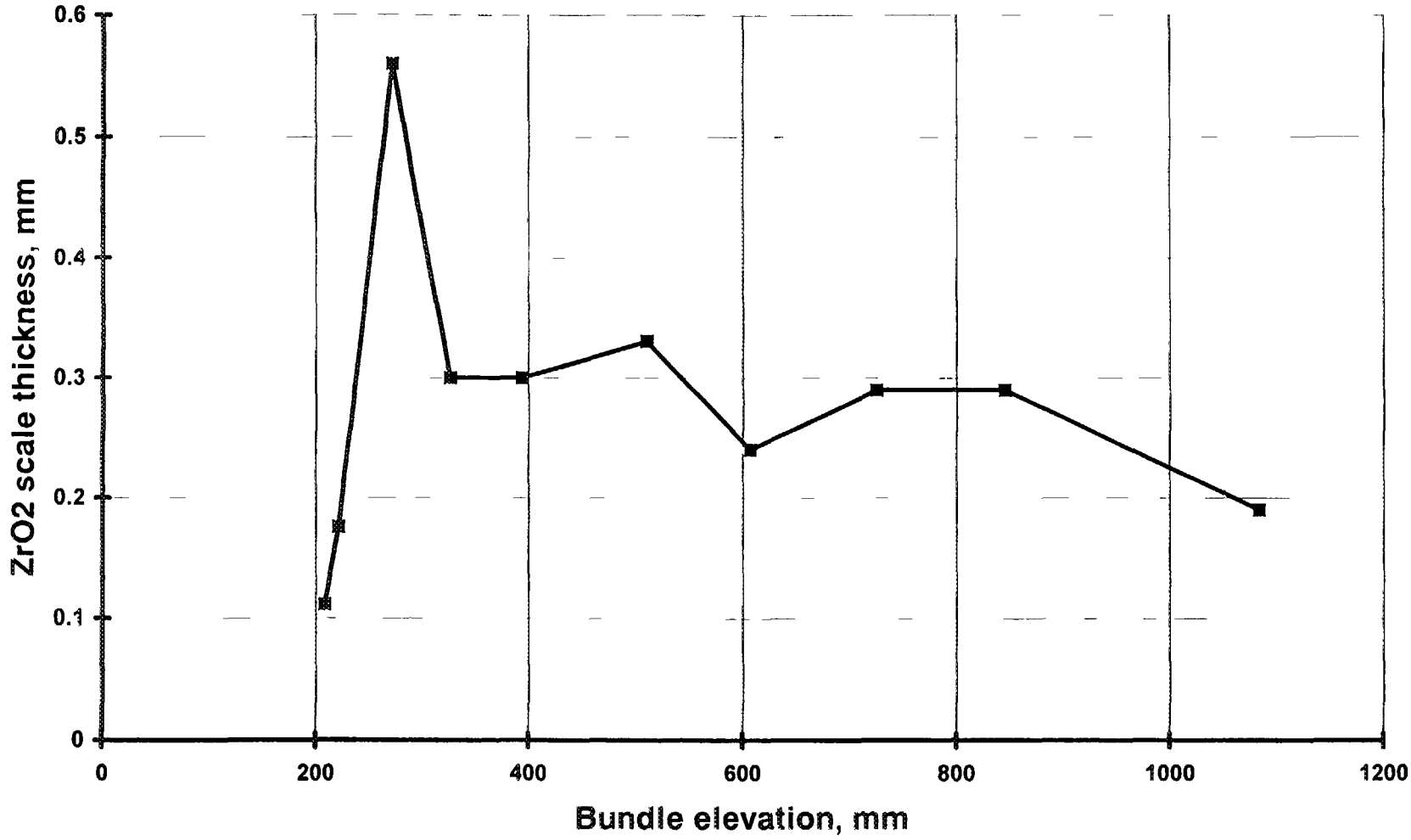

Fig.10 Profile of cladding oxidation along the bundle CORA-W2.

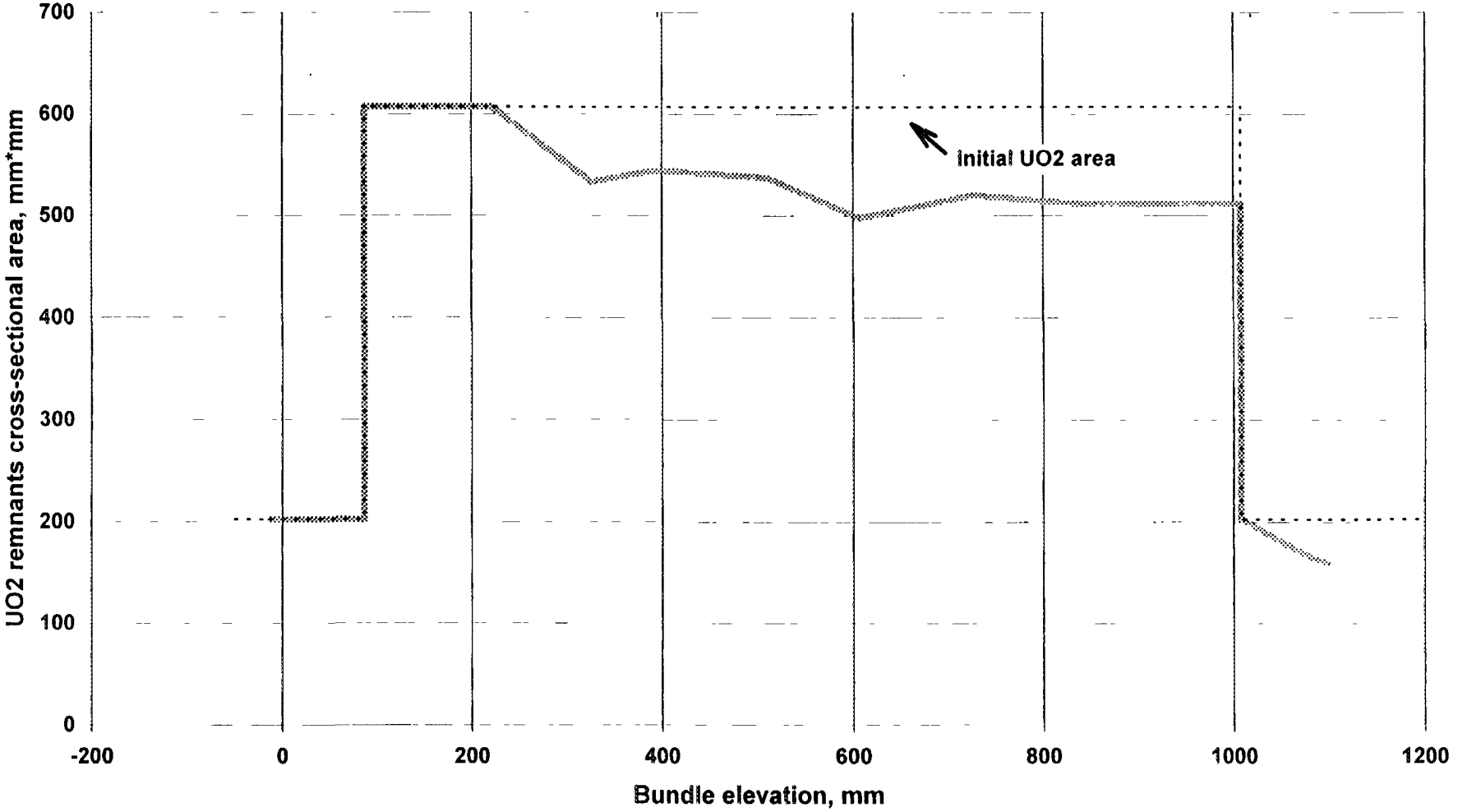

Fig.11 Axial profile of the UO2 pellets cross sectional area after the test CORA-W2.

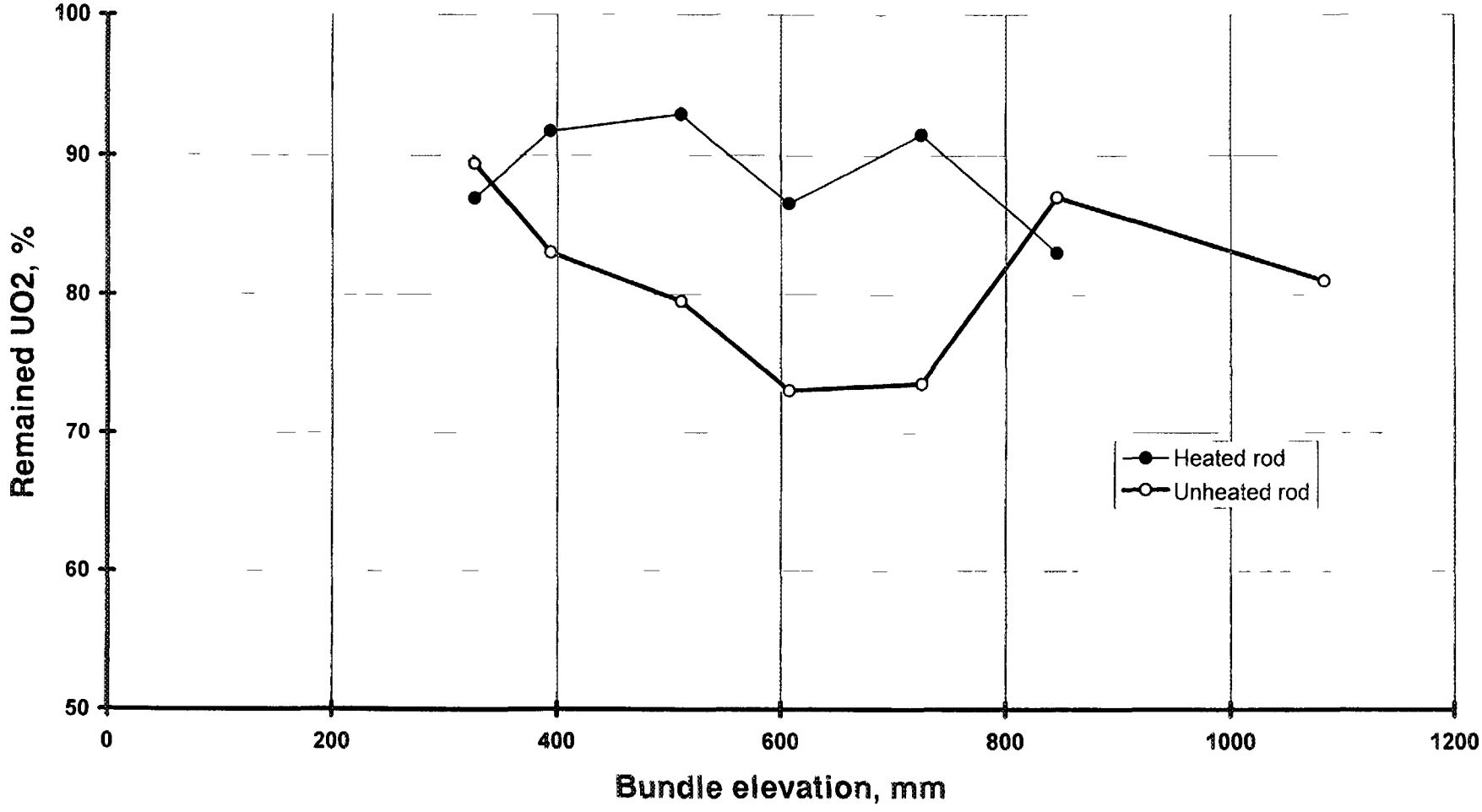

Fig.12 Damage profile of UO2 pellets.

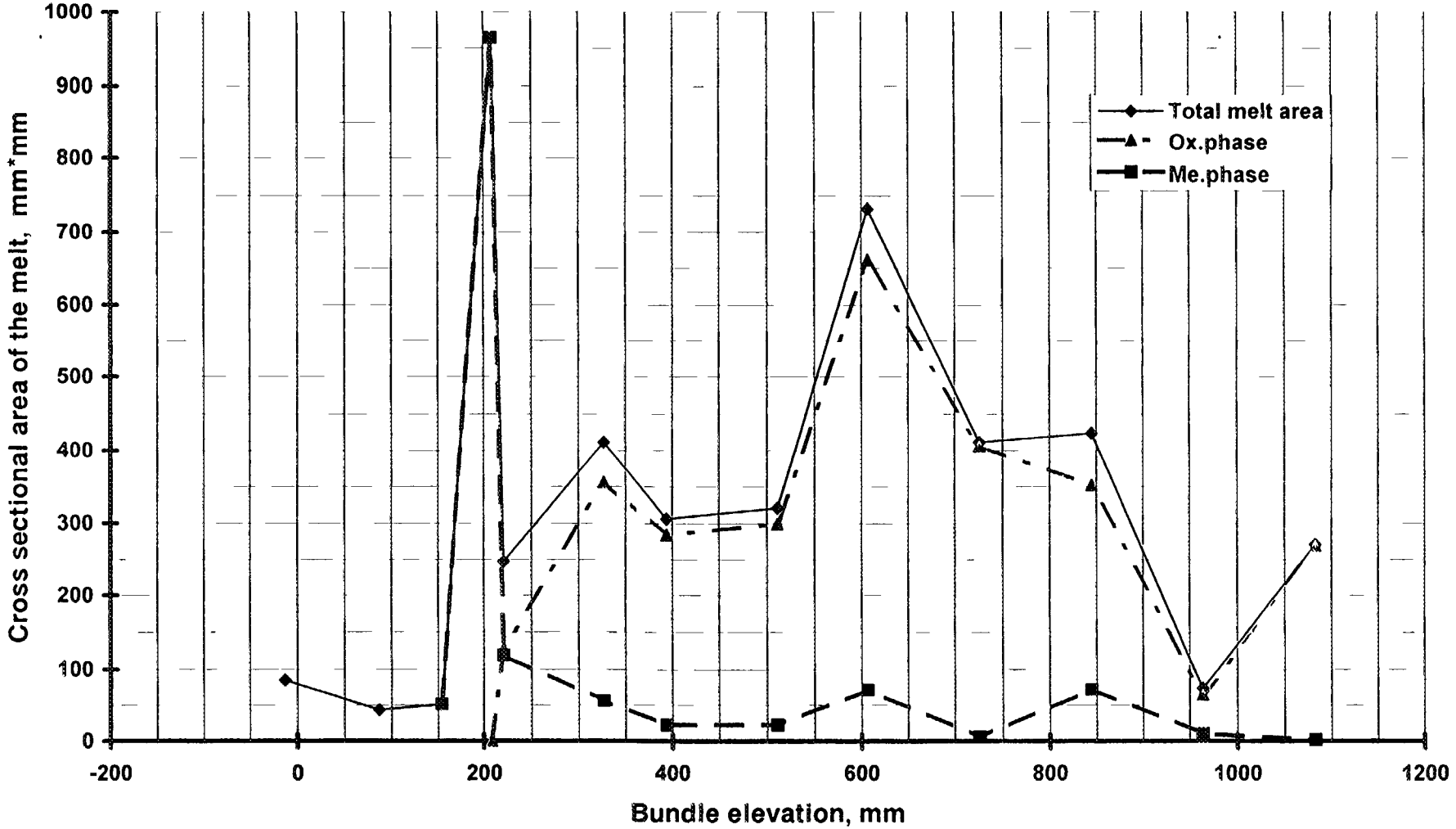

Fig.13 Axial profile of the core materials melt cross-sectional area

estimate a relocated melt oxidation the cross-sectional area or the oxidized and metallic parts of the melt were measured separately. In the case of the
phase under investigation consisted of the metallic and ceramic grains mixture, the image analysis of the microstructures was used for separation of the metallic and oxidized parts of this phase.
As one can see from the Fig. 13, the main part of the relocated melt were oxidized and most likely, that core melt flowing finished before the end of the test. The metallic part of the melt consists mainly at the stainless steel melt, originated from the absorber rod cladding and guide tube, that formed a lower blockage, and separated stainless steel droplets remained in the oxidized matrix at the oxidized core melt in the upper part of the bundle.

Conclusions.

The data of the posttest microstructural investigation and quantitative parameter measurements present a consistent picture of the VVER-type bundle behavior under SFD conditions.

The experiment realized led to a better understanding of the severe fuel damage processes in the VVER core.

In general, the VVER fuel bundles behaviour in the early stage of the loss-of-coolant accident is similar to the behaviour of the PWR bundles.

The results obtained from the posttest bundle examination consist a data base for the comparison with the analytical predictions of the bundle behaviour by the codes.

REFERENCES

1. Posttest Examination of the VVER-1000 Fuel Rod Bundle CORA-W2,

FZKA 5570 (1995)

2. S. Hagen, P. Hofmann, V. Noack, G. Schanz, G. Schumacher, L. Sepold "Behavior of a VVER-1000 Fuel Element with Boron Carbide/Steel Absorber
Tested under Severe Fuel Damage Conditions in the CORA Facility",

KfK 5363 (1994).

3. K. Minato, W. Hering, S. Hagen "Zircaloy Oxidation and Cladding Deformation in PWR-Specific CORA Experiments", KfK 4827 (1991).

THE FISSION PRODUCT AND ACTINIDE RELEASE AT HIGH TEMPERATURE IN PWR FUEL RODS: THE VERCORS SAFETY PROGRAMME

G DUCROS, B. ANDRE, M. TOURASSE
Commissariat à l'Energie Atomique, Grenoble

D. MARO
Commissariat à l'Energie Atomique,
Institut de Protection et de Sûreté Nucléaire

France

Abstract

Analytical fission product release tests under severe accident conditions have been initiated by the French Protection and Safety Institute (IPSN) and Electricité de France (EDF). They have been conducted at the Centre d'Etudes Nucléaires de Grenoble (CEA-CENG). Since 1983, the HEVA programme has been extended by the current VERCORS programme in 1989 with higher fuel temperature (2600K).

For these tests, industrial fuel from French PWR reactor plants is used. In order to rebuilt the short-lived fission product inventory, a re-irradiation is performed in the SILOE reactor, prior to the test.

The device is equipped with three gamma spectrometers that allow on-line measurements on fission product and actinide release kinetic. The post-test characterisation includes gamma spectrometry, ceramography, scanning electron microscopy, gamma emission tomography. This gives a full overview of both fission product and fuel rod behaviours.

This paper deals with the dependence of fission product and actinides release with temperature and environmental conditions (oxidising or reducing conditions). The results obtained with VERCORS 4 experiment (38 GWd/tU, 2570 K, reducing conditions) are detailed. The comparison with the previous tests in lower thermal conditions (VERCORS 1 and 2) or oxidising conditions (VERCORS 3) gives information on the key parameters.

For further needs in relation with fuel meltdown conditions, the modifications of the VERCORS loop and of the on-line instrumentation that are planned to be operational by the beginning of 1996 are presented.

1. INTRODUCTION

The VERCORS programme extends the HEVA experimental programme, which has been previously presented during the last IAEA TCM held in 1992 at Cadarache, France [1], [2]. It is devoted to the source term of fission products (FP) released from Pressurised Water Reactor (PWR) fuel samples during a sequence representative of a severe accident. This programme, implemented by the Nuclear Reactor Division of the French Atomic Energy Commission, CEA, is defined by the "Institut de Protection et du Sûreté Nucléaire" (Nuclear Protection and Safety Institute - IPSN) and confounded by IPSN and "Electricité de France" (EDF. French Electricity Board).

6 VERCORS tests have been conducted since 1989 with higher fuel temperature (2600K) as former HEVA tests, in order to measure the release of low volatile FP and actinides. The results obtained with the VERCORS 4 experiment, performed in reducing conditions are detailed. Some comparison with previous tests in lower thermal conditions or oxidising conditions are presented.

2. AIMS OF THE VERCORS PROGRAMME

The aims of the programme are as follows :

- to improve and validate models used in the ESCADRE system codes describing the risks of fission product transfer into the environment during a severe accident,
- to create a realistic data bank for computing the behaviour of FP in the primary circuit and the containment and, as a result, for assessing the potential waste. Essentially, this could lead to the re-evaluation of safety margin on envelope data currently available.

The measurements taken during the tests are thus aimed at characterising :

- the release kinetics and the total release of FP, actinides and structural materials as a function of fuel temperature and oxidising/reducing conditions of the environment,
- the aerosol source as a function of temperature, of dilution in the vector gas and of structure materials present,
- the chemical behaviour of the FP in the fluid and in their interaction with the walls.

3. EXPERIMENTAL DEVICE

The experiments are conducted in a shielded hot cell of the LAMA, Grenoble Nuclear Research Centre Hot Laboratory.

3.1. Fuel sample

The test fuel sample comprises a fuel rod section from an EDF power plant and includes three pellets in their original cladding. Two half-pellets of depleted uranium oxide are placed on each side of the test sample and held in place by crimping the cladding. The sample is maintained vertically on a zirconia crucible (latter in a thoria crucible for the test designed to reach the fuel melting temperature).
This fuel is re-irradiated at low power, about 15 $W.cm^{-}$, in the SILOE experimental reactor in Grenoble during a week, in order to recreate the most important short-lived FP for the purpose of safety-related analysis. These short-lived FP include volatile FP (tellurium and iodine), gases (xenon) and the less volatile FP (molybdenum, barium/lanthanum, ruthenium, cerium, zirconium, etc.). The accident sequence takes place about 30 hours after the re-irradiation of the fuel rod.

3.2. Hot cell lay out

The experimental device (figure 1) includes, the following main components, in the fluid flow direction :

- a supply of steam and hydrogen constituting the fluid in which the experiment is conducted,
- a supply of helium for protecting the susceptor (tungsten or graphite) of the HF furnace against oxidisation caused by the steam,
- a superheater to heat the fluid to 1100K,
- an induction furnace for heating the sample to high temperature, 2600 K at present (fuel melting temperature by the end of the year). It comprises, from the inside to the outside two concentric channels dynamically sealed by a stack of dense zirconia sleeves (the internal channel containing the sample is flowed with steam and hydrogen, the external channel containing the susceptor (graphite or tungsten) is protected by the helium flow

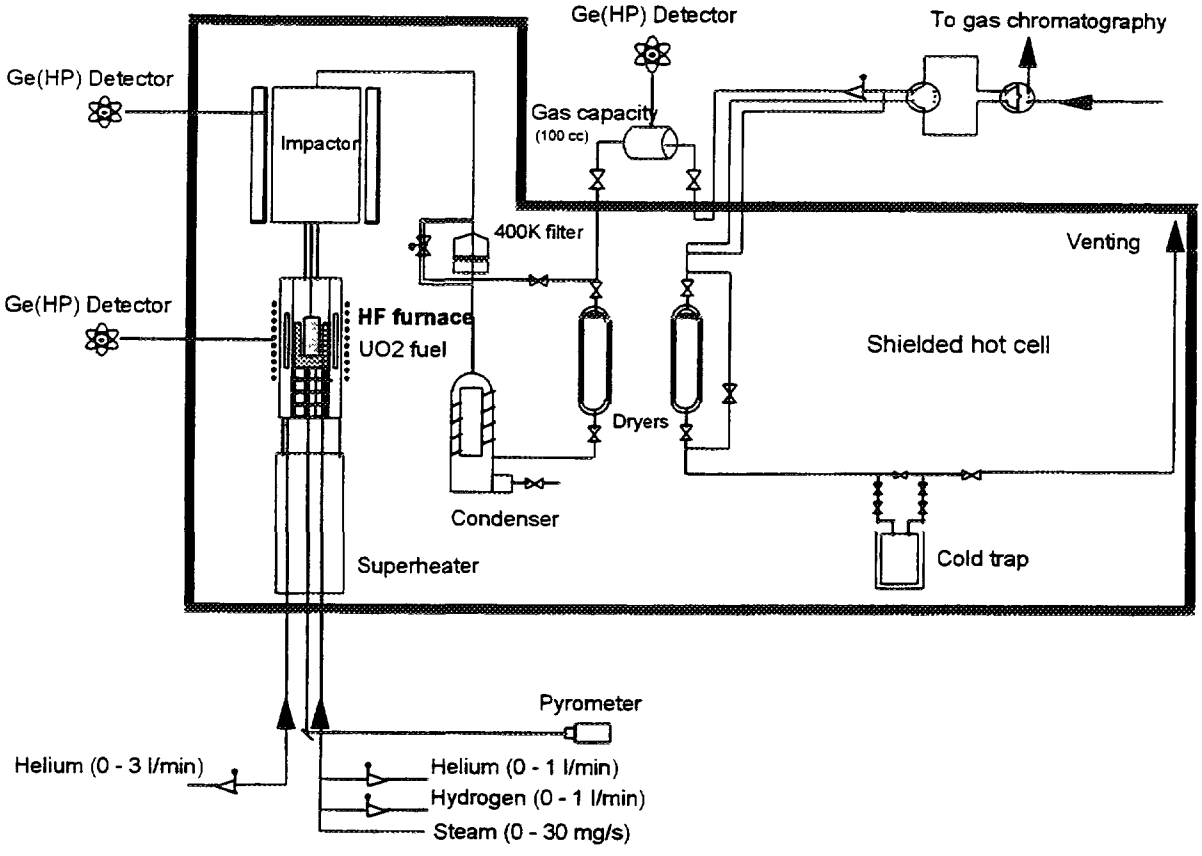

Figure 1 : VERCORS DEVICE IN HOT CELL

with a slightly higher pressure than the internal channel), a double layer heat insulator (dense zirconia and alumina), a quartz tube, constituting the furnace chamber, and the furnace coils,

- a junction zone, with a zirconia tube internal channel, linking the furnace to the impactor,
- a cascade impactor, placed in a resistance furnace with an adjustable temperature range of 500 K to 1000 K, which traps the aerosols on different stages according to their dimensions,
- a filter, heated at 400 K, which traps non-gaseous forms of iodine at this temperature,
- a condenser and dryers (silica gel and molecular sieve) for collecting the steam,
- a cold trap (charcoal adsorber cooled by liquid nitrogen) for trapping noble gases.

3.3. On line instrumentation and post test analyses

Apart from the traditional analogical measurements of temperature, flow rate, pressure, the on-line instrumentation have been improved since the HEVA tests. In particular for the following instruments :

- a radiation pyrometer, calibrated between 1300K and 3300K, for measuring the crucible temperature (from VERCORS 3 onwards),
- an on-line gas chromatography (from VERCORS 2 onwards) located between the two dryers and used to measure hydrogen emission kinetics during the cladding oxidation phase. This device can also be used to quantify the volume of extraneous CO resulting from possible oxidation (particularly from susceptor when made of graphite).

Moreover three complementary gamma spectrometry stations measure FP release kinetics :

- one station focused on the fuel rod (originally in place since HEVA 3),
- one station focused on the top of the impactor, filter and last stages (from HEVA 7 onwards),
- one station for taking measurements of isotopes of xenon (133, 133m and 135) and krypton (85) in the gas flow after the condenser (from VERCORS 2 onwards).

These three gamma spectrometry stations are composed of a portable liquid nitrogen-cooled Ge (High Purity) detector, an electronic device, for signal shaping and storage, fitted with a rack unit for correcting pile-up counting losses in order to obtain spectra at a high rate (up to 1 spectrum.min^{-1}). Compensation better than 5% is guaranteed up to 150.000 pulses.$^{-1}$, the limit of the counting rate defined for the tests. The spectra data processing is made through a code, developed in the laboratory, suitable for the complex spectra due to the abundant short lived FP leading to numerous gamma rays interferences. This code includes modules which make the automatic identification of the peaks, the fitting of the gaussian curves, the correction of multiplets and interferences and the calculation of the number of measured nuclides based on an established yield curve (self calibration or calibration with a multiline standard).

After the test, the fuel is embedded in situ with an epoxy resin and X-rayed. A longitudinal gamma scanning of the fuel is conducted to measure the final FP inventory in order to calculate the quantitative fraction of FP emitted by the fuel during the test. All the components of the loop (impactor stages, filters, condenser, dryers, etc.) are then gamma-scanned to measure and locate the PF released during the test and to draw up a balance of these FP. For some tests, a non destructive transversal gamma scanning is carried out for several angles of incidence to determine the spatial location of the FP remaining inside the fuel and analyse probable interactions of these FP with cladding components (traps of tellurium or barium in the cladding, delaying their emission) [3].

A ceramographic examination is carried out on each pellet of the fuel rod to analyse the changes in the microstructure of the cladding and the fuel.

Physico-chemical analyses are then carried out on samples of the loop after dismantling, especially on the plates of the impactor and on the zirconia tube linking the furnace and the impactor. The basic method used is scanning electron microscopy combined with an analysis of X-ray emitted (SEM/EDX), performed in the LAMA laboratory and in collaboration with the AEA-Winfrith laboratories. Some XPS and XRD analysises have been conducted on selected samples.

Table I : VERCORS TEST GRID

VERCORS TEST	1	2	3	4	5	6
Fuel burnup (GWd/tU)	43	38	38	38	38	# 55
Reirradiation	SILOE	SILOE	SILOE	SILOE	SILOE	SILOE
Heat up rate (K/s)	1	1	1	1	1	1
Max fuel temp. (K)	2130	2150 (*)	2570	2570	2570 (*)	2620
Plateau duration (min)	17	13	15	30	30	30
Injected gas during plateau (mg/s) :						
H2	0,05	0,5	0,5	0,2	0	0,5
H2O	2,5	25	25	0	25	25
He				8		
Impactor temp. (K)	870	870	870	870	870	870
Date of test	21/11/1989	06/06/1990	14/04/1992	22/06/1993	30/11/1993	07/06/1994

(*) : Several plateaus at low temperature (between 1070 and 1770K) before accidental simulation

4. PARAMETER VARIATIONS AND TEST GRID

The parameters that can be varied are the temperature plateau, the temperature ramp and the burn-up of the fuel sample, the temperature of the impactor, the fluid composition and flow rate (steam and/or hydrogen) The test grid (table I) shows how the programme has been implemented.

VERCORS 1 and VERCORS 2 were made at a temperature around 2100K, the same temperature as the most previous HEVA tests :

- at a low fluid flow of steam and hydrogen (high concentration of the FP in the fluid flow) for VERCORS 1,
- at a high fluid flow of steam and hydrogen, and with several plateaux at low temperature (between 1070 and 1770K) before accidental simulation for VERCORS 2.

The next four tests, from VERCORS 3 to VERCORS 6, were all performed at about 2600K (probably slightly higher for VERCORS 6) :

- in a mixed steam and hydrogen atmosphere for VERCORS 3,
- in pure hydrogen during the high temperature plateau for VERCORS 4 (and after a pre-oxidising phase of the clad),
- in pure steam during the high temperature plateau for VERCORS 5,
- in a mixed steam and hydrogen atmosphere for VERCORS 6 and a high burn-up fuel (55 GWd/tU).

The high temperature plateau was maintained 30 min for the last three tests and only 15 min for VERCORS 3, because of a blockage of the loop on the last stage of the impactor, due to large release of aerosols.

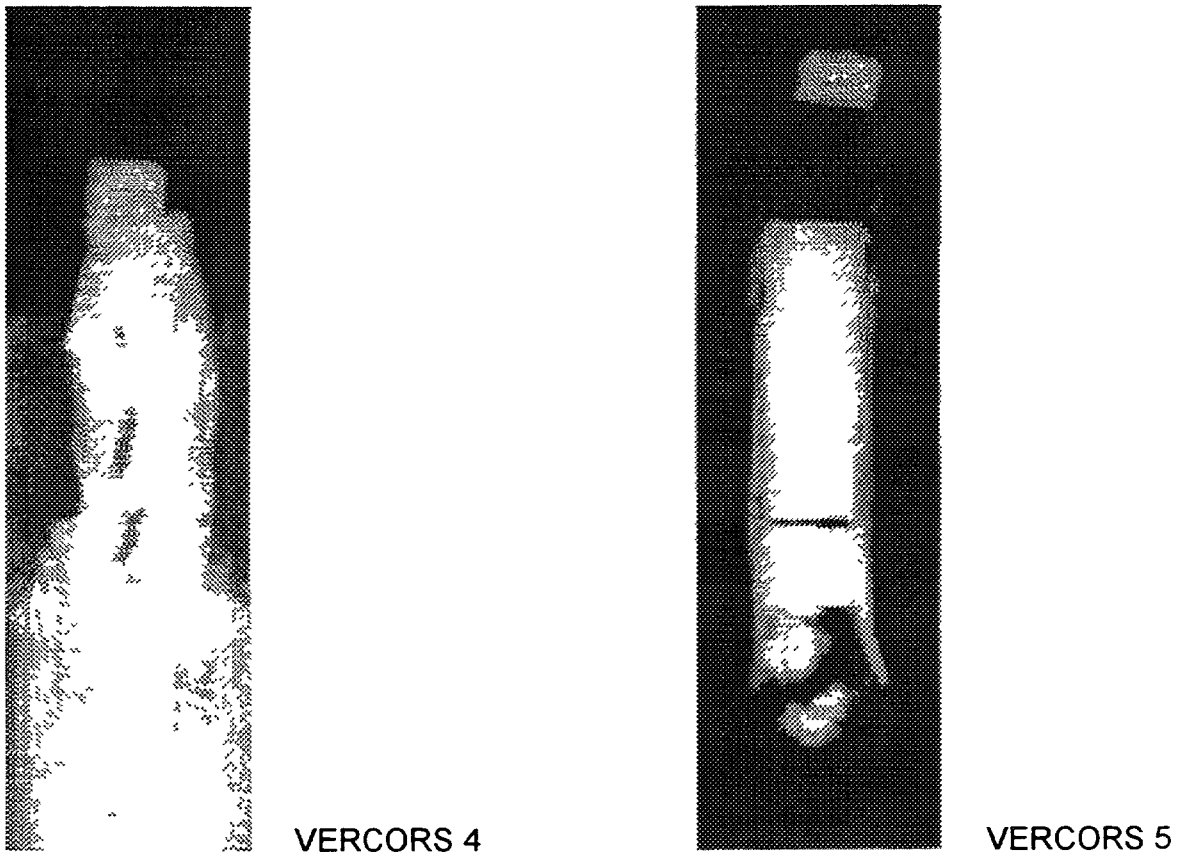

Figure 2 : X-ray radiography of VERCORS fuel samples after the test

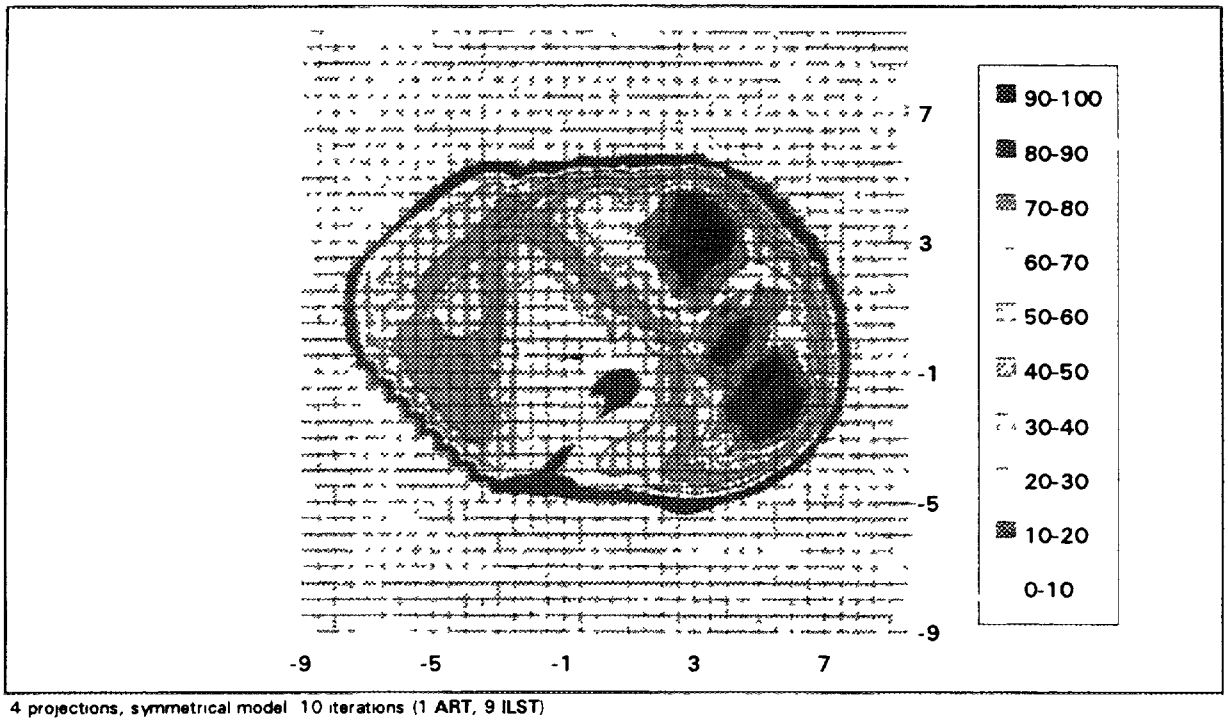

Figure 3 : Gamma emission tomography of Zr95 in the fuel after VERCORS 4 test

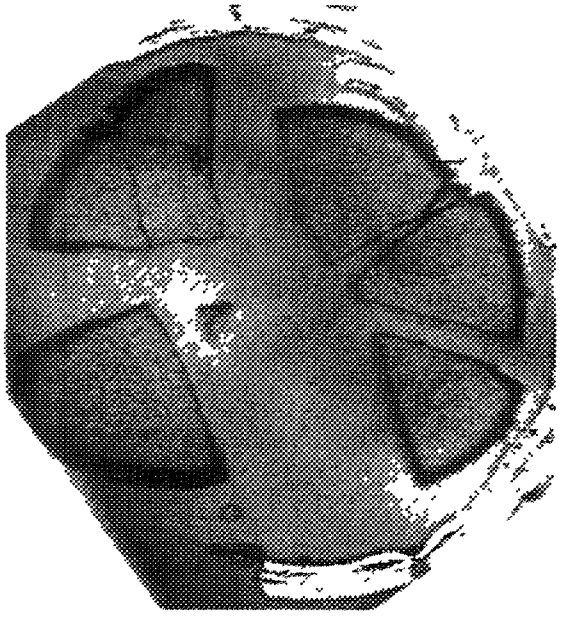

Figure 4 : Ceramography of VERCORS 4 fuel after the test

5. RESULTS OF VERCORS 4 EXPERIMENT

The main results presented in this section are obtained from VERCORS 4 test, the last test from which all the results are now available. Comparison with other tests will be made to give information on the key parameters such as temperature, environmental conditions and burn-up of the fuel [4], [5].

5.1. Fuel behaviour at 2600K

Figure 2 compares the X-ray radiography of the fuel sample after VERCORS 4 and VERCORS 5 tests. VERCORS 4, performed in pure hydrogen atmosphere, shows a fuel with large split up for the three original pellets ; on the opposite, VERCORS 5, performed in pure steam atmosphere, shows a fuel, which has significantly swollen, but has maintained its total integrity. For both tests, the non irradiated half pellets appear intact (except the lower half pellet from VERCORS 5 which is broken), emphasising a different behaviour between irradiated and non irradiated fuel.

Figures 3 and 4 compare gamma emission tomography of Zr95, which is a fuel tracer, with ceramographic examination of the fuel after the VERCORS 4 test [3]. The tomographic image, obtained by deconvolution of only 4 transversal acquisitions at 45° intervals, shows that the fuel has been severely damaged and relocated at least in two well separated parts. This is a useful information as it can be obtained by a non destructive way prior to the ceramographic examinations. More comprehensive transversal acquisitions, constituted of 18 projections every 10° were performed on VERCORS 5 fuel, producing a better spatial resolution, both for fuel tracers (Zr95), and more volatile FP (Cs137, Ba140). The ceramography confirms the tomographic analyses by showing a fuel which is radially cracked and separated in several pieces. Moreover, the microstructure of the fuel shows a wide intergranular and intragranular porosity (foaming aspect) and a wide peripheral zone about 500 mm thick of very large opened porosity, from which volatile FP have been completely released.

TABLE II : MEASURED RELEASED FRACTIONS OF GAMMA EMITTERS

Element	Gamma emitters (Half life)	Vercors 1	Vercors 2	Vercors 3	Vercors 4
Srontium	Sr91 (9,5 h)/Y91m (0,8 h)				< 8%
Yttrium	Y93 (10,1 h)			17%	
Zirconium	Zr95 (64,0 d), Zr97 (16,9 h)				< 2%
Molybdenum	Mo99 (2,8 d)		15%	42%	47%
Ruthenium	Ru103 (39,3 d), Ru106 (1,0 y)			0,36%	7%
Rhodium	Rh105 (35,4 h)			0,52%	45%
Antimony	Sb125 (2,8 y), Sb127 (3,9 d)	2%	7%	69%	97%
Tellurium	Te131m (1,3 d), Te132 (3,3 d)	4%	18%	76%	100%
Iodine	I131 (8,0 d), I133 (20,8 h)	30%	23%	70%	87%
Xenon	Xe133 (5,2 d), Xe135 (9,1 h)	33%	23%	77%	86%
Cesium	Cs134 (2,1 y), Cs137 (30,2 y)	42%	30%	70%	93%
Barium	Ba140 (12,8 d)	4%	4%	13%	66%
Lathanum	La140 (1,7 d)			< 4%	< 2%
Cerium	Ce141 (32,5 d), Ce143 (1,4 d)				3%
Europium	Eu154 (8,8 y)			9%	< 5%
Neptunium	Np238 (2,1 d), Np239 (2,4 d)	0,006%	0,016%	0,40%	6%

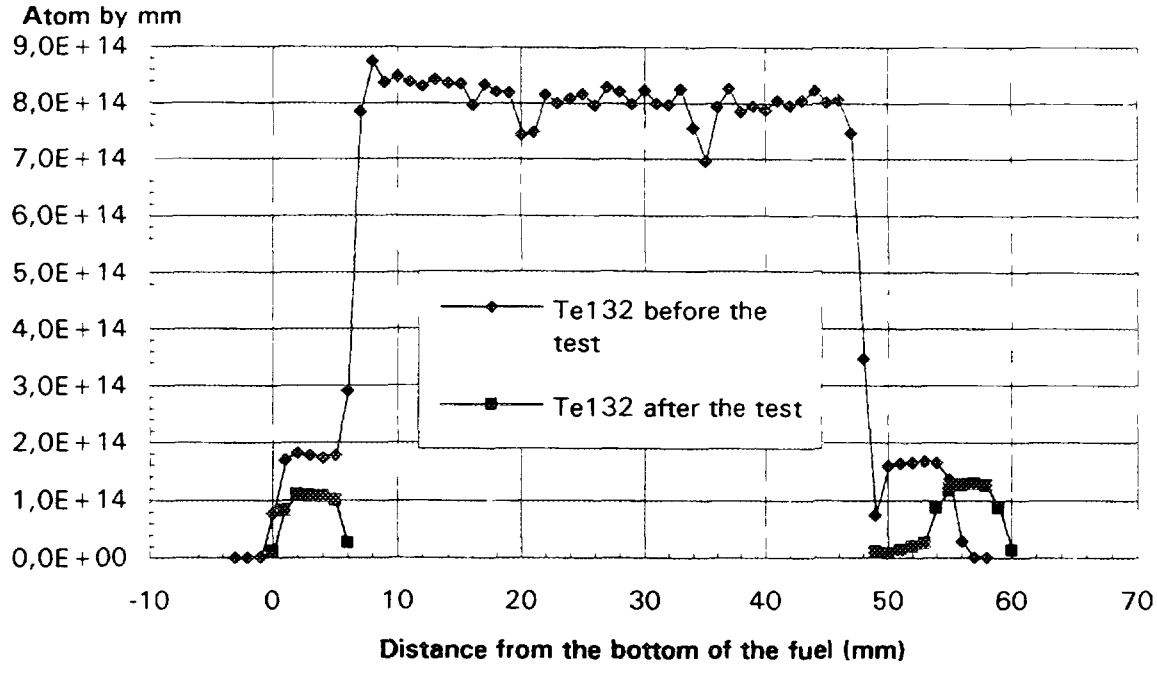

Figure 5 : Te132 inside the fuel before and after VERCORS 4 test

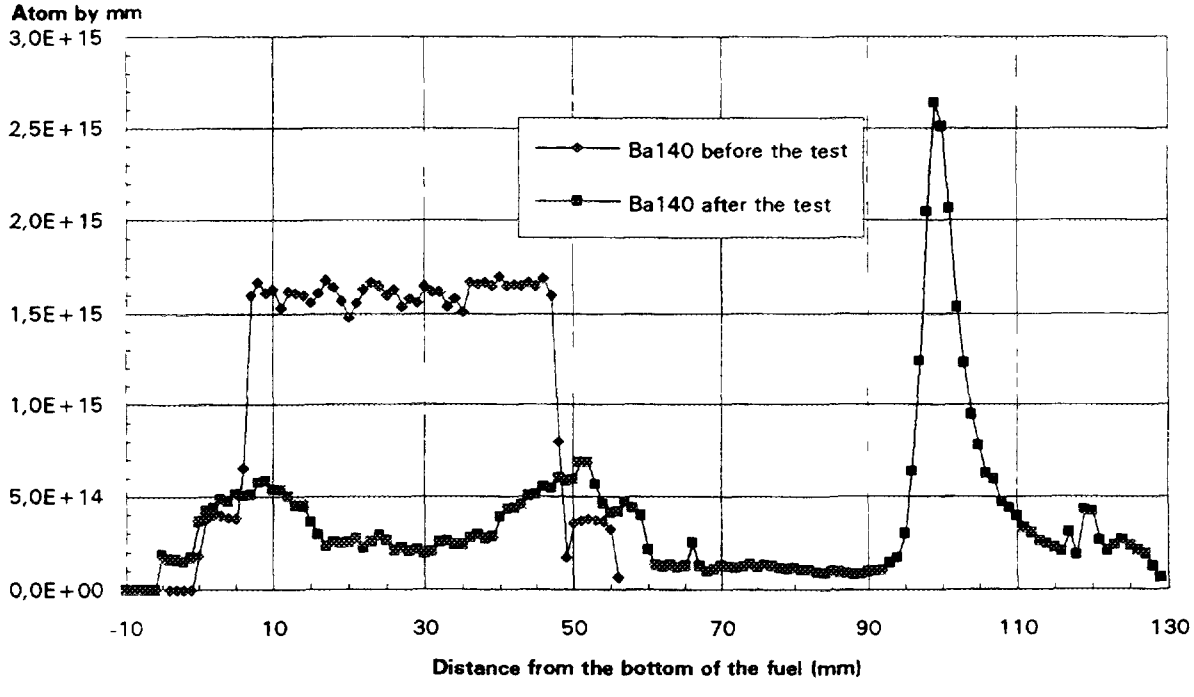

Figure 6 : Ba140 inside the fuel and the zirconia tube surrounding the fuel before and after VERCORS 4 test

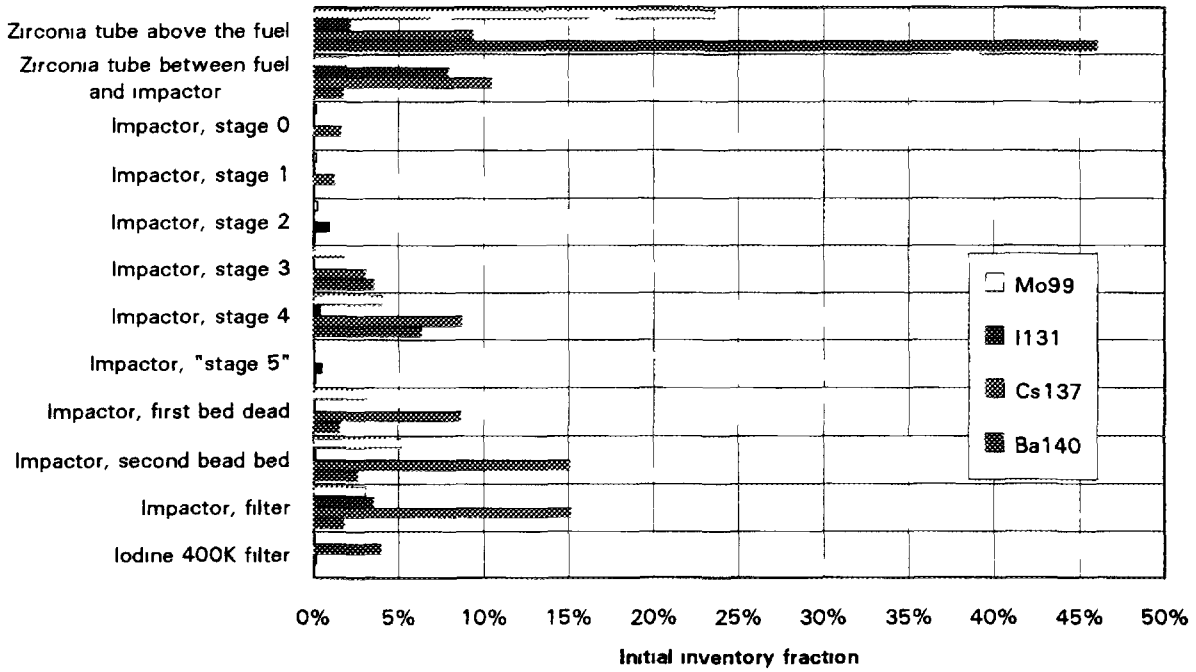

Figure 7 : Distribution of Mo99, I131, Cs137, Ba140 along the loop after VERCORS 4 test

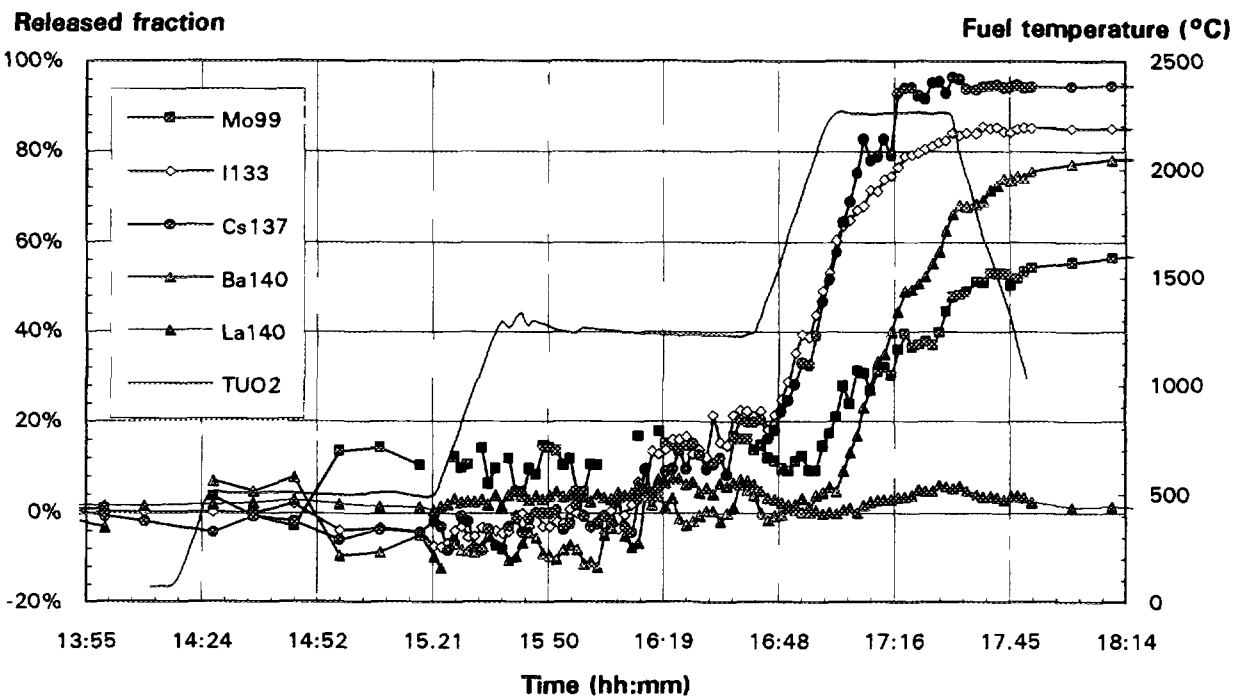

Figure 8 : Release kinetic of Mo99, I133, Cs137, Ba140, La140 on VERCORS 4 test

5.2. Fission products release

5.2.1. Total release

The released fractions of all the FP, measured by gamma spectrometry from the first four VERCORS tests are given in table II. From VERCORS 1 and 2, apart the volatile species, only Mo, Sb and Ba had a measurable release. It should be noticed that Np was identified with a very small amount in the cold trap, downstream the loop. From VERCORS 3 and 4, performed at higher temperature, other low volatile FP were measured. Accordingly to their release at 2600K, FP can be classified in four categories :

- usual volatile species, Cs, I, Te, with nearly complete release, but not total release for I and Cs, which can form some less volatile compound at high temperature with another elements (in particular U, or Mo can be associated with Cs and retained a few percentage of cesium initial inventory) [3], [6],
- semi volatile species, composed of Sb, Mo, Ba, Rh, with a total release close to the release of volatile species, especially for Sb. These elements present both non volatile forms, deposited close to the fuel, and volatile forms, deposited far away downstream the loop,
- low volatile species, composed of Ru, Ce, Np and also Sr, Eu to be confirmed, with a significant release fraction, ranged from 2% to 10%, and deposits exclusively located upstream in the loop, very close to the fuel. Among these elements can be noticed the actinide Np, which is more volatile than U,
- non volatile species, composed of Zr, La, Nd, with no significant release in this range of temperature.

Other elements, non measurable through gamma spectrometry, are detected by SEM/EDS (see § 5.3), but this technique is not able to give the total release or the release kinetic of these elements ; it only gives a release indication.

5.2.2. Deposits along the loop

Longitudinal gamma scanning of the fuel after the test, then of all the components of the loop after dismantling, allow to measure and locate the FP deposition. For instance, figure 5 gives the distribution of Te132 inside the fuel before and after the test, showing the great difference of behaviour between the three original irradiated pellets, completely depleted in Te132, and the non irradiated half pellets, with a released fraction of only 33%.

Figure 6 gives in the same way the distribution of Ba140 inside the fuel before the test, and inside the fuel and the upper part of the zirconia tube surrounding the fuel after the test ; 38% of Ba140 released, over a total fraction released of 66%, is deposited in a non volatile form about 40 mm above the fuel.

To complete this post test analysis, figure 7 is an example of the distribution of Mo99, I131, Ba140 and Cs137 along the loop after the test. This result emphasises in particular the specific behaviour of iodine, composed of a significative amount of very volatile forms, going through the last filter of the impactor (at 870K) and being totally trapped in the filter maintained at 400K.

5.2.3. Release kinetic

The three complementary on line gamma spectrometers, previously described, allow a good measurement of the FP release kinetic.

The release kinetic from the central pellet of the fuel is given on figure 8 for Mo99, I133, Ba140, La140 and Cs137. Volatile species (I133 and Cs137) have the same kinetic, their release being increased during the heat up of the fuel between 1520K and 2600K, when the release of the semi volatile species (Mo99 and Ba140) is delayed and occurs at the beginning of the high temperature plateau. Notice the great release of Ba140 and the total lack of release of his daughter La140.

The release rate of noble gases, measured after the condenser, is given on figure 9 for Xe133,

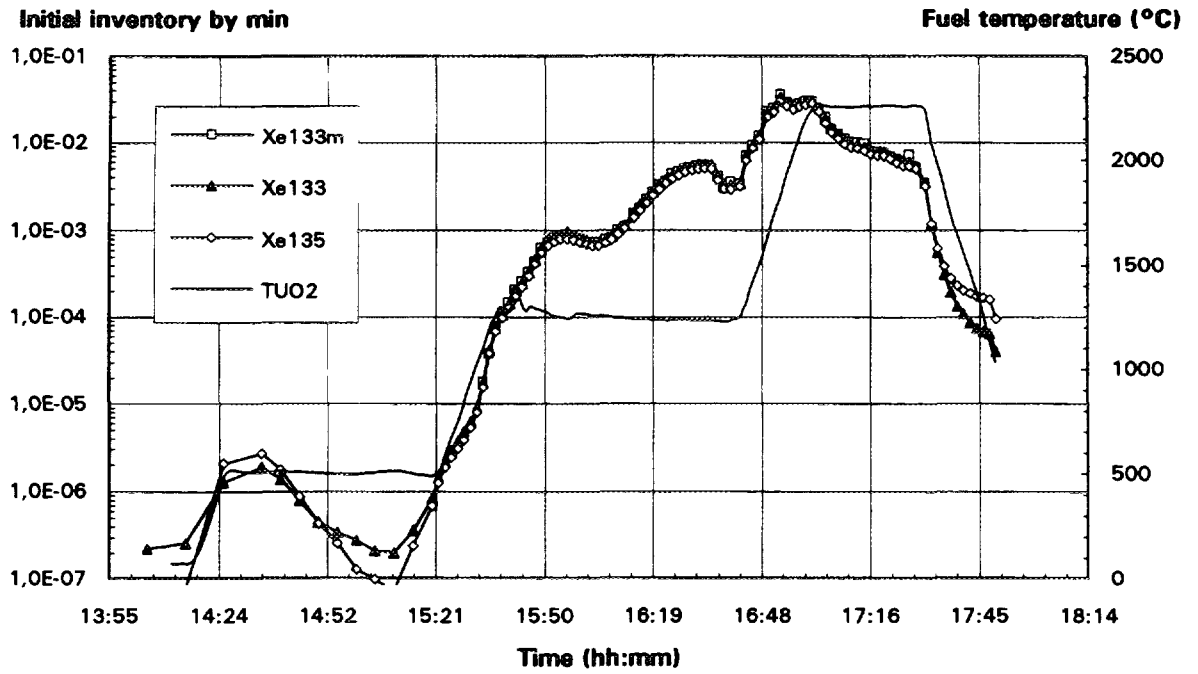

Figure 9 : Release rate kinetic of xenon on VERCORS 4 test

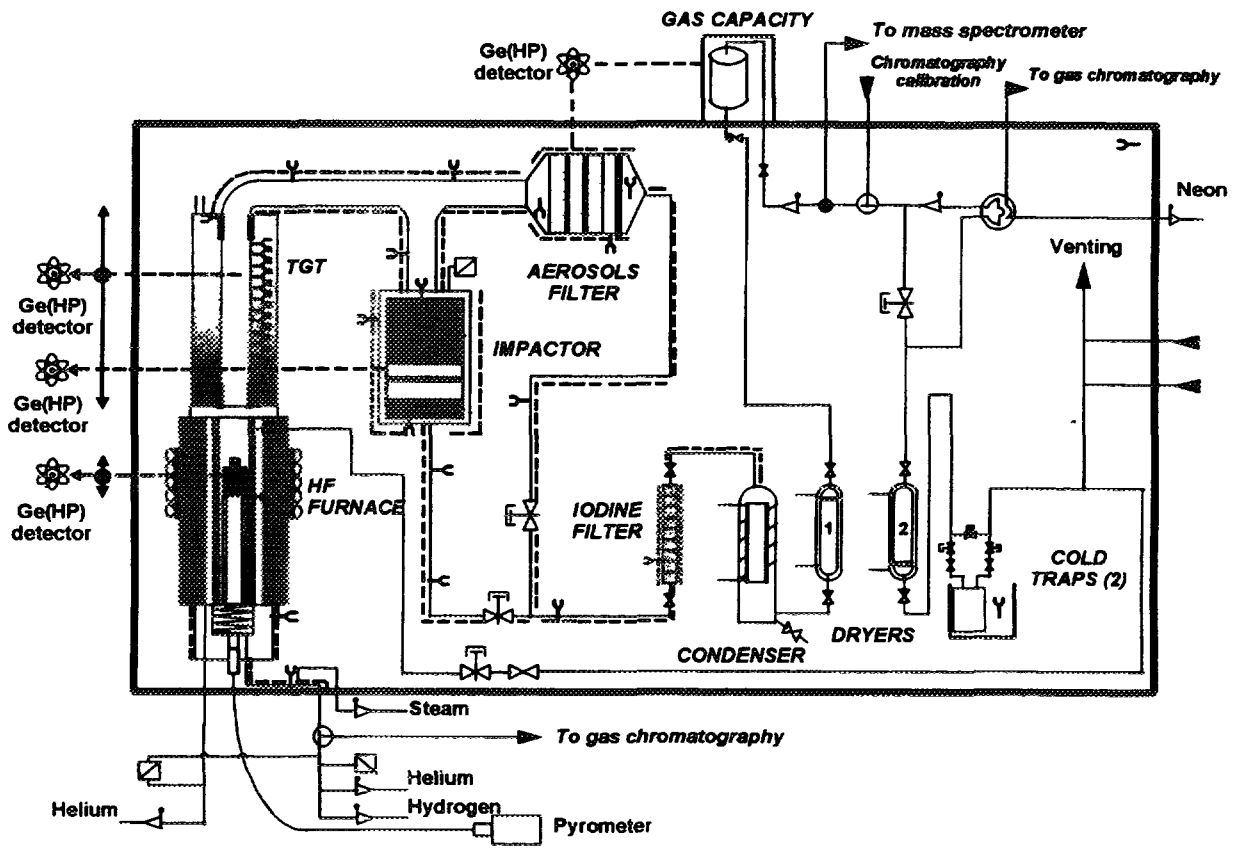

Figure 10 : VERCORS HT NEW DEVICE IN HOT CELL (Operational beginning 1996)

Xe133m and Xe135. A first gust occurs at the beginning of the conditioning plateau (800K under He), followed by two another gusts during the pre-oxidising plateau (1520K under steam and hydrogen). The third gust is synchronous with the first arrival of iodine and cesium in the impactor, probably correlated with more oxidising conditions, due to the end of the cladding oxidation. Lastly the maximum release rate occurs during the heat up to the high temperature plateau.

5.3. Electron microscopy of aerosols

In the first instance this analysis aims at characterising those elements that could not be identified through gamma spectrometry. Samples come from the impactor plates.
Global morphology of the aerosols showed very thin particles with a mean diameter ranging from 0,1 to 0,3 mm, probably transported within aggregate form. Elemental compositions determined by energy dispersive spectrometry (EDS) associated with the scanning electron microscopy (SEM) revealed a great amount of U (up to 60% of atomic concentration of main elements). Sn and Pd were identified in less amount than U. Among FP simultaneous detections of Cs and Mo on all samples, suggest the formation of cesium molybdate.

6. FUTURE PROSPECTS

In order to reach the fuel melting temperature, a new loop is under construction within a wider shielded cell. On line instrumentation will be improved, with :

- a thermal gradient tube 0,7 m long, just downstream the fuel furnace, devoted to the study of the vapour phase deposition and the FP deposits,
- the moving of the impactor on a derived circuit, working in a more suitable sequential mode,
- a specific iodine filter, dividing the chemical species.

This new device (figure 10), called VERCORS HT (High Temperature), is especially conceived in order to extend the release rate and deposits data of low volatile FP and actinides between 2600K and 3100K, and to study the chemical forms of iodine. The next test, VERCORS HT1 will be performed at the beginning of 1996.

Another device with less on-line instrumentation, called VERCORS RT (Transuranic Release), is also under preparation, in order to have a better measurement of the total amount of actinides release, not measurable through gamma spectrometry (U, Np, Pu, Am, Cm). Balance will be made by chemical analysis (particularly ICPAES) after dissolution of both the fuel sample and a trapping filter located just downstream the fuel and collecting all the released elements.

7. CONCLUSION

The VERCORS programme represents a step forwards in the knowledge and the accuracy of the source term. Following the HEVA programme, which had contributed to the main data of volatile FP, the VERCORS tests have extend the data base up to 2600K :

- confirming the nearly total release of volatile species Cs, I and Te,
- measuring the release of low volatile species and classifying them in three categories : "semi volatile" (Sb, Mo, Ba, Rh), "low volatile" (Ru, Ce, Np, Sr, Eu) and "non volatile" (Zr, La, Nd).

The further experiments VERCORS HT and RT will be focused on the release of low volatile FP and actinides, and chemical forms of iodine, up to the fuel melting temperature.

REFERENCES

[1] : J.P. LEVEQUE, G. LHIAUBET, D. BOULAUD, "The HEVA experimental program", TCM IAEA Cadarache 1992.

[2] : J.P. LEVEQUE, B. ANDRE, G. DUCROS, G. LE MAROIS, G. LHIAUBET, "The HEVA experimental program", Nuclear Technology, Vol. 108, Oct. 1994.

[3] : G. DUCROS, E. CONFORT, P. DREVON, "Non destructive location of fission products in a damaged fuel rod section using gamma-emission tomography", TCM IAEA on recent developments on post-irradiation examination techniques for water reactor fuel, Cadarache 1994.

[4] : B. ANDRE, G. DUCROS, M. TOURASSE, D. MARO, "Fission product release and PWR fuel behaviour at 2600K under steam and hydrogen : the VERCORS tests", Spring CSARP meeting, Bethesda, 1995.

[5] : G. DUCROS, B. ANDRE, M. TOURASSE, D. MARO, "The VERCORS safety program, source term analytical study with special emphasis on the release of non volatile fission products and transuranic elements", Spring CSARP meeting, Bethesda, 1995.

[6] : R.R. HOBBINS, D.A. PETTI, D.L. HAGRMAN, "Fission product release from fuel under severe accident conditions", Nuclear Technology, Vol. 101, Mar 1993.

ASSESSMENT OF THE MODIFIED ICARE2 CODE OXYGEN DIFFUSION MODEL FOR UO2/Zr(SOLID)/H2O INTERACTIONS

A.M. VOLTCHEK, A.E. KISSELEV, V.F. STRIZHOV
Institute of Nuclear Safety,
Moscow, Russian Federation

A. PORRACCHIA, R. GONZALEZ, P. CHATELARD
Institut de Protection et de Sûreté Nucléaire,
France

Abstract

In this paper the results of the code-to-data and code-to-code comparisons for verification of the new ICARE2 oxygen diffusion model (module UZRO) are reported. The separate-effect test data Prater - Courtright and Hofmann were examined in temperature range 1200 - 2273 K. The main objective of this research is the evaluation of the applicability of the diffusion approach at very high temperatures, T > 1773 K, when the oxidation heat release become so high that, in integral experimental facilities, it actually determines the heat up rate of the bundle. It is shown that good agreement exists between experiments of Prater - Courtright (isothermal temperature regimes) and Hofmann (transients), both experimental sets may be described in the framework of the same oxygen diffusion model. The parabolic approach (Prater-Courtright correlations) underpredicts the oxide layer thickness in the finite cladding geometry by 25-40%.

1. INTRODUCTION

The severe fuel damage (SFD) phenomena in various types of reactors have been the subject of research for many years. The development and validation of the integral codes, devoted to core degradation analysis, are a part of national analytical programs. The collaboration between different groups provides a new step in understanding of physical processes during SFD accidents. The presented report concerns the activities of two institutes - NSI RAS (Russia) and IPSN (France) - for the development of new detailed mechanistic models of different SFD phenomena, their implementation in the ICARE2 code (France) and validation against various experimental data.

The ICARE2 code has been developed in IPSN since 1987 [1]. The code allows a mechanistic description of all the major degradation phenomena on the basement of the models for thermalhydraulics, heat transfer, main chemical reactions, mechanical destruction of fuel rods, etc. Complexity of the described object required generalisation of the code and development of more physically grounded models for most crucial events, occurring in the core during an accident transient. Primary detailed mechanistic modules were developed in NSI RAS in the frame of the SVECHA package in 1991 (see [2]). They include the following modules:

UZRO - chemical interactions UO2/Zr/H2O ([3]),

DROP - melt relocation,

CROX -mechanical behaviour of the fuel cladding.

These modules were successfully implemented into the ICARE2 V2 mod1 code in collaboration with IPSN. The extensive assessment of the modified version V2 mod1 was performed in 1993-1994 against in-pile integral tests PHEBUS SFD B9+ (ISP-28) and PBF SFD 1.4 and the out-of pile experiment CORA-13 (ISP-31)

The ICARE2 V2 mod2 version with implemented SVECHA package was recently released (1995).

This report concerns the assessment of the modified ICARE2 code module UZRO to the separate effect tests [4], [5] and the code-to-code comparisons.

2. OVERVIEW OF THE ICARE2 CODE MODULES.

The ICARE2 code is composed of a set of modules, each addressing a specific phenomenon of the early and late phase of core degradation. Table I shows the main modules used for the current analysis of separate effect tests.

The thermalhydraulic solution is based on a multi-channel modeling without cross-flows. Heat and mass transfer between different components of the bundle are described by separate modules. Exchange of information about physical state of the bundle goes throughout a common database. This modular structure possesses great flexibility and allows further development of any element.

The version V2 mod1 contains modules which were based on a simplified physical approach. This concerns, in particular, the parabolic scaling for chemical fuel/clad or clad/steam interactions, movement with constant velocity of relocated melt and unilayer cladding structure for description of mechanical behaviour. For detailed analyses of these processes, the modules developed in NSI RAS were adopted and installed in the code during 1992-94. This new approach allows the description of accident transient on a deeper physical level of accuracy, remaining the old ones as user options. Table II presents the comparison between the two modeling approaches.

Table I Main models of the ICARE2 code, used for the analysis of separate effect tests [3], [4].

Module	Modeling approach
Multi-channel thermalhydraulics	1-D gaseous flow: steam - non condensable gas mixture, change of geometry due to relocation
Heat transfer	radiation in participative gas, convection, conduction in radial and axial directions
Chemical interactions UO2/Zr/H_2O	Two levels of modeling can be used: primary ICARE2 models or detailed mechanistic models (see Table II)

Table II. Comparison between two modeling approaches.

Physical phenomena	V2 mod1 version	V2 mod2 (option for SVECHA modules)
Zry oxidation	parabolic correlations for ZrO2 thickness growth and oxygen mass gain	Modeling of chemical interactions in the framework of oxygen diffusion theory, temperature range 1200 \SYMBOL 184 \f "Symbol" 3000 K (module UZRO)
UO2 dissolution by solid Zry	parabolic correlations for intermediate layers thickness growth	
UO2 dissolution by molten Zry	parabolic correlations or convective Kim-Olander model	
U-Zr-O melt oxidation	parabolic correlations, analogous to Zry oxidation	

The module UZRO has been developed in NSI since 1991. The objective of this development was to improve the prediction of experimental results, given by the existing integral codes. A short description of the module implemented into the ICARE2 code is presented below.

The oxygen diffusion theory is the physical basement of the module forms for the chemical interactions $UO_2/Zr/H_2O$ in temperature range 1200 ÷ 3000 K. The main phenomena described by UZRO are the following:

- Oxidation of solid and liquid Zry cladding;
- Dissolution of UO_2 by molten and solid Zry;
- Cladding internal oxidation (double side oxidation);
- "Chemical thinning" (or complete dissolution) of oxide layer in conditions of limited steam supply ("starvation");
- Oxidation of U-Zr-O melts after relocation.

The model takes into account the coupling of Zr/steam (outside) and Zr/UO_2 (inside) interactions, tetragonal-to-cubic transition in zirconia (1773 < T < 2650 K), equilibrium composition of U-Zr-O mixtures. The calculation procedure gives the solution of the oxygen diffusion equations in the multilayered structure (7 and more layers) of different phases formed in the course of the UO_2/Zr/steam interactions. The numerical method of the module allows to reduce partial derivative equations for the real diffusion process to ordinary derivative equations (the method with analogous idea was realised in [6] for description of corrosion couple metal + oxide in Zry cladding). Thus the calculations become more simple, than for more sophisticated and time consuming methods (see, for example [7]) and comparable (in computation time and memory request consumption) with the empirical correlation approach.

Currently the module UZRO is coupled with the module of mechanical behavior (module CROX). The latter uses the information about layers system and performs the analysis of the cladding mechanical state in terms of a multilayer structure (α-Zr, β-Zr, α-Zr + β-Zr, ZrO_2) [8]. The correct description of the α-Zr(O) layer is very important for the mechanical behaviour module as this layer plays the main role in the strengthening of the metallic part of the cladding.

3. ALTERNATIVE DATABASES FOR ZRY OXIDATION.

As a rule in all current severe accident codes the $UO_2/Zr/H_2O$ interactions are represented by the parabolic rate equations developed from laboratory experiments in isothermal conditions and unlimited steam environment. For the UO_2/Zr(solid) interaction the experimental data were obtain in [9]. There have been many measurements of the parabolic rate constants for Zircaloy oxidation for the temperatures 1273 — 1773 K. The results obtained by different groups for the oxide scale growth and oxygen uptake seems to be close to each other in the range of the experimental error. At higher temperatures T > 1773 K there are only two sets of measurements [4] and [10] for which the results differ significantly by the order ~ 100 %. At extremely high temperatures T > 2100 K the data source reported in [4] remains the only one. Fig. 1 summaries the above statements and presents the parabolic rate constants for averaged oxide scale growth $K_{ox} = L_{ox} / \sqrt{t}$. For comparison at lowei temperatures the data obtained in [5] for isothermal regimes are given along with Prater et al [4] and Urbanic et al [10].

For application of diffusion-theory analyses the equilibrium oxygen concentrations and diffusion coefficients for all phases are needed.

The assessed binary diagram Zr-O of Abriata et al [10] specifies the available upper and lower limits of oxygen phase concentrations and is shown on Fig. 2. The researches in equilibrium Zr-O diagrams resulted in prediction of the following phase sequences during Zr-O oxidation:

- T < Tct: 3 layers - β-Zr, α-Zr(O) and ZrO_2(tet)
- Tct < T < Te: 4 layers - β-Zr, α-Zr(O), ZrO_2(cub) and ZrO_2(tet)
- Te < T < Tcub: 3 layers - Zr-O melt, ZrO_2(cub) and ZrO_2(tet)
- Tcub < T < Tmelt: 2 layers - Zr-O melt and ZrO_2(cub)

The kinetic consequences of additional, more complicated layers sequences are not well pronounced and detected in corrosion experiments.

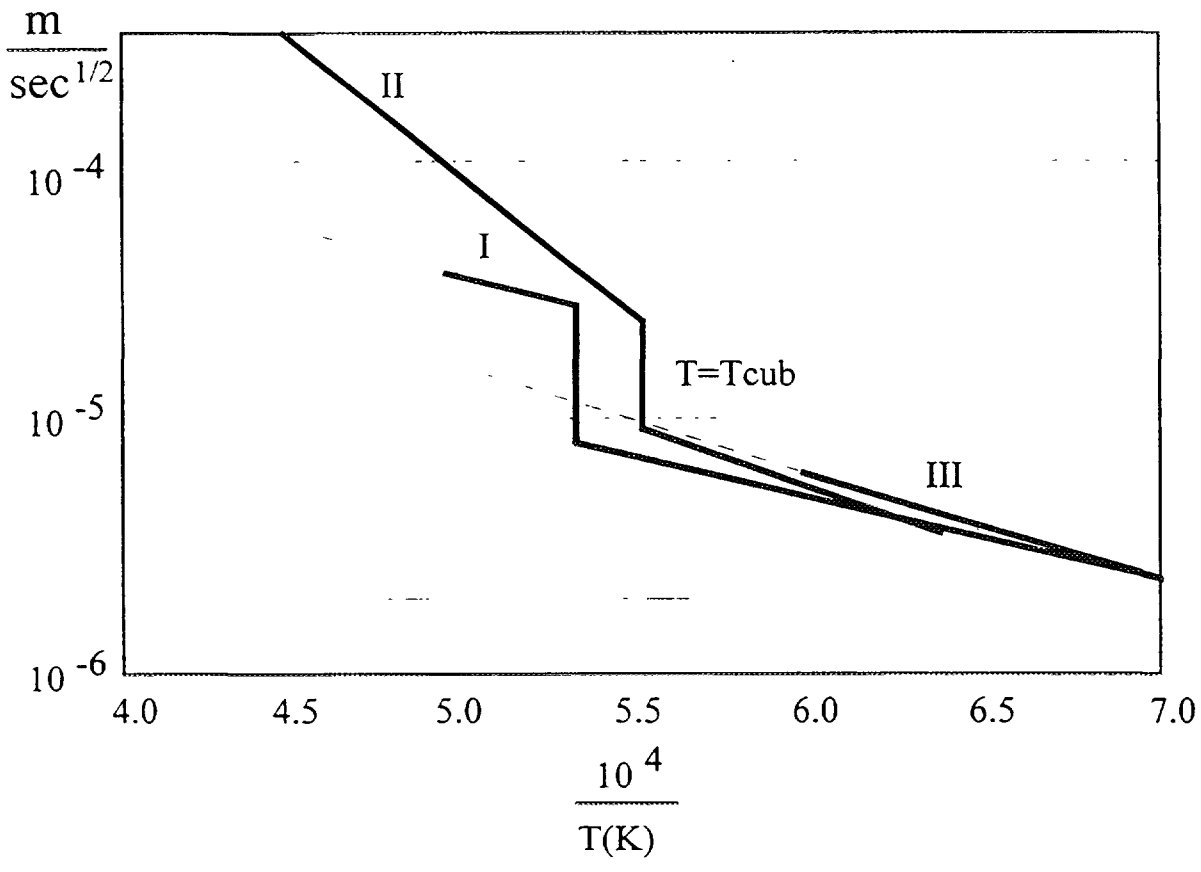

Fig.1. Alternative correlations in parabolic scaling for oxide scale growth: I — Urbanic - Heidrick [8], II — Prater - Courtright [3] ,.III — Hofmann [4].

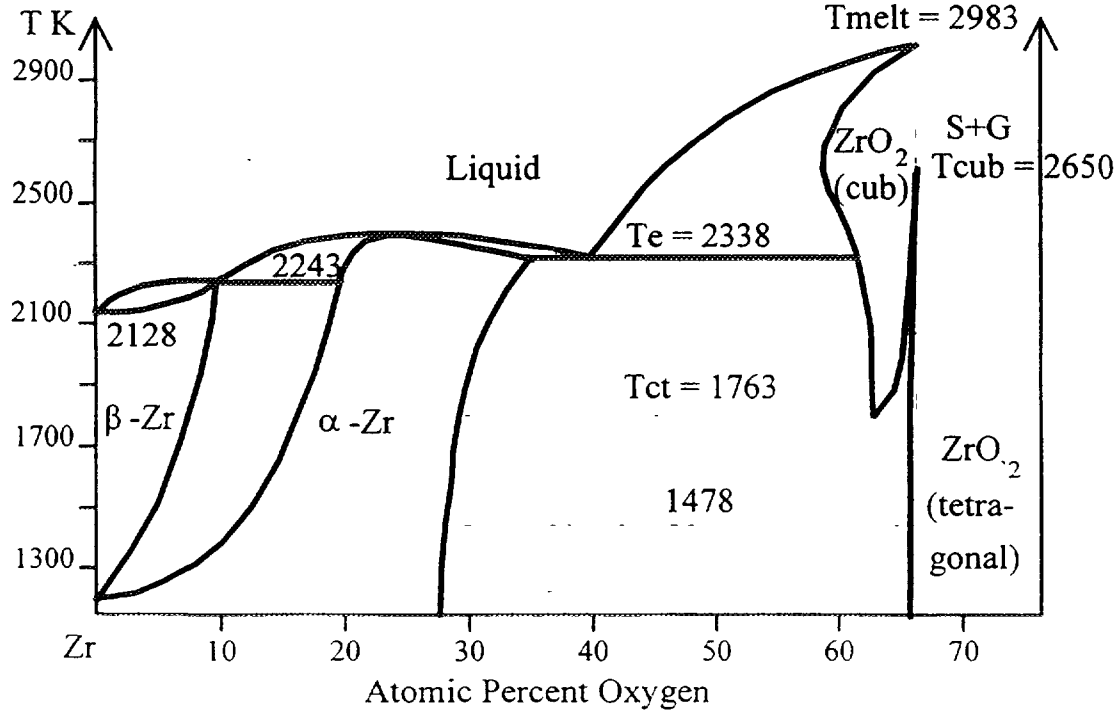

Fig.2. Oxygen boundary concentrations according to binary Zr-O phase diagram

Table III. Oxygen diffusion coefficients, D = A·exp(-B/T).

Phase	Notation	A	B
ZrO2(tet.)	Dtet	$3.705 \cdot 10^{-7}$	19773
ZrO2(cub.)	Dcub	$8.72 \cdot 10^{-4}$	24141
Zr-O melt	Dmelt	0.595	41221

The diffusion coefficients of β-Zr and α-Zr(O) are reported in literature [12]. There are no direct measurements of diffusion coefficients in tetragonal and cubic phases of zirconia and molten Zry. These quantities can be obtained from the exact solution to the diffusion equations for isothermal oxidation in infinite media with parabolic rate constants growth for α-Zr(O) and ZrO_2 layers known from the experiment . This relationship has been derived (among others) by Pawel [13] (considering both the α and β phases of Zr) and Olander [14] (in which the entire metal phase is treated as α-Zr and duplex oxide at temperatures higher than Tct as single homogenized oxide layer).

Our analysis involves all possible layer structures listed above. For the first version of UZRO [3] the data reported by Urbanic et al [10] were used to obtain the diffusion coefficients in tetragonal and cubic phases of zirconia. The current version is based on the experimental set of Prater et al [4]. The oxygen diffusivity in molten Zry was calculated taking into account the kinetics of dissolution of ZrO_2 by molten Zry reported in [15]. The diffusion coefficients which depends only on temperature and which are used in current version are listed in Table III.

4. TRANSIENT EXPERIMENTS.

The out-of-pile experiments [5] were performed in an (Ar + 25 %O_2) gas mixture in high temperature/high pressure apparatus. The tests were made using short cladding tube specimens with stoichiometric high-density UO_2 pellets and Zry cladding with an outside diameter 10.75 mm and a wall thickness of 0.72 mm. The specimen located in a high-pressure vessel was inductively heated. The external overpressure was about 40 bar in most of the experiments to obtain close contact between the pellet and the cladding.

Transient temperature experiments were performed to find out the conditions when an uncontrolled temperature escalation takes place during heat up. The temperature history of the specimen is shown on the Fig. 3. The heat-up and cool-down rates ±dT/dt were equal 0.25, 1, 5, 10 K/s. The maximum temperature Tmax varied between 1273 and 2273 K. The holding time at maximum temperatures was 10 s. At temperatures above the melting point of Zircaloy (~ 2040 K) a part of cladding melted. However, due to the oxide shell, which formed on the cladding surface, the molten material remained in place.

Due to oxygen uptake by the Zry cladding from the reaction with gaseous oxygen and from the reaction with UO_2 various intermediate oxygen-stabilised phases were formed and their thicknesses were determined metallographically. The sequence of phases (layers) inside cladding at all temperatures for isothermal (T < 1673 K) and transient experiments was the following (from inside to outside)

$$UO_2 \rightarrow [\alpha\text{-Zr(O)} + (U,Zr)] \rightarrow (U,Zr)\text{alloy} \rightarrow \alpha\text{-Zr(O)} \rightarrow \beta\text{-Zr} \rightarrow \alpha\text{-Zr(O)} \rightarrow ZrO_2$$

The intermediate α-Zr(O) +(U,Zr), (U,Zr)alloy and first α-Zr(O) layers were formed due to the UO_2/Zr interaction, the outer layers of α-Zr(O) and ZrO_2 — due to oxidation. With increasing time the β-phase of the cladding disappears due to oxygen uptake and transformation into α-Zr(O). Since the cladding thickness is small the external and internal oxygen uptake influence each other and an accelerated reaction-layer growth was observed at longer reaction times.

5. CODE-TO DATA AND CODE-TO-CODE COMPARISONS.

5.1 Isothermal experiments.

The first calculations performed by the ICARE2 code UZRO module were made to determine the oxidation kinetics of isothermal regimes at high temperatures. Fig. 4 and 5 presents the comparison between calculated and measured parabolic rate constants for the oxidation process. The rate constants Kox for the thicknesses of zirconia (duplex oxide scale at high temperatures T > 1773 K) and K_α for α-Zr(o) are plotted versus inverse temperature.

The parabolic constant Kox increases upon reaching the temperature of tetragonal-to-cubic transition Tct = 1763 K. The increase appears due to higher oxygen diffusivity and wider range of O/Zr ratio in cubic oxide in comparison with the tetragonal one. The simple parabolic scaling proposed in [4] involves discontinuous change of Kox. The diffusion model predicts smooth increase due to the continuous growth of cubic oxide O/Zr ratio range and differs from the predictions of simple approach in temperature range 1773 – 1900K. It should be noted that separate measurements of Kox at these temperatures made in [4] and [10] are close to the predictions of diffusion theory in the range of experimental error.

At higher temperatures T > 1900 K the current UZRO module gives the same results for isothermal regimes in infinite media as parabolic correlations [4] and is close to experimental measurements. Small decrease in Kox (7 %) upon reaching the melting point of the metallic part of the cladding (T = 2273 K) is due to the simplified modeling assumptions for this phenomena and does not lead to the discrepancy with the experiment.

Concerning the predictions of the diffusion model for the α-Zr(O) layer one may see a good agreement with the experiment taking into account that Kα(T) is a smooth function of temperature as Kox(T) due to the reasons mentioned above.

5.2 Transient experiments.

Calculations with the ICARE2 code modules ZROX + UZRS (options URBANIC and PRATER) and UZRO were performed for temperature transients [5] at all heat-up rates and all maximum temperatures. Figs. 6, 7 and 8 presents the calculation results for the evolution of cladding layers at heat-up rate dT/dt = 1 K/s and maximum temperature Tmax = 1873 K. On these figures the positions of different layers in the radial direction (mm) are plotted versus time. External overpressure was not introduced in simulations, only the pellet-cladding gap was eliminated to provide good contact between both components of fuel rod. The gap, seen on the Figs 6-8, appears in such conditions at cool-down stage due to the change of the cladding mechanical state. This phenomenon does not influence the final composition of the cladding as internal UO2/Zr/H_2O interactions at the instant of gap appearance become negligible.

The good agreement with the experiment exists for both modeling approahes for the UO2/Zr (solid) interaction. This modeling does not include the description of such details of the interaction as instability of the (U,Zr)alloy layer and formation of liquid globules [5]. But the extent of the UO_2 pellet thinning and the thicknesses of the interaction zone α-Zr(O) +(U,Zr), (U,Zr)alloy and first α-Zr(O) are correctly predicted. The process of UO_2/Zr interaction stopped with the disappearance of β-Zr that is adequately described by both models.

The main difference in the code-to-data comparisons appears in the modeling of the oxide scale. The Urbanic-Heidrick's correlation underpredicts the oxide scale by the order of 100%. The underprediction of the Prater-Courtright correlation is much lower and results of the diffusion model are the closest ones. Note that at the end of the transient the primary β-Zr is totally consumed and transformed into α-Zr(O).

To give the quantitative assessment of the difference between all three models, calculated over measured zirconia thicknesses after transients are plotted against maximum temperatures at different heat-up rates on Figs. 9-11. At temperatures higher than 1773 K the underprediction of

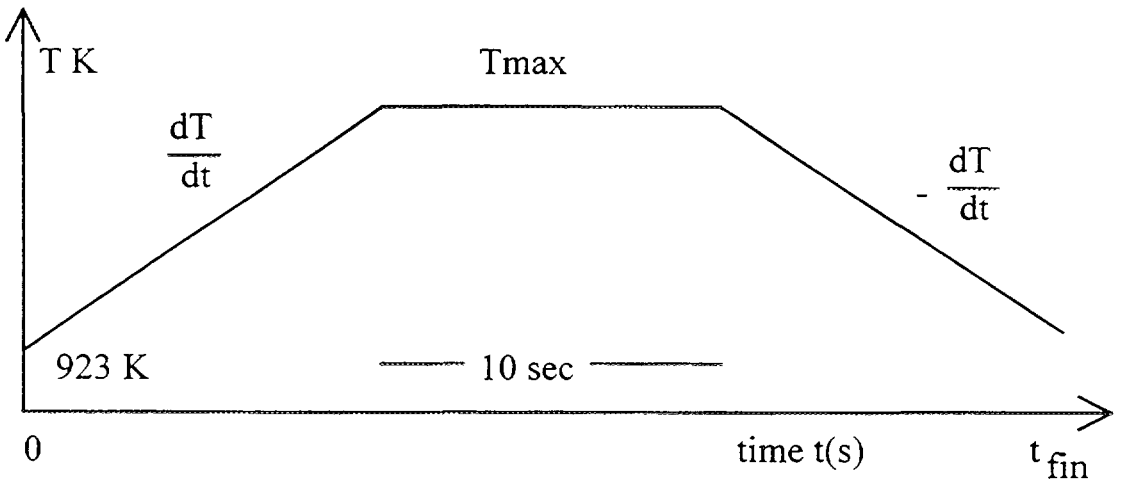

Fig. 3. Transient experiments [3], temperature history.

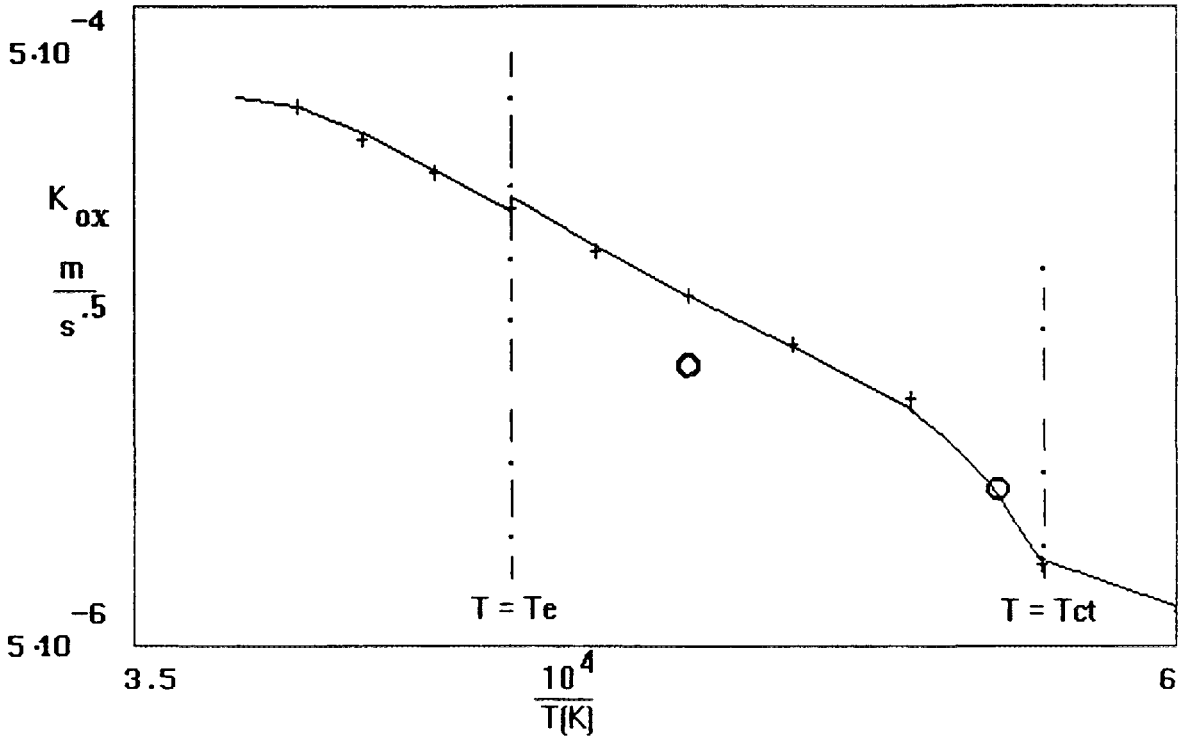

Fig. 4. Parabolic constants ($K_{ox} = L_{ox} / \sqrt{t}$) for oxide at high temperatures. + — Prater-Courtright. o - Urbanic, solid line — analytical calculations.

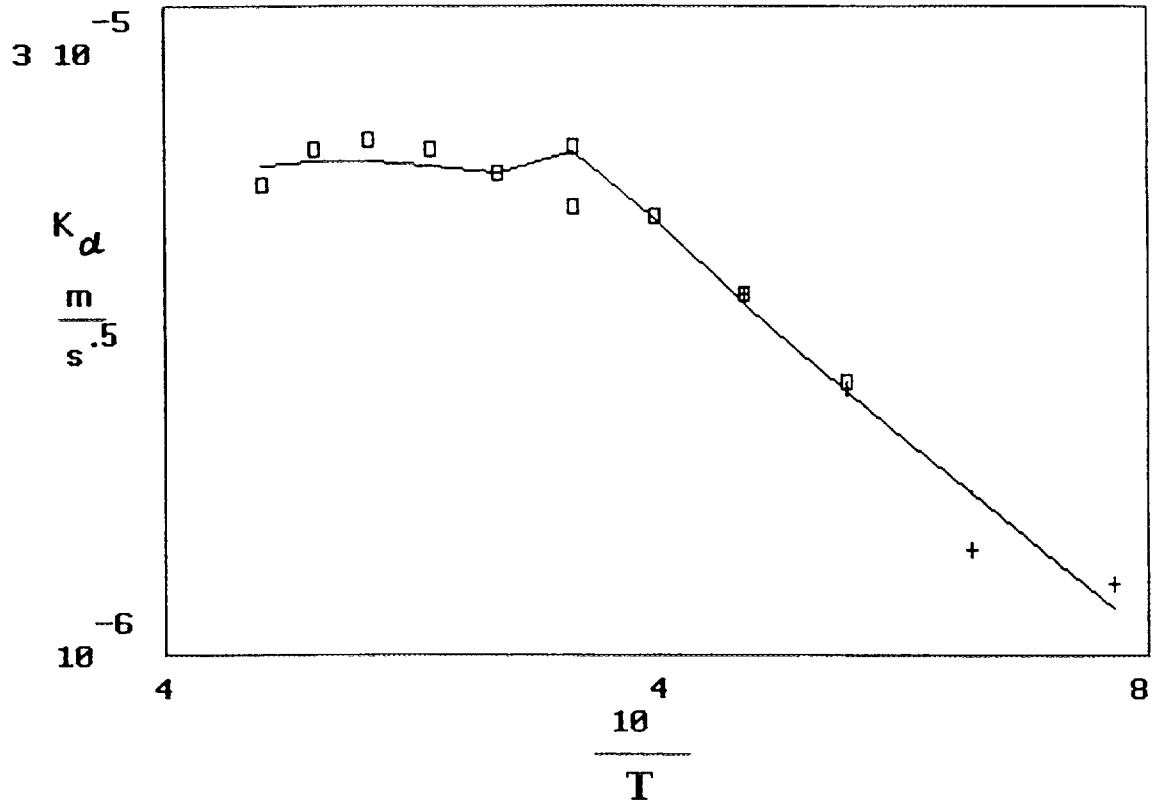

Fig 5 Parabolic constants ($K_\alpha = L_\alpha / \sqrt{t}$) for α - Zr(O) at high temperatures, (+) — Hofmann, □ — Prater, solid line — analytical calculations

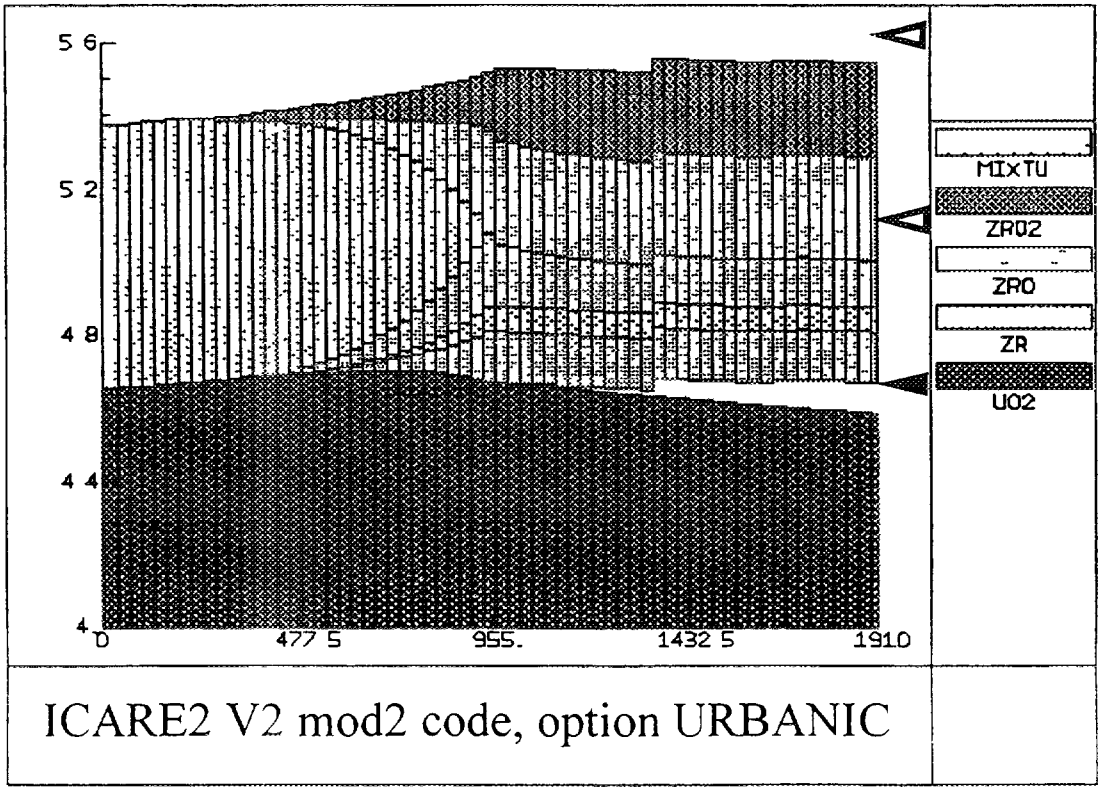

Fig 6 Calculated layers evolution for the transient dT/dt = 1 K/s, Tmax = 1873 K, option URBANIC, ◀ — internal cladding surface (in experiment UO_2/Zr interface), ◁ — position of zirconia layer in experiment

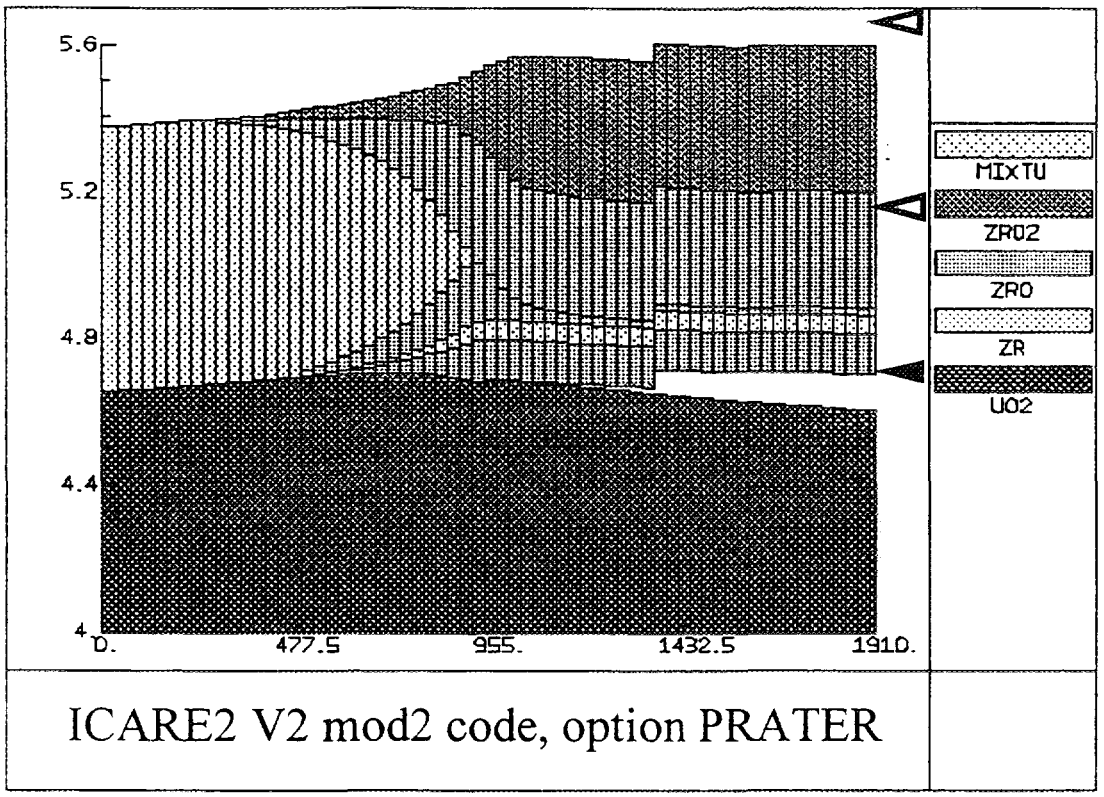

Fig. 7. Calculated layers evolution for the transient dT/dt = 1 K/s, Tmax = 1873 K, option PRATER.

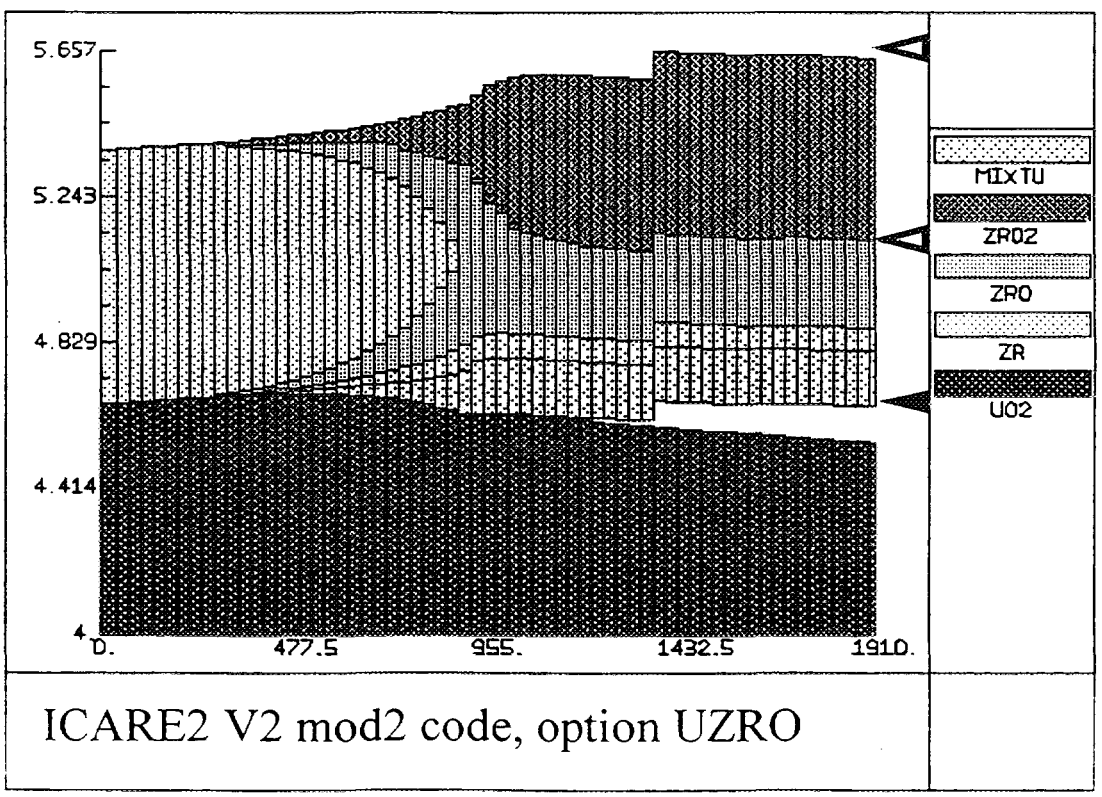

Fig. 8. Calculated layers evolution for the transient dT/dt = 1 K/s, Tmax = 1873 K, option UZRO.

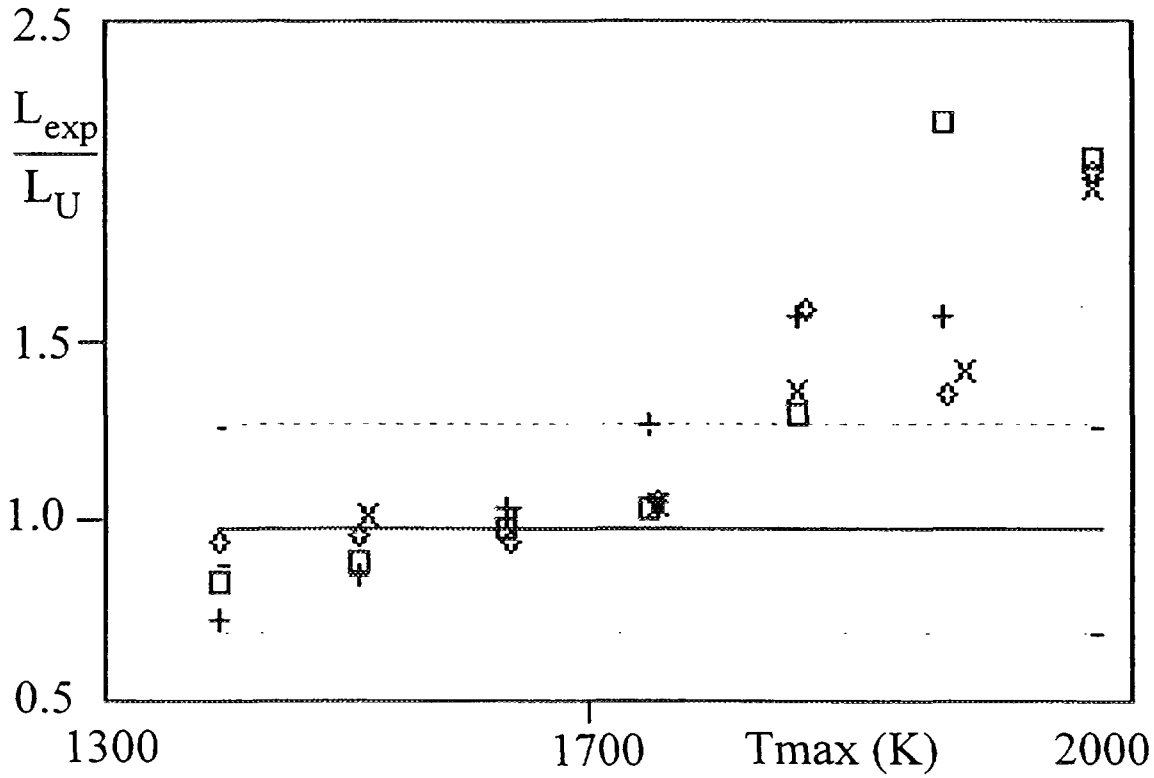

Fig. 9. Calculated over measured zirconia thickness after transients: L_{exp}, L_U — measured and calculated (option URBANIC) thicknesses of oxide layer after transient. + — dT/dt = 0.25 K/s, □ — dT/dt = 1 K/s, ◊ — dT/dt = 5 K/s, × — dT/dt = 10 K/s.

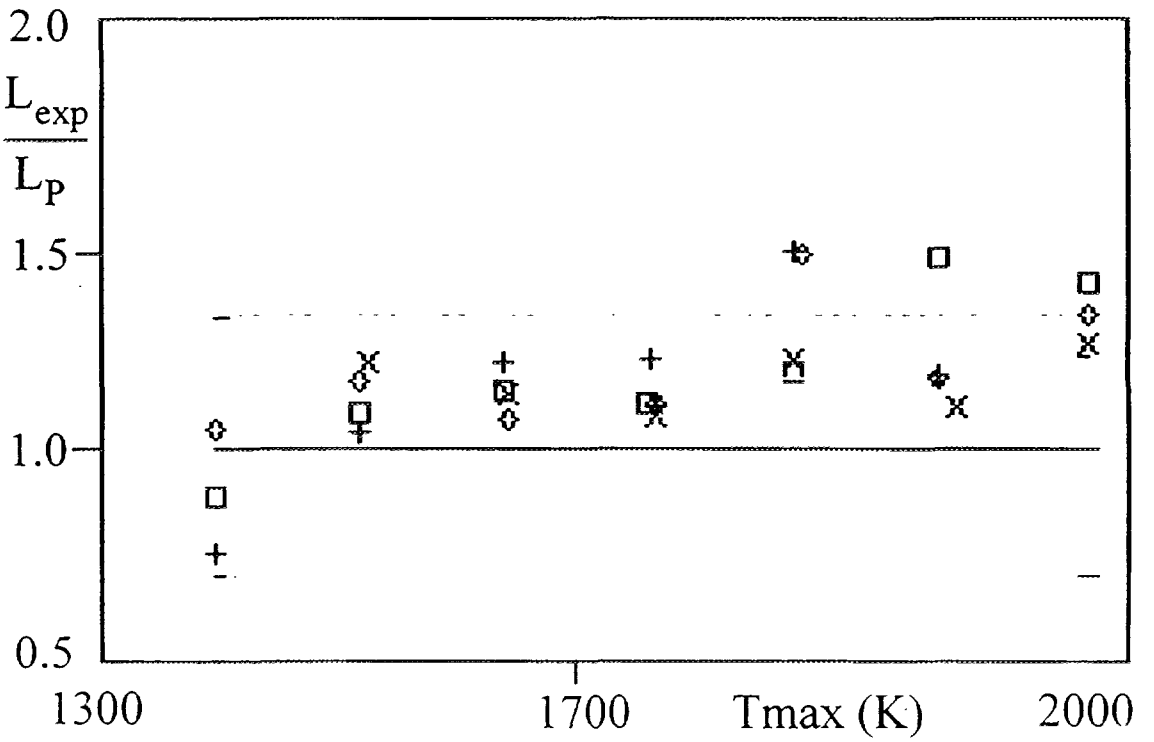

Fig. 10. Calculated over measured zirconia thickness after transients: L_{exp}, Lp — measured and calculated (option PRATER), thicknesses of oxide layer after transient.

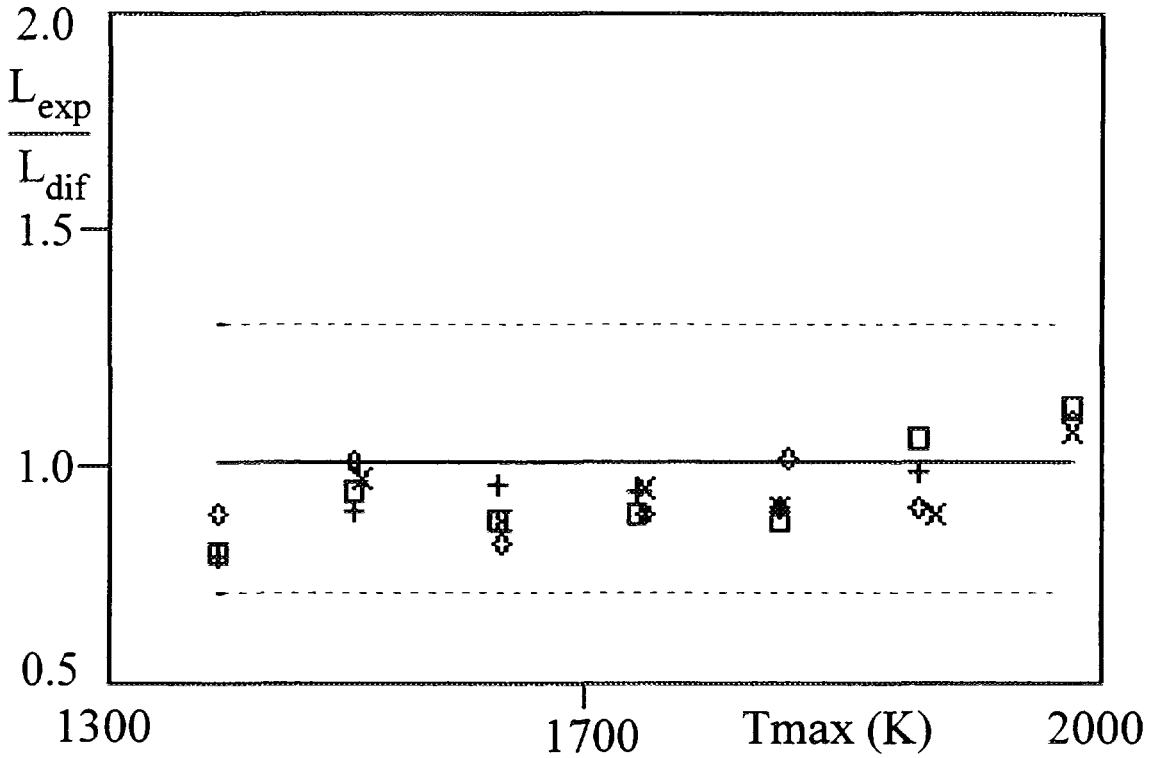

Fig. 11. Calculated over measured zirconia thickness after transients: L_{exp}, L_{dif} — measured and calculated (option UZRO) thicknesses of oxide layer after transient, + — dT/dt = 0.25 K/s, □ — dT/dt = 1 K/s, ◊ — dT/dt = 5 K/s, × — dT/dt = 10 K/s.

Urbanic-Heidrick's correlation is about 50-100% (Fig. 9), the difference between Prater-Courtright correlation and the experiment is about 20-50% (Fig. 10), depending on heat-up rates, the predictions of oxygen diffusion theory are in the range of the experimental error (Fig. 11). As the main difference between the results obtained using Prater-Courtright's correlation and diffusion model corresponds to heat-up rates 0.25 and 1.0 K/s for which the β phase disappears during the transients. The subsequent acceleration of oxide scale growth due to effects of finite cladding geometry is about 25 - 40%.

At the late stage of cladding oxidation the metallic part of the cladding consists of α-Zr(O). Therefore the oxygen mass gain rate Kt for the cladding is changed along with the oxide thickness growth Kox in comparison with the primary layer configuration. The relationship between these parabolic constants provides the formula [13,14], which is valid for all periods of oxidation process:

$$Kt \cdot Kox = 0.5\ Dox\ \Delta C, \quad (1)$$

where Dox - diffusion coefficient, ΔC - upper and lower oxygen concentrations in oxide scale.

The above formula (1) predicts the decrease of oxygen mass gain for α-Zr(O) oxidation, this decrease being of the order of 25 - 40% from the current assessment.

6. CONCLUSIONS.

Current assessment allows the following conclusions about the different models of the ICARE2 code for the physical processes during pellet/cladding/steam interactions.

I. Interaction UO_2/Zr (solid).

1. Calculated and measured parameters are in satisfactory agreement.
2. Parabolic scaling and diffusion theory predictions are close to each other for any instant of interaction.

II. Oxidation of the Zry cladding.

1. The predicted extent of the cladding oxidation during transients substantially depends on the modeling approach.
2. Among the parabolic scaling models the best agreement with the transient experimental data is obtained with the model based on Prater-Courtright's correlation (underestimation of oxide layer thickness at T > 1800 K ∝50%.)
3. The predictions of oxygen diffusion theory based on first principles are in the range of experimental error for isothermal and transient tests.

III. Coupling of Zr/H2O (outside) and Zr/UO2 (inside) interactions.

1. The process of Zr/UO_2 interaction is ceased with disappearance of β-Zr that is adequately described by both models.
2. The oxide layer growth in finite cladding geometry with disappearance of β-Zr is accelerated by 25 - 40%, the effect being taken into account only by the diffusion theory.

REFERENCES

[1] R. Gonzalez, P. Chatelard, F. Jacq. ICARE2 - A computer program for severe core damage analysis in LWRs. Note technique SEMAR 93 / 33. Cadarache, le 07/05/ 93.

[2] Code Package SVECHA. Modeling of Core Degradation Phenomena at Severe Accidents. Preprint NSI-RAS No NSI-18-94, Moscow, 1994.

[3] A.M. Voltchek, A.E. Kisselev. On the Modeling of the Pellet/Cladding/Steam Interactions in the Framework of the Oxygen Diffusion Theory. Proc. of ARS'94 Int. Topical Meeting on Advanced Reactors Safety, Pittsburgh, PA, April 17-21, pp.583-590.

[4] J.T. Prater, E.L. Courtright, "High-Temperature Oxidation of Zircaloy-4 in Steam and Steam-Hydrogen Environments", NUREG/CR-4476, PNL-5558, U.S. NRC,(1986).

[5] P. Hofmann, H.J. Neitzel, "Experimental and Theoretical Results of Cladding Oxidation under Severe Fuel Damage Conditions", Zirconium in tne Nuclear Industry: 7th Int. Symp., ASTM STP 939, Philadelphia, 1987.

[6] M. Moalem, D.R. Olander, Oxidation of Zircaloy by Steam. J.Nuc.Mat., 182 (1991), .97-109.

[7] P.Hofmann, H.J. Neitzel, E.A. Garcia, Chemical interactions of Zircaloy-4 Tubing with UO2 Fuel at Temperatures Between 900 and 2000 C, KfK-4422, 1988.

[8] N. Yamshchikov, Deformation Behavior of Oxidised Fuel Cladding. Preprint NSI--5--93. Moscow: Nuclear Safety Institute, January 1993.

[9] P. Hofmann and D.K. Kerwin-Peck, UO2/Zircaloy-4 Chemical Interactions and Reaction Kinetics from 1000 to 1700o C under Isothermal Conditions. KfK-3552, Kernforschungszentrum Karlsruhe, (1983).

[10] V.F. Urbanic, T.R. Heidrick, "High-Temperature Oxidation of Zircaloy-2 and Zircaloy-4 by Steam", J.Nuc.Mat., 75 (1978), pp. 251-261.

[11] J .P. Abriata, J. Garces and R. Versaci, "The O-Zr (Oxygen- Zirconium) System", Bull. of Alloy Phase Diag., 7, No 2 (1986), 116.

[12] R.C. Reid and T.K. Sherwood, "The Properties of Gases and Liquids, Their Estimation and Correlation", 2nd Ed, Mcgraw-Hill, New-York (1966).

[13] R. E. Pawel, J. Electrochem. Soc., 126 (1979), 1111.

[14] D. R. Olander, Material-Chemistry and Transport Modeling for Severe Accident Analysis in Light-Water Reactors. I. External cladding oxidation", Univ. California Lawrence Berkeley Lab. Report, June, (1993), private communication.

[15] P. Hofmann et al. Mechanishes und Chemisches Verhalten von Zircaloy-4 Hullrohren und UO2-Brennstoff bei honen Temperaturen, KfK 4100, Kernforschungszentrum Karlsruhe (1987).

PHEBUS FPTO TEST: STATUS OF INTERPRETATION OF THE BUNDLE DEGRADATION USING ICARE2

B. ADROGUER, C. JAMOND, S. BOURDON, G. RÉPETTO
Institut de Protection et de Sûreté Nucléaire
CEA/Cadarache, Saint-Paul-lez-Durance,
France

S. EDERLI
ENEA, Casaccia-Roma, Italy

I. SHEPHERD
European Commission Joint Research Centre,
Ispra, Italy

Abstract

The aim of the international PHEBUS FP Programme is to investigate in an in-pile facility various phenomena governing degradation of fuel as well as release, transportation and deposition of fission products in LWR severe accident conditions. This paper gives a summary on the current analysis of the core degradation aspect of the first FPT0 test using the ICARE2 code. Results show a core degradation far beyond any other test that has been performed in the past. The current interpretation illustrates difficulties to analyse complex phenomena which characterise the late phase of core degradation such as loss of rod-like geometry and large molten pool formation. The overall movement of material during the test is largely understood. Weaknesses in current models to predict severe degradation are identified and new development efforts are launched. Lessons learnt from FPT0 are applied in preparing the next FPT1 test.

1.INTRODUCTION

The investigation of severe accidents in LWRs from the point of view of consequence assessment (Source Term) and the evaluation of possible accident mitigation measures is an important task both for the European Commission's Joint Research Centre (JRC) and for the "Institut de Protection et de Sûreté Nucléaire" (IPSN).

The PHEBUS-FP programme is the centre piece of the current work aimed at studying in an in-pile facility the degradation of fuel rods and the Fission Product (FP) release and behaviour in the reactor circuit and the containment vessel [1]. Emphasis is on chemical effects and the six tests are carefully chosen to cover a range of conditions likely to be found in a severe accident. The first test FPT0 was performed in December 1993.

The specific objective of the FPT0 core aspect was to investigate FP release from trace irradiated PWR fuel under severe accident conditions characterised by significant fuel rod degradation and melting under low pressure and oxidising conditions. Objectives were fulfilled and show a core degradation progression in the late phase far beyond any other integral Severe Fuel Damage (SFD) experiment that has been performed up to now [2] : PBF SFD, PHEBUS SFD, CORA, FLHT, LOFT-FP-2.

This paper describes the current status of the analysis of core degradation aspects using the mechanistic ICARE2 code which is under development by IPSN at Cadarache. This code has been validated up to 2800 K on the early phase of core degradation with tests of different Severe Fuel Damage programmes [2-4] characterized by a limited loss of rod like geometry and cooling atmospheres mainly with steam starvation or pure reducing conditions. ICARE2 is the main tool currently used by JRC-Ispra and IPSN to prepare and analyse PHEBUS FP tests.

2.DESCRIPTION OF THE PHEBUS FACILITY AND OF THE TEST DEVICE

2.1. PHEBUS facility

The PHEBUS FP facility mainly consists of a driver core, a FP circuit and a pressurised water loop :

- the driver core (PWR type fuel rods of 0.8 m fissile length) supplies the test fuel bundle with nuclear power.
- the FP circuit is scaled to represent the core and coolant circuit of a light water reactor. The main components are several gas injection lines (steam, hydrogen, helium or nitrogen), a test bundle device and the FP circuit with a U tube (steam generator simulator) and a containment tank.
- the pressurised water loop is used as a cooling circuit of the bundle during the irradiation phase (2.5 MPa, 333K) and of the Inconel pressure tube during the degradation phase (2.5 MPa, 438K).

2.2. Test device and experimental bundle

The test device located in a cell on the vertical axis and mid-zone of the reactor (Fig 1) consists in a bundle of 20 fresh fuel rods (10.5 kg of UO_2) 1 meter long with zircaloy claddings and a central absorber rod (80% Silver-15% Indium-5% Cadmium) with stainless steel cladding housed in a zircaloy guide tube.

The in-pile device involves from the bottom to the top : the inlet valve (allowing to shift from irradiation phase to degradation and FP release condition), the bundle and the vertical line (beginning of FP circuit). All elevations in this paper are referenced to the bottom of the fissile length in the bundle (Fig.1).

The 21 rods (20 fuel rods and one absorber rod), are maintained by two spacer grids (Zircaloy type with inconel springs), 43 mm high located on either side of the mid plane and four zircaloy stiffeners. A radial cross section is given in Fig 2. The bundle is surrounded by two stabilised zirconia cylinders and a pressure tube of inconel (6 mm) coated on its internal face by a spray of dense zirconia (1 mm).These three structures are separated by two gaps in cold conditions.

2.3. Instrumentation and test parameter monitoring

The total power generated in the fuel assembly is deduced from the core power measurement and the coupling factor between the driver core and the test bundle.

Different kinds of thermocouples (TCs) at several radial and axial locations allowed temperatures measurements of fuel centrelines, guide tube, stiffeners, outlet fluid (with W/Re TCs), inlet fluid and thermal shroud (with K type TCs). These TCs were developed for the previous PHEBUS SFD programme. The fuel thermocouples measured temperatures up to 2700 K. After their failure, the heat up was controlled by shroud K type TCs.

An On Line optical Aerosol density Monitor (OLAM) is incorporated at the horizontal part of the experimental FP circuit. This instrument measures the attenuation of light across two path lengths during the bundle FP release phase. Its has been adapted by EG & G, Idaho Falls, from a similar instrument used in PBF SFD 1-4 test. For this first test this OLAM gave only qualitative information on aerosols production.

3.FPT0 CONDITIONS

3.1. Irradiation phase.

In order to provide fission products, the bundle was irradiated during 213 h (from November 21th to November 30th 1993 in the PHEBUS reactor) at powers ranging from 230 to

250 Kw (average linear power around 120 W/cm). During this phase, the fuel rods reached a maximum temperature of ~ 1000 K.

After shutdown and before the experimental phase, a transition phase of 36 hours was necessary for preparation of the circuits : closing the inlet foot valve, drying of the bundle, pre-heating of the FP circuits.

3.2. Experimental phase.

The transient was performed in four parts (Fig 3):

- the 1st part (0 - 10000 s) was a thermal calibration phase to check the thermal response of the bundle. Comparison with the pre-test calculation was performed in order to adjust the power increase.
- the 2nd part (10000 - 13700 s) named the oxidation phase, was monitored by linear increases of the power and large increase of the mass flow rate (from 0.5 to 3 g/s).
- the 3rd part (13700 - 18138 s) was the heat up phase during which the liquefaction and relocation of fuel was reached. This phase was performed by reducing the steam flow rate (most of the material had oxidized so there was no need to maintain a high flow rate in order to avoid local steam starvation) and increasing the nuclear power. During the last 70 seconds of this period, several events, in particular a number of temperature responses of external shroud TCs, led to the shutdown of the reactor at t=18138 seconds. The maximum bundle power reached was about 50kW.
- the 4th part (duration : 40mn) was the cooling phase. The steam flow rate was maintained to transport the FPs and aerosols to the outlet circuit.

4.MEASURED BUNDLE DEGRADATION BEHAVIOUR AND FINAL VIEW

An analysis of the measurements, especially, but not only, from the measurements of aerosol density downstream of the bundle on a pipe diameter using the OLAM (Fig. 4) indicated a number of events. Combined with an analysis of calculational results, these events were identified as :

Event 1 : Clad failure of pressurised rods during the calibration phase at ~ 1050 K

Event 2 : Control rod failure around 1500 K followed by an increase of aerosol and Indium release (gamma spectrometers in the FP line) when melting of steel is reached (~ 1700 K). This event was not clearly indicated by OLAM signals.

Event 3 : Clad oxidation escalation at ~ 12000 s, Zr melting, large aerosol production

Event 4 : Relocation of fuel rod materials to lower elevations after 14500 s

Event 5 : Large aerosol production at 15200 s probably due to a sudden peak of mass flow rate after a large flow area blockage due to the formation of a molten pool

Event 6 : Final fuel motion just before the reactor shut down.

The destructive and the non-destructive examinations of the bundle are described in an other paper of the conference [5]. The gamma-scanning results are shown in the Figure 5. The Cobalt-60 coming from the activation of the Inconel tube shows the irradiation axial flux profile. The axial distribution of the Zr-95 (fuel material indicator) and the Ag 110 m (activation of control rod silver) show material relocations by comparison with Co 60. In particular control rod material is mainly accumulated under 0.15 m.

The radiography (Fig. 6) and the 52 transmission tomographies gave respectively a general picture and very detailed information about the final state of the degraded bundle.

1 - lower 0 - 0.15 m zone : almost intact bundle with some relocated materials
2 - just under the lower spacer grid over 0.10 m length, an ingot of frozen materials
3 - over 0.15 m above the lower grid, only a peripheral crust is remaining on the shroud
4 - over 0.35 m under the upper grid, a central cavity surrounded by remaining damaged external rods
5 - above the upper grid over 0.25 m length, rods with significant UO_2 dissolution and quite complete inner rod disappearance near the spacer grid.

In summary FPT0 reached a more advanced state of bundle degradation than any previous SFD experiments. Indeed, about 50 % of the fuel relocated either in solid or molten states creating a molten pool near the lower grid and an upper cavity laying above.

As a consequence of the very large degradation of the bundle, a large fraction of the volatile fission product is (more than 50 %) were released and carried out to the containment.

The kinetics of the FP release is currently under evaluation. However it was clearly observed a close coupling between main fuel rod degradation events and FP release, in particular a reduction of the release during a molten pool formation. These aspects are not considered in this paper.

An overview of the different aspects of FPT0 is given in [6]. The following sections are mainly devoted to the analysis of the fuel rod degradation aspects.

5.STATUS OF INTERPRETATION

The interpretation effort is currently carried out within the framework of the PHEBUS FP Scientific Analysis Working Group (SAWG). Code degradation results and calculations are shared and discussed between the organisations involved in the PHEBUS FP programme. The main codes used are ICARE2, ATHLET-CD, KESS, SCDAP/RELAP5, MAAP and MELCOR.

In this section the current status of the ICARE2 post-test calculations performed by IPSN and JRC are presented using the V2 Mod1 and V2 Mod2 versions. This code was extensively used to prepare the test [7]. A reference post-test calculation (ICARE2 - V2Mod1) performed with actual boundary conditions and revised material properties is presented. Additional sensitivity studies have been done in particular for identification of the damage progression.

The bundle was modelled with 11 axial meshes, and different components representing inner and outer rods, the Ag-In-Cd control rod with its Zr-guide tube and two spacer-grids. The insulating shroud around the bundle was modelled by two ZrO_2 insulating layers, two annular gaps and an external Inconel tube (Fig. 7).

Previous calculations [8] showed relatively correct calculations of temperatures and H_2 production during the initial calculation phase (0 - 12000 s) and the following clad oxidation period [12000 - 13700 s] characterized by a downward evolution of a strong clad oxidation front. Nevertheless UO_2 dissolution by molten Zr and related relocation were not sufficient to induce during this period or just after the large fuel slumping observed in the test.

A critical review of the experimental database (CORA, PBF SFD) and additional sensitivity studies with ICARE2 enabled the improvement of the input data deck, in particular regarding the user-specified melt relocation conditions. The modelling of Zr upper plugs of rods and the modelling of the shroud gap closure due to the thermal expansion of the two insulating ZrO_2 cylinders were improved. Physical models regarding chemical interaction were unchanged compared to [8]

5.1 Thermal and oxidation behaviour

Calculated and measured temperatures are shown on Fig.8 to 11 at 0.8, 0.7, 0.4 and 0.3 m. These figures show temperatures of the fuel and inside the ZrO_2 shroud at two radial positions : middle and outer surface of the external ZrO_2 insulating layer. The two first calibration plateaux performed before 6000 s are accurately predicted but are not considered in these figures. Comparisons start at the beginning of the 3rd plateau at 6000 s.

Fuel rod temperatures

After calculation of the cladding burst as in the test (event (1) on Fig. 4), the correct prediction of the 3rd plateau shows that global heat losses through the shroud at low temperature

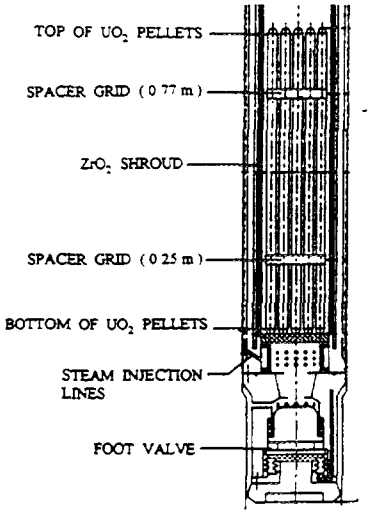

Fig. 1 : Axial cross section of bundle

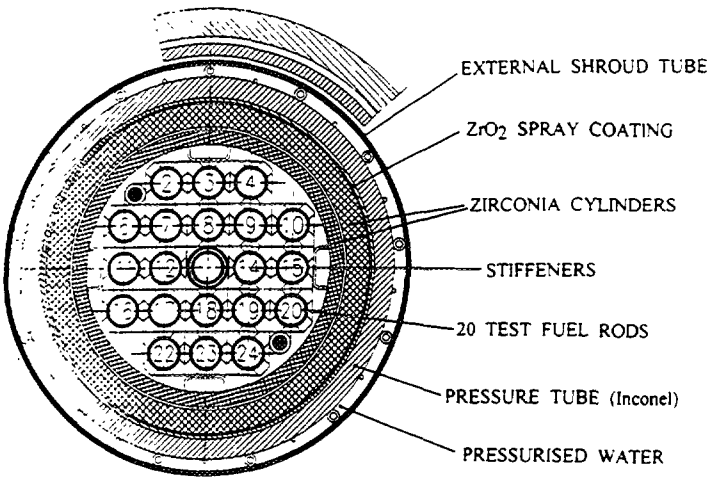

Fig. 2 : Radial cross section

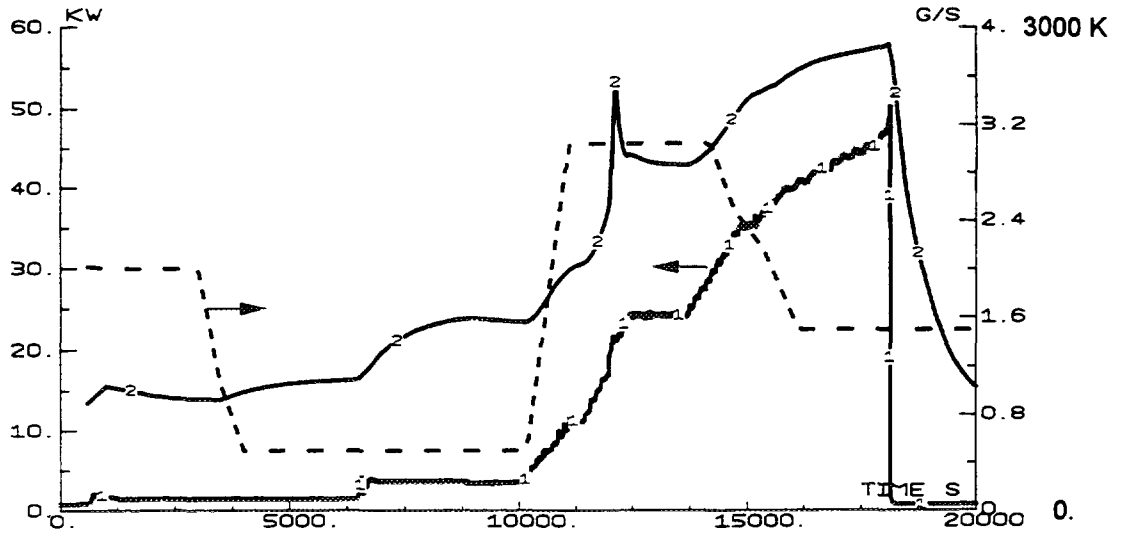

Fig. 3 : Bundle power, mass flow rate scenario and calculated fuel temperature (2) at 0.7 m

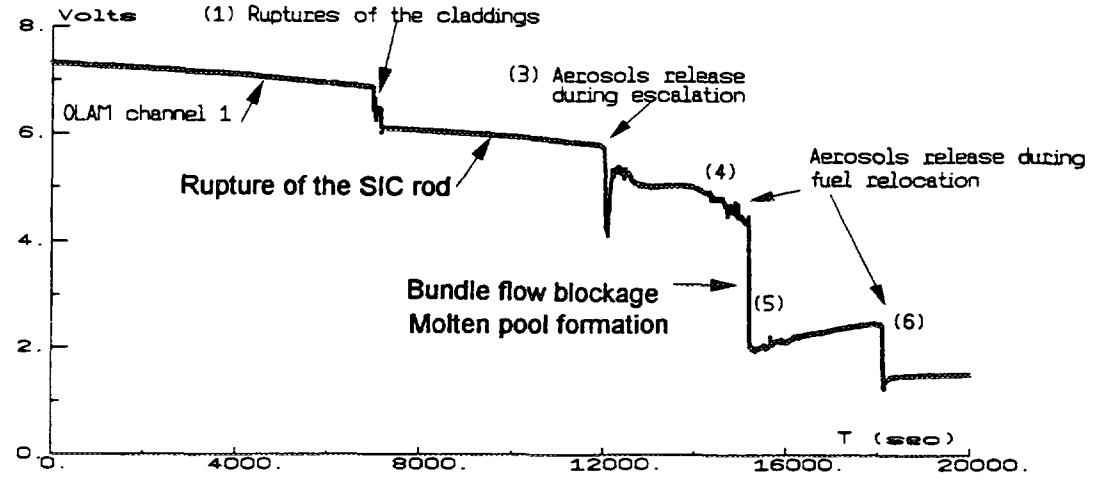

Fig. 4 : OLAM signal through the pipe diameter

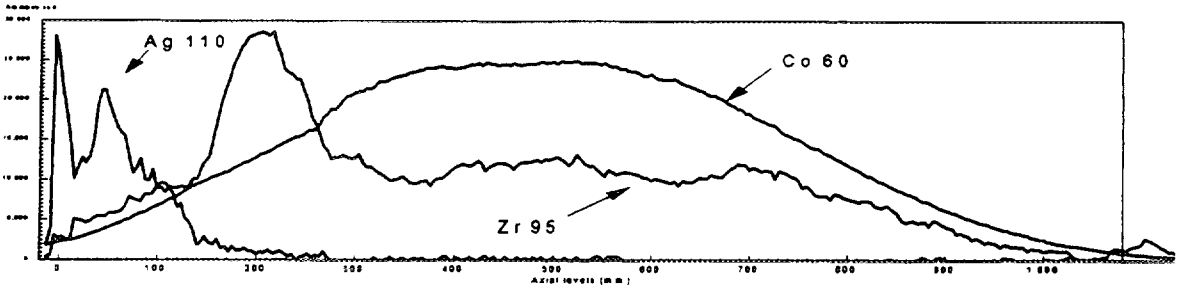

Fig. 5 : Gamma-scanning

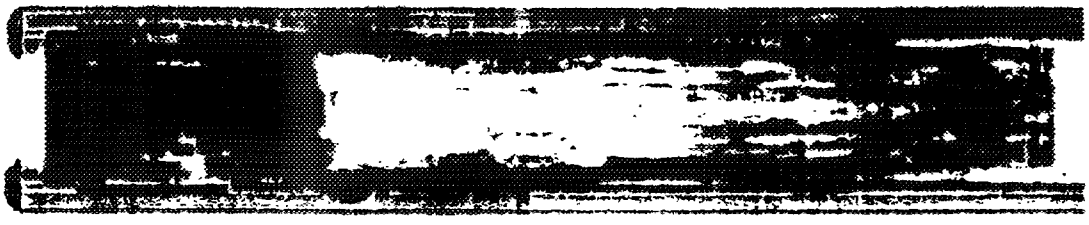

Fig. 6 : Radiography

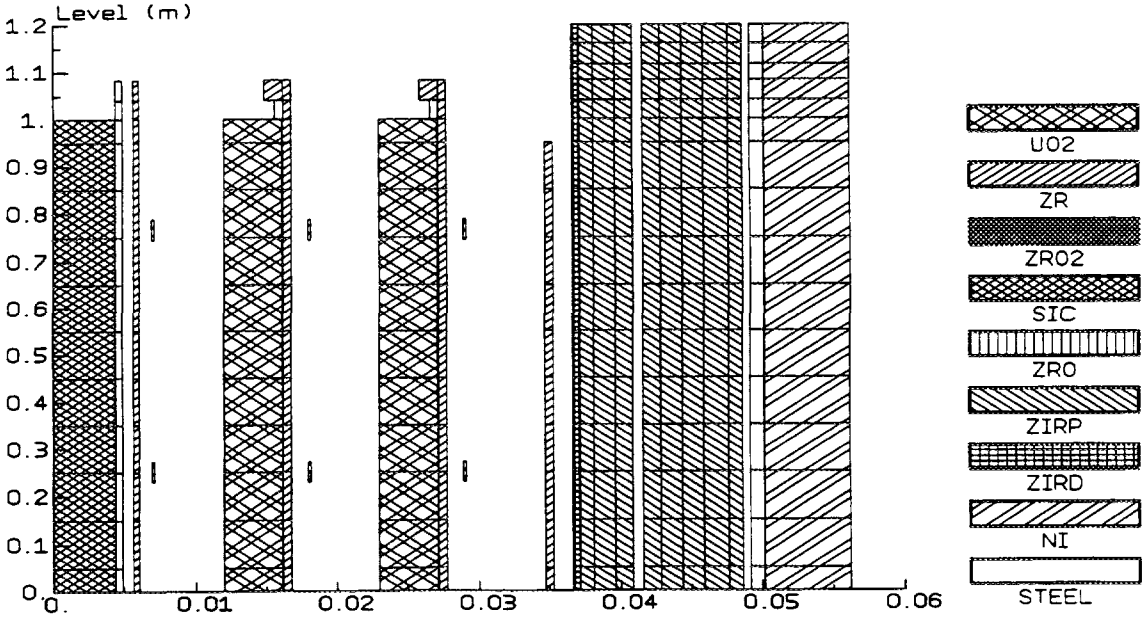

Fig. 7 : ICARE2 model of FPT0 bundle ; Axial meshes and different components ; SIC (Ag-In-Cd) control rod, ZIRD (porous ZrO_2 layers), Ni (Inconel pressure tube)

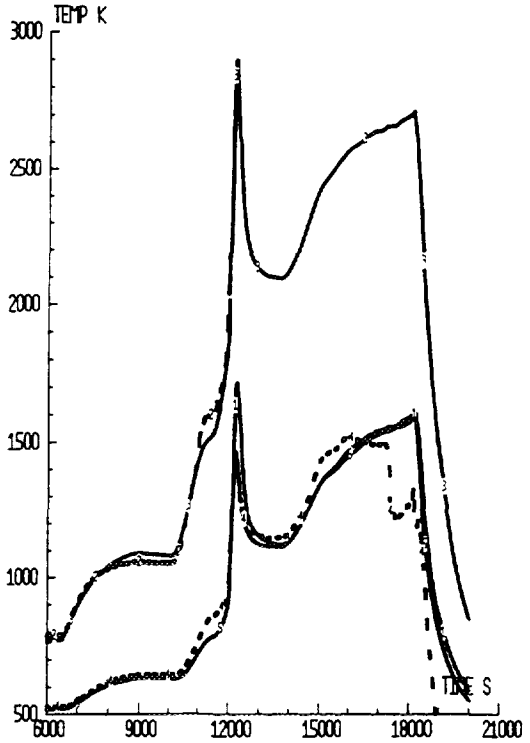

Fig. 8 : Fuel and inner shroud temp., 0.8 m
Measurements : (2) fuel, (4) int. shroud
ICARE2 : (3) fuel, (1) int. shroud

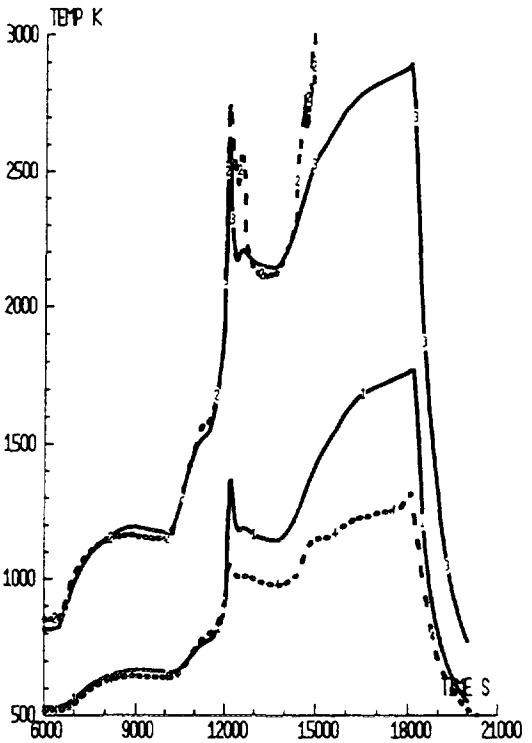

Fig. 9 : Fuel and inner shroud temp., 0.7 m
Measurements : (2) fuel, (4) int. shroud
ICARE2 : (3) fuel, (1) int. shroud

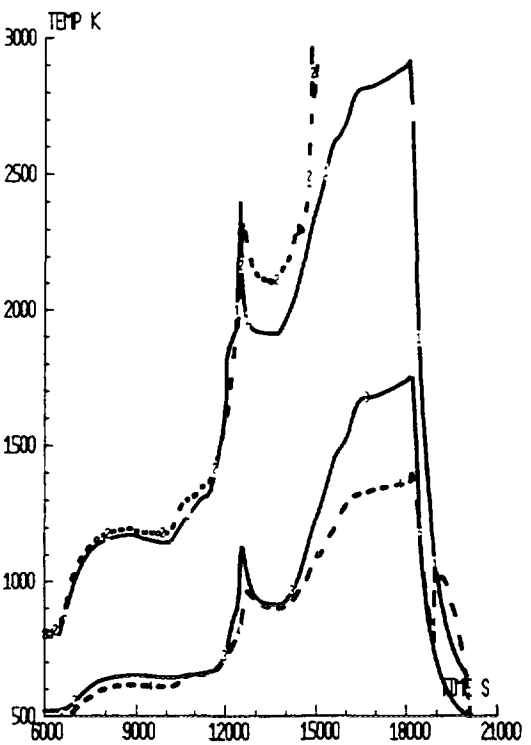

Fig. 10 : Fuel and inner shroud temp., 0.4 m
Measurements : (2) fuel, (4) int. shroud
ICARE2 : (1) fuel, (3) int. shroud

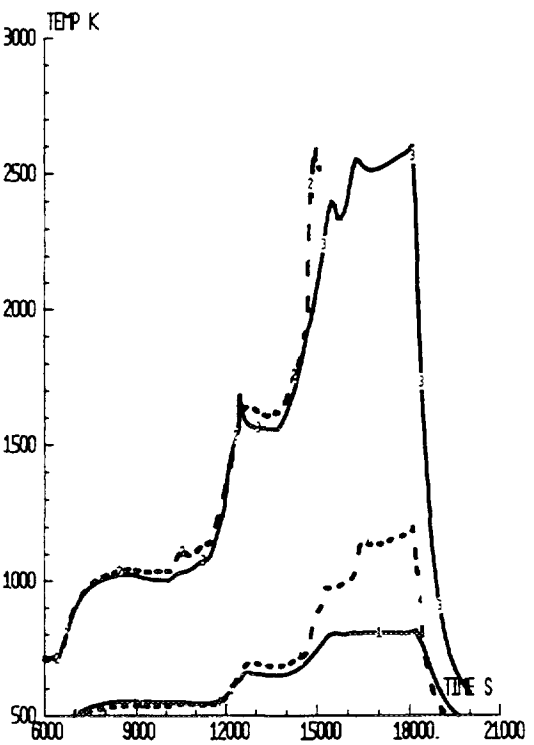

Fig. 11 : Fuel and inner shroud temp., 0.3 m
Measurements : (2) fuel, (4) outer shroud
ICARE2 : (3) fuel, (1) outer shroud

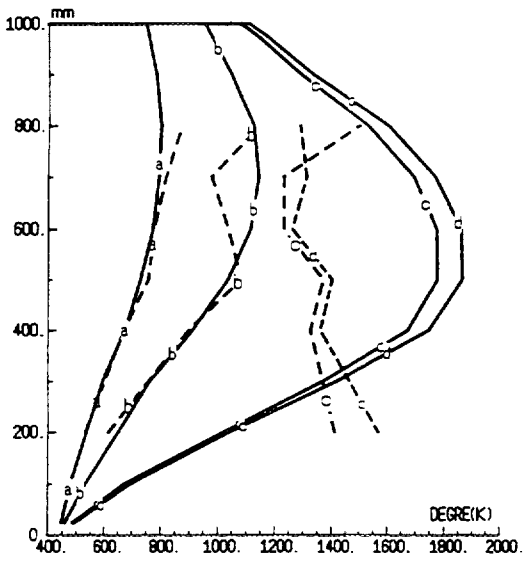

Fig. 12 : Axial shroud temp. profiles at 11700 s (a), 13700 s (b), 16700 s (c), 18100 s (d), Measurements : (dot lines), ICARE2 (solid lines)

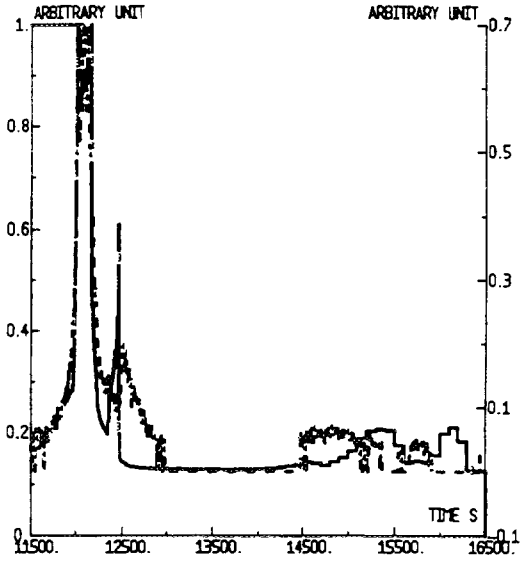

Fig. 13 : H_2 production rate Experiment (estimation) : (4) ICARE2 calculation : (3)

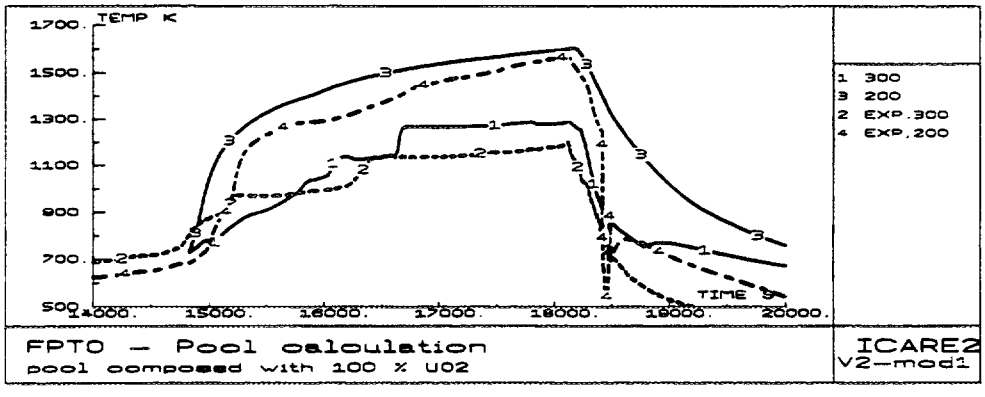

Fig. 14 : ICARE2 calculation with a molten pool ; int. (0.2 m) and ext. (0.3 m) shroud temp. ; Measurements : (4) at 0.2 m, (2) at 0.3 m ; ICARE2 : (3) at 0.2 m, (1) at 0.3 m

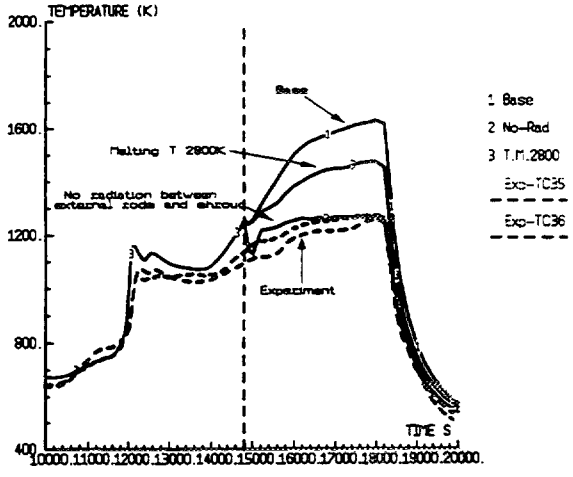

Fig. 15 : Debris bed configuration ; shroud temp. at 0.6 m, ICARE2 (1; 2; 3)

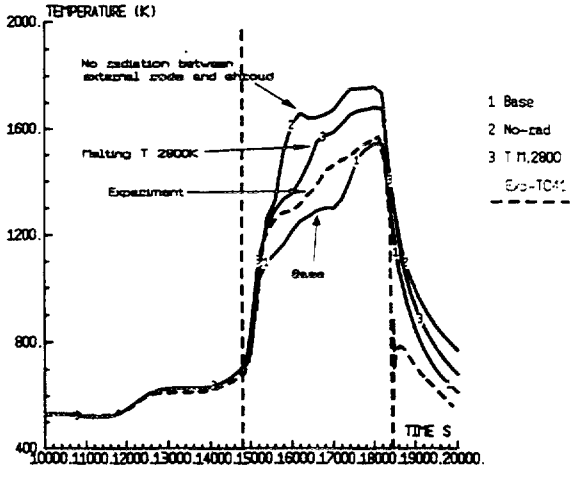

Fig. 16 : Debris bed configuration ; shroud temp. at 0.2 m, ICARE2 (1; 2; 3)

are correctly modelled. Energy balance calculations show that most of the nuclear power is dissipated through the shroud : ~ 80 % from the 3rd plateau up to the final heat-up phase except during the strong clad oxidation escalation period observed in the 0.4 - 1 m zone between 12000 and 12400 s [8]. This strong heating period (~ 10 K/s) of the hot zone (0.8 / 0.7 m) at about 12000 s is correctly calculated, the oxidation power is twice the nuclear power and the melting point of non oxidised Zr is reached before total oxidation. Fuel TCs operated up to 2700 K at 0.7 m. A large release of aerosol was detected by the OLAM (event (3) on Fig. 4) at 12000 s.

The oxidation front and the related temperature escalation are calculated to move down rapidly from the hot zone (0.9 m - 0.7 m) at 12000 s to 0.4 m at 12400 s. Then a slower downward progression of the oxidation escalation front is predicted ; it is located at 0.3 m at 14500 s and 0.2 m at 16000 s. This final progression of the oxidation front is confirmed by the late H_2 production deduced from temperature measurements and heat transfer considerations in the steam generator (see below).

No steam starved condition is calculated during this oxidation period. The calculated temperature evolution is globally consistent with measurements at different elevations. A precise examination of temperature measurements show that the downward progression of the oxidation front is accompanied by local and sudden temperature increase (particularly at 0.4 m) indicative of simultaneous material relocations. This suggests that melt progression could be driven by the oxidation front. This is consistent with the calculation which indicates that during the oxidation escalation, the melting temperature of Zr was reached leading to a simultaneous UO_2 and ZrO_2 dissolution by molten Zr.

These competitive interactions, which are calculated by ICARE2, can be stopped by the mechanical failure of the external clad ZrO_2 layer which trigger relocation of the U-Zr-O melt entrapped inside the cladding. This event was well predicted between the two spacer-grids imposing the same user-specified failure criteria than in the previous calculations [8] ($T > 2600$ K and thickness of $ZrO_2 < 0.25$ mm or $T > 2700$ K). In general the calculations are rather sensitive to these criteria. In earlier calculations for CORA, PBF, PHEBUS-SFD, lower temperature values were used. In FPT0, the temperature criterium was revised to maintain intact the clad for longer in order to favour fuel dissolution and higher peak temperatures. In the revised calculation the amount of melt relocated after the ZrO_2 failure was changed. It is now limited to 60 % instead of 100 % (this partial relocation was clearly observed in CORA tests). Using this option, the peak temperature in the upper zone (0.75, 0.95 m) is increased by 200 K due to the oxidation of the in place molten Zr and local fuel temperatures are raised to 2800/2900 K. At these temperatures, liquefaction of UO_2 - ZrO_2 oxides are possible due to eutectic formation. The maximum temperature which is now 200 K greater than the TC indications is plausible because TCs are known to underestimate temperatures above 2600 K due to the degradation of the electric resistivity of their insulator [9].

Under the upper grid, fuel temperatures are not significantly different from the previous calculation, in spite of the prediction of a progressive U-Zr-O melt relocation to 0.4 m and finally on the lower grid (between 12000 s and 12500 s).

Shroud temperatures

Following the oxidation phase the thermocouples within the bundle become unreliable and the most reliable indicator of behaviour comes from the thermocouples within and outside the shroud.

Between 12000 s and 13700 s, in spite of a tendency to overestimate local temperatures in the 0.6-0.7 m zone the overall temperature behaviour of the shroud is well calculated up to 13700 s. At 0.5 m an azimuthal temperature difference of 150 K was measured in the shroud either due to non uniform outer gap distribution or asymmetries in the flow area blockage near the lower spacer grid.

After 13700 - 14000 s, code-to-data comparisons indicate.

- a correct agreement at 0.8 m (Fig. 8) up to 17300 s when the sudden TC decrease is unclear,

- a progressive overestimation of temperatures between 0.4 and 0.7 from 14800 s to 15200 s. Then, the large overestimation is maintained up to the end of test (Fig. 9 and 10),
- a significant underprediction of temperatures at 0.3 and 0.2 m after 15200 s (Fig. 11).

Sensitivity studies aimed at checking uncertainties on the shroud conductivity and external gap closure could not explain these discrepancies. As discussed later, this is indicative of the large fuel material relocation from the mid-plane to the lower spacer-grid. Because the bundle is heated by the nuclear power generated in the UO_2 this fuel relocation modified the axial power profile. This is illustrated on Figure 12 which shows code-to-data comparisons of the axial temperature profiles in the shroud at different times.

This figure clearly illustrates that the large fuel relocation which occurred after 14800 s is still not calculated as in the previous calculations [8] in spite of recent improvements of the ICARE2 modelling of FPT0. However the calculation suggested that at about 14500 s the temperature of the central zone of the bundle prior to relocation was about 2400 - 2500 K. At this relatively low level of temperature no data from other experiments (CORA, PBF-SFD, PHEBUS-SFD, ...) have indicated a so large fuel liquefaction and relocation. This point is discussed further on.

5.2 Hydrogen production

Calculated and measured total H_2 production indicate the same trend as in the previous calculations ; a rapid production rate corresponding to the early oxidation and a large amount of H_2 generated in between 12000 and 12400 s.

More than 70 % of the Zr inventory had been consumed during this period. The oxidation of the U-Zr-O melt which remains entrapped in the rods after clad failure enabled a slight increase of the early H_2 production and an improved agreement with the H_2 rate derived from heat transfer considerations in the downstream steam generator (Fig. 13).

A detailed ICARE2 analysis of H_2 production indicates that during the early oxidation escalation (12000 - 12400 s), a small amount of Zr was melted before total oxidation. (In the calculation, the resulting UO_2 liquefaction by this molten Zr occurred mainly above the upper grid and to a less extent ($\sim$ 1 %) between the two spacer-grids). The delayed H_2 production observed between 14500 and 16000 s is consistent with the calculated delayed H_2 which results on the clad oxidation at lower levels (under 0.35 m).

ICARE2 calculations have been done using double-sided oxidation in the cladding burst zone (over 0.3 m around the burst). A sensitivity calculation with no internal clad oxidation indicated lower peak temperature during the oxidation period but slightly more UO_2 dissolution in the mid bundle zone. These effects are not sufficient to affect significantly the prediction of the following rod degradation.

5.3 Control rod degradation

Unchanged calculated results have been obtained because no modelling improvements of the control rod model could be done.

- The early failure of the Ag-In-Cd control rod measured by gamma spectrometry (Indium) at 10780 s is not predicted. This failure is probably due to a local clad-guide tube eutectic formation not considered by the code.
- The rod degradation progression is calculated to be driven by the progression of the melting front of the stainless steel cladding. This is consistent with various temperature measurements and with the OLAM signal.
- The possible interaction between Ag-In-Cd material and surrounding cladding is not taken into account in ICARE2. This prevent any calculation of early UO_2 dissolution by the resulting low temperature Zr-Ag melts.

- The grid located just under the rods is not considered in the calculations. In this condition the Ag-In-Cd melts are predicted to be relocated to too low an elevation. Part of these mixtures are relocated in FPT0 at the entrance of the bundle between 0 and 0.15 m (Fig. 5).

5.4 Fuel rod degradation

In spite of recent improvements of the ICARE2 modelling of FPT0, the code fails to calculate the large bundle degradation observed from the post-test tomographies. This large degradation seems to have taken place after 14800 s as inferred in particular from the code-to-data comparisons of the thermal behaviour of the insulating shroud. Main results of the reference calculations are :

(a) UO_2 dissolution and relocation in the upper zone : Above the upper spacer-grid and during the early oxidation period (12000 s - 12400 s), ICARE2 predicts Zr melting, local UO_2 dissolution and U-Zr-O melt relocation on the upper spacer-grid [8]. The amount of Zr assigned to the rod upper plugs has been corrected (reduction of ~ 45 %). After melting, the corresponding Zr-rich melt which is imposed to be relocated on the upper grid is accordingly reduced. The corresponding impact on the local UO_2 dissolution at 0.8 m is significantly reduced (from 25 % to ~ 5 %). This interaction is presently underestimated compared to local fuel dissolution observed on tomographies.

(b) UO_2 dissolution and relocation in the mid-bundle zone : Between the two spacer-grids, the UO_2 dissolution by molten Zr (few %) and relocation are significantly underestimated. In general, sensitivity studies on modelling or experimental uncertainties were unable to change the tendency of the calculation and the rod like geometry was always calculated unchanged at the end of the test. There is one exception, increasing the solubility limit of UO_2 in the melt enable the prediction of a large amount of UO_2 liquefaction. Whatever the prediction of the UO_2 dissolution the code cannot calculate fuel rod slumping and the related transition to a debris bed configuration.

(c) Molten pool formation : There was undoubtedly an event at 15200 s (event (5) on Fig. 4) that cause a large bundle blockage around the lower spacer-grid for a while. This blockage was later cleared by the formation of a chimney through the relocated materials. Different measurements in particular coolant temperatures and OLAM signals gave evidence of this event which was assigned to the formation of a molten pool. Local tomographies confirm also the location of a molten pool above the lower grid during part of the heat up phase of the test.

The flexibility of ICARE2 enabled a user-imposed molten pool located between 0.25 m (lower spacer-grid location) and 0.32 m (to account for the accumulation of the inner ring rods). The pool conductivity is increased to simulate the internal convective transfer at the location and just under the pool. The local nuclear power is re-calculated to account for the neutronic self-shielding effect. The local flow area blockage of the molten pool is supposed to suppress any convective transfer just under the pool at 0.2 m. Demonstration calculations initiated at 14800 s with 50 % and 100 % of UO_2 in the pool enabled to reproduce the shroud temperatures behaviour measured at 0.2 and 0.3 m, in particular the rapid temperature increase observed after 15000 s (Fig. 14). This calculation confirms the hypothesis of a molten pool at the onset of the heat up phase.

(d) Loss of rod geometry : The cause of the partial loss of rod geometry which leads to the molten pool formation is still unclear. Different scenarios are possible [6] [8] in particular :

- Relocation of metal-rich melts (Ag-Zr-Fe mixtures, U-Zr-O melts) in the mid-bundle zone during the initial oxidation escalation followed by repetitive melting-local fuel rod dissolution-relocating-re-heating processes up to a final slumping at 15200 s on the lower spacer grid.

- Formation at about 14800 s of a solid debris bed (zone with a local loss of rod like geometry) in between the two spacer-grids due to the dislocation of inner ring rods. The thermal shock produced by the peak temperature at 12000 s could be a cause of the rod embrittlement. The melting of debris due to degraded heat exchanges produces enough melt which relocate to fill quite totally the flow area above the lower spacer grid at 15200 s.

Demonstration calculations using the recent V2 Mod2 version of ICARE2 were performed using a debris bed model. The debris configuration was imposed at 14800 s with initial temperatures given by a standard bundle calculation (fuel temperature ~ 2450 K). Only the inner rods located between 0.18 and 0.80 m were imposed to be in a debris configuration (external rods remain in place as observed on tomographies). The porosity was supposed unchanged (no compaction during the loss of rod geometry). Inside the debris bed only equivalent conductive transfers (conduction plus radiation) are considered including exchanges between debris and embedded outer rods. Convective and radiative transfers are only considered between the debris bed and the shroud. Radiative transfers are defined between external outer rods and shroud and the free debris surface and shroud. Axial radiative transfers are not considered. Calculations indicate a rapid transition of 200 s between solid debris and a molten pool configuration with an upper cavity laying above [4]. The amount of relocated fuel on the lower grid depends on the geometry considered to define external radiative transfer with the shroud. The fuel liquefaction temperature considered is also a sensitive parameter. The impact of debris bed formation on the thermal response of the shroud is illustrated on Fig. 15 and 16 respectively at 0.6 and 0.2 m. Sensitivities to the UO_2 liquefaction temperature and radiative transfers between external rods and shroud is illustrated. These results indicate that the hypothesis of a debris bed formation in FPT0 cannot be ruled out to explain the rapid and continuous transition between a rod like geometry and a molten pool configuration. Large uncertainties are related to the definition of radiative transfers with the shroud.

(e) Final degradation events : No indication of large movements occurred after the formation of the molten pool until 18068 s. At this time a final fuel motion was observed (event (6) on Fig. 4) characterized in particular by a large release of aerosol and power increase in the driver core. The shutdown was triggered 70 s after the onset of the fuel motion. Two explanations are under study :

- The upper spacer grid failed and induced the relocation of surrounding U-rich mixtures into the molten pool above the lower spacer grid (higher power zone), reheating and crust failure.
- Silver within the molten pool crust vaporised (T ~ 2630 K at 2 bars). The two-phase mixture induces upward pool swelling and corresponding fuel movement to a higher power zone.

The final power increase could have been the cause of the relocation of the molten pool from the position above the lower spacer grid to a lower position. Investigations are underway based on current post irradiation examinations, reactor physics calculations and ICARE2 analyses of the final behaviour of the molten pool.

6.SUMMARY AND CONCLUSIONS

The first FPT0 test of the PHEBUS FP programme indicates a large rod degradation far beyond that observed in any previous SFD tests. It provides an unexpected early loss of rod-like geometry and formation of a molten pool under strongly oxidising conditions. In addition the following phenomena were observed :

- a very sharp clad oxidation escalation (~ 10 K/s) followed by a steep temperature decrease when Zr is totally oxidised
- a significant UO_2 dissolution and relocation
- a quite total flow blockage just after the inner rod slumping

ICARE2 V2 Mod1 was the main code used by IPSN and JRC to prepare and analyse the FPT0 test. This code is validated against a large validation matrix and showed correct calculations of most of the degradation phenomena. Nevertheless it fails to predict the severe fuel rod degradation which occurred in FPT0. The loss of rod geometry happened at a temperature that was lower that had been measured in earlier experiments where the rods had remained intact. So temperature could not be the cause of the slumped. FPT0 had a combination of real fuel, very oxidising atmosphere and a high peak temperature during oxidation (possibly ~ 2900 K) followed by a rapid cooling (thermal shock).This combination was unique.

Main results of the code-to-data comparisons are :

- A correct prediction of the overall thermal and oxidation behaviour of the bundle up to the end of the oxidation phase.

- The unexpected large dissolution of fuel which occurred during the oxidation phase is underestimated even after tuning. This could result from the early UO_2 dissolution by Zr-control rod mixtures which can develop above 1500 K. This interaction is not taken into account by ICARE2 V2 Mod1. In addition, UO_2 dissolution by molten Zr under high oxidising conditions could be underestimated. The uncertainty on the UO_2 solubility limit in melts could be a cause of this weakness.

- The loss of rod-like geometry which occurred on inner rods in the mid-zone of the bundle is not calculated. The current version of ICARE2 cannot simulate the slumping of solid components. The possible formation of an early solid debris configuration in the inner zone of the bundle could not be totally ruled out.

- Between fuel dissolution and loss of geometry the main cause of rod slumping is unclear. Whatever the basic phenomena which drives the rod slumping, several ICARE2 sensitivity calculations indicated that this process should involve both chemical interactions which lower the liquefaction temperature of UO_2 and reduction of radiative heat transfer with the surrounding shroud.

- In spite of the well identified ICARE2 weaknesses, the flexibility of the code enabled the user to impose core configurations e.g. local debris bed, molten pools or specific relocations. This approach was useful for understanding the overall behaviour of the degradation.

- Lessons learned from FPT0 are applied to the preparation of the next FPT1 test foreseen with similar core conditions but irradiated fuel.

- ICARE2 modelling developments on the late phase aspects of the core degradation are promoted to facilitate the preparation and interpretation of future PHEBUS FP test.

REFERENCES

[1] TATTEGRAIN, A., CLEMENT, B., GONNIER, C., FASOLI-STELLA, P., Von der HARDT, P. and LECOMTE, C., "The PHEBUS FP programme. Contribution to Reactor Containment Safety Research". 3rd Intern. Conf. on Containment Design and Operation, Toronto, Ontario, Canada. October 19-21, 1994.

[2] HASTE, T., ADROGUER, B., BROCKMEIER, U., HOFMANN, P., MÜLLER, K. and PEZZILLI, M., "In-Vessel Core Degradation in LWR Severe Accidents : A State of the Art Report", Update Jan. 1991 - June 1995, AEA/CS R1025/W, August 1995.

[3] GONZALEZ, R., ADROGUER, B., CHATELARD, P, and CRESTIA, J.C., "Status of ICARE2 V2 code and overview of its validation".
NURETH 6, Grenoble. October, 5-8, 1993

[4] SERRE, F., JAMOND, C., EDERLI, S., ADROGUER, B., CHATELARD, P. and FICHOT, F., "Status of the ICARE2 Code Assessment, Illustration on PHEBUS FPT0 Experiment", IAEA Tech. Committee Meeting on Advances in and Experience with Accident Consequences Analysis, Vienna, 27-29 Sept. 1995.

[5] BLANC, J.Y., CLEMENT, B. and Von der HARDT, P., "Fuel Bundle Examination Techniques for the Phebus Fission Product test", this conference.

[6] SCHWARZ, M. and JONES, A.V., "Analytical Interpretation of FPT0 and Preparation of Future PHEBUS FP Tests". ENS TOPSAFE'95, Budapest September 24-27, 1995.

[7] SHEPERD, I. and SERRE, F., "Precalculations for the bundle for the first PHEBUS FP test FPT0", IAEA Tech. Committee Meeting on Behaviour of Core Materials and Fission Product Release in Accident Conditions in L.W.R., Aix-en-Provence, March 1992.

[8] JAMOND, C., ADROGUER, B., BOURDON, S., EDERLI, S. and REPETTO, G., "Status of the FPT0 Interpretation with ICARE2 Mod1 Code", International Seminar on Heat and Mass Transfer in Severe Reactor Accidents, Cesme, Turkey, May 21-26, 1995.

[9] GAUNTT, L., Personal Communication, Sandia National Laboratories, 1995.

FEATURES OF RAPTA-SFD CODE MODELLING OF CHEMICAL INTERACTIONS OF BASIC MATERIALS OF THE VVER ACTIVE ZONE IN ACCIDENT CONDITIONS WITH SEVERE FUEL DAMAGE

Yu.K. BIBILASHVILI, N.B. SOKOLOV,
A.V. SALATOV, O.A. NECHAEVA,
L.N. ANDREYEVA-ANDRIEVSKAYA, F.Yu. VLASOV
All-Russian Institute of Inorganic Materials,
Moscow, Russian Federation

Abstract

A brief description of RAPTA-SFD code intended for computer simulations of VVER-type fuel elements (simulator or absorber element) in conditions of accident with severe damage of fuel. Presented are models of chemical interactions of basic materials of the active zone, emphasized are special features of their application in carrying out of the CORA-W2 experiment within the framework of International Standard Problem ISP-36. Results obtained confirm expediency of phenomenological models application.

1. Brief Description of the Code

Model of damage of a single fuel element of water-cooled power reactor in conditions of accident with severe damage of fuel is important as an element of the general model of damage of the active zone of a reactor describing the first stage of the latter. The object of RAPTA-SFD calculational analysis is a single fuel element (simulator or absorber element) of a rod type.

RAPTA-SFD code is developed basing on RAPTA-5 version intended for calculation of fuel elements behaviour in design accident modes through including of the following models:
- boundary conditions (related to modelling of special experiments, for example CORA-W2);
- model of heat and mass transfer at melting;
- model of boron carbide absorber element with stainless steel cladding;
- models of high-temperature chemical interaction of basic materials of the VVER active zone.

The present version of RAPTA-SFD code is created in 1993 - 94 as a result of works under International Standard Problem ISP-36.

In the code the algorithm of numerical integration of the system of non- stationary equations of balance of heat of elementary volumes of multi-layered cylindric domain is implemented taking into consideration variations of its geometry at each time step. Geometric variations account for thermal elastic deformations of fuel and cladding, creep deformations of the cladding, building up of layers of chemical interactions of materials and displacement of melt. Axial discretization of a cylindric domain can be arbitrary. The problem is solved in axial-symmetric formulation. Within each axial region all parameters describing the state of simulation are assumed independent of the axial coordinate.

Phenomenological model of melt displacement uses conservation laws for mass and heat. Displacement of a melted volume is simulated through variation of lengths and temperatures of corresponding layers of a cylindric domain within the boundaries of adjacent axial regions.

Model of boundary conditions on the outer surface of a simulation takes into consideration convection heat exchange with the stream of single-phase coolant (steam, steam/argon mixture) and radiation heat exchange with surrounding surfaces. Simulation of a 19-rod assembly of CORA-W2 was carried out by means of iterative calculations of single representative simulator from periphery to center and vice versa. With this, calculations for outer layer simulator was carried out simultaneously with calculations of multi-layered heat insulation shroud of the assembly.

Results of RAPTA-SFD calculations are arranged in compliance with requirements of ISP-36 [1] and they include large information concerning energy balance, temperature mode, local and integral characteristics of chemical interactions and displacements of melted volumes.

Usage in this code version of simple phenomenological models for description of interrelated chemical and physical processes enable one to rapidly assess the condition of the fuel. These models imply expert setting of a number of parameters values of which can be determined from the results of experimental modelling. The above applies to a considerable extent to simulation of high-temperature chemical interactions of basic materials of VVER active zone in conditions of accident with severe damage of fuel.

2. Models of High-Temperature Chemical Interactions

Phenomenological models of chemical interactions use parabolic dependence of the measure of reaction W on time t at isothermal conditions:

$$W^2 = K_p\, t, \quad \text{where } K_p = A \exp (-B / T),$$

A, B being empirical coefficients, T - temperature, K.

Kinetics of the reaction in non-isothermal conditions is determined from a recurrent relation taking into account previous reaction history.

In RAPTA-SFD code, models of the following chemical reactions are implemented:

- oxidation of Zr1%Nb by steam (actual dependence);
- interaction of Zr1%Nb with UO_2;
- oxidation of stainless steel X18H10T by steam;
- interaction of stainless steel with B_4C;
- interaction of Zr1%Nb with stainless steel;
- dissolution of UO_2 by melted zirconium.

Empiric coefficients of these models have been determined from the results of laboratory experimental investigation of chemical interaction in temperature range specific for severe accidents [2 - 4] (Table 1).

The most reliable measure of steam/zirconium reaction determined in experiments on oxidation of fuel cladding samples is weight increase of oxygen per unit surface area. The absorbed oxygen forms a layer of stoichiometry zirconium dioxide and a layer of a-Zr stabilized by oxygen depths of which can also be used as a measure of reaction. In the result of the reaction hydrogen is liberated, the amount of this hydrogen is determined on the basis of reaction equation. Rate of hydrogen liberation by a structure being oxidized is determined via integration over the structure active surface (assembly of fuel elements and shroud). Heat production of steam/zirconium reaction is estimated as ca 6.5 MJ/kgZr which causes strong influence of steam/zirconium reaction to temperature mode, especially at temperatures above 1500 ^{o}C when acceleration of reaction occurs due to alteration of structure of oxide film.

Eutectic interaction of uranium dioxide with Zr1%Nb alloy (as well as with zircaloy) results in creation of three specific layers (Table 1) in which intermetallic inclusions (U, Zr) can exist in liquid state at relatively not high temperatures. However, within the period from the onset of this reaction to achieving of cladding melting point (characteristic for CORA-W2 experiment), layers of considerable thickness do not manage to build up.

Rate of reaction of stainless steel oxidation by steam is comparable to the rate of steam/zirconium reaction. Reaction can also lead to hydrogen release, the measure of reaction used being the specific weight increase of oxygen. Analysis of values of specific heats of oxidation enables one to conclude that the heat effect of this reaction is an order of magnitude less than that for steam/zirconium one.

Interaction of stainless steel with boron carbide leads to propagation of interaction layer mainly into the depth of the cladding. This leads to emerging of fusible eutectics. Experiments on samples have shown that melting occurs at the temperature of 1200 ^{o}C (melting point of chromium/nickel steels of austenite class constitutes 1400 to 1425 ^{o}C) . The melt of control rod is occured significantly earler than fuel element. The remained boron carbide, evidently, partially flakes off and partially is dissolved in melt. Melt of the control rod coming to adjacent fuel elements initiates the reaction of

TABLE 1. SUMMARY OF MODELS OF CHEMICAL INTERACTIONS OF MATERIALS OF VVER ACTIVE ZONE IMPLEMENTED IN RAPTA-SFD CODE

Interaction type	Measure of reaction, dimension	Temperature range, $\hat{E}^*$	Coefficients		Ref.
			A	Â	
Zr1%Nb + H_2O	Weight gain, mg/ñm^2	1273 - 1773 1773 - 1873	1.59 10^5 9.825 10^5	23040 20800	/1/
	ZrO_2 thickness, ñm	1273 - 1773 1773 - 1873	0.00519 0.01772	15355 14680	/1/
	Thickness of ZrO_2 + a-Zr(O), ñm	1273 - 1773 1773 - 1873	0.0144 0.516	14088 19520	/1/
Zr1%Nb + UO_2	Layer-1 tickness, ñm [a-$Zr(O)_a$+(U,Zr)]	1273 - 1873	5.42	30191	/1/
	Layer-2 tickness, ñm [layer-1 + (U,Zr)]	1273 - 1873	62.68	32247	
	Layer-3 tickness, ñm [layer-2 +a-$Zr(O)_b$]	1273 - 1873	1.8548	22568	
X18H10T + H_2O	Weight gain, mg/dm^2	1073 - 1373	3.607 10^{13}	35210	/1/
X18H10T + B_4C	Layer tickness in cladding, ñm	1073 - 1473	3180	34600	/1/
Zr1%Nb + X18H10T	Layer tickness in cladding, ñì	1173 - 1583	3.717 10^{13}	66140	/2/
Dissolution of UO_2 in Zr melt	wt% UO_2 - 35.8%	2223 - 2523	1.0196 10^{15}	81450	/3/

* Temperature ranges for which experimental data are available

zirconium dissolution which is simulated in RAPTA-SFD code using kinetics of interaction of Zr1%Nb with stainless steel in their solid state.

Zr1%Nb alloy interaction with stainless steel (spacer grids) results in creation of interaction layers. Eutectics (Zr-Fe, Zr-Ni) have low melting point (less than 1000 ^oC) and can be sites of origin for structure melting. This reaction is counteracted by existing oxide films on original materials.

Reaction of uranium dioxide dissolution in zirconium melt is the most essential for determining of the amount and the composition of energy-releasing melt (corium). UO_2 solubility in Zr melt is very high, and the weight concentration of the former essentially instantly reaches 35.8%. For integral features of interaction a major role is played by time and scale factors.

3. Some Peculiarities and Results of Modelling

In Figs. 1 - 7 some results of RAPTA-SFD code simulation of CORA-W2 experiment are shown. In each figure 3 curves are presented: 1 - the plot obtained in the result of direct measurements in the course of the experiment with possible subsequent processing or in the result of post-test investigation of the assembly [5]; 2 - calculational curve obtained as the result of "blind" calculation within the framework of ISP-36; 3 - curve obtained as the result of final corrected calculations.

As it was mentioned above, RAPTA-SFD code uses several parameters set forth from expert reasoning based on experimental information. Thus, debugging of the code for calculations under ISP-36 was carried out using the known results of CORA-W1 experiment. In choice of parameter values the following factors were taken into consideration:

- uranium melting point was not reached;
- axial discretization in calculational model should not lead to considerable steps of functions describing processes of hydrogen generation and melt flow down.

Let us focus on choice of calculational parameters of RAPTA-SFD code and on their influence on simulation results.

Mass transfer model uses a parameter essentially influencing the temperature mode and the kinetics of chemical interactions. This is the rate of leaving by a melted ring volume from the boundaries of the axial region which is not to be identified with melt flow rate. Change in volumes of material in melting region and lower adjacent regions is accounted for by changing of layer thicknesses of uniform material. Temperature of the layer similar to incoming melt is adjusted through averaging over mass. With this, the melt "solidifies" if this temperature happens to be less than the preset temperature of motion begining onset. This procedure is applied sequentially for each integration step and for each axial region from top to bottom.

In conduction of "blind" simulation under ISP-36 the rate of melt flow away was assumed 1 mm/s (which proved to be an underestimate), and the relocated melt was joined to a single adjacent region. This led to melt "delay", to considerable overestimation of temperature level after fuel element claddings melting and to an error in determination of lower level of solidified melt. In the corrected calculation the rate was set 3 mm/s and relocated melt being distributed among 2 lower adjacent regions. This permitted us to obtain more satisfactory calculated results in simulation of temperature mode (Fig. 1, 2) and of melt relocation which could be assessed, for example, by height distribution of assembly cros- section blockage (fig. 3) or by share of dissolved uranium dioxide (fig. 4). In both calculation versions higher values of blocking compared to those measured in post-test investigations have been obtained. The following reasons for computer overestimation of blockage: interaction between boron carbide and steam, drop of material parts to outside of bundle active zone, increasing of shroud restricted area due to deformation in the experiment were not take into account. However, form of axial distribution as a result of corrected calculation has fair agreement with experiment. It should be also emphasized that this rate parameter essentially influences kinetics of chemical interactions through time and temperature factors.

Dependencies used for calculation of kinetics of chemical interactions permit to determine their local features. In obtaining of integral features of some materials interactions in conditions of fuel elements assembly one should bear in mind uncertainity in actual values of reagents contact area. This applies first of all to the process of uranium dioxide dissolution by zirconium melt. In the "blind" calculation reagents contact area was assumed to constitute 10 per cent of area of the fuel rod outer surface. This value in corrected calculation being set to 15 per cent. In both cases a realistic estimate of maximum local share of dissolved uranium dioxide was obtained, in the second case the height distribution of this value being closer to measured one (fig. 4).

One of the most important aspects of fuel behaviour in condition of severe accident influencing temperature mode and degradation processes is steam/zirconium reaction. Extrapolation of oxidation law beyond the limits of temperature range of experimental data can lead to the need to account for

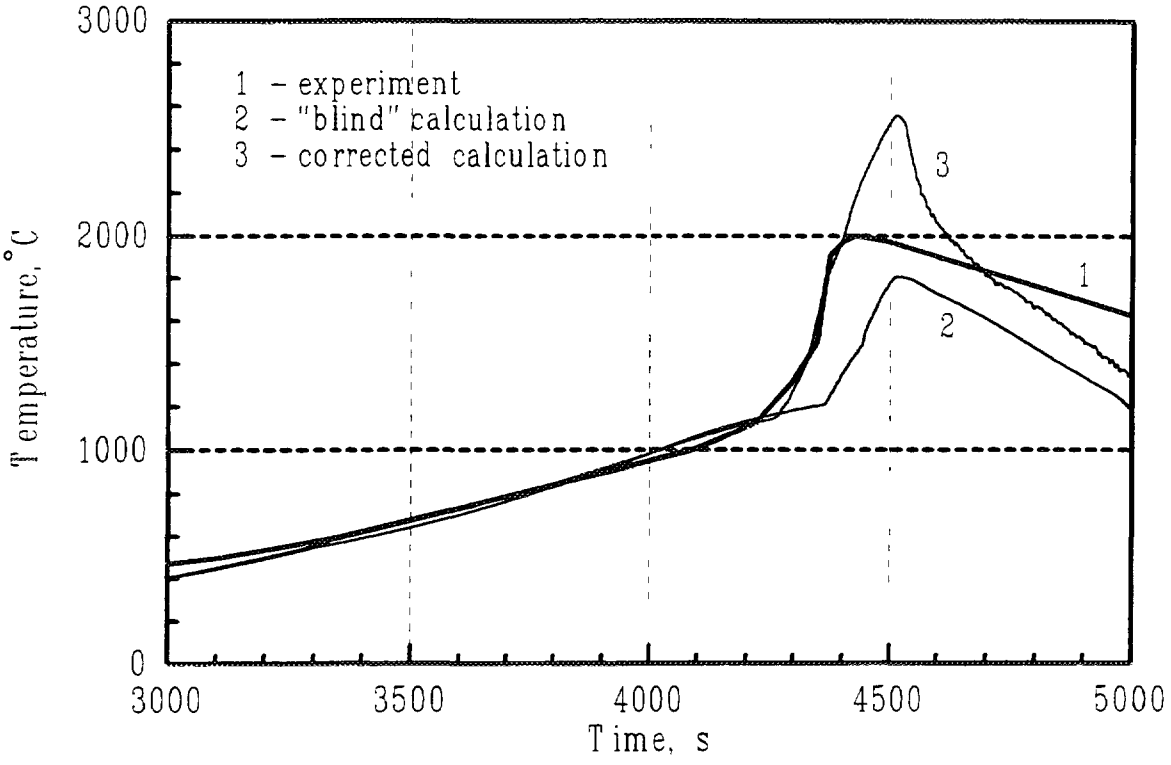

Fig. 1. CORA-W2 Experiment. Temperature mode of fuel elements simulation. Height coordinate 550 mm.

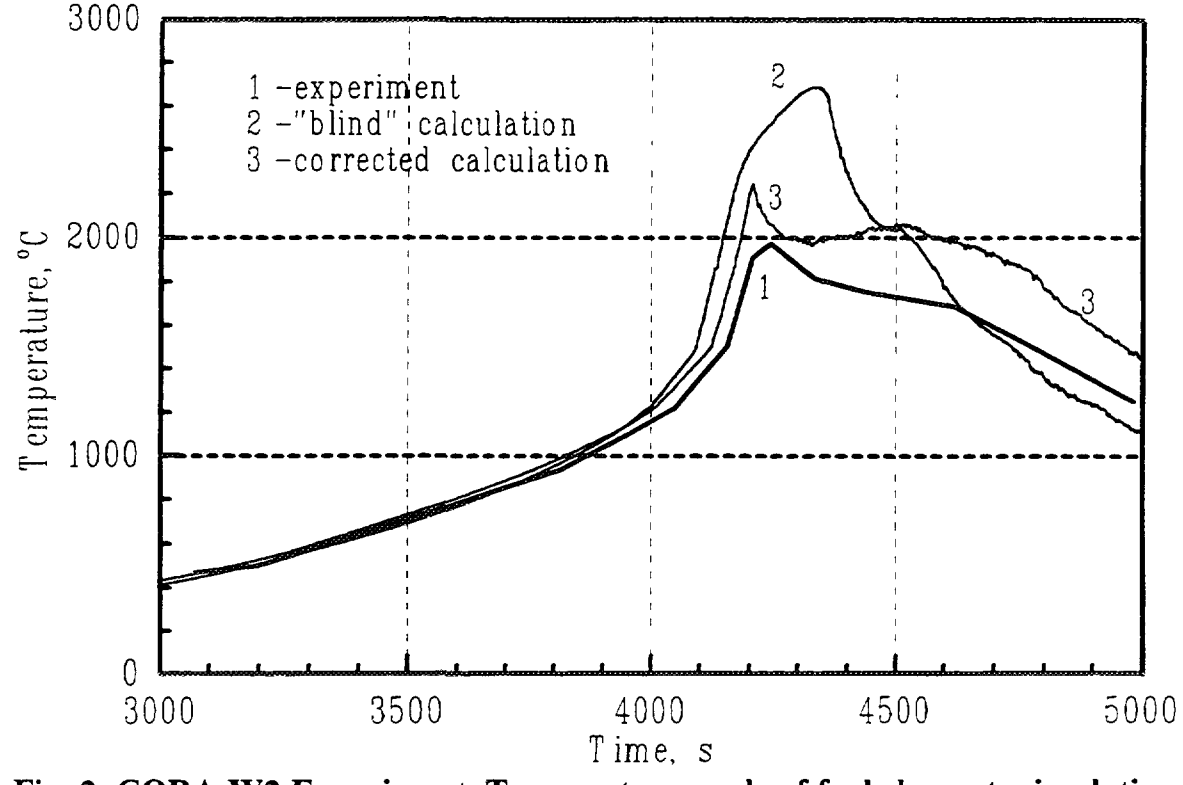

Fig. 2. CORA-W2 Experiment. Temperature mode of fuel elements simulation. Height coordinate 950 mm.

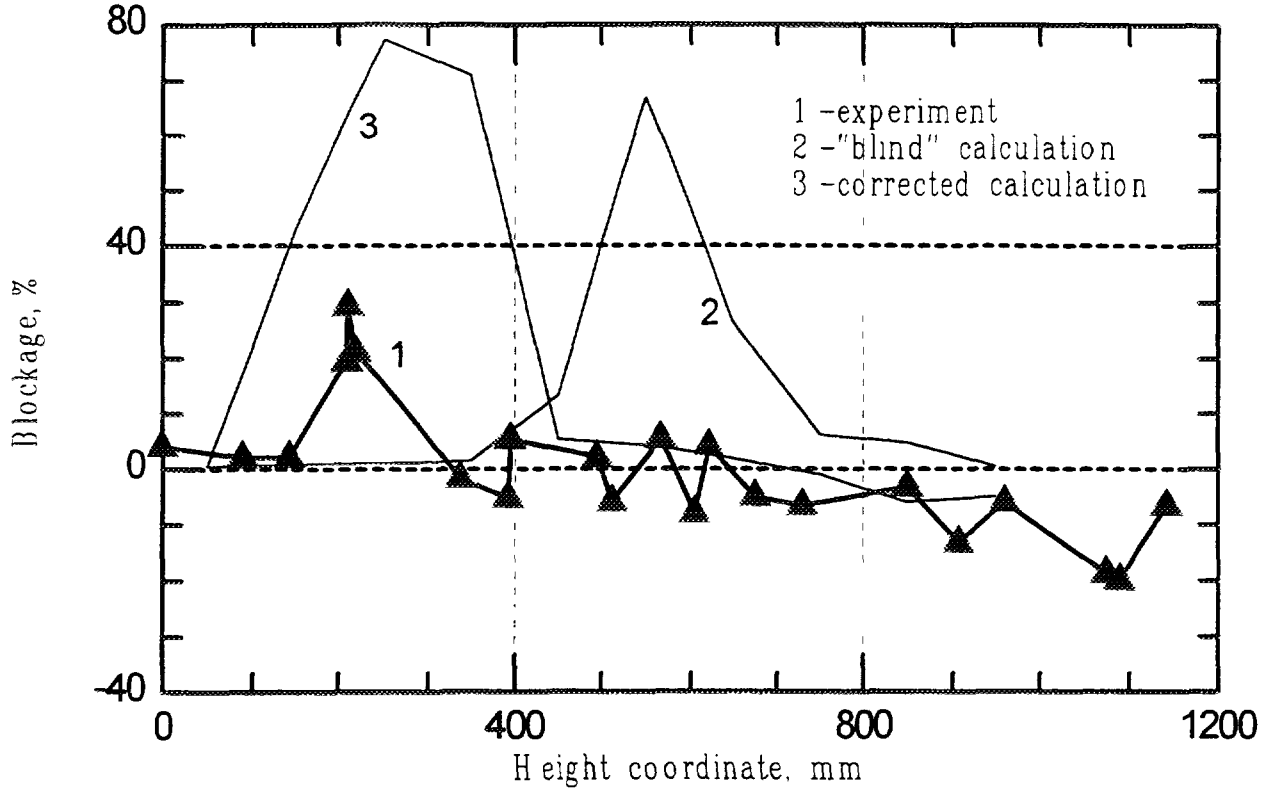

Fig. 3. CORA-W2 Experiment. Blockage distribution of cross section over height of the bundle.

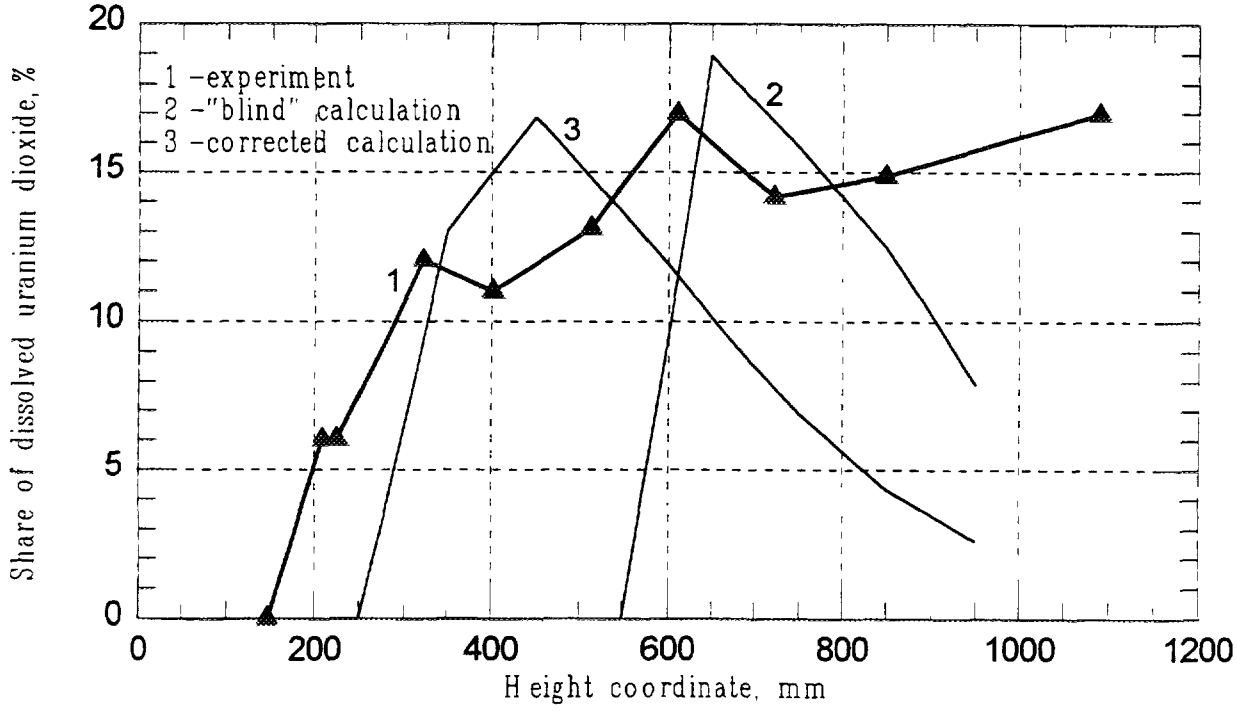

Fig. 4. CORA-W2 Experiment. Distribution of the share of uranium dioxide dissolved by zirconium melt over height of the bundle.

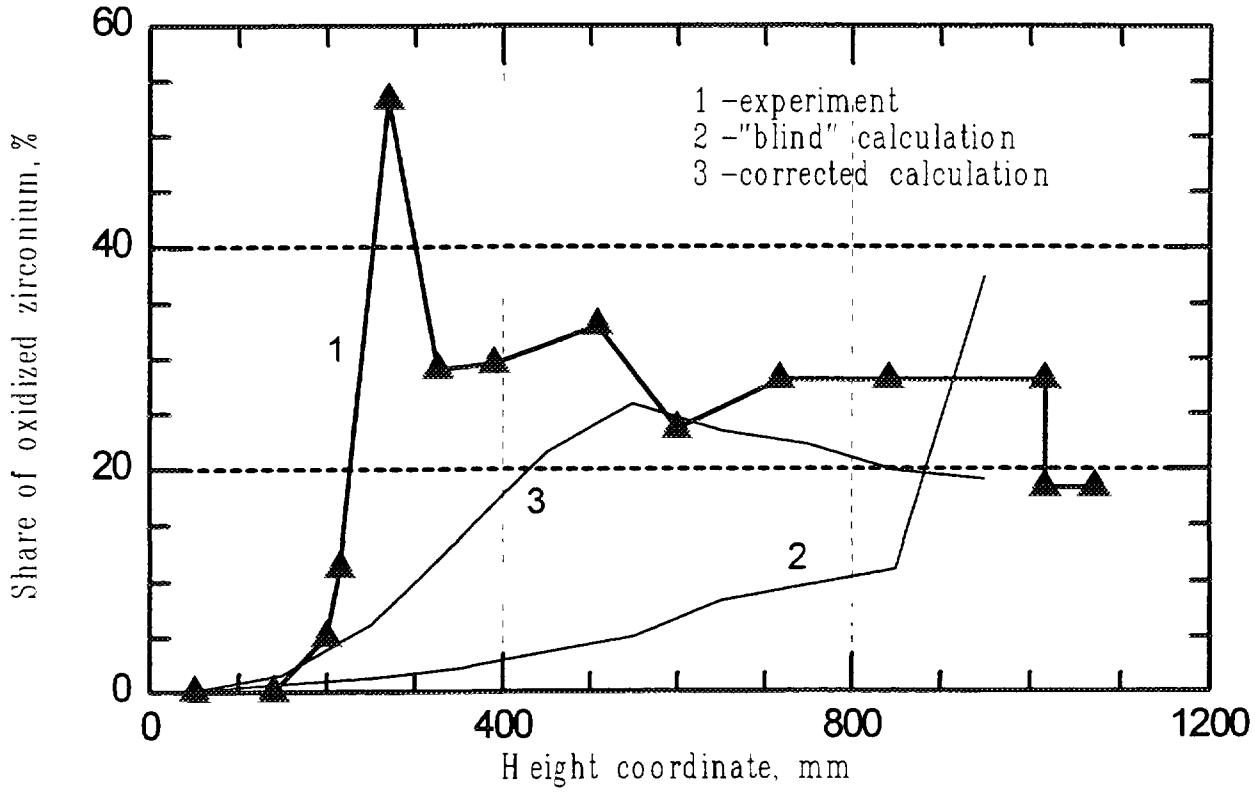

Fig. 5. CORA-W2 Experiment. Distribution of the share of oxidized zirconium in original position over height of the bundle

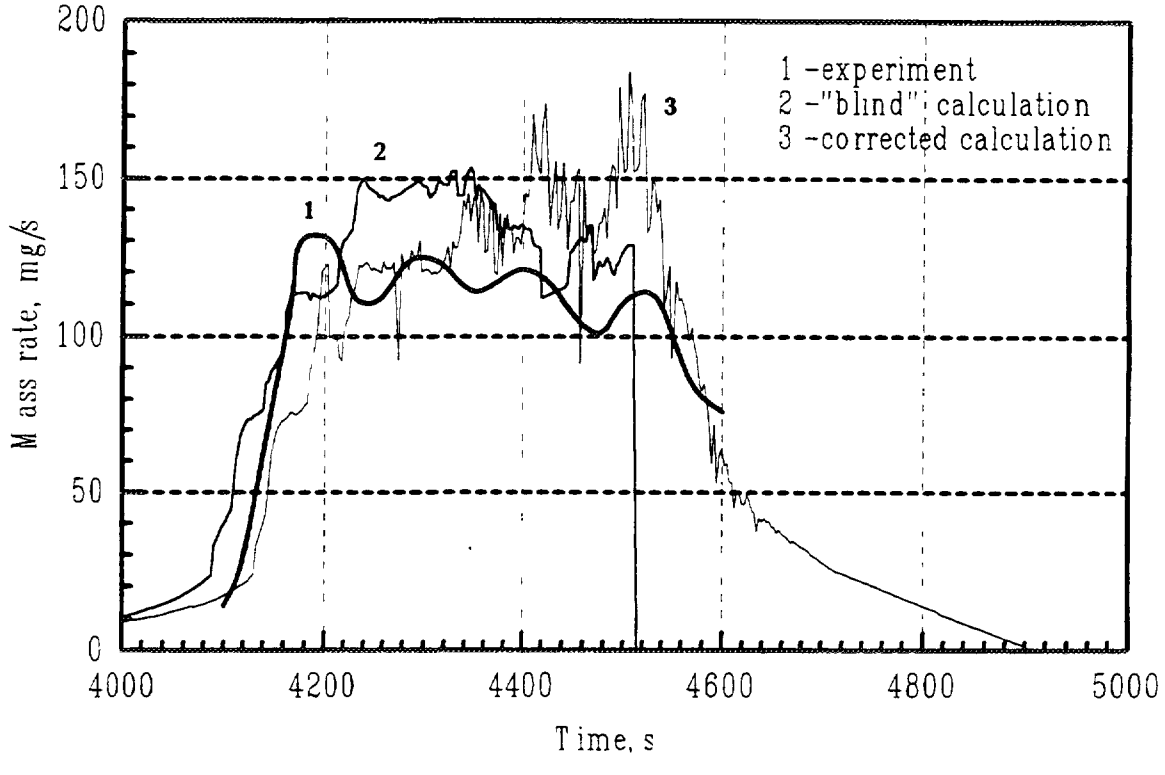

Fig. 6. CORA-W2 Experiment. Rate of hydrogen production (Bundle + Shroud).

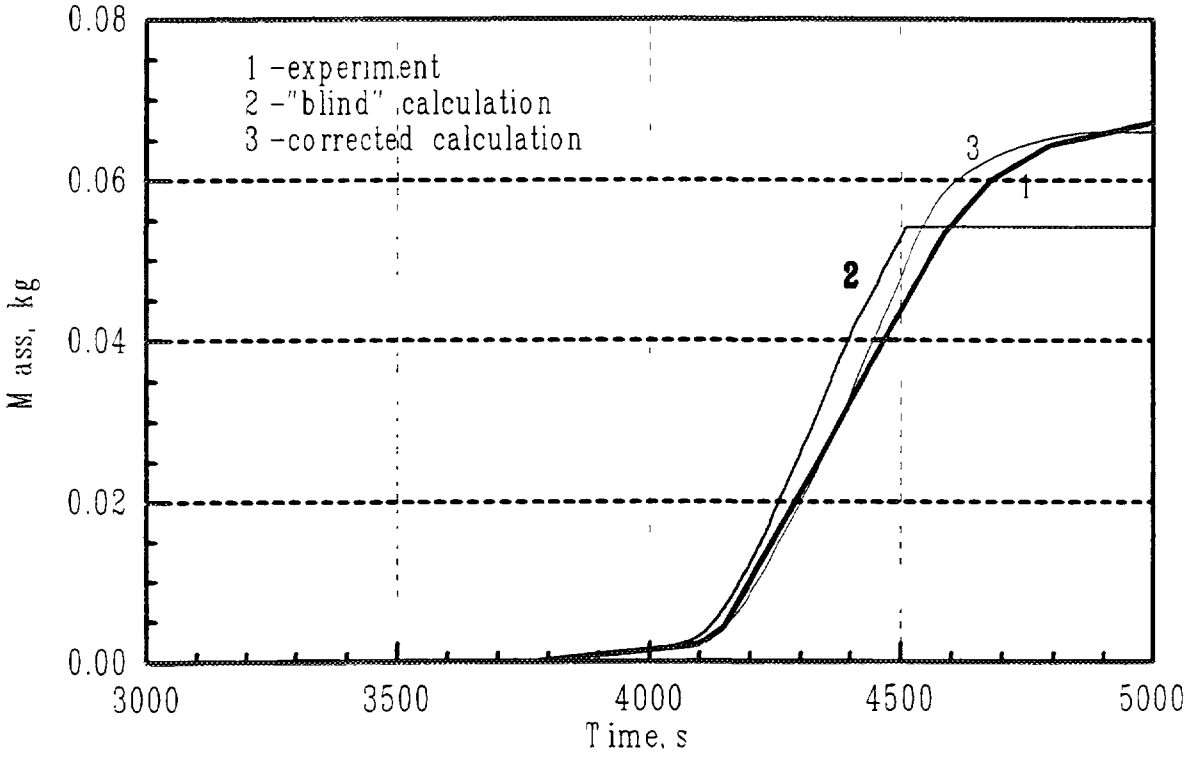

Fig. 7. CORA-W2 Experiment. Total hydrogen yield (Bundle + Shroud).

"steam hunger". In conduction of "blind" and corrected calculation the rate of specific weight gain oxygen was limited by the value of steam flow rate through the assembly divided by total zirconium surface area of the assembly. In corrected version the residual steam flow after valve shutting was taken into account. In the "blind" calculation it was assumed that after melt relocation onto an axial region oxidation of original zirconium in this region stops and oxidation of relocated melt continuing. In the corrected calculation oxygen weight gain in the axial region containing relocated melt was divided to original and relocated zirconium proportionally to their masses. This permitted to obtain better result in assessment of height distribution of assembly oxidized zirconium prior to its melting (fig. 5). In both calculations fair agreement of hydrogen generation rate and of its total yield with experiment values has been obtained (fig. 6,7).

Conclusion

Henceforth, simulation of CORA-W2 experiment by RAPTA-SFD code has shown that usage of relatively simple phenomenological models could give good results. Application of phenomenological models of chemical interactions and mass transfer is related to the necessity of assuming of several expert parameters. Reliable values of these parameters could be determined on the basis of integral experiments, such as CORA-W1, CORA-W2. The similar possibilities are possessed by the experimental unit PARAMETER (Research Scientific Institute of Scientific and Production Amalgamation "Looch", Moscow, RF) on which two similar experiments with 7-rod assemblies have been carried out in 1993 - 94. It seems expedient to continue such experimental investigations of fuel behaviour expanding the range of loading conditions (rate of heating, inner fuel element pressure, heat transport medium parameters). This would strengthen the base of experimental data for assessments of possibilities to control severe accident as well as for development and verification of calculational codes intended for fuel licensing.

REFERENCES

[1] M. FIRNHABER, K. TRAMBAUER, S. HAGEN, P. HOFMANN, L.EGOROVA. Specification of the International Standart Problem ISP36: CORA-W2 Experiment on Severe Fuel Damage. February 1994.

[2] SOKOLOV, N.B., ANDREEVA-ANDRIEVSKAYA, L.N., VLASOV, F.Yu., NECHAEVA, O.A., SALATOV, A.V., TONKOV, V.Yu., KARPOV, V.M. Kinetics of Interaction between Materials in Water-Cooled Power Reactor Core. Recomendations for Application within the Framework of the Intrnational Standard Problem for Cora-W2 Experiment. All-Research Institute of Inorganic Materials named after Academican A.A.Bochvar, 1993, -18p.

[3] VLASOV, Fu.V., DEGALTSEV, Yu.G., KOVALEV, A.M. Temperature-Time Characteristics of the Interactions of Materials the Core of VVER Type of Reactors. Recomendations for Application within the Framework of the Intrnational Standard Problem for Cora-W2 Experiment. Russian Research Center "Kurchatov Institute", 1993, -7p.

[4] HOFMANN, P., UETSUKA, H., WILHELM, A.N., GARCIA, E.A. Dissolution of solid UO_2 by molten zircaloy and its modelling. In: Severe Accidents in Nuclear Power Plants, Proceedings of a Symposium, Sorrento, 21-25 March 1988, Jointly organized by IAEA and NEA (OECD), IAEA-SM-296/1, p.3-17.

[5] International Standard Problem ISP-36: CORA-W2 Experiment on Severe Fuel Damage for a Russian Type PWR. Comparison Report (Draft). GRS, Koln, Germany, 1995.

[6] International Standard Problem ISP-36: CORA-W2 Experiment on Severe Fuel Damage. Code RAPTA-SFD blind Calculations of CORA- W2 Experiments. ARSRIIM, Moscow, 1994.

STUDY OF CORIUM RADIAL SPREADING BETWEEN FUEL RODS IN A PWR CORE

S. ROCHE, J.M. GATT
DER/SERA/LAPE,
CEA/Cadarache,
Saint-Paul-lez-Durance,
France

Abstract

In the framework of severe accident studies for PWR like Three Mile Island Unit 2 (TMI-2), the reactor core essentially constituted of fuel rods begins to heat and then to melt. During the early degradation phase, a melt (essentially UO2 and ZrO2) that constitutes the corium flows first along the rods, and after a blockage formation, may radially propagate towards the core periphery.

A simplified model has been elaborated to study the corium freezing phenomena during its crossflow between the fuel rods. The corium spreads on an horizontal support made, of either a corium crust, or a grid assembly.

The model solves numerically the interface energy balance equation at the solid-liquid corium interface and the monodimensionnal heat balance equation in transient process with convective terms and heat source (residual power). "Zukauskas" correlations are used to calculate heat transfer coefficients.

The model can be integrated in severe accident codes like ICARE II (IPSN) describing the in-vessel degradation scenarios.

1. INTRODUCTION

We have to solve a corium phase-change liquid-solid problem during corium spreading between the fuel rods. The fuel rods are considered as smooth tubes and they are arranged in an in-line tube bank (see Fig.1). The first row represents the corium inlet in the tube bank. The fuel rods stay at a constant temperature less than the corium melting temperature. A simplified model has been elaborated to study the corium freezing phenomena during its crossflow between the fuel rods. The model solves numerically two equations : the interface energy balance equation at the solid-liquid corium interface and the monodimensionnal heat balance equation in transient process with convective terms and heat source (residual power). The first equation determines the corium crust thickness which forms around the fuel rods. The second equation calculates the temperature evolution of the corium which flows between the fuel rods in the direction of the flow.

2. DETERMINATION OF THE CORIUM CRUST THICKNESS

The corium is a mixture of different components (UO2, ZrO2, Steel, ...). In the present study, the corium is considered like a pure material. The phase change takes place at a discrete temperature T_f , and the solid and liquid phases are separated by a sharp moving interface. The requirement on the continuity of temperature at the solid liquid interface is given by :

$$T_s(r,t) = T_l(r,t) = T_f$$

where $T_s(r,t)$ et $T_l(r,t)$ are respectively the temperatures of the solid and the liquid phases, and T_f is the melting (or solidification) temperature. The energy equation at the solid-liquid interface for the

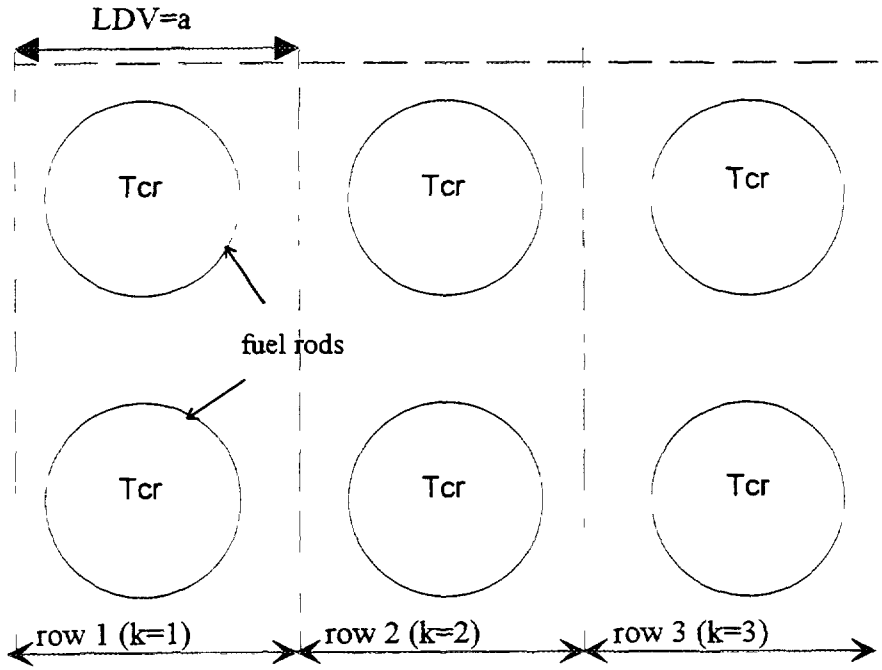

$$t'(1)=\frac{LDV}{U_{max}^{n'}} \qquad t'(2)=\frac{LDV}{U_{max}^{n'}} \qquad t'(3)=\frac{LDV}{U_{max}^{n'}}$$

Fig.1 Cross-sectional view of fuel rods arranged in an in-line tube bank

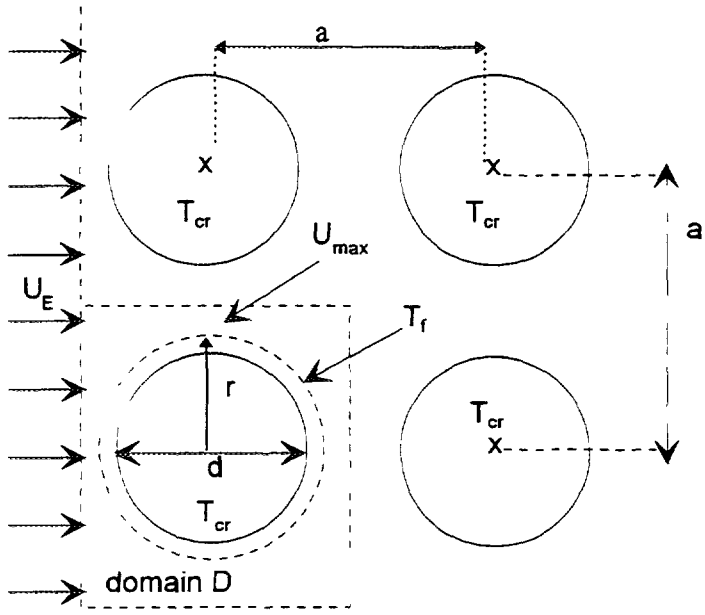

Fig. 2. Interface energy balance equation solved in the domain D

solidification problem [1] can be stated as :

$$\varphi_l - \varphi_s = \rho_s L \frac{dr}{dt} \qquad (1)$$

where φ_l et φ_s are the heat fluxes (in W/m^2), L is the latent heat of melting per unit mass of the material (in J/kg) and ρ is the density (in kg/m^3). If the heat transfer on the liquid side is controlled by convection characterized by a heat transfer coefficient h_m, and on the solid side by conduction, the equation (1) can be written :

$$\lambda_s \frac{\partial T_s}{\partial r} - h_m \left(T_M - T_f\right) = \rho_s L \frac{dr}{dt} \qquad (2)$$

where T_M is the inlet temperature of the liquid corium in every row. By considering the conduction phenomenon has reached the steady state in the solid phase, the term $\lambda_s \frac{\partial T_s}{\partial r}$ can be written in cylindrical coordinates :

$$\lambda_s \frac{\partial T_s}{\partial r} = \lambda_s \frac{\left(T_f - T_{cr}\right)}{r \ln\left(2r / d\right)}$$

Equation (2) can be stated as :

$$\lambda_s \frac{\left(T_f - T_{cr}\right)}{r \ln\left(2r / d\right)} - h_m \left(T_M - T_f\right) = \rho_s L \frac{dr}{dt} \qquad (3)$$

This energy balance equation is solved in a domain D. It is indicated by a dotted-lined square on figure 2. The maximum radius r_{max} cannot exceed the value a/2.

2.1 Assumptions

- The corium crust is concentric with the fuel rod.
- The fuel rod temperature is constant.
- The corium density does not change with phase change.
- The inlet temperature T_M represents the inlet temperature of the liquid corium in every row. This temperature changes with the time step except for the first row where T_M is considered constant. T_M is defined in the paragraph 4.

2.2 Zukauskas correlations [2]

Zukauskas has established correlations which determine the mean Nusselt number of a crossflow in an in-lined or staggered tube bank. Heat transfer in the first row of tube bank is generally different compared to the heat transfer in the inner rows. It principally depends on the Reynolds number value, the tube bank arrangement and the intertubular spacing. Above a Reynolds number of 10^3, the flow turbulence in intertubular spacing of the tube bank increases and heat transfer in inner rows becomes more intensive than in the first row. Turbulence is generated by the first rows of tubes and affects heat transfer in inner rows. Thus, for the first row of in-line tube banks, the mean Nusselt number Nu_m is given by Zukauskas as follows :

- If $1 \leq Re_{max} \leq 10^2$ then $Nu_m = 1.02 \cdot Re_{max}^{0.36} \cdot Pr_l^{0.36} \cdot \left(\frac{Pr_l}{Pr_s}\right)^{0.25}$
- If $10^2 \leq Re_{max} \leq 1.5.10^3$ then $Nu_m = 0.7 \cdot Re_{max}^{0.45} \cdot Pr_l^{0.36} \cdot \left(\frac{Pr_l}{Pr_s}\right)^{0.25}$

For the inner rows, the mean Nusselt number Nu_m is given as follows :

- If $1 \leq Re_{max} \leq 10^2$ then $Nu_m = 0.9 . Re_{max}^{0.4} . Pr_l^{0.36} . \left(\frac{Pr_l}{Pr_s}\right)^{0.25}$
- If $10^2 \leq Re_{max} \leq 10^3$ then $Nu_m = 0.52 . Re_{max}^{0.5} . Pr_l^{0.36} . \left(\frac{Pr_l}{Pr_s}\right)^{0.25}$
- If $10^3 \leq Re_{max} \leq 2.10^5$ then $Nu_m = 0.27 . Re_{max}^{0.63} . Pr_l^{0.36} . \left(\frac{Pr_l}{Pr_s}\right)^{0.25}$

The heat transfer coefficients h_m are determined by the expression : $h_m = \lambda_l . Nu_m / d$. In these correlations, the Reynolds number Re_{max} is defined by the maximum corium velocity between the neighboring tubes, U_{max}. This velocity is determined as follows :

$$U_{max} = U_E \frac{a}{a - 2r}$$

where U_E is the inlet velocity of the corium in the tube bank. U_{max} is obtained by the balance flow rate equation in the tube bank [3]. The velocity U_{max} has a finite value : in the present study, when the Reynolds number Re_{max} exceeds the value 2.10^5, the velocity stops to change. The pressure losses are not considered.

2.3 Discretization of equation (3)

$$r^{n+1} = r^n + \frac{\lambda_S . \Delta t}{\rho_S . L} \cdot \frac{(T_f - T_{cr})}{r^n . \ln(2r^n / d)} - \frac{h_m . \Delta t}{\rho_S . L} (T_M^n(k) - T_f \qquad (4)$$

The inlet temperature $T_M^n(k)$ of the liquid corium changes with the time step and with the row. This evolution is determined by the solution of a second equation, the heat balance equation.

3. DETERMINATION OF THE TEMPERATURE EVOLUTION OF THE LIQUID CORIUM

The heat balance equation determines the temperature evolution of the corium which flows between the fuel rods in the x direction of the flow.

3.1 Study domain

The heat balance equation is solved in the domain V shown by the dotted line rectangle in figure 3. The domain V represents the liquid corium crossing between the tubes. The domain decreases widthwise when the crust appears around the tubes, the crust growth being determined by equation (4). The temperature of the longitudinal wall of the domain V is equal to the melting temperature of the corium T_f. The length of the domain V (LDV) is equal to the tube bank pitch (a). The heat balance equation can be stated as :

$$\frac{\partial T}{\partial t} + U_{max} \frac{\partial T}{\partial x} = \frac{h_m (T_f - T)}{e . \rho . Cp} + \frac{q}{\rho . Cp} \qquad (5)$$

The conduction terms are neglected because the Peclet number is more than 10.

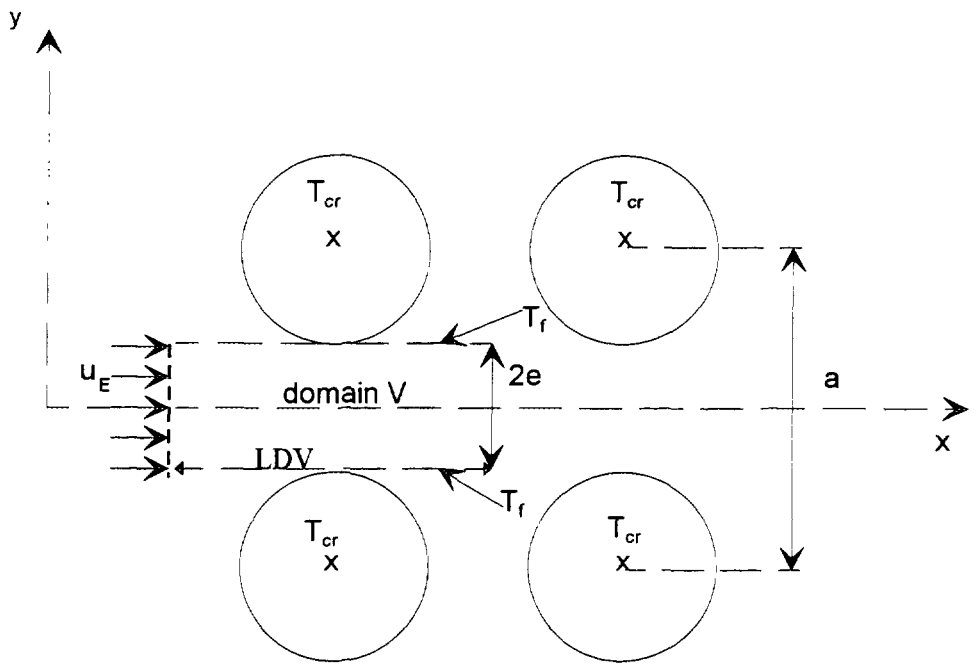

Fig. 3. Heat balance equation solved in the domain V

3.2 Discretization of the equation

The equation is discretized with an explicit finite difference scheme. We use an upwind scheme [4] to avoid the possible instability due to a centered discretization :

$$T_i^{n+1}(k) = \frac{U_{max}^n . \Delta t}{\Delta x} . T_{i-1}^n(k) + \left[1 - \frac{U_{max}^n . \Delta t}{\Delta x} - \frac{h_m^n . \Delta t}{e^n . \rho . Cp} \right] . T_i^n(k) + \frac{\Delta t}{\rho . Cp} \left[q + \frac{h_m^n}{e^n} T_f \right] \qquad (6)$$

with :

$$U_{max}^n = U_E \frac{a}{a - 2r^n} \qquad e^n = (a - 2r^n)/2 \qquad h_m^n = \lambda_S . Nu_m^n / d$$

The upwind scheme of equation (6) is stable if the time step Δt is less than the rate $\frac{\Delta x}{U_{max}}$.

4. THE HEAT BALANCE EQUATION COUPLING WITH THE INTERFACE ENERGY BALANCE EQUATION

The corium crust thickness which forms around the fuel rods is calculated by equation (4). However, the corium temperature is decreasing as and when the corium penetrates in the banks. This temperature can be obtained by equation (6) which determines the liquid corium temperature evolution according to corium spreading in the tube bank. Each temperature $T_i^n(k)$ is calculated in each row of the tube bank during a local time $t_{lo}(k)$. $T_i^n(k)$ depends on the local time $t_{lo}(k)$ defined by $t_{lo}(k) = t_g - \Sigma t'$. $\Sigma t'$ is the sum of the time t' necessary for the corium to cross the $(k-1)^{th}$ precedent rows. t_g is the global time in the bank (see Fig.1). The time t' necessary for the corium to cross the row k (domain V) is defined by the following expression :

$$t'(k) = \frac{LDV}{U_{max}^{n'}}$$

The domain V only varies in width, its length stays constant and equal to LDV. The global time t_g is the time of corium spreading in the tube bank. For example, in the $(k+1)^{th}$ row, t_g is equal to the sum of the time t' necessary for the corium to cross the first k rows plus the local time $t_{lo}(k+1)$ of the $(k+1)^{th}$ row.

In the first row, the boundary conditions are :

$$T_M^n(1) = T_E \quad T_i^0(1) = T_I \qquad T_0^{n>0}(1) = T_E$$

From the second row, we have :

$$T_M^n(k+1) = T_{LDV}^{n+n'}(k)$$
$$T_0^n(k+1) = T_{LDV}^{n+n'}(k)$$
$$T_i^0(k+1) = T_{LDV}^{n'}(k)$$

where : $T_{LDV}^{n'}(k)$: temperature at the end of the k^{th} row at the time t'(k).

$T_M^n(k+1)$: inlet temperature of the $(k+1)^{th}$ row at the time $t_{lo}(k+1)$.

The maximum corium spreading in the tube bank (blocking) is reached when the liquid corium temperature $T_i^n(k)$ in the domain V is equal to the solidification temperature of the corium.

5. APPLICATION

5.1 Physical characteristics and parameters

The fuel rods are arranged in an in-line tube bank with a pitch equal to 12.6 mm. The fuel rod diameter is equal to 9.5 mm, the intertubular spacing is then equal to 3.1 mm. The dimensions and arrangement of the tube bank correspond to the fuel rod assembly in a PWR core. In the present numerical example, the inlet velocity of the corium is chosen equal to 5.10^{-2} m/s. This value is generally used in computer codes describing invessel degradation scenarios to represent the corium spreading velocity in the core. The melting temperature is set at 2800 K, the inlet temperature of the bank T_E is equal to 3000 K, the fuel rod temperature takes the value 2000 K. The physical characteristics of the corium used in the numerical application are :

$\rho = 8.10^3$ kg/m^3 $\qquad \lambda = 3$ W/m.K $\qquad Cp = 5.10^2$ J/kg.K

$\mu = 5.10^{-3}$ kg/m.s $\qquad L = 3.10^5$ J/kg $\qquad q = 2.10^6$ W/m^3.

The minimum Reynolds number for the corium flowing is equal to 760.

5.2 Results

Figures 4 to 9 show the evolution of the corium crust thickness as a function of the global time t_g and the location of the fuel rod in the bank. There is a time lag between the successive rows about the start of crust formation to take into account the necessary time for the corium to cross a row. From a time t_{lo}, the crust thickness in a row does not progress and the steady-state is reached. When the corium penetrates into the tube bank, the maximum crust thickens more and more. At the 20^{th} row, the corium spreading stops, the corium crust entirely fills the intratubular spacing. The corium has crossed twenty rows : this corresponds to the crossing of a fuel rod assembly in a PWR core (17 rows) plus three rows in a neighboring assembly. Figure 10 shows the variation of the liquid corium temperature with the corium penetration into the tube bank. This variation is determined when the corium crust has reached its maximum thickness in every row. We can notice that the residual power q included in the source term given in the equation (5) has no influence. This term is negligible compared with the convection term.

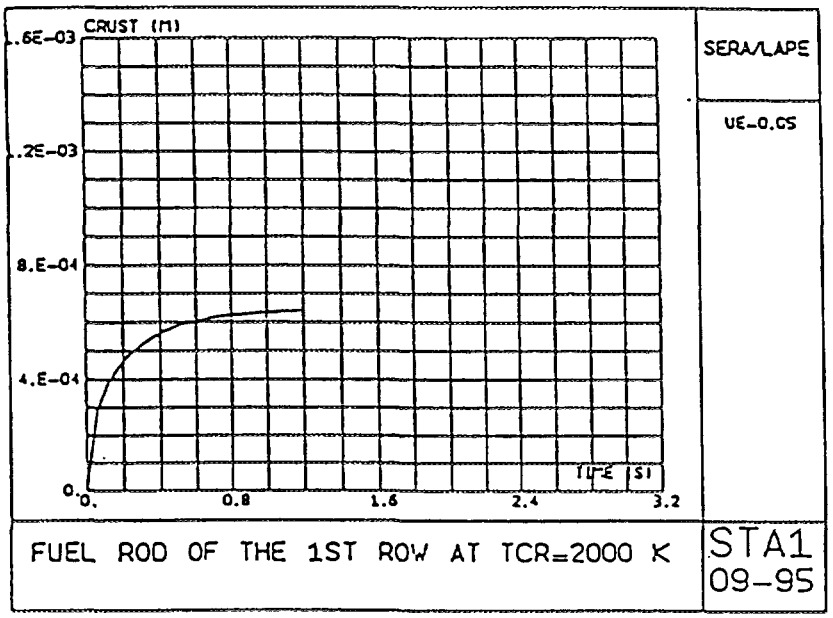

Fig. 4: Evolution of the corium crust thickness with the global time t, (I st row).

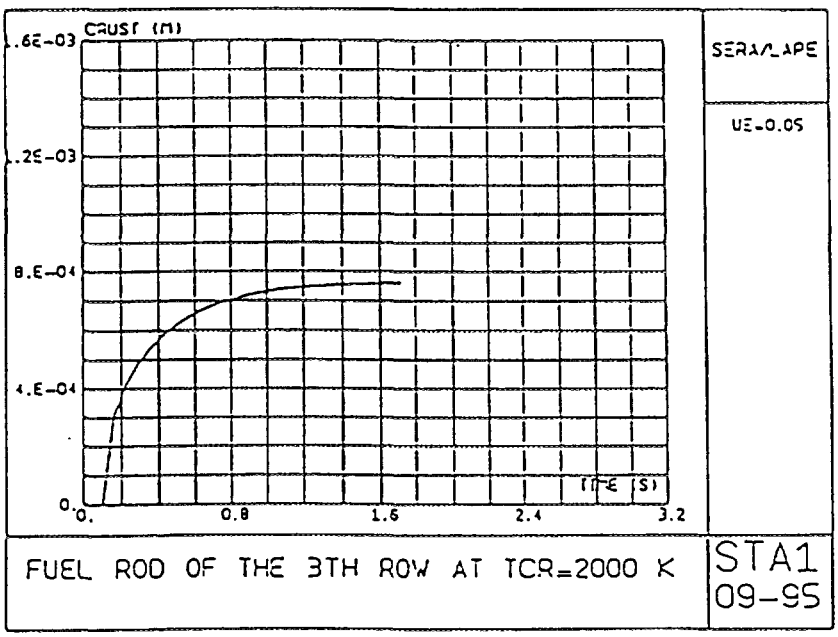

Fig. 5: Evolution of the corium crust thickness with the global time t, (3th row).

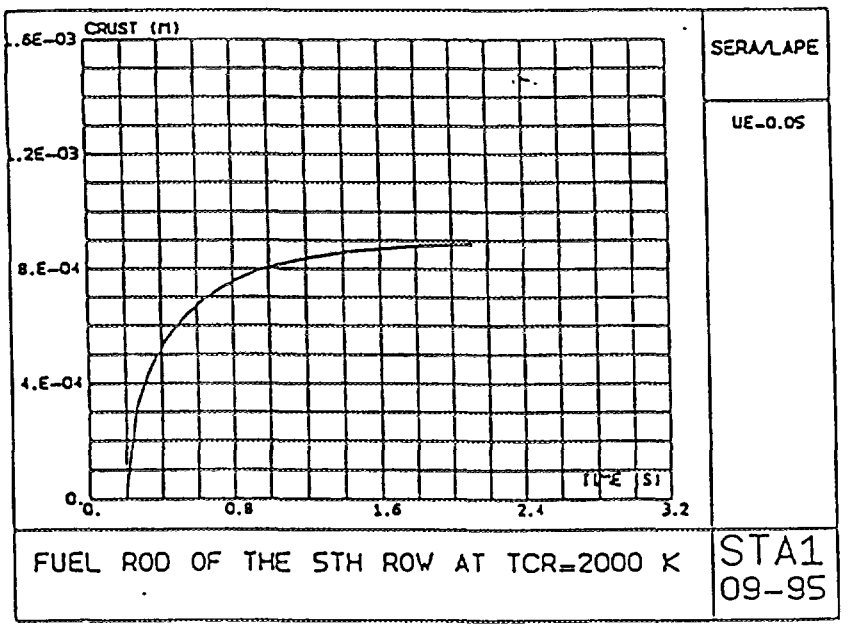

Fig. 6: Evolution of the corium crust thickness with the global time t, (5th row).

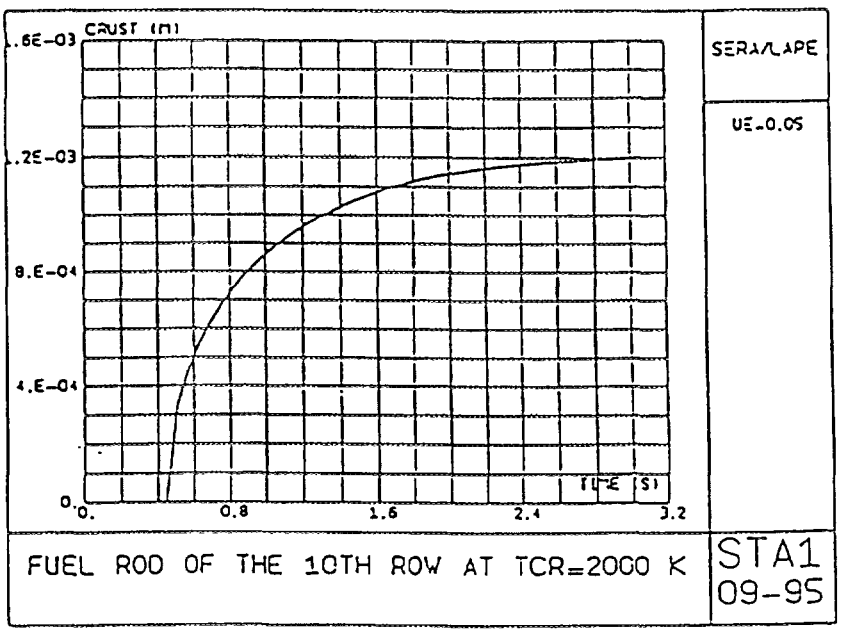

Fig. 7: Evolution of the corium crust thickness with the global time t, (10th row).

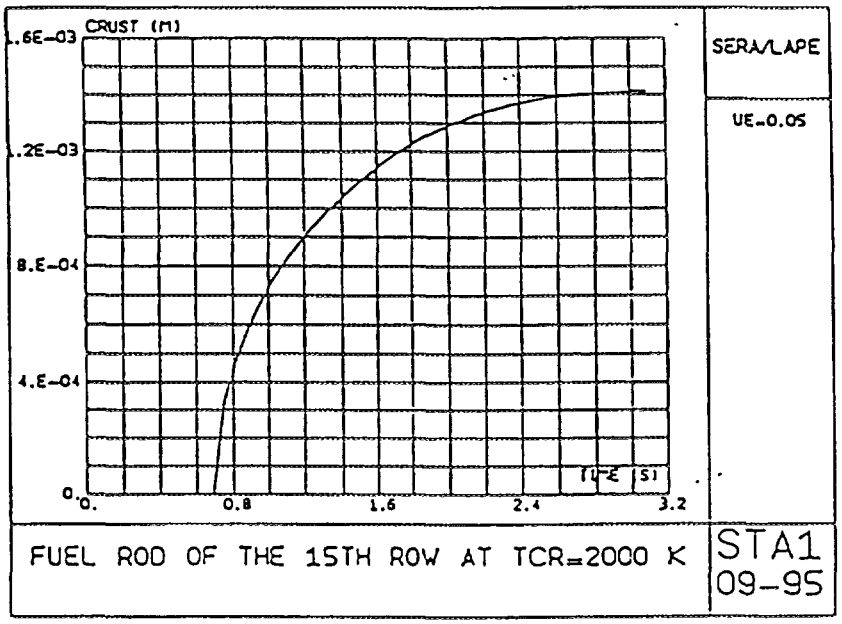

Fig. 8: Evolution of the corium crust thickness with the global time t, (I 5th row).

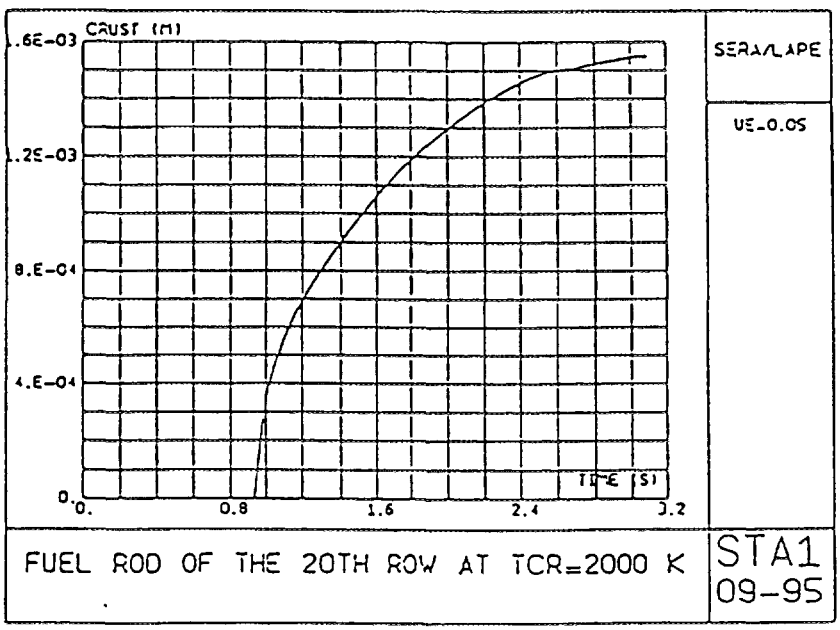

Fig. 9: Evolution of the corium crust thickness with the global time t, (20th row).

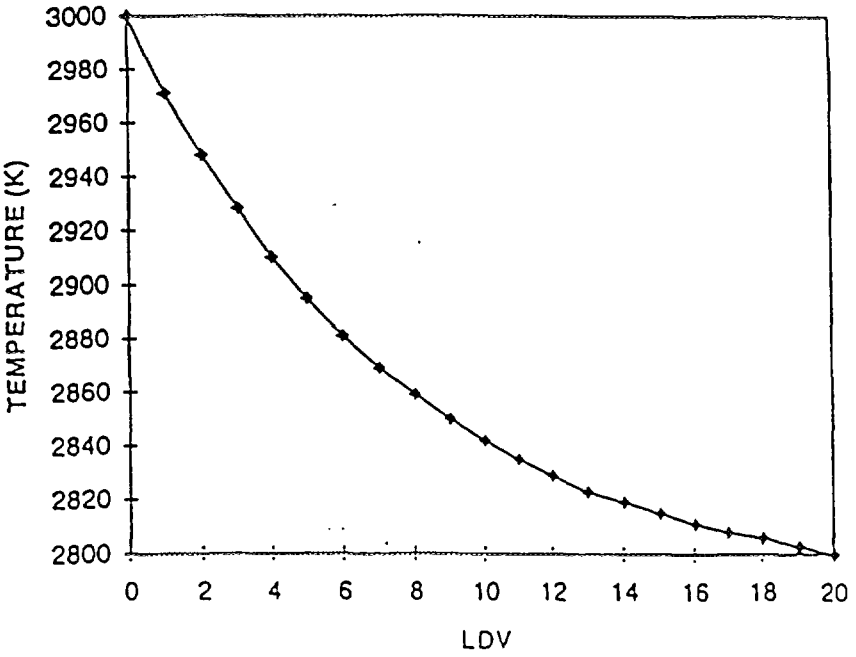

Fig. 10: Evolution of the liquid corium temperature with the corium penetration in the tube bank

6. CONCLUSION

A simplified model for the study of corium freezing phenomena during its crossflow between fuel rods has been elaborated. The model is based on two equations which are solved numerically : the interface energy balance equation and the heat balance equation. The model calculates the crust thickness which forms around the fuel rods. It also determines the liquid corium temperature which spreads between the fuel rods and the progression of the corium flowing in the tube bank till blockage. It should be noted that this model is in the process of being validated with the MARCUS code developed by IUSTI [5]. This code simulates numerically non-isothermal flows by a finite element method. After its validation, the model can be integrated in severe accident codes like ICARE II (IPSN) describing the in-vessel degradation scenarios.

REFERENCES

[1] OZISIK, M.N. , Heat Conduction, John Wiley and Sons, (1980).

[2] ZUKAUSKAS, A. , ULINSKAS, U. , Heat Transfer In Tube Banks In Cross Flow, Hemisphere Publishing Corporation. (1988).

[3] WHITE, F.M. , Heat Transfer, Addison-Wesley Publishing Company, (1984) 588 pp.

[4] PATANKAR, S.V. , Numerical Heat Transfer And Fluid Flow, Hemisphere Publishing Corporation, (1980) 197 pp.

[5] JAEGER, M. ,MEDALE, M. ,LOCK, N. ,MARTIN, R. , "A finite element model for thermal incompressible flows with moving free boundaries", Heat Transfer, Vol.2, (1994) 373-378.

FUEL BEHAVIOUR IN RIA CONDITIONS

(Session D)

Chairmen

J.P. BRETON
France

A.V. GORYACHEV
Russian Federation

NSRR EXPERIMENT WITH 50 MWd/kgU PWR FUEL UNDER AN RIA CONDITION

T. FUKETA, K. ISHIJIMA, Y. MORI,
H. SASAJIMA, T. FUJISHIRO
Department of Reactor Safety Research,
Japan Atomic Energy Research Institute,
Tokai Research Establishment,
Tokai, Japan

Abstract

Results obtained in the NSRR power burst experiments with irradiated PWR fuel rods with fuel burnup up to 50 MWd/kgU are described and discussed in this paper. Data concerning test method, test fuel rod, pulse irradiation, transient records during the pulse and post irradiation examination are described, and interpretations and discussions on fission gas release and fuel pellet fragmentation are presented. During the pulse-irradiation experiment with 50 MWd/kgU PWR fuel rod, the fuel rod failed at considerably low energy deposition level, and large amount of fission gas release and fragmentation of fuel pellets were observed.

INTRODUCTION

To provide a data base for the regulatory guide of light water reactors, behavior of reactor fuels during off-normal and postulated accident conditions such as reactivity-initiated accident (RIA) is being studied in the Nuclear Safety Research Reactor (NSRR) program of the Japan Atomic Energy Research Institute (JAERI). Numerous experiments using pulse irradiation capability of the NSRR have been performed to evaluate the thresholds, modes, and consequences of fuel rod failure in terms of the fuel enthalpy, the coolant conditions, and the fuel design. The current safety evaluation guideline for the reactivity-initiated events in light water reactors (LWRs) was established by the Nuclear Safety Commission of Japan in 1984, and based mainly on the results of the NSRR experiments. In the guideline, an absolute limit of fuel enthalpy during an RIA is defined as 963 J/g fuel (230 cal/g fuel) to avoid mechanical forces generation. The guideline also defines an allowable limit of fuel enthalpy for fuel design as a function of difference between rod internal pressure and system pressure. When fuel rod internal pressure is lower than external pressure, the limit is 712 J/g fuel (170 cal/g fuel). All of the NSRR data used for the guideline were limited to those derived from the experiments with fresh, i.e. un-irradiated fuel rods. For this reason, the current Japanese guideline adopted a peak fuel enthalpy of 356 J/g fuel (85 cal/g fuel) as a provisional failure threshold of pre-irradiated fuel rod during an RIA; and this failure threshold is used to evaluate number of failed pre-irradiated fuel rods, and to assess source term regarding fission gas release in a postulated RIA. This failure threshold enthalpy of 356 J/g fuel was derived from only one experiment, i.e. the test 859 performed in the Special Power Excursion Reactor Test program in the Capsule Driver Core facility (SPERT/CDC) [Miller 1970, 1976], and hence the current guideline noted that the failure threshold should be revised by the NSRR experiments with pre-irradiated fuel rods. In addition to the requirements for the regulation, the burnup effect becomes one of a primary concern in the field of fuel behavior study since economics and prudent utilization of natural resources have provided strong incentives for extending the burnup levels of fuel operating in commercial power-producing LWRs. The burnup limits in Japan have been increased from 39 MWd/kgU to 48 MWd/kgU for PWRs and 50 MWd/kgU for BWRs, and further increase of the limits to 55 MWd/kgU is in consideration. In these conditions, a series of experiments with pre-irradiated fuel rods were newly initiated in July 1989 as a part of the NSRR program after the completion of necessary modifications

of the experimental facilities. This paper describes the results obtained from the NSRR experiments with irradiated PWR fuels, including 50 MWd/kgU PWR fuels (the HBO fuels).

EXPERIMENTAL METHOD AND TEST CONDITION

Pulse Irradiation in the NSRR

The NSRR is a modified TRIGA-ACPR (Annular Core Pulse Reactor) of which salient features are the large pulsing power capability which allows the moderately enriched fuel to be heated by nuclear fission to temperature above the melting point of UO_2; and large (22 cm in diameter) dry irradiation space located in the center of the reactor core which can accommodate a sizable experiment. **Figure 1** shows NSRR power histories of \$4.6, \$3.6 and \$3.0 reactivity insertion, which are recorded during tests HBO-3, -4 and -2, respectively. Shape of reactor power history depends on the inserted reactivity, and the smaller pulse becomes broader. While the full width at half maximum (FWHM) in \$4.6 pulse is 4.4 ms, that in \$3.0 pulse is 6.9 ms.

Energy Deposition and Peak Fuel Enthalpy

The energy deposited to a test fuel during pulse irradiation, is a key attribute among test conditions, which represents magnitude of power burst. To evaluate the energy deposition, number of fissions generated during the pulse irradiation is obtained from gamma-ray measurement of sample solution from post-pulse fuel pellet. Because additional burnup during the pulse irradiation is much smaller than that accumulated during base irradiation in a commercial power-producing reactor, only short life fission products are used for evaluating the number of fissions during the pulse irradiation. Fission product Ba-140, with a half life of 12.75 days, is selected for the evaluation. In order to reduce high gamma ray background from Cs-137 and other fission products, chemical separation scheme is applied to the sample solution. Unless otherwise noted, the "energy deposition", Q_t, denotes the radial average total energy deposition per unit mass of fuel (J/g fuel or cal/g fuel) in this paper. Since the energy deposition includes an energy released during runout phase, one should know an amount of energy promptly generated at pulse for assessment of fuel behavior. The prompt energy deposition, Q_p, can be calculated by using a ratio Q_p/Q_t, which is provided from an analysis with EUREKA code [Ishikawa et al.] as a function of an inserted reactivity. Since the NSRR transient is extremely fast, the prompt energy deposition becomes identical to peak fuel enthalpy under adiabatic assumption.

Test Capsule and Instrumentation

The experimental capsule used in the pulse irradiation is a newly developed double-container system for the irradiated fuel rod test in the NSRR. **Figure 2** shows a schematic diagram of the capsule. The outer capsule is a sealed container of 130 mm in inner diameter and 1,250 mm in height, and the inner capsule is a sealed pressure vessel of 72 mm in inner diameter and 680 mm in height. In terms of the design of the capsule, the easiness of assembling and disassembling works by the remote handling system is one of primary concern as well as the structural strength. The capsule contains an instrumented test fuel rod with stagnant water at atmospheric pressure and ambient temperature.

The instrumentation used in the pulse irradiation is illustrated in **Fig. 3**. Cladding surface temperatures are measured by 0.2 mm bare-wire R type (Pt/Pt-13%Rh) thermocouples (T/Cs) spot-welded to the cladding at three elevations. Coolant water temperature is measured by sheathed K type (CA) thermocouples (1 mm in diameter) near the cladding surface at top of the test fuel rod and/or center of the fuel stack. A strain gauge type pressure sensor is installed at the bottom of the inner capsule to measure the increase of capsule internal pressure. A foil type strain gauge was attached at axial center on the outer surface of the inner capsule wall to measure the deformation of capsule. In some experiments, sensors for axial elongations of pellet stack and cladding tube are instrumented.

Test Fuel Rod

In a series of the irradiated PWR fuel experiments, four different test fuels have been refabricated from full-size commercial reactor fuels, and subjected to the pulse irradiation in the NSRR. The test

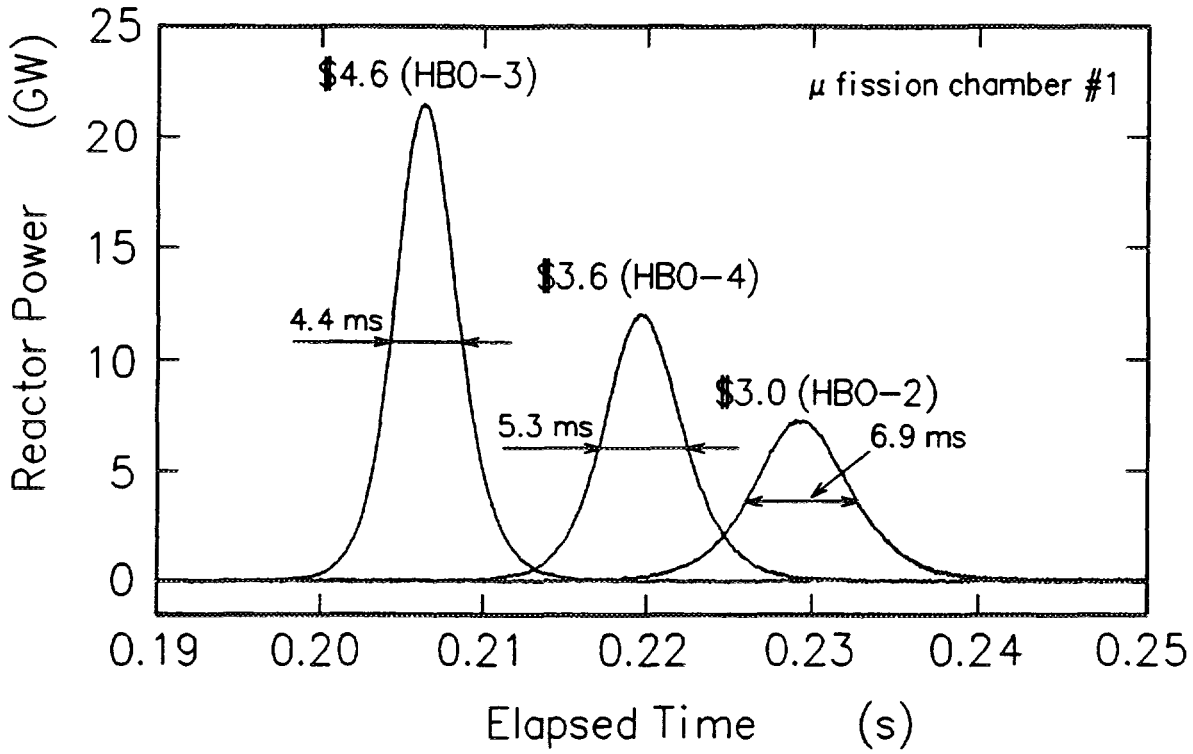

Fig. 1 Power histories during pulse-irradiations for the Test HBO-2, -3 and -4

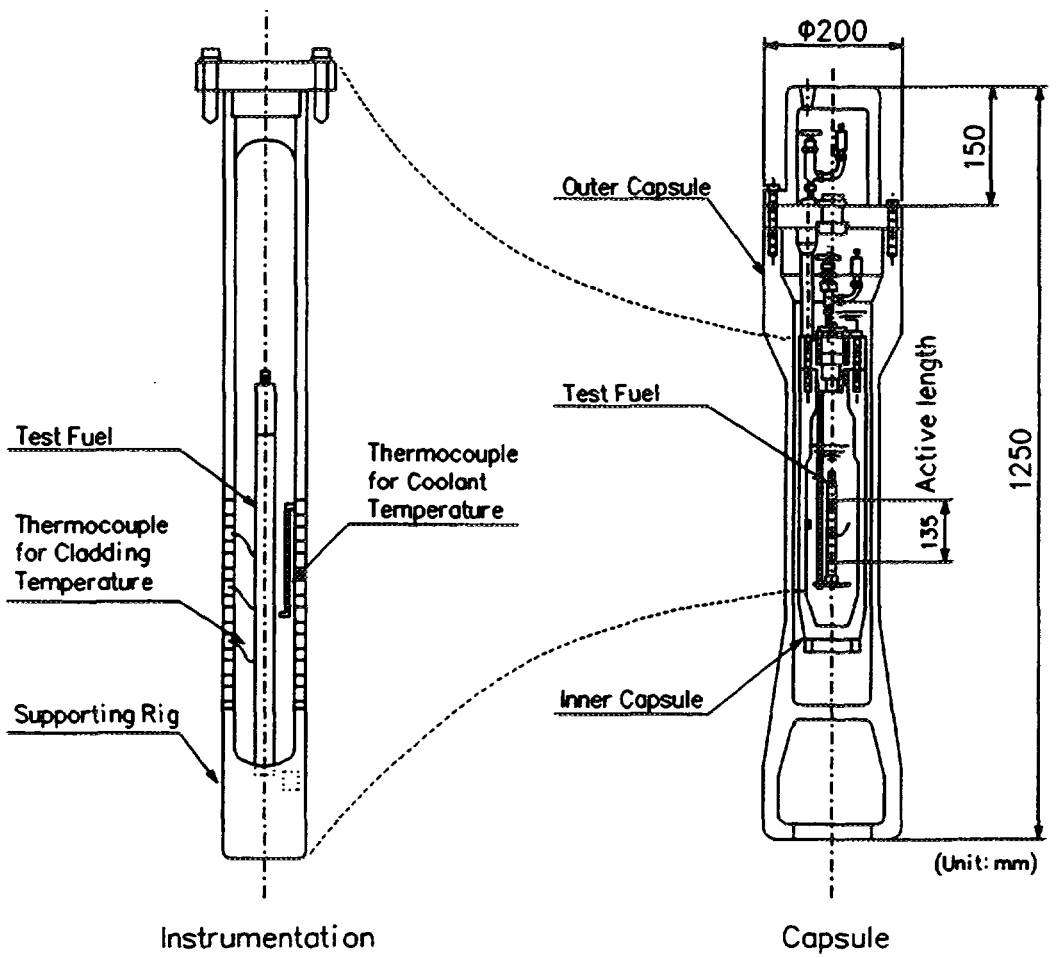

Fig. 2 Schematics of experimental capsule for pulse-irradiation

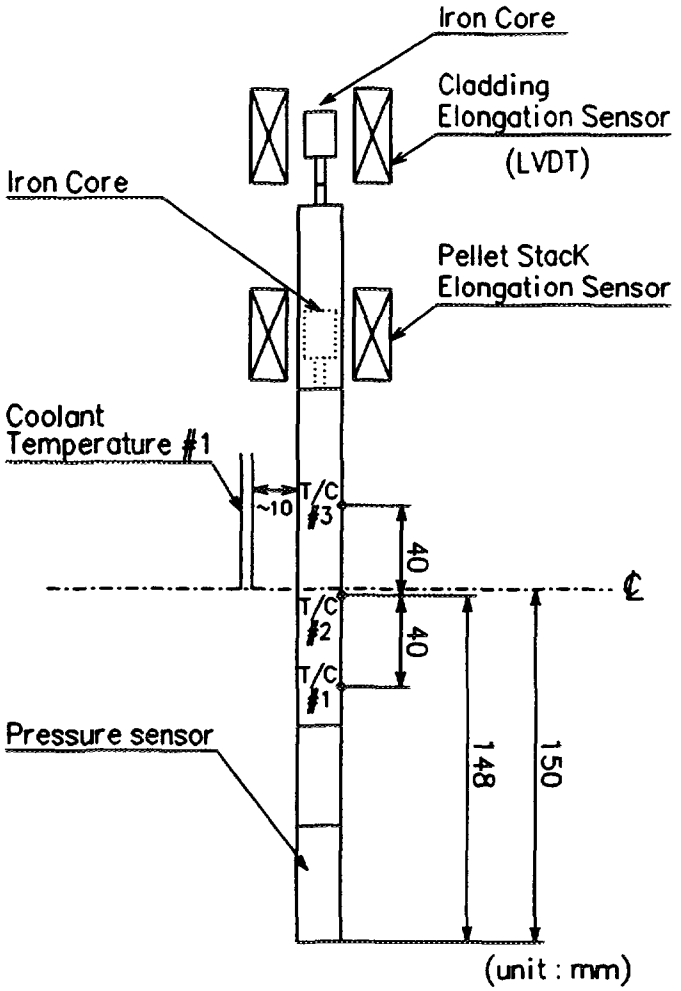

Fig. 3 Instrumentations for pulse-irradiation experiment

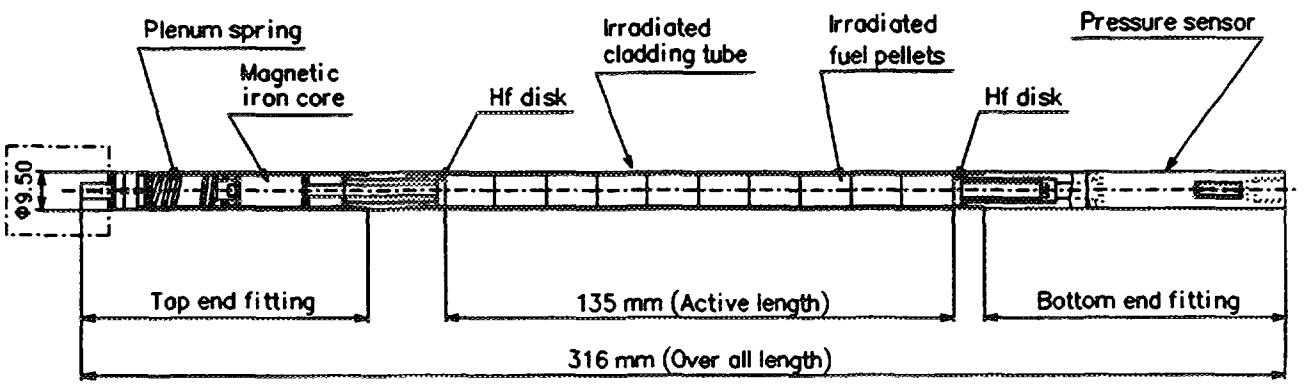

Fig. 4 Schematics of the HBO test fuel (segmented 50 MWd/kgU PWR fuel)

Table 1 Base-irradiation conditions

Test Fuel ID	Reactor	Initial Enrichment (%)	Irradiation cycle	Start of irradiation	End of irradiation	Fuel burnup (MWd/kgU)	LHGR (kW/m)	
							Average	Last cycle
HBO	Ohi unit #1	3.2	4	June, 1981	Dec., 1987	50.4	16.1	15.4
OI	Ohi unit #2	3.2	2	Dec., 1985	Aug., 1988	39.2	20.7	20.5
MH	Mihama unit #2	2.6	4	June, 1978	Aug., 1983	38.9	19.8	19.3
GK	Genkai unit #1	3.4	3	Feb., 1975	Feb., 1979	42.1	20.1	19.8

Table 2 As-fabricated fuel rod specifications

Fuel ID	Fuel type	Cladding			Fuel pellet			Radial P/C gap
		O.D.	I.D.	Thickness	O.D.	Height	Shape	
HBO	17×17	9.5	8.36	0.57	8.19	13.5	Dished & Chamfered	0.084
OI		9.5	8.22	0.64	8.05	9.5	Dished & Chamfered	0.085
MH, GK	14×14	10.72	9.48	0.62	9.29	15.2	Dished & Chamfered	0.095

(unit : mm)

Table 3 Test fuel rod specifications

Test Fuel ID	Total Length	Active Fuel Stack	Cladding O.D.	Radial P/C gap
HBO	308	135	9.444 ± 0.002	< 0.01
OI	306	133	9.470 ± 0.002	0.02
MH	300	121.6	10.656 ± 0.001	0.02
GK	300	121.6	10.666 ± 0.002	0.02

Table 4 Pulse-irradiation condition

Test ID	Fuel Burnup (MWd/kgU)	Date of Pulse	Inserted Reactivity ($)	Energy Deposition (J/g fuel)	(cal/g fuel)	Peak Fuel Enthalpy (J/g fuel)	(cal/g fuel)
HBO-1	50.4	Feb. 16, 1994	4.6	390	93	305	73
HBO-2		Mar. 25, 1994	3.0	215	51	157	37
HBO-3		Oct. 19, 1994	4.6	397	95	310	74
HBO-4		Jan. 24, 1995	3.6	279	67	211	50
OI-1	39.2	Nov. 10, 1992	4.5	571	136	444	106
OI-2		Jan. 27, 1993	4.6	581	139	453	108
MH-1	38.9	Nov. 28, 1989	3.4	262	63	196	47
MH-2		Mar 8, 1990	3.8	301	72	228	55
MH-3		Oct. 31, 1990	4.3	363	87	280	67
GK-1	42.1	Mar. 12, 1991	4.3	505	121	389	93
GK-2		Mar. 17, 1992	4.2	490	117	377	90

fuels consist of the MH, GK, OI and HBO test fuels (acronyms for the fuels irradiated in the **Mi**hama, **G**enkai, **O**hi reactors and **H**igh **B**urnup fuels irradiated in the **O**hi reactor, respectively). Irradiation history in the commercial reactor is a key attribute in this program. Fuel burnup and linear heat generation rate (LHGR) during the base-irradiation are listed in **Table 1**. Preceding to the extension of PWR fuel burnup limit from 39 MWd/kgU to 48 MWd/kgU, the demonstration program of high burnup fuel had been performed in the Ohi unit #1 reactor. The HBO test fuel had been irradiated in this program, and the fuel burnup reached 50.4 MWd/kgU.

As-fabricated, initial fuel specifications are listed in **Table 2**. The MH and GK fuels are 14×14 PWR type, and have the same dimensional configurations. While the OI and HBO fuels are 17×17 type, they have different cladding thickness and pellet outer diameter since fuel manufacturer of each fuel is different. It should be noted that the HBO fuel was not newly designed and manufactured for the high burnup application.

Dimensional data of the short-sized test fuel rods are listed in **Table 3**. The radial distance between cladding inner surface and fuel pellet (P/C gap) listed in the table is obtained from metallography for arbitrary horizontal cross-section (round slice). As it can be seen in this table, the P/C gap of the HBO test fuels is smaller than those of the other test fuels, since creep down of the cladding exceeded and the linear heat generation rate in the last irradiation cycle is lower in the high burnup HBO test fuel. As an example, the HBO test fuel rod is illustrated in **Fig. 4**.

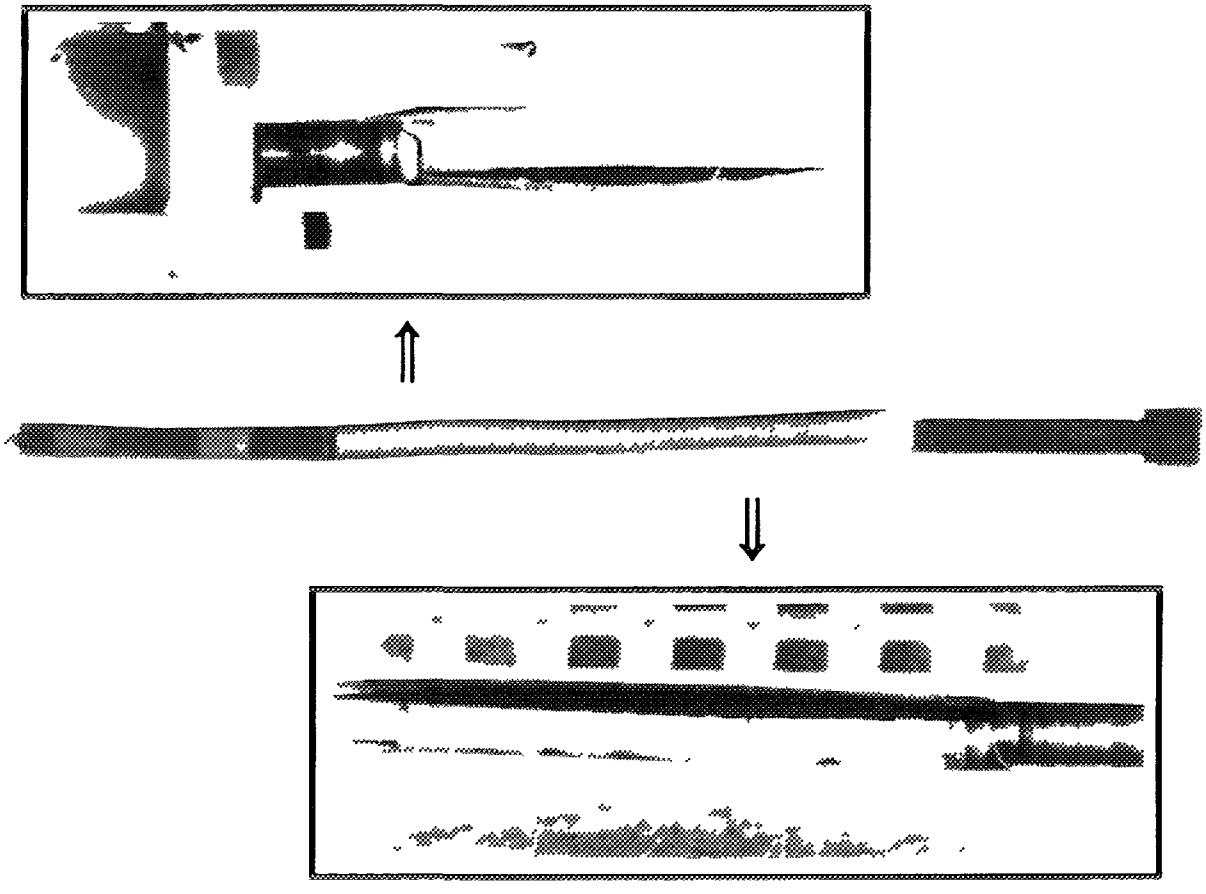

Fig. 5 Post-test appearance of the HBO-1 test fuel

Pulse-irradiation Condition

The pulse-irradiation conditions including the energy deposition and peak fuel enthalpy are listed in **Table 4**. The Tests HBO-1, HBO-3 and OI-2 were performed with the maximum pulse of the NSRR. Because of high burnup and small number of residual fissile in the HBO fuel, peak fuel enthalpy was restricted to 310 J/g fuel (74 cal/g fuel). The Test KF-1 (referred as GK-3 in some documents) is excluded from the table, since the experiment is atypical. The fuel rod used in the Test KF-1 was exposed to excessive load follow operations with several hundred cycles in the Japan Materials Testing Reactor (JMTR).

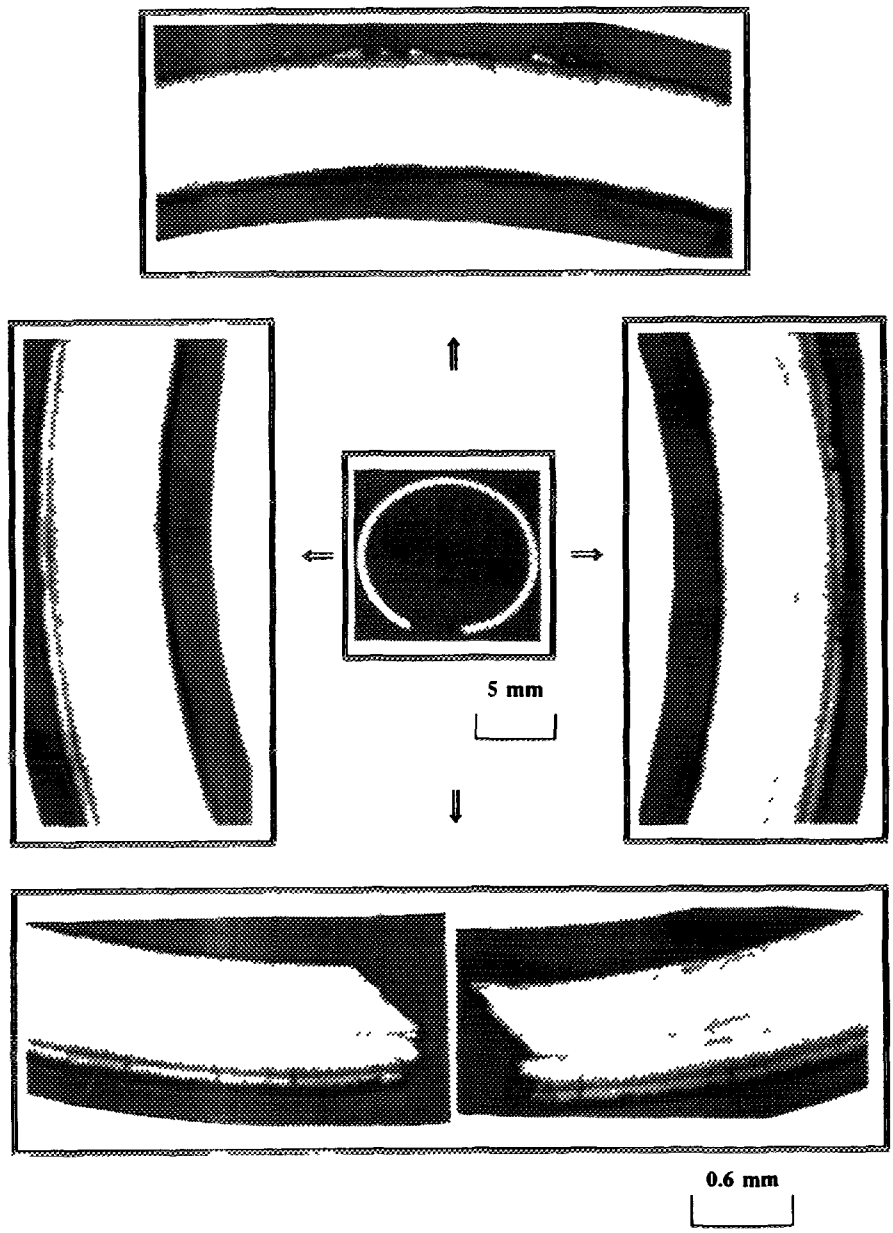

Fig. 6 Horizontal cross-section of the cladding failed in the Test HBO-1

RESULTS AND DISCUSSION

Appearance of Post-test Fuel Rod

The first test in a series of experiments with the HBO fuels, the Test HBO-1, resulted in fuel failure, while the other irradiated PWR experiments, including the Tests HBO-2, -3 and -4, remained no failure. **Figure 5** shows post-test appearance of the HBO-1 test fuel. Axial cracking of the cladding in entire region corresponding to the fuel stack occurred. The fractures are similar to those occurred by hydride-assisted PCMI in the SPERT 859 experiment. **Figure 6** shows horizontal cross-section of the failed cladding. Considerable hydride deposition and oval deformation can be seen in the figure. Residual hoop strain at a failed position is estimated as approximately 2%, which is much larger than that observed in un-irradiated fuel experiments. This could be caused by severe creep down of the cladding and large transient swelling of the high burnup fuel. Many small cracks vertical to the cladding outer surface were also found in outside oxide layer and radially localized hydride layer. Large wall-through cracks were originated from some of these crack tips and showed a feature of ductile fracture in the inner cladding region. The average hydrogen absorption in the cladding is approximately 190 ppm.

All of fuel pellets did not stay inside the rod, and were found in the capsule water as fragmented debris. Since the collected fuel pellets are finely fragmented, it can be thought that the fuel pellets are expelled from the fractured opening during the pulse. However, it can be also expected that the pellets dropped from the horizontal break after the pulse. The break can be seen at the bottom end of fuel active region.

Transient Record

Figure 7 illustrates the transient records of the reactor power, cladding surface temperature, fuel rod internal pressure and capsule internal pressure during the pulse-irradiation of the Test HBO-1 with the peak fuel enthalpy of 305 J/g fuel (73 cal/g fuel). Thermo-couple failure and spikes in capsule and fuel rod internal pressure histories observed simultaneously. This indicates an occurrence of cladding failure. The energy deposition at failure is approximately 250 J/g fuel (60 cal/g fuel). The early failure when the cladding surface temperature remains about 50 deg C indicates cladding cracking caused by pellet cladding mechanical interaction (PCMI). Although all of the fuel pellets was expelled or dropped from the rod and was recovered as finely fragmented debris, the transient records did not show pressure generation indicating an occurrence of molten fuel-coolant interaction. Because of the fuel failure in the Test HBO-1, pellet stack and cladding elongations were not successfully measured.

Fuel Deformation

Residual hoop strain was obtained from dimensional measurements on the post-test fuel rods. The residual hoop stain is shown in **Fig. 8** as a function of the peak fuel enthalpy. The strain becomes larger in the increased peak fuel enthalpy. In relatively low peak fuel enthalpy range, 250 J/g fuel (60 cal/g fuel) or lower, the Tests HBO resulted in larger strain than those in the Tests MH, as it was expected from the thinner pre-pulse P/C gap in the HBO test fuel. On the other hand, the strain of the Test HBO-3 with the peak fuel enthalpy of 310 J/g fuel (74 cal/g fuel) was almost same with that in the Test MH-3 with the peak fuel enthalpy of 280 J/g fuel (67 cal/g fuel). It should be noted that the Tests GK-1 and OI-2 resulted in no failure although the strains in these experiments exceeded 2% and 4%, respectively.

Fission Gas Release

After the pulse irradiation, rod-average fission gas release was destructively measured for the test rod by rod puncture and gas analysis. The fission gas release during the pulse-irradiation is shown in **Fig. 9** as a function of the peak fuel enthalpy. Fission gas release from the HBO fuel during base-irradiation was 0.49%. On the other hand, significant fission gas release occurred in the pulse-irradiation of the Tests HBO. Fission gas release is 17.7% even in the Test HBO-2 with the peak fuel enthalpy of 157 J/g fuel (37 cal/g fuel), and reaches 22.7% in the Test HBO-3. It should be noted that the fission gas release in the Test HBO-2 is higher than the release in the Test GK-1 with the peak fuel enthalpy of 389 J/g fuel (93 cal/g fuel). The data shown in Figs. 8 and 9 indicate that

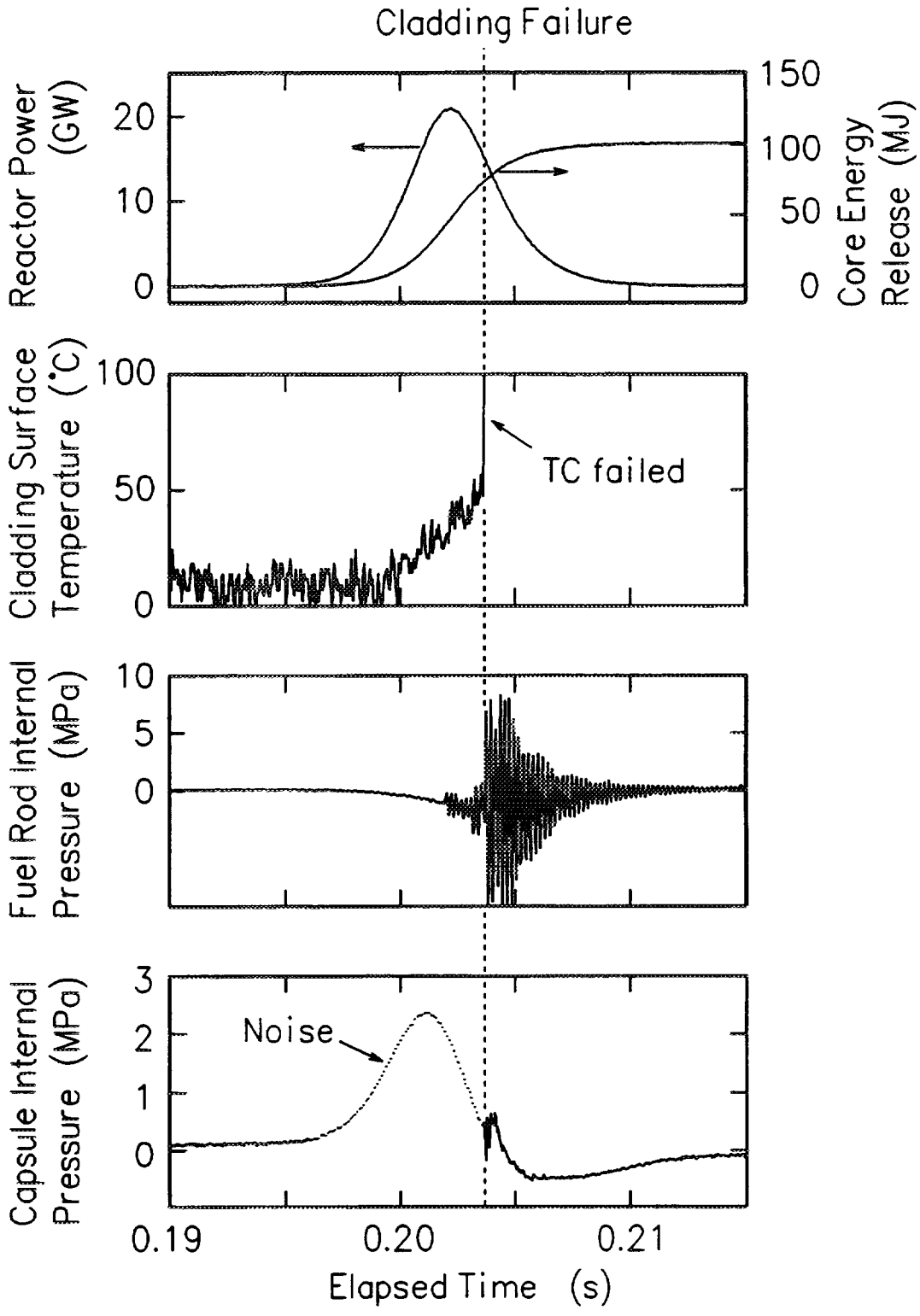

Fig. 7 Transient records of reactor power, cladding surface temperature, fuel rod internal pressure and capsule internal pressure during the pulse-irradiation of the Test HBO-1

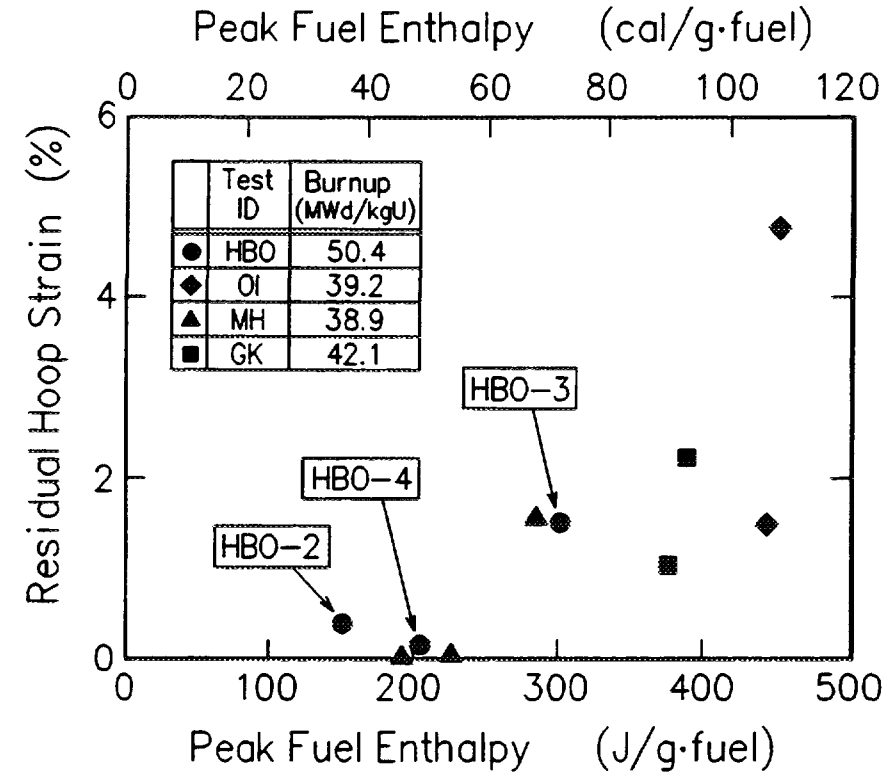

Fig. 8 Residual hoop stain as a function of peak fuel enthalpy

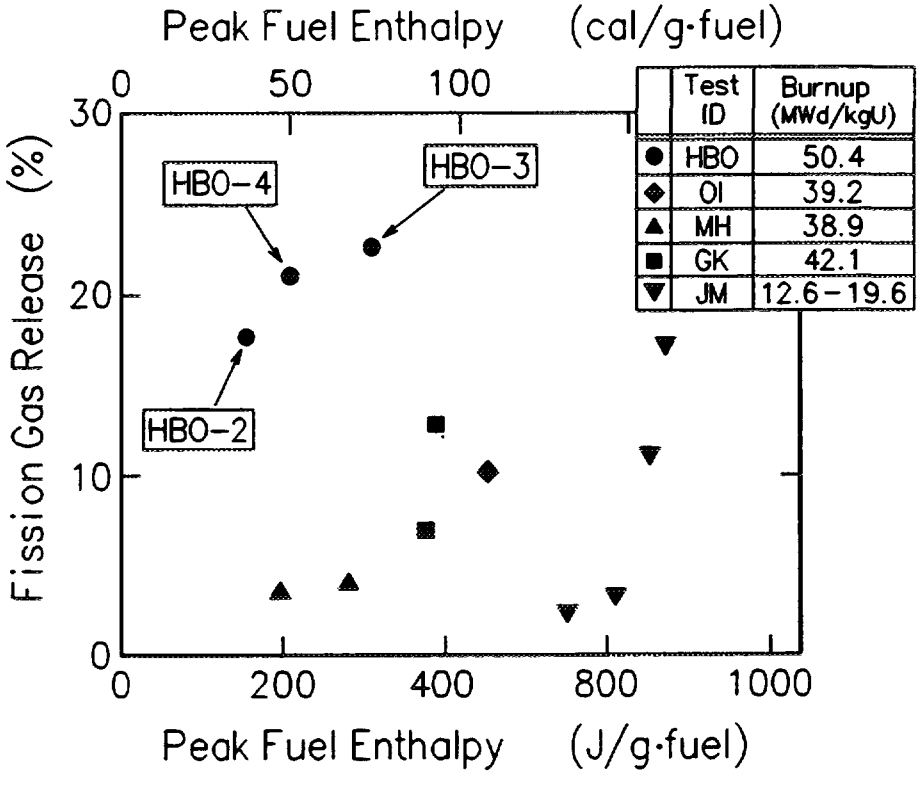

Fig. 9 Fission gas release during the pulse-irradiation as a function of the peak fuel enthalpy

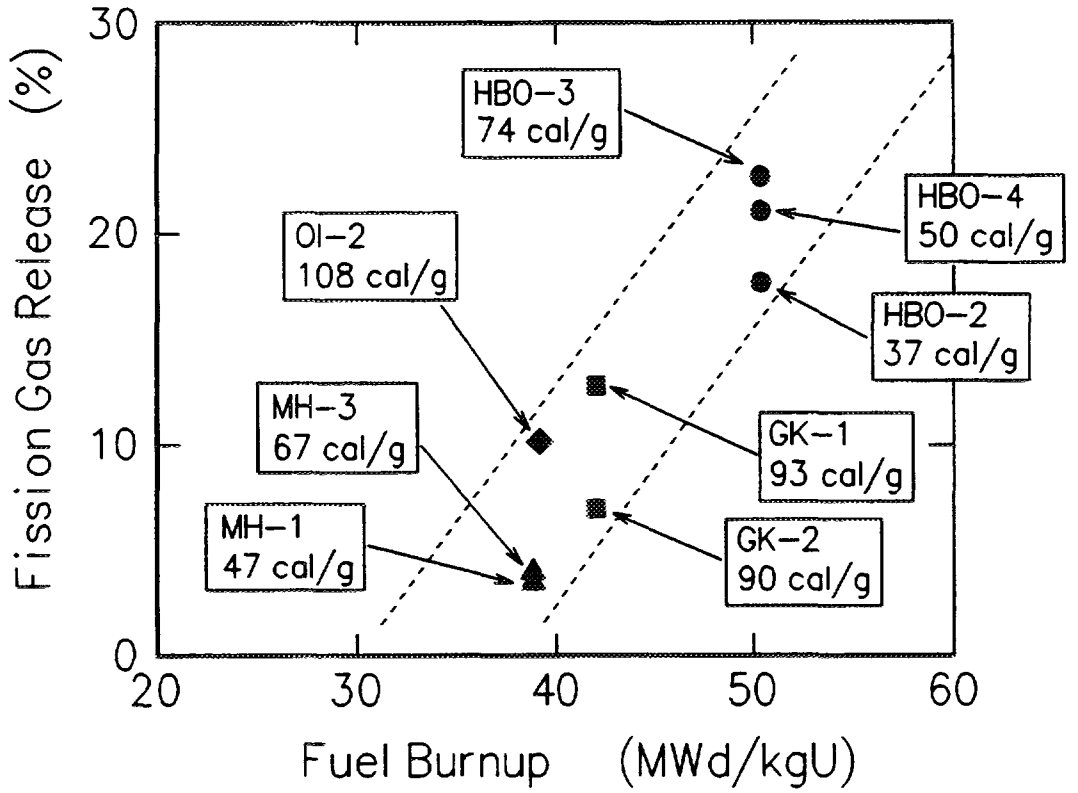

Fig. 10 Fission gas release as a function of fuel burnup

the significant fission gas release in the Tests HBO occurred with relatively small fuel swelling. **Figure 10** shows the fission gas release as a function of the fuel burnup. Higher fuel burnup correlates with the higher fission gas release.

Fuel Pellet Fragmentation

The fuel pellets were found as finely fragmented particles after the Test HBO-1. A particle size distribution of the Test HBO-1 fuel is given in **Table 5**. The fragmented fuel debris were sieved to obtain the particle size distribution. Since the fuel was highly radioactive, the variation of mesh size was restricted to only two, and the mesh openings for the sieves were 500 μm and 50 μm. The result shows an occurrence of intensive fragmentation. About 90% of recovered particles are smaller than 500 μm, and a half or more is smaller than 50 μm. Regarding destructive forces generation, fragmented particle size distribution has been examined also in NSRR high energy deposition experiments with fresh, un-irradiated fuels [Fuketa and Fujishiro]. In the fresh fuel experiment with an energy deposition of 1600 J/g fuel (380 cal/g fuel) or higher, partly molten fuel ejected from the rod and fragmented fuel particles were recovered. As for fresh fuel rods, more than a half of debris are larger than 100 μm even in the experiment with an energy deposition of 2100 J/g fuel (500 cal/g fuel). The fuel recovered in the Test HBO-1 became the finest particles in the NSRR program. Optical and scanning electron microscopy (SEM) and electron probe microanalysis (EPMA) are in planning stage for relatively large fragmented fuel particle.

The radially averaged peak fuel enthalpy in the Test HBO-1 is only 306 J/g fuel (73 cal/g fuel), and corresponding fuel temperature is well below the melting point. It is naturally accepted that the fuel pellets of the Test HBO-1 have not melted during the experiment. During the PIE process, once-molten, spherical particle was not observed. Hence, one can hardly expect an occurrence of molten fuel-coolant interaction, or steam explosion. However, it seems premature to deny the possibility of mechanical forces generation caused by vigorous boiling. Since surface area of the finely fragmented

Table 5 Particle size of recovered fragmented fuel in the Test HBO-1

		Mass (g)	% in initial mass	% in total collected
Collected fuel particles	$d \geq 500\ \mu m$	4.78	6.5	9.7
	$500\ \mu m \geq d \geq 50\ \mu m$	17.81	24.3	36.0
	$50\ \mu m \geq d$	26.84	36.7	54.3
	Total collected	49.43	67.5	100
Un-collected fuel pellets		23.78	32.5	
Initial mass (fuel pellets before pulse)		73.21	100	

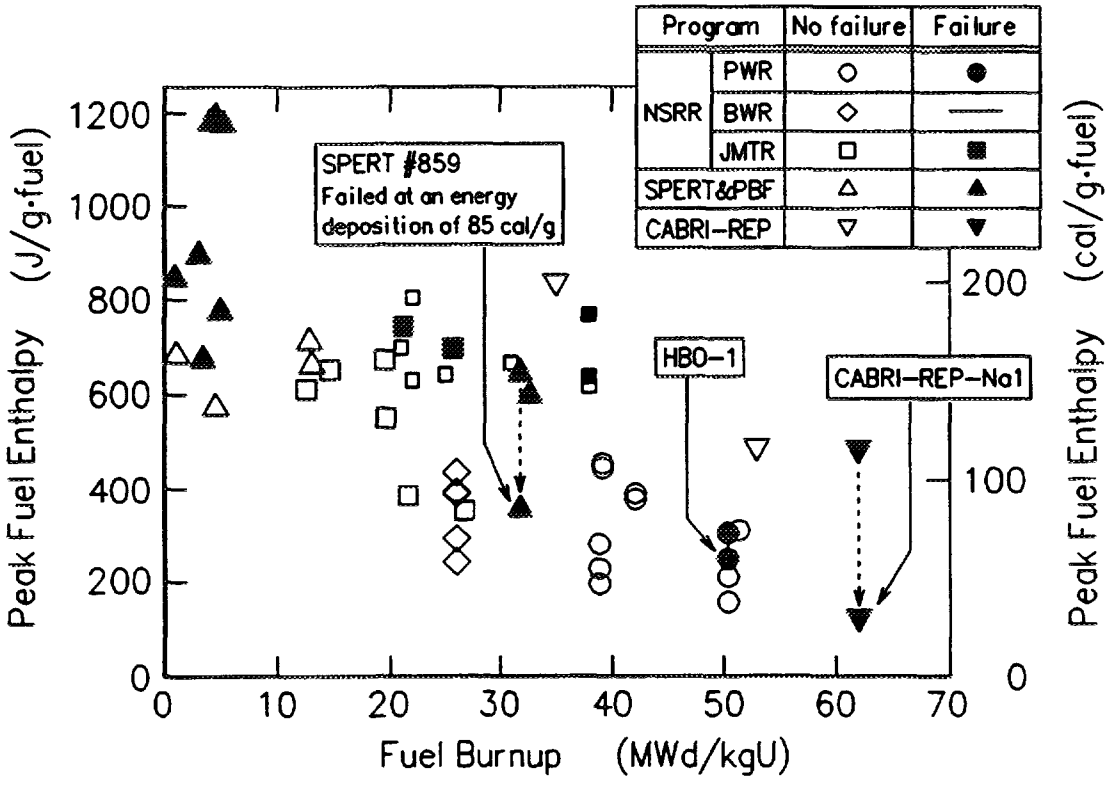

Fig. 11 Fuel burnup and peak enthalpy in irradiated fuel experiments

fuel particles is considerably large, prompt contact of the particles with coolant water may generate mechanical force, especially under stagnant and high subcooling coolant and atmospheric pressure conditions of the NSRR experiment.

Fuel Failure

Figure 11 summarizes fuel burnup of subjected test fuels and peak fuel enthalpy during transients in RIA experiments [MacDonald et al., Schmitz et al.]. Fuel integrity have been demonstrated at the peak fuel enthalpy below 450 J/g fuel (108 cal/g fuel) for the fuel burnup of 42 MWd/kgU or lower. The data in the figure, however, suggests decreased failure threshold in high burnup region in terms of peak fuel enthalpy. Fission gas accumulation and its rapid expansion may contribute to the significant fuel swelling which has been observed in the NSRR experiments. The swelling has a potential to cause PCMI, and possibly in combination with decreased cladding integrity, to generate the cladding failure.

SUMMARY AND CONCLUSIONS

The Test HBO-1 with a 50 MWd/kgU PWR fuel resulted in fuel failure at the energy deposition of approximately 250 J/g fuel (60 cal/g fuel). The results suggest possible reduction of failure threshold for high burnup fuels, and indicate that PCMI with swelling of the fuel pellets leads to the failure. Rapid thermal expansion of accumulated fission gas can intensify the swelling and fission gas release, and subsequent fuel fragmentation to extremely small particles.

The 50 MWd/kgU fuel rods in three experiments following to the Test HBO-1 survived through the transients with peak fuel enthalpy ranged from 157 to 310 J/g fuel (37 to 74 cal/g fuel). However, significant fission gas release up to 22.7% occurred.

Further investigations on fuel failure mechanisms through in-pile integrated experiments, out-of-pile separate effect tests and phenomenological modeling could contribute to "accident-conscious" fuel design to avoid fuel failure and excessive fission gas release.

ACKNOWLEDGEMENTS

The HBO test series have been performed as a collaboration program between JAERI and Mitsubishi Heavy Industries, LTD. by using fuel rods transferred from Kansai Electric Power Company. The authors would like to acknowledge and express their appreciation for the time and effort devoted by numerous engineers and technicians in Reactivity Accident Research Laboratory, NSRR Operation Division, Department of Hot Laboratories and Analytical Chemistry Laboratory, JAERI. They also acknowledge the support and help of individuals and other organizations too numerous to cite, whose contribution were critical to the success of the program

REFERENCES

Fuketa, T. and Fujishiro, T., "Generation of Destructive Forces During Fuel/Coolant Interactions Under Severe Reactivity Initiated Accident Conditions", *Nucl. Eng. Des.*, **146**, 181 (1994).

Ishikawa, M., Ohnishi, N., Kanbayashi, Y., Kuge, Y. and Takeuchi, E., "EUREKA: A Computer Code for Uranium-Oxide Fueled Water Cooled Reactor Kinetics", JAERI 1235, (Sep. 1974).

MacDonald, P. E., Seiffert, S. L., Martinson, Z. R., McCardel, R. K., Owen, D. E. and Fukuda, S. K., "Assessment of Light-Water-Reactor Fuel Damage During a Reactivity-Initiated Accident", *Nucl. Safety*, **21**, 582 (1980).

Miller, R. W., "The Effects of Burnup on Fuel Failure: I. Power Burst Tests on Low Burnup UO_2 Fuel Rods", IN-ITR-113, Idaho Nuclear Corporation (July 1970).

Miller, R. W., "The Effects of Burnup on Fuel Failure: Power Burst Tests on Fuel Rods with 13,000 and 32,000 MWd/MTU Burnup", ANCR-1280/TID-4500, R63, Aerojet Nuclear Company (Jan. 1976).

Schmitz, F., Papin, J., Haessler, M., Nervi, J. C. and Permezel, P., "Investigation of the Behaviorof High Burn-up PWR Fuel Under RIA Conditions in the CABRI Test Reactor", *22nd Water Reactor Safety Information Mtg.*, Bethesda, Maryland, Oct. 24-26, (1994).

THE BEHAVIOUR OF IRRADIATED FUEL UNDER RIA TRANSIENTS: INTERPRETATION OF THE CABRI EXPERIMENTS

J. PAPIN, H. RIGAT, J.P. BRETON, F. SCHMITZ
Institut de Protection et de Sûreté Nucléaire
CEA/Cadarache, Saint-Paul-lez-Durance,
France

Abstract

Paper presents the results of investigation of highly irradiated PWR fuel behaviour under fast power transients conducted in a sodium loop of CABRI reactor, as well as the results on development and validation of computer code SCANAIR.

I. INTRODUCTION

The CABRI experimental programme has been designed in the frame of the safety studies related to the Reactivity Initiated Accidents and in view of the future burn-up increase in the French PWRs [1], [2]. It is performed under the collaboration between Nuclear Safety and Protection Institute (IPSN) and Electricité de France (EDF).

The aim of this programme is to investigate the behaviour of highly irradiated fuel under fast power transients and to provide knowledge on the physical phenomena for the development and validation of the computer code SCANAIR elaborated at IPSN [3].

Up to the years 90 s, the available data base (SPERT, PBF experiments) has been limited to fresh or low irradiated fuel (up to 30 GWd/t) and has served as a basis for the establishment of the safety criteria which are presently independent of burn-up level.

However, several aspects of the high irradiation level may affect the fuel rod behaviour under RIA transient such as :

- the important clad oxidation with possible spallation of the zirconia layer leading to clad embrittlement and reduction of the mechanical strength,
- the high fission gas retention which induces transient fuel swelling and thus strong pellet-clad mechanical interaction (PCMI),
- the presence of the "rim" zone with high porosity, high local burn-up and plutonium content, and small grains structure.

As a consequence, early rod failure followed by dispersion of finely fragmented fuel with fuel coolant interaction (FCI) might be expected.

A first analysis of the recent NSRR tests with irradiated fuel [4] clearly showed that due to PCMI, early rod failure occurs with cold clad : such mechanism appears different from the case of fresh fuel rods in which clad failure occurs lately after DNB at quenching.

The low influence of the clad-coolant heat transfer during the initial phase of the fast power transient allowed in a first step, to define experiments in the CABRI sodium loop with the objective of determination of the fuel enthalpy threshold for rod failure and onset of fuel ejection.

Table 1 : RIA TESTS MATRIX IN CABRI SODIUM LOOP

Name (date)	Fuel Rod	Maximum mean fuel enthalpy (cal/g)	Remarks
REP Na1 (11/93)	EDF, 63 Gwd/t (4.5 %) grid levels 5/6 Fabrice rod : 569 mm	115	failure fast pulse
REP Na2 (06/94)	BR3, 33 Gwd/t (6.85 %) no rod conditioning (1 m length)	200	no failure fast pulse
REP Na3 (10/94)	EDF, 52 Gwd/t (4.5 %) grid levels 5/6 segmented rod (440 mm)	125	no failure fast pulse
REP Na4 (07/95)	EDF, 63 Gwd/t (4.5 %) grid levels 5/6 Fabrice rod : 571 mm	~ 100	no failure reactor type ramp
REP Na5 (05/95)	EDF, 63 Gwd/t (4.5 %) grid levels 2/3 Fabrice rod : 571 mn	~ 115	no failure fast pulse
REP Na6 (95)	Mox 3 cycles Fabrice rod	~ 140	ramp to be defined
REP Na7 (96)	Mox 4 cycles Fabrice rod	~ 125	ramp to be defined
REP Na8 (96)	EDF, ≥ 58 Gwd/t (4.5 %) grid level 4/5	~ 125	ramp to be defined
REP Na9 (96)	Mox 2 cycles Fabrice rod	~ 180	ramp to be defined

This experimental programme, still underway, consists of six tests with UO_2 rods and three tests using MOX fuel to be realised up to end of 96 (see matrix, table 1) with as main parameter the burn-up level from 30 to 65 GWd/t.

In this paper, we will concentrate on the analysis of the three first UO_2 tests REP Na1, REP Na2, REP Na3 with some elements on REP Na4 and REP Na5.

The interpretation of these tests is based on the experimental results including non-destructive and destructive examinations as discussed in [5] and [6] and on the quantitative analysis performed with the SCANAIR code [3].

Evaluation of open issues and future tasks will be discussed.

TABLE 2 : MAIN CHARACTERISTICS OF THE TESTS

	REP Na1	REP Na2	REP Na3	REP Na4	REP Na5
Test fuel rod fissile length (mm)	EDF/Fabrice 569	BR3 rod 1000	EDF/segmented 440	EDF/Fabrice 571	EDF/Fabrice 571
Cladding	standard	standard	improved	standard	standard
Pint-Pchannel (b)	0.	0.	2.	2.	2.
Enrichment (%)	4.5	6.85	4.5	4.5	4.5
Burn-up (Gwd/t) (max. rod)	63.8	33.	52.8	62.3	64.3
Corrosion thickness (μ)	80	4	40	80	20
Gap gas composition	83.3% He + 16.7% Xe	He	He	He	He
Test energy deposition (cal/g) at 0.4 s	110	211	120	95 (at 1.2 s)	105
Power pulse width (ms)	9.5	9.5	9.5	# 60.	9.
Diametral maximum clad strain (mean value, %)	-	3.5	2.1	not yet available	not yet available
Rod failure	yes	no	no	no	no
Maximal clad elongation (mm)	-	10	6	not yet available	not yet available
Maximal fuel elongation (mm)	-	4	not available	not yet available	not yet available
Transient FGR (%)		5.5	13.4	not yet available	not yet available

II. DESCRIPTION OF THE CABRI REP Na TESTS

1) Tests conditions

The REP Na tests are performed in the sodium loop located in the centre of the CABRI reactor. The experimental procedure and the instrumentation for test diagnostic are discussed in [5].

The coolant channel conditions are the following :

- sodium inlet temperature : 280°C,
- sodium velocity : 4 m/s,
- coolant outlet pressure : 2 b

Except the pressure level, these thermal-hydraulic conditions simulate the PWR reactor hot-stand-by state.

The power transient is initiated from initial zero power and has a 9.5 ms half width : such rapid power pulse is consistent with the existing RIA data base (SPERT, NSRR tests). The energy deposition corresponds to the maximum power of the CABRI driver core.

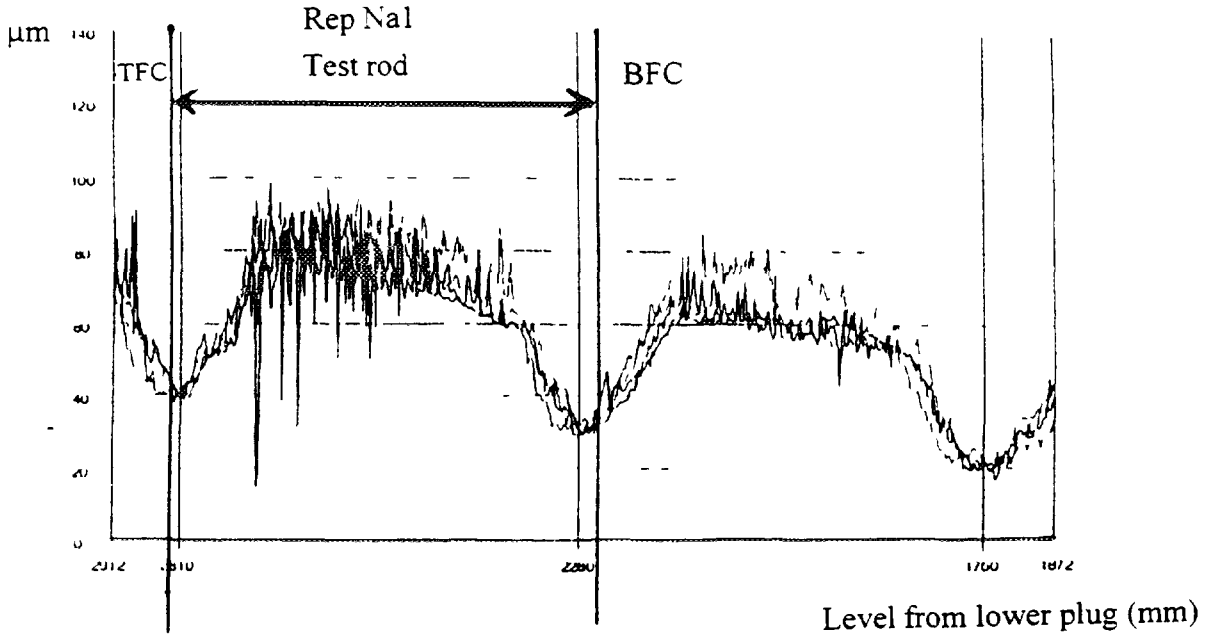

FIG. 1. Oxide thickness on the part of the PWR rod QO_2 for CABRI Rep Na 1 test.

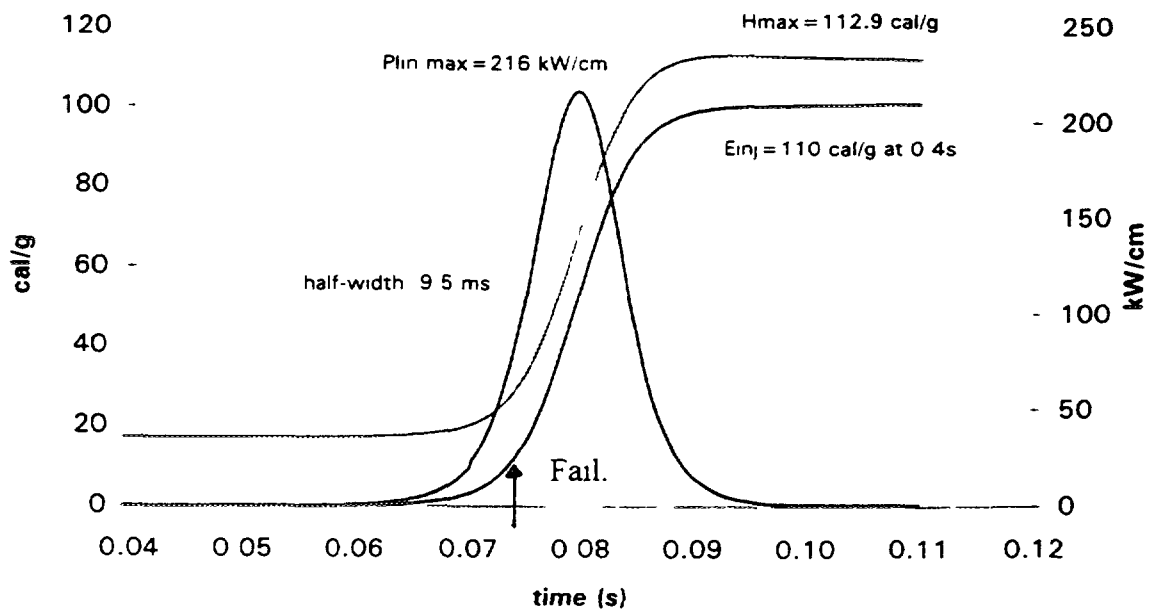

FIG. 2. Lineic power, injected energy and fuel enthalpy at Peak Power Node Rep Na 1.

In the future tests, power pulses with larger half width (25 to 60 ms), will be realised in order to better simulate reactor transients.

The axial power profile along the test rod is of cosine shape following the CABRI flux and the radial power profile depends on the self-shielding varying with the rod burn-up (maximum power in the periphery of the rod).

The main characteristics of the tests REP Na1 to 5 are summarised in table 2.

Special features of the rods may be noticed :

- the presence of the rim zone in REP Na1, 4, 5 (200 µm thickness) and REP Na3 (100 µm thickness) due to the high burn-up level of the rods,
- the important clad corrosion in REP Na1 (standard cladding) with hydrogen content up to 700 ppm, spallation and scaling off of the zirconia layer (fig. 1).

2) Main features of the quantitative analysis with the SCANAIR code

The SCANAIR code [3] describes the fuel and clad thermo-mechanical behaviour during fast power transients starting from the initial state of the fuel rods given by the irradiation codes such as TOSURA-REP (IPSN) or METEOR (CEA/DRN).

The fuel swelling induced by fission gases is taken into account based on intra-granular and inter-granular gas behaviour.

The deformation induced by the presence of cracks is described and the plastic strains are given by the Prandtl-Reuss laws.

The fuel creep mechanism is only simulated by a softening temperature but the clad creep is not described (no clad ballooning description in the present version).

The main points to be compared to the experimental results are the clad and fuel elongations, the clad plastic deformation if any, and the fission gas release from fuel due to the transient.

III. THE REP Na1 TEST

The main result of this test is the occurrence of an early rod failure when only 11.7 cal/g [5] has been injected at peak power node (PPN). At the location of the first failure, 8.75 cm above bottom of fissile length, the energy deposition is 8.9 cal/g due to the axial power profile. Taking into account the initial fuel enthalpy of 17.1 cal/g the rod failure occurred with a maximum fuel enthalpy of 29 cal/g at PPN (see fig. 2) and 26 cal/g at failure level.

The rod failure led to fuel ejection into liquid sodium with sodium flow ejection and pressure peaks of 9-10 b.

The evolution of the channel voiding zone and of the temperature given by the thermocouples are understood as due to the passage of hot gases from the fuel.

A partial blockage of the test channel has been observed (reduced residual flow).

1) **Analysis of the failure scenario**

At the time of failure no significant fuel and clad heat-up nor clad deformation are expected as confirmed by the SCANAIR code which indicates a maximum fuel temperature in the periphery of the pellet of 600°C at PPN (fig. 3) and no clad plastic deformation.

The detailed examinations of the clad showed multiple failure sites with cracks of brittle type and axial propagation [6]. They also evidenced the presence of a multitude of hydride accumulations with crack initiation in the external part.

Such features are similar to the pre-test observations made on twin samples and indicate that those hydrides were present in the clad before the CABRI test as a result of the scaling-off of the zirconia layer.

Indeed, in case of high burn-up fuel rods similar to REP Na1, the disappearance of the zirconia layer at some places has also been observed in association with hydride accumulation, so called "sun burst" : this can be explained by precipitation of the hydrides due to creation of a cold point in the clad after contact with coolant (no more thermal insulation by the ZrO_2 layer).

On the other hand, measurement of H_2 content in the REP Na1 clad after test, indicated no modification of the mean hydrogen concentration which is a confirmation of the absence of hydriding during the test.

Concerning the fuel, the main outcomes from the post test examinations are the following :

- large fuel swelling (5 to 10 %) occurred along the test pin, after clad failure,
- loss of cohesion at the grain boundary is observed and may result from over pressurisation of the grain boundary gases during the fast power pulse,
- the total amount of fuel loss is evaluated to 6 g (hodoscope) but is not only due to the rim particles entrainment ; fuel fragments ($\varnothing > 40$ µm) from the inner fuel part have also been ejected out of the rod,
- total scaling off of the zirconia layer,
- no release of intragranular gases has been observed (EPMA) indicating that the driving force for fuel pressurisation resulted from inter-granular and porosity gases.

So, as a summary, the rod failure in REP Na1 can be understood as the result of :

- the action of the rim zone in which the rapid temperature transient above the irradiation conditions creates gas pressurisation and fuel fragmentation, loading the clad ; indeed at such enthalpy level ($\approx$ 30 cal/g), the classical fuel swelling resulting from diffusion process cannot be activitated and cannot take part in the clad loading.
- the low mechanical resistance of the clad due to high corrosion level with spalling zirconia which favours hydride concentration and thus embrittlement.

Such a mechanism is confirmed by the absence of failure in REP Na3 and REP Na5 with high burn-up fuel rods (52.8 and 64.3 GWd/t respectively) and thus presence of rim zone but with lower oxidation level (40 µm and 20 µm respectively) and without spallation.

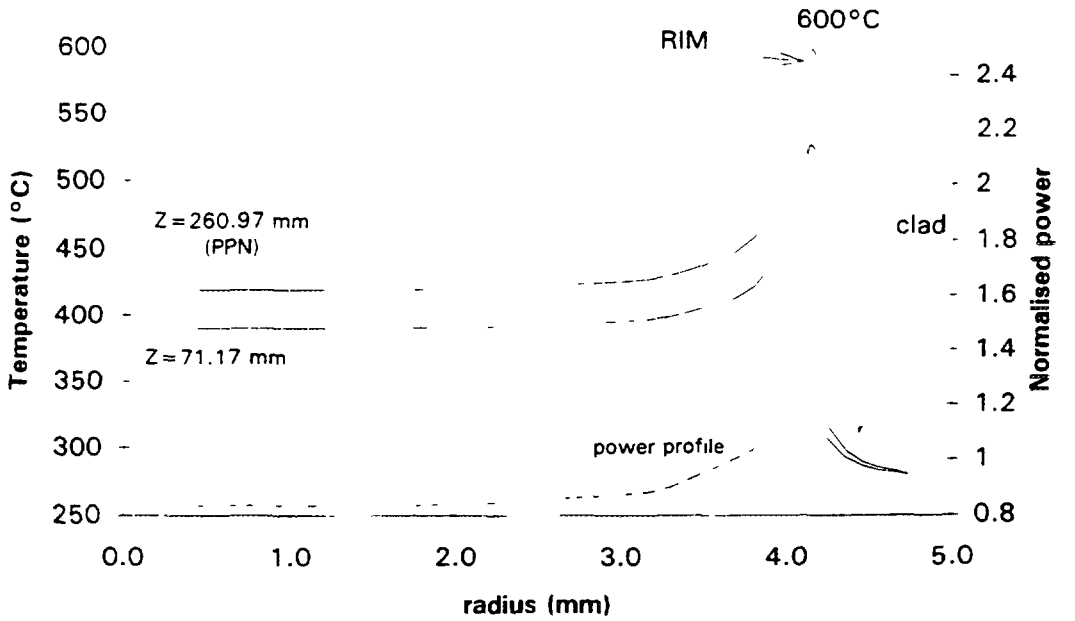

FIG. 3. Rep Na 1: Temperature (radial distribution) at failure time (# 74 ms) SCANAIR results.

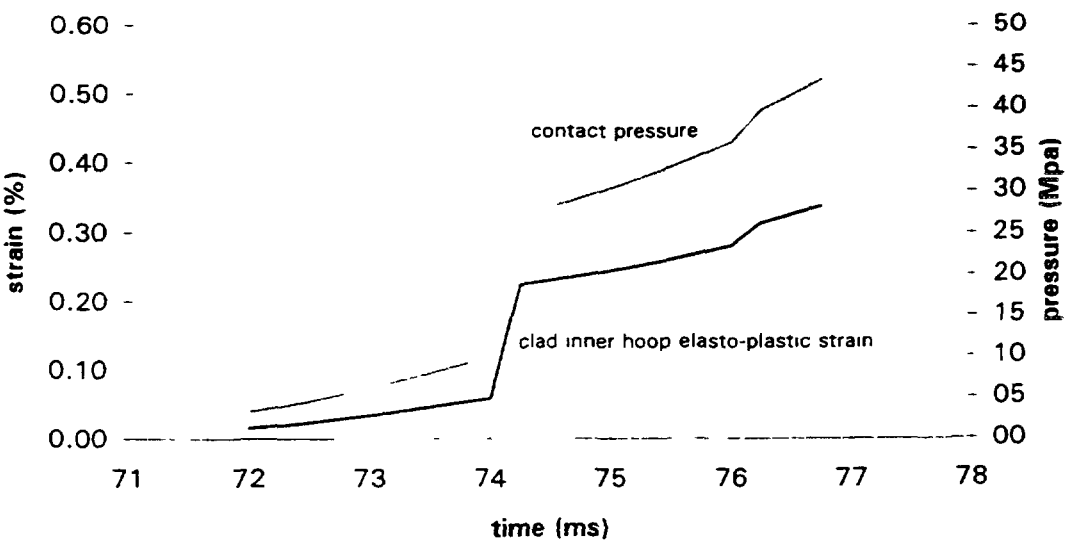

FIG. 4. Rep Na 1: clad elasto-plastic strain and contact pressure at failure location. SCANIAR results.

In the recent test REP Na4 with similar burn-up and oxide thickness as in REP Na1, two parameters have been changed simultaneously : the power transient half-width of 60 ms and the state of the zirconia layer without any spallation. The absence of failure in this test seems, to be rather related to the uniform oxidation layer.

Another important outcome from REP Na1 test is that after failure the fuel dispersion occurred with solid fragmented fuel.

2) Description with SCANAIR

In the SCANAIR code (version 2.2), the simulation of the rim behaviour is made with the following assumptions :

- the grain boundary fragmentation is due to overpressurisation of the gas bubbles compared to equilibrium state,
- after fragmentation and due to high porosity of the rim zone, the fuel behaves as a mixture of gas and particles (hydrostatic behaviour) with direct loading on the clad .

The application to REP Na1 (fig. 4) shows that at the time of experimental failure, the fuel fragmentation in the rim leads to a sharp increase of the contact pressure (up to 270 b) and thus to a high clad strain rate, with no plastic clad deformation.

Uncertainty on the contact pressure may be related to the knowledge of the initial state of the fuel rod (gas quantity in the rim zone, threshold for fragmentation).

However such contact pressure may lead to clad failure when applied on initially brittle clad at temperature of 280°C and especially with high strain rate of more than 1/s.

At the present time, the clad mechanical behaviour in such conditions is not known and this underlines the need to perform mechanical testing in the transverse direction [7] with clad samples from similar rods as the test rod (local hydriding).

IV. THE REP Na 2 AND REP Na 3 TESTS

IV.1. Analysis of the experimental results

In the REP Na2 test using a BR3 Rod irradiated to 33 GWd/t with very low oxidation level, the fast power pulse injected 211 cal/g at 0.4 s while in REP Na3, using an EDF segmented rod of 52.8 GWd/t burn-up with 40 µm of oxide layer, the energy injection has been 120 cal/g at 0.4 s.

In both tests, the rod did not fail but significant clad plastic deformation has been obtained.

In REP Na2, there is evidence of a pronounced "bamboo effect" with maximum deformation at the edges of the pellets reaching 4.2 % at PPN while the mean value is 3.5 % (fig. 5). Such feature is the classical result of a plastic deformation due to pellet-clad mechanical interaction with parabolic temperature profile inside the fuel (as in operating conditions).

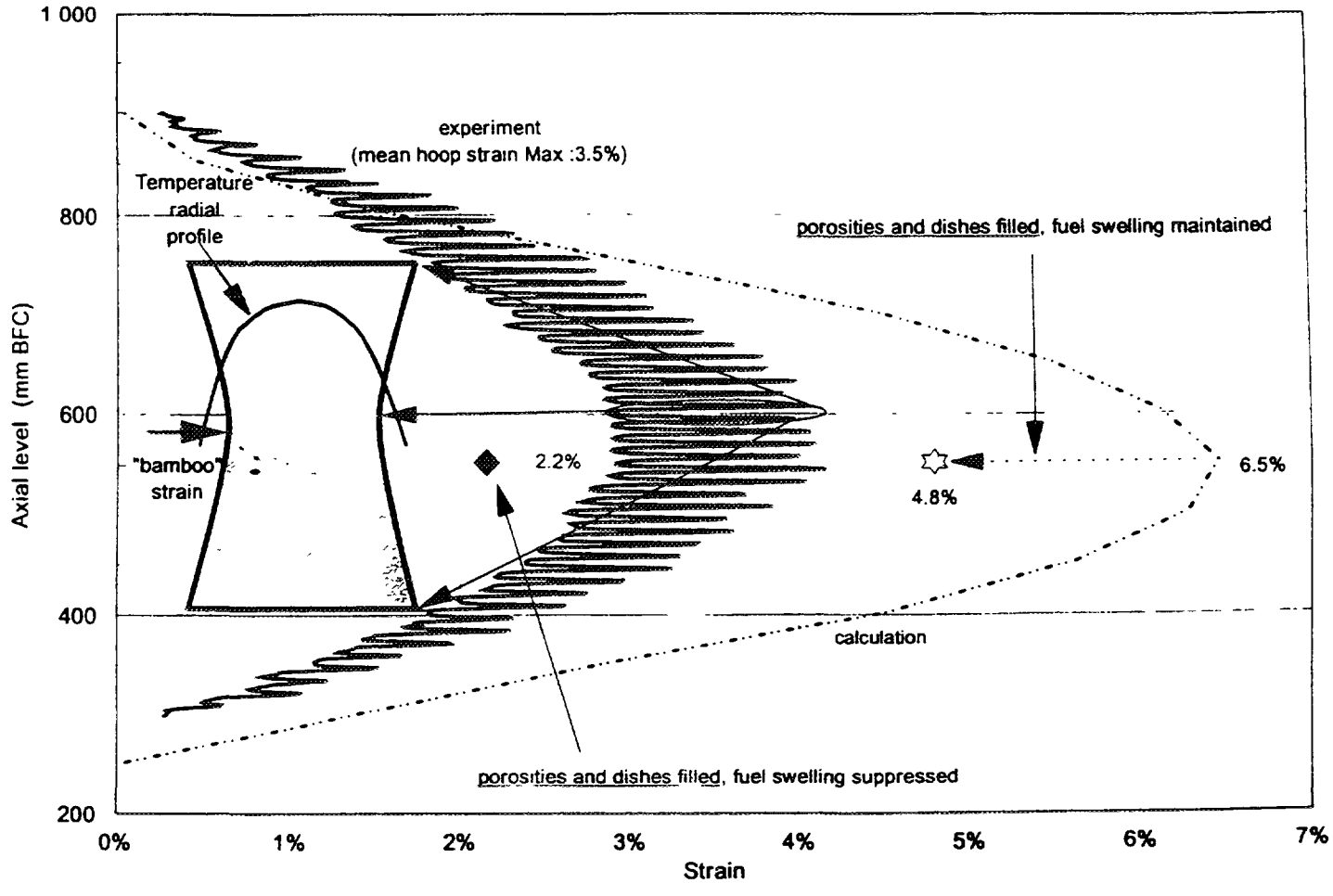

FIG. 5. Calculated clad plastic hoop strain axial profile.

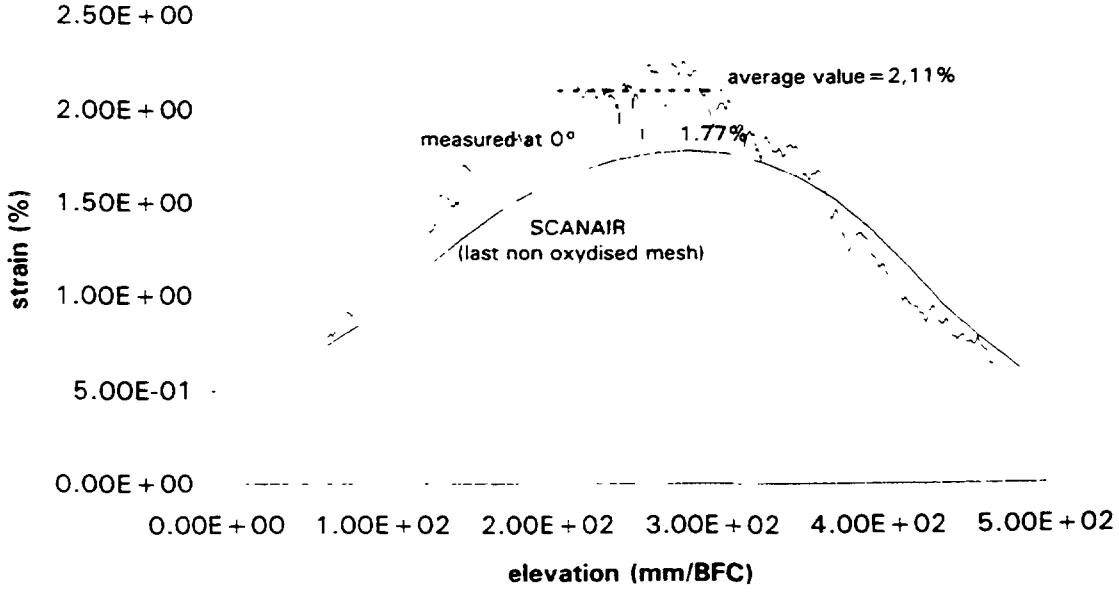

FIG. 6. Axial profile of clad plastic hoop strain reference case REPNA 3.

In REP Na3, the clad deformation shows maximum values at the mid-height of the pellets, the mean value being 2.1 % at PPN (fig. 6). This shape may be explained by a clad loading with maximum fuel temperature in the peripheral part as it occurs in the first phase of fast power transients due to the radial power profile with maximum power in periphery (Pperiphery/Pcenter : 2.56 in REP Na3, 1.9 in REP Na2).

Nevertheless, in both tests, the axial profile of the mean deformation follows the axial power profile (cosine shape).

The occurrence of significant clad deformation is consistent with :

- the transient volume change as shown by the sodium flow expulsion [5] which is more pronounced in REP Na2 than in REP Na3 according to the different amplitudes of clad deformation,
- the measurement of the fuel and clad elongations as given in Table 2.

On the other hand, the destructive examinations of the REP Na2 rod showed :

- a total filling of the pellet dishings which traduces a highly plastic fuel behaviour due to high temperature level in the test,

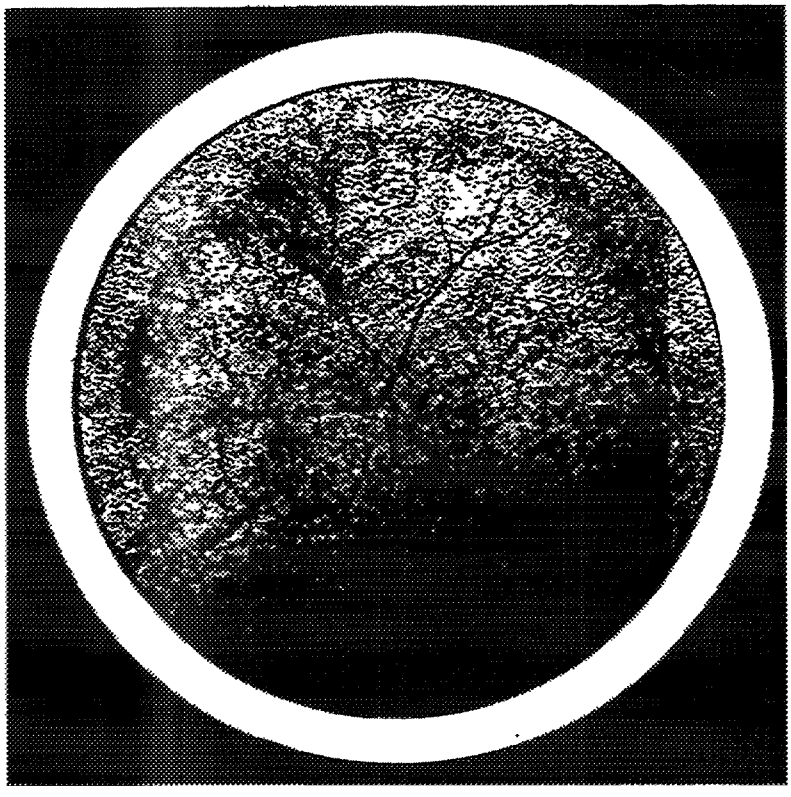

1 mm

REP Na 2 CR1 519.5 mm/bcf

FIG. 7 Radial cut at 519.5 mm from bottom of fissile column.

- inside the fuel, the formation of a radial zone in the periphery of the pellets, with high porosity and loss of grain cohesion (fig. 7) ; this results from fuel fragmentation due to grain boundary separation in the region where maximum fuel temperature is reached.

At the present time, the destructive examinations of REP Na3 are not completed but no evidence of filling of the pellet dishings is found.

The fission gas release measurements indicated a release of 5.5 % in REP Na2 (21.7 cm^3 NTP) and 13.4 % (45 cm^3 NTP) in REP Na3. Taking into account the difference of the rods burn-up and the associated gas retention, these results show that the fission gas release is highly correlated to the irradiation level.

IV.2. SCANAIR results

Both tests have been calculated with the Scanair code (version 2.2) on the basis of the initial state of the rods given by the TOSURA-REP results and taking into account the presence of the clad oxide layer (thermal effect).

IV.2.1. REP Na2

Due to the high energy injection, the calculated maximum fuel enthalpy (radially averaged) is 206 cal/g (at 95 ms) and the maximum fuel temperature reaches only very temporarily 2815°C (at PPN) which is close to melting temperature.

The fig. 8 shows the radial profile of the fuel temperature at different times in the transient. We can note that after 250 ms, the radial profile becomes of parabolic shape and that high temperature level is maintained in the centre of the fuel (above 2000°C up to 3.5 s) : this contributes to activate fuel swelling and explains the clad deformation shape ("bamboo").

The calculated maximum plastic clad deformation reaches 6.5 % (fig. 5) which is over-estimated compared to the mean experimental value of 3.5 % (no description of the bi-dimensional effect in SCANAIR). A sensitivity study has shown that this result cannot be explained by the uncertainty on the clad mechanical properties.

However, such over-estimation is consistent with the absence of description in SCANAIR of the filling of dishings volume due to creep mechanism at high temperature level and with the assumption that the fuel porosity is maintained even under significant fuel swelling (not justified at high temperature level).

Substracting those volume contributions from the fuel swelling would lead to a clad deformation of 4.8 % still higher than the experimental value. On the other hand, the clad deformation which would result of the only contribution of the fuel dilatation (without swelling) would reach 2.2 % : this confirms the role of the fuel swelling in the REP Na2 clad loading, with however over-estimation at high temperature by the present SCANAIR modelling

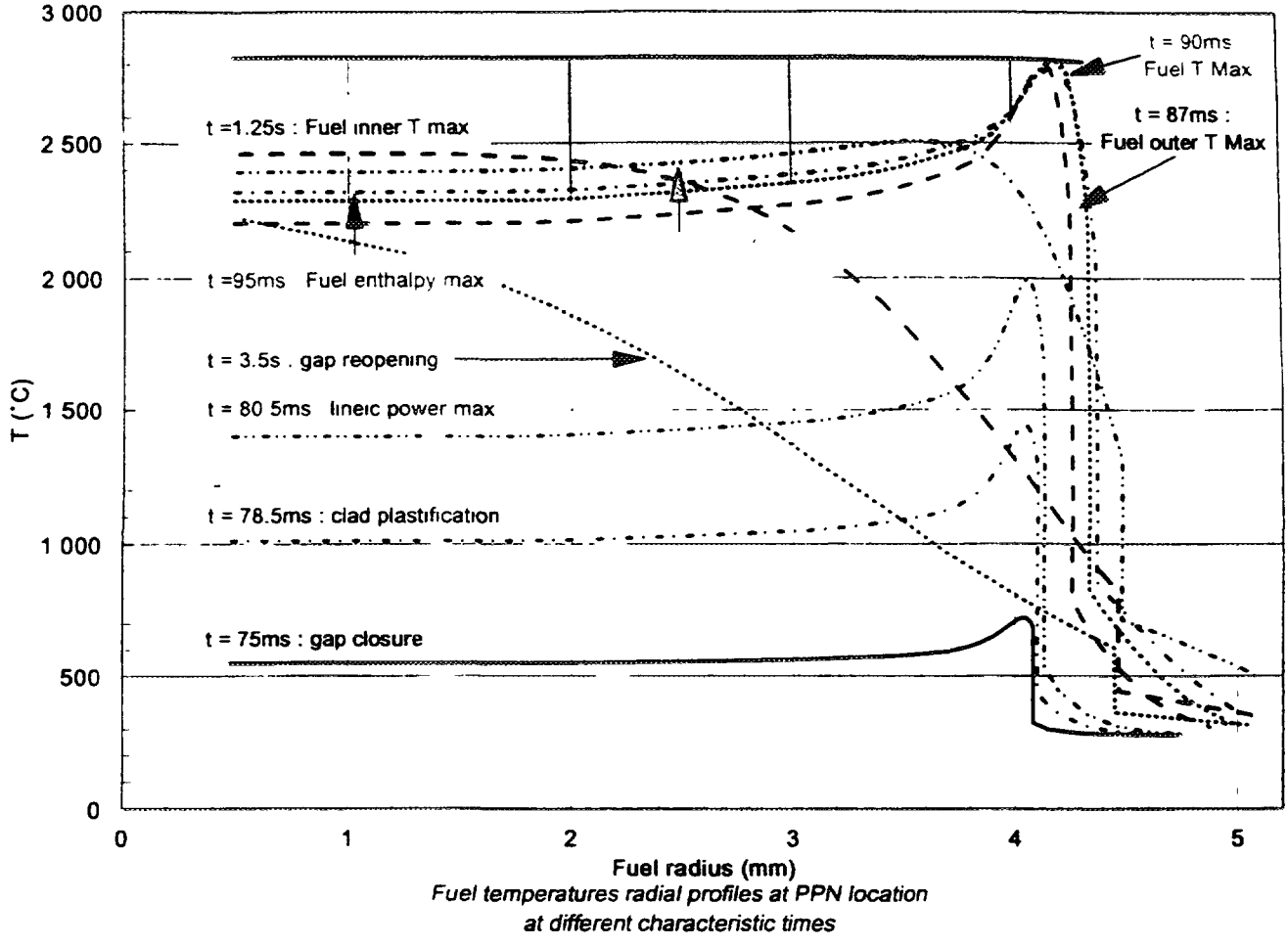

FIG. 8. Fuel temperatures radial profiles at PPN location at different characteristic times.

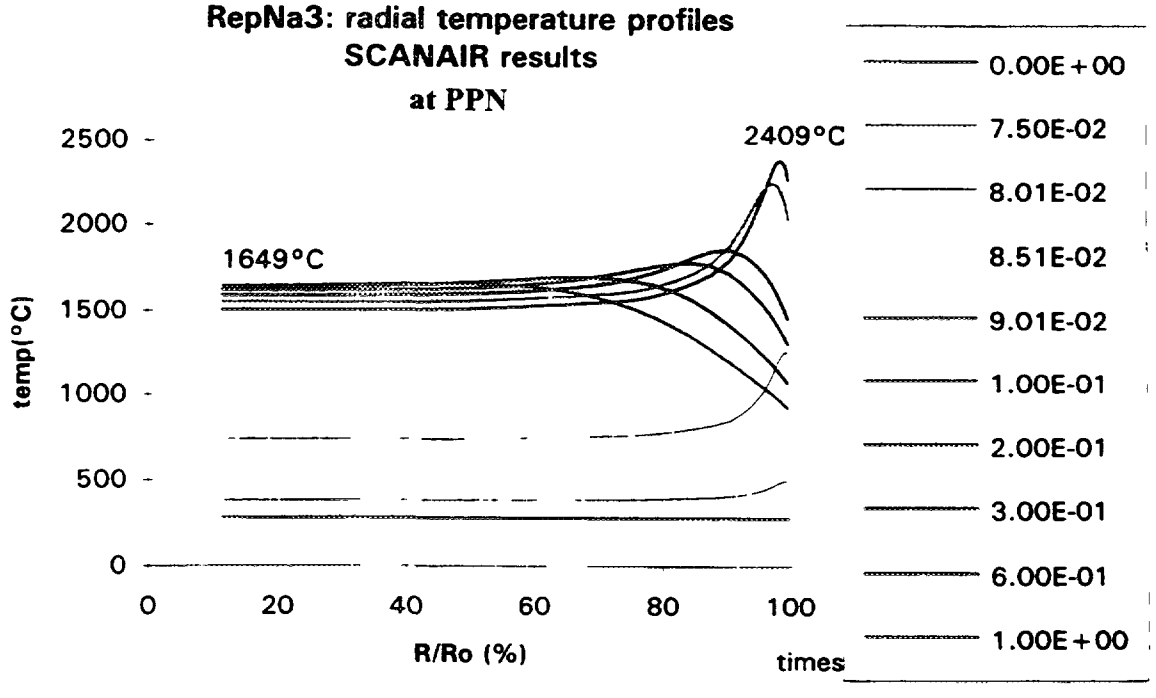

FIG. 9. Rep Na 3: radial temperature profiles SCANAIR results at PPN.

Such over-prediction is also reflected by the calculated maximum fuel and clad elongations.

Fuel fragmentation due to the rapid temperature increase is found in the pellet periphery consistently with the evidence of the porous zone seen on the radial cuts.

The calculated fission gas release amounts to 17 cm^3 NTP in reasonable agreement with the measurement (21.7 cm^3 NTP).

IV.2.2. REP Na3

The best-estimate description of REP Na3 with SCANAIR has been obtained with the upper limit of energy injection within the uncertainty margin (125 cal/g at 0.4 s) and led to a maximum fuel enthalpy of 131 cal/g.

The figure 9 shows the radial temperature profile at different times with a maximum temperature of about 2410°C reached in the pellet periphery at 90 ms.

The main difference compared to the REP Na 2 test is the fact that the temperature in the fuel centre stays below 1650°C (higher than 2000°C in REP Na2) which reduces the fission gases induced swelling for clad loading.

In REP Na3, the clad deformation occurred in the first phase of the transient and reached 1.8 % (fig. 6) slightly below the experimental value of 2.1 %. In REP Na2, such kind of deformation has been erased by the continuous loading due to the high temperature level under cosine radial profile.

The calculated maximum clad elongation (7.7 mm) and the residual fuel elongation (1.2 mm) are in reasonable agreement with the experimental values (respectively 6 mm and 3 mm ± 2 mm).

The calculated fission gas release due to migration of intra-granular gases to porosities (free volume) amounts to 20 cm^3 to be compared to 45 cm^3 measured. At high burn-up this might be explained by additional gas release from gases retained inside the porosities at end of irradiation and will be taken into account in the future development of the SCANAIR code.

V. DISCUSSION OF THE RESULTS AND OPEN ISSUES

The interpretation of the first CABRI REP Na tests has shown that with irradiated PWR rods, significant clad deformation and even rod failure may be obtained under RIA transients.

These results may be related to the fast power transient (9.5 ms half width compared to 30 - 80 ms in reactor situation).

Indeed a sensitivity study performed with SCANAIR with different pulse half-widths (9, 20, 60 ms) has shown that with similar total energy injection, a fast power pulse (hw = 9 ms) leads to higher fuel temperature and clad deformation than a slower transient (hw = 20.60 ms).

From the analysis of the tests, we can postulate different phases of the clad loading scenario with rod failure potential during a RIA transient as illustrated by the following scheme :

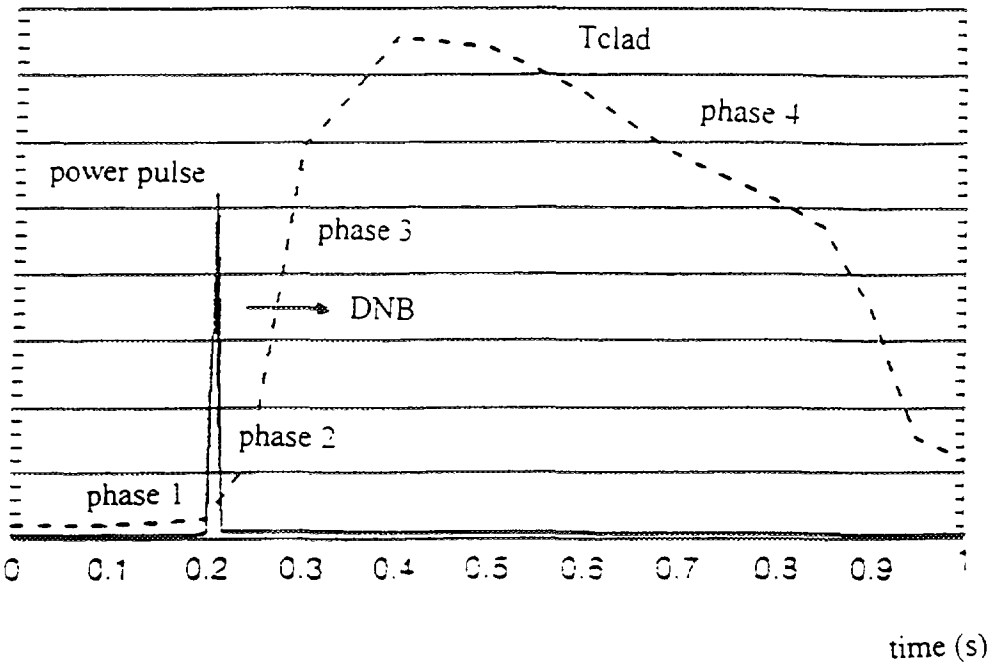

In a very early phase (some ms), rod failure may occur due to gas pressurisation and fuel fragmentation with brittle cladding (rim behaviour, REP Na1).

In a second phase (up to hundred ms), strong pellet-clad mechanical interaction may occur due to thermal fuel dilatation and swelling and is increased with energy deposition and burn-up level (REP Na2, REP Na3, NSRR tests [4]).

In the reactor situation with pressurised water environment, a third and fourth phases may appear due to departure from nucleate boiling (DNB) occurrence.

In this case, due to the lower clad-coolant heat transfer, the fuel temperature will be maintained at high temperature level during a longer time leading, in spite of clad dilatation, to continuous clad loading if sufficient energy is injected.

Indeed, the REP Na2 rod would have certainly encountered DNB in pressurised water conditions due to less efficient cooling with water compared to sodium and this would have most likely led to rod failure. This might also be true for REP Na3 and REP Na5.

Finally, in a fourth phase, clad ballooning might occur after sufficient gas release and clad heating (long term event) and lead to failure under quenching.

The two last situations are not addressed presently neither by the CABRI REP Na tests nor by other available tests.

In fact, a pressurised water loop associated to an in-pile power transient facility does not exist world-wide

In fact, a pressurised water loop associated to an in-pile power transient facility does not exist world-wide.

At the present time, the only investigation in realistic thermal hydraulic conditions concern the determination of clad-coolant heat transfer correlation under fast power transients (out of pile experiments underway in CEA).

A project study to implement a pressurized water loop in the CABRI reactor has been initiated [8] based on the need of representativity for fission gas behaviour, DNB occurrence and post-DNB phenomenology.

Without availability of a fully representative test facility, two major points must be studied by analytical testing for a better description in SCANAIR of the thermo-mechanical rod behaviour :

- the fission gases behaviour from initial state during the whole transient with gas pressurisation in the rim zone, fuel fragmentation, fuel swelling, gas release ; analytical tests have been proposed in NSRR facility but their feasibility is not reached,

- the clad mechanical properties, in particular for highly corroded clad as in REP Na1 [7].

VI. CONCLUSION.

The first CABRI REP Na tests have shown that highly irradiated fuel (up to 63 Gwd/t) submitted to a RIA transient may experience early rod failure with solid fuel ejection into the coolant. Such behaviour has been understood as the result of gas pressurisation inside the rim zone and clad embrittlement due to the spallation of the oxide layer and related hydride accumulation.

In case of less oxidised clad (REP Na3, REP Na5) and/or lower burn-up (REP Na2), the experiments have demonstrated a satisfying rod behaviour with nevertheless significant clad deformation due to fuel thermal dilatation and fuel swelling, function of the energy injection.

The fuel ejection in REP Na1 and the evidence of fuel fragmentation in the hot fuel zone in the other tests, underlined the fact that in case of rod failure, fragmented solid fuel (down to 0.1 μm) with associated fission gases is already available for fuel-coolant interaction with a potential high energy conversion rate.

It must be stated that such tests in the CABRI sodium loop are not fully representative of the whole sequence of a RIA due to the impossibility to study the long-term phenomena (occurrence of DNB, post-DNB events).

However, the first analysis with the SCANAIR code has succeeded to explain the mechanism for clad loading but additional knowledge is needed for better quantification of the results in the field of gases behaviour (initial state, transient behaviour) and clad mechanical properties. The analytical experiments which are underway should improve the quantification of the results.

Future REP Na tests will concern the effect of wider power transients and the study of the MOX fuel behaviour at different irradiation levels.

REFERENCES

[1] J. PAPIN, J.P. MERLE.
Irradiated fuel behaviour during reactivity initiated accidents in LWR : status of research and development studies in France.
21st WRSM, Bethesda, USA, Oct. 93.

[2] F. SCHMITZ, J. PAPIN, M. HAESSLER, J.C. NERVI, P. PERMEZEL.
Investigation of the behaviour of high burn-up PWR fuel under RIA conditions in the CABRI test reactor.
22nd WRSM, Bethesda, USA, Oct 94.

[3] J.C. LATCHE, F. LAMARE, M. CRANGA.
Computing Reactivity Initiated Accidents in PWRs.
SMIRT 13th, Porto Alegre, Brésil, August 95.

[4] K. ISHIJIMA, T. FUJISHIRO, K. SHIBA.
Behaviour of pre-irradiated LWR fuel rods under Reactivity Initiated Accident Conditions.
AIEA Technical Committee Meeting, TECDOC 706 Aix en Provence, March 92.

[5] M.C. ANSELMET-VITIELLO
The experimental test programme for the study of high burn-up PWR rods under RIA conditions in the CABRI core.
This meeting

[6] P. MENUT, D. LESPIAUX, M. TROTABAS.
Cladding and fuel modifications of a 60 GWd/t irradiated rod during a power transient performed in the CABRI reactor.
This meeting

[7] M. BALOURDET, C. BERNAUDAT.
Tensile properties of irradiated zircaloy-4 cladding submitted to fast transient loading
This meeting.

[8] J. FURLAN, M. HAESSLER, F. SCHMITZ, J. PAPIN, A. TATTEGRAIN
The project to implement into CABRI a pressurised water loop. Motivations and objectives of the future test program.
This meeting.

LIST OF PARTICIPANTS

CZECH REPUBLIC

L. Belovsky	Nuclear Research Institute Rez, plc 250 68 Rez
R. Rehacek	State Office for Nuclear Safety Slezská 9 120 29 Prague 2

BELGIUM

B. Boesmans	Belgatom Ariane Avenue 7 1200 Brussels

FRANCE

J P. Breton	IPSN/DRS - CEN CADARACHE - BAT. 702 F-13108 Saint-Paul-lez-Durance
J.-Y. Blanc	CEA-DRN/DMT/SEMI/LECM 91191 Gif-sur-Yvette
G Ducros	CEA/DRN/DTP Rue des Martyrs 17 38054 Grenoble
B Adroguer	Institut de Protection et de Sûreté Nucléaire (IPSN), CE Cadarache 13108 St. Paul-lez-Durance
J.P. Mardon	FRAMATOME Nuclear Fuel Rue Juliette Recamier 10 69456 Lyon Cedex 06
J.-M. Gatt	DER/SERA/LAPE CE Cadarache 13108 St. Paul-lez-Durance Cedex

INDIA

P. Balakrishna	Nuclear Fuel Complex Hyderabad 500 062

JAPAN

K. Ishijima	Tokai Research Establishment JAERI, 2-4 Shirakata-Shirane Tokai-mura, Naka-gun Ibaraki-ken 319-11

UKRAINE

A.A. Afanasyev	Ukrainian State Committee on Nuclear Power Utilization "GOSKOMATOM" 9/11 Arsenalnaya st. 252011 Kiev
V.S.Krasnorutskiy E.A.Reznichenko	National Science Centre "Kharkov Physical and Technology Institute" 310108, Kharkov, Akademicheskay str.,1

U S A

R. Moore	Department of Energy, NE-50 Washington D.C. 20585

RUSSIAN FEDERATION

V.B. Ivanov V.P. Smirnov V.A. Krasnoselov Yu. Shtuckert V.A. Ovchinnikov V.M. Makhin A.V. Goryachev I.A. Kungurtzev V.G. Dvoretsky V.N. Golovanov	State Scientific Centre Research Institute of Atomic Reactors 433510 Dimitrovgrad, Ulyanovsk Region
N.B. Sokolov A.V. Salatov L.N. Andreeva-Andrievskaja	State Scientific Centre All-Russia Research Institute of Inorganic Materials (VNIINM), Rogova 5

E.K. Karasev

Research and Development Institute of PowerEngineering (NIKIET)
101000 Moscow

K.N. Koscheev

SF NIKIET
624051 Zarechny, Sverdlovsk Region

A.M. Voltchek

IBRAE RAN
Nuclear Safety Institute
Russian Academy of Science

A.K. Kiselev

113191, B.Tulskaya, 52, Moscow

V.M. Trojanov

Institute of Physics and Power Engineering

P.S. Pometko

249020 Bondarenko Sq. 1
Obninsk, Kaluga Region

V.B. Ponomarenko

Moscow Polymetal Plant
49, Kashirskoye Shosse
115409, Moscow

L. Egorova

Kurchatov Institute
123182 Moscow

V.Doil'nitsyna

All-Russia Research Institute
of Power Technology (VNIPIET)
S.-Peterburg, Savushkina, 83.

IAEA

G. Sukhanov

International Atomic Energy Agency
Wagramer Strasse 5, P.O.Box 100
A-1400 Vienna, Austria